Title
Exotic Phases and Phase Transitions in Quantum Matter

Author
Wu, Xiaochuan

Publication Date
2022

Peer reviewed|Thesis/dissertation

University of California
Santa Barbara

Exotic Phases and Phase Transitions in Quantum Matter

A dissertation submitted in partial satisfaction
of the requirements for the degree

Doctor of Philosophy
in
Physics

by

Xiaochuan Wu

Committee in charge:

Professor Cenke Xu, Chair
Professor Matthew P. A. Fisher
Professor Andrea F. Young

September 2022

The Dissertation of Xiaochuan Wu is approved.

Professor Matthew P. A. Fisher

Professor Andrea F. Young

Professor Cenke Xu, Committee Chair

July 2022

Exotic Phases and Phase Transitions in Quantum Matter

by

Xiaochuan Wu

Acknowledgements

Over the past five years, I was unavoidably asked by many people on various occasions, "when are you going to graduate?" A little bit surprising to everybody, my instinctive answer is always, "I am not sure yet, but I do not want to graduate." I know it is partly due to the beautiful weather in Santa Barbara. However, the most important reason is that working with my advisor Cenke Xu has been such an enjoyable experience. I have benefited immensely from his patient guidance, constant encouragement, and generous support. I am amazed by Cenke's capability to identify interesting universal physics and make connections to experimental realities. I learned to appreciate and share his taste for problems in condensed matter physics. In addition, his enthusiasm can often give me a lot of courage to face challenging problems. I am deeply grateful that I could always get a timely response whenever I contacted him, even during the hard times of the epidemic.

I would like to express my deepest appreciation to professors Matthew P. A. Fisher and Andrea F. Young for servings on my committee. Their advice and questions helped me improve and think more deeply about my research area.

I want to mention this thesis would not be possible without the contributions of Chao-Ming Jian, who has acted, in many ways, as my second advisor. Chao-Ming is extremely helpful and always has a clear explanation for my questions. Discussions with him continually broadened my horizons and shed new light on my knowledge. I cannot thank Chao-Ming enough for the collaborations and guidance over the years and the support for my postdoc application.

During the past two years, I learned a lot from Leon Balents. I greatly appreciate that Leon allowed me to attend his group meetings. Thanks to Leon, I also had an unforgettable experience collaborating with Pengcheng Dai's experimental group. (Special thanks to Michael Flynn and Tong Chen for this project.) I am deeply impressed by

Leon's style of doing physics, marked by a deep insight into experimental data combined with brilliant technical skills in theory. In addition, I would like to acknowledge that Leon has selflessly helped me with the postdoc application.

I want to thank the other group member and long-time collaborator, Yichen Xu, and I enjoyed our free-ranging discussions inside and outside physics. In addition, I have been fortunate to collaborate with many outstanding researchers, including Wenjie Ji, Mengxing Ye, Zhu-Xi Luo, Xiao Chen, Anna Keselman, Haoyu Guo, etc.

To the previous group member Zhen Bi, I am deeply grateful for your help with my application for UCSB graduate school and, later, my postdoc application. Although we have not worked together, you are a role model that I can look up to.

I was fortunate to be a teaching assistant for Anthony Zee. I will never forget the long walk with Tony from the classroom to KITP. Tony's advice on how to be a good theoretical scientist is invaluable to me.

There are many other local peers to whom I owe thanks. To Chunxiao Liu, I am deeply in debt for all your help over the years. You gave me valuable advice and suggestions on the advancement exam presentation, the postdoc interviews, etc. I also want to thank you for the spontaneous and enjoyable conversations on a broad range of topics in physics. To Yaodong Li, thanks for being such a good roommate (and office mate). I had lots of fun living with you during the first year. I want to thank Chaitanya Murthy for organizing Many-Body Journal Club and Kasra Hejazi, Alan Tran, Yubi Chen, Taka Park, Mark Arildsen (in addition to Chunxiao and Yaodong) for the exciting discussions. I missed the old days when everybody was still at UCSB, and we could meet in person!

I want to acknowledge illuminating conversations with other condensed-matter community members, including Peng Ye, Yuan-Ming Lu, Shinsei Ryu, Meng Cheng, Sung-Sik Lee, Chong Wang, Yin-Chen He, Yichen Hu, Dan Mao, Ya-Hui Zhang, Xiao-Qi Sun, Yingfei Gu, Wenbo Fu, Rui-Xing Zhang, Yu-Ping Lin, Umang Mehta, Gang Chen, Kaix-

iang Su, Nayan Myerson-Jain, Yinhan Zhang, Oguzhan Can, etc. I especially want to thank Christopher Herzog for kindly meeting with Yichen Hu and me several times and educating us on many topics in high-energy theory.

Going further into the past, I am deeply grateful for the support from Ran Cheng, Di Xiao, Zhenyu Zhang, and Guo-Zhu Liu before I came to UCSB. I also want to thank some of my classmates/friends from college. I greatly value the friendship of Haoxin Zhou, my classmate at both USTC and UCSB. Thanks, Wenxia Wang, my college roommate, for being in touch for so many years and sharing interesting news with me. Thanks, Ji Zou, Shang Ren, and Hantao Zhang, for enjoyable conversations on a broad range of topics. Their enthusiasm for physics is contagious!

Over the past five years, I have been fortunate to make many friends both in and outside physics. I enjoyed playing basketball weekly with Lizhong Zhang, Kai Yu, Wangzhou Wu, Shuai Shao, etc. In addition, I am deeply grateful that Lizhong gave me a place to stay when I had a hard time looking for an apartment. I would also like to thank other friends who helped me and made my graduate school memorable, including Zhiran Zhang, Jiaoyue Yuan, Zhitao Chen, Wayne Weng, Tianji Cai, Yunlin Zeng, Suoqing Ji, Haoxiang Wang, Siyu He, Yizhou He, Andi Li, Hongbo Cai, Yufeng Shen, etc.

My special gratitude goes to my girlfriend Qianru Yang, who has been a source of constant love, support, and encouragement during my adventure of being a Ph.D. student. Despite the long spatial distance and 3 hours of the time difference between CA and PA, our past five years have been amazing. I look forward to our next journey!

Finally, I want to thank my parents, to whom my gratitude is beyond words. My father, who also majored in physics in college, instilled a love of natural science in me at an early age. In addition, my mother took excellent care of various aspects of my life during my growing up. All these years, they have provided me with an infinite amount of financial and emotional support. Without their loving care and encouragement

throughout my life, I would not have made it this far.

Curriculum Vitæ

Xiaochuan Wu

Education

2017 - 2022	PhD in Physics (Expected), University of California, Santa Barbara
2017 - 2020	MA in Physics, University of California, Santa Barbara
2011 - 2015	BS in Physics, University of Science and Technology of China

Awards and Honors

2020	UCSB Physics Summer Fellowship
2018	Gary T. and Corinne M. Horowitz Graduate Student Fellowship

Publications

19. *Deconfined quantum critical point with non-locality*
    Yichen Xu, **X.W.**, Cenke Xu,
    preprint arXiv:2206.14222
18. *Diffusive excitonic bands from frustrated triangular sublattice in a singlet-ground-state system*
    Bin Gao, Tong Chen, **X.W.**, Michael Flynn, Chunruo Duan, Lebing Chen, Chien-Lung Huang, Jesse Liebman, Shuyi Li, Feng Ye, Matthew Stone, Andrey Podlesnyak, Douglas Abernathy, Devashibhai Adroja, Manh Duc Le, Qingzhen Huang, Andriy Nevidomskyy, Emilia Morosan, Leon Balents, Pengcheng Dai
    (submitted to journal)
17. *A construction of exotic metallic states*
    X.W., Yichen Xu, Mengxing Ye, Zhu-Xi Luo, Cenke Xu,
    preprint arXiv:2203.14168, to appear in Chen-Ning Yang Centenary Festschrift
16. *Interaction-driven metal-insulator transition with charge fractionalization*
    Yichen Xu, **X.W.**, Zhu-Xi Luo, Meng-Xing Ye, Chao-Ming Jian, Cenke Xu,
    Phys. Rev. X 12, 021067 (2022)
15. *Universal features of higher-form symmetries at phase transitions*
    X.W., Chao-Ming Jian, Cenke Xu,
    SciPost Phys. 11, 033 (2021)
14. *Categorical symmetries at criticality*
    X.W., Wenjie Ji, Cenke Xu,
    J. Stat. Mech. 073101 (2021)

13. *Physics of symmetry protected topological phases involving higher symmetries and its applications*
    Chao-Ming Jian, **X.W.**, Yichen Xu, Cenke Xu,
    Phys. Rev. B 103, 064426 (2021)

12. *Continuous Néel-VBS quantum phase transition in non-local one-dimensional systems with SO(3) symmetry*
    Chao-Ming Jian, Yichen Xu, **X.W.**, Cenke Xu,
    SciPost Phys. 10, 033 (2021)

11. *Topological edge and interface states at bulk disorder-to-order quantum critical points*
    Yichen Xu, **X.W.**, Chao-Ming Jian, Cenke Xu,
    Phys. Rev. B 101, 184419 (2020)

10. *Boundary criticality of topological quantum phase transitions in two-dimensional systems*
    X.W., Yichen Xu, Hao Geng, Chao-Ming Jian, Cenke Xu,
    Phys. Rev. B 101, 174406 (2020)

9. *Non-Landau quantum phase transitions and nearly-marginal non-Fermi liquid*
    Yichen Xu, Hao Geng, **X.W.**, Chao-Ming Jian, Cenke Xu,
    J. Stat. Mech. 073102 (2020)

8. *Orbital order and possible non-Fermi liquid in Moiré systems*
    Yichen Xu, **X.W.**, Chao-Ming Jian, Cenke Xu,
    Phys. Rev. B 101, 205426 (2020)

7. *Interacting valley Chern insulator and its topological imprint on Moiré superconductors*
    X.W., Yichen Xu, Chao-Ming Jian, Cenke Xu,
    Phys. Rev. B 100, 155138 (2019)

6. *Lattice models for non-Fermi liquids with tunable transport scalings*
    X.W., Chao-Ming Jian, Cenke Xu,
    Phys. Rev. B 100, 075101 (2019)

5. *Ferromagnetism and spin-valley liquid states in Moiré correlated insulators*
    X.W., Anna Keselman, Chao-Ming Jian, Kelly Ann Pawlak, Cenke Xu,
    Phys. Rev. B 100, 024421 (2019)

4. *Coupled-wire description of the correlated physics in twisted bilayer graphene*
    X.W., Chao-Ming Jian, Cenke Xu,
    Phys. Rev. B 99, 161405(R) (2019)

3. *Emergent superconductivity in the weak Mott insulator phase of bilayer graphene Moiré superlattice*
    X.W., Kelly Ann Pawlak, Chao-Ming Jian, Cenke Xu,
    preprint arXiv:1805.06906

2. *Candidate theory for the strange metal phase at a finite-energy window*
   X.W., Xiao Chen, Chao-Ming Jian, Yi-Zhuang You, Cenke Xu,
   Phys. Rev. B 98, 165117 (2018)

1. *Spin-mechanical inertia in antiferromagnets*
   Ran Cheng, **X.W.**, Di Xiao,
   Phys. Rev. B 96, 054409 (2017)

Abstract

Exotic Phases and Phase Transitions in Quantum Matter

by

Xiaochuan Wu

This dissertation is devoted to the theoretical study of strongly correlated quantum many-body systems. The central theme is to understand the universal properties of quantum matter from the perspective of renormalization group (RG) fixed points. The guiding principles are provided by symmetries and 't Hooft anomalies, which are both preserved under RG flow and serve to constrain physical properties. The main body of this dissertation can be divided into four main parts.

The first part concerns boundary critical phenomena associated with symmetry-protected topological (SPT) phases and unconventional quantum phase transitions. Our results include new stable boundary phases and exotic boundary phase transitions in various dimensions. For example, a continuous Néel-VBS transition can be potentially realized at the 1+1D boundary of a 2+1D SPT state protected by SO(3) symmetry.

The second part is about two strongly correlated Moiré materials. *(1)* The band topology in twisted bilayer graphene (TBG) severely complicates the standard lattice model descriptions. Therefore, we seek an alternative and provide a coupled-wire framework describing the correlated physics in TBG. *(2)* As for the experimentally observed continuous metal-insulator transition in $MoTe_2/WSe_2$ heterobilayer, we provide a theoretical proposal involving charge fractionalization, which potentially explains the observed anomalously large critical resistivity.

The third part concerns exotic metallic states beyond Landau Fermi liquid theory. We study the problem mainly from two approaches. *(1)* In the perturbative RG approach, we show analytically controlled examples of marginal Fermi liquids involving non-Landau quantum critical points. In addition, we show charge fractionalization naturally leads to the bad metal behavior at low temperatures. *(2)* The other approach is based on exactly solvable toy models for quantum matter without quasiparticles. We construct a square-lattice model for the strange metal phase and generalize it for non-Fermi liquids with tunable transport scalings.

The fourth part is about generalized symmetries and their 't Hooft anomalies. *(1)* We illustrate how to unambiguously characterize generalized symmetries (including higher-form symmetries, categorical symmetries, and subsystem symmetries) at quantum phase transitions. *(2)* We discuss physical constructions and classifications of SPT states involving higher-form symmetries. Special attention is paid to anomaly constraints for condensed matter systems such as quantum dimer models.

Contents

List of Figures

List of Tables

Permissions and Attributions

1. The content of Sec. 2.1 is the result of a collaboration with Chao-Ming Jian, Yichen Xu, and Cenke Xu, and has previously published (on 12 February 2021) in SciPost Phys. 10, 033 (2021), licensed under the Creative Commons Attribution 4.0 License together with an author copyright.

2. The content of Sec. 2.2 is the result of a collaboration with Yichen Xu, Hao Geng, Chao-Ming Jian, and Cenke Xu, and has previously published (on 5 May 2020) in Phys. Rev. B 101, 174406 (2020). © The American Physical Society. Reproduced with permission. All rights reserved.

3. The content of Sec. 2.3 is the result of a collaboration with Yichen Xu, Chao-Ming Jian, and Cenke Xu , and has previously published (on 18 May 2020) in Phys. Rev. B 101, 184419 (2020). © The American Physical Society. Reproduced with permission. All rights reserved.

4. The content of Sec. 3.1 and App. B.1 is the result of a collaboration with Chao-Ming Jian and Cenke Xu, and has previously published (on 17 April 2019) in Phys. Rev. B 99, 161405(R) (2019). © The American Physical Society. Reproduced with permission. All rights reserved.

5. The content of Sec. 3.2 and App. B.2 is the result of a collaboration with Yichen

Xu, Mengxing Ye, Zhu-Xi Luo, Chao-Ming Jian, and Cenke Xu, and has previously published (on 28 June 2022) in Phys. Rev. X 12, 021067 (2022). © The American Physical Society. Reproduced with permission. All rights reserved.

6. The content of Sec. 4.1 is the result of a collaboration with Yichen Xu, Hao Geng, Chao-Ming Jian, and Cenke Xu, and is from a preprint of the article before peer review or editing, as submitted (on 5 March 2020) by an author to Journal of Statistical Mechanics: Theory and Experiment. IOP Publishing Ltd is not responsible for any errors or omissions in this version of the manuscript or any version derived from it. The version of record is available online at J. Stat. Mech. 073102 (2020). © IOP Publishing. Reproduced with permission. All rights reserved.

7. The content of Sec. 4.2 is the result of a collaboration with Yichen Xu, Mengxing Ye, Zhu-Xi Luo, and Cenke Xu, and has previously appeared in arXiv:2203.14168.

8. The content of Sec. 4.3 is the result of a collaboration with Xiao Chen, Chao-Ming Jian, Yi-Zhuang You, and Cenke Xu, and has previously published (on 11 October 2018) in Phys. Rev. B 98, 165117 (2018). © The American Physical Society. Reproduced with permission. All rights reserved.

9. The content of Sec. 4.4 and App. B.3 is the result of a collaboration with Chao-Ming Jian and Cenke Xu, and has previously published (on 1 August 2019) in Phys. Rev. B 100, 075101 (2019). © The American Physical Society. Reproduced with permission. All rights reserved.

10. The content of Sec. 5.1 and App. B.4 is the result of a collaboration with Wenjie Ji and Cenke Xu, and is from a preprint of the article before peer review or editing, as submitted (on 16 February 2021) by an author to Journal of Statistical Mechanics: Theory and Experiment. IOP Publishing Ltd is not responsible for any errors or

omissions in this version of the manuscript or any version derived from it. The version of record is available online at J. Stat. Mech. 073101 (2021). © IOP Publishing. Reproduced with permission. All rights reserved.

11. The content of Sec. 5.2 and App. A.4 is the result of a collaboration with Chao-Ming Jian and Cenke Xu, and has previously published (on 18 August 2021) in SciPost Phys. 11, 033 (2021), licensed under the Creative Commons Attribution 4.0 License together with an author copyright.

12. The content of Sec. 5.3 is the result of a collaboration with Chao-Ming Jian, Yichen Xu, and Cenke Xu , and has previously published (on 22 February 2021) in Phys. Rev. B 103, 064426 (2021). © The American Physical Society. Reproduced with permission. All rights reserved.

Chapter 1

Introduction

Condensed matter physics is a branch of physics that studies the macroscopic properties of many quantum particles that form the matter in our universe. In principle, one could describe each quantum mechanical particle by its Schrödinger equation, and try to understand the whole system by solving around 10^{23} coupled equations. However, this is a task virtually unreachable with today's computational power. In fact, in most cases, we do not need to take track of all fundamental constituents of matter, and it is possible to make progress by isolating a few relevant variables that characterize the system's behaviors on a particular time or length scale. The emergent physics laws are sometimes very simple and appealing. What's more, due to the correlations between many particles, the emergent laws can be very different from the microscopic description of each individual. The philosophy of "more is different" has been demonstrated over and over again in the history of condensed matter physics. In addition to *emergence*, the other central theme of modern physics is *universality*, which is the observation that very different microscopic systems can have identical long-distance and low-energy properties. The idea serves to unify the experimental and numerical data from wildly different systems under different conditions.

The interacting electrons in crystalline solids are historically the playground for condensed matter physics. Much of our understanding of quantum many-electron systems is based on two cornerstones, namely Landau's Fermi liquid theory [8] and Landau's symmetry-breaking theory of phase transitions [9]. Landau's Fermi liquid theory is a perturbation theory based on the assumption that collective excitations above an electronic ground state can be described by long-lived quasiparticles which resemble the original electrons (i.e., they carry the same quantum numbers and statistics). It successfully describes all ordinary metals. Landau's symmetry-breaking theory provides a general understanding of conventional phases of matter (e.g., liquid crystal states, superfluid, ferromagnetic and antiferromagnetic states, etc). It points out that different phases really correspond to different symmetries in the organizations of the constituents of matter. Landau (together with Ginzburg) also laid out the foundation of the theoretical description of phase transitions. With the help of renormalization group (RG) machinery, all universal properties of conventional phase transitions can be systematically understood within the so-called Landau-Ginzburg-Wilson-Fisher (LGWF) paradigm. From a modern point of view, both Landau Fermi liquids and Landau phase transitions can be identified as RG fixed points. We see that the notions of emergence and universality are deeply rooted in the foundations of condensed matter physics.

Although the two theoretical frameworks by Landau are so successful, it is not the end of the story. The discovery of a wide range of exotic phenomena in the past few decades challenges conventional paradigm and deserves new languages and conceptual advances. In very recent years, it turned out that, with certain generalizations of symmetries, the Landau paradigm can even incorporate many examples that were once believed to be outside the paradigm. We are going mention some examples that are relevant to the dissertation (instead of examples in historical order).

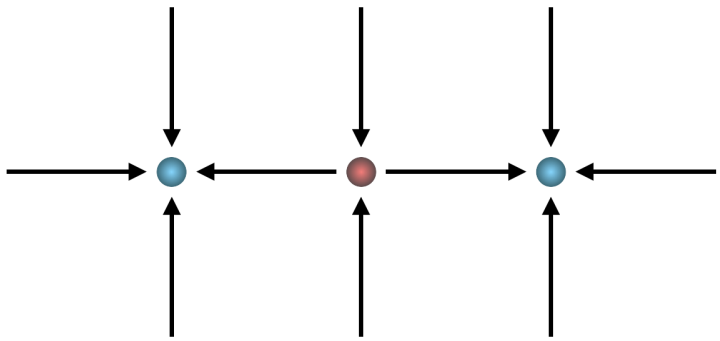

Figure 1.1: Understanding universal properties of classical or quantum matter by renormalization group (RG) fixed points. In the parameter space, attractive RG fixed points (in blue) represent stable phases, and RG fixed points with repulsive directions (in red) represent critical points of phase transitions.

This is an outline of the introductory chapter [1]. In Sec. 1.1 and Sec. 1.2, we introduce the Landau symmetry paradigm of conventional phase transitions and related boundary critical phenomena. In Sec. 1.3, we discuss various metallic states that are beyond the Landau quasiparticle paradigm. Sec. 1.4 is about unconventional quantum phase transitions, and our focus will be on two examples, deconfined quantum critical points (DQCPs) and continuous metal-insulator transitions. Sec. 1.5 serves as an introduction to the extended Landau paradigm based on generalized symmetries and anomalies. Sec. 1.6 concerns a type of experimental platforms for exotic phases and phase transitions, the strongly correlated Moiré materials.

[1] It is nearly impossible to make our notations consistent everywhere throughout the dissertation. All the sections in the main body (Sec. 2.1,2.2,2.3,3.1,3.2,4.1,4.2,4.3,4.4,5.3,5.1,5.2) are from different publications, and they are considered self-contained. In the introductory chapter, we try to make things as consistent as possible. Dimensionality is important in discussing phases of matter, but related notations may be confusing sometimes. Let us add some clarifications here. For bulk or boundary quantum phase transitions (with dynamical exponent $z = 1$) in D spacetime dimensions, we use $d = D-1$ to denote the spatial dimension or the boundary (spacetime) dimension. The notation "2+1D system" (or "$(2+1)d$ system" in later chapters) means a system in $2+1$ spacetime dimensions, "$2d$ system" means a system in 2 spatial dimensions, and "3D O(N) universality class" means the universality class of classical phase transitions in 3 spatial dimensions or quantum phase transitions in $2+1$ spacetime dimensions. In discussing classical boundary phase transitions, we still use D to denote the total dimension and $d = D-1$ the boundary dimension, but now they both are spatial.

1.1 Landau Symmetry Paradigm

Provided a sufficiently large piece of material, we can measure some of its macroscopic properties (e.g., magnetization, compressibility, and susceptibility). Then we can divide it into two halves and do the measurement again under the same external conditions (i.e., the same temperature, pressure, etc.). Usually, we would find that each part has the same macroscopic properties compared to those of the whole. But if we keep dividing the system, the "self-similarity" will break down at a certain point, and the length scale phenomenologically defines the correlation length ξ of the material. We are interested in the situation when the length scale ξ diverges. In this case, the theoretical description of the system only depends on a set of universal data, which is universal in the sense that wildly different systems may share the same theoretical description. From the point of view of renormalization group (RG), a system with $\xi \to +\infty$ is at an RG fixed point. If the RG fixed point is attractive, it represents a stable phase of matter. While if the RG fixed point is repulsive, it describes a continuous phase transition, which is the point where the macroscopic properties of the system change qualitatively. In the Landau paradigm, phases of matter are labeled by how they represent their symmetries, particularly whether the symmetries are spontaneously broken or not. For a continuous transitions between different phases, the set of universal data only depends on the space(-time) dimensions and the symmetry group.

1.1.1 Classical Phase Transitions

The classic example of universality is that of symmetry-breaking transitions at finite temperature T. The correlation length ξ at such transitions typically diverges as

$$\xi \sim |T - T_c|^{-\nu}, \tag{1.1}$$

where T_c is the critical temperature of the transition, and ν is the correlation length exponent. The transition happens as a consequence of the competition between energy E and entropy S, since we need to minimize the free energy

$$F = E - TS. \tag{1.2}$$

At low-temperature T, the entropy S becomes unimportant, and we essentially need to minimize the energy E. While for high-temperature T, the entropy S becomes the dominant term in the free energy, and we need to maximize S. Since entropy refers to the level of disorder, randomness, or uncertainty in the thermodynamic system, we can intuitively understand this is an "order-to-disorder" phase transition.

The Landau theory of phase transition is based on a key concept called order parameter. By definition, an order parameter ϕ must transform nontrivially under the symmetry group G of the system. One can evaluate the expectation value $\langle\phi\rangle$ under different external conditions (i.e., at different temperatures in classical phase transitions). The low-temperature phase with $\langle\phi\rangle \neq 0$ is called an ordered phase, and the high-temperature phase with $\langle\phi\rangle = 0$ is called disordered. The different phases can also be characterized by the correlation function $\langle\phi(\boldsymbol{x})\phi(0)\rangle$, which is a measurable quantity in experiments. In the disordered phase, we have the *short-range correlation* $\langle\phi(\boldsymbol{x})\phi(0)\rangle \sim \exp(-|\boldsymbol{x}|/\xi)$, which is exponentially decay. At the critical point, ξ diverges and the correlation obeys the power law $\langle\phi(\boldsymbol{x})\phi(0)\rangle \sim 1/|\boldsymbol{x}|^{2\Delta[\phi]}$, where $\Delta[\phi]$ is called the scaling dimension of ϕ. While in the ordered phase, we have the *long-range correlation* $\langle\phi(\boldsymbol{x})\phi(0)\rangle \sim$ const. As we will see in Sec. 1.5, Sec. 5.1, and Sec. 5.2, for generalized symmetries (e.g., higher-form symmetries and subsystem symmetries), the concepts of short-range and long-range correlations (with certain generalizations of $\langle\phi(\boldsymbol{x})\phi(0)\rangle$) can still be used to distinguish different phases of matter.

	exponent	definition	conditions
specific heat	α	$C \sim \lvert t\rvert^{-\alpha}$	$h = 0, t \to 0$
order parameter	β	$\phi \sim (-t)^{\beta}$	$h = 0, t \to 0^-$
susceptibility	γ	$\chi \sim \lvert t\rvert^{-\gamma}$	$h = 0, t \to 0$
critical isotherm	δ	$\phi \sim \lvert h\rvert^{1/\delta}$	$h \to 0, t = 0$
correlation length	ν	$\xi \sim \lvert t\rvert^{-\nu}$	$h = 0, t \to 0$
correlation function	η	$\langle \phi(\boldsymbol{x})\phi(0)\rangle \sim \lvert \boldsymbol{x}\rvert^{-(d-2+\eta)}$	$h = 0, t \to 0$

Table 1.1: The definitions of critical exponents in classical phase transitions, where $t = (T - T_c)/T_c$ is the rescaled temperature and h is the symmetry-breaking field conjugate to the order parameter ϕ.

In the ordered phase, the condensation $\langle\phi\rangle \neq 0$ could be invariant under a subgroup $H \subseteq G$, and G is said to be spontaneously broken down to H. The inequivalent ground states with the same free energy form a manifold G/H. The critical theory can be equally well formulated using the Landau-Ginzburg model of the order parameter ϕ or the non-linear sigma model (NLSM) with the target space G/H.

Let us first look at the Landau-Ginzburg formulation. We consider the expansion of the free energy around the critical point

$$\mathcal{S}[\phi] = \int \mathrm{d}^d\boldsymbol{x}\, |\partial_{\boldsymbol{x}}\phi|^2 + r\,|\phi|^2 + u\,|\phi|^4 - h\cdot\phi + \dots \tag{1.3}$$

where d is the spatial dimension, and we have included an external field h conjugate to ϕ. In this simple example, the RG flow in the vicinity of the critical point is controlled by only two relevant scaling variables $r \sim t = (T - T_c)/T_c$ and h. In addition to the correlation length Eq. 1.1, various physical quantities exhibit universal scaling behaviors

with the critical exponents defined in TABLE. 1.1. They satisfy the following relations

$$\text{scaling relations:} \qquad 2-\alpha = 2\beta+\gamma \quad \text{(Rushbrooke law)}, \tag{1.4}$$

$$\gamma = \beta(\delta-1) \quad \text{(Widom law)}; \tag{1.5}$$

$$\text{hyperscaling relations:} \qquad \gamma = \nu(2-\eta) \quad \text{(Fisher law)}, \tag{1.6}$$

$$2-\alpha = \nu d \quad \text{(Josephson law)}. \tag{1.7}$$

There are only two independent degrees of freedom. Namely, we can express

$$\alpha = 2-\nu d, \quad \beta = \frac{1}{2}\nu(d+\eta-2), \quad \gamma = \nu(2-\eta), \quad \delta = \frac{d-\eta+2}{d+\eta-2} \tag{1.8}$$

in terms of η and ν. All critical exponents are uniquely determined by the symmetry group G (which specifies ϕ) and the dimension d. To determine their numerical values, one needs to evaluate the RG flow of Eq. 1.3. Perhaps the quickest way to obtain the leading-order result in $d = 4-\epsilon$ expansion is to use the conformal perturbation theory (i.e., the method of OPE) introduced in Appendix A.1. One only needs to work out the fusion algebra of operators ϕ^2 and ϕ^4 by counting symmetry factors. Then the beta functions are readily read from Eq. A.14. For O(N) model, the anomalous dimension η to leading order $O(\epsilon)$ is zero, and the exponent ν is given by the scaling dimension of r

$$\nu^{-1} = \Delta[r] = 2 - \frac{N+2}{N+8}\epsilon + O(\epsilon^2). \tag{1.9}$$

We will extensively use the method of OPE for RG calculations in this dissertation.

According to the Calla-Coleman-Wess-Zumino coset construction [10, 11], the same

Wilson-Fisher fixed point is expected to be described by the NLSM

$$\mathcal{S}[\varphi] = \frac{1}{2}\int g_{ab}\mathrm{d}\varphi^a \wedge \star\mathrm{d}\varphi^b, \tag{1.10}$$

where φ^a and g_{ab} are the coordinate and the metric on the ground-state manifold G/H. To compare with the O(N) Landau-Ginzburg model, we take the groups $G = \mathrm{O}(N)$ and $H = \mathrm{O}(N-1)$. The space of ground states is the coset space

$$\varphi \in G/H = \frac{\mathrm{O}(N)}{\mathrm{O}(N-1)} = S^{N-1}. \tag{1.11}$$

The Nambu-Goldstone theorem guarantees there are Goldstone gapless modes when a continuous symmetry is spontaneously broken. There is a Goldstone mode for each broken symmetry generator, so the total number is

$$\#\text{ Goldstone modes} = \mathrm{dim}G - \mathrm{dim}H = \frac{N(N-1)}{2} - \frac{(N-1)(N-2)}{2} = N-1, \tag{1.12}$$

which is indeed the dimension of the sphere S^{N-1}. We can try to reproduce the critical exponents using $d = 2+\epsilon$ expansion. Since the target space S^{N-1} is highly symmetric, perhaps the quickest way to obtain the RG flow of NLSM is to use the Ricci flow method introduced in Appendix. A.2. There is a fixed point at Eq. A.46, which leads to

$$\nu^{-1} = \epsilon + O(\epsilon^2), \qquad \eta = \frac{\epsilon}{N-2} + O(\epsilon^2). \tag{1.13}$$

We can compare the numerical values for three-dimensional O(3) model in TABLE. 1.2 by extrapolating $\epsilon \to 1$. We can see the leading-order $d = 2+\epsilon$ expansion is not very satisfactory. Nonetheless, by going to higher powers in ϵ, one can try more sophisticated matching techniques to compare the two expansions.

	η	ν
mean-field	0	1/2
$d = 4 - \epsilon$	0	0.647
$d = 2 + \epsilon$	1	1
actual	0.0386	0.702

Table 1.2: The comparison of the leading-order $d = 4 - \epsilon$ expansion and $d = 2 + \epsilon$ expansion for 3D O(3) universality class.

One may wonder if quantum mechanics is essential in classical phase transitions at finite temperatures. At microscopic scales, quantum mechanics is crucial in understanding the existence of various ordered phases (at finite temperatures), such as superconductivity and magnetism. However, quantum fluctuations are not necessarily important for the macroscopic critical behaviors at phase transitions. There is a typical time scale for the correlation of order parameters $\tau_c \sim \xi^z \sim |t|^{-\nu z}$ where z is called the dynamical exponent. It leads to a typical energy scale $\omega_c \sim \xi^{-z} \sim |t|^{\nu z}$. Quantum fluctuations are more important than thermal fluctuations only when $\omega_c \gg T$ (where $\hbar = k_B = 1$). However, for any continuous transition at T_c, quantum mechanics becomes unimportant when $T_c^{1/(\nu z)} \gg |t| \to 0$ (which means $\omega_c \ll T$). In conclusion, only classical thermal fluctuations dominate at the macroscopic scales that control the critical behaviors.

1.1.2 Quantum Phase Transitions

In recent years, lots of efforts have been devoted to understanding phase transitions at zero temperature. As we have mentioned before, when $T = 0$ we essentially need to minimize the ground-state energy. In many cases, the minimization is not a trivial task since there are non-commutative terms in the quantum Hamiltonian. When different terms dominate, the macroscopic properties could be qualitatively different, and there could be a continuous transition (which is driven by quantum fluctuations instead of

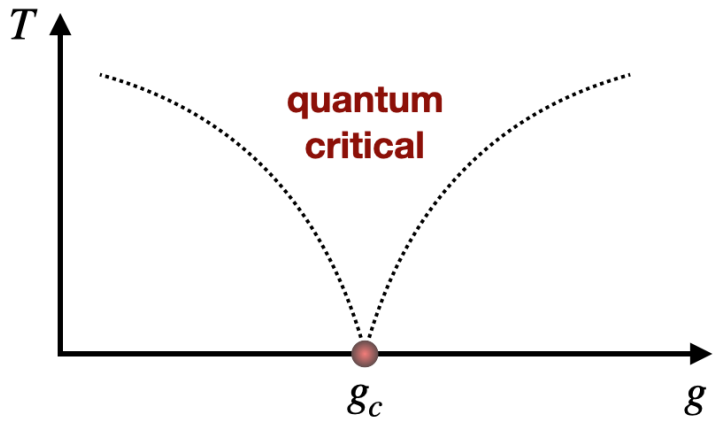

Figure 1.2: The schematic phase diagram for a quantum critical point at $g = g_c$.

thermal fluctuations.). The correlation length typically diverges as

$$\xi \sim |g - g_c|^{-\nu}, \tag{1.14}$$

where g_c is the critical value of the tuning parameter g. In quantum mechanical systems with the dispersion relation $\omega \sim k^z$, there is an associated vanishing energy scale

$$\omega_c \sim \xi^{-z} \sim |g - g_c|^{z\nu}, \tag{1.15}$$

where z is called the dynamical exponent.

In experiments, we can never reach the absolute zero temperature. Given a quantum critical point, what we would observe is the "quantum critical fan" shown in FIG. 1.2. To understand what is going on, we can take a conventional quantum critical point and consider the Landau expansion of free energy

$$\mathcal{Z} = \mathrm{Tr} e^{-\hat{H}/T} = \int \mathcal{D}[\phi] e^{-\mathcal{S}[\phi]}, \tag{1.16}$$

$$\mathcal{S}[\phi] = \int_{-\frac{1}{2T}}^{+\frac{1}{2T}} \mathrm{d}\tau \int \mathrm{d}^d \boldsymbol{x} \, |\partial_\tau \phi|^{2/z} + |\partial_{\boldsymbol{x}} \phi|^2 + r \, |\phi|^2 + u \, |\phi|^4 - h \cdot \phi + \ldots \tag{1.17}$$

where $r \sim (g - g_c)$ is the tuning parameter for the condensation of ϕ. In momentum space, the Lagrangian reads $\mathcal{L} \sim |\omega_n|^{2/z} + |\boldsymbol{p}|^2 + \ldots$ where $\omega_n = 2\pi T n$ is the bosonic Matsubara frequency. Something special happens at the energy scale of T

$$|\boldsymbol{p}|^2 \sim |\omega_n|^{2/z} \sim T^{2/z} \quad \Longrightarrow \quad \omega_c \sim |g - g_c|^{z\nu} \sim \xi^{-z} \sim |\boldsymbol{p}|^z \sim T. \tag{1.18}$$

If the temperature T is much higher than ω_c, the configurations with $\omega_n \neq 0$ are strongly suppressed (due to $|\omega_n|^{2/z} \gg |\boldsymbol{p}|^2$ in the action) and give very little contribution to the functional integral. Therefore, the partition function is dominated by configurations which are independent of τ and we can replace $\int_{-\frac{1}{2T}}^{+\frac{1}{2T}} \mathrm{d}\tau \to 1/T$. We effectively have a classical theory in d dimensions, which is out of the quantum critical region. On the other hand, at very low temperature $T \to 0$, we can replace $\int_{-\frac{1}{2T}}^{+\frac{1}{2T}} \mathrm{d}\tau \to \int_{-\infty}^{+\infty} \mathrm{d}\tau$ and obtain a quantum critical theory in $d+1$ (or effectively $d+z$) dimensions. The quantum critical point controls the physics inside the region $\omega_c \sim |g - g_c|^{z\nu} < T$, and the critical region looks like a fan (shown in FIG. 1.2). If one is interested in the dynamics of the system, the thermal equilibration time τ_{eq} behaves quite differently in the two regimes [12]

$$\begin{cases} \tau_{\mathrm{eq}} \gg 1/T & \omega_c > T \\ \tau_{\mathrm{eq}} \sim 1/T & \omega_c < T \end{cases}. \tag{1.19}$$

For conventional quantum phase transitions, various discussions in Sec. 1.1.1 also apply. We only need to pay attention to the difference in dimensionality.

In the most general sense, as long as a critical point enjoys certain continuous symmetry, one can define the conserved Noether current J and its conductivity, which is a measurable quantity. Namely, we can look at the superfluid-insulator transition in $d = 2$, which is described by Eq. 1.17 with $z = 1$ and ϕ being a U(1) order parameter. Before

doing any calculation, we can try some dimensional analysis for the conductivity

$$\sigma \sim \frac{e^2}{h} a^{2-d}, \tag{1.20}$$

where a is certain length scale. We immediately see that $d = 2$ is special since the conductivity σ can be a dimensionless number independent of any length scale, which is a universal quantity associated with the critical point. The fascinating transport properties have attracted a series of experimental and theoretical studies. To compare theories and experiments, an important point needs to be made. In terms of the magnitudes of frequency ω and temperature T, there are two important regimes. When $\omega \gg T$, the charged excitations created by the external fields are mainly responsible for transport, and the collision with thermally excited carriers can be neglected. This limit makes theorists' life much easier since we can only focus on the ground-state properties which are described by a conformal field theory (CFT). In any CFT_3 [2], the two-point correlation of conserved current $J(\tau, \boldsymbol{x})$ has the structure

$$\langle J_\mu(x) J_\nu(0) \rangle = \frac{C_J}{|x|^4} \left(\delta_{\mu\nu} - \frac{2x_\mu x_\nu}{|x|^2} \right), \tag{1.21}$$

where the current central charge $C_J \sim \sigma$ (which belongs to universal CFT data) can be analytically computed using various techniques. However, all experiments are performed at low but nonzero temperatures T, and frequencies ω easily satisfy $\omega \ll T$. In this regime, the transport is dominated by repeated inelastic scattering between thermally excited carriers. In general, the conductivity has the expression

$$\sigma(\omega) = \frac{e^2}{h} \Sigma \left(\frac{\hbar\omega}{k_B T} \right), \tag{1.22}$$

[2] The notation CFT_D means conformal field theory in D dimensions.

$\Sigma(0)$	$\Sigma(\infty)$	
≈ 1		experiment in PRL 62, 2180 (1989)
	0.315	ϵ-expansion in PRB 8883 (1996)
1.037	0.3927	ϵ-expansion in PRB 56, 8714 (1997)
1.068		large-N in PRB 86, 245102 (2012)
	0.359(4)	Monte Carlo in PRL 112, 030402 (2014)
	0.355155(11)	conformal bootstrap in JHEP 2020, 142 (2020)

Table 1.3: Some existing results about the universal conductivity Eq. 1.22 (under the limit $\omega/T \to 0$ or $\omega/T \to \infty$) at the XY fixed point in $D = 2 + 1$.

where $\Sigma(\omega/T)$ is a scaling function, which is universal but hard to entirely determined theoretically. Some existing results regarding the two limiting cases are summarized in TABLE. 1.3. Maybe we can trust $\Sigma(\infty) \approx 0.36$ from the conformal bootstrap result and $\Sigma(0) \approx 1$ from the experiment. In both cases, the resistivity $\rho = \sigma^{-1}$ is an order of one quantity in the unit of h/e^2. In Sec. 5.2, we are going to make some conceptual connections between the current central charge C_J defined in Eq. 1.21 to the universal behaviors of higher-form symmetries. In Sec. 3.2, we will discuss the critical transport at a continuous Mott transition, which is beyond the conventional Landau paradigm.

The phase transitions driven by quantum fluctuations have much richer possibilities than classical phase transitions. One important reason is that the Berry phase term can not be neglected at zero temperature. For example, quantum antiferromagnets in $d = 2$ are described by O(3) NLSM (defined in Eq. 1.10 with $G = \mathrm{SU}(2)$ and $H = \mathrm{U}(1)$) together with the summation of all single-spin Berry phase terms (see e.g. [13])

$$\mathcal{S}[\mathbf{n}] = \mathtt{i}S \sum_j \mathcal{S}_{\mathrm{WZ}}[\mathbf{n}_j] + \frac{1}{2g} \int \mathrm{d}\tau \mathrm{d}^2\boldsymbol{x}((\partial_\tau \mathbf{n})^2 + (\partial_{\boldsymbol{x}} \mathbf{n})^2), \tag{1.23}$$

$$\mathcal{S}_{\mathrm{WZ}}[\mathbf{n}] = \int_0^\beta \mathrm{d}\tau \int_0^1 \mathrm{d}u \mathbf{n} \cdot (\partial_\tau \mathbf{n} \times \partial_u \mathbf{n}), \tag{1.24}$$

where $\mathbf{n}$ is a O(3) unit vector (i.e., the Néel order parameter) defined on each site j. In the Wess-Zumino term $\mathcal{S}_{\mathrm{WZ}}[\mathbf{n}]$, one has to extend the definition of $\mathbf{n}$ to another

direction u with the boundary conditions $\mathbf{n}(\tau, u = 0) = (0, 0, 1)$ and $\mathbf{n}(\tau, u = 1) = \mathbf{n}(\tau)$. This consideration leads to the possibility of a direct continuous transition between two symmetry-breaking phases, the Néel phase and the VBS phase, on the square lattice (see Ref. [14] and references therein). But in Landau's language, the competition between the two order parameters can only lead to either the coexistence of two phases or a first-order transition, i.e., a continuous phase transition without fine-tuning is not possible. We will explain the continuous Néel-VBS transition in slightly more detail in Sec. 1.4.1.

In view of the Landau paradigm, it seems the disordered phase (without breaking any ordinary symmetry) is a featureless gapped phase. But this conclusion was overturned by many examples in the past few decades. Namely, some gapped systems have robust gapless boundary states (e.g., topological insulators and topological superconductors). Some other gapped systems have robust ground-state degeneracy which depends on the topology of the spatial manifold (e.g., gapped spin liquids and fractional quantum hall states). The first types of states are related to 't Hooft anomalies of (internal and spacetime) symmetries. The second types of state are actually spontaneous symmetry-breaking states of generalized symmetries instead of ordinary symmetries. We will explain all these topics in slightly more detail in Sec. 1.5.

1.1.3 Topological Defects & Dualities

In the previous discussions, the degrees of freedom at a critical point is described by the fluctuating order parameter ϕ, and the phase transition is driven by the condensation of ϕ which breaks the symmetry group G down to H. Usually, there is a dual version of the story, i.e., the ordered phase can be destroyed by the condensation or proliferation of the topological defects associated with G/H. In general, p-dimensional topological defects in $D = d + 1$ spacetime dimensions are classified by the homotopy group $\pi_{d-p-1}(G/H)$

in space or $\pi_{D-p-1}(G/H)$ in spacetime. The topological defects defined in space only are usually referred to as "solitons". They can be viewed as particles with their own dynamics, and they can condense. While the spacetime topological defects are usually referred as "instantons", which can be viewed as events. They have nonzero contributions to the path integral, which can be relevant or irrelevant under RG. The relevant case corresponds to the proliferation of instantons. After introducing the concepts, we can look at some simple examples of quantum phase transitions in low dimensions.

Ising domain wall The simplest example is the Ising domain wall characterized by $\pi_0(\mathbb{Z}_2) = \mathbb{Z}_2$. Let us look at the transverse Ising chain

$$H = -J \sum_j \sigma_j^3 \sigma_{j+1}^3 - h \sum_j \sigma_j^1, \tag{1.25}$$

where σ_j^1 and σ_j^3 are Pauli matrices on site j. There is a global $\mathbb{Z}_2$ symmetry which takes $\sigma_j^3 \to -\sigma_j^3$. (The Landau order parameter should be the coarse-graining of σ_j^3.) The phase with $J/h \gg 1$ spontaneously breaks $\mathbb{Z}_2$, and the phase with $J/h \ll 1$ preserves the symmetry. We can equally well describe the transition using the other set of variables via $\sigma_j^3 \sigma_{j+1}^3 = \tau_{\bar{j}}^1$ and $\sigma_j^1 = \tau_{\bar{j}-1}^3 \tau_{\bar{j}}^3$. The dual Hamiltonian now reads

$$H = -J \sum_{\bar{j}} \tau_{\bar{j}}^1 - h \sum_{\bar{j}} \tau_{\bar{j}-1}^3 \tau_{\bar{j}}^3, \tag{1.26}$$

where $\tau_{\bar{j}}^3$ is the Ising domain wall. When $J/h \ll 1$, $\tau_{\bar{j}}^3$ will condense and destroy the $\mathbb{Z}_2$ ordered phase. This is usually referred to as Kramers-Wannier duality [15]. It is remarkable that the model is self-dual, which implies the critical point is right at $J = h$. The duality also poses a question about how to understand symmetry at the critical point. (Is it enlarged by another $\mathbb{Z}_2$ that takes $\tau_{\bar{j}}^3 \to -\tau_{\bar{j}}^3$?) We will get back to this

point in Sec. 1.5.1, Sec. 5.1, Sec. 5.2, and Appendix. A.4 (also see Ref. [16]).

Superfluid vortex The second example is about the superfluid vortex characterized by $\pi_1(\mathrm{U}(1)) = \mathbb{Z}$. The superfluid-insulator transition in $D = 2+1$ is believed to be described by the abelian Higgs model (due to Peskin [17] and Dasgupta-Halperin [18])

$$\mathcal{L} = \frac{1}{2e^2} f \wedge \star f + |\mathrm{D}_a \tilde{\phi}|^2 + \tilde{r}|\tilde{\phi}|^2 + \tilde{u}|\tilde{\phi}|^4 + \ldots, \tag{1.27}$$

where $f = \mathrm{d}a$ is the gauge curvature, and $\mathrm{D}_a = \mathrm{d} - \mathtt{i}a$ is the gauge covariant derivative. We call the gauge field non-compact in the sense that there is $\mathrm{U}(1)_m$ symmetry for the conservation of the topological current $J_m^\mu = \frac{1}{4\pi}\varepsilon^{\mu\nu\rho} f_{\nu\rho}$. The physical meaning of $\tilde{\phi}$ is the vortex at the superfluid-insulator transition. To see how Eq. 1.27 is dual to Eq. 1.17 with a U(1) order parameter ϕ, let us first understand what phases Eq. 1.27 describes. In the Coulomb phase with $\tilde{r} \gg e^4 > 0$, we can integrate out $\tilde{\phi}$ which is gapped, which leaves the free Maxwell theory below the scale of $\tilde{r}$ (in the field-strength formulation [19])

$$\mathcal{Z} = \int \mathcal{D}[f] \exp\left(- \int \frac{1}{2e^2} f \wedge \star f + \frac{\mathtt{i}}{2\pi} \vartheta (\mathrm{d}f) \right), \tag{1.28}$$

where a Lagrangian multiplier $\vartheta(x)$ is introduced to impose the Bianchi identity $\mathrm{d}f = 0$. The Dirac quantization condition $\frac{1}{2\pi}\int \mathrm{d}f \in \mathbb{Z}$ leads to the periodicity $\vartheta \simeq \vartheta + 2\pi$. We see that a charge-$q_m$ monopole operator can be implemented as $\mathcal{M}(x) \sim e^{\mathtt{i}q_m \vartheta(x)}$, since the insertion of $\mathcal{M}(x)$ in the path integral leads to $\partial_\mu J_m^\mu(x) = q_m \delta^3(x)$. After integrating out f, we are left with the effective action for the gapless dual photon ϑ

$$\mathcal{S}[\vartheta] = \int \mathrm{d}^3x \frac{e^2}{8\pi^2} \partial_\mu \vartheta \partial_\mu \vartheta = \int \frac{e^2}{2} \frac{\mathrm{d}\vartheta}{2\pi} \wedge \star \frac{\mathrm{d}\vartheta}{2\pi}. \tag{1.29}$$

In this formulation, the $\mathrm{U}(1)_m$ symmetry is manifested as $\vartheta \to \vartheta + \alpha$, and the Noether current is $J_m^\mu = \frac{e^2}{(2\pi)^2}\partial^\mu \vartheta$. It is clear that we can interpret ϑ as the Goldstone mode of the spontaneously broken $\mathrm{U}(1)_m$ symmetry. In the Higgs phase with $r \ll -e^4 < 0$, the condensation of $\tilde{\phi}$ gives the dual photon ϑ a mass. The monopole operator $\mathcal{M} \sim e^{\mathtt{i} q_m \vartheta}$ has a short-range correlation, which means the $\mathrm{U}(1)_m$ symmetry is preserved. The observations imply that the Higgs transition in Eq. 1.27 indeed corresponds to a Landau transition for the $\mathrm{U}(1)_m$ symmetry. We can identify the Landau order parameter ϕ in eq. 1.17 to the charge-1 monopole operator $\phi \sim e^{\mathtt{i}\vartheta}$ in the theory eq. 1.27. Furthermore, inside the superfluid phase, an isolated vortex of ϕ has logarithmically divergent energy, which is in perfect agreement with the behavior of $\tilde{\phi}$ in the Coulomb phase. In principle, the duality can be verified by evaluating the critical exponents from both theories. Especially the scaling dimensions of the following operators should be equal to each other

$$\Delta[\phi] = \Delta[\mathcal{M}_{q_m=1}], \qquad \Delta[|\phi|] = \Delta[|\tilde{\phi}|]. \tag{1.30}$$

However, the critical point $|\tilde{r}| \ll e^4$ is strongly coupled in IR, and we do not have an analytical control. Fortunately, the existing numerical works seem to be very supportive.

Néel skyrmion Let us consider spin-1/2 quantum antiferromagnets on the the square lattice, which can be described by Eq. 1.23. The Néel order parameter $\mathbf{n}$ enjoys the homotopy group $\pi_2(S^2) = \mathbb{Z}$, where $S^2 = G/H = \mathrm{SU}(2)/\mathrm{U}(1)$ is the famous Hopf fibration. It allows skyrmion defects in space and hedgehog events in spacetime, such that each hedgehog corresponds to a tunneling event of the skyrmion number

$$Q = \frac{1}{4\pi}\int \mathrm{d}x\mathrm{d}y(\partial_x \mathbf{n} \times \partial_y \mathbf{n}) \cdot \mathbf{n} \in \mathbb{Z}. \tag{1.31}$$

The proliferation of hedgehog events necessarily destroys the Néel order. However, this case is more nontrivial than the previous examples. According to the Lieb-Schultz-Mattis (LSM) theorem [20, 21, 22], for a spin system with translation and spin rotation symmetries and half-integer spin per unit cell, the ground state must be gapless or gapped with degeneracy. Therefore, a conventional Néel order-to-disorder transition can not exist in ordinary spin-1/2 systems on the square lattice. The resolution is based on the observation by Haldane [23] and Read-Sachdev [24, 25] that the hedgehog defects must transform nontrivially under lattice translation. Therefore, the proliferation leads to a lattice symmetry-breaking phase. If continuous, this transition is, of course, beyond the Landau paradigm. We leave the discussion of the critical theory to Sec 1.4.1.

In recent years, the study of non-supersymmetric dualities around quantum critical points has been quite fruitful. In addition to the previously mentioned bosonic particle-vortex duality, there is a $\mathrm{SL}(2,\mathbb{Z})$ web of dualities that relates gauged/ungauged Wilson-Fisher bosons and gauged/ungauged Dirac fermions (see Ref. [26, 27] for review). Generalizing the ideas to $D = 2+1$ CFTs with $\mathrm{U}(1)^N$ symmetry, one finds a $\mathrm{Sp}(2N,\mathbb{Z})$ duality web [28, 29]. In particular, the $\mathrm{Sp}(4,\mathbb{Z})$ duality web can be applied to the easy-plane version of the Néel-VBS transition on the square lattice [14] (also see Sec. 1.4.1).

1.2 Boundary Critical Phenomena

In Sec. 1.1, we have considered critical behaviors of systems under the thermodynamic limit (i.e., the infinity volume limit). But any experimental sample in the lab can never be truly infinitely large. Provided that the system size is sufficiently larger than the correlation length, the scaling behaviors in Sec. 1.1 are, of course, valid deep into the bulk. But what happens at the boundary is an experimental relevant excellent question, as one would generally expect a different set of critical exponents at the boundary. The

study of conventional Landau transitions with boundaries has a long history (see Ref. [30, 31, 32] and references therein). It has recently attracted renewed attention due to the connections to the physics of symmetry-protected topological (SPT) phases [33, 34, 35, 36, 37, 38, 39, 40]. A nontrivial SPT state typically has protected gapless boundary modes, and one may wonder if the boundary modes are stable if the bulk is at criticality and becomes gapless. From a theoretical point of view, one concerns the RG flow for coupled degrees of freedom from different dimensions, and the problems of gapless boundaries (and defects) offer exciting opportunities to realize new fixed points and universal physics. Namely, for a 3-dimensional system with boundaries, the projection of bulk-boundary couplings to the boundary usually leads to nonlocal interactions. Even if we start with a purely local lattice model, the 2-dimensional boundary is capable of escaping from the Mermin-Wagner theorem. (The statement and proof of the Mermin-Wagner theorem are given in the discussion around Eq. 1.120.) In Sec. 2.1, we will discuss the possibility of a continuous Néel-VBS transition on the boundary of the $(2+1)$-dimensional Affleck-Kennedy-Lieb-Tasaki (AKLT) state.

But before moving to the exciting physics associated with boundaries and defects in Chap. 2, in this introductory section, let us introduce conventional boundary phase transitions and the theoretical methods to explore them. In this section, the transitions can be either classical or quantum. We use D to denote the bulk dimension (i.e., spatial dimension in classical phase transitions or spacetime dimension in quantum phase transitions), and the boundary dimension is given by $d = D - 1$.

1.2.1 Boundary Universality Classes

In general, given a bulk universality class, there exist several distinct boundary universality classes. For conventional phase transitions, much physics can already be under-

stood by looking at the classical ferromagnetic spin model

$$H/T = -K_1 \sum_{\langle i,j\rangle \in \partial X} \vec{S}_i \cdot \vec{S}_j - K \sum_{\langle i,j\rangle \notin \partial X} \vec{S}_i \cdot \vec{S}_j, \tag{1.32}$$

where $\vec{S}_j$ are classical O(N) spins on the lattice X, and the nearest neighbor coupling is taken to be K_1 for links between boundary sites and K for all other links. Let us first consider the case $D > 3$ such that the boundary is above its own lower critical dimension (which is 2 for the continuous symmetry O(N) with $N \geq 2$). In other words, the boundary can become ordered itself even if decoupled from the bulk. (The case of $D = 3$ will be commented on later.) We would not expect the bulk phase to depend on the boundary coupling K_1 for such a local Hamiltonian. But the boundary should be sensitive to what happens in the bulk. At a large bulk coupling $K > K_c$ (or a low temperature $T < T_c$), the bulk phase should be ordered. Due to the coupling to the bulk, the boundary will see a background mean-field from the ordered bulk, leading to symmetry breaking at the boundary. In the bulk disordered phase with a small $K < K_c$ (or a high temperature $T > T_c$), the boundary phase depends on K_1. One can define the ratio $\kappa = K_1/K$. Under the small κ limit, the boundary will be in the same phase as the bulk. But when κ is sufficiently large, the boundary can be ordered, disordered, or critical depending on the temperature. Thus, there is a critical value κ_c, which leads to three boundary universality classes. When $\kappa < \kappa_c$, the boundary undergoes the same transition at the bulk critical point. This is called an ordinary transition. When $\kappa > \kappa_c$, the boundary is already ordered at the bulk critical point, which is called an extraordinary transition. The multicritical point with $\kappa = \kappa_c$ and $K = K_c$ is called a special transition. We summarize the phase diagram in FIG. 1.3.

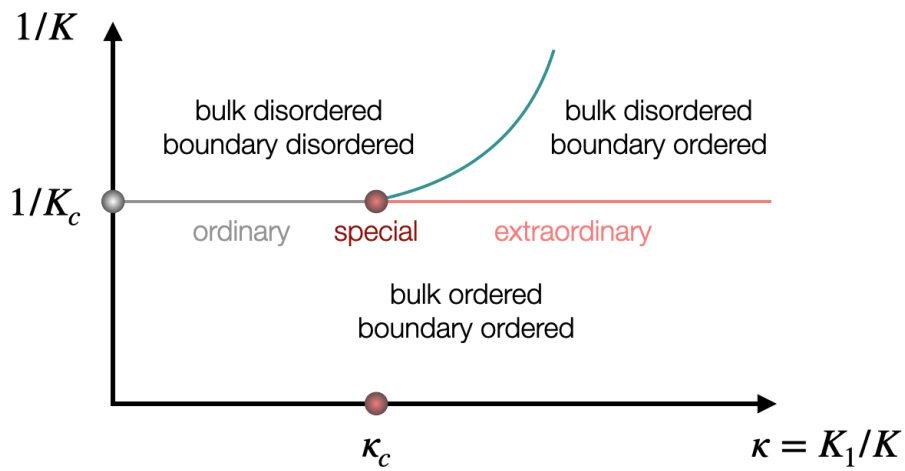

Figure 1.3: The schematic phase diagram for a ferromagnet with a boundary (described by Eq. 1.32). The dimension of the boundary is assumed to be higher than its own lower critical dimension.

To explore the critical behaviors, we can write down the continuum field theory

$$\mathcal{S} = \int_X \mathrm{d}^D x(|\partial\phi|^2 + r|\phi|^2 + u|\phi|^4 + \ldots) + \int_{\partial X} \mathrm{d}^{D-1} x(r_1|\phi|^2 + \ldots), \tag{1.33}$$

where X is a D-dimensional spatial (or spacetime) manifold for classical (or quantum) phase transitions. To understand why $|\phi|^4$ boundary term is not included, one should note that its bare scaling dimension is $\epsilon - 1$ in the $D = 4 - \epsilon$ expansion for the bulk Wilson-Fisher fixed points. Thus, the $|\phi|^4$ boundary term is irrelevant. For the case of Eq. 1.32 (and FIG. 1.3 in $D > 3$), the order parameter ϕ is the coarse-grained object of $\vec{S}_j$. The relations between the coupling constants are $r \sim (1/K - 1/K_c)$ and $r_1 \sim (\kappa - \kappa_c)$. We can see the three boundary universality classes are given by

$$\text{ordinary: } r_1 \to +\infty, \qquad \text{special: } r_1 \to 0, \qquad \text{extraordinary: } r_1 \to -\infty. \tag{1.34}$$

The case of $D = 3$ is special, since the boundary reaches its lower critical dimension. For O(2) symmetry, we need to replace the boundary ordered phase (when bulk is dis-

ordered) in FIG. 1.3 to quasi-long-range order. Recently, Metlitski [41] suggests that in the case of $\kappa > \kappa_c$ at $K = K_c$, the order parameter has the logarithmic correlation

$$\langle \phi(x)\phi(x')\rangle \sim \frac{1}{(\log|x-x'|)^q}, \qquad x, x' \in \partial X, \tag{1.35}$$

where q is a universal exponent. This is called the extraordinary-log universality class in Ref. [41]. What about $N > 2$? It is known that under the $N \to +\infty$ limit, one only has an ordinary transition without a special fixed point. For finite N, Ref. [41] suggests that there is a critical value N_c such that the case of $2 < N < N_c$ at bulk criticality is qualitatively the same as the case of $N = 2$. But the precise value of N_c and what will happen when N is slightly larger than N_c are not entirely conclusive at this stage. The results about classical O(N) transitions in Ref. [41] are potentially related to the Néel-VBS quantum phase transition discussed in Sec. 2.1, where we have considered a spin-1/2 quantum spin chain on the boundary of a two-dimensional bulk with SO(3) symmetry. Compared to the classical model, we also need to add a topological θ-term in our boundary theory. It is an open question whether the "Néel phase" that we found is a truly long-range ordered phase or an extraordinary-log phase. This part of the phase diagram is out of the reach of our perturbative RG calculation around the boundary critical point.

1.2.2 Example–Ordinary Transition

In this section, we use an example to illustrate why the bulk criticality is unaffected by the boundary and how the boundary scaling dimensions are calculated. (This section is a bit technical and could be skipped if you are not interested in the details.)

For illustrative purposes, let us consider the semi-infinite U(N) model on the manifold

$X = \{(\mathtt{x}, y) \in \mathbb{R}^D | 0 \leq y < \infty\}$ which will be used in Sec. 2.2

$$\mathcal{S} = \int \mathrm{d}^{D-1}\mathtt{x} \left[r_1 |\phi(\mathtt{x}, 0)|^2 + \int_0^{+\infty} \mathrm{d}y |\partial\phi|^2 + r|\phi|^2 + u|\phi|^4 + \ldots \right], \tag{1.36}$$

where we parametrize the D-dimensional coordinate as $x = (\mathtt{x}, y)$, and the boundary ∂X is given by $y = 0$. In this section, we will use the notations for dimensionality

$$d = (\text{boundary dimension}), \qquad D = (\text{bulk dimension}) = d + 1. \tag{1.37}$$

Method of images The boundary condition of the propagator of ϕ is given by

$$\begin{aligned} \partial_y G(\mathtt{x}, y \to 0; \mathtt{x}', y') &= r_1 G(\mathtt{x}, y \to 0; \mathtt{x}', y'), \\ \partial_{y'} G(\mathtt{x}, y; \mathtt{x}', y' \to 0) &= r_1 G(\mathtt{x}, y; \mathtt{x}', y' \to 0). \end{aligned} \tag{1.38}$$

Since the system has translation invariance alone direction of $\mathtt{x}$, $G(\mathtt{x}, y; \mathtt{x}', y')$ can be written as $G(\mathtt{x} - \mathtt{x}'; y, y')$. The free propagator (after the partial Fourier transformation $\mathtt{x} \to \mathtt{p}$) that satisfies the boundary condition is

$$G(\mathtt{p}; y, y') = \frac{2\pi^{\frac{d+1}{2}}}{\Gamma(\frac{d-1}{2})} \frac{1}{\Omega} \left(e^{-\Omega|y-y'|} + \frac{\Omega - r_1}{\Omega + r_1} e^{-\Omega|y+y'|} \right) \quad \text{with} \quad \Omega = \sqrt{\mathtt{p}^2 + r}. \tag{1.39}$$

We call the first term ($\sim e^{-\Omega|y-y'|}$) the bulk part $G_{\mathfrak{B}}$ and the second term ($\sim e^{-\Omega|y+y'|}$) the image part $G_{\mathfrak{I}}$. The bulk part $G_{\mathfrak{B}}$ is the expression that one would get for an infinite system with any boundary

$$G_{\mathfrak{B}}(x - x') = \frac{1}{|x - x'|^{d-1}} \quad (\text{at bulk criticality } r = 0)\,. \tag{1.40}$$

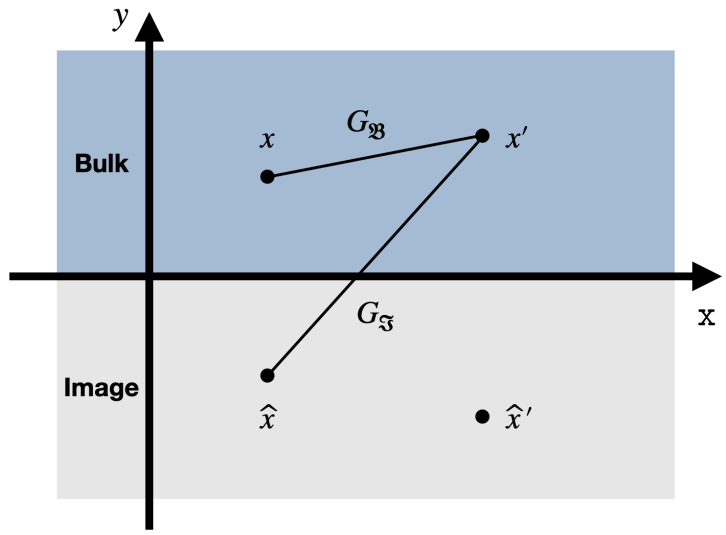

Figure 1.4: The illustration of the method of images in boundary critical problems. The total propagator is given by $G = G_{\mathfrak{B}} + G_{\mathfrak{J}}$ where the bulk part $\mathfrak{B}$ depends on the distance $|x - x'|$ and the image part $G_{\mathfrak{J}}$ is a function of $|x - \widehat{x'}| = |\widehat{x} - x'|$.

The image part only depends on the distance $|x - \widehat{x'}| = |\widehat{x} - x'|$, where $\widehat{x} = (\mathtt{x}, -y)$ denotes the imagine of $x = (\mathtt{x}, y)$. Namely, we have the two prototype boundary conditions (b.c.)

$$G_{\mathfrak{J}}(x, x') = \begin{cases} -G_{\mathfrak{B}}(x - \widehat{x'}) & \text{Dirichlet b.c. under } r_1 \to +\infty \\ +G_{\mathfrak{B}}(x - \widehat{x'}) & \text{Neumann b.c. under } r_1 \to -\infty \end{cases} . \tag{1.41}$$

It is important to notice that the UV singularities in $G_{\mathfrak{B}}$ and $G_{\mathfrak{J}}$ are quite different. The bulk part $G_{\mathfrak{B}}(x - x')$ always has a UV singularity when $x = x' \in X$. However, the image part $G_{\mathfrak{J}}(x, x')$ only diverges at the boundary $x = \widehat{x'} \in \partial X$.

Ordinary transition Let us focus on the boundary universality class with $r_1 \to +\infty$. There is a subtle point about how to define the boundary fields properly, since $\phi(\mathtt{x}, y = 0)$ vanishes under the large r_1 limit. One way to solve this problem is to use the boundary

condition to rewrite the boundary mass term

$$\partial_y \phi(\mathtt{x}, y=0) = r_1 \phi(\mathtt{x}, y=0) \qquad \Longrightarrow \qquad r_1 |\phi|^2 = |\partial_y \phi|^2 / r_1 \tag{1.42}$$

and consider the leading-order perturbative expansion in terms of $1/r_1$. In other words, we use $\partial_y \phi$ to represent the boundary order parameter. It makes sense since ϕ and $\partial_y \phi$ (on the boundary) transform in the same way under symmetries. In the real-space RG approach introduced in Appendix A.1, the operators of interest are the following

$$\begin{aligned} &\Phi_4 =: (\phi^\dagger \phi)^2 : -2\,(N+1)\,(2y)^{1-d} : \phi^\dagger \phi : \qquad \Phi_2 =: \phi^\dagger \phi : \qquad \Psi_2 =: \phi^2 : \\ &\Phi_1^\perp = \partial_y \phi|_{y=0} \qquad \Psi_2^\perp =: (\partial_y \phi)^2 : |_{y=0} \end{aligned} \tag{1.43}$$

where the boundary operators are labeled by $\perp$ (to remind ourselves that they involve a derivative normal to the boundary). We define their coupling constants as

$$u\Phi_4, \quad r\Phi_2, \quad w\Psi_2, \quad h_\perp \Phi_1^\perp, \quad w_\perp \Psi_2^\perp. \tag{1.44}$$

Bulk critical point We can prove the image part $G_{\mathfrak{I}}$ do not contribute to the scaling dimensions of bulk operators. We first observe that $G_{\mathfrak{I}}$ does not contribute to any OPE linear in $G = G_{\mathfrak{B}} + G_{\mathfrak{I}}$ simply because $G_{\mathfrak{I}}$ is UV-finite in bulk. One example is

$$: |\phi(\mathtt{x}_1, y_1)|^2 : \phi(\mathtt{x}_2, y_2) = G_{\mathfrak{B}}(\mathtt{x}_1 - \mathtt{x}_2; y_1 - y_2)\phi(\mathtt{x}_2, y_2) + \ldots \tag{1.45}$$

Then we consider slightly more complicated OPEs which are proportional to $G^2 = G_{\mathfrak{B}}^2 + 2G_{\mathfrak{B}}G_{\mathfrak{I}} + G_{\mathfrak{I}}^2$. For example, we can look at

$$: |\phi(\mathtt{x}_1, y_1)|^4 :: |\phi(\mathtt{x}_2, y_2)|^2 := 2(N+1)(G_{\mathfrak{B}}^2 + 2G_{\mathfrak{B}}G_{\mathfrak{I}}) : |\phi(\mathtt{x}_2, y_2)|^2 : + \ldots, \tag{1.46}$$

where $G_{\mathfrak{B}}G_{\mathfrak{J}}$ should be kept due to the UV divergence in $G_{\mathfrak{B}}$. To proceed, we plug it into Eq. A.13, and we have $G_{\mathfrak{B}}^2 \sim a^{-2(d-1)}$ and $G_{\mathfrak{B}}G_{\mathfrak{J}} \sim a^{-(d-1)}$ within the thin shell $a < ((\mathtt{x}_1 - \mathtt{x}_2)^2 + (y_1 - y_2)^2)^{1/2} < ae^{\delta\ell}$, where a is the real-space UV cut off. It is clear that only $G_{\mathfrak{B}}^2$ will generate the bulk operator $\int d^d\mathtt{x}dya^{-2}\left|\phi\right|^2$, and $G_{\mathfrak{B}}G_{\mathfrak{J}}$ vanishes as $e^{-(d-1)\ell}$ under RG. The OPEs involving higher powers of G can be analyzed in the same way. Finally, we find only $G_{\mathfrak{B}}$ contributes, and the bulk critical point is identical to the standard Wilson-Fisher fixed point. The bulk RG flow can be found in Eq. A.26.

Boundary scaling dimensions The boundary operators will be generated by bulk-boundary interactions. It is convenient to split Φ_4 into two operators $\Phi_{4,1} =: (\phi^\dagger\phi)^2 :$ and $\Phi_{4,2} = -2\left(N+1\right)\left(2y\right)^{1-d} : \phi^\dagger\phi :$. Just by counting all possible Wick contractions, we have the following bulk-boundary OPEs

$$
\begin{aligned}
[\Phi_{4,2}] \times [\Phi_1^\perp] &= -2(N+1)[\Phi_1^\perp] + \dots \\
[\Phi_{4,2}] \times [\Psi_2^\perp] &= -4(N+1)[\Psi_2^\perp] + \dots \\
[\Phi_{4,1}] \times [\Psi_2^\perp] &= 2[\Psi_2^\perp] + \dots
\end{aligned}
\tag{1.47}
$$

from which we read the coefficient C_{ijk} in Eq. A.31. In addition, we need to evaluate the dimensionless factor Υ_{ijk} in Eq. A.31

$$
\begin{aligned}
\Upsilon(\Phi_{4,2}, \Phi_1^\perp, \Phi_1^\perp) = \Upsilon(\Phi_{4,2}, \Psi_2^\perp, \Psi_2^\perp) &= \frac{1}{S_d}\int_{\text{half-shell}} \frac{\mathrm{d}^d\mathtt{x}_1\mathrm{d}y}{a^{(2d+1)-2(d-1)}} \frac{(d-1)(2y)^{3-d}}{2((\mathtt{x}_1-\mathtt{x}_2)^2+y^2)^{\frac{d+1}{2}}} = \frac{1}{2} \\
\Upsilon(\Phi_{4,1}, \Psi_2^\perp, \Psi_2^\perp) &= \frac{1}{S_d}\int_{\text{half-shell}} \frac{\mathrm{d}^d\mathtt{x}_1\mathrm{d}y}{a^{(2d+1)-2(d-1)}} \frac{4(d-1)^2y^4}{((\mathtt{x}_1-\mathtt{x}_2)^2+y^2)^{d+1}} = 1,
\end{aligned}
\tag{1.48}
$$

where $S_d = 2\pi^{\frac{d+1}{2}}/\Gamma(\frac{d+1}{2})$ is the surface area of d-sphere. Finally, the one-loop beta functions of boundary couplings can be directly read from Eq. A.33

$$\begin{aligned}\frac{dh_\perp}{dl} &= \frac{d-1}{2}h_\perp + 2(N+1)h_\perp u + \dots \\ \frac{dw_\perp}{dl} &= -w_\perp + 4(N+1)w_\perp u - 4w_\perp u + \dots\end{aligned} \tag{1.49}$$

which leads to the boundary scaling dimensions

$$\Delta[\Phi_1^\perp] = \frac{d+1}{2} - \frac{N+1}{2\,(N+4)}\epsilon, \qquad \Delta[\Psi_2^\perp] = (d+1) - \frac{N}{N+4}\epsilon. \tag{1.50}$$

These results will be used in Sec. 2.2.

The theoretical machinery illustrated in this example (i.e., the combination of conformal perturbation theory and method of images) is very powerful (also see Ref. [30]). It can be applied to other boundary critical problems as well.

1.3 Beyond Landau Fermi Liquids

The other side of the world of condensed matter physics is about understanding metals, such as a piece of iron, copper, or silver, that are ubiquitous in our daily lives. Landau's fermi liquid (FL) theory [8] has served as the paradigm of our understanding of conducting electrons. Landau's great insight is that despite interactions between electrons, they retain their identity as quasiparticles, which carry the same quantum numbers as electrons and have a diverging lifetime at low energies. The "quasiparticle assumption" leads to various universal properties that have been experimentally verified in a wide range of materials. From a theoretical perspective, based on modern RG treatment [42], one can show that Landau's assumption is valid in quite general considerations.

With the discovery of cuprate high-temperature superconductors, heavy fermion compounds, iron pnictides, and twisted bilayer graphene, people have found more and more experimental signatures (typically close to some quantum critical points in metals) that are not consistent with the universal predictions from the quasiparticle paradigm. These exotic metallic states are generally termed non-fermi liquids (NFLs). The theoretical study of NLFs is incredibly challenging. On the one hand, the system is below the upper critical dimension and exhibits strong quantum fluctuations. On the other hand, the extended fermi-surface manifold hosts a large number of gapless excitations. The combination of the two features makes perturbative RG calculations especially hard. Despite the efforts from the last three decades (see e.g. [43, 44, 45, 46, 47, 48, 49, 50, 51, 52, 53]), there is still no satisfying expansion method that is commonly accepted. In the past few years, the Sachdev-Ye-Kitaev (SYK) model [54, 55], which is an exactly solvable model under a certain theoretical limit, has attracted a lot of attention since it provides a controlled approach to model metallic states without quasiparticles (see Ref. [56] and references therein). Very recently, people have started to understand the universal features of metals (e.g., Luttinger theorem) in view of symmetries, anomalies, and multidimensional bosonization (see e.g. [57, 58, 59]).

1.3.1 Experimental Signatures

Since the criterion for non-fermi liquid behaviors is usually based on "what it is not" rather than "what it is," we will begin by quickly reviewing some properties of fermi liquids and related experimental signatures of the breakdown of quasiparticle paradigm.

To describe fermi liquids, we can start with non-interacting electrons

$$H = \sum_{\boldsymbol{k}} \epsilon_{\boldsymbol{k}} c_{\boldsymbol{k}}^{\dagger} c_{\boldsymbol{k}} \tag{1.51}$$

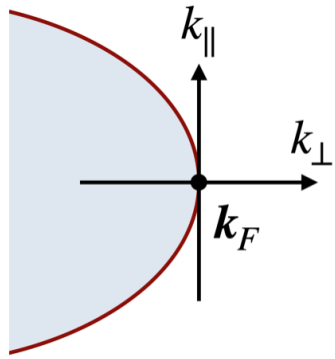

Figure 1.5: The low-energy expansion Eq. 1.52 around the fermi wave vector $\boldsymbol{k}_F$. The component $k_\perp$ is in the direction of fermi velocity, and $\boldsymbol{k}_\parallel$ is in the $(d-1)$-dimensional tangent space of the fermi-surface manifold.

where $c_{\boldsymbol{k}}$ is the electron operator with momentum $\boldsymbol{k}$, and the band structure $\epsilon_{\boldsymbol{k}}$ is determined by the underlying microscopic physics. In our notation, the chemical potential μ is absorbed in $\epsilon_{\boldsymbol{k}}$, and the location of the fermi surface (FS) in the Brillouin zone is given by $\epsilon_{\boldsymbol{k}} = 0$, which separates occupied and unoccupied states at zero temperature. The $(d+1)$-dimensional low-energy theory is given by the expansion $\epsilon_{\boldsymbol{k}+\boldsymbol{k}_F} \approx v_F k_\perp + \kappa \boldsymbol{k}_\parallel^2$ around any momentum on the fermi surface $\boldsymbol{k}_F \in \mathrm{FS}$ (shown in FIG. 1.5)

$$\mathcal{S}_F = \int \mathrm{d}\tau \mathrm{d}x_\perp \mathrm{d}^{d-1}\boldsymbol{x}_\parallel \psi^\dagger (\partial_\tau - \mathtt{i} v_F \nabla_\perp - \kappa \boldsymbol{\nabla}_\parallel^2)\psi, \tag{1.52}$$

where $x_\perp$ denotes the normal direction of the FS and $\boldsymbol{x}_\parallel$ is a $(d-1)$-dimensional vector in the tangent space of the FS. The coefficient v_F is called the fermi velocity, and κ is the FS curvature. Both v_F and κ generally depend on the location of $\boldsymbol{k}_F \in \mathrm{FS}$. Eq. 1.52 is usually the starting point of theoretical analysis of the properties of metals.

Quasiparticle decay rate The abundance of gapless excitations around the FS will interact with each other and result in quasiparticle decay. We can calculate the fermion

self-energy due to four-fermion scatterings

$\Sigma_\psi(\mathtt{i}\omega, \boldsymbol{k}) =$ 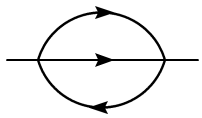 $\sim \begin{cases} \mathtt{i}\omega^2 \mathrm{sgn}(\omega) \log(\Lambda/|\omega|)/(v_F^2\kappa) & d = 2 \\ \mathtt{i}\omega^2 \mathrm{sgn}(\omega) \Lambda^{d-2}/(v_F^2\kappa) & d > 2 \end{cases}, \tag{1.53}$

where Λ is a momentum-space UV cut-off. It physically means the quasiparticle decay rate scales as $1/\tau_{\mathrm{qp}} \sim T^2$, which is much smaller than the quasiparticle energy. It justifies Landau's assumption about long-lived quasiparticles in FLs. The decay rate can be measured in angle-resolved photoemission spectroscopy (ARPES) experiments [60]. In a number of experimental systems (see e.g. [61, 62]), people found $1/\tau_{\mathrm{qp}} \sim T$, which signals the breakdown of the quasiparticle concept.

T-dependence of resistivity Closely related to the quasiparticle decay rate is the momentum relaxation rate, which determines the electrical transport properties. After considering Umklapp scatterings, one can show that it still scales as $\sim T^2$. Therefore, the low-temperature resistivity of fermi liquids is commonly

$$\rho \sim \rho_0 + T^2, \tag{1.54}$$

where ρ_0 denotes the impurity contribution. (Notice that we have neglected the scatterings between phonons and electrons. When the temperature T is much lower than the Debye temperature T_D, phonon contribution $\sim T^{d+2}$ is not as relevant as the electron-electron scattering contribution $\sim T^2$. In the other region $T \gg T_D$, the electron-phonon scattering mechanism largely dominates the transport and gives $\rho \sim T$.) A famous departure from the FL resistivity is the strange metal phase in cuprate high-temperature superconductors (see e.g. [63, 64, 65, 66, 67] and Ref. [68] for a recent review), which has linear-T resistivity at low temperatures $T \ll T_D$. The strange metal behavior was also

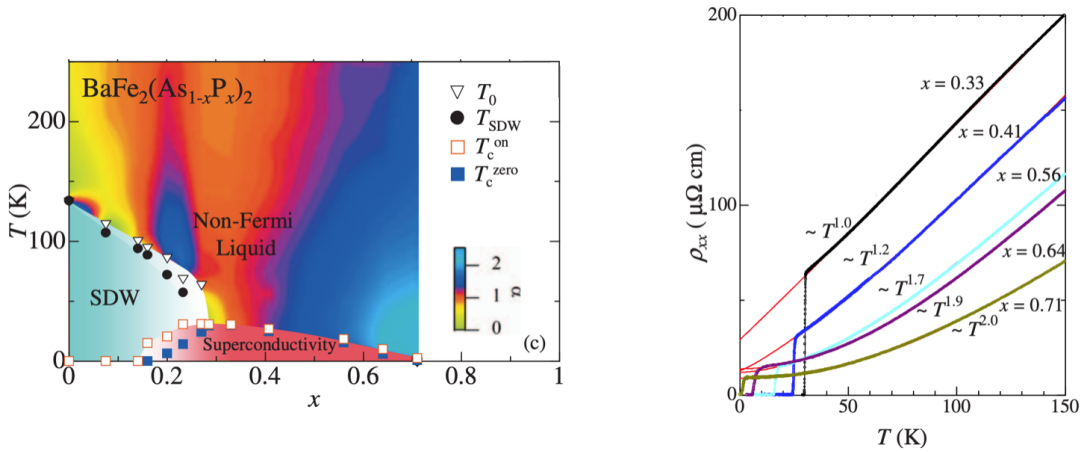

Figure 1.6: The resistivity exponent α in $\Delta\rho \sim T^{\alpha}$ versus x in $BaFe_2(As_{1-x}P_x)_2$ (Figures from Ref. [1] with permission).

observed in various heavy-fermion compounds (see Ref. [69] for a review) and recently in twisted bilayer graphene [70, 71]. In addition to linear-T behavior, other transport scalings have also been observed [72, 73, 74, 75, 76, 77, 1]

$$\rho \sim \rho_0 + T^{\alpha}, \qquad 1 \leq \alpha < 2, \tag{1.55}$$

where α is usually tunable by varying the charge carrier density. See FIG. 1.6 for a set of experimental data for the isovalent doped pnictide $BaFe_2(As_{1-x}P_x)_2$.

Mott-Ioffe-Regel limit There is an upper bound for the electrical resistivity for the so-called "good metals," which is good in the sense that we have the well-defined semi-classical wave-packet description of electrons. At the simplest level, we can describe the electrical resistivity by the Drude formula. A majority of the systems in this dissertation are in (quasi) two spatial dimensions, and we can write

$$\rho = \frac{h}{e^2}\frac{1}{k_F l_m} \leq \frac{h}{e^2}, \tag{1.56}$$

where k_F is the fermi wave vector, and l_m is the scattering mean free path. Due to the Heisenberg uncertainty principle, we need $k_F l_m \geq 1$, which gives rise to the upper bound h/e^2, sometimes referred to as the Mott-Ioffe-Regel (MIR) limit. Any compressible system going beyond the MIR limit is called a "bad metal" [78, 79, 80], and we no longer have a valid Boltzmann transport theory based on quasiparticle pictures.

1.3.2 Phase Transitions in Metals

In this section, we want to understand spontaneous symmetry breaking in metals. In Sec. 1.1, the critical theory (for insulators) is governed by a fluctuating bosonic order parameter. The situation becomes much more complicated in metals since there are a large number of fermionic excitations around the fermi surface. For simplicity, we consider the order parameters at zero momentum in this section, such as ferromagnetic order and nematic order. (We do not consider spin-density-wave and charge-density-wave orders.) In practice, we can start with a FL described by Eq. 1.52 and couple it to a bosonic order parameter ϕ through a Yukawa interaction, where ϕ is described by the Landau theory Eq. 1.17. At present, no RG treatment completely solves this problem in two spatial dimensions. The original attempt at the problem, known as the Hertz-Millis theory [81, 82], has tried to evade the difficulties associated with the FS by integrating out the fermion part. But it has some serious pitfalls [83, 84]. We will briefly review the Hertz-Millis approach and then discuss an ϵ-expansion method first considered by Nayak-Wilczek [45, 46] (also see Ref. [85], Sec. 4.1, and Appendix. A.3).

Hertz-Millis theory In principle, by integrating out the FS, the effective Landau action Eq. 1.17 receives corrections of all orders in ϕ

$$\delta\mathcal{S}[\phi] = \sum_{n=2}^{+\infty}\prod_{i=1}^{n}\int \mathrm{d}^{d+1}q_i\Gamma^{(n)}(q_1,\ldots,q_n)\phi(q_1)\ldots\phi(q_n)\delta^{d+1}(q_1+\ldots+q_n), \tag{1.57}$$

where $q = (\omega, \boldsymbol{q})$ includes frequency and momentum. In general, the interaction vertex $\Gamma^{(n)}$ could be singular and non-local. The basic assumption in the Hertz-Millis approach is that one can truncate the infinite series in Eq. 1.57 at second order. Considering the Yukawa interaction between bosons and fermions, one finds the one-loop boson self-energy

$$\Sigma_\phi(\mathtt{i}\omega, \boldsymbol{p}) = \quad = \gamma\frac{|\omega|}{|\boldsymbol{p}_\parallel|} \tag{1.58}$$

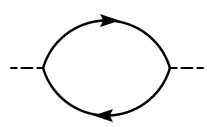

where $\boldsymbol{p}_\parallel$ is tangent to the FS manifold. The coefficient γ is related to the fermi velocity v_F and the FS curvature κ as $\gamma \sim \Lambda^{d-2}/(v_F\kappa)$, where Λ is a momentum-space UV cut-off. Adding this term to the Landau action 1.17, we obtain the Hertz action

$$\mathcal{S}[\phi] = \int \frac{\mathrm{d}\omega\mathrm{d}^d\boldsymbol{k}}{(2\pi)^{d+1}}\left(\gamma\frac{|\omega|}{|\boldsymbol{k}|} + |\boldsymbol{k}|^2 + r\right)|\phi(\omega,\boldsymbol{k})|^2 + u\int \mathrm{d}\tau\mathrm{d}^d\boldsymbol{x}\,|\phi|^4\,, \tag{1.59}$$

where we have averaged the boson self-energy over different patches on the FS. The first singular term is called the Landau damping term, which means the order parameter ϕ can decay into particle-hole excitations around the FS. The original term $|\partial_\tau\phi|^2$ is no longer relevant, and the dynamical exponent is modified to $z = 3$. Under the scale transformation of coordinates $\boldsymbol{x} \to \boldsymbol{x}e^{-\ell}$ and $\tau \to \tau e^{-z\ell}$, we have the scaling dimension

$$\Delta[\phi] = \frac{d+z-2}{2} \qquad \Longrightarrow \qquad \frac{\mathrm{d}u}{\mathrm{d}\ell} = (4-d-z)\,u \tag{1.60}$$

at the Gaussian fixed point. Therefore, when $d > 1$ (provided that $z = 3$) the u-term is irrelevant, and the critical theory is simply given by the Gaussian part of Eq. 1.59. There are several reasons to suspect that the Hertz-Millis theory is incomplete. In the justification of the Gaussian fixed point, the fermion-boson Yukawa coupling has not been checked carefully, which could be relevant. The feedback of bosons to fermions also has been completely ignored. In fact, the one-loop fermion self-energy in $d = 2$ satisfies

$$\Sigma_\psi(\mathtt{i}\omega, \boldsymbol{k}) = \sim -\mathtt{i}|\omega|^{2/3}\mathrm{sgn}(\omega). \tag{1.61}$$

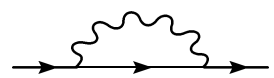

The Landau quasiparticles become ill-defined, which means the procedure of integrating out the FL part is not going to be self-consistent. From another perspective, neglecting higher-order terms in Eq. 1.57 is also suspicious since they could be highly singular terms.

Perturbative NFL fixed points Let us consider a more careful treatment of the problem in $d = 2$. We couple the single-patch theory Eq. 1.52 to the boson sector

$$\begin{aligned} \mathcal{S}[\phi] &= \int \frac{\mathrm{d}\omega \mathrm{d}k_\perp \mathrm{d}k_\parallel}{(2\pi)^3} \left(\gamma \frac{|\omega|}{|k_\parallel|} + |k_\parallel|^{z_\phi - 1} \right) |\phi(\omega, \boldsymbol{k})|^2 , \\ \mathcal{S}_{\text{Yukawa}} &= g \int \mathrm{d}\tau \mathrm{d}x_\perp \mathrm{d}x_\parallel \phi \psi^\dagger \psi, \end{aligned} \tag{1.62}$$

where z_ϕ is the boson dynamical exponent. To have a theoretical control of the system, we introduce $z_\phi = 2 + \epsilon$ and consider the perturbative RG calculation under a small ϵ expansion. The details can be found in Sec. 4.1 (also see Ref. [45, 46, 85]). To leading-order in ϵ, there is a new fixed point $g^2 = 2\pi^2 v_F \epsilon$, and the fermion propagator becomes

$$G_\psi(\mathtt{i}\omega, \boldsymbol{p}) = \frac{1}{\mathtt{i}|\omega|^{1-\epsilon/2}\mathrm{sgn}(\omega) - v_F p_\perp - \kappa p_\parallel^2}, \tag{1.63}$$

which no longer has a quasiparticle pole. Within this framework, we can show that the system flows to a NFL fixed point. But the physical value of the boson dynamical exponent is $z_\phi = 3$, which means we need to extrapolate $\epsilon \to 1$. The validity of the small ϵ expansion is not really justified. In Sec. 4.1, we will consider a situation where ϵ is naturally small, and we indeed have a controlled expansion. In that case, the boson sector no longer undergoes a Landau-type transition but a deconfined quantum phase transition (which will be introduced in Sec. 1.4.1). There are also other scenarios where similar NFL fixed points show up. The gapless bosons could be emergent gauge fields other than quantum critical modes. Namely, the problem of FS states coupled to dynamical U(1) gauge fields appears for the spinon FS at the continuous metal-insulator transition [86, 87] (which will be introduced in Sec. 1.4.2), and the FS of composite fermions in the Halperin-Lee-Read theory [88] for the half-filled Landau level. In Sec. 4.2, we will add one more example about metallic states with charge fractionalization. A technical generalization of the perturbative RG to the case of non-abelian gauge fields is in need (see Appendix. A.3 for details, also see Ref. [89]). As we will see in Sec. 4.2 and Sec. 3.2, charge fractionalization also provides a simple physical picture to construct bad metals with resistivity beyond the MIR limit 1.56 at low temperatures.

1.3.3 Large-N Solvable Models

In the last section, we start with free fermions and try to show the RG flow to a NFL fixed point. Recently, there has been another popular approach that directly gives us a NFL fixed point. This approach is based on an exactly solvable quantum mechanical model called the Sachdev-Ye-Kitaev (SYK) model (see Ref. [56] and references therein).

The SYK model with $(q/2)$-body interactions of complex fermions (which is usually

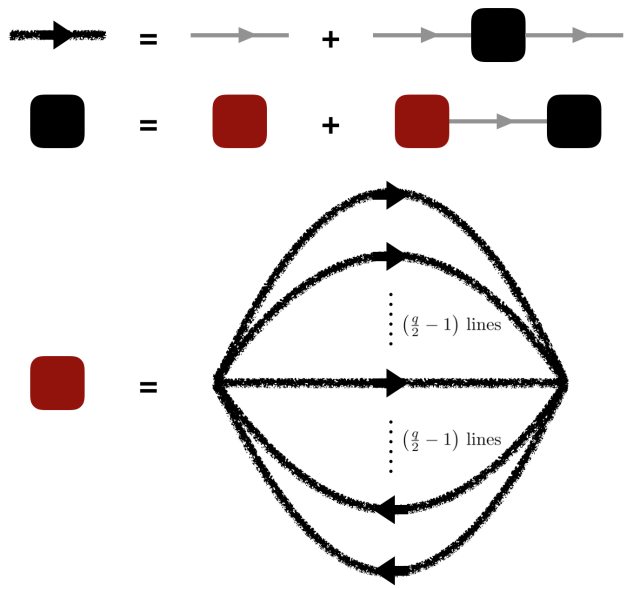

Figure 1.7: The diagrammatic representation of the Schwinger-Dyson equation in the complex SYK_q model Eq. 1.64. The self-energy only contains melon diagrams.

referred to as the complex SYK_q model) can be written as

$$H_{\mathrm{SYK}} = \sum_{\{i\},\{j\}=1}^{N} U_{i_1\ldots i_{\frac{q}{2}},j_1\ldots j_{\frac{q}{2}}} c_{i_1}^\dagger \ldots c_{i_{\frac{q}{2}}}^\dagger c_{j_1} \ldots c_{j_{\frac{q}{2}}} - \mu \sum_{i=1}^{N} c_i^\dagger c_i, \tag{1.64}$$

where N is an integer, and q is an even integer. The antisymmetric random couplings $U_{i_1\ldots i_{\frac{q}{2}},j_1\ldots j_{\frac{q}{2}}} = U_{[i_1\ldots i_{\frac{q}{2}}],[j_1\ldots j_{\frac{q}{2}}]}$ are Gaussian distributed complex variables which satisfy

$$U^*_{i_1\ldots i_{\frac{q}{2}},j_1\ldots j_{\frac{q}{2}}} = U_{j_1\ldots j_{\frac{q}{2}},i_1\ldots i_{\frac{q}{2}}}, \qquad \overline{U_{i_1\ldots i_{\frac{q}{2}},j_1\ldots j_{\frac{q}{2}}}} = 0, \qquad \overline{(U_{i_1\ldots i_{\frac{q}{2}},j_1\ldots j_{\frac{q}{2}}})^2} \sim \frac{U^2}{N^{q-1}}. \tag{1.65}$$

Under the large-N limit, only the melon diagrams (shown in FIG. 1.7) contribute to the self-energy Σ, and the Schwinger-Dyson equation reads

$$G(\mathtt{i}\omega) = \frac{1}{\mathtt{i}\omega + \mu - \Sigma(\mathtt{i}\omega)}, \qquad \Sigma(\tau) = -(-1)^{\frac{q}{2}} U^2 [G(\tau)]^{\frac{q}{2}} [G(-\tau)]^{\frac{q}{2}-1}, \tag{1.66}$$

The two-point Green function is solved as $G(\tau) \sim \mathrm{sgn}(\tau)/(U|\tau|)^{2/q}$, which gives the fermion scaling dimension at the SYK_q fixed point

$$\Delta[c] = 1/q. \tag{1.67}$$

To build a lattice model for NFLs, we consider a collection of strongly interacting quantum dots shown in FIG. 1.8. In each dot labeled by the site index x, there are a large number of fermions described by the complex SYK model Eq. 1.64. Between nearest neighbor quantum dots, we turn on a random hopping term

$$H = \sum_x H_{\mathrm{SYK}}[c_{i,x}] + \sum_{\langle x,x'\rangle} (t_{ij,xx'} c^\dagger_{i,x} c_{j,x'} + \mathrm{h.c.}), \tag{1.68}$$

where $t_{ij,xx'}$ are also Gaussian distributed variables satisfying $\overline{(t_{ij,xx'})^2} \sim t^2/N$. Under the strong coupling limit $U \gg t$, the physic is dominated by the SYK_q fixed point ($q \geq 4$) which is far away from the free-fermion fixed point. We should pay attention that the single-particle hopping is relevant under RG, which becomes non-perturbative at the energy scale $\sim t^2/U$. Therefore, the NFL fixed point is only expected within a finite temperature window. If one is careful enough, there is also a superconducting pairing instability, which will be discussed in detail in Sec. 4.3.

The lattice model Eq. 1.68 enjoys a U(1) global symmetry. Therefore, we can define its electrical current which is written in terms of fermion bilinears. At the SYK fixed point, the exponent $\alpha = 2(1 - 2\Delta[c])$ in the resistivity Eq. 1.55 is determined by the fermion scaling dimension Eq. 1.67. It is remarkable that $q = 4$ leads to strange metal behavior $\rho \sim \rho_0 + T$ and four-fermion interactions are natural in condensed matter systems.

There are, however, several unrealistic features in the approach mentioned above. To describe the strange metal phase in cuprates, we would like to know how to realize SYK

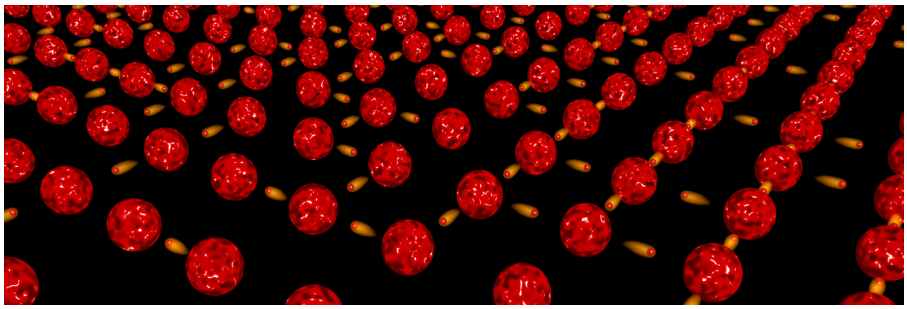

Figure 1.8: The typical setup for non-fermi liquids (NFLs) built from SYK models. One can build a lattice model using a collection of strongly correlated quantum dots. In each quantum dot, a large number of fermions interact with each other through a random coupling U (see Eq. 1.64). Between any pair of nearest neighbor quantum dots, there is a random hopping term t (see Eq. 1.68). Under the strong coupling limit $U \gg t$, the NFL behaviors are expected within the finite temperature window $T \sim (t^2/U, U)$. (Figure credit to Leon Balents.)

physics without quenched disorder (without randomness), and with only a few orbitals of fermions per site. Such a square-lattice model will be constructed in Sec. 4.3. In addition to the Hubbard model, we also turn on a plaquette spin-singlet ring exchange, which describes the tunneling between two singlets on the diagonal of the plaquette on the square lattice. Under a certain theoretical limit, this model has the same conformal solution as the original SYK model. Another question is about how to realize the transport scalings $1 < \alpha < 2$ in Eq. 1.55. In the SYK_q construction, it seems we can take $q > 4$. But the physics dominated by higher-order interactions seems unrealistic. In Sec. 4.4, we are going to present a generalization of the model in Sec. 4.3, which can realize $1 < \alpha < 2$ with four-fermion interactions. The exponent α is tunable by changing charge density which mimics the behavior in experimental systems (see FIG. 1.6 for example).

1.4 Unconventional Phase Transitions

There are a large number of quantum phases known to be beyond the Landau paradigm (strictly speaking, based on 0-form symmetries), including topological orders (such as gapped spin liquids and fractional quantum Hall states), symmetry-protected

topological (SPT) phases (such as electronic topological insulators and topological superconductors), gapless states with fractionalization (such as Dirac spin liquids, spinon fermi-surface states, and composite fermi liquids in the half-filled Landau level), gapped fractons, etc. Any quantum phase transition that involves such an exotic quantum phase is usually referred to as an example of unconventional phase transitions. Furthermore, as we have mentioned before, a direct continuous phase transition between two Landau symmetry-breaking phases is also unconventional. Based on the Lieb-Schultz-Mattis (LSM) theorem [20, 21, 22] and its various generalizations (see e.g. [90, 91, 92, 93, 94, 95]), a non-degenerate gapped ground state is forbidden in the presence of certain lattice and internal symmetries, and hence Landau-type order-to-disorder transitions are not possible in these situations. Our natural expectation is that unconventional quantum phase transitions should be ubiquitous. In this introductory section, we are going to mention two types of examples that are highly relevant to the later part of the dissertation.

1.4.1 Deconfined Quantum Criticality

This section concerns quantum phase transitions between two Landau-ordered phases that necessarily involve fractionalized degrees of freedom. We will start with the example of isotropic Néel-VBS transition to illustrate the simple pictures and physical properties behind this new paradigm. An exotic quantum phase transition sometimes involves emergent symmetries at the critical point, which is hard to fully understand by looking at a particular critical theory in the UV. A good understanding comes from a web of dualities, which will be illustrated using the example of easy-plane Néel-VBS transition. Finally, we will briefly mention the superfluid-insulator transition at fractional fillings, which is very useful for Sec. 1.6 and Sec. 3.2.

Isotropic Néel-VBS Transition

We continue the discussion of the Néel-VBS transition on the square lattice. In Sec. 1.1.3, we have already mentioned that the topological defect of the Néel order parameter carries lattice symmetry. Let us first explain this in slightly more detail. A crucial observation is that the Berry phase term in Eq. 1.23 takes a nontrivial value in the presence of hedgehog events (i.e., the tunneling events of the skyrmion number Eq. 1.31). As shown in Ref. [23, 24, 25], if the order parameter has hedgehogs with charge $q_{\bar{j}} \in \mathbb{Z}$ localized on the plaquette of dual lattice site $\bar{j}$, the Berry phase term equals to

$$\mathcal{S}_B = \mathtt{i}\pi S \sum_{\bar{j}} \zeta_{\bar{j}} q_{\bar{j}}, \tag{1.69}$$

where $S = 1/2$ is the spin value, and $\zeta_{\bar{j}}$ takes a value from $0, 1, 2, 3$ depending on whether the dual lattice site $\bar{j} = (\bar{j}_x, \bar{j}_y)$ is $(\text{even}, \text{even})$, $(\text{even}, \text{odd})$, $(\text{odd}, \text{even})$, or (odd, odd). The implication is that charge-1 hedgehog events occurring on nearby dual lattice sites interfere destructively and do not survive in the continuum field theory. Only hedgehog events with $q_{\bar{j}} = 4$ contribute to the critical theory. Under a four-fold lattice rotation C_4, the hedgehog operator $\mathcal{M}$ transforms as $\mathcal{M}(\boldsymbol{x}) \to \mathtt{i}\mathcal{M}(C_4\boldsymbol{x})$. Therefore, $\mathcal{M}$ can be identified as the VBS operator, and the quadrupled hedgehog term is allowed

$$\delta\mathcal{L} = \lambda_4(\mathcal{M}^4 + (\mathcal{M}^\dagger)^4). \tag{1.70}$$

Using the famous Hopf fibration, the critical theory Eq. 1.23 can be formulated as the non-compact $\mathbb{C}\mathrm{P}^1$ ($\mathrm{NC}\mathbb{C}\mathrm{P}^1$) model (i.e., the two-flavor bosonic QED_3)

$$\mathcal{L} = \mathrm{d}b \wedge \star\mathrm{d}b + |\mathrm{D}_b z|^2 + r|z|^2 + u(|z|^2)^2 + \dots \tag{1.71}$$

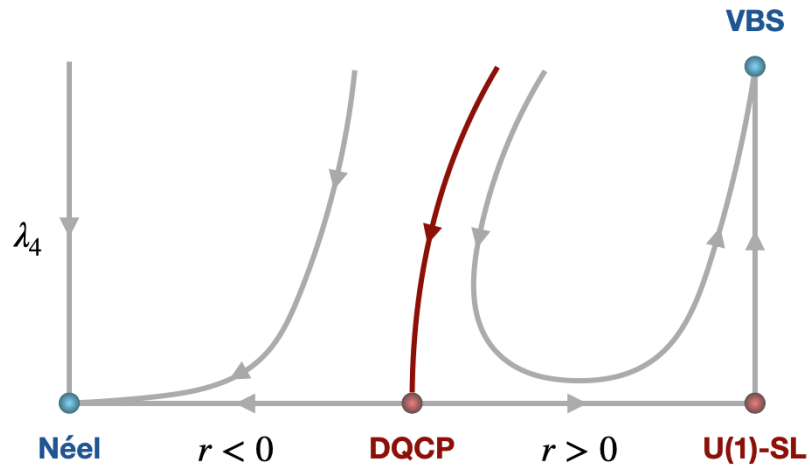

Figure 1.9: The schematic RG flow diagram of the continuous Néel-VBS transition, where r is the coupling that drives the transition, and λ_4 is the 4-monopole fugacity.

where the two-component spinon $z = (z_1, z_2)$ is related to the Néel order as $n_i = z^\dagger \sigma^i z$ with $i = 1, 2, 3$, and $\mathrm{D}_b = \mathrm{d} - \mathtt{i} b$ is the covariant derivative for the emergent abelian gauge field b. Since the skyrmion number Eq. 1.31 translates to $Q = \frac{1}{2\pi}\int \mathrm{d}b$, the monopole operator of b is identified as the hedgehog operator $\mathcal{M}$. When $r < 0$, the spinon condensation $\langle z_\alpha \rangle \neq 0$ describes the Néel state with $\langle \mathbf{n} \rangle = \langle z_\alpha^\dagger \rangle \boldsymbol{\sigma}_{\alpha\beta} \langle z_\beta \rangle \neq 0$. When $r > 0$, the spinon is gapped, the Coulomb phase is a U(1) spin liquid. However, away from the critical point at $r = 0$, the Coulomb phase is unstable due to charge-4 monopole events, and finally the gauge field will confine. The monopole proliferation breaks the lattice symmetry and leads to the VBS order. The schematic RG flow is shown in FIG. 1.9. There are two divergent length scales at the critical point, one is the spin correlation length, and the other is the confinement length.

In the previous discussion, our starting point is the O(3) NLSM Eq. 1.23 in terms of the Néel order parameter. In fact, the critical theory Eq. 1.71 can be understood from another perspective [96]. We can start with the VBS ordered state on the square lattice, and try to draw its topological defect which is a $\mathbb{Z}_4$ vortex (shown in FIG. 1.10). We immediately see that the vortex core is a free spin-1/2 moment, which transforms

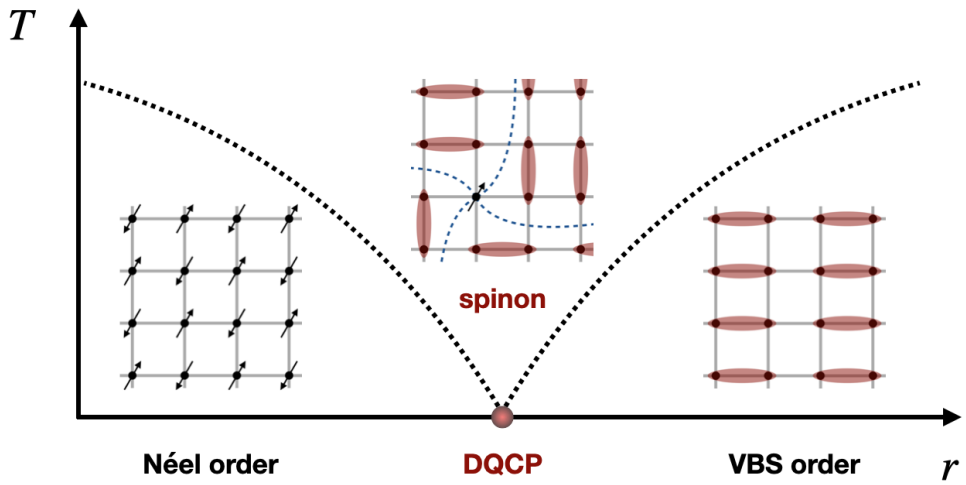

Figure 1.10: The phase diagram of the continuous Néel-VBS transition on the square lattice. The degrees of freedom at the critical point are deconfined spinon excitations.

nontrivially under the SU(2) symmetry. To destroy the VBS order, we can condense the $\mathbb{Z}_4$ vortices, which breaks the SU(2) spin symmetry and leads to the Néel order. In the field-theoretical description, the VBS order is described by a discrete $\mathbb{Z}_4$ clock order parameter. We recognize that the domain walls of the VBS order can be understood as electric field lines of the dual $\mathbb{Z}_4$ gauge theory, and the $\mathbb{Z}_4$ vortex carries a $\mathbb{Z}_4$ gauge charge. At the critical point, $\mathbb{Z}_4$ can be embedded into U(1), since the $\mathbb{Z}_4$ clock anisotropy is irrelevant (e.g., the 3D $\mathbb{Z}_4$ clock model belongs to the 3D XY universality class). Therefore, we arrive at the same field theory Eq. 1.71 for the vortex of the VBS order.

Emergent SO(5) symmetry At the critical point, an enlarged SO(5) symmetry has been numerically observed [97], which rotates the Néel and VBS order parameters

$$(n_1, n_2, n_3, n_4, n_5) \sim (z^\dagger \sigma^1 z, z^\dagger \sigma^2 z, z^\dagger \sigma^3 z, 2\mathrm{Re}\mathcal{M}_b, 2\mathrm{Im}\mathcal{M}_b). \tag{1.72}$$

Recently, the emergent SO(5) symmetry was theoretically rationalized using a web of dualities [98] between self-dual NC$\mathbb{C}$P^1 models and self-dual QED-Gross-Neveu models

(with hints from the NLSM by Senthil-Fisher [99]). The scaling dimension of the SO(5) vector was numerically found to be ~ 0.62 on the largest system so far, which is lower than the bound of 0.76 from the conformal bootstrap [100]. The nature of this transition is currently under debate. But there is no question that a continuous deconfined quantum critical point (DQCP) can exist. Namely, one could consider a version in SU(N) spin systems with a sufficiently large N. It is theoretically confirmed that the critical theory flows to a CFT in the IR.

Experimental signatures The fractionalization of Landau order parameters at the critical point has important implications for experimental observables. For example, the Néel order has a very large anomalous dimension η which is far away from the Wilson-Fisher result (see TABLE. 1.2). If we use the spinon mean-field value in $D = 2+1$ to do the estimation

$$\langle \mathbf{n}(x)\mathbf{n}(0)\rangle \sim \langle z^\dagger(x)\boldsymbol{\sigma} z(x) z^\dagger(0)\boldsymbol{\sigma} z(0)\rangle \sim \frac{1}{|x|^{2(D-2)}} = \frac{1}{|x|^{D-2+\eta}}, \tag{1.73}$$

we find η is an order of one quantity. In Sec. 4.1, we will calculate scaling dimensions in some examples more seriously under the large-N expansion.

Easy-Plane Néel-VBS Transition

Let us turn on an easy-plane anisotropy $(n_3)^2 = |z_1|^4 - 2|z_1|^2|z_2|^2 + |z_2|^4$. The SU(2) symmetry is broken down to the in-plane U(1) rotation of (n_1, n_2) around the z-axis and the Ising $\mathbb{Z}_2$ spin reflection $n_3 \to -n_3$ along the z-axis. The in-plane U(1) symmetry can be described by the complex order parameter $\Phi_B = n_1 + \mathtt{i} n_2 = 2z_1^\dagger z_2$ (or $\Phi_B^\dagger =$

$n_1 - \mathtt{i}n_2 = 2z_2^\dagger z_1$). Since $n_3 = |z_1|^2 - |z_2|^2$, the ordering in the x-y plane corresponds to

$$|\langle z_1 \rangle| = |\langle z_2 \rangle| \neq 0. \tag{1.74}$$

We should notice that this is not as simple as a 3D XY transition. In the vortex core of $\Phi_B = n_1 + \mathtt{i}n_2$, the XY order (n_1, n_2) vanishes, and the z-component has two choices $n_3 = \pm 1$, which are related via the Ising symmetry $n_3 \to -n_3$. The topological defects are actually merons (half-skyrmions) of the O(3) order parameter $\mathbf{n}$. The tunneling between two different merons is a monopole event. In view of the expression $\Phi_B = 2z_1^* z_2$, we can see that a 2π-vortex of Φ_B can be realized by a 2π-vortex of z_2 or a 2π-antivortex of z_1. In the vortex core, $n_3 = |z_1|^2 - |z_2|^2$ is positive or negative depending on which condensate $\langle z_{1,2} \rangle$ is destroyed by its vortex. Based on the $[\mathrm{U}(1)^B \rtimes \mathbb{Z}_2^{\mathrm{spin}}] \times \mathrm{U}(1)^C$ symmetry (where $\mathrm{U}(1)^B$ is the in-plane spin rotation of (n_1, n_2), $\mathbb{Z}_2^{\mathrm{spin}}$ is the Ising symmetry $n_3 \to -n_3$, and $\mathrm{U}(1)^C$ forbids the monopole events of $\mathbf{n}$), we can formulate the critical theory as

$$\mathcal{L} = |\mathrm{D}_b z_1|^2 + |\mathrm{D}_{b+B} z_2|^2 + |z_1|^4 + |z_2|^4 - \frac{\mathtt{i}}{2\pi} b \mathrm{d}C, \tag{1.75}$$

where B is the $\mathrm{U}(1)^B$ background field, and C is the $\mathrm{U}(1)^C$ background field. All coupling constants are neglected for simplicity. Under $\mathbb{Z}_2^{\mathrm{spin}}$ symmetry, we interchange z_1 and z_2. The Néel-VBS transition is driven by a single mass term $rz^\dagger z = r(|z_1|^2 + |z_2|^2)$. When z_1, z_2 condense simultaneously (which preserves $\mathbb{Z}_2^{\mathrm{spin}}$), the gauge field b is Higgsed, $\mathrm{U}(1)^B$ symmetry is broken and $\mathrm{U}(1)^C$ symmetry is preserved. This is the in-plane Néel ordered state. When z_1, z_2 are gapped, $\mathrm{U}(1)^B$ symmetry is preserved, and we are left with gapless b right at the DQCP. However, b will eventually confine. The $\mathrm{U}(1)^C$ symmetry-breaking phase corresponds to the VBS order.

Emergent O(4) symmetry Similar to the isotropic Néel-VBS transition, the easy-plane case has an enlarged symmetry at the critical point and enjoys a duality web [98, 27] under $\mathrm{Sp}(4,\mathbb{Z})$ duality transformations. Let us be more precise about the dual theories which include a pair of self-dual two-flavor bosonic QED_3 (i.e., a pair of easy-plane $\mathrm{NC}\mathbb{C}\mathrm{P}^1$ models) and a pair of self-dual two-flavor fermionic QED_3

$$\begin{aligned}
& \mathcal{L}_{\mathrm{bQED}} = |\mathrm{D}_{b+X} z_1|^2 + |z_1|^4 + |\mathrm{D}_{b+Y} z_2|^2 + |z_2|^4 - \frac{\mathtt{i}}{2\pi} b\mathrm{d}(X+Y) - \frac{\mathtt{i}}{2\pi} Y\mathrm{d}X \\
\leftrightarrow \quad & \tilde{\mathcal{L}}_{\mathrm{bQED}} = |\mathrm{D}_{\tilde{b}-Y} \phi_1|^2 + |\phi_1|^4 + |\mathrm{D}_{\tilde{b}+X} \phi_2|^2 + |\phi_2|^4 - \frac{\mathtt{i}}{2\pi} \tilde{b}\mathrm{d}(X-Y) + \frac{\mathtt{i}}{2\pi} Y\mathrm{d}X \\
\leftrightarrow \quad & \mathcal{L}_{\mathrm{fQED}} = \bar{\psi}_1 \not{D}_{a+X} \psi_1 + \bar{\psi}_2 \not{D}_{a-X} \psi_2 - \frac{\mathtt{i}}{4\pi} a\mathrm{d}a - \frac{\mathtt{i}}{2\pi} a\mathrm{d}Y + \frac{\mathtt{i}}{4\pi} Y\mathrm{d}Y - \mathtt{i}2\mathrm{CS}_g \\
\leftrightarrow \quad & \tilde{\mathcal{L}}_{\mathrm{fQED}} = \bar{\chi}_1 \not{D}_{\tilde{a}-Y} \chi_1 + \bar{\chi}_2 \not{D}_{\tilde{a}+Y} \chi_2 - \frac{\mathtt{i}}{4\pi} \tilde{a}\mathrm{d}\tilde{a} - \frac{\mathtt{i}}{2\pi} \tilde{a}\mathrm{d}X + \frac{\mathtt{i}}{4\pi} X\mathrm{d}X - \mathtt{i}2\mathrm{CS}_g
\end{aligned} \tag{1.76}$$

where the original background fields are $B = Y - X$ and $C = Y + X$, $b, \tilde{b}$ are dynamical U(1) gauge fields, and $a, \tilde{a}$ are dynamical Spin^c connections. The gravitational Chern-Simons term CS_g is normalized such that the thermal Hall conductance is $\kappa_{xy} = \pi^2 k_B^2 T/(6h)$. Our convention about the regularization of Dirac fermions is the same as Ref. [26, 27]. The Néel $\mathrm{U}(1)^B$ order Φ_B and the VBS $\mathrm{U}(1)^C$ order Φ_C are represented by the following operators in the different dual theories

$$(\Phi_B, \Phi_C) \sim (z_1^\dagger z_2, \mathcal{M}_b) \sim (\mathcal{M}_{\tilde{b}}^\dagger, \phi_1^\dagger \phi_2) \sim (\psi_2^\dagger \mathcal{M}_a, \psi_1^\dagger \mathcal{M}_a) \sim ((\chi_1^\dagger \mathcal{M}_{\tilde{a}})^\dagger, \chi_2^\dagger \mathcal{M}_{\tilde{a}}), \tag{1.77}$$

where $\mathcal{M}_a$ (or $\mathcal{M}_b$) is the monopole operator of a (or b), and $\psi_1^\dagger \mathcal{M}_a$ denotes a monopole of a with a fermion zero mode of ψ_1 filled. Provided that the duality web is valid, we observe that the global symmetry group is much larger than one would expect based on Eq. 1.75. Let us take a closer look at the symmetries in the fermionic theories [98, 27, 101, 102]. In $\mathcal{L}_{\mathrm{fQED}}[\psi, a]$, the global symmetry group is $\mathrm{SU}(2)^X \times \mathrm{Pin}^-(2)^Y/\mathbb{Z}_2$. The explicit background field X couples to $\mathrm{U}(1)^X \subseteq \mathrm{SU}(2)^X$, and Y couples to $\mathrm{U}(1)^Y \subseteq \mathrm{Pin}^-(2)^Y$.

There is also a charge conjugation $\mathcal{C}^Y : Y \to -Y, a \to -a, X \to X, \psi \to \mathtt{i}\sigma^2\bar{\psi}$ that commutes with $\mathrm{SU}(2)^X$. The notation $\mathrm{Pin}^-(2)^Y$ means $(\mathcal{C}^Y)^2 = -\mathbf{1}$. In addition, we should pay attention that global symmetries only act on gauge-invariant operators. Any composite operator of $\psi, \bar{\psi}$ should carry the $\mathrm{U}(1)^X$ charge $q_X =$ even and the $\mathrm{U}(1)^Y$ charge $q_Y = 0$. Any gauge-invariant monopole is filled with a fermion zero mode and carries $(q_Y = 1, q_X = \pm 1)$. More generally, it is easy to see that all gauge-invariant operators satisfy $q_X + q_Y \in 2\mathbb{Z}$. Similar agreements hold for $\tilde{\mathcal{L}}_{\mathrm{fQED}}[\chi, \tilde{a}]$, and the symmetry group is $\mathrm{Pin}^-(2)^X \times \mathrm{SU}(2)^Y/\mathbb{Z}_2$. Therefore, we find the symmetry at the critical point is at least as large as $\mathrm{SO}(4) = \mathrm{SU}(2)^X \times \mathrm{SU}(2)^Y/\mathbb{Z}_2$. Notice that there is an extra self-dual symmetry between the two fermionic theories

$$\mathbb{Z}_2^{\mathrm{fdual}}: \quad X \leftrightarrow Y, \quad (\psi_1, \psi_2) \leftrightarrow (\chi_2, \chi_1), \quad a \leftrightarrow \tilde{a}, \quad (\Phi_B, \Phi_C) \leftrightarrow (\Phi_B^\dagger, \Phi_C). \tag{1.78}$$

In conclusion, the symmetry group is enlarged from G_{UV} to G_{IR} at critical point

$$G_{\mathrm{UV}} = \begin{cases} [\mathrm{U}(1)^{Y-X} \rtimes \mathbb{Z}_2] \times \mathrm{U}(1)^{Y+X} & \mathcal{L}_{\mathrm{bQED}} \\ \mathrm{U}(1)^{Y-X} \times [\mathrm{U}(1)^{Y+X} \rtimes \mathbb{Z}_2] & \tilde{\mathcal{L}}_{\mathrm{bQED}} \\ \mathrm{SU}(2)^X \times \mathrm{Pin}^-(2)^Y/\mathbb{Z}_2 & \mathcal{L}_{\mathrm{fQED}} \\ \mathrm{Pin}^-(2)^X \times \mathrm{SU}(2)^Y/\mathbb{Z}_2 & \tilde{\mathcal{L}}_{\mathrm{fQED}} \end{cases},$$
$$G_{\mathrm{IR}} = \frac{\mathrm{SU}(2)^X \times \mathrm{SU}(2)^Y}{\mathbb{Z}_2} \rtimes \mathbb{Z}_2 = \mathrm{SO}(4) \rtimes \mathbb{Z}_2 = \mathrm{O}(4). \tag{1.79}$$

It is easy to check the four-component vector (n_1, n_2, n_3, n_4) that transforms under $\mathrm{O}(4)$ is related to the Néel and VBS order parameters as

$$(\Phi_B, \Phi_C) \sim (n_1 + \mathtt{i}n_2, n_3 + \mathtt{i}n_4). \tag{1.80}$$

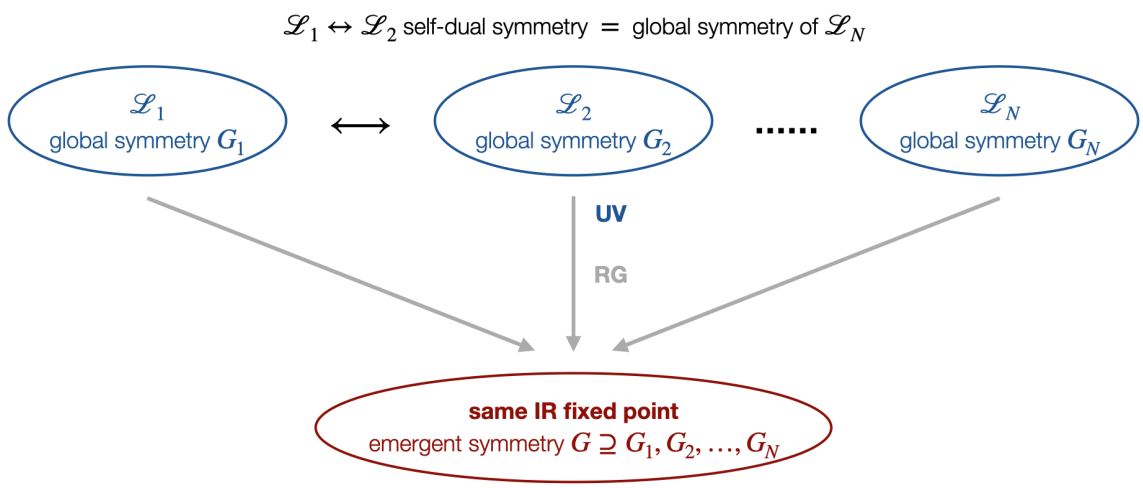

Figure 1.11: The structure of UV and IR symmetries in a web of dualities.

In principle, the enlarged O(4) symmetry can be proven by explicitly checking the scaling dimensions $\Delta[\Phi_B] = \Delta[\Phi_C]$. But all of them are strongly coupled field theories, and we do not have good analytical control. Nevertheless, symmetry enhancement is a comment feature of dualities, the logic of which is summarized in FIG. 1.11.

Self-dual symmetries We first notice that the self-dual $\mathbb{Z}_2^{\text{fdual}}$ symmetry in Eq. 1.78 is identified as the spin-flip $\mathbb{Z}_2^{\text{spin}}$ symmetry in the bosonic theories

$$\mathbb{Z}_2^{\text{fdual}} = \mathbb{Z}_2^{\text{spin}} : \quad (z_1, z_2) \leftrightarrow (z_2, z_1), \quad b \leftrightarrow b, \quad (\phi_1, \phi_2) \leftrightarrow (\phi_2^\dagger, \phi_1^\dagger), \quad \tilde{b} \leftrightarrow -\tilde{b}. \tag{1.81}$$

We should note that only $B = Y - X$ and $C = Y + X$ are properly quantized background fields, which transform as $B \to -B$ and $C = C$ (according to $X \leftrightarrow Y$). We find both dual bosonic theories get an extra term under the $\mathbb{Z}_2^{\text{spin}}$ symmetry

$$\begin{aligned}
\mathcal{L} &= |D_b z_1|^2 + |z_1|^4 + |D_{b+B} z_2|^2 + |z_2|^4 - \frac{\mathtt{i}}{2\pi} b \mathrm{d}C \quad \xrightarrow{\mathbb{Z}_2} \quad \mathcal{L} - \frac{\mathtt{i}}{2\pi} B \mathrm{d}C, \\
\tilde{\mathcal{L}} &= |D_{\tilde{b}-C} \phi_1|^2 + |\phi_1|^4 + |D_{\tilde{b}} \phi_2|^2 + |\phi_2|^4 + \frac{\mathtt{i}}{2\pi} \tilde{b} \mathrm{d}B \quad \xrightarrow{\mathbb{Z}_2} \quad \tilde{\mathcal{L}} - \frac{\mathtt{i}}{2\pi} B \mathrm{d}C,
\end{aligned} \tag{1.82}$$

where $-\frac{\mathtt{i}}{2\pi}X\mathrm{d}X$ has been added to both theories $\mathcal{L}_{\mathrm{bQED}}$ and $\tilde{\mathcal{L}}_{\mathrm{bQED}}$ in Eq. 1.76. The same behavior is also manifested under the self-dual $\mathbb{Z}_2^{\mathrm{fdual}}$ symmetry of fermionic theories

$$\begin{aligned} &\mathcal{L}_{\mathrm{fQED}} = \bar{\psi}_1 \not{D}_a \psi_1 + \bar{\psi}_2 \not{D}_{a-C+B} \psi_2 - \mathtt{i}\mathrm{CS}[a+B] + \frac{\mathtt{i}}{2}\mathrm{CS}[C+B] - \mathtt{i}2\mathrm{CS}_g \\ \leftrightarrow \quad &\tilde{\mathcal{L}}_{\mathrm{fQED}} = \bar{\chi}_1 \not{D}_{\tilde{a}-C-B} \chi_1 + \bar{\chi}_2 \not{D}_{\tilde{a}} \chi_2 - \mathtt{i}\mathrm{CS}[\tilde{a}-B] + \frac{\mathtt{i}}{2}\mathrm{CS}[C-B] - \mathtt{i}2\mathrm{CS}_g \end{aligned} \tag{1.83}$$

where the notation $\mathrm{CS}[A] = \frac{\mathtt{i}}{4\pi}A\mathrm{d}A$ has been used. Except for $\frac{\mathtt{i}}{2}\mathrm{CS}[C \pm B]$, all the other Chern-Simons terms are properly normalized. To make the expressions well-defined, we could add $-\frac{\mathtt{i}}{2\pi}X\mathrm{d}X$ on both sides. Then one theory has an additional term $\frac{\mathtt{i}}{2\pi}B\mathrm{d}C$ compared to the other. In conclusion, from both sides, we find $\mathbb{Z}_2^{\mathrm{spin}} = \mathbb{Z}_2^{\mathrm{fdual}}$ is anomalous. One way to make the continuum field theory consistent is to put the system on the boundary of a $(3+1)$-dimensional bulk manifold W_4 (see Sec. 1.5.2 for a general introduction to 't Hooft anomalies)

$$\mathcal{S} = \int_{\partial W_4} \mathcal{L} - \mathtt{i}\pi \int_{W_4} \frac{\mathrm{d}B}{2\pi} \wedge \frac{\mathrm{d}C}{2\pi}, \tag{1.84}$$

where the bulk topological term describes a SPT state with $[\mathrm{U}(1) \rtimes \mathbb{Z}_2] \times \mathrm{U}(1)$ symmetry. From a microscopic point of view, deconfined criticality can nevertheless be realized in two-dimensional lattice models because lattice rotation symmetries are not on-site, and therefore can be implemented in a seemingly anomalous fashion in the continuum theory. There is also a self-dual $\mathbb{Z}_2^{\mathrm{bdual}}$ symmetry between the two bosonic theories

$$\mathbb{Z}_2^{\mathrm{bdual}}: \quad Y \leftrightarrow -Y (\text{or } B \leftrightarrow -C), \quad (z_1, z_2) \leftrightarrow (\phi_2, \phi_1), \quad b \leftrightarrow \tilde{b}, \quad \Phi_B \leftrightarrow \Phi_C^\dagger. \tag{1.85}$$

It turns out to be an explicit global $\mathbb{Z}_2^\chi$ symmetry of the fermion χ, which is a subgroup of the $\mathrm{SU}(2)^Y$ flavor symmetry

$$\mathrm{SU}(2)^Y \supseteq \mathbb{Z}_2^{\mathrm{bdual}} = \mathbb{Z}_2^\chi : \quad X \leftrightarrow X, \quad Y \leftrightarrow -Y, \quad (\chi_1, \chi_2) \leftrightarrow (\chi_2, \chi_1), \quad \tilde{a} \leftrightarrow \tilde{a}. \tag{1.86}$$

In conclusion, we have seen that a certain $\mathbb{Z}_2$ global symmetry of one theory in the duality web is not manifested as a symmetry of the other theory but the self-dual symmetry between a pair of dual theories. The logic is summarized in FIG. 1.11.

Superfluid-Insulator Transition at Fractional Fillings

A famous example that realizes a conventional quantum phase transition in the 3D XY universality class is the Bose-Hubbard model at integer fillings [103]. The model has a global U(1) symmetry that corresponds to the conservation of the total boson number, and the spontaneous breaking of the U(1) symmetry realizes an insulator-to-superfluid transition. The critical point can be described by the Landau theory Eq. 1.17 with $z = 1, d = 2$ or the dual vortex theory Eq. 1.27. The situation, however, will be very different if we consider the Bose-Hubbard model at fractional fillings [104, 105] since the LSM theorem forbids a non-degenerate disordered state that preserves lattice symmetries. It resembles what we have encountered in the Néel-VBS transition. One possible resolution is that the insulating state is actually a commensurate density-wave state which spontaneously breaks lattice translation symmetry. (It can also be a topologically ordered state which will be discussed in Sec. 3.2.) This transition between two Landau-ordered phases is again an example of deconfined quantum criticality.

Under the particle-vortex duality introduced in Sec. 1.1.3, the critical theory can be

formulated in terms of the dual vortex fields φ_I

$$\mathcal{L} = \sum_{I=1}^{N} \left(|(\partial - \mathtt{i}a)\varphi_I|^2 + r|\varphi_I|^2 \right) + u \left(\sum_{I=1}^{N} |\varphi_I|^2 \right)^2 - \frac{\mathtt{i}}{2\pi} a \wedge \mathrm{d}A + \dots \tag{1.87}$$

where all PSG-allowed terms [3] should be included. The dynamical U(1) gauge field a is defined by $\mathrm{d}a = \star 2\pi J$, where J is the conserved U(1) current coupled to the background field A. The dual vortex theory looks very different compared to Eq. 1.17, since the vortex band structure has multiple minima $\boldsymbol{Q}_1, \boldsymbol{Q}_2, \dots, \boldsymbol{Q}_N$ in the Brillouin zone which leads to multiple dual vortex fields φ_I under the low-energy expansion

$$\varphi(\boldsymbol{x}) = \sum_{I=1}^{N} \varphi_I e^{\mathtt{i}\boldsymbol{Q}_I \cdot \boldsymbol{x}}. \tag{1.88}$$

The vortex condensation carries finite momentum and therefore breaks translation symmetry. This is the density-wave insulating state that we are after. On the other hand, when the vortex band is gapped, we are left with the Coulomb phase, where the photon corresponds to the Goldstone mode in the superfluid phase.

Similar to the Néel-VBS transition mentioned above, the superfluid-insulator transition also involves symmetry fractionalization. Let us consider the dual vortex $\tilde{\varphi}_I$ of each low-energy vortex field φ_I. The dual critical theory reads

$$\mathcal{L} = \sum_{I=1}^{N} \left| \left(\partial - \mathtt{i}\tilde{a}^I - \mathtt{i}\frac{e}{N} A \right) \tilde{\varphi}_I \right|^2 + \tilde{r}|\tilde{\varphi}_I|^2 + \dots \quad \text{where} \quad \sum_{I=1}^{N} \tilde{a}^I = 0. \tag{1.89}$$

We clearly see that each charge carrier $\tilde{\varphi}_I$ has a fractional charge e/N of the background field A. The charge fractionalization is only expected right at the critical point. When charge carriers $\tilde{\varphi}_I$ are gapped, the gauge fields $\tilde{a}^I$ will confine due to the proliferation of

[3] The concept of projective symmetry group (PSG) is introduced in Ref. [106]

monopoles carrying lattice translation symmetry.

1.4.2 Mott Metal-Insulator Transition

Understanding metal-insulator transitions (MITs) is one of the oldest yet one of the fundamentally least understood problems in condensed matter physics. Strictly speaking, a sharp difference between a metal and an insulator only exists at zero temperature. We can look at the electrical resistivity ρ at $T = 0$. A vanishing resistivity $\rho = 0$ means a superconducting phase, an infinity resistivity $\rho = +\infty$ means an insulating phase, and any finite value $0 < \rho < +\infty$ means a metal phase. At any finite temperature $T > 0$, an insulator typically has activated behavior $\rho(T) \sim e^{\Delta/T}$ where Δ is the charge gap, and an ordinary metal has $\rho(T) \sim \rho_0 + T^2$ according to fermi liquid theory (see Sec. 1.3.1). Therefore, sometimes people use the sign of $\mathrm{d}\rho/\mathrm{d}T$ to distinguish between metals and insulators. But various mechanisms may complicate the situation, and $\rho(T)$ could be a non-monotonic function. A sharp transition between two zero-temperature phases is a quantum phase transition. It is believed to be outside the Landau paradigm since no obvious Landau order parameter can fully describe the transition.

The simplest MIT can be understood at the level of band theory. We know the material is an insulator when the fermi level lies in the band gap (i.e., the occupied bands are fully filled), and partially filled bands give a metal. Therefore, changing the particle filling factor can induce a metal-insulator transition. However, if we are interested in the transition at fixed fractional particle filling, how would an insulator be even possible within the band theory picture? One resolution by Slater [107] is that the metal undergoes a certain symmetry-breaking transition that breaks the original lattice translation symmetry. For example, an antiferromagnetic order leads to unit cell doubling and gap opening at the new Brillouin zone boundary.

There are two main exceptions to the simple picture of band theory. The first type is the disorder-driven MIT. Introducing quenched disorder into a metal can change the electron wave function from spatially extended to localized, known as Anderson localization [108]. Our focus will be on the second type, the interaction-driven MIT, also known as the Mott transition [109]. The most studied model showing such a transition is the one-band Hubbard model

$$H = -\sum_{\langle i,j \rangle} \sum_{\alpha=\uparrow,\downarrow} t_{ij}(c^\dagger_{i,\alpha} c_{j,\alpha} + c^\dagger_{j,\alpha} c_{i,\alpha}) + U \sum_j n_{j,\uparrow} n_{j,\downarrow}, \tag{1.90}$$

where $c^\dagger_{j,\alpha}$ is the creation operator for an electron with spin α on site j, and $n_{j,\alpha} = c^\dagger_{j,\alpha} c_{j,\alpha}$ is the density operator. Let us fix the particle density at half-filling. There is a competition between the hopping energy t and the on-site Coulomb repulsion U. When $t/U \gg 1$, we know from band theory that it has to be a metal (if without translation symmetry breaking). The other limit $t/U \ll 1$ prevents doubly occupied sites and hence completely suppresses the electric current. The value of t/U (i.e., the bandwidth) is generally tunable in different correlated materials by changing external parameters. Namely, the Mott organic material κ-$(ET)_2Cu_2(CN)_3$ is tuned by pressure [110], and the TMD Morié bilayer $MoTe_2/WSe_2$ is tuned by a displacement field [4]. According to Mott [109], the bandwidth-tuned MIT is a first-order transition. The argument is that the carrier density is smaller with decreasing t/U, and the screening of long-range Coulomb interaction becomes ineffective, leading to the formation of particle-hole bound states. However, we want to mention the old argument may not apply to the TMD Morié system [4] since the nearby gates still screen the Coulomb interaction.

Continuous Mott Transition

A theoretical proposal for interaction-driven continuous MIT was systematically studied by Senthil [86, 87]. In order to make the electronic fermi surface disappear abruptly in a continuous fashion, a neutral fermi surface remains on the insulator side. It necessarily involves spin-charge separation. One type of parton construction is

$$c_{j,\alpha} = b_j f_{j,\alpha}, \tag{1.91}$$

where each electron $c_{j,\alpha}$ is fractionalized into a spinless bosonic chargon b_j which carries the electric charge and a charge neutral fermionic spinon $f_{j,\alpha}$ which carries the spin quantum number. There is a U(1) gauge redundancy, i.e., the electron operator is invariant under the local gauge transformation $b_j \to b_j e^{\mathtt{i}\theta_j}, f_{j,\alpha} \to e^{-\mathtt{i}\theta_j}$, which leads to a dynamical U(1) gauge field $a_\mu = (a_\tau, \boldsymbol{a})$ that couples b and f. Close to the critical point, the low-energy field theory can be written as

$$\mathcal{L} = \mathcal{L}[f,a] + \mathcal{L}[b,a] + \mathcal{L}[a] + \mathcal{L}[b,f] + \ldots, \tag{1.92}$$

$$\mathcal{L}[f,a] = f_\alpha^\dagger(\partial_\tau - \mathtt{i}a_\tau - \mu_f + \mathcal{E}(\nabla - \mathtt{i}\boldsymbol{a}))f_\alpha, \tag{1.93}$$

$$\mathcal{L}[b,a] = |(\partial_\mu - \mathtt{i}a_\mu)b|^2 + r|b|^2 + u|b|^4 + \ldots, \tag{1.94}$$

$$\mathcal{L}[a] = \frac{1}{e^2}(\varepsilon_{\mu\nu\rho}\partial_\nu a_\rho)^2, \qquad \mathcal{L}[b,f] = |b|^2 f_\alpha^\dagger f_\alpha, \tag{1.95}$$

where $\mathcal{E}(\boldsymbol{k})$ denotes the spinon mean-field dispersion. The transition is controlled by a single parameter $r \sim (g_c - g)$ where $g = t/U$. When $r > 0$, the chargon b is gapped, and we are left with a spinon fermi-surface state, which corresponds to a spin-liquid Mott insulator. When $r < 0$, the chargon condensation will Higgs the gauge field a, and the system goes back to a fermi-surface state of the original electron $c \sim \langle b \rangle f$.

There are some salient features associated with this critical theory. Although we

should start with a compact U(1) gauge field a_μ in the microscopic derivation, the monopole events are strongly suppressed by the spinon fermi surface, and therefore a_μ becomes non-compact in the critical theory. Another important feature is that the chargon sector is dynamically decoupled from the rest, and the boson condensation transition belongs to the 3D XY universality class. We first check the spinon-chargon coupling $\mathcal{L}[b, f] = O_b f^\dagger f$ where $O_b = |b|^2$ carries zero momentum. (The case of O_b with a finite momentum will considered in Sec. 3.2.) As we have discussed in Sec. 1.3.2, a Landau damping term will be generated

$$\mathcal{S}_{\text{eff}}[b] \supset \int \frac{\mathrm{d}\omega \mathrm{d}^2\boldsymbol{k}}{(2\pi)^3} \tilde{\gamma} \frac{|\omega|}{|\boldsymbol{k}|} \left|O_b(\omega, \boldsymbol{k})\right|^2 . \tag{1.96}$$

The scaling dimension of O_b at the 3D XY fixed point is $\Delta[O_b] = 3 - 1/\nu$ where the exponent ν is defined in TABLE. 1.1. The coupling $\tilde{\gamma}$ can be seen to be irrelevant since $\Delta[O_b] > 3/2$ is satisfied. (If O_b is a density-wave order, then the generated term is instead $\mathcal{L} \sim |\omega| \, |O_b|^2$, and one needs $\Delta[O_b] > 1$ for dynamical decoupling.) The second task is to examine whether the gauge field will affect the critical point of the chargon sector. We first notice that the effective action of the transverse gauge field becomes

$$\mathcal{S}_{\text{eff}}[a] = \int \frac{\mathrm{d}\omega \mathrm{d}^2\boldsymbol{k}}{(2\pi)^3} \left(\gamma_f \frac{|\omega|}{|\boldsymbol{k}|} + v_b |k| + \frac{|k|^2}{e^2} \right) \left|a(\omega, \boldsymbol{k})\right|^2 , \tag{1.97}$$

where the γ_f term describes the Landau damping due to spinon fermi surface, and the v_b term is the chargon contribution. It resembles Eq. 1.62 with the dynamical exponent $z = 2$, which leads to a marginal fermi liquid fixed point of the spinon-gauge system. At the critical point of the chargon sector, ω and $\boldsymbol{k}$ should scale identically. Therefore, the γ_f term in Eq. 1.97 behaves like a mass term and quenches the effects of the gauge field fluctuations. In conclusion, the chargon condensation identifies the 3D XY transition.

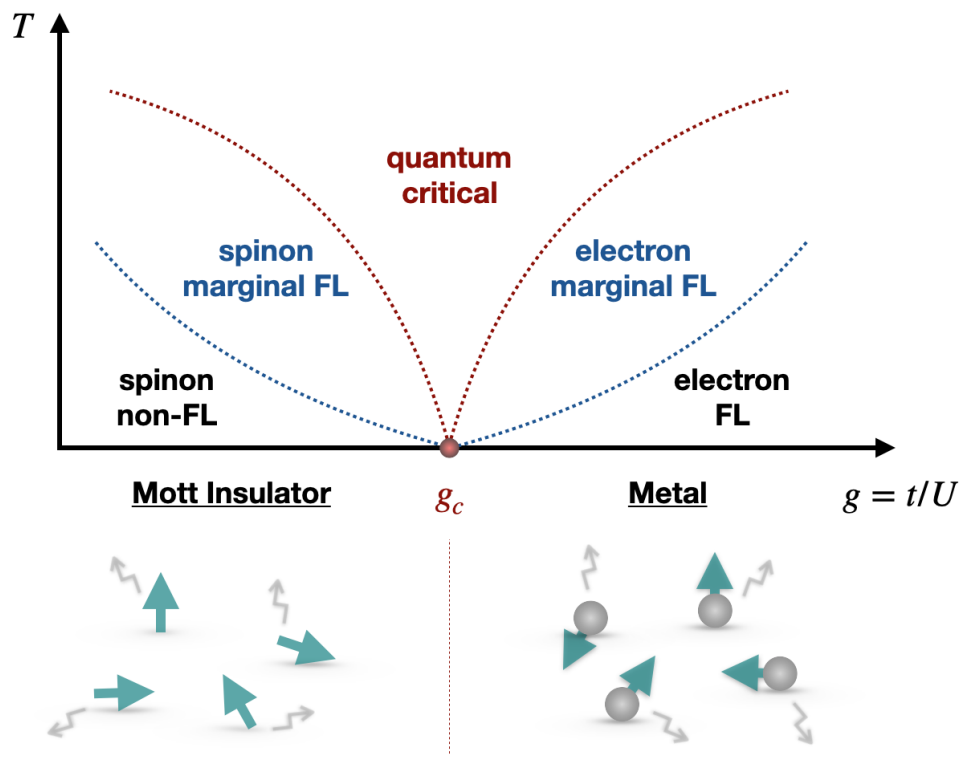

Figure 1.12: The schematic phase diagram of the continuous Mott metal-insulator transition involving spin-charge separation. The transition is driven by the chargon condensation which belongs to the 3D XY universality class. One has two crossover scales $T_{**} < T_*$ on both sides of the phase diagram. When $T_{**} < T < T_*$, one has marginal fermi-liquid states for electrons and spinons. Only below the much lower scale $T < T_{**}$, one has an electron fermi liquid and a spinon non-fermi liquid.

Finally, we want to mention that this transition has richer crossover phenomena than the single critical fan shown in FIG. 1.2. From Sec. 1.1.2, we know there is a crossover temperature scale $T_* \sim |g - g_c|^\nu$ for the XY transition. But after the chargon condensation, the gauge field will not immediately feel the Higgs mechanism and will continue to affect the dynamical properties of the fermi-surface state. Only below a lower temperature scale $T_{**} \sim |g - g_c|^{2\nu}$, we have the electron fermi-liquid state. Similar considerations apply to the insulating side as well. The spin-gauge system will not immediately feel the chargon gap until a lower energy scale. There is a crossover of the gauge field dynamical exponent from $z = 2$ to $z = 3$ (with/without the v_b term in Eq. 1.97). As for the spinon fermi-surface state, this is a crossover from marginal fermi liquid to non-fermi liquid. We summarize the phase diagram in FIG. 1.12.

Experimental Signatures

There are various physical properties of the proposed continuous Mott transition that can be checked in experimental systems. If we approach from the fermi-liquid side, the quasiparticle residue Z will behave as

$$Z \sim \frac{|g - g_c|^{2\beta}}{\log(1/|g - g_c|)}, \tag{1.98}$$

where the critical exponent (defined in TABLE. 1.1) is roughly $\beta \approx 0.33$ at the 3D XY fixed point. In addition, the electron effective mass will diverge logarithmically

$$m_* \sim \log(1/|g - g_c|), \tag{1.99}$$

which can be detected via the Kadowaki-Woods scaling in the transport measurement. There are also thermodynamic signatures. Namely, the specific heat at the critical point is

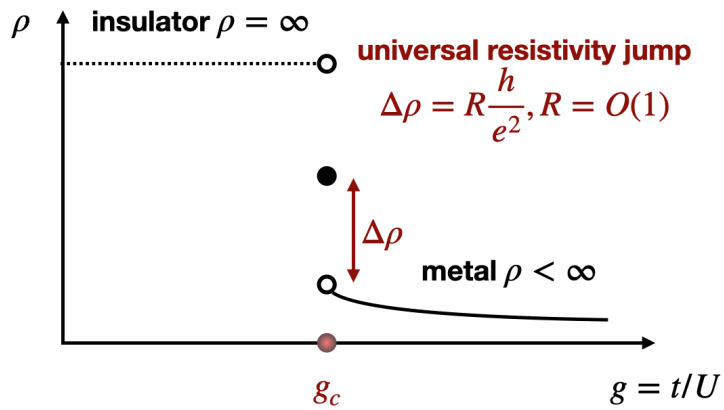

Figure 1.13: The predicted universal resistivity jump $\Delta\rho = Rh/e^2$ at the continuous Mott transition, where R is the is of the order $1 < R < 10$ (expected).

dominated by the spinon-gauge contribution, which has the marginal fermi-liquid scaling

$$C \sim T \log(1/T). \tag{1.100}$$

One particularly interesting prediction is the universal resistivity jump at the transition. According to the Ioffe-Larkin rule, the total electrical resistivity is given by $\rho = \rho_f + \rho_b$, where ρ_f is the spinon contribution and ρ_b is the chargon contribution. In the insulating phase at $T = 0$, the gapped chargon sector has $\rho_b = +\infty$, and therefore the total resistivity is $\rho = +\infty$. In the metallic phase at $T = 0$, the chargon superfluid has $\rho_b = 0$, and therefore $\rho = \rho_f$ is totally determined by the fermi-surface state. In principle, ρ_f can be nonzero due to some weak disorder (which is weak in the sense that the localization effect is negligible). There is something very interesting right at the transition. According to Sec. 1.1.2, the critical bosons at the 3D XY transition should have a universal resistivity $\rho_b = Rh/e^2$. Consequently, if we approach from the metal side, there is a universal resistivity jump right at the critical point

$$\rho = \rho_f + R\frac{h}{e^2}. \tag{1.101}$$

In general, R is a universal scaling function of ω/T. But only the two limits $\omega/T \to \infty$ and $\omega/T \to 0$ are more accessible in theoretical calculations. The simpler case $\rho_b(\infty) \approx 3h/e^2$ is determined by the ground-state properties and identifies the 3D XY result in TABLE. 1.3. As for $\rho_b(0)$, one also needs to consider the scattering between critical bosons and damped gauge fields, and therefore $\rho_b(0)$ is expected to be larger than the result in TABLE. 1.3. A large-N calculation is provided by Ref. [111], which gives $\rho_b(0) \approx 7.93h/e^2$. One may not take this number too seriously, but $1 < R < 10$ is still expected. If one finds a huge resistivity jump with $R \gg 10$ in an experimental system, the theoretical construction may need serious modifications.

One may wonder if there are available experimental realizations of this theoretical proposal. There is a claimed continuous metal-insulator transition in the organic system κ-$(ET)_2Cu_2(CN)_3$ [110] which is also a spin-liquid candidate because no magnetic order has been found at very low temperatures. Although the early specific heat data support the proposed spinon fermi-surface state [112], the thermal transport appears to show a gap [113], and the recent electron spin resonance measurement also confirms the spin gap [114]. Another potential realization is the TMD Morié bilayer $MoTe_2/WSe_2$ [4]. But the observed critical resistivity seems to be much larger than the prediction. We will get back to this point in Sec. 1.6.

1.5 Generalized Landau Paradigm

The concept of symmetry has long been a guiding principle in different areas of physics. If a system has a certain symmetry, then we know immediately that the states are organized according to the representations of the symmetry group. Symmetries also provide superselection rules that tell us which physical processes are allowed. If a symmetry is continuous, then the Noether theorem leads to a local conserved current. Our

modern understanding of phases of matter and phase transitions is based on RG flows (see FIG. 1.1). Under coarse-graining, a lot of information gets lost. But symmetries are always preserved under RG. (Symmetries can be spontaneously broken, but local operators are still in the representations of the symmetry group.) Therefore, symmetries are at least part of the information that completely determines the universal properties of any quantum many-body system. Namely, as reviewed in Sec. 1.1, conventional phases of matter are labeled by how they represent their symmetries, and critical properties at Landau phase transitions are entirely determined by the symmetry group and the dimensionality. Furthermore, a global symmetry can sometimes be anomalous, meaning it can not be consistently promoted to a local one (i.e., gauge symmetry). The inconsistency (called 't Hooft anomaly) is always preserved under RG, making symmetries even more powerful in constraining low-energy dynamics.

The concept of symmetry has also been evolving with time (see Ref. [115, 116] and references therein). With certain generalizations of symmetries, many famous non-Landau phases of matter, such as topological orders, fracton phases, and SPT phases, can actually be understood in a flavor similar to the Landau paradigm, namely by how the states represent their symmetries. The purpose of this section is to briefly introduce some of the recent developments.

1.5.1 Generalized Symmetries

There are two features of ordinary symmetries: *(1)* symmetries are acting on zero-dimensional objects, e.g., quantum numbers are carried by quasiparticles; *(2)* symmetry transformations form a group structure. For the purpose of understanding universal properties of quantum matter, both of them can be generalized. Namely, one can define symmetries acting on higher-dimensional objects such as loops and membranes [117]. One

step further, a symmetry algebra does not have to be a group algebra, which can even be a fusion category algebra [118, 119]. The generalized symmetries not only provide new organizing principles of known phases of matter, but can also have 't Hooft anomalies constraining low-energy dynamics of strongly correlated systems.

Higher-Form Symmetries

Ordinary symmetries To set the stage for subsequent generalizations, we summarize some basic facts about ordinary global symmetries. The charged operators are 0-dimensional objects, and therefore ordinary symmetries are called 0-from symmetries. Let us denote the $(d+1)$-dimensional spacetime manifold by Y_{d+1}, which is given by the foliation of spatial slices denoted by $X_d \subseteq Y_{d+1}$. For each symmetry group element $\mathbf{g} \in G$, there is a unitary (or anti-unitary) operator $U(\mathbf{g}; M_d)$ associated with a d-dimensional manifold $M_d \subseteq Y_{d+1}$ that satisfies the group algebra

$$U(\mathbf{g}; M_d)U(\mathbf{h}; M_d) = U(\mathbf{gh}; M_d) \quad \text{for} \quad \forall \mathbf{g}, \mathbf{h} \in G. \tag{1.102}$$

The symmetry transformation on a charged operator $V(\text{pt})$ defined on the point $\text{pt} \in X_d$ is implemented via the equal-time commutation relation

$$U(\mathbf{g}; X_d)V_a(\text{pt})U^\dagger(\mathbf{g}; X_d) = R_{ab}(\mathbf{g})V_b(\text{pt}) \quad \text{for} \quad \forall \mathbf{g} \in G, \tag{1.103}$$

where $R_{ab}(\mathbf{g})$ is the representation of the group element $\mathbf{g} \in G$. We recall that the equal-time commutation relation should be understood as a time-ordered product. In the point-splitting definition, the charged object $V(\text{pt})$ at the time t is sandwiched by $U(\mathbf{g}; X_d^+)$ and $U^\dagger(\mathbf{g}; X_d^-)$ at $t+\epsilon$ and $t-\epsilon$ respectively. We can define a d-dimensional manifold M_d by gluing the two spatial slices $M_d = X_d^+ \cup (-X_d^-)$, which is topologically equivalent to a

sphere $M_d \cong S^d$ surrounding pt (see FIG. 1.14). The equal-time commutator Eq. 1.103 then becomes the time-ordered operator equation (i.e., the Ward identity)

$$U(\mathbf{g}; M_d)V_a(\mathrm{pt}) = R_{ab}(\mathbf{g})V_b(\mathrm{pt}). \tag{1.104}$$

Written in this way, the Ward identity 1.104 holds for both continuous and discrete symmetries. For each group generator $\mathbf{t} \in G$, we say there is a charge $Q(M_d) = U(\mathbf{t}; M_d)$ associated with the manifold M_d. If the symmetry is continuous, the conserved charge $Q(M_d)$ is given by integrating the Noether 1-form current J

$$Q(M_d) = \int_{M_d} \star J, \tag{1.105}$$

where $\mathrm{d} \star J = 0$ implies the conservation law. For the group element $\mathbf{g} = e^{\mathbf{i}\alpha\mathbf{t}}$, we have

$$U(e^{\mathbf{i}\alpha\mathbf{t}}; M_d) = e^{\mathbf{i}\alpha Q(M_d)}. \tag{1.106}$$

The nonlocal operator $U(\mathbf{g}; M_d)$ is usually referred to as a symmetry defect. For Lorentz invariant field theories, the symmetry defect $U(\mathbf{g}; M_d)$ is topological because its correlation functions are not affected by any continuous deformation of M_d without passing through other charged objects. The topological invariance is a fancy way of stating the conservation law. For non-relativistic theories, including lattice models, we can not freely deform M_d in the total spacetime. The symmetry defect is not topological. But we still have conservation laws based on deformations in restricted directions.

A helpful perspective is to regard the existence of defect operators and associated Ward identities (i.e., conservation laws) as the definition of any symmetries [4].

[4] There is a subtle point that symmetries may be inexplicit sometimes, and not all charged objects are necessarily present in the Hilbert space. But inexplicit symmetries can still be defined by the existence of conservation laws. The concepts are clarified in Appendix. A.4

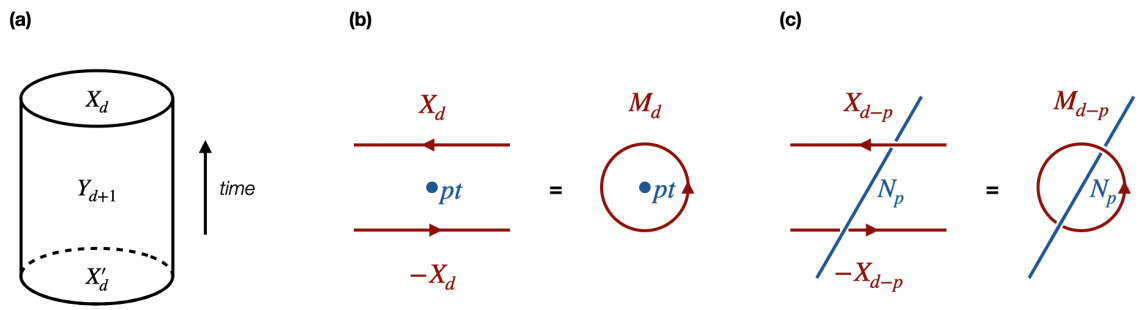

Figure 1.14: (a) The spacetime manifold Y_{d+1} given by the foliation of spatial slices X_d. (b) The equal-time commutator 1.103 for ordinary symmetry transformations is deformed to a linked configuration Eq. 1.104 of d-dimensional symmetry defects $U(M_d)$ and charged particles $V(\text{pt})$. (c) The equal-time commutator 1.108 for p-form symmetry transformations is deformed to a linked configuration Eq. 1.107 of $(d-p)$-dimensional symmetry defects $U(M_{d-p})$ and charged p-sheets $V(N_p)$.

p-form symmetries We are ready to consider the generalization to higher-form symmetries [117]. A charged object $V(N_p)$ is supported on a p-dimensional manifold N_p. Let us call it charged p-sheet. The Ward identity Eq. 1.104 is generalized to

$$U(\mathbf{g}; M_{d-p})V(N_p) = R(\mathbf{g})^{\mathrm{Lk}(M_{d-p},N_p)}V(N_p), \tag{1.107}$$

where the symmetry defect $U(\mathbf{g}; M_{d-p})$ is associated with a group element $\mathbf{g} \in G^{(p)}$ and a $(d-p)$-cycle M_{d-p}, $R(\mathbf{g})$ is a representation of the group $G^{(p)}$, and $\mathrm{Lk}(M_{d-p}, N_p)$ denotes the linking number between M_{d-p} and N_p. See FIG. 1.14 for an illustration of how it is deformed from the equal-time commutator

$$U(\mathbf{g}; X_{d-p})V(N_p)U^\dagger(\mathbf{g}; X_{d-p}) = R(\mathbf{g})^{\#(X_{d-p},N_p)}V(N_p), \tag{1.108}$$

where $X_{d-p} \subseteq X_d$ is a spatial submanifold, and $\#(N_p, X_{d-p})$ denotes its intersection number number with N_p. By definition, the symmetry defects satisfy the group algebra

$$U(\mathbf{g}; M_{d-p})U(\mathbf{h}; M_{d-p}) = U(\mathbf{gh}; M_{d-p}) \quad \text{for} \quad \forall \mathbf{g}, \mathbf{h} \in G^{(p)}. \tag{1.109}$$

For Lorentz invariant field theories on a simply connected spacetime manifold Y_{d+1}, the symmetry defects are topological and the group $G^{(p)}$ when $p > 0$ has to be abelian. (We do not exclude the possibility of nonabelian higher-form symmetries in field theories on topologically nontrivial manifolds or nonrelativistic lattice models.) For any generator $\mathbf{t}$ in a continuous symmetry group, there is a conserved $(p+1)$-form current $J^{(p+1)}$ which satisfies $\mathrm{d} \star J^{(p+1)} = 0$. The conserved charge Q is associated with M_{d-p}

$$Q(M_{d-p}) = \int_{M_{d-p}} \star J^{(p+1)}. \tag{1.110}$$

For the group element $\mathbf{g} = e^{\mathbf{i}\alpha\mathbf{t}}$, we still have $U(e^{\mathbf{i}\alpha\mathbf{t}}; M_{d-p}) = e^{\mathbf{i}\alpha Q(M_{d-p})}$.

Physical examples of higher-form symmetries The concept of 1-form symmetry can be associated with conserved gauge fluxes through a $(d-1)$-dimensional subsystem M_{d-1}. Namely, Maxwell theory in $d = 3$ without magnetic monopoles has a continuous 1-form symmetry (denoted by $\mathrm{U}(1)_m^{(1)}$) with the conserved current $J_m = \star f/2\pi$, where $f = \mathrm{d}a$ is the gauge curvature. The conservation law is simply due to the Bianchi identity $\mathrm{d}f = 0$, and the charged objects are 't Hooft lines. If no electric charge is present, there is a second conserved 1-form current $J_e = f/e^2$ (for $\mathrm{U}(1)_e^{(1)}$ symmetry) in view of the Maxwell equation $\mathrm{d} \star f = 0$. The objects that transform under $\mathrm{U}(1)_e^{(1)}$ are Wilson lines. In addition, it is not surprising that discrete gauge theories enjoy discrete 1-form symmetries. In $\mathbb{Z}_2$ gauge theory with exact Gaussian law constraint, the electric fluxes through a closed surface are conserved mod 2. Furthermore, continuous gauge theories can have discrete 1-form symmetries if only certain matter fields are allowed. For U(1) gauge theory with only even electric charges, the Gauss law $\nabla \cdot \boldsymbol{E} \in 2\mathbb{Z}$ again means the electric fluxes are conserved mod 2. For SU(2) gauge theory with only adjoint matter fields, the gauge group center $\mathbb{Z}_2$ gives rise to a 1-form symmetry. Therefore, the different

gauge fields (with gauge groups $\mathbb{Z}_2, \mathrm{U}(1), \mathrm{SU}(2)$, etc) can share the $\mathbb{Z}_2^{(1)}$ 1-form symmetry depending on the matter fields.

Other Generalized Symmetries

Subsystem symmetries In non-relativistic theories, the notation of symmetry can also be generalized by defining symmetry transformations independently on rigid subspaces of space X_d. This type of generalized symmetry is called subsystem symmetry. An example in $d = 2$ with U(1) subsystem symmetry has been considered in Ref. [120]

$$\mathcal{L} = \frac{1}{2U}(\partial_\tau \theta)^2 + \frac{K}{2}(\partial_x \partial_y \theta)^2, \tag{1.111}$$

where $\theta \simeq \theta + 2\pi$ is a compact scalar. It is invariant under the symmetry transformation

$$\theta(\tau, x, y) \to \theta(\tau, x, y) + f(x) + g(y), \tag{1.112}$$

where f, g are arbitrary functions of one spatial coordinate. The Noether currents are $J_\tau = \frac{1}{U}\partial_\tau \theta$ and $J_{xy} = -K\partial_x \partial_y \theta$ which satisfy the dipole conservation law $\partial_\tau J_\tau + \partial_x \partial_y J_{xy} = 0$. There are a large number of conserved charges labeled by one spatial coordinate

$$Q_x(x) = \int \mathrm{d}y J_\tau, \qquad Q_y(y) = \int \mathrm{d}x J_\tau. \tag{1.113}$$

We observe the restricted mobility of charged objects since x or y needs to be specified. A more extensive discussion of related lattice models can be found in Sec. 5.1. Subsystem symmetries are also crucial in understanding fracton phases of matter. In such a gapped phase, one typically has a large ground state degeneracy growing exponentially with system size and has excitations with restricted mobility. Some fracton models can be realized by gauging subsystem symmetries (see Ref. [116, 115] for a list of references).

Categorical symmetries A further generalization is that the fusion of symmetry defects Eq. 1.109 does not have to obey a group algebra. More generally, it can be

$$\mathbf{t}_a \times \mathbf{t}_b = \sum_c \mathrm{N}_{ab}^c \mathbf{t}_c, , \tag{1.114}$$

where N_{ab}^c are non-negative integers that satisfy the commutative and associative relations

$$\mathrm{N}_{ab}^c = \mathrm{N}_{ba}^c, \qquad \sum_d \mathrm{N}_{ab}^d \mathrm{N}_{dc}^f = \sum_d \mathrm{N}_{ac}^d \mathrm{N}_{bd}^f. \tag{1.115}$$

One can understand Eq. 1.114 as the fusion algebra of anyons $\mathbf{t}_a$ in a topological order or the OPE of primary fields $\mathbf{t}_a$ in a rational CFT. There are currently two perspectives about generalizing the notion of symmetries based on Eq. 1.114. The perspective taken by Ref. [119] is based on duality walls. The simplest example is the Ising CFT that describes the critical transverse Ising chain introduced in Sec. 1.1.3. The duality wall $\mathcal{N}$ is defined as a defect operator such that when we pass through the wall, we act by the Kramers-Wannier duality interchanging the spin and the domain wall. Together with the ordinary $\mathbb{Z}_2$ symmetry defect η, they form the algebra $\eta \times \eta = 1$, $\eta \times \mathcal{N} = \mathcal{N} \times \eta = \mathcal{N}$, and $\mathcal{N} \times \mathcal{N} = 1 + \eta$, which identity the fusion algebra Eq. 1.114 for Ising anyons. The second perspective that will be taken in Sec. 5.1 and Sec. 5.2 is based on Ref. [118]. We want to understand emergent symmetries at quantum critical points by looking at dual theories in the same spirit as FIG. 1.11. Let us again look at the transverse Ising chain. We have seen in Sec. 1.1.3 that there is a $\mathbb{Z}_2$ symmetry in the spin description and another $\tilde{\mathbb{Z}}_2$ symmetry in the domain-wall description. Is the symmetry simply enlarged to $\mathbb{Z}_2 \times \tilde{\mathbb{Z}}_2$? The answer is no since the symmetry charges have nontrivial π mutual statistics. To make the two symmetries on equal footing, one also needs to project all symmetry-breaking states to the symmetric sector (e.g., the cat state $|\uparrow, \ldots, \uparrow\rangle \pm |\downarrow, \ldots, \downarrow\rangle$). The idea of

Ref. [118] is to put the system on the boundary of the $\mathbb{Z}_2$ topological order in $d = 2$. There are four types of excitations $\{1, e, m, f\}$, where e and m have π mutual statistics. The two gapped edge phases are given by e condensation and m condensation. The fusion rules Eq. 1.114 in this case are $e \times e = 1$, $m \times m = 1$, $f \times f = 1$, and $e \times m = f$.

Spontaneous Symmetry Breaking (SSB)

Generalized symmetries can be spontaneously broken, which leads to generalized Landau phases of matter. In this section, we first illustrate how to characterize whether the system is in the symmetric (Sym) phase or the spontaneous symmetry breaking (SSB) phase. Then we will briefly discuss the physical consequences of the SSB of higher-form symmetries. For simplicity, we assume the spacetime manifold Y_{d+1} is simply connected such that all higher-form symmetries are abelian.

Order diagnosis operators To set the stage for subsequent generalizations, let us first review some facts about 0-form symmetries from Sec. 1.1. In order to distinguish the two phases, we can define a nonlocal operator called order diagnosis operator (ODO) using the Landau order parameter $\phi(\boldsymbol{x})$

$$\mathcal{O}_{\boldsymbol{x},\boldsymbol{x}'} = \phi^\dagger(\boldsymbol{x})\phi(\boldsymbol{x}'). \tag{1.116}$$

The order parameter $\phi(\boldsymbol{x})$ transforms under the unitary representation of the global symmetry group $\phi(\boldsymbol{x}) \to \mathcal{U}\phi(\boldsymbol{x})$, and accordingly the ODO is symmetry invariant. One can imagine $\mathcal{O}_{\boldsymbol{x},\boldsymbol{x}'}$ is associated with a line with two ends $\boldsymbol{x}$ and $\boldsymbol{x}'$. One can stretch the

line and check the scaling behavior of $\langle \mathcal{O}_{\boldsymbol{x},\boldsymbol{x}'} \rangle$, which defines the two phases

$$\langle \mathcal{O}_{\boldsymbol{x},\boldsymbol{x}'} \rangle \sim \begin{cases} \exp(-|\boldsymbol{x}-\boldsymbol{x}'|/\xi) & \text{Sym} \\ \text{const.} & \text{SSB} \end{cases} \tag{1.117}$$

where ξ is the correlation length. This is the criterion for short-range and long-range correlations mentioned in Sec. 1.1.1. The generalization to p-form symmetries is straightforward. The ODO is a nonlocal operator $\mathcal{O}_C^{(p)}$ associated with a p-dimensional boundary $C_p = \partial A_{p+1}$ (e.g., a Wilson p-sheet supported on a trivial p-cycle C_p). We can deform $C_p = \partial A_{p+1}$ and check the scaling behavior of the expectation value

$$\langle \mathcal{O}_C^{(p)} \rangle \sim \begin{cases} \exp(-t_{p+1}\text{Vol}(A_{p+1})) & \text{Sym} \\ \exp(-t_p \text{Vol}(C_p)) & \text{SSB} \end{cases} \tag{1.118}$$

where t_p and t_{p+1} are nonuniversal coefficients. When $p = 0$, Eq. 1.118 reduces back to Eq. 1.117. When $p = 1$, the Wilson loop's area-law and perimeter-law behaviors mark the confined and deconfined phases of 1-form gauge fields. For subsystem symmetries, ODOs can be defined accordingly, with special forms and behaviors. Some examples of subsystem ODOs will be discussed in Sec. 5.1.

Explicit and inexplicit symmetries Our motivation of introducing the concept of ODO in Ref. [121, 122] is to treat categorical symmetries (defined in the way of Ref. [118]). If we do not go to one-higher dimension (do not introduce the bulk topological order), the dual symmetry is inexplicit and elusive to understand. For example, let us take the transverse Ising chain with periodic boundary conditions. In the original Ising spin Hilbert space, only states with an even number of domain walls are allowed. Therefore, there is no charged object that transforms nontrivially under the dual $\tilde{\mathbb{Z}}_2$ symmetry. In

other words, we are not able to define the Landau order parameter for $\tilde{\mathbb{Z}}_2$ in the original Hilbert space. There is also no ground-state degeneracy when $\tilde{\mathbb{Z}}_2$ is spontaneously broken. However, the ODO for $\tilde{\mathbb{Z}}_2$ can still be defined in the original Ising model, and can characterize the phases of $\tilde{\mathbb{Z}}_2$ without any ambiguity. See Appendix. A.4 for a more detailed illustration. From the perspective of categorical symmetries, we also observe some similarities between Landau transitions and DQCPs introduced in Sec. 1.4.1. Namely, the $\mathbb{Z}_2$ defect is charged under the $\tilde{\mathbb{Z}}_2$ symmetry, while the $\tilde{\mathbb{Z}}_2$ defect is charged under the $\mathbb{Z}_2$ symmetry. The condensation of one type of defect will break one symmetry and preserve the other. There is, however, a key difference. In the Landau transition, the symmetry is explicit, while the dual symmetry is inexplicit. But in the DQCP, both the Néel and VBS order parameters carry explicit symmetries.

Coulomb phase as SSB We know photons are gapless in our universe. A satisfying understanding comes from interpreting photons as Goldstone modes of a $\mathrm{U}(1)^{(1)}$ 1-form symmetry. The Goldstone theorem for continuous higher-form symmetries guarantees that Goldstone modes are gapless. In general, when a $\mathrm{U}(1)^{(p)}$ p-form symmetry is spontaneously broken, one has a gapless p-form field $a^{(p)}$

$$\mathcal{S}[a^{(p)}] = \int_{Y_{d+1}} \frac{1}{2e^2} \mathrm{d}a^{(p)} \wedge \star \mathrm{d}a^{(p)} + \dots \tag{1.119}$$

When $p = 0$, $a^{(p)}$ reduces to a compact scalar. When $p \geq 1$, $a^{(p)}$ is a p-form gauge field. This is the familiar Coulomb phase of gauge theories. There is a p-form generalization of the *Mermin-Wagner theorem*, which states that the SSB of continuous symmetries is only possible when $d > p + 1$. It can be understood from the IR divergence of the ODO

$\mathcal{O}_C^{(p)} = \exp(\mathtt{i}\int_{C_p} a^{(p)})$ for the continuous p-form symmetry, i.e.,

$$-\log\langle\mathcal{O}_C^{(p)}\rangle = \frac{1}{2}\int_{C_p}\int_{C_p} \mathrm{d}^p x \wedge \mathrm{d}^p y D(x-y) \sim \frac{e^2 L^p}{2}\int \frac{\mathrm{d}^{d+1-p}k}{(2\pi)^{d+1-p}}\frac{1}{|k_\perp|^2}, \tag{1.120}$$

where the propagator of $a^{(p)}$ satisfies $D(k) \sim e^2/|k|^2$, L is the linear length scale of C_p, and $k_\perp$ represents the momentum perpendicular to C_p. When $d < p+1$, the momentum integral is IR divergent, which means long-wavelength fluctuations will destroy the would-be long-range order. When $d > p+1$, the UV divergence in $-\log\langle\mathcal{O}_C^{(p)}\rangle \sim L^p \sim \mathrm{Vol}(C_p)$ can be absorbed by local counterterms, and the SSB phase is stable. In the marginal case $d = p+1$, we have $-\log\langle\mathcal{O}_C^{(p)}\rangle \sim L^p \log L$, which is in between the perimeter law $\mathrm{Vol}(C_p) \sim L^p$ and the area law $\mathrm{Vol}(A_{p+1}) \sim L^{p+1}$. One example is the free QED_3 (with $d = 2$ and $p = 1$). There is a logarithmic potential between test charged particles, which is an extremely mild form of confinement. It can be linearly confined due to monopole proliferation, a higher-form analog of the vortex proliferation in the Kosterlitz-Thouless transition. As we have seen in Sec. 1.4.1, this mechanism is essential in realizing DQCPs. Namely, when the spinons are gapped, the emergent U(1) gauge field is going to confine due to the condensation of the VBS order parameter.

Topological order as SSB Discrete p-form symmetries can be spontaneously broken in spatial dimension $d > p$, which is one dimension lower than continuous symmetries. In $d = 2$, abelian topological orders are described by deconfined topological gauge theories with 1-form symmetries spontaneously broken. Namely, the $\nu = 1/k$ Laughlin state is described by the U(1) Chern-Simons theory at level k

$$\mathcal{S} = \frac{\mathtt{i}k}{4\pi}\int_{Y_3} a \wedge \mathrm{d}a. \tag{1.121}$$

The system has a $\mathbb{Z}_k^{(1)}$ 1-form symmetry with the symmetry defects given by the Wilson loops

$$U_m(M_1) = \exp\left(\mathtt{i}m \int_{M_1} a\right), \qquad m = 0, 1 \ldots, k-1. \tag{1.122}$$

In this case, the charged objects are the Wilson loops themselves. The Ward identity Eq. 1.107 is given by the braiding of the Wilson loops

$$U_m(M_1)U_n(N_1) = (e^{\mathtt{i}2\pi mn/k})^{\mathrm{Lk}(M_1,N_1)} U_n(N_1), \tag{1.123}$$

where $\mathrm{Lk}(M_1, N_1)$ is the linking number between the two 1-cycles M_1 and N_1. This is a symmetry since the Chern-Simons action is invariant under $a \to a + \gamma/k$, where γ is a flat connection with $\int_{\text{1-cycle}} \gamma \in 2\pi\mathbb{Z}$. The fact that the symmetry generators are charged under the symmetry, indicates the symmetry is actually anomalous. (We will define the anomaly more precisely in Sec. 1.5.2.) More generally, all abelian topological orders are described by the K-matrix Chern-Simons theories

$$\mathcal{S} = \frac{\mathtt{i}K_{IJ}}{4\pi} \int_{Y_3} a^I \wedge \mathrm{d}a^J, \tag{1.124}$$

where a^I are abelian 1-form gauge fields, and the invertible K-matrix satisfies $K_{IJ} = K_{JI} \in \mathbb{Z}$. There are 1-form symmetries generated by the Wilson loops

$$U_{\boldsymbol{l}}(M_1) = \exp\left(\mathtt{i} \int_{M_1} \boldsymbol{l}^{\mathsf{T}} a\right), \tag{1.125}$$

where each $\boldsymbol{l}$ is an integer-valued vector, sometimes referred to as a quasiparticle vector. The symmetry transformation Eq. 1.107 is again given by nontrivial self or mutual

braiding of quasiparticles

$$U_{\boldsymbol{m}}(M_1)U_{\boldsymbol{n}}(N_1) = (e^{\mathtt{i}2\pi \boldsymbol{m}^{\mathsf{T}} K^{-1} \boldsymbol{n}})^{\mathrm{Lk}(M_1,N_1)} U_{\boldsymbol{n}}(N_1), \tag{1.126}$$

where $\boldsymbol{m}, \boldsymbol{n}$ are quasiparticle vectors, and M_1, N_1 are 1-cycles. In this context, gauging 1-form symmetries corresponds to the condensation of anyons, and nontrivial self statistics (or mutual statistics) are interpreted as anomalies (or mixed anomalies). Based on the Haldane null vector condition [123, 124, 125], each gapped boundary of an abelian topological order is characterized by a non-anomalous subgroup of 1-form symmetries.

1.5.2 Anomalies & Constraints

So far, we have encountered many examples of 't Hooft anomalies without mentioning their common properties and defining features. In this section, we give a general discussion and provide more examples of 't Hooft anomalies of higher-form symmetries.

't Hooft anomalies If a system on a $(d+1)$-dimensional manifold Y_{d+1} enjoys a global symmetry, one can couple it to a non-dynamical background gauge field A. We denote its partition function by $\mathcal{Z}[Y_{d+1}, A]$. Depending on the context, A could be a background connection for ordinary/generalized symmetries or a Riemannian metric for spacetime symmetries. It may also contain discrete topological data, such as a spin structure in theories with fermions. The 't Hooft anomaly is defined by the non-invariance of $\mathcal{Z}[Y_{d+1}, A]$ under background gauge transformations $A \to A^\lambda$

$$\mathcal{Z}[Y, A^\lambda] = \mathcal{Z}[Y, A] \exp\left(-\mathtt{i} \int_Y \alpha[\lambda, A]\right), \tag{1.127}$$

where gauge parameters are generally denoted by λ, and $\alpha[\lambda, A]$ is a local functional that can not be removed by any local counterterms. From the perspective of anomaly inflow, the phase ambiguity can be removed by introducing a higher-dimensional bulk W_{d+2} such that $\partial W_{d+2} = Y_{d+1}$. The bulk response functional $\omega[A]$ satisfies

$$\exp\left(\mathtt{i}\int_W \omega[A^\lambda] - \mathtt{i}\int_W \omega[A]\right) = \exp\left(\mathtt{i}\int_{\partial W} \alpha[\lambda, A]\right). \tag{1.128}$$

In other words, the system can be made gauge-invariant by including a bulk extension

$$\widehat{\mathcal{Z}}[W, A] = \mathcal{Z}_{\text{bulk}}[W, A]\mathcal{Z}[\partial W, A], \qquad \mathcal{Z}_{\text{bulk}}[W, A] = \exp\left(\mathtt{i}\int_W \omega[A]\right), \tag{1.129}$$

which satisfies $\widehat{\mathcal{Z}}[W, A] = \widehat{\mathcal{Z}}[W, A^\lambda]$. The gauge non-invariance of $\mathcal{Z}[Y, A]$ is translated to the W-dependence of the gauge-invariant $\widehat{\mathcal{Z}}[W, A]$ with $\partial W = Y$. For two different bulk extensions W and W', the total partition functions $\widehat{\mathcal{Z}}$ differ by

$$\frac{\widehat{\mathcal{Z}}[W', A]}{\widehat{\mathcal{Z}}[W, A]} = \exp\left(\mathtt{i}\int_{W'} \omega[A] - \mathtt{i}\int_W \omega[A]\right) = \mathcal{Z}_{\text{bulk}}[W' \cup (-W), A] \neq 1, \tag{1.130}$$

where $W' \cup (-W)$ is a $(d+2)$-cycle (see FIG. 1.15). We can reverse the logic and say the 't Hooft anomaly is detected in a gauge-invariant way by $\mathcal{Z}_{\text{bulk}}[C_{d+2}, A] \neq 1$ where $\partial C_{d+2} = 0$. The physical meaning of $\mathcal{Z}_{\text{bulk}}[W, A]$ is the response theory of a nontrivial SPT state in $d+2$ spacetime dimensions. It is famously a non-Landau phase (see Ref. [126] for a review), but nevertheless can still be characterized by how symmetries are realized at the boundary. Under RG flow, the local functional $\omega[A]$ can only change continuously and therefore stays in the same topological class. The anomaly matching between UV and IR serves as a powerful tool in constraining low-energy properties nonperturbatively. The nontrivial phase factor in Eq. 1.127 means there can not be a non-degenerate gapped ground state on Y. It gives rise to an LSM-type theorem, meaning the ground state must

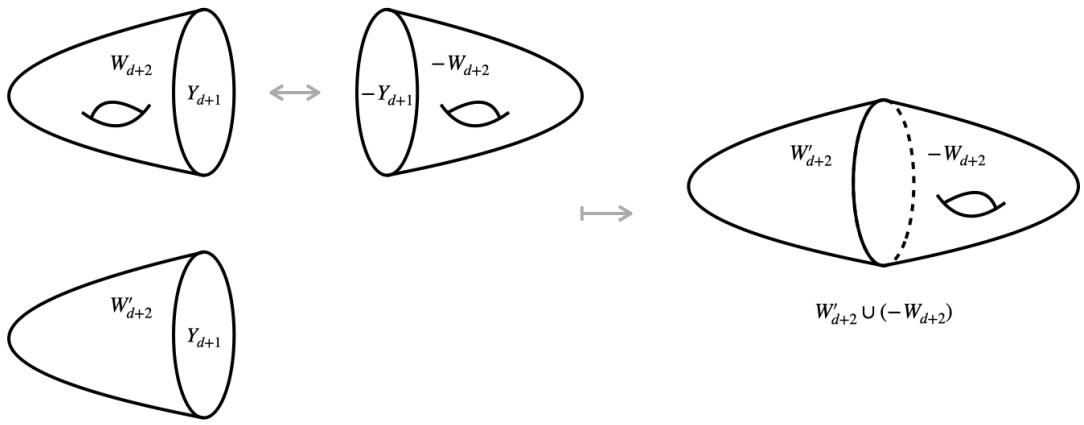

Figure 1.15: The schematic pictures of two bulk extensions W_{d+2}, W'_{d+2} for Y_{d+1}, the reversal $-W_{d+2}$ of W_{d+2}, and the glued manifold $W'_{d+2} \cup (-W_{d+2})$.

be either gapless, symmetry-broken, or topologically ordered.

Mixed anomaly of two $\mathrm{U}(1)^{(1)}$ 1-form symmetries in 3+1D Maxwell theory For free gapless photons, we have mentioned there are $\mathrm{U}(1)_e^{(1)}$ and $\mathrm{U}(1)_m^{(1)}$ 1-form symmetries from the Maxwell equation and the Bianchi identity. We can introduce two 2-form background fields B_e, B_m for them respectively

$$\mathcal{S} = \int_{Y_4} \frac{1}{2e^2}(\mathrm{d}a + B_e) \wedge \star(\mathrm{d}a + B_e) - \frac{\mathtt{i}}{2\pi} B_m \wedge \mathrm{d}a, \tag{1.131}$$

where a is the dynamical U(1) gauge field in the Maxwell theory. The background gauge transformations for $\mathrm{U}(1)_e^{(1)}$ and $\mathrm{U}(1)_m^{(1)}$ are given by

$$B_e^{(2)} \to B_e^{(2)} - \mathrm{d}\lambda_e^{(1)}, \quad a^{(1)} \to a^{(1)} + \lambda_e^{(1)}, \tag{1.132}$$

$$B_m^{(2)} \to B_m^{(2)} - \mathrm{d}\lambda_m^{(1)}, \quad \tilde{a}^{(1)} \to \tilde{a}^{(1)} + \lambda_m^{(1)}, \tag{1.133}$$

where λ_e, λ_m are 1-form parameters, and the dual gauge field $\tilde{a}$ is defined by $\mathrm{d}\tilde{a} = \frac{2\pi}{e^2} \star \mathrm{d}a$. The Maxwell action is clearly not gauge-invariant under the simultaneous transformations of $\mathrm{U}(1)_e^{(1)}$ and $\mathrm{U}(1)_m^{(1)}$. We find an example of $\alpha = \frac{\mathtt{i}}{2\pi} B_m \mathrm{d}\lambda_e$ in Eq. 1.127. To make it

gauge-invariant, we consider an extension to a 4+1D bulk W_5 such that $Y_4 = \partial W_5$

$$\widehat{\mathcal{S}} = \int_{\partial W_5} \frac{1}{2e^2}(\mathrm{d}a + B_e) \wedge \star(\mathrm{d}a + B_e) - \int_{W_5} \frac{\mathtt{i}}{2\pi}\mathrm{d}B_m \wedge (\mathrm{d}a + B_e), \tag{1.134}$$

The price we pay is that now $\widehat{\mathcal{S}}$ depends on the extension W_5. Namely, we check the difference between two different extensions W_5 and W_5'

$$\widehat{\mathcal{S}}[W_5'] - \widehat{\mathcal{S}}[W_5] = \int_{W_5' \cup (-W_5)} \frac{-\mathtt{i}}{2\pi}\mathrm{d}B_m \wedge (\mathrm{d}a + B_e) = \int_{\text{5-cycle}} \frac{-\mathtt{i}}{2\pi}\mathrm{d}B_m \wedge B_e. \tag{1.135}$$

We find an example of the bulk topological term $\omega = \frac{-\mathtt{i}}{2\pi}\mathrm{d}B_m \wedge B_e$ in Eq. 1.129.

Mixed anomaly of two $\mathbb{Z}_2^{(1)}$ 1-form symmetries in 2+1D toric code Let us consider a simple example of Eq. 1.124 with

$$K = \begin{pmatrix} 0 & 2 \\ 2 & 0 \end{pmatrix}, \tag{1.136}$$

which describes the $\mathbb{Z}_2$ toric code model (i.e., the $\mathbb{Z}_2$ topological order). In the K-matrix theory, the e particle and the m particle are give by the integer vectors

$$\boldsymbol{l}_e = \begin{pmatrix} 1 \\ 0 \end{pmatrix}, \qquad \boldsymbol{l}_m = \begin{pmatrix} 0 \\ 1 \end{pmatrix}. \tag{1.137}$$

The system has two $\mathbb{Z}_2^{(1)}$ 1-form symmetries generated by the Wilson loops

$$U_e(M_1) = \exp\left(\mathtt{i}\int_{M_1} \boldsymbol{l}_e^{\mathsf{T}} a\right), \qquad U_m(N_1) = \exp\left(\mathtt{i}\int_{N_1} \boldsymbol{l}_m^{\mathsf{T}} a\right). \tag{1.138}$$

where M_1, N_1 are 1-cycles. The two symmetry generators are mutually charged under each other. From Eq. 1.126, we have the two $\mathbb{Z}_2^{(1)}$ symmetry transformations

$$U_e(M_1)U_m(N_1) = (-1)^{\mathrm{Lk}(M_1,N_1)}\, U_m(N_1), \tag{1.139}$$

$$U_m(N_1)U_e(M_1) = (-1)^{\mathrm{Lk}(M_1,N_1)}\, U_e(M_1). \tag{1.140}$$

We can couple the system to two background 2-form $\mathbb{Z}_2$ gauge fields B_e and B_m

$$\mathcal{S} = \frac{\mathtt{i}}{2\pi}\int_{Y_3} a_e \wedge (\mathrm{d}a_m + B_m) + a_m \wedge (\mathrm{d}a_e + B_e). \tag{1.141}$$

where $a_e = \boldsymbol{l}_e^{\mathsf{T}} a$ and $a_m = \boldsymbol{l}_m^{\mathsf{T}} a$. Under the two $\mathbb{Z}_2^{(1)}$ background gauge transformations

$$B_e^{(2)} \to B_e^{(2)} - \mathrm{d}\lambda_e^{(1)}, \quad a_e^{(1)} \to a_e^{(1)} + \lambda_e^{(1)}/2, \tag{1.142}$$

$$B_m^{(2)} \to B_m^{(2)} - \mathrm{d}\lambda_m^{(1)}, \quad a_m^{(1)} \to a_m^{(1)} + \lambda_m^{(1)}/2, \tag{1.143}$$

the partition function Eq. 1.127 has a phase ambiguity $\alpha = \frac{\mathtt{i}}{4\pi}(\lambda_e \mathrm{d}\lambda_m - \lambda_e B_m - \lambda_m B_e)$, which can be canceled by introducing a bulk term Eq. 1.129 in one higher dimension

$$\int_{W_4} \omega = \mathtt{i}\pi \int_{W_4} \frac{B_e}{2\pi} \wedge \frac{B_m}{2\pi} \quad \text{where} \quad \partial W_4 = Y_3. \tag{1.144}$$

How do we connect the gauge invariance of Eq. 1.141 to the braiding of Wilson loops? We first notice that the background fields should be understood as $B_e/2\pi, B_m/2\pi \in H^2(Y_3, \mathbb{Z}_2)$. Under the Poincaré duality $H^2(Y_3, \mathbb{Z}_2) \simeq H_1(Y_3, \mathbb{Z}_2)$, they correspond to two 1-cycles $C_e, C_m \in H_1(Y_3, \mathbb{Z}_2)$ such that $\int_Y \eta \wedge B/2\pi = \int_C \eta$ for any 1-form η. The action

Eq. 1.141 now becomes

$$\mathcal{S} = \frac{\mathtt{i}}{2\pi}\int_{Y_3}(a_e \wedge \mathrm{d}a_m + a_m \wedge \mathrm{d}a_e) + \mathtt{i}\int_{C_m} a_e + \mathtt{i}\int_{C_e} a_m. \tag{1.145}$$

Therefore, introducing background fields B_e, B_m is equivalent to inserting the Wilson loops $U_e(C_m), U_m(C_e)$ in the partition function. The gauge transformation of B_e, B_m amounts to deforming the Wilson loops. Hence, the partition function is not gauge-invariant due to nontrivial braiding statistics between e and m particles. Finally, let us mention an interesting manifestation of the bulk mixed anomaly in the edge theory of toric code. The two gapped edge phases (i.e., e condensation and m condensation) correspond to gauging one of the two $\mathbb{Z}_2^{(1)}$ symmetries. At the domain wall between two different gapped edge regions, there is a localized Majorana zero mode!

We will get back to 't Hooft anomalies of higher-form symmetries in Sec. 5.3. A lot more examples in various dimensions will be constructed and classified based on physical arguments. Our special attention is paid to the generalized LSM theorem for condensed matter systems such as quantum dimer models.

1.6 Strongly Correlated Moiré Materials

Quantum materials in two (spatial) dimensions are fascinating. On the one hand, they are allowed to have various symmetry-breaking orders (recall the Mermin-Wagner theorem Eq. 1.120 for 0-form symmetries). On the other hand, they have enhanced quantum effects compared to $3d$ materials, which leads to exotic electronic and magnetic properties. With the recent advancements in the fabrication methods of $2d$ atomic crystals, a large number of Van der Waals heterostructures are realized in the labs by stacking $2d$ materials [127, 128]. Examples include the combinations of graphene, hexagonal boron

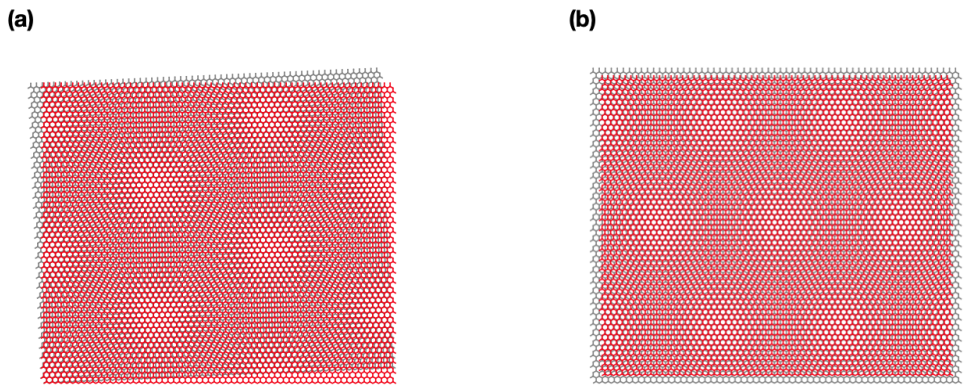

Figure 1.16: The Moiré pattern formed by bilayer honeycomb lattices: (a) with a small twisting angle; (b) with a small lattice constant mismatch.

nitride (hBN), transition-metal dichalcogenides (TMDs), etc. Adding a lattice mismatch (e.g., a twisting angle or a difference in lattice constants) to two-layer $2d$ materials opens a whole new realm of electronic states. A new periodic structure emerges at a larger distance, known as Moiré superlattice (see FIG. 1.16). The Moiré pattern acts as a long-wavelength modulating potential dramatically affecting the electronic band structures. The resulting emergent physical properties often differ qualitatively from the underlying monolayers. Namely, many correlated phenomena have been experimentally observed in graphene-based Moiré systems [2, 3, 129, 130, 131, 132, 133, 134, 135, 70, 136], which are tantalizingly similar to those seen in cuprate high-temperature superconductors. In conventional strongly correlated materials, experimentally controlled knobs are often limited due to the comparative lack of tenability of conventional chemical compounds. But Moiré heterostructures provide a highly tunable platform by changing the external parameters such as gating, straining, packing, and twist angle. It is promising that many paradigmatic theoretical models, such as the Hubbard model, can be simulated in the lab by the versatile Moiré heterostructures [137].

Magic-Angle Twisted Bilayer Graphene

The correlated physics in Moiré materials was first reported by Ref. [2, 3]. Both Mott insulating states and superconducting states were observed in twisted bilayer graphene at a "magic angle" of around 1.1 degrees. These experiments built on earlier theoretical predictions [138, 139] about the existence of exceptionally narrow and isolated bands on the Moiré superlattice at certain twisting angles. As shown in FIG. 1.17.(a), two Dirac cones near either valley mix through the interlayer hybridization, which leads to an energy gap around $2w$. At the magic angle, the interlayer hybridization energy $2w$ is comparable to the energy difference $\hbar v_0 k_\theta$ between two Dirac cones at the intersection point, where v_0 is the single-layer fermi velocity. It leads to a strong renormalization of the fermi velocity v_F, and the layer hybridized states are pushed toward narrow bands close to zero energy. The Moiré flat bands enable electronic correlations to play the dominant role in many material properties. The observed phase diagram FIG. 1.17.(c) exhibits some similarities to those seen in strongly correlated unconventional superconducting materials. If one compares the ratios between the superconducting critical temperatures T_c and the fermi temperatures T_F in various systems in FIG. 1.17.(d), the magic-angle twisted bilayer graphene is actually located above the trend line on which most cuprates, heavy-fermion, and organic superconductors lie. It looks appealing to construct a Hubbard model on the Moiré superlattice, using the fact that the electron density is strongly concentrated in the regions with AA stacking, as shown in FIG 1.17.(b). However, band topology severely complicates the problem, as one runs into the Wannier obstruction in writing down a tight-binding model that involves flat bands alone. Careful considerations lead to exceedingly complicated models (see e.g. [140, 141] for early works), which are hard to make progress analytically.

There are many analogies between correlated physics in graphene Moiré materials

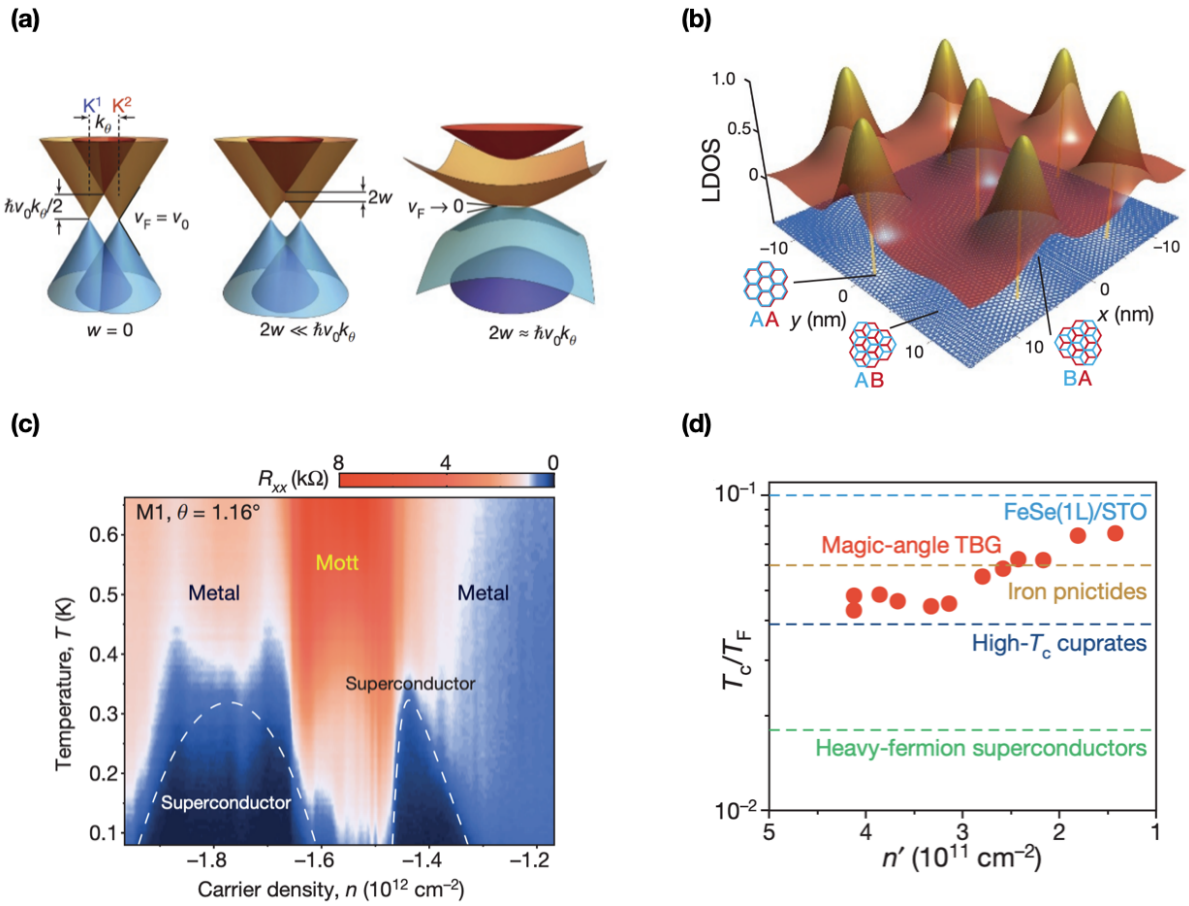

Figure 1.17: (a) Illustration of the effect of interlayer hybridization on Moiré bands; (b) Normalized local density of states (LDOS) calculated for the flat bands at the twisting angle $\theta = 1.08^{\circ}$; The phase diagram at the twisting angle $\theta = 1.16^{\circ}$; (d) The comparison of the ratios of critical temperatures and fermi temperatures in different superconducting materials. (Figures from Ref. [2, 3] with permission.)

and quantum Hall physics. Some connections between the flat bands and the lowest Landau level can be made by looking at a simplified chiral model (see Ref. [142] for a review). Alternatively, in Sec. 3.1, we will make progress by generalizing another theoretical framework existing in quantum Hall physics, the coupled-wire network construction. Namely, the Chalker-Coddington model [143, 144] has been used to describe quantum states with the similar topological obstruction. Our network model is constructed by the conducting wires along the AB/BA domain walls on the Moiré superlattice. These domains are enlarged due to lattice relaxation, and are driven into the quantum valley Hall insulators under a out-of-plane displacement field. The non-interacting physics in such a network has already been addressed in Ref. [145]. In Sec. 3.1, using the powerful techniques of 1+1D conformal field theory, we are able to incorporate a correlated insulator as well as superconductivity.

TMD Heterobilayer ($MoTe_2/WSe_2$) without Twisting

The other Moiré material relevant to this dissertation is the TMD heterobilayer $MoTe_2/WSe_2$. TMD-based Moiré systems (including heterobilayers and twisted homobilayers) and twisted bilayer graphene (TBG) differ in important ways. In TBG, in addition to spin, the band has valley degeneracy to an excellent approximation, and the interlayer hybridization is relatively weak. As a result, completely filled flat bands allow 8 electrons. For TMDs, as shown in FIG. 1.18.(a), every single layer has fewer degrees of freedom since strong spin-orbit coupling locks the spin and valley quantum numbers. In addition, the TMD-Moiré bands are dominated by one of the two layers, since in twisted homobilayers the hybridization energy between layers is strong, and the band offset is large in heterobilayers. TMD Moiré materials are strongly correlated electron systems since the hopping energy around 1-10 meV is significantly smaller than the local Coulomb repulsion around 50-100 meV. Most importantly, the flat band is topologically trivial,

and there is no Wannier obstruction. Consequently, we can write down a single-band Hubbard model Eq. 1.90 on the Moiré triangular lattice [146].

In Ref. [4], a bandwidth-tuned continuous metal-insulator transition at half-filling is observed in the TMD heterobilayer $MoTe_2/WSe_2$ without twisting. There is a 7% lattice mismatch, which leads to a Moiré triangular superlattice schematically shown in FIG. 1.16.(b). There are various experimental evidences that support the transition being continuous. If one approaches the transition from the insulating side, the charge gap vanishes continuously. From the metal side, the electron effective mass (extracted from Kadowaki–Woods scaling in transport measurements) diverges near the critical point. The temperature-dependent resistivity also exhibits scaling collapse. As for magnetic properties, the system does not show any sign of long-range ordering in the insulating phase, and the magnetic susceptibility shows a smooth dependence on the electric field across the transition. It is believed to be an interaction-driven transition instead of a disorder-driven one, supported by the estimation that the half-band filling density is two orders of magnitude larger than the disorder density [4].

Putting everything together, it seems to be an ideal realization of the theoretical construction introduced in Sec. 1.4.2. But there is one experimental feature that is really puzzling. As shown in FIG. 1.18.(c), the critical resistivity is huge compared to h/e^2. (This is also significantly larger than the experimental data from other $2d$ materials, see e.g. [147].) According to the Ioffe-Larkin rule, the total electrical resistivity $\rho = \rho_f + \rho_b$ has contributions from spinons f and chargons b. The spinon fermi-surface contribution ρ_f is likely from weak disorder scattering and is expected to be below the Mott-Ioffe-Regel limit (recall Eq. 1.56). As we illustrated in Sec. 1.4.2, the chargon contribution ρ_b (i.e., the universal resistivity jump) is also an order of one quantity in the unit of h/e^2. Therefore, the total critical resistivity should not be significantly larger than h/e^2, which is in conflict with FIG. 1.18.(c). One possible resolution will be discussed in detail in

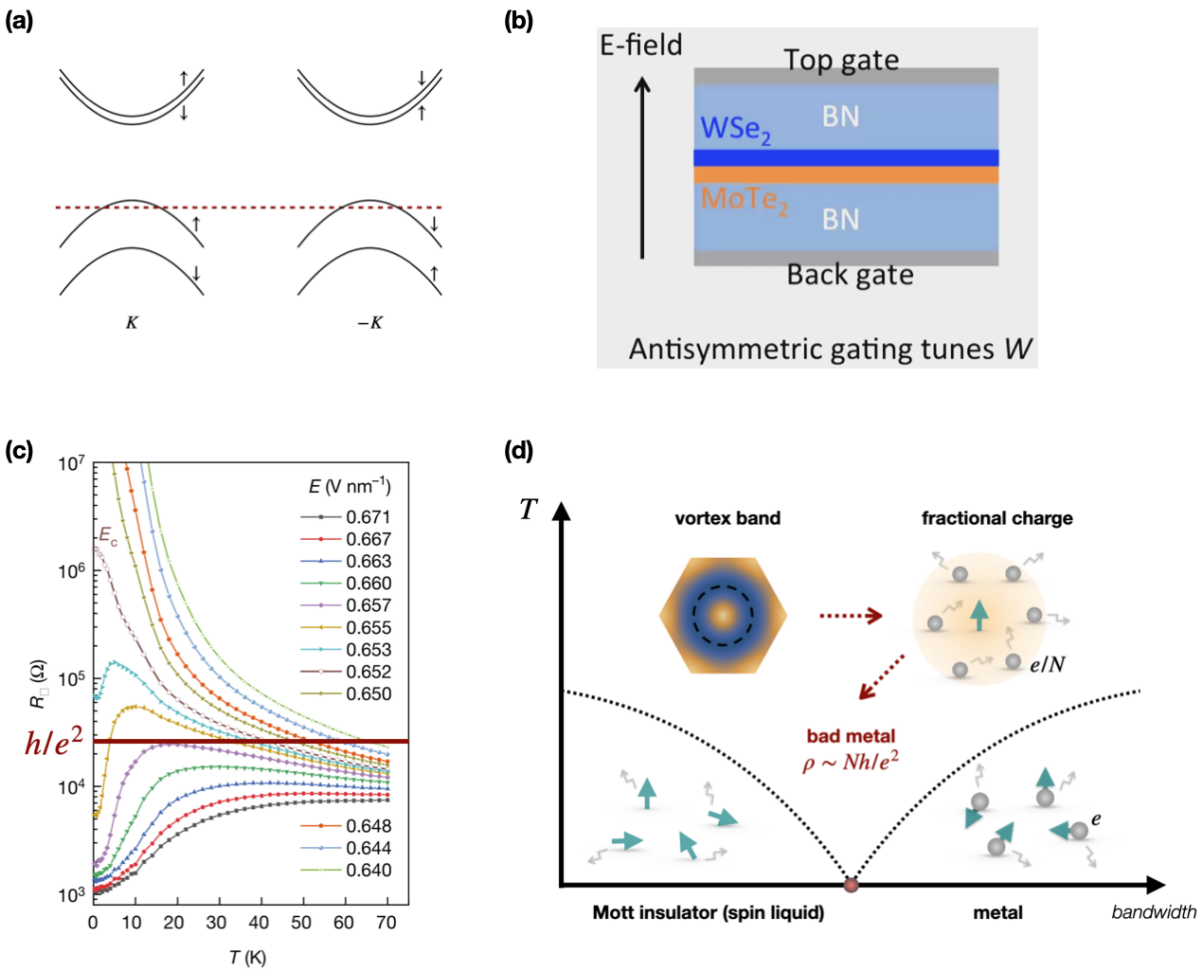

Figure 1.18: (a) The schematic band structure of monolayer TMD at two valleys. The valence bands have a large splitting due to strong spin-orbit coupling. (b) (Figure credit to Kin Fai Mak.) The experimental setup for the continuous Mott transition [4] where the bandwidth is tuned by an out-of-plane electric field. (3) (Figure from Ref. [4] with permission.) The temperature dependence of the resistivity at fixed half-filling under varying electric fields. The critical point is labeled by E_c. (4) The schematic phase diagram based on the theoretical proposal in Sec. 3.2. In addition to spin-charge separation, it involves charge fractionalization at the critical point, naturally leading to a large critical resistivity.

Sec. 3.2. We propose a new parton construction $c_{j,\alpha} = f_{j,\alpha} b_{j,\alpha}$ such that each electron $c_{j,\alpha}$ in each valley (or spin) $\alpha = \uparrow, \downarrow$ is fractionalized into a spinon $f_{j,\alpha}$ and a chargon $b_{j,\alpha}$. This is supported by the microscopic symmetries of the system (see Sec. 3.2 for details). As required by the Lieb-Schultz-Mattis theorem, the chargon sector now at fractional fillings must undergo a more exotic transition instead of the XY transition described in Sec. 1.4.2. One scenario is introduced in Sec. 1.4.1, which exhibits charge fractionalization at the critical point, and significantly enhances the value of ρ_b. Our new construction with charge fractionalization naturally leads to a large total critical resistivity. The schematic phase diagram is shown in FIG. 1.18.(d).

1.7 Summary

We set up the stage in this chapter by introducing *(1)* the conventional Landau symmetry paradigm, including bulk and boundary phase transitions; *(2)* the extended Landau symmetry paradigm based on generalized symmetries and 't Hooft anomalies; *(3)* strongly correlated metals beyond Landau-Fermi liquid theory; *(4)* a highly tunable experimental platform for exotic phases and phases transitions, the strongly correlated Moiré materials. In the main body of the dissertation, we will continue to explore these topics. Chap. 2 is about boundary phases and boundary phase transitions, Chap. 3 concerns Moiré quantum matter, Chap. 4 presents our theoretical constructions of exotic metals, and Chap. 5 is about characterizations and applications of generalized symmetries and anomalies in condensed matter systems.

Chapter 2

Quantum Phase Transitions with Non-Locality

In Sec. 1.2, we have seen interesting boundary critical phenomena associated with conventional symmetry-breaking transitions. In this chapter, we are going to explore the interplay of gapless boundaries (or defects) and unconventional quantum phase transitions introduced in Sec. 1.4.

One dimensional ($1d$) interacting systems with local Hamiltonians can be studied with various well-developed analytical methods. Recently novel $1d$ physics was found numerically in systems with either spatially nonlocal interactions, or at the $1d$ boundary of $2d$ quantum critical points, and the critical fluctuation in the bulk also yields effective nonlocal interactions at the boundary. Sec. 2.1 studies the edge states at the $1d$ boundary of $2d$ strongly interacting symmetry protected topological (SPT) states, when the bulk is driven to a disorder-order phase transition. We will take the $2d$ Affleck-Kennedy-Lieb-Tasaki (AKLT) state as an example, which is a SPT state protected by the SO(3) spin symmetry and spatial translation. We found that the original $(1+1)d$ boundary conformal field theory of the AKLT state is unstable due to coupling to the boundary

avatar of the bulk quantum critical fluctuations. When the bulk is fixed at the quantum critical point, within the accuracy of our expansion method, we find that by tuning one parameter at the boundary, there is a generic direct transition between the long-range antiferromagnetic Néel order and the valence bond solid (VBS) order. This transition is very similar to the Néel-VBS transition recently found in numerical simulation of a spin-1/2 chain with nonlocal spatial interactions. Connections between our analytical studies and recent numerical results concerning the edge states of the $2d$ AKLT-like state at a bulk quantum phase transition will also be discussed.

In Sec. 2.2, we discuss the boundary critical behaviors of two dimensional quantum phase transitions with fractionalized degrees of freedom in the bulk, motivated by the fact that usually it is the $1d$ boundary that is exposed and can be conveniently probed in many experimental platforms. In particular, we mainly discuss boundary criticality of two examples: *(1)* the quantum phase transition between a $2d$ Z_2 topological order and an ordered phase with spontaneous symmetry breaking; *(2)* the continuous quantum phase transition between metal and a particular type of Mott insulator (U(1) spin liquid). This theoretical study could be relevant to many purely $2d$ systems, where recent experiments have found correlated insulator, superconductor, and metal in the same phase diagram.

In Sec. 2.3, we study the interplay between two nontrivial boundary effects: *(1)* the two-dimensional ($2d$) edge states of three dimensional ($3d$) strongly interacting bosonic symmetry protected topological states, and *(2)* the boundary fluctuations of $3d$ bulk disorder-to-order phase transitions. We then generalize our study to $2d$ gapless states localized at an interface embedded in a $3d$ bulk, when the bulk undergoes a quantum phase transition. Our study is based on generic long-wavelength descriptions of these systems and controlled analytic calculations. Our results are summarized as follows: (i.) The edge state of a prototype bosonic symmetry protected states can be driven to a new fixed point by coupling to the boundary fluctuations of a bulk quantum phase transition;

($ii.$) the states localized at a $2d$ interface of a $3d$ SU(N) quantum antiferromagnet may be driven to a new fixed point by coupling to the bulk quantum critical modes. The properties of the new fixed points identified are also studied.

2.1 Continuous Néel-VBS Transition in Non-Local $1d$ Systems

Our understanding of one dimensional ($1d$) quantum many-body systems with local Hamiltonians is far more complete compared with higher dimensional systems, since many powerful analytical methods such as Bethe ansatz [148], Virasoro algebra [149], etc. are applicable only to $1d$ systems (or $(1+1)d$ space-time). We also understand that $1d$ systems have many unique features that are fundamentally different from higher dimensions. For example, with local Hamiltonians, generally there can not be spontaneous continuous symmetry breaking in $(1+1)d$ even at zero temperature (with exceptions of the scenarios when a fully polarized ferromagnet is the exact ground state), the closest one can possibly get is a quasi-long range power-law correlation of order parameters that transform nontrivially under a continuous symmetry. There is also no topological order in $1d$ systems analogous to fractional quantum Hall states which have a gap and simultaneously ground state topological degeneracy [150]. This means that many phenomena that are found in higher dimensions do not occur in $1d$ systems.

To seek for richer physics in one dimensional systems, we need to explore beyond the restriction of local Hamiltonians. One way to get around this restriction is to consider $1d$ systems at the boundary of a $2d$ systems, and drive the $2d$ bulk to a quantum phase transition. The physics becomes especially interesting when the disordered phase in the phase diagram of the $2d$ bulk is a symmetry protected topological (SPT) phase, which

already has topologically protected $1d$ edge state. The interplay between the topological edge state and gapless quantum critical modes can lead to very nontrivial physics, which has been studied through numerical methods recently [151, 152, 37, 38]. One can also directly turn on nonlocal spatial interaction in a $1d$ Hamiltonian. $1d$ quantum spin chains with nonlocal spatial interactions have also been studied recently, and very intriguing physics was found [153, 154]. We will discuss the results of these numerical works later in this paper.

In this work we investigate the $2d$ SPT state protected by symmetry $\mathrm{SO}(3) \times G$, where $\mathrm{SO}(3)$ is the ordinary spin symmetry, while G is a discrete symmetry, which could be an onsite unitary Z_2 symmetry, or an anti-unitary time-reversal Z_2^T. G can also be a lattice symmetry such as translation by one lattice constant. For example, when G is the translation along the $\hat{x}$ axis (T_x), this state can be realized as the Affleck-Kennedy-Lieb-Tasaki (AKLT) state of the spin-2 system on a $2d$ square lattice [155]. In the example of spin-2 AKLT state, there is a chain of dangling spin-1/2 at the boundary of the system, as long as the boundary is along the $\hat{x}$ axis and preserves the translation symmetry T_x. The nature of the SPT states, and the Lieb-Shultz-Mattis (LSM) theorem [20, 21, 22] guarantee that this boundary system cannot be trivially gapped, *i.e.* it must be either gapless, or gapped but degenerate (For a closed $1d$ system without $0d$ boundaries, a generic ground state degeneracy can only originate from spontaneous discrete symmetry breaking [150]). In this work we will take the AKLT state as an example, but our results can be straightforwardly generalized to other discrete symmetries G.

Our study will mainly focus on the $1d$ boundary of strongly interacting $2d$ bosonic SPT phases, using a controlled renormalization group method. We would like to mention that previous literature has discussed the coupling between quantum criticality and topologically localized gapless states in various fermionic topological insulators [39]; other approaches such as constructing soluble models and various numerical methods have also

been used to study edge states of interacting SPT states at a bulk quantum criticality [33, 34, 35]. Our main finding is that there is a generic continuous quantum phase transition between a long range antiferromagnetic Néel order which spontaneously breaks the SO(3) spin symmetry, and a valence bond solid state, at the $1d$ boundary of an AKLT state that couples to the bulk quantum critical modes. The bulk quantum critical modes effectively yield nonlocal interactions at the $1d$ boundary, which makes the long range Néel order possible.

In principle the $1d$ boundary of this AKLT state should be effectively described by an extended Heisenberg model

$$H = \sum_j J\vec{S}_j \cdot \vec{S}_{j+1} + \cdots \tag{2.1}$$

where $\vec{S}_j$ is the spin-1/2 operator, and the ellipsis includes other possible terms allowed by SO(3) $\times T_x$. The ground state of Eq. 2.1 depends on the entire lattice Hamiltonian. But a useful starting point of analyzing this boundary system is the $\mathrm{SU}(2)_1$ conformal field theory (CFT) described by the following Hamiltonian in the infrared limit:

$$H_0 = \int dx \frac{1}{3 \cdot 2\pi}(\vec{J}_L \cdot \vec{J}_L + \vec{J}_R \cdot \vec{J}_R). \tag{2.2}$$

The $\mathrm{SU}(2)_1$ CFT has a larger symmetry than the lattice Hamiltonian Eq. 2.2, since $\vec{J}_L$ and $\vec{J}_R$ generate the $\mathrm{SU}(2)_{L,R}$ symmetries for the left and right chiral modes respectively. The relation between the microscopic operator $\vec{S}$ and the low energy field is [156]

$$\vec{S}(x) \sim \frac{1}{2\pi}(\vec{J}_L(x) + \vec{J}_R(x)) + (-1)^x \vec{n}(x), \tag{2.3}$$

where $\vec{n}(x)$ is the Néel order parameter at the boundary. $\vec{J}_{L,R}$ both have scaling dimension

+1 at the $\mathrm{SU}(2)_1$ CFT fixed point, while $\vec{n}(x)$ has scaling dimension 1/2 at the $\mathrm{SU}(2)_1$ CFT.

The diagonal SU(2) symmetry (simultaneous SU(2) rotation between the left and right modes) corresponds to the original SO(3) spin symmetry on the lattice scale. And because the lattice Hamiltonian has a lower symmetry than the infrared theory Eq. 2.2, another term is allowed in the low energy Hamiltonian:

$$H_1 = \int dx\ \lambda \vec{J}_L \cdot \vec{J}_R. \tag{2.4}$$

Since $\vec{J}_{L,R}$ have scaling dimension +1, power-counting indicates the coefficient λ has scaling dimension 0. Depending on the sign of λ, this term can be either marginally relevant or marginally irrelevant. When λ is negative and marginally irrelevant the system flows back to the $\mathrm{SU}(2)_1$ CFT with an enlarged $\mathrm{SU}(2)_L \times \mathrm{SU}(2)_R$ symmetry. When this term is positive and marginally relevant, it will flow to infinite (nonperturbative) and generate a mass gap, which based on the nature of the SPT phase would imply that the system spontaneously breaks the discrete symmetry G. For example, when this system is realized as the AKLT state, and G is the translation T_x, the LSM theorem demands that when the boundary of the system generates a mass gap, it spontaneously breaks the translation symmetry and develops a nonzero expectation value of a dimerized valence bond solid (VBS) order: $v \sim (-1)^j \vec{S}_j \cdot \vec{S}_{j+1}$. As a side-note, we emphasize that the state we are studying here is different from the SO(3) or SU(2) SPT state defined through the group cohomology of SO(3) or SU(2) [157, 158, 159], since in those states the symmetry acts chirally, *i.e.* it only acts on either the left or right modes. While in our case the spin symmetry acts on both the left and right modes of the $1d$ boundary, and another discrete symmetry such as translation is demanded.

Our goal is to study the edge states when the bulk undergoes a disorder-order quantum

phase transition, and the disordered phase of the bulk phase diagram is the AKLT state. The quantum critical fluctuation in the bulk may affect the edge of the AKLT state. To study the interplay between the topologically protected edge states, and the quantum critical modes, we adopt the "two layer" picture used in Ref. [160]: in layer-1, the system remains a gapped AKLT state in the bulk with solid edge states described by Eq. 2.1 and Eq. 2.2; in layer-2 the system undergoes a phase transition between an ordinary *trivial* disordered phase and an ordered phase. These two systems are glued together at the boundary. We have used the common wisdom that the transition between the SPT phase and the ordered phase is generically in the same universality class as the transition between an ordinary disordered phase and an ordered phase [1]. We will discuss two kinds of ordered phases: an SO(3) antiferromagnetic order, and an Ising-like VBS order that spontaneously breaks T_x, assuming the boundary is at $y = 0$. In the bulk the two disorder-order transitions under discussion correspond to the three dimensional ($3D$) SO(3) and Ising Wilson-Fisher transitions respectively, which can be studied through a standard $\epsilon = 4 - D$ expansion, where $D = 2 + 1$ is the space-time dimension in the bulk. We only extend the bulk dimensionality of layer-2 to $3 - \epsilon$ spatial dimensions, while the layer-1 still has a two-dimensional bulk and one-dimensional boundary.

We denote the bulk SO(3) antiferromagnetic order parameter, and the Ising-VBS order parameter in layer-2 as $\vec{\phi}$ and ϕ respectively, which should couple to the Néel order parameter $\vec{n}$ and the VBS order parameter v at the boundary theory of layer-1, and this coupling could lead to new physics in the infrared. However, $\vec{\phi}$ and ϕ do not directly couple to $\vec{n}$ and v due to the boundary condition of the Wilson-Fisher fixed point. Assuming the boundary of the $2d$ system is at $y = 0$, the most natural boundary

[1] This statement can be inferred based on the observation that, the topological effects of many of the SPT states can be captured by a nonlinear Sigma model plus a topological $\Theta-$term at $\Theta = 2\pi$ [161, 162]. The $\Theta = 2\pi$ topological term reduces precisely to a boundary term, and we do not expect this topological term to change the bulk universality class.

condition for fields $\vec{\phi}, \phi$ would be $\vec{\phi}(y = 0) = \phi(y = 0) = 0$ [2]. Then the leading nonvanishing boundary fields with the same quantum number as $\vec{\phi}$ and ϕ are $\vec{\Phi} \sim \partial_y \vec{\phi}$ and $\Phi \sim \partial_y \phi$ [163].

The SO(3) order parameter $\vec{\phi}$ and the Ising order parameter ϕ will not become critical simultaneously without fine-tuning, but they can be treated in the same framework. The boundary quantum critical modes $\vec{\Phi}$ and Φ couple to the fields at the boundary of layer-1 through the following terms in the action

$$\begin{aligned}\mathcal{S} = &\int d^2\mathbf{x} g_n \vec{\Phi}(\mathbf{x}) \cdot \vec{n}(\mathbf{x}) + g_v \Phi(\mathbf{x}) v(\mathbf{x}) \\ &+ \int d^2\mathbf{x} d^2\mathbf{x}' \frac{1}{2} \Phi^a(\mathbf{x}) C_n^{-1}(\mathbf{x}, \mathbf{x}')_{ab} \Phi^b(\mathbf{x}') \\ &+ \int d^2\mathbf{x} d^2\mathbf{x}' \frac{1}{2} \Phi(\mathbf{x}) C_v^{-1}(\mathbf{x}, \mathbf{x}') \Phi(\mathbf{x}'),\end{aligned} \tag{2.5}$$

where $\mathbf{x} = (x, \tau)$ is the space-time coordinate. $C_n(\mathbf{x}, \mathbf{x}')_{ab}$ and $C_v(\mathbf{x}, \mathbf{x}')$ are the normalized correlation functions of Φ^a and Φ at the boundary:

$$\begin{aligned}C_n(\mathbf{x}, 0)_{ab} &= \langle \Phi^a(x, \tau) \Phi^b(0, 0) \rangle = \frac{\delta_{ab}}{(x^2 + \tau^2)^{3/2 - \epsilon_n}}, \\ C_v(\mathbf{x}, 0) &= \langle \Phi(x, \tau) \Phi(0, 0) \rangle = \frac{1}{(x^2 + \tau^2)^{3/2 - \epsilon_v}}.\end{aligned} \tag{2.6}$$

The scaling dimension of $\vec{\Phi}$ and Φ is $\Delta_n = D/2 - \epsilon_n + O(\epsilon^2)$ and $\Delta_v = D/2 - \epsilon_v + O(\epsilon^2)$, where $D = 3$ is the bulk space-time dimension. $\epsilon_{n/v}$ can be computed again through the $\epsilon = (4 - D)$ expansion, following the calculation of boundary criticality of the Wilson-Fisher fixed points [163, 164, 165, 166, 167]: for an O(N) Wilson-Fisher fixed point in

[2] This boundary condition corresponds to the "ordinary transition" in the standard boundary criticality literatures; other possibilities can also occur such as special and extraordinary boundary transitions [163].

the bulk, the scaling dimension of the boundary modes of the order parameter is

$$\Delta_{\mathrm{O}(N)} = \frac{D}{2} - \frac{N+2}{2(N+8)}\epsilon + O(\epsilon^2). \tag{2.7}$$

In our case $\epsilon_{n/v} = \epsilon(N+2)/(2(N+8))$ with $N = 3, 1$ respectively. We again stress that the ϵ dimensionality was introduced for layer-2 only. The effective action of $\vec{\Phi}$ and Φ in Eq. 2.5 already received leading order correction from the $\epsilon-$expansion due to the self-interaction of the bulk critical modes. These effective actions can in principle receive further corrections from the g_v and g_n couplings with the boundary fields $\vec{n}$ and v, but this correction should be at least at the order of g_n^2, g_v^2, which will be at higher order of $\epsilon-$expansion. As we can see later, the main physics we will discuss is at the vicinity of a fixed point where $g_n, g_v \sim \epsilon$.

Eq. 2.2, 2.4, 2.5 together can be viewed as an effective non-local $1d$ theory, and this theory will be the starting point of our discussion hereafter. Considering the fact that the scaling dimension of both the Néel and VBS order parameter at the $\mathrm{SU}(2)_1$ CFT is $1/2$, to the leading order of ϵ expansion, the scaling dimensions of the coupling constants must be

$$\Delta_{g_n} = \epsilon_n + O(\epsilon^2), \qquad \Delta_{g_v} = \epsilon_v + O(\epsilon^2), \qquad \epsilon_n = \frac{5}{22}\epsilon, \qquad \epsilon_v = \frac{1}{6}\epsilon. \tag{2.8}$$

$g_{n/v}$ are hence weakly relevant assuming a small parameter ϵ. Hence the $\mathrm{SU}(2)_1$ CFT at the boundary of the AKLT state will be unstable against coupling to the quantum critical modes, while fortunately due to the weak relevance of the coupling constants, this effect can be studied perturbatively.

To proceed we need to compute the coupled renormalization group (RG) flow of λ and $g_{n/v}$ in Eq. 2.4 and Eq. 2.5. The RG equations can be derived based on the following

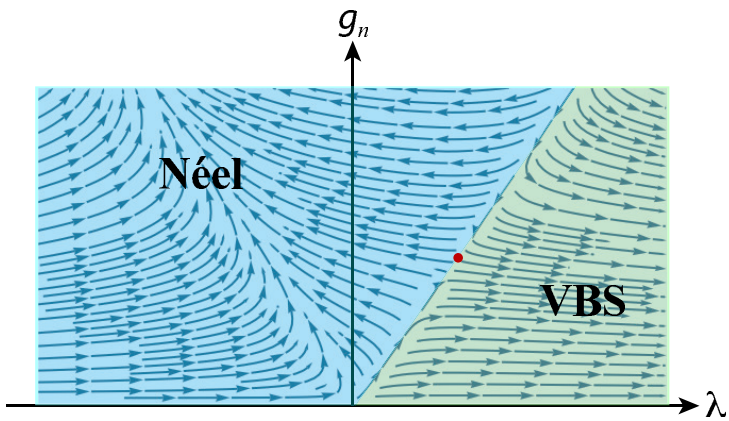

Figure 2.1: The coupled RG flow of λ and g_n based on Eq. 2.11. A new fixed point $(\lambda^*, g_n^*) = (\frac{2\epsilon_n}{\pi}, \frac{4\epsilon_n}{\pi})$ is found, which separates two phases: the phase where $\lambda \to +\infty$ is the VBS phase, and the phase with $(\lambda, g_n) \to (-\infty, +\infty)$ is the long range Néel order at the $1d$ boundary. But on the Néel order side of the phase diagram, the RG flow is complicated and nonmonotonic, hence it may take a long RG scale, or a large system size to finally reveal the true long range order.

operator product expansion (OPE):

$$
\begin{aligned}
&J_L^a(z)n^b(w,\bar{w}) \sim \frac{1}{2}\frac{1}{z-w}\left(\mathrm{i}\delta_{ab}v(w,\bar{w}) + \mathrm{i}\epsilon_{abc}n^c(w,\bar{w})\right), \\
&J_R^a(\bar{z})n^b(w,\bar{w}) \sim \frac{1}{2}\frac{1}{\bar{z}-\bar{w}}\left(-\mathrm{i}\delta_{ab}v(w,\bar{w}) + \mathrm{i}\epsilon_{abc}n^c(w,\bar{w})\right), \\
&J_L^a(z)v(w,\bar{w}) \sim -\frac{1}{2}\frac{\mathrm{i}}{z-w}n^a(w,\bar{w}), \qquad J_R^a(\bar{z})v(w,\bar{w}) \sim \frac{1}{2}\frac{\mathrm{i}}{\bar{z}-\bar{w}}n^a(w,\bar{w}), \\
&\left(\sum_a n^a(z,\bar{z})\Phi^a(z,\bar{z})\right)\left(\sum_b n^b(w,\bar{w})\Phi^b(w,\bar{w})\right) \\
&\sim \frac{3}{2}\frac{1}{|z-w|^4} + \frac{1}{2}\frac{1}{|z-w|^2}\sum_{a=1,2,3} J_L^a(w)J_R^a(\bar{w}) + \frac{3}{4}\frac{1}{(\bar{z}-\bar{w})^2}T_L(w) + \frac{3}{4}\frac{1}{(z-w)^2}T_R(\bar{w}) + ..., \\
&\left(v(z,\bar{z})\Phi(z,\bar{z})\right)\left(v(w,\bar{w})\Phi(w,\bar{w})\right) \\
&\sim \frac{1}{2}\frac{1}{|z-w|^4} - \frac{1}{2}\frac{1}{|z-w|^2}\sum_{a=1,2,3} J_L^a(w)J_R^a(\bar{w}) + \frac{1}{4}\frac{1}{(\bar{z}-\bar{w})^2}T_L(w) + \frac{1}{4}\frac{1}{(z-w)^2}T_R(\bar{w}) + ..., \\
&\left(\sum_{a=1,2,3} J_L^a(z)J_R^a(\bar{z})\right)\left(\sum_{b=1,2,3} J_L^b(w)J_R^b(\bar{w})\right) \\
&\sim \frac{3}{4}\frac{1}{|z-w|^4} - \frac{2}{|z-w|^2}\sum_{a=1,2,3} J_L^a(w)J_R^a(\bar{w}) + \frac{3}{2}\frac{1}{(\bar{z}-\bar{w})^2}T_L(w) + \frac{3}{2}\frac{1}{(z-w)^2}T_R(\bar{w}) + ...
\end{aligned}
\tag{2.9}
$$

In these equations, z and w are the chiral coordinates ($z = \tau + \mathrm{i}x$); and the ellipsis contains less singular terms of the OPEs. The fields $T_{L/R}$ are the energy-momentum

tensor of the left and right movers, which are given via the Suguwara construction by $T_L = \frac{1}{3}\sum_a : J_L^a J_L^a :$ and $T_R = \frac{1}{3}\sum_a : J_R^a J_R^a :$. Notice the form of energy-momentum tensors is similar to the Hamiltonian Eq. 2.2 but with an extra factor of 2π. The OPEs above involving the fields Φ^a and Φ are derived to the leading order of $\epsilon_{n/v}$.

These OPEs are sufficient to derive the desired RG equations to the second order of the coupling constants. For example, using the first two lines of Eq. 2.9, we can derive another set of secondary OPEs:

$$\begin{aligned}
&\left(\sum_{a=1,2,3} J_L^a(z) J_R^a(\bar{z})\right)\left(\sum_b n^b(w,\bar{w})\Phi^b(w,\bar{w})\right) \sim \frac{1}{4}\frac{1}{|z-w|^2}\left(\sum_b n^b(w,\bar{w})\Phi^b(w,\bar{w})\right), \\
&\left(\sum_{a=1,2,3} J_L^a(z) J_R^a(\bar{z})\right)\left(v(w,\bar{w})\Phi(w,\bar{w})\right) \sim -\frac{3}{4}\frac{1}{|z-w|^2}\left(v(w,\bar{w})\Phi(w,\bar{w})\right).
\end{aligned} \tag{2.10}$$

The coupled RG equations (beta functions) for λ and $g_{n/v}$ then read

$$\begin{aligned}
\beta(\lambda) &= \frac{d\lambda}{d\ln l} = 2\pi\lambda^2 - \frac{\pi}{2}g_n^2 + \frac{\pi}{2}g_v^2, \\
\beta(g_n) &= \frac{dg_n}{d\ln l} = \epsilon_n g_n - \frac{\pi}{2}\lambda g_n, \\
\beta(g_v) &= \frac{dg_v}{d\ln l} = \epsilon_v g_v + \frac{3\pi}{2}\lambda g_v.
\end{aligned} \tag{2.11}$$

These RG equations are valid as long as we restrict our analysis to the parameter region with $\lambda, g_n, g_v \sim \epsilon$, since every term in the RG equations Eq. 2.11 would be at the same order of ϵ^2.

As we explained before, there is no general reason for $\vec{\phi}, \phi$ to become critical simultaneously in the bulk. Hence let us ignore the Φ field first, and consider the coupled RG equation for λ, g_n only. If there is no bulk quantum critical modes, an initial positive value $\lambda = \lambda_0$ will be marginally relevant, and open up an energy gap when it flows to positive infinite. According to the LSM theorem, and the nature of the SPT state, this $1d$ boundary cannot be trivially gapped, hence a nonperturbative positive λ would drive

the system into an SO(3) invariant VBS state with spontaneous symmetry breaking of translation symmetry T_x. But by coupling to the boundary modes $\vec{\Phi}$ of quantum critical fluctuation, the beta functions have an new unstable fixed point at

$$(\lambda^*, g_n^*) = \left(\frac{2\epsilon_n}{\pi},\ \frac{4\epsilon_n}{\pi}\right). \tag{2.12}$$

The two eigenvectors of RG flow expanded at the new fixed point have scaling dimensions $(8.9\epsilon_n, -0.89\epsilon_n)$.

Of course the RG analysis above is only at the leading nontrivial order of $\epsilon-$expansion, and at this order of accuracy, no other fixed point is found in the phase diagram. The new fixed point found above separates two phases: phase I where λ flows to positive infinity, and phase II where λ and g_n flow to negative and positive infinity respectively. Then both phases no longer have scaling invariance, so both phases should have certain long range order considering the fact that there is no topological order in one dimension [150]. Phase I with $\lambda \to +\infty$ is the dimerized VBS phase as we discussed before; phase II with $(\lambda, g_n) \to (-\infty, +\infty)$ should be a Néel ordered phase, *i.e.* the $1d$ boundary can develop the Néel order before the bulk, even though the bulk is still at a quantum critical point. A negative λ would enhance the correlation of the Néel order parameter, and after integrating out $\vec{\Phi}$, a long range interaction proportional g^2 would be generated between the Néel order parameters. Hence the infrared limits $\lambda \to -\infty$ and $g \to +\infty$ of phase II both favor the long range Néel order.

The correlation length critical exponent ν of this Néel-VBS transition is $\nu \sim 1/(8.9\epsilon_n)$. At the transition point $(\lambda^*, g_n^*) = (2\epsilon_n/\pi, 4\epsilon_n/\pi)$, the scaling dimensions of the Néel and VBS order parameters can again be computed to the leading order of $\epsilon-$expansion:

$$\Delta_{\vec{n}} = \frac{1}{2} + \frac{\pi\lambda^*}{2} = \frac{1}{2} + \epsilon_n, \qquad \Delta_v = \frac{1}{2} - \frac{3\pi\lambda^*}{2} = \frac{1}{2} - 3\epsilon_n. \tag{2.13}$$

One can see that compared with the $\mathrm{SU}(2)_1$ CFT, the Néel order correlation is suppressed while the VBS order correlation is enhanced at the new transition fixed point, since $\lambda^* > 0$. This also implies that this Néel-VBS transition has no enlarged symmetry of $\mathrm{SU}(2)_L \times \mathrm{SU}(2)_R$. An enlarged $\mathrm{SU}(2)_L \times \mathrm{SU}(2)_R \sim \mathrm{SO}(4)$ symmetry would guarantee that the Néel and VBS order parameters have the same scaling dimension, because $(\vec{n}, v)$ transform as a vector under SO(4). Many previous studies suggest that at an unconventional quantum critical point between two phases with different spontaneous symmetry breaking, an enlarged emergent symmetry in the infrared is often expected due to a series of dualities [168, 169, 170, 98, 171, 172, 173]. But in our current case we expect the infrared symmetry at the Néel-VBS transition is still the microscopic symmetry $\mathrm{SO}(3) \times G$.

As we mentioned before, suppose we integrate out the field $\vec{\Phi}$ in Eq. 2.5, a long range interaction in space-time will be generated between the Néel order parameter. The scenario is similar to the spin-1/2 chain with a long range spin-spin interaction, the only difference is that in the latter case the long range interaction is instantaneous and only nonlocal in space. Recently a direct transition between the Néel and VBS order was found in a spin-1/2 chain with nonlocal two-spin interaction and local four-spin interaction [153, 154]. It was found numerically that at the direct Néel-VBS transition the scaling dimension of the Néel order parameter is greater than the VBS order parameter, which is fundamentally different from the $\mathrm{SU}(2)_1$ CFT, but consistent with our RG calculations Eq. 2.13. We also note that a previous RG analysis was performed for $1d$ spin-1/2 system with an instantaneous nonlocal spin interaction, but the Néel-VBS transition was not found therein. Instead the previous analysis identified a transition between the true long range Néel order and a quasi-long range order at the parameter region $\epsilon_n < 0$ and $\lambda < 0$ with our notation [174].

So far we have assumed that the fields $\vec{n}, v$ and $\vec{\Phi}, \Phi$ have the same velocity in our

effective $1d$ theory Eq. 2.5, hence the theory we considered so far has a Lorentz invariance. We can also turn on a weak velocity difference between these two sets of fields, and analyze how it flows under RG. This velocity anisotropy corresponds to modifying the correlation function of $\vec{\Phi}$:

$$C_n(\mathbf{x},0)_{ab} = \langle \Phi^a(x,\tau)\Phi^b(0,0)\rangle = \frac{\delta_{ab}}{\left((1-\frac{\delta v}{2})^2 x^2 + (1+\frac{\delta v}{2})^2\tau^2\right)^{3/2}}. \tag{2.14}$$

Here we have assumed that the velocity of $\vec{\Phi}$ exceeds the velocity of $\vec{n}$ by a factor of $(1+\delta v)$ (to the first order of δv). We have taken $\epsilon_n = 0$ for the leading order calculation. δv can flow under RG as it is the "seed" for velocity difference. Based on symmetry, the RG flow of δv should look like

$$\frac{d\delta v}{d\ln l} = -\alpha g_n^2 \delta v. \tag{2.15}$$

And eventually we will plug in the fixed point value of $g_n = g_n^*$. Based on previous experience, at an interacting fixed point, a weak velocity anisotropy is often irrelevant [175, 176], since intuitively in the infrared all the interacting modes are expected to have the same velocity. Hence we expect $\alpha > 0$, *i.e.* a weak velocity difference between the boundary and bulk will be irrelevant at the Néel-VBS transition fixed point.

To evaluate α, we expand the correlation function of $\vec{\Phi}$ to the leading order of δv:

$$C_n(\mathbf{x},0) = \frac{1}{|z|^3} - \frac{3}{2}\frac{\delta v}{|z|^5}\frac{z^2+\bar{z}^2}{2} + O(\delta v^2) \tag{2.16}$$

Using the OPEs in Eq. 2.10, the second order perturabtion of g_n would generate the

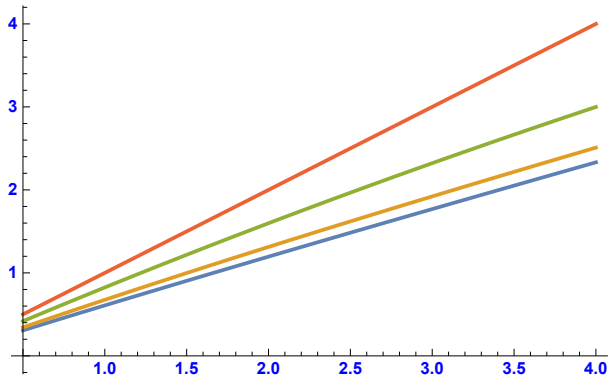

Figure 2.2: The plot of $\ln[3\pi G_n(\mathbf{k})(1 + A(g_n^{*\prime})^2)]$ against $\ln[1/|\mathbf{k}|]$, where $G_n(\mathbf{k})$ is given by Eq. 2.20. From top to bottom, $A(g_n^{*\prime})^2 = 0, 1/2, 2$, and 5.

following term:

$$
\begin{aligned}
&-\frac{1}{2}g_n^2\left(\sum_a n^a(z,\bar{z})\Phi^a(z,\bar{z})\right)\left(\sum_b n^b(w,\bar{w})\Phi^b(w,\bar{w})\right) \\
&\sim -\frac{3g_n^2}{4|z-w|^4} - g_n^2\frac{1}{4}\frac{1}{|z-w|^2}\sum_{a=1,2,3} J_L^a(w)J_R^a(\bar{w}) + g_n^2\delta v\frac{9}{32}\frac{1}{|z-w|^2}\left(T_L(w)+T_R(\bar{w})\right)+\cdots
\end{aligned}
\tag{2.17}
$$

Here we only kept the terms that will lead to nonzero effect under real space RG. The last term in Eq. 2.17 would contribute a renormalization (or acceleration) for the velocity of $\vec{n}$. Under rescaling, the ratio between the two velocities reduces by a factor:

$$
1+\delta v \to \frac{1+\delta v}{1+g_n^2\delta v\frac{9\pi^2}{8}\ln l}, \tag{2.18}
$$

which leads to the RG equation for δv:

$$
\frac{d\delta v}{d\ln l} = -\frac{9\pi^2}{8}(g_n^*)^2\delta v, \tag{2.19}
$$

which confirms our expectation that δv is an irrelevant perturbation at the Néel-VBS transition fixed point.

Suppose we start with $\delta v > 0$, namely the velocity of $\vec{n}$ is smaller than $\vec{\Phi}$, the velocity of $\vec{n}$ will increase under RG. This means that in this case the system will qualitatively

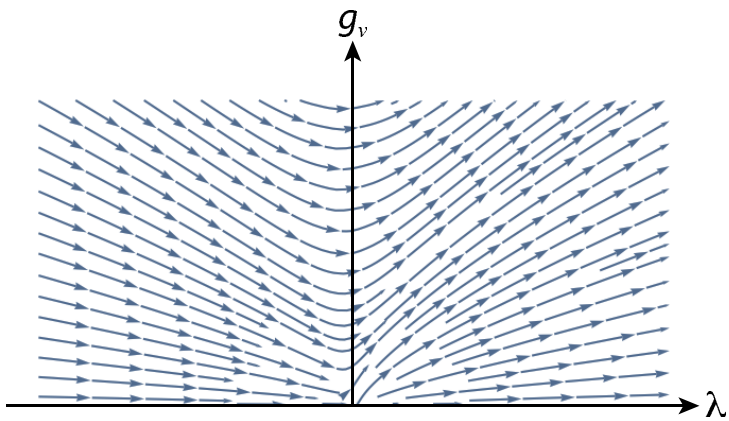

Figure 2.3: The RG flow of (λ, g_v). As long as the initial value g_v is nonzero, both parameters will flow to positive infinity, which implies that the boundary will likely develop the Ising-VBS order before the bulk.

behave like $z < 1$, where z is the dynamic critical exponent (not to confuse with the chiral coordinate). On the contrary, if we start with $\delta v < 0$, the velocity of $\vec{n}$ would decrease under RG, which means that effectively $z > 1$. The former scenario is analogous to a spin chain with instantaneous spatial nonlocal interaction [154], which is equivalent to taking the velocity of the effective action of $\vec{\Phi}$ and Φ to infinity in our effective $1d$ theory Eq. 2.5. Although our calculation is for $\delta v > 0$, rather than taking the velocity in the $\vec{\Phi}$ action to be infinity, the "acceleration" of the modes derived here (including $z < 0$) is qualitatively consistent with what was observed in Ref. [154] at the Néel-VBS transition in a spin-1/2 chain with nonlocal spatial interactions.

In the phase diagram Fig. 2.1, on the side of the Néel order, the path of the RG flow towards the long range order can be complicated. It may take a long RG scale and hence large system size to reveal the true long range order. For example, on part of the phase diagram, λ changes its sign and eventually flow away to the negative nonperturbative regime. While λ changes sign, g_n first decreases its magnitude from the initial value g_0, then after reaching its minimum $g_n^{*\prime}$ along the RG flow, g_n keeps increasing and eventually become nonperturbative. Hence it is possible that for a relatively large intermediate scale, the system behaves like $g_n \sim g_n^{*\prime}$. The effect of this nonmonotonic RG flow can be illustrated by a simple perturbation theory to the correlation function of the Néel order

parameter:

$$G_n(\mathbf{x}) = \langle \vec{n}(\mathbf{x}) \cdot \vec{n}(0) \rangle \sim \frac{3}{2}\frac{1}{|\mathbf{x}|} + \frac{3}{4}\int d^2\mathbf{x}_1 d^2\mathbf{x}_2 \frac{(g_n^{*\prime})^2}{|\mathbf{x}-\mathbf{x}_1||\mathbf{x}_1-\mathbf{x}_2|^{3-2\epsilon_n}|\mathbf{x}_2|} + O(g_n^{*\prime})^4 + \cdots . \quad (2.20)$$

Hence $G_n(\mathbf{k})$ in the momentum-frequency space $\mathbf{k} = (k, \omega)$ reads

$$G_n(\mathbf{k}) \sim \frac{1}{G^{(0)}(\mathbf{k})^{-1} - \Sigma(\mathbf{k})}, \quad (2.21)$$

where $G^{(0)}(\mathbf{k}) = 3\pi/|\mathbf{k}|$, $\Sigma(\mathbf{k}) = -A(g_n^{*\prime})^2|\mathbf{k}|^{1-2\epsilon_n}/(3\pi)$, and $A > 0$ for $0 < \epsilon_n < 1/2$. The system will have enhanced spin-spin correlation function compared with the $\mathrm{SU}(2)_1$ CFT of the spin-1/2 chain, as was observed in numerical simulations [151, 37, 38]. The mixture of the two terms in $G^{-1}(\mathbf{k})$ may yield results that appear to be power-law correlation with different scaling dimensions, which is illustrated in Fig. 2.2, where we have fixed $\epsilon_n = 5/22\epsilon$ but chosen different $g_n^{*\prime}$. This nonuniversal power-law like scaling of spin correlation was also observed in recent numerics concerning the edge states of the AKLT state during a bulk phase transition [37, 38].

Now we briefly consider the situation when the bulk undergoes a disorder-order quantum phase transition between the AKLT state and the Ising like VBS order, which is described by order parameter ϕ. The boundary mode of ϕ is $\Phi \sim \partial_y \phi$, and it couples to the VBS order parameter v at the boundary CFT. In this case, the coupled RG flow of λ and g_v in Eq. 2.5 is relatively simple: as long as we start with nonzero (λ_0, g_{v0}), both g_v and λ quite generally flow to positive infinity, which corresponds to a nonzero long range order of v. Hence the $1d$ boundary of the system should develop the Ising-VBS order before the bulk. when the bulk is tuned closer and closer to a VBS (Ising) transition, the boundary will go through a transition between the gapless $\mathrm{SU}(2)_1$ CFT state to a VBS phase, before the bulk actually hits criticality. This boundary transition should be in the same universality class as the transition from an $\mathrm{SU}(2)_1$ CFT to a VBS phase in a purely

one-dimensional spin-1/2 chain with both nearest and next nearest neighbor Heisenberg interactions (see, for example, Ref. 177 for the one-dimensional transition). We note that this transition is not an ordinary $1+1d$ Ising transition and, hence, is different from the "extraordinary transition" studied in the standard boundary criticality literature. But if we start with a negative initial value λ_0, it may take a long RG time before the coupling constants become positive and nonperturbative. Hence the VBS order parameter may still appear to have quasi long range correlation for a finite system.

In conclusion, we have found that there can be a direct continuous quantum phase transition between the long range antiferromagnetic Néel order, and the VBS order, in an effective $1d$ spin-1/2 system with nonlocal interactions (Eq. 2.5). Due to the nonlocality of the model, even in a $1d$ system with a continuous SO(3) spin symmetry there can be a long range Néel order. Within the accuracy of our method, the effective spin-1/2 system Eq. 2.5 arises from coupling the $1d$ boundary of a $2d$ SPT phase to bulk quantum critical modes. Our results were drawn from a controlled renormalization group study, and the critical exponents extracted (including the anomalous dimensions of order parameters and the dynamical exponent) are qualitatively consistent with the Néel-VBS transition found numerically in recent simulation of a spin-1/2 chain with spatially instantaneous nonlocal interactions [153, 154]. If a $1d$ system has local interactions only, there can only be spontaneous discrete symmetry breaking. Previous numerical and analytical works [178, 179, 180] have studied the analogue of deconfined quantum critical point between two phases that spontaneously break different discrete symmetries.

2.2 Boundary Criticality of $2d$ Topological Phase Transitions

2.2.1 Introduction

Two dimensional quantum many body systems at zero temperature gave us a plethora of exotic phenomena beyond the classical wisdom of phases of matter. These phenomena include topological orders [181, 150], symmetry protected topological orders [157, 158] (generalization of topological insulators), and unconventional quantum phase transitions beyond the Landau's paradigm [182, 183, 184, 185, 186, 187]. The unconventional quantum phase transitions usually have very distinct universal scalings compared with the ordinary $(2+1)d$ Landau's transitions. These unconventional quantum phase transitions, or unconventional quantum critical points (QCP), could happen between two ordinary Landau's phases with different patterns of spontaneous symmetry breaking [182, 183], they can also happen between a topological order and an ordered phase [184, 185, 186]. Although many appealing numerical evidences of these unconventional QCPs have been found [188, 189, 190, 191], direct clear experimental observation of these unconventional QCPs is still demanded.

To identify an unconventional QCP in an experimental system, we need to measure the correlation functions and scaling dimensions of various operators at this QCP, and compare the results with analytical predictions. In this work we do not attempt to propose a particular experimental system that realizes one of the unconventional QCPs, instead we try to address one general issue that many experimental platforms would face, platforms where potentially these unconventional QCPs can be found. In numerical simulations of a QCP, correlation functions and scalings in the bulk can be directly computed. But experimentally many purely $2d$ systems of interests are sandwiched between

other auxiliary layers in a Van der Waals heterostructure [128]. Hence the bulk of the $2d$ system is often not exposed for probing for many experimental techniques. Instead, the $1d$ boundary of the $2d$ system is exposed and can often be probed directly. Based on the early studies of the boundary of Wilson-Fisher fixed points [192, 164, 165, 166] and the boundary of two dimensional conformal field theories [193], we learned that the scaling of operators at the boundary of a system can be very different from the bulk, hence the previous calculations about unconventional QCPs in the bulk may not be so relevant to many experimental platforms. We need to restudy the critical exponents at the $1d$ boundary of the system in order to compare with future experimental observations.

2.2.2 Boundary Criticality of Z_2 Topological Transition

In this section we discuss the boundary critical behaviors of a $2d$ topological quantum phase transition between a fully gapped Z_2 topological order, and an ordered phase which spontaneously breaks the global symmetry of the system and has no topological order. We assume that the "electric gauge particle" (the so called $e-$anyon) of the Z_2 topological order is an $N-$component complex boson b_a. This topological transition is described by the following field theory:

$$\mathcal{S} = \int d\tau d^2x \ \sum_{a=1}^{N} |\partial\phi_a|^2 + r|\phi_a|^2 + g(\sum_{a=1}^{N} |\phi|_a^2)^2, \tag{2.22}$$

where the complex scalar ϕ_a is the low energy field of anyon b_a, and it is coupled to a Z_2 gauge field which is not written explicitly. Because a Z_2 gauge field does not have gapless gauge boson, it does not contribute any infrared corrections to gauge invariant operators. When $r > r_c$, ϕ_a is disordered and the system is a Z_2 topological order which is also the deconfined phase of the Z_2 gauge field; when $r < r_c$, ϕ_a condenses and destroy the Z_2 topological order through the Higgs mechanism, and the condensate of ϕ_a has

ground state manifold S^{2N-1}/Z_2, where S^{2N-1} is a $2N-1$ dimensional sphere.

This theory Eq. 2.22 with different N can be realized in various scenarios. For $N=1$, this theory can be realized as the transition between a $2d$ superconductor and a Z_2 spin liquid. Similar unconventional topological transitions have been observed in numerical simulations in lattice spin (or quantum boson) models [184, 185], and theoretical predictions of the bulk critical exponents have been confirmed quantitatively. In this realization the boson b can be introduced by formally fractionalizing the electron operator on the lattice as

$$c_{j,\alpha} = f_{j,\alpha} b_j, \tag{2.23}$$

where b_j is a charge-carrying bosonic "rotor", $f_{j,\alpha}$ is the fermionic parton that carries the spin quantum number. $f_{j,\alpha}$ and b_j share a U(1) gauge symmetry, and the Z_2 topological order is constructed by assuming that b_j has a finite mass gap, while $f_{j,\alpha}$ forms a superconductor at the mean field level, which breaks the U(1) gauge symmetry down to Z_2. The quantum phase transition between the superconductor and the Z_2 topological is described by Eq. 2.22 with $N=1$. In the condensate of ϕ ($r < r_c$), the physical pairing symmetry of the superconductor is inherited from the mean field band structure of f_α. The long range Coulomb interaction between charge carriers is often screened by auxiliary layers such as metallic gages in experimental systems, hence in Eq. 2.22 there is only a short range interaction. Eq. 2.22 with $N=1$ is often referred to as the "XY*" transition. In the dual picture, starting from the superconducing phase, the XY* transition can also be viewed as the condensation of double vortices of the superconductor.

Eq. 2.22 with even N and $N \geq 2$ can be realized in Sp(N) spin systems, as the Z_2 spin liquid can be naturally constructed in Sp(N) spin systems. $b_a \sim \phi_a$ is introduced as the fractionalized Schwinger boson of the spin system, and the Z_2 topological order emerges

when a pair of b_a (which forms a Sp(N) singlet) condenses on the lattice [194, 195]. In particular, when $N = 2$, the theory Eq. 2.22 can be realized as the quantum phase transition between a Z_2 topological order and a noncollinear spin density wave of spin-1/2 systems on a frustrated lattice, for example the so-called 120° antiferromagnetic state on the triangular lattice [186]. The order parameter of the noncollinear spin order of a fully SU(2) invariant Hamiltonian will form a ground state manifold SO(3), which is equivalent to $\mathrm{SU}(2)/Z_2 = S^3/Z_2$, where the Z_2 is identified as the Z_2 gauge group, and also the center of the spin SU(2) group. The gauge invariant order parameter can be constructed with the low energy field ϕ_a as

$$\vec{N}_1 = \mathrm{Re}[\phi^t \mathrm{i}\sigma^2 \vec{\sigma}\phi], \quad \vec{N}_2 = \mathrm{Im}[\phi^t \mathrm{i}\sigma^2 \vec{\sigma}\phi], \quad \vec{N}_3 = \phi^\dagger \vec{\sigma}\phi, \tag{2.24}$$

and one can show that $\vec{N}_i$ are three orthogonal vectors. In this case theory Eq. 2.22 is referred to as the O(4)* transition, because there is an emergent O(4) symmetry that rotates between the four component real vector $(\mathrm{Re}[\phi_1], \mathrm{Im}[\phi_1], \mathrm{Re}[\phi_2], \mathrm{Im}[\phi_2])$. Other systems can potentially realize the theory with larger$-N$, for instance spin systems with Sp(4) symmetry can be realized in spin-3/2 cold atom systems [196].

We are most interested in the composite operator $\sum_a \phi_a^2$, which is invariant under the Z_2 gauge symmetry, but transforms nontrivially under the physical symmetry, hence it is a physical order parameter. When $N = 1$, in the condensate of ϕ (or b_j), the electron operator has a finite overlap with the fermionic parton operator $c_{j,\alpha} \sim f_{j,\alpha}\langle\phi\rangle$, hence the superconductor order parameter $\Delta \sim \langle\phi^2\rangle$. In the bulk the scaling dimension of ϕ^2 can be extracted through the standard ϵ expansion or numerical simulation [197]. Near the critical point the superconductor order parameter should scale as $\Delta \sim |r|^\beta$, where $\beta = [\phi^2]\nu$ and $[\phi^2]$ is the scaling dimension of operator ϕ^2. At the XY* critical point the exponent $\nu \sim 2/3$. When $N = 2$, the composite operator $\sum_a \phi_a^2$ is one component of the

spin order parameter of the noncollinear spin density wave.

All the results above are only valid in the $2d$ bulk. But in experiments on the boundary (as we discussed previously, it is the boundary that is exposed and hence can be probed conveniently), many of the critical exponents are modified. We now consider a system whose $2d$ bulk is in the semi-infinite xz plane with $z > 0$, with a $1d$ boundary at $z = 0$. For simplicity, let us tentatively ignore the Z_2 gauge field, and view ϕ_a as a physical order parameter. The most natural boundary condition is the Dirichlet boundary condition, *i.e.* the field vanishes at the boundary and also outside of the system $z \leq 0$. The boundary condition of the system can be imposed by turning on a large $c|\phi_a|^2$ term along the boundary, which fixes $\phi_a(\mathbf{x}, z = 0) = 0$, where $\mathbf{x} = (\tau, x)$.

At the mean field level, the correlation function of the ϕ_a field near the boundary can be computed using the "image method" [192]:

$$\begin{aligned} G(\mathbf{x}_1 - \mathbf{x}_2, z_1, z_2) &= \langle \phi_a(\mathbf{x}_1, z_1)\phi_a^*(\mathbf{x}_2, z_2)\rangle \\ &= G(\mathbf{x}_1 - \mathbf{x}_2, z_1 - z_2)_{\text{bulk}} - G(\mathbf{x}_1 - \mathbf{x}_2, z_1 + z_2)_{\text{bulk}}. \end{aligned} \tag{2.25}$$

where $G_{\text{bulk}} = \langle \phi_a(\mathbf{x}_1, z_1)\phi_a^*(\mathbf{x}_2, z_2)\rangle_{\text{bulk}}$ is the bulk correlation function far from the boundary. Notice that the boundary breaks the translation symmetry along the z direction, hence the full expression of the correlation function near the boundary is no longer a function of $z_1 - z_2$. The expression in Eq. 2.25 guarantees that the correlation function satisfies $G(\mathbf{x}_1 - \mathbf{x}_2, 0, z_2) = G(\mathbf{x}_1 - \mathbf{x}_2, z_1, 0) = 0$, which is consistent with the boundary condition. The fact that the correlation function of the ϕ_a field vanishes at the boundary means that ϕ_a itself is no longer the leading representation of the field at the boundary $z = 0$. Instead, another field with the same symmetry and quantum number

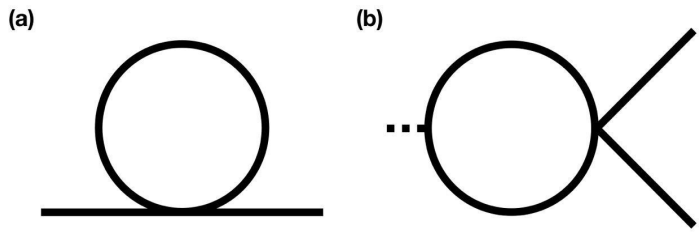

Figure 2.4: The diagrams that renormalize Φ_2 at the first order of ϵ. In the bulk the first diagram only shifts the mass of ϕ_a, but at the boundary it makes a nontrivial contribution to the wave function renormalization.

at the boundary,

$$\Phi_{1,a} = \partial_z \phi_a, \tag{2.26}$$

should be viewed as the leading representation of the field near the boundary. In fact, since $\Phi_{1,a}$ and ϕ_a have the same symmetry transformation near the boundary, an external field that couples to ϕ_a should also couple to $\partial_z \phi_a$. At the mean field level, a typical configuration of ϕ_a scales as $\phi_a(\mathbf{x}, z) \sim z$ near the boundary, hence $\Phi_{1,a} = \partial_z \phi_a$ is not suppressed by the boundary condition. Also, the correlation function of $\Phi_{1,a}$ at the boundary does not vanish, and at the mean field level it has scaling dimension $[\Phi_{1,a}] = [\phi_a] + 1 = D/2$, where D is the total space-time dimension of the bulk.

The gauge invariant order parameter $\sum_a \phi_a^2$ we are interested in reduces to $\Phi_2 = \sum_a \Phi_{1,a}^2$ at the boundary, and it has scaling dimension $[\Phi_2] = D$ at the mean field level. If the Z_2 gauge field is ignored, the correlation function of $\Phi_{1,a}$ at the boundary reads

$$\langle \Phi_{1,a}(\mathbf{x}_1) \Phi_{1,a}^*(\mathbf{x}_2) \rangle = \lim_{z_1, z_2 \to 0} \partial_{z_1} \partial_{z_2} G(\mathbf{x}_1 - \mathbf{x}_2, z_1, z_2), \tag{2.27}$$

where $G(\mathbf{x}_1 - \mathbf{x}_2, z_1, z_2)$ is still given by the image method Eq. 2.25. If we assume that

G_{bulk} takes the standard form at the Gaussian fixed point

$$\langle \phi_a(\mathbf{x}_1, z_1)\phi_a^*(\mathbf{x}_2, z_2)\rangle_{\text{bulk}} = \frac{1}{(|\mathbf{x}_1 - \mathbf{x}_2|^2 + (z_1 - z_2)^2)^{\frac{D-2}{2}}}, \tag{2.28}$$

the boundary correlation function of $\Phi_{1,a}$ at the mean field level reads

$$\langle \Phi_{1,a}(\mathbf{x}_1)\Phi_{1,a}^*(\mathbf{x}_2)\rangle = \frac{2(D-2)}{|\mathbf{x}_1 - \mathbf{x}_2|^D}. \tag{2.29}$$

At the Gaussian fixed point, the correlation function of Φ_2 can be derived using the Wick theorem:

$$\langle \Phi_2(\mathbf{x}_1)\Phi_2^*(\mathbf{x}_2)\rangle = \sum_a \langle \Phi_{1,a}(\mathbf{x}_1)\Phi_{1,a}^*(\mathbf{x}_2)\rangle^2 \sim \frac{1}{|\mathbf{x}_1 - \mathbf{x}_2|^{2D}}. \tag{2.30}$$

The scaling dimension of Φ_2 will acquire further correction from interaction, which can be computed through the $\epsilon = (4 - D)$ expansion. Interestingly, at the leading ϵ order, $[\Phi_2]$ will receive corrections from both wave function renormalization and vertex corrections:

$$[\Phi_2] = D + 2\delta_{wf} + \delta_v. \tag{2.31}$$

The wave function renormalization δ_{wf} can be extracted from the previously calculated $\epsilon-$expansion of the anomalous dimension at the boundary of the Wilson-Fisher fixed points, *i.e.*

$$[\Phi_{1,a}] = \frac{D}{2} + \delta_{wf} = \frac{D}{2} - \frac{N+1}{2(N+4)}\epsilon. \tag{2.32}$$

In contrast, in the bulk renormalization group (RG) analysis of the Wilson-Fisher fixed

point, the wave function renormalization only appears at the second and higher order of ϵ expansion.

The vertex correction is most conveniently computed using the standard real-space RG, since now the momentum along the $\hat{z}$ direction is no longer conserved. We will use the following operator-product-expansion (OPE) between $\Phi_2(\mathbf{x}, 0)$ and the interaction term in Eq. 2.22 (Fig. 2.4b), where $\Phi_2(\mathbf{x}, 0)$ is defined as $\Phi_2(\mathbf{x}, 0) = \lim_{z\to 0} \left(\partial_z \phi(\mathbf{x}, z)\right)^2$:

$$\begin{aligned}\Phi_2(\mathbf{x}, 0) g \left(\sum_a \phi_a^*(\mathbf{x}', z')\phi_a(\mathbf{x}', z')\right)^2 &= 2g \lim_{z\to 0} (\partial_z G(\mathbf{x}-\mathbf{x}', z, z'))^2 \sum_a \phi_a^2(\mathbf{x}', z') \\ &\sim \frac{32 z'^4 g}{((\mathbf{x}-\mathbf{x}')^2 + z'^2)^4} \lim_{z\to 0} \left(\partial_z \phi(\mathbf{x}, z)\right)^2 . \end{aligned} \tag{2.33}$$

Notice that like all the $4-\epsilon$ expansions, the OPE and loop integrals were performed by assuming the bulk system is in a four dimensional space-time. Under rescaling $\mathbf{x} \to \mathbf{x}/b$, through the vertex correction the operator Φ_2 will acquire a correction

$$\delta\Phi_2 = -\Phi_2 \int_{a/b}^{a} 4\pi r^2 dr \int_0^{+\infty} dz' \, \frac{32 z'^4 g}{(r^2 + z'^2)^4} = -4g\pi^2 (\ln b)\, \Phi_2. \tag{2.34}$$

The integral of z' is within the upper semi-infinite plane $z' > 0$.

Using epsilon expansion, g will flow from the noninteracting Gaussian fixed point to an interacting fixed point $g_* = \epsilon/(4(N+4)\pi^2)$. Plugging the fixed point value of g into Eq. 2.34, we obtain the vertex correction

$$\delta_v = \frac{\epsilon}{N+4}. \tag{2.35}$$

The wave function renormalization δ_{wf} can be reproduced in the same way through OPE (Fig. 2.4a). Eventually the scaling dimension of the gauge invariant order parameter Φ_2

at the boundary is

$$[\Phi_2] = D - \frac{N\epsilon}{N+4}. \tag{2.36}$$

We have also confirmed these calculations through direct computation of the correlation function of Φ_2 near the boundary (with diagrams in Fig. 2.5).

As we discussed before, the case with $N = 1$ can be realized as the transition between a Z_2 topological order and a superconductor. If the system is probed from the boundary, in the ordered phase but close to the critical point, the superconductor order parameter should scale with the tuning parameter r as

$$\Delta \sim |r|^{[\Phi_2]\nu} \sim |r|^{1.87}, \tag{2.37}$$

and we have taken $\nu \sim 2/3$ for the XY* fixed point [197].

For $N = 2$, the Φ_2 operator is one component of the noncollinear spin order of a SU(2) spin system, which scales as

$$\langle \vec{S} \rangle \sim \Phi_2 \sim |r|^{[\Phi_2]\nu} = |r|^{1.97} \tag{2.38}$$

Again, we have taken $\nu = 0.74$ for the O(4)* fixed point [197]. As a comparison, in the $2d$ bulk Φ_2 should scale with r as $\Phi_2 \sim |r|^{0.82}(N = 1)$ and $\Phi_2 \sim |r|^{0.87}(N = 2)$ respectively, which is significantly different from the boundary scaling.

When $N = 1$, the action Eq. 2.22 may or may not allow an extra chemical potential term $\mu\phi^*\partial_\tau\phi$, depending on whether the system has a (emergent) particle-hole symmetry $\phi \to \phi^*$ or not. With nonzero μ the system has the same scaling as a mean field transition (with logarithmic corrections) as the total space-time dimension is effectively $D = 2 + d = 4$, and g is marginally irrelevant. In this case the scaling dimension of the

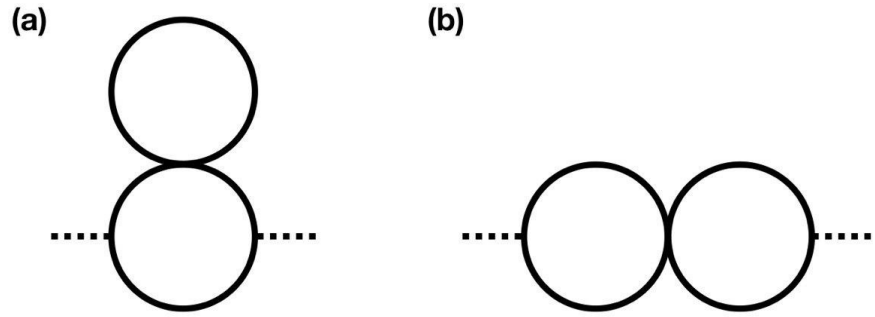

Figure 2.5: The renormalization of operator Φ_2 at the leading order of ϵ can also be computed directly using the correlation functions in this figure.

Cooper pair at the boundary becomes $[\Phi^2]_{\mu\neq 0} = D = 4$, and $\nu = 1/2$ as in the mean field transition.

The boundary scaling is valid as long as we consider correlation function $G(\mathbf{x}_1 - \mathbf{x}_2, z_1, z_2)$ with $|\mathbf{x}_1 - \mathbf{x}_2| \gg z_1, z_2$. Right at the boundary of a $2d$ Z_2 topological order, the gauge field is confined, due to the condensation of the $m-$anyons of the Z_2 topological order at the boundary (the boundary of a Z_2 topological order can also have $e-$anyon condensate, but since in our case the $e-$anyons carry nontrivial symmetry transformations, we assume our boundary always has $m-$anyon condensate). Near the boundary, the system still has a finite confinement length $\xi(z)$ as a function of z, *i.e.* the distance from the boundary, due to the "proximity effect" of the $m-$condensation at the boundary. In order to guarantee that we can approximately assume a deconfined Z_2 gauge field near the boundary, we need $\xi(z) \gg z$.

The most convenient way to estimate the confinement length $\xi(z)$ close to the boundary, is to evaluate the energy cost of two gauge charged particles separated with distance x near the boundary. This energy cost can be estimated in the "dual" Hamiltonian of a Z_2 gauge theory, which is a $(2+1)d$ quantum Ising model: $H_{\text{dual}} = \sum_{\bar{j}} -h\tau^x_{\bar{j}} - \sum_{\mu=x,y} J_{\bar{j},\mu}\tau^z_{\bar{j}}\tau^z_{\bar{j}+\mu}$, where $\tau^x_{\bar{j}}$, $\tau^z_{\bar{j}}$ are a pair of Pauli operators defined on the dual lattice sites $\bar{j}$. The dual Ising operator $\tau^z_{\bar{j}}$ is a creation/annihilation operator of the Z_2 gauge

flux. A confined (and deconfined) phase of the Z_2 gauge field corresponds to the ordered (and disordered) phase of the dual quantum Ising model with nonzero (and zero) expectation value $\langle\tau^z\rangle$ [198]. If there is a pair of static $e-$particles with Z_2 gauge charges separated with distance x, this system is dual to a frustrated Ising model with $J_{\bar{j},\mu} = -J$ on the links along the branch-cut that connects the two particles, while $J_{\bar{j},\mu} = +J$ everywhere else. The energy cost of the two separated static particles corresponds to the energy difference between this frustrated Ising model nonuniform $J_{\bar{j},\mu}$, and the case with uniform $J_{\bar{j},\mu}$. Then if $\tau^z_{\bar{j}}$ has a nonzero expectation value $\langle\tau^z\rangle$, the pair of Z_2-gauge charges will approximately cost energy $E \sim J\langle\tau^z\rangle^2 x$, *i.e.* the system is in a confined phase with a linear confining potential between the two Z_2 gauge charges, and the confinement length is roughly $\xi \sim 1/(J\langle\tau^z\rangle^2)$. In our system with a boundary at $z = 0$, although $\langle\tau^z\rangle$ is nonzero at the boundary, its expectation value decays exponentially with z because the Z_2 gauge field is in a deconfined phase deep in the bulk with $\langle\tau^z\rangle = 0$. Hence the confinement length $\xi(z)$ also increases with z exponentially, and we can safely assume that the Z_2 gauge field is still approximately deconfined near the boundary.

2.2.3 Boundary Properties of Continuous Mott Transition

Another unconventional quantum phase transition that can happen in $2d$ systems is the continuous metal-insulator transition, where the insulator is a U(1) liquid phase with a fermi surface of the fermionic parton $f_{j,\alpha}$. Both $f_{j,\alpha}$ and b_j are coupled to an emergent U(1) gauge field, which is presumably deconfined in the $2d$ bulk due to the existence of the Fermi surface and finite density of states of the matter fields. The critical behavior of this transition in the bulk was studied in Ref. 199, and it is again described by the condensation of b_j, but in this case b_j is coupled to an dynamic U(1) gauge field a_μ.

Although there is a gapless gauge field a_μ in the bulk, the gauge field dynamics is

over-damped by the fermi surface of f_α through a term $\mathcal{S}_{\text{damp}} \sim \frac{1}{e^2}\sum_{\omega,\vec{q}}|a^t_{\omega,q}|^2\frac{|\omega|}{|q|}$ based on the standard Hertz-Millis formalism [81, 82], where a^t is the transverse mode of the gauge field. A simple power-counting would suggest that the gauge coupling e^2 becomes irrelevant at the transition where b_j condenses, for both $\mu = 0$ and $\mu \neq 0$. Hence the universality class of this transition does not receive relevant infrared corrections from the gauge field. Moreover, the direct density-density interaction between the bosonic and fermionic partons also does not lead to relevant effects [199]. Hence the metal-insulator transition can still be described by Eq. 2.22. The quasiparticle residue is proportional to $|\langle b\rangle|$, and the electron Green's function is proportional to $|\langle b\rangle|^2$. Hence if one probes from the boundary, the local density of states of electrons at low energy, which is proportional to the electron Green's function, scales with the tuning parameter r as

$$\rho \sim |\langle\Phi_1\rangle^2| \sim |r|^{2[\Phi_1]\nu}. \tag{2.39}$$

For $\mu = 0$, $[\Phi_1]$ is calculated in Eq. 2.32, and $\nu \sim 2/3$; for $\mu \neq 0$, $[\Phi_1] = 2$ and $\nu = 1/2$.

Again we need to address the question of confinement length near the boundary, and demonstrate that $\xi(z) \gg z$. A pure U(1) gauge field in $(2+1)d$ is dual to a scalar boson $\varphi \sim \exp(\mathrm{i}\theta)$ which physically is the Dirac monopole operator, and the confined phase of a U(1) gauge field corresponds to a phase with a pinned nonzero expectation value of φ. A U(1) gauged particle becomes a vortex of θ in the dual formalism, and in a deconfined phase a vortex costs logarithmically divergent energy; but if φ has a pinned nonzero expectation value, a vortex will cost linearly diverging energy and hence confined. Now suppose we consider a pair of gauge charged particles separated at distance x, the energy cost will be roughly $x\langle\varphi\rangle^2$. Hence we need to evaluate $\langle\varphi(z)\rangle$ as a function of z away from the boundary, assuming a nonzero expectation value of φ at the boundary $\varphi_0 = \langle\varphi(z=0)\rangle$. $\langle\varphi(z)\rangle$ can be inferred from the correlation function $\langle\varphi(z)\rangle \sim \langle\varphi(z)\varphi(0)^*\rangle \sim$

$\exp(\langle\theta(z)\theta(0)\rangle)$.

A $(2+1)d$ pure U(1) gauge field without the matter field is dual to a scalar boson model with an ordinary action $\mathcal{S} \sim \int d^2x d\tau \rho_s(\partial_\mu\theta)^2$, then θ has a positive scaling dimension $[\theta] = 1/2$. The correlation function of θ reads $\langle\theta(r)\theta(0)\rangle \sim 1/r$, which makes the correlation function of the monopole operator saturates to a nonzero value as $r \to \infty$. Hence a positive scaling dimension of θ in the dual action renders the confinement of the compact gauge field in $(2+1)d$. If θ has a negative scaling dimension in its (dual) action, the correlation function of φ will decay exponentially. Then the confinement length $\xi(z) \sim 1/\langle\varphi(z)\rangle^2 \sim 1/\langle\varphi(z)\varphi(0)^*\rangle^2$ will grow exponentially with z in the bulk away from the boundary. And since $\xi(z) \gg z$, the boundary scaling behavior calculated in this work can be applied under the assumption that the gauge field is sufficiently deconfined near the boundary since the confinement length is long enough in the vicinity of the boundary.

Now we need to derive the dual action for θ more carefully. Schematically the action for the transverse gauge field is

$$\mathcal{S} = \sum_{\omega,\vec{q}} \frac{1}{2}\left(\frac{1}{e^2}\frac{|\omega|}{q} + c^2q^2\right)|a^t|^2. \tag{2.40}$$

The canonical conjugate field of $\vec{a}$, *i.e.* the electric field of the gauge field is defined as $\vec{E} = \delta\mathcal{L}/\delta\dot{\vec{a}}$, hence $\vec{E}_{\omega,\vec{q}} \sim \vec{a}_{\omega,\vec{q}}/(e^2q)$, hence the action can also be written as

$$\mathcal{S} = \sum_{\omega,\vec{q}} \frac{e^2}{2}|\omega||\vec{q}||\vec{E}_{\omega,\vec{q}}|^2 + \frac{c^2}{2}q^2|a^t_{\omega,\vec{q}}|^2. \tag{2.41}$$

Then we can use the standard duality transformation that preserves the commutation relation between the canonical conjugate variables $\vec{E}$ and $\vec{A}$: $\vec{E} = \vec{\nabla}\theta$, $\vec{\nabla}\times\vec{a} = n$, where n is the flux density, or the particle density conjugate to θ. Eventually the dual action

reads

$$\mathcal{S}_d = \sum_{\omega,\vec{q}} \frac{1}{2} \left(e^2 |\omega| q^3 + \frac{1}{c^2} \omega^2 \right) |\theta_{\omega,\vec{q}}|^2. \tag{2.42}$$

Indeed, $\theta(\mathbf{x}, \tau)$ has a negative scaling dimension in this dual action, which is consistent with our expectation that $\langle \varphi(z) \rangle$ decays exponentially in the bulk, hence the gauge field is still approximately deconfined in the vicinity of the boundary.

2.2.4 Discussion

In this work we computed the boundary universal scaling behaviors of a class of deconfined quantum phase transitions, which is relevant to future realization of these exotic transitions in experimental systems. From the perspective of the pure Laudau's paradigm, the cases we study correspond to the "ordinary transitions" of boundary CFT [192], meaning the bulk will enter an ordered phase before the boundary, which we believe is the most natural case in real systems. Measurement of the scaling laws we calculated depends on the specific realization of the theory Eq. 2.22. For example, if the $N = 1$ theory is realized (as we proposed in this work) as the transition between the Z_2 spin liquid to superconductor, the amplitude of the Cooper pair at the boundary predicted in our calculation can be measured through the Josephson effect by building a junction between the boundary of the system and another ordinary bulk superconductor, as the Josephson current is proportional to the amplitude of the superconductor order parameter near the boundary. The Josephson current should follow the same scaling law as Eq. 2.37.

The studies in this work can be naturally generalized to higher dimensions. If there is a deconfined QCP between the Z_2 topological order and an ordered phase in the $(3+1)d$ bulk, at its $(2+1)d$ boundary the gauge invariant order parameter Φ_2 has precise scaling

dimension $[\Phi_2] = 4$, since in the bulk this transition is described by a mean field theory and received no extra corrections.

The direct transition between the Néel and valance bond solid (VBS) order is another type of deconfined QCP that has attracted a great deal of attentions. The boundary effect of this deconfined QCP is more complex than the situations we have considered because the boundary breaks the lattice symmetry, hence the boundary condition would couple to the VBS order parameter. Another interesting scenario worth studying is the boundary scaling of a bulk transition between a symmetry protected topological (SPT) states and an ordered phase which spontaneously breaks part of the defining symmetries of the SPT phase. Although the bulk transition should belong to the same universality class as the ordinary Ginzburg-Landau transition, its boundary is expected to be very different due to the existence of symmetry protected nontrivial boundary states even in the SPT phase. Efforts have been made along this direction including numerical simulation [200] and construction of exactly soluble models [201]. We will leave these subjects to future studies.

2.3 Topological Edge and Interface States at $3d$ Bulk Criticality

2.3.1 Introduction

The most prominent feature of topological insulators (TI) [202, 203, 204, 205, 206, 207, 208] and more generally symmetry protected topological (SPT) states [157, 158] is the contrast between the boundary and the bulk of the system. In particular the $2d$ edge of $3d$ SPT states hosts the most diverse zoo of exotic phenomena that keep attracting attentions and efforts from theoretical physics. It has been shown that many

exotic phenomena such as anomalous topological order [209, 210, 211, 212, 213, 214, 215], deconfined quantum critical points [161], self-dual field theories [168, 170, 169, 98] can all occur on the $2d$ edge of $3d$ SPT stats. Sometimes the symmetry of the system is secretly realized as a self-dual transformation of the field theories at the boundary [216, 172]. All these suggest that the $2d$ boundary of a $3d$ system is an ideal platform of studying physics beyond the standard frameworks of condensed matter theory.

On the other hand, even the boundary of an ordinary Landau-Ginzburg type of quantum phase transition can have nontrivial behaviors. It was studied and understood in the past that the boundary of a bulk conformal field theory (CFT) follows a very different critical behavior from the bulk [163, 193, 164, 165, 166, 167], due to the strong boundary condition imposed on the CFT. The boundary fluctuations (or the boundary CFT) of the Landau-Ginzburg phase transitions were studied through the standard $\epsilon-$expansion, and it was shown that the critical exponents are very different from the bulk. Hence if experiments are performed at the boundary of the system, one should refer to the predictions of the boundary instead of the bulk CFT. These two different boundary effects were studied separately in the past. In this work we will study the interplay of these two distinct boundary effects. Our goal is to seek for new physics, ideally new fixed points under renormalization group (RG) flow due to the coupling of the two boundary effects.

For our purpose we give the system under study a virtual two-layer structure Fig. 2.6: layer-1 is a SPT state with nontrivial edge states, and it is not tuned to a bulk phase transition; layer-2 is a topological trivial system which undergoes an ordinary Landau-Ginzburg disorder-to-order phase transition. Then as a starting point we assume a weak coupling between the boundary of the two layers, and study the RG flow of the coupling. Besides the edge state localized at the boundary of a SPT state, we will also consider symmetry protected gapless states localized at a $2d$ interface embedded in a $3d$ bulk. We

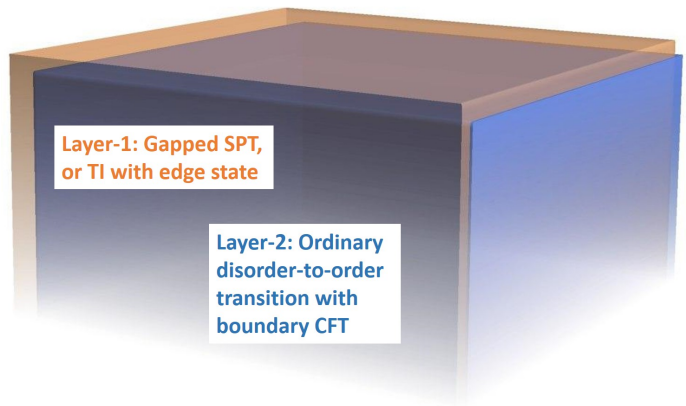

Figure 2.6: We view the system under study as a two layer system. Layer-1 is a SPT or TI with nontrivial edge states; layer-2 is an ordinary disorder-to-order phase transition whose order parameter at the boundary follows the scaling of boundary CFT. The boundary of the entire system may flow to new fixed points due to the coupling between the two layers.

will demonstrate that in several cases, including the edge state of a prototype bosonic SPT state, the $2d$ boundary or interface will flow to a new fixed point due to the bulk quantum phase transition.

Previous works have explored related ideas with different approaches. Exactly soluble $1d$ and $2d$ Hamiltonians have been constructed for gapless systems with protected edge states [33]; fate of edge states was also studied for $1d$ and $2d$ SPT states [34, 35, 36, 37, 38]. But the $2d$ edge of $3d$ bosonic SPT systems coupled with boundary modes which originate from bulk quantum critical points, *i.e.* the situation that potentially hosts the richest and most exotic phenomena, have not been studied to our knowledge. We note that the interaction between bulk quantum critical modes and the boundary of free or weakly interacting fermion topological insulator (or topological superconductor) was studied in Ref. 39, but the coupling in that case was strongly irrelevant hence will not lead to new physics in the infrared (we will review the interplay between the bulk quantum critical modes and the edge states of free fermion topological insulator in the next section). We will focus on bosonic SPT state with intrinsic strong interaction in this work. We use

the generic long wavelength field theory description of both the bulk bosonic SPT states and the edge states. Due to the lack of exact results of strongly interacting $(2+1)d$ field theories, we seek for a controlled calculation procedure that allows us to identify new fixed points under RG flow. Indeed, in several scenarios we will explore in this work, new fixed points are identified based on controlled calculations.

2.3.2 Edge States of $3d$ SPT at Bulk QCP

Edge States of Non-Interacting $3d$ TIs

We first consider the edge state of $3d$ topological insulator (TI) and symmetry protected topological states. The edge state of free fermion TI is described by the action

$$\mathcal{S} = \int d^2x d\tau \sum_{\alpha=1}^{N_f} \bar{\psi}_\alpha \gamma_\mu \partial_\mu \psi_\alpha, \tag{2.43}$$

with $\gamma^1 = \sigma^2$, $\gamma^2 = -\sigma^1$, $\gamma^0 = \sigma^3$, $\bar{\psi} = \psi^\dagger \gamma^0$. Based on the "ten-fold way classification" [206, 207, 208], for the AIII class, at the noninteracting level the TI is always nontrivial and topologically different from each other for arbitrary integer$-N_f$; while for the AII class the TI is nontrivial only for odd integer N_f, and they are all topologically equivalent to the simplest case with $N_f = 1$. In both cases the fermion mass term $\sum_\alpha \bar{\psi}_\alpha \psi_\alpha$ is forbidden by the time-reversal symmetry. Hence let us consider the disorder-to-order phase transition in the $3d$ bulk associated with a spontaneous time-reversal symmetry breaking, which is described by an ordinary $(3+1)d$ Landau-Ginzburg quantum Ising theory:

$$\mathcal{S}_b = \int d^3x d\tau \ (\partial\phi)^2 + u\phi^4. \tag{2.44}$$

Because u is a marginally irrelevant coupling at the $(3+1)d$ noninteracting Gaussian fixed point, the scaling dimension of ϕ in the bulk is precisely $[\phi] = 1$.

Here we stress that the disorder-to-order transition is driven by the physics in the bulk. Without the bulk, the boundary alone does not support an ordered phase. To study the fate of the edge state when the bulk is tuned to the quantum critical point, we view the bulk as a "two layer" system (Fig. 2.6): layer-1 is a $3d$ TI which is not tuned to the quantum phase transition; while layer-2 is at the disorder-to-order bulk quantum phase transition between a time-reversal invariant trivial insulator and a spontaneous time-reversal symmetry breaking phase. Now both layers have nontrivial physics at the edge. The quantum critical fluctuation (from layer-2) at the $2d$ boundary must satisfy the boundary scaling law. When we impose the most natural boundary condition $\phi(z \geq 0) = 0$, the leading field at the boundary which carries the same quantum number as ϕ is $\Phi \sim \partial_z \phi$. Since ϕ has scaling dimension 1, Φ should have scaling dimension $[\Phi] = 2$, *i.e.*

$$\langle \Phi(\mathbf{x}, z=0)\Phi(0, z=0)\rangle \sim 1/|\mathbf{x}|^4, \tag{2.45}$$

where $\mathbf{x} = (\tau, x, y)$. Eq. 2.45 is a much weaker correlation than ϕ in the bulk (more detailed derivation of boundary correlation functions can be found in Ref. 163, 164, 165, 166).

Now we turn on coupling between the $2d$ boundaries of the two layers. The edge state of the TI in layer-1 is affected by the boundary fluctuations of layer-2 through the "proximity effect". The coupling between the two layers at the $2d$ boundary is described by the following term in the action:

$$\mathcal{S}_c = \int d^2x d\tau \sum_\alpha g\Phi\bar{\psi}_\alpha\psi_\alpha. \tag{2.46}$$

Since $\Phi \sim \partial_z \phi$ has scaling dimension 2, g will have scaling dimension $[g] = -1$, *i.e.* it is strongly irrelevant. This conclusion is consistent with previous study Ref. 39. A negative "mass term" Φ^2 will be generated through the standard fermion loop diagram, but since Φ has scaling dimension 2, this mass term will be irrelevant. Hence the edge state of a $3d$ TI is stable even at the bulk quantum critical point where the time-reversal symmetry is spontaneously broken, and the properties of the edge states (such as electron Green's function) should be identical to the edge state of TI in the infrared. To make the coupling g relevant, the quantum critical modes also need to localize on the boundary, which is one of the situations studied in Ref. 39.

Edge States of Bosonic SPT States

The situation of bosonic SPT phases can be much more interesting. The bosonic SPT state can only exist in strongly interacting systems. We use the prototype $3d$ bosonic SPT phase with $(\mathrm{U}(1) \times \mathrm{U}(1)) \times Z_2^T$ symmetry as an example, since this phase can be viewed as the parent state of many $3d$ bosonic SPT phases by breaking the symmetry down to its subgroups, without fully trivializing the SPT phase. The topological feature of this phase can be conveniently captured by the following nonlinear sigma model in the $(3+1)d$ bulk [161, 217]:

$$\mathcal{S} = \int d^3x d\tau \; \frac{1}{g}(\partial \boldsymbol{n})^2 + \frac{\mathrm{i}2\pi}{\Omega_4} \epsilon_{abcde} n^a \partial_x n^b \partial_y n^c \partial_z n^d \partial_\tau n^e, \tag{2.47}$$

where $\boldsymbol{n}$ is a five component vector field with unit length, and Ω_4 is the volume of the four dimension sphere with unit radius. (n_1, n_2), and (n_3, n_4) transform as a vector under the two U(1) symmetries respectively, and the Z_2^T changes the sign of all components of the vector $\boldsymbol{n}$. The nonlinear sigma model Eq. 2.47 is invariant under all the transformations.

The $2d$ edge state of this SPT phase can be described by the following $(2+1)d$ action:

$$\mathcal{S} = \int d^2x d\tau \sum_{\alpha=1,2} |(\partial - \mathrm{i}a)z_\alpha|^2 + r|z_\alpha|^2 + u|z_\alpha|^4 + \frac{1}{e^2}(\mathrm{d}a)^2, \tag{2.48}$$

where a_μ is a noncompact U(1) gauge field. The theory Eq. 2.48 is referred to as the "easy-plane noncompact CP^1" (EP-NCCP^1) model. We are most interested in the point $r = 0$. The term $\sum_\alpha r|z_\alpha|^2$ would be forbidden if there is an extra Z_2 self-dual symmetry that exchanges the two U(1) symmetries [218], while without the self-duality symmetry r needs to be tuned to zero, and the point $r = 0$ becomes the transition point between two ordered phases that spontaneously breaks the two U(1) symmetries respectively [182, 183]. At $r = 0$, starting with the UV fixed point with noninteracting z_α and a_μ, both u and e are expected (though not proven) to flow to a fixed point with $u = u_*$, $e = e_*$.

The putative conformal field theory at $r = 0$ and its fate under coupling to the boundary fluctuations (boundary modes) of the bulk quantum critical points is the goal of our study in this section. As was discussed in previous literatures, it is expected that there is an emergent O(4) symmetry in Eq. 2.48 at $r = 0$, when we fully explore all the duality features of Eq. 2.48 [218, 168, 170, 171, 169, 98, 172]. In the EP-NCCP^1 action, the following operators form a vector under O(4):

$$(n_1, n_2, n_3, n_4) \sim (z^\dagger \sigma^1 z,\ z^\dagger \sigma^2 z,\ \mathrm{Re}[\mathcal{M}_a],\ \mathrm{Im}[\mathcal{M}_a]), \tag{2.49}$$

where $\mathcal{M}_a$ is the monopole operator (the operator that annihilates a quantized flux of a_μ). In the equation above, (n_1, n_2) and (n_3, n_4) form vectors under the two U(1) symmetries respectively. The emergent O(4) includes the self-dual Z_2 symmetry of the EP-NCCP^1, *i.e.* the operation that exchanges the two U(1) symmetries.

Now we consider the $3d$ bulk quantum phase transition between the SPT phase and

the ordered phases that break part of the defining symmetries of the SPT phase. We first consider two order parameters: ϕ_0, ϕ_3. ϕ_0 is the order parameter that corresponds to the self-dual Z_2 symmetry; and ϕ_3 is a singlet under the emergent SO(4) but odd under the improper rotation of the emergent O(4), and also odd under Z_2^T. Again we view our system as a two layer structure: layer-1 is a SPT phase with solid edge states described by Eq. 2.48; layer-2 is a topological-trivial system that undergoes the transition of condensation of either ϕ_0 or ϕ_3. Both order parameters have an ordinary mean field like transition in the bulk of layer-2. Again at the boundary, both order parameters will have very different scalings from the bulk. We assume that system under study fills the entire semi-infinite space at $z < 0$, then at the boundary plane $z = 0$, the most natural boundary condition is that $\phi_0(z \geq 0) = \phi_3(z \geq 0) = 0$, hence all order parameters near but inside the bulk should be replaced by the following representations: $\Phi_0 \sim \partial_z \phi_0$, $\Phi_3 \sim \partial_z \phi_3$. Both order parameters have scaling dimensions 2 at the $(2+1)d$ boundary of layer-2.

Now we couple Φ_0 and Φ_3 to the edge states of layer-1. The coupling will take the following form:

$$\mathcal{L}_{c0} = \sum_{\alpha} g_0 \Phi_0 |z_\alpha|^2, \qquad \mathcal{L}_{c3} = g_3 \Phi_3 z^\dagger \sigma^3 z. \tag{2.50}$$

The RG flow of coupling constants $g_{0,3}$ can be systematically evaluated in certain large$-N$ generalization of the action in Eq. 2.48:

$$\mathcal{S} = \int d^2x d\tau \sum_{\alpha=1,2} \sum_{j=1}^{N/2} |(\partial - \mathrm{i}a) z_{j,\alpha}|^2 + u(\sum_j |z_{j,\alpha}|^2)^2. \tag{2.51}$$

The large$-N$ generalization facilitate calculations of the RG flow, but the down side is that the duality structure and emergent symmetries no longer exist for $N > 2$. In the

large$-N$ limit of Eq. 2.51, the scaling dimension of the operators under study is

$$N \to +\infty : \quad [z^\dagger \sigma^3 z] = [|z|^2] = 2. \tag{2.52}$$

In the equation above, each operator has a sum of index j, which was not written explicitly. Apparently coupling constants $g_{0,3}$ are both irrelevant with large$-N$ due to the weakened boundary correlation of Φ_0 and Φ_3.

We are seeking for more interesting scenarios when the boundary is driven to a new fixed point due to the bulk quantum criticality. For this purpose we consider another order parameter $\vec{\phi}$ which transforms as a vector under one of the two U(1) symmetries. Here we no longer assume the Z_2 self-dual symmetry on the lattice scale. Again at the boundary $\vec{\phi}$ should be replaced by $\vec{\Phi} \sim \partial_z \vec{\phi}$. At the $2d$ boundary, the coupling between $\vec{\Phi}$ and the edge state of layer-2 reads

$$\mathcal{L}_{cv} = g_v \left(\Phi_1 z^\dagger \sigma^1 z + \Phi_2 z^\dagger \sigma^2 z \right). \tag{2.53}$$

In the large$-N$ limit of Eq. 2.51, the scaling dimension of the operators under study is

$$N \to +\infty : \quad [z^\dagger \sigma^1 z] = [z^\dagger \sigma^2 z] = 1. \tag{2.54}$$

Hence g_v is marginal in the large$-N$ limit, and there is a chance that g_v could drive the system to a new fixed point with $1/N$ corrections.

We introduce the following action in order to compute the RG flow of g_v with finite but large N:

$$\mathcal{S} = \int d^2x d\tau \sum_{\alpha=1,2} \sum_{j=1}^{N/2} |(\partial - \mathrm{i}a) z_{j,\alpha}|^2 + \mathrm{i}\lambda_+ |z_{j,\alpha}|^2 + \mathrm{i}\lambda_- z_j^\dagger \sigma^3 z_j + \mathrm{i} g_v \vec{\Phi} \cdot z_j^\dagger \vec{\sigma} z_j + \frac{1}{2} \vec{\Phi} \cdot \frac{1}{|\partial|} \vec{\Phi}. \tag{2.55}$$

The $\lambda_\pm$ are two Hubbard-Stratonovich (HS) fields introduced for the standard $1/N$

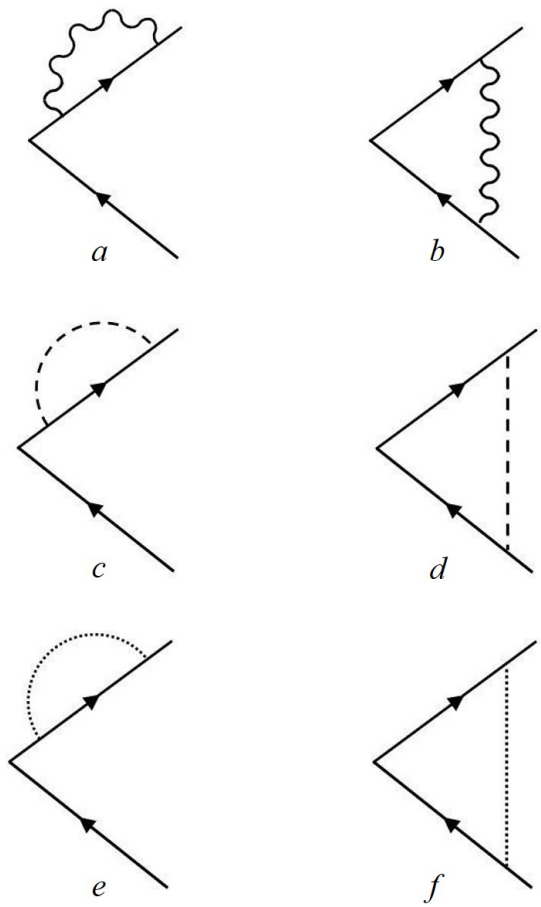

Figure 2.7: (a, b) the $1/N$ contribution to $z^\dagger\sigma^{1,2}z$ and $\bar{\psi}\tau^{1,2}\psi$ from the gauge field fluctuation, the solid lines represent either the propagator of z_α or ψ_α, the wavy line represents the propagator of the photon; (c, d) the $1/N$ contribution to $z^\dagger\vec{\sigma}z$ from $\lambda_\pm$ in Eq. 2.55; (e, f) the contribution to B in Eq. 2.56.

calculations [219, 220]. The scaling of $|z|^2$ and $z^\dagger\sigma^3 z$ in Eq. 2.51 are replaced by the HS fields λ_+, λ_- in the new action Eq. 2.55 respectively. A coefficient "i" is introduced in the definition of g_v by redefining $\Phi \to \mathrm{i}\Phi$ for convenience of calculation.

The schematic beta function of g_v reads

$$\frac{dg_v}{d\ln l} = (1 - \Delta_v)g_v - Bg_v^3 + O(v^5). \tag{2.56}$$

Δ_v is the scaling dimension of $z_j^\dagger\vec{\sigma}z_j$ in the large$-N$ generalization of the EP-NCCP^1

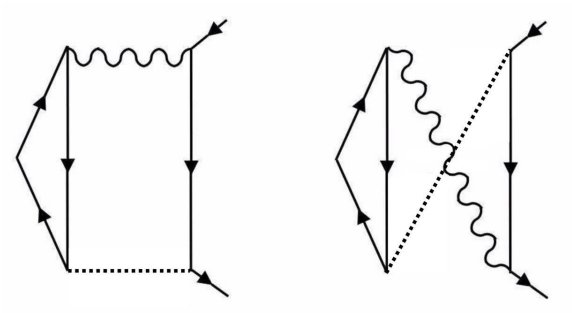

Figure 2.8: The two diagrams at g_v^3 order which cancel each other for arbitrary gauge choices.

model Eq. 2.51, with $\vec{\sigma} = (\sigma^1, \sigma^2)$. The standard $1/N$ calculation leads to

$$\Delta_v = 1 - \frac{56}{3\pi^2 N} + O(\frac{1}{N^2}). \tag{2.57}$$

The $1/N$ correction of Δ_v comes from diagram Fig. 2.7$(a-d)$, where the wavy line is the gauge boson propagator, and the dashed line represents propagators of both $\lambda_\pm$. The first term of Eq. 2.57 implies that g_v is indeed weakly relevant with finite but large$-N$.

The constant B in the beta function arises from the operator product expansion of the coupling term Eq. 2.53, which is equivalent to the diagrams Fig. 2.7e, f. This computation leads to $B = 1/(3\pi^2)$. The two diagrams in Fig. 2.8 which are also at g_v^3 order cancel each other for arbitrary gauge choices. Similar two-loop diagrams at the same order of $1/N$ do not enter the RG equation due to lack of logarithmic contribution, as was explained in Ref. 220. $\vec{\Phi}$ does not receive a wave function renormalization due to the singular form of its action. Hence with finite but large$-N$, g_v indeed flows to a new fixed point:

$$g_{v*}^2 = \frac{56}{N} + O(\frac{1}{N^2}). \tag{2.58}$$

We stress that this result is drawn from a controlled calculation and it is valid to the

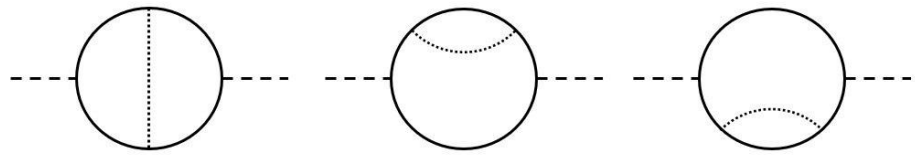

Figure 2.9: The g_v^2 diagrams that contributes to the scaling dimension of $[\lambda_+]$. Here the solid line represents the propagator of $z_{j,\alpha}$, the dotted line represents the vector operator $\vec{\Phi}$, and the dashed line represents λ_+.

leading order of $1/N$.

As we explained before, the point $r = 0$ is a direct transition between two ordered phases that spontaneously break the two U(1) symmetries. This transition will be driven to a new fixed point by coupling to the boundary fluctuations of bulk critical points as we demonstrated above. At this new fixed point, the critical exponent ν follows from the relation

$$\nu^{-1} = 3 - [\lambda_+]. \tag{2.59}$$

To evaluate the scaling dimension $[\lambda_+]$ we have to incorporate the contributions of g_v^2 from the diagrams shown in Fig. 2.9, and combined with $1/N$ calculations performed previously [221, 220]. Then in the end we obtain

$$\nu_*^{-1} = 1 + \frac{160}{3\pi^2 N} + \frac{4g_{v*}^2}{3\pi^2} + O(1/N^2) = 1 + \frac{128}{\pi^2 N} + O(1/N^2). \tag{2.60}$$

Again, there are other loop diagrams which appear to be at the same order of $1/N$ but do not make any logarithmic contributions [220].

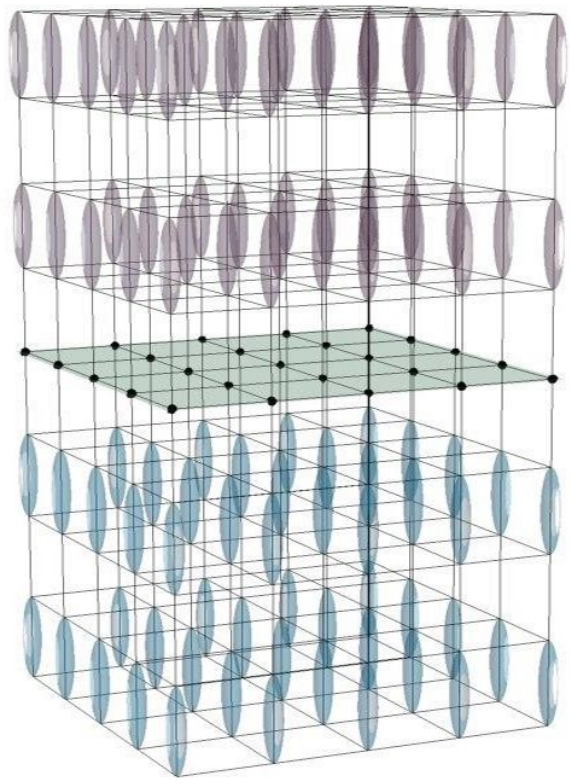

Figure 2.10: We consider a SU(N) antiferromagnet with self-conjugate representation on each site. The system forms a background VBS pattern, with opposite dimerizations between semi-infinite spaces $z > 0$ and $z < 0$. There is a $2d$ antiferromagnet localized at the interface $z = 0$, and the entire bulk can undergo phase transition simultaneously due to the mirror (reflection) symmetry that connects the two sides of the domain wall.

2.3.3 Interface States Embedded in $3d$ Bulk

Interface states of Non-Interacting electron systems

In previous examples we studied topological edge states at the boundary of a $3d$ system. In this section we will consider the $2d$ states localized at an interface ($z = 0$) in a $3d$ space, when the entire $3d$ bulk (for both $z > 0$ and $z < 0$ semi-infinite spaces) undergoes a phase transition simultaneously. Without fine-tuning, we need to assume an extra reflection symmetry $z \to -z$ that connects the two sides of the interface, which guarantees a simultaneous phase transition in the entire system. In this case there is no

physical reason to impose the strong boundary condition at the interface embedded in the $3d$ space, hence the quantum critical modes at the interface follow the ordinary bulk scalings, instead of the weakened correlation of boundary CFT.

Again we will consider free fermion systems first. Let us first recall that the AIII class TI has a $\mathbb{Z}$ classification which is characterized by a topological index n_T. n_T will appear as the coefficient of the electromagnetic response of the TI: $\mathcal{L} \sim i\pi n_T \mathbf{E} \cdot \mathbf{B}$. n_T must change sign under spatial reflection transformation $\mathcal{M}_z : z \to -z$. To construct the desired system, we assume the semi-infinite space $z < 0$ is occupied with the AIII class TI with Hamiltonian $\hat{H}$, whose topological index is n_T; and its "reflection conjugate" $\mathcal{M}_z^{-1}\hat{H}\mathcal{M}_z$ fills the semi-infinite space $z > 0$. Then there are $N_f = 2n_T$ flavors of massless Dirac fermions localized at the $2d$ plane $z = 0$, which are still protected by time-reversal symmetry. Now we assume the entire bulk undergoes a quantum phase transition with a spontaneous time-reversal symmetry breaking, whose order parameter couples to the domain wall Dirac fermions as

$$\mathcal{S} = \int d^2x d\tau \sum_{\alpha=1}^{N_f} \bar{\psi}_\alpha \gamma_\mu \partial_\mu \psi_\alpha + g\phi\bar{\psi}_\alpha\psi_\alpha + \frac{1}{2}\phi(-\partial^2)^{1/2}\phi. \tag{2.61}$$

The last term in the action is still defined in the $(2+1)d$ interface, and it reproduces the correlation of ϕ in the bulk: $\langle\phi(0)\phi(r)\rangle \sim 1/r^2$. We stress that, since now the order parameter resides in the entire bulk, ϕ no longer obeys the boundary scaling as we discussed in previous examples. A negative boson mass term $-r\phi^2$ can be generated through the standard fermion mass loop diagram, hence we need to tune an extra term at the interface to make sure the mass term of ϕ vanishes.

In this case the coupling constant g is a marginal perturbation based on simple power-counting. But g will flow under renormalization group (RG) with loop corrections

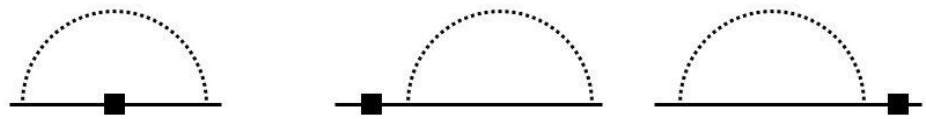

Figure 2.11: The Feynman diagrams that renormalizes the extra velocity δ in Eq. 2.63. The box represents the vertex δ, and all three diagrams contributes to the fermion self-energy and renormalize δ.

in Fig. 2.7(e, f):

$$\beta(g) = \frac{dg}{d\ln l} = -\frac{2}{3\pi^2}g^3 + O(g^5). \tag{2.62}$$

Hence even in this case, the coupling between the domain wall states and the bulk quantum critical modes is perturbatively marginally irrelevant.

So far we have assumed that the velocity of the interface state is identical with the bulk. Now let us tune the velocity of the domain wall Dirac fermions slightly different, which can be captured by the following term in the Lagrangian:

$$\sum_\alpha \delta\bar{\psi}_\alpha(\gamma^1\partial_x + \gamma^2\partial_y - 2\gamma^3\partial_3)\psi_\alpha. \tag{2.63}$$

δ defined above is an eigenvector under the leading order RG flow. With the loop diagrams in Fig. 2.11, we obtain the leading order beta function of δ:

$$\beta(\delta) = \frac{d\delta}{d\ln l} = -\frac{1}{5\pi^2}g^2\delta. \tag{2.64}$$

Together with $\beta(g)$, the velocity anisotropy is also perturbatively irrelevant.

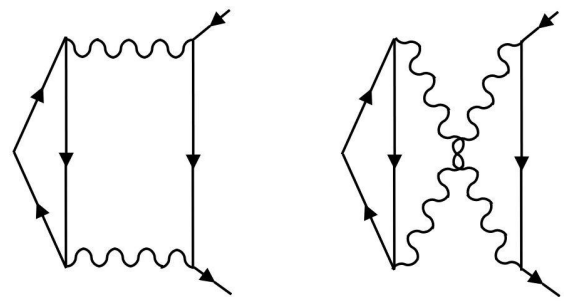

Figure 2.12: The extra diagrams that contribute to the scaling dimension of $\sum_\alpha \bar{\psi}_\alpha \psi_\alpha$ at the leading order of $1/N_f$ in QED_3. Again the wavy lines are photon propagators.

Interface States of Quantum Antiferromagnet

We now consider a SU(N) quantum antiferromagnet on a tetragonal lattice with a self-conjugate representation on each site (we assume N is an even integer). With large$-N$, an antiferromagentic Heisenberg SU(N) model has a dimerized ground state [222, 223] where the two SU(N) spins on two nearest neighbor sites form a spin singlet (valence bond). We consider the following background configuration of valence bond solid (VBS): the spins form VBS along the $\hat{z}$ direction which spontaneously break the translation symmetry, while there is a domain wall between two opposite dimerizations at the $2d$ XY plane $z = 0$, namely $z = 0$ is still a mirror plane of the system (Fig. 2.10). In each $1d$ chain along the $\hat{z}$ direction, there is a dangling self-conjugate SU(N) spin localized on the site at the domain wall. Hence the $2d$ domain wall is effectively a SU(N) antiferromagnet on a square lattice.

One state of SU(N) antiferromagnet which is the "parent" state of many orders and topological orders on the square lattice, is the gapless $\pi-$flux U(1) spin liquid [224, 175]. At low energy this spin liquid is described by the following action of $(2+1)d$ quantum

electrodynamics (QED_3):

$$\mathcal{S} = \int d^2x d\tau \sum_{\alpha=1}^{N_f} \bar{\psi}_\alpha \gamma_\mu (\partial_\mu - \mathrm{i} a_\mu) \psi_\alpha + \cdots \tag{2.65}$$

ψ_α is $N_f = 2N$ flavors of $2-$component Dirac fermions, and they are the low energy Dirac fermion modes of the slave fermion $f_{j,\alpha}$ defined as $\hat{S}_j^b = f_{j,\alpha}^\dagger T_{\alpha\beta}^b f_{j,\beta}$, T^b with $b = 1 \cdots N^2 - 1$ are the fundamental representation of the SU(N) Lie Algebra. Besides the spin components, there is an extra two dimensional internal space which corresponds to two Dirac points in the Brillouin zone. There is an emergent SU(N_f) flavor symmetry in QED_3 which includes both the SU(N) spin symmetry and discrete lattice symmetry.

It is known that when N_f is greater than a critical integer, the QED_3 is a conformal field theory (CFT). We will consider the fate of this CFT when the three dimensional bulk is driven to a quantum phase transition. We will first consider a disorder-to-order quantum phase transition, where the ordered phase spontaneously breaks the time-reversal and parity symmetry of the XY plane. Notice that due to the reflection symmetry $z \to -z$ of the background VBS configuration, the two sides of the domain wall will reach the quantum critical point simultaneously. The bulk transition is still described by Eq. 2.44. When we couple the Ising order parameter ϕ to the domain wall QED_3, the total $(2+1)d$ action reads

$$\mathcal{S} = \int d^2x d\tau \sum_{\alpha=1}^{N_f} \bar{\psi}_\alpha \gamma_\mu (\partial_\mu - \mathrm{i} a_\mu) \psi_\alpha + g\phi\bar{\psi}_\alpha\psi_\alpha + \frac{1}{2}\phi(-\partial^2)^{1/2}\phi. \tag{2.66}$$

If the gauge field fluctuation is ignored, or equivalently in the large$-N_f$ limit, the scaling dimension of $\bar{\psi}\psi$ is $[\bar{\psi}\psi] = 2$, and hence the scaling dimension of g is $[g] = 0$, *i.e.* g is a marginal perturbation. The $1/N_f$ correction to the RG flow arises from the Feynman

diagrams (Fig. 2.7(a, b) and Fig. 2.12) which involves one or two photon propagators:

$$G^a_{\mu\nu}(\vec{p}) = \frac{16}{N_f p}\left(\delta_{\mu\nu} - \frac{p_\mu p_\nu}{p^2}\right). \tag{2.67}$$

Again in this case the fermions will generate a mass term for the order parameter at the interface, which we need to tune to zero. At the leading order of $1/N_f$ the corrected beta function for g reads

$$\beta(g) = \frac{dg}{d\ln l} = -\frac{128}{3\pi^2 N_f} g - \frac{2}{3\pi^2} g^3 + O(g^3). \tag{2.68}$$

But this beta function does not lead to a new unitary fixed point other than the decoupled fixed point $g = 0$. Hence in this case the domain wall state is decoupled from the bulk quantum critical modes in the infrared limit.

A more interesting scenario is when the bulk undergoes a transition which spontaneously breaks the translation and C_4 rotation symmetry by developing an extra VBS order within the XY plane. The inplane VBS order parameters are $V_x \sim \bar{\psi}\tau^1\psi$, and $V_y \sim \bar{\psi}\tau^2\psi$, where $\tau^{1,2}$ are the Pauli matrices operating in the Dirac valley space. The coupling between the VBS order parameter and the domain wall QED$_3$ reads

$$\mathcal{S}_c = \int d^2x d\tau \; g\left(\phi^*\bar{\psi}\tau^-\psi + \phi\bar{\psi}\tau^+\psi\right) + \phi^*(-\partial^2)^{1/2}\phi. \tag{2.69}$$

Here $\tau^\pm = (\tau^1 \pm \mathrm{i}\tau^2)/2$. The scaling dimension of the VBS order parameter at the QED$_3$ fixed point has been computed previously [175, 225, 226]: $[\bar{\psi}\tau^a\psi] = 2 - 64/(3\pi^2 N_f)$, and the beta function of g to the leading order of $1/N_f$ reads

$$\beta(g) = \frac{64}{3\pi^2 N_f} g - \frac{1}{6\pi^2} g^3 + O(g^3). \tag{2.70}$$

In the large$-N_f$ limit, the coupling g is marginally irrelevant; but with finite and large$-N_f$, g is weakly relevant at the noninteracting fixed point, and it will flow to an interacting fixed point

$$g_*^2 = \frac{128}{N_f} + O(\frac{1}{N_f^2}). \tag{2.71}$$

This new fixed point will break the emergent SU(N_f) flavor symmetry down to SU(N) $\times$ $U(1)$ symmetry, where U(1) corresponds to the rotation of the Dirac valley space. The following gauge invariant operators receive different corrections to their scaling dimensions from coupling to the bulk quantum critical modes:

$$\begin{aligned}
[\bar{\psi}\psi] &= 2 + \frac{128}{3\pi^2 N_f} + \frac{2}{3\pi^2} g_*^2 + O(1/N_f^2), \\
[\bar{\psi}T^b\psi] &= 2 - \frac{64}{3\pi^2 N_f} + \frac{2}{3\pi^2} g_*^2 + O(1/N_f^2), \\
[\bar{\psi}\tau^3\psi] &= 2 - \frac{64}{3\pi^2 N_f} - \frac{1}{3\pi^2} g_*^2 + O(1/N_f^2), \\
[\bar{\psi}\tau^{1,2}\psi] &= 2 - \frac{64}{3\pi^2 N_f} + \frac{1}{6\pi^2} g_*^2.
\end{aligned} \tag{2.72}$$

The operators $\bar{\psi}\tau^{1,2}\psi$ have exactly scaling dimension 2, the Feynman diagram contributions from Fig. 2.7 cancel each other for operator $\bar{\psi}\tau^{1,2}\psi$ as they should. Notice that the last three operators in Eq. 2.72 should have the same scaling dimension in the original QED_3 fixed point due to the large SU(N_f) flavor symmetry, but at this new fixed point they will acquire different corrections.

Another interesting scenario is that the bulk is at a critical point whose order parameter couples to the Ising like operator $\bar{\psi}\tau^3\psi$, which breaks the inplane parity but

preserves the time-reversal:

$$\mathcal{S}_c = \int d^2x d\tau \; g\phi\bar{\psi}\tau^3\psi + \frac{1}{2}\phi(-\partial^2)^{1/2}\phi. \tag{2.73}$$

The microsopic representation of the operator $\bar{\psi}\tau^3\psi$ can be found in Ref. 175. The beta function of the coupling g reads

$$\beta(g) = \frac{64}{3\pi^2 N_f} g - \frac{2}{3\pi^2} g^3 + O(g^3), \tag{2.74}$$

and once again there is new stable fixed point $g_*^2 = 32/N_f + O(1/N_f^2)$. And at this fixed point,

$$\begin{aligned}
[\bar{\psi}\psi] &= 2 + \frac{128}{3\pi^2 N_f} + \frac{2}{3\pi^2} g_*^2 + O(1/N_f^2), \\
[\bar{\psi}T^b\psi] &= 2 - \frac{64}{3\pi^2 N_f} + \frac{2}{3\pi^2} g_*^2 + O(1/N_f^2), \\
[\bar{\psi}\tau^{1,2}\psi] &= 2 - \frac{64}{3\pi^2 N_f} - \frac{1}{3\pi^2} g_*^2 + O(1/N_f^2), \\
[\bar{\psi}\tau^3\psi] &= 2 - \frac{64}{3\pi^2 N_f} + \frac{2}{3\pi^2} g_*^2.
\end{aligned} \tag{2.75}$$

The domain wall state considered here is formally equivalent to the boundary state of a $3d$ bosonic SPT state with pSU(N) $\times$ U(1) symmetry, which can also be embedded to the $3d$ SPT with pSU(N_f) symmetry discussed in Ref. 162. This SPT state can be constructed as follows: we first break the U(1) symmetry in the $3d$ bulk by driving the bulk $z < 0$ into a superfluid phase, and then decorate the vortex loop of the superfluid phase with a $1d$ Haldane phase with pSU(N) symmetry [227, 228, 229, 230]. Eventually we proliferate the decorated vortex loops to restore all the symmetries in the bulk. A $1d$ pSU(N) Haldane phase can be constructed as a spin-chain with a pSU(N) spin on each site, and there is a dangling self-conjugate representation of SU(N) on each end of the

chain. And this dangling spin will also exist in the U(1) vortex at the boundary of the pSU(N) $\times$ U(1) SPT state. Notice that the self-conjugate representation of SU(N) is a projective representation of pSU(N).

2.3.4 Discussion

In this work we systematically studied the interplay of two different nontrivial boundary effects: the $2d$ edge states of $3d$ symmetry protected topological states, and the boundary fluctuations of $3d$ bulk quantum phase transitions. New fixed points were identified through generic field theory descriptions of these systems and controlled calculations. We then generalized our study to the $2d$ states localized at the interface embedded in the $3d$ bulk.

The last case studied in Eq. 2.74, 2.75 is special when $N_f = 2$, and when the gauge field is noncompact. This is the theory that has been shown to be dual to the EP-NCCP^1 model [171, 98] studied in Eq. 2.48, the operator $\sum_\alpha r|z_\alpha|^2$ is dual to $r\bar{\psi}\tau^3\psi$, and both theories are self-dual. By coupling the operator $\bar{\psi}\tau^3\psi$ to the bulk critical modes (rather than the boundary fluctuations of the bulk critical points), we have shown that this $(2+1)d$ theory is driven to a new fixed point, and the self-duality structure still holds. The self-duality transformation of Eq. 2.48 now is combined with the Ising symmetry of the order parameter ϕ. However, the O(4) emergent symmetry no longer exists at this new fixed point, due to the nonzero fixed point of g in Eq. 2.73.

The methodology used in this work can have many potential extensions. We can apply the same field theory and RG calculation to the $1d$ boundary of $2d$ SPT states (for instance the AKLT state), which was studied through exactly soluble lattice Hamiltonians [33] and also numerical methods [36, 37, 38]. Also, $1d$ defect in a $3d$ topological state can also have gapless modes [231, 232], it would be interesting to investigate the fate

of a $1d$ defect embedded in a $3d$ bulk at the bulk quantum phase transition. Defects of free or weakly interacting fermionic topological insulator and topological superconductor coupled with bulk critical modes was studied in Ref. 39, but we expect the defect of an intrinsic strongly interacting topological state can lead to much richer physics. Last but not least, the "higher order topological insulator" has nontrivial modes localized at the corner instead of the boundary of the system [233]. The coupling between the bulk quantum critical points and corner topological modes is also worth exploration.

Chapter 3

Quantum Phase Transitions in Moiré Systems

In this chapter, we continue to discuss the two examples of strongly correlated Moiré materials introduced in Sec. 1.6, i.e., the magic-angle twisted bilayer graphene and the TMD heterobilayer $MoTe_2/WSe_2$.

Since the discovery of superconductivity and correlated insulator at fractional electron fillings in the twisted bilayer graphene, most theoretical efforts have been focused on describing this system in terms of an effective extended Hubbard model. However, it was recognized that an exact tight-binding model on the Moiré superlattice which captures all the subtleties of the bands can be exceedingly complicated. In Sec. 3.1, we pursue an alternative framework of coupled wires to describe the system based on the observation that the lattice relaxation effect is strong at a small twist angle, which substantially enlarges the AB and BA stacking domains. Under an out-of-plane electric field which can have multiple origins, the low energy physics of the system is dominated by interconnected wires with (approximately) gapless $1d$ conducting quantum valley hall domain wall states. We demonstrate that the Coulomb interaction likely renders the wires a $U(2)_2$ $(1+1)d$

conformal field theory with a tunable Luttinger parameter for the charge $U(1)$ sector. Spin triplet and singlet Cooper pair operator both have quasi-long range order in this CFT. The junction between the wires at the AA stacking islands can lead to either a two-dimensional superconductor or an insulator.

It has been proposed that an extended version of the Hubbard model which potentially hosts rich correlated physics may be well simulated by the transition metal dichalcogenide (TMD) Moiré heterostructures. Motivated by recent reports of continuous metal-insulator transition (MIT) at half-filling, as well as correlated insulators at various fractional fillings in TMD Moiré heterostructures, in Sec. 3.2, we propose a theory for the potentially continuous MIT with fractionalized electric charges. The charge fractionalization at the MIT will lead to various experimental observable effects, such as a large critical resistivity as well as large universal resistivity jump at the continuous MIT. These predictions are different from previously proposed theory for interaction-driven continuous MIT. Physics in phases near the MIT will also be discussed.

3.1 Coupled-Wire Description of Correlated Physics in Twisted Bilayer Graphene

Surprising correlated physics such as superconductivity and correlated insulator at fractional electron fillings away from charge neutrality has been discovered in different systems with Moiré superlattices [234, 235, 236, 237], which motivated a series of active theoretical studies [238, 239, 240, 241, 242, 243, 244, 245, 246, 247, 248, 249, 250, 251, 36, 252, 253, 254, 141, 255, 256, 257, 258]. These systems have narrow electron bandwidth near charge neutrality [259, 260, 261, 262], hence interaction effects are significantly enhanced. In several systems that are microscopically different, for example, (1) the

heterostructure of trilayer graphene (TLG) and hexagonal boron nitride (hBN), and (2) twisted bilayer graphene (TBG), (3) twisted double bilayer graphene (TDBG) [263], insulating behavior was observed at commensurate fractional fillings away from the charge neutral point [234, 235, 237]; superconductivity has been observed in all these systems near the insulator phases [236, 237, 264, 263].

A consensus of the mechanism for the observed insulator and superconductor has not yet been reached. A minimal triangular lattice extended Hubbard model [238] at least describes the TLG/hBN heterostructure and twisted double bilayer graphene with certain out-of-plane electric field (displacement field) [239, 265, 266, 267], since in these cases there is no symmetry protected band touching below the fermi energy, and the isolated narrow band has trivial topology. This minimal model would then naturally predict either a spin-triplet [238] or spin-singlet $d + id$ topological superconductor [240], depending on the sign of the Hund's coupling. Signatures of spin triplet pairing predicted in Ref. [238] was recently found in TDBG [263], though further experiments are demanded to determine the exact pairing symmetry.

On the contrary, for one of the systems, *i.t.* the TBG, it was recognized that a standard tight binding model on the superlattice that captures all the subtleties of the band structure can be exceedingly complicated, and it may demand as many as ten bands for each valley and each spin component [140, 268], which makes analytical or numerical studies of this system very difficult. These results suggest that an alternative theoretical framework to understand the observed correlated physics is highly desired for the TBG. Here we pursue a coupled wire network framework to describe the TBG with a small twisted angle. A similar description based on coupled wires, such as the Chalker-Coddington model [143, 144], has been used to describe states without local Wannier orbitals. But in TBG, the coupled wire network description is not just motivated by theoretical convenience, it is also physically realistic, based on the following observations:

(1) At small twisted angle, the lattice relaxation and deformation effect is expected to be strong, and lead to substantially enlarged AB and BA stacking domains [5, 6], and narrow $1d$ domain walls.

(2) A displacement field will drive an AB (or BA) stacking bilayer graphene into a "quantum valley Hall insulator" [269, 270, 271, 272, 273, 274, 275], and this displacement field can be turned on manually experimentally [237], or intrinsically exists in the system due to lack of $\hat{z} \to -\hat{z}$ reflection symmetry (strongly asymmetric response to the displacement field was indeed observed in Ref. [237]), or even be generated spontaneously due to interaction [276]. Compared with a single layer graphene, in an AB (or BA) stacking bilayer graphene, interaction has much stronger effects due to the quadratic band touching at each valley [277, 278, 279, 280, 281].

(3) Under a uniform displacement field (regardless of its origin), the AB and BA stacking domains are quantum valley Hall insulators with opposite valley Hall conductivities, and they are separated by domain walls with conducting $1d$ states. The long wavelength modulation of the entire system prohibits large momentum transfer, hence the valley quantum number is approximately conserved, and the domain wall states are approximately gapless. These conducting wires (AB/BA domain walls) have been observed directly in numerics [282] and experiment on TBG [7, 283].

In fact, an effective network model has been proposed to describe the noninteracting physics of the system [145]. In the current work we will focus on the correlated phenomena. Along each $1d$ wire, there are four counter-propagating localized electron modes, which without interaction would constitute the $U(4)_1$ conformal field theory (CFT). The $1d$ fermions carry three quantum numbers: valley (L, R), spin $(\uparrow, \downarrow)$, and channel $(1, 2)$

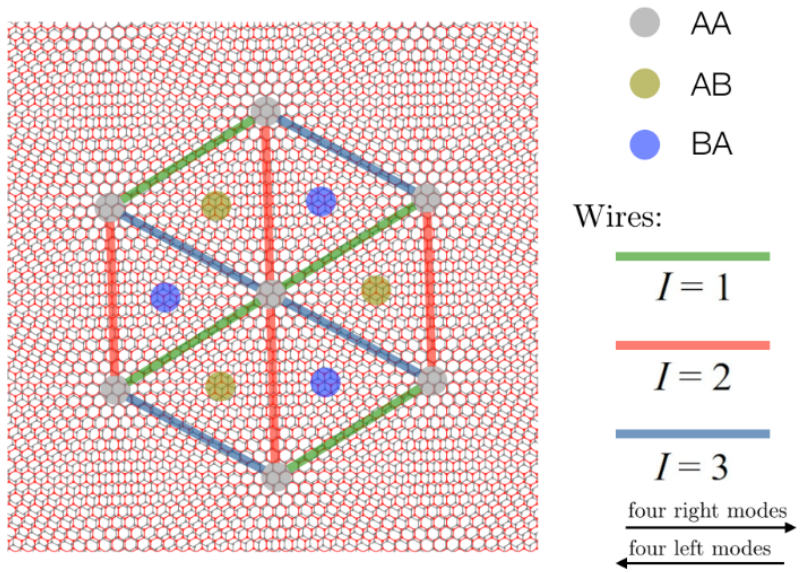

Figure 3.1: The Moiré superlattice of TBG. If the lattice relaxation and deformation effect is taken into account [5, 6, 7], the AB/BA stacking domains would be substantially enlarged. There are four (two channels and two spin components) left moving fermion modes and four right moving modes along each wire (AB/BA domain wall). The left and right moving fermions differ by a large lattice momentum (orthogonal to the wires) which is the size of the Brillouin zone of the original honeycomb lattice.

index (Fig. 3.1):

$$H = \int dx \sum_{c=1,2} \sum_{\alpha=\uparrow,\downarrow} iv(\psi^\dagger_{L,c,\alpha}\partial_x\psi_{L,c,\alpha} - \psi^\dagger_{R,c,\alpha}\partial_x\psi_{R,c\alpha}). \tag{3.1}$$

The left and right moving modes come from two different valleys (which differ by a large momentum orthogonal to the wire), and each valley will contribute two channels of chiral fermions, each with two degenerate spin components. The displacement field in experiment (for instance 0.5V/nm) corresponds to a much higher energy scale compared with the sub kelvin environment of the experiments. Thus we can safely assume that the quantum valley Hall insulators are rather robust and these $1d$ wires, which form a triangular lattice network, are dominating the low energy physics.

The most important interaction in the system is still the Coulomb interaction. The

most noticeable effect of the Coulomb interaction is to energetically favor two electrons to form a "channel-singlet" state, which is very similar to the mechanism of the standard Hund's rule in transition metals. Let us consider two electrons with the following two-body wave functions $\Psi_A(\mathbf{x}_1, \mathbf{x}_2)$ and $\Psi_B(\mathbf{x}_1, \mathbf{x}_2)$ ($\mathbf{x}_1$, $\mathbf{x}_2$ are $2d$ coordinates):

$$\begin{aligned}\Psi_A(\mathbf{x}_1, \mathbf{x}_2) \sim\ & \varphi_{L,1}(\mathbf{x}_1)\varphi_{R,2}(\mathbf{x}_2) - \varphi_{L,2}(\mathbf{x}_1)\varphi_{R,1}(\mathbf{x}_2) \\ & + \varphi_{R,1}(\mathbf{x}_1)\varphi_{L,2}(\mathbf{x}_2) - \varphi_{R,2}(\mathbf{x}_1)\varphi_{L,1}(\mathbf{x}_2), \qquad (3.2)\\ \Psi_B(\mathbf{x}_1, \mathbf{x}_2) \sim\ & \varphi_{L,1}(\mathbf{x}_1)\varphi_{R,2}(\mathbf{x}_2) - \varphi_{L,2}(\mathbf{x}_1)\varphi_{R,1}(\mathbf{x}_2) \\ & - \varphi_{R,1}(\mathbf{x}_1)\varphi_{L,2}(\mathbf{x}_2) + \varphi_{R,2}(\mathbf{x}_1)\varphi_{L,1}(\mathbf{x}_2). \qquad (3.3)\end{aligned}$$

Here $\varphi_{L,1}(\mathbf{x})$ represents the spatial wave function of the left-moving fermions (which comes from one of the two valleys) at channel 1. Both states $\Psi_{A,B}$ are "channel singlet" states (they are antisymmetric in the channel indices), while Ψ_A is symmetric in the valley space, Ψ_B is antisymmetric in the valley space. The spin space wave function was not written down but can be straightforwardly inferred. Both states cost low energy under Coulomb interaction, *i.e.* they have considerable lower energy compared with states that are symmetric in the channel space, and this energy difference is not suppressed by large momentum transfer (more detailed estimate will be given in the supplementary material). Thus the channel space is analogous to the gauged "color space" of spin chains [284, 285], which must form a color singlet state.

A $U(4)_1$ CFT can be decomposed as

$$U(4)_1 \sim U(1)_4^e \oplus SU(2)_2^s \oplus SU(2)_2^c, \qquad (3.4)$$

where $SU(2)_2^c$ corresponds to the sector of the channel space. The interaction effect discussed in the previous paragraph contributes to the marginally relevant term $\lambda \mathcal{J}_L^c \cdot \mathcal{J}_R^c$

in the CFT, where $\mathcal{J}^c_{L,R}$ are the left and right Kac-Moody currents of the channel space, and it will gap out the $SU(2)^c_2$ sector of the CFT. The residual degrees of freedom would form CFT

$$U(2)_2 \sim U(1)^e_4 \oplus SU(2)^s_2. \tag{3.5}$$

The $U(1)^e_4$ sector of the CFT corresponds to the charge degrees of freedom, and it can be represented by a pair of conjugate bosons θ and ϕ which satisfy $[\nabla_x\phi, \theta] = [\nabla_x\theta, \phi] = i$. The $SU(2)^s_2$ corresponds to the spin degrees of freedom, and as we discussed before, due to the prohibition of large momentum transfer, the left and right modes have approximately separate spin $SU(2)$ symmetries. The $SU(2)^s_2$ CFT can be represented by a $(1+1)d$ nonlinear sigma model whose order parameter is a $SU(2)$ matrix $g_{\alpha\beta}$, plus a Wess-Zumino-Witten term at level-2 [286]. The left and right spin symmetry acts on $g_{\alpha\beta}$ as the left and right $SU(2)$ transformations.

Physical operators can be represented as CFT fields. For example, a fermion mass operator (which is a back-scattering term) can be written as [286]

$$\hat{M}_{\alpha\beta} = \sum_c \psi^\dagger_{L,c,\alpha}\psi_{R,c,\beta} \sim \exp\left(i\sqrt{\pi}\phi\right) g_{\alpha\beta}, \tag{3.6}$$

where $g_{\alpha\beta}$ is the spin $SU(2)$ matrix order parameter mentioned previously. Notice that the mass operator must be a channel singlet, because otherwise it must involve the $SU(2)^c_2$ sector, which as we argued is already gapped out.

Likewise, a Cooper pair operator can be written as

$$\hat{\Delta}_{\alpha\beta} = \epsilon_{\alpha\gamma}\epsilon_{cd}\psi_{L,c,\gamma}\psi_{R,d,\beta} \sim \exp\left(i\sqrt{\pi}\theta\right) g_{\alpha\beta}, \tag{3.7}$$

θ and ϕ are the pair of conjugate bosons that describe the charge sector of the CFT. The

representation of the mass operator $\hat{M}_{\alpha\beta}$ is given in Ref. [286]. The Cooper pair operator representation can be inferred by defining a new set of fermions: $\tilde{\psi}_L = \epsilon\epsilon\psi_L^\dagger$, $\tilde{\psi}_R = \psi_R$, where the two ϵ matrices act in the spin and channel indices respectively. The fermion operator $\tilde{\psi}_L$ transforms exactly the same as ψ_L in the channel and spin space, but carries opposite charge. The Cooper pair operator in Eq. 3.7 becomes precisely the mass term (backscattering) between $\tilde{\psi}_L$ and $\tilde{\psi}_R$.

The Cooper pair operator $\hat{\Delta}_{\alpha\beta}$ is a channel singlet pairing. The pairing matrix $\hat{\Delta}_{\alpha\beta}$ can always be expanded as a four component vector $(\Delta^0, \vec{\Delta})$:

$$\hat{\Delta}_{\alpha\beta} = \Delta^0 \mathbf{1}_{2\times 2} + i\vec{\Delta}\cdot\vec{\sigma}. \tag{3.8}$$

Here Δ^0 is a spin singlet pairing order parameter, while $\vec{\Delta}$ is a spin triplet pairing order parameter. Together they form a four component vector representation under the $SO(4) \sim SU(2)_L \times SU(2)_R$ symmetry. Without a further Hund's (or anti-Hund's) coupling that favors either spin triplet or singlet pairing, these four components pairing order parameters are all degenerate. In the supplementary material, we discuss a different method to obtain the CFT field expressions Eq. 3.6 and Eq. 3.7 where the fermion mass and the Cooper pair operators are treated on equal footing.

The scaling dimensions of the fermion mass and Cooper pair operators are

$$[\hat{M}_{\alpha\beta}] = \frac{3}{8} + \frac{1}{4K}, \qquad [\hat{\Delta}_{\alpha\beta}] = \frac{3}{8} + \frac{K}{4}, \tag{3.9}$$

where 3/8 comes from the scaling dimension of the g matrix order parameter in the $SU(2)_2^s$ CFT, and K is the Luttinger parameter in the $U(1)_4^e$ CFT. Soon we will see that these scaling dimensions will determine whether the system becomes superconductor or insulator due to wire junctions at the AA islands. Notice that both $\hat{M}_{\alpha\beta}$ and $\hat{\Delta}_{\alpha\beta}$

can simultaneously have lower scaling dimensions (which implies enhanced correlation) compared with noninteracting $1d$ fermion systems, where both operators have scaling dimensions 1. Thus the interaction which gaps out the $SU(2)^c$ channel space indeed enhances the system's tendency to form superconductor and insulator.

The $U(1)_4^e$ CFT deserves some clarifications. It can always be written as a free boson theory with the Hamiltonian:

$$H = \int dx \, \frac{1}{2K}(\nabla_x \theta)^2 + \frac{K}{2}(\nabla_x \phi)^2. \tag{3.10}$$

θ and ϕ are a pair of conjugate bosons. We can fermionize this theory through standard procedure, and define new fermion operators as

$$C_{L,R} \sim \eta_{L,R} \exp(i\sqrt{\pi}\theta \pm i\sqrt{\pi}\phi), \tag{3.11}$$

where $\eta_{L,R}$ are the Klein factors. Then the Cooper pair and the mass term of the new fermion $C_{L,R}$ should be represented as $\exp(i\sqrt{4\pi}\theta)$, and $\exp(i\sqrt{4\pi}\phi)$. But these Cooper pairs should correspond to the charge$-4e$ bound state of the electrons, and the mass term should correspond to a two electron backscattering. This is because under the assumption of separate left and right spin $SU(2)$ symmetries, a charge$-2e$ Cooper pair, or a singlet electron back scattering term, cannot be invariant under the $SU(2)_L \times SU(2)_R$ spin symmetry. Later we will show that the charge$-4e$ $U(1)^e$ sector may become relevant to the finite temperature physics of the system.

The $1d$ CFTs will intersect at the AA stacking islands, and due to the lattice relaxation and deformation, the size of the AA stacking islands has shrunk [5]. Let us first look at a single AA island which is a junction between CFTs along three directions. At this junction, the Cooper pairs can tunnel between $1d$ CFTs along different wires. This

Josephson tunnelling between CFTs can be described by a $(0+1)d$ action at the junction

$$\mathcal{S} = \int d\tau \sum_{I,J} u_0 \Delta^{0\dagger}_{\hat{e}_I} \Delta^0_{\hat{e}_J} + u_1 \vec{\Delta}^\dagger_{\hat{e}_I} \cdot \vec{\Delta}_{\hat{e}_J}, \tag{3.12}$$

$\hat{e}_I$ with $I = 1, 2, 3$ represent wires along three directions that meet at this junction. The scaling dimension of u_0 and u_1 are both $[u_0] = [u_1] = 1/4 - K/2$, where K is the Luttinger parameter in Eq. 3.10, thus when $K < 1/2$ even a single junction Josephson Cooper pair tunnelling becomes relevant, and we expect this Josephson tunnelling to drive the entire system into a superconductor. If we take into account of the tunnelling between parallel wires, which happens along the entire $1d$ wires rather than one junction, then this parallel tunnelling will be relevant and the entire system becomes a superconductor for $K < 5/2$.

Here we allow u_0 and u_1 to be different, which breaks the two separate $SU(2)$ spin symmetries to its diagonal spin $SU(2)$ symmetry. The AA island has shrunk substantially due to lattice relaxation, thus the potential modulates at a shorter length scale compared with other regions of the system, which enhances the large momentum transfer and leads to the mixing between the left and right $SU(2)$ symmetries. If u_0 dominate u_1, the system would favor to form a global spin singlet pairing. Now the global structure of the system can be mapped to the following classical XY model:

$$H \sim \sum_{\vec{r}} -V \sum_{I=1}^{3} \cos(\theta^I_{\vec{r}} - \theta^I_{\vec{r}+a\hat{e}_I}) + u_0 \sum_{I,J=1}^{3} \cos(\theta^I_{\vec{r}} - \theta^J_{\vec{r}}) + \cdots \tag{3.13}$$

Here $\vec{r}$ denote the AA stacking islands of the lattice, and $\hat{e}_I$ with $I = 1, 2, 3$ are unit vectors along the wires (Fig. 3.1). a is the distance between two AA stacking islands, and $\theta^I_{\vec{r}}$ is the phase angle of the spin singlet Cooper pair of wire along direction $\hat{e}_I$. The ellipsis in Eq. 3.13 represent other weaker terms allowed by symmetry in the system

Here naturally $V > 0$, which reflects the fact that along each wire the superconduc-

wires	$u_0 < 0$, s-wave pairing	$u_0 > 0$, $d + id$ or $d - id$ pairing
$I = 1$	Δ	Δ
$I = 2$	Δ	$\Delta e^{\pm i \frac{2\pi}{3}}$
$I = 3$	Δ	$\Delta e^{\mp i \frac{2\pi}{3}}$

Table 3.1: The SC order parameter along different wires, with $u_0 < 0$ and $u_0 > 0$ in Eq. 3.13. The index I refers to the wires in Fig. 3.1.

tor order parameter has a quasi long range order and prefers the Cooper pair to have a uniform pairing phase along the wire. Then when $u_0 < 0$, the Josephson couplings between different wires are "unfrustrated", hence the entire system should form a spin singlet $s-$wave pairing with a uniform pairing phase; while when $u_0 > 0$, the Josephson coupling between wires along three directions is "frustrated". The two terms in Eq. 3.13 demands a uniform θ^I along direction $\hat{e}_I$, while wires that intersect each other at one island will have Cooper pair phases which differ from each other by ± 120 degrees. Then the pairing symmetry of the entire system is identical to the $d + id$ (or $d - id$) pairing, as under a spatial 60 degree rotation (a cyclic permutation between wires along three directions), the pairing phase angle changes by ± 120 degrees. This $d + id$ pairing superconductor is a singlet of spin, valley, and channel indices.

When u_1 dominates u_0 in Eq. 3.12, the system will form a spin triplet superconductor. As an example let us assume that $\vec{\Delta}_{\hat{e}_I}(\vec{r}) = \exp(i\theta^I_{\vec{r}})\vec{n}^I_{\vec{r}}$ (the real and imaginary parts of the spin triplet Cooper pair are parallel with each other), which is similar to the so called "polar state" of Bose-Einstein condensate (BEC) of the spin-1 spinor cold atoms [287, 288, 289]. Then the effective Hamiltonian of the coupled Josephson wires reads

$$H \sim \sum_{\vec{r}} -V \sum_{I=1}^{3} \vec{n}^I_{\vec{r}} \cdot \vec{n}^I_{\vec{r}+a\hat{e}_I} \cos(\theta^I_{\vec{r}} - \theta^I_{\vec{r}+a\hat{e}_I}) + u_1 \sum_{I,J=1}^{3} \vec{n}^I_{\vec{r}} \cdot \vec{n}^J_{\vec{r}} \cos(\theta^I_{\vec{r}} - \theta^J_{\vec{r}}) + \cdots \quad (3.14)$$

When $u_1 < 0$, the system forms a uniform $s-$wave spin triplet pairing. When $u_1 > 0$,

again the Josephson coupling on every AA island is frustrated, then the system either forms a uniform state of θ, with a 120 degree "antiferromagnetic" pattern of $\vec{n}$, or forms a $d+id$ pattern of θ, with a "ferromagnetic" state of $\vec{n}$. Other symmetry allowed terms, or quantum fluctuation may lift the degeneracy of the two scenarios described above.

There is a Z_2 gauge transformation shared between $\exp(i\theta^I_{\vec{r}})$ and $\vec{n}^I_{\vec{r}}$, *i.e.* the spin triplet pairing order parameter is invariant under $\vec{n}^I_{\vec{r}} \to -\vec{n}^I_{\vec{r}}$ and $\theta^I_{\vec{r}} \to \theta^I_{\vec{r}} + \pi$. At any finite temperature, the vectors $\vec{n}^I_{\vec{r}}$ will be disordered due to thermal fluctuation because this system is purely two dimensional, then as was predicted in Ref. [238], the superconductor vortex at finite temperature will carry magnetic flux quantized as $nhc/(4e)$. This means that the charge sector will form an effective charge$-4e$ superconductor with algebraic correlation of charge$-4e$ order parameters. This charge-$4e$ superconductor is qualitatively the same as the Cooper pair of the fermions $C_{L,R}$ defined before. The same logic led to fractionalized vortices of the polar state of spin-1 BEC, which was confirmed numerically in Ref. [289].

At the AA islands, symmetry also allows charge backscattering within each wire. The charge sector of the system is described by the C fermions defined in Eq. 3.11. C_L and C_R come from two different valleys in the bulk, which project to the same momentum (Dirac crossing) along the $1d$ domain wall. Upon doping away from charge neutrality, the $C_{L,R}$ fermion will acquire a fermi wave vector $\pm\delta k_f$ away from the Dirac crossing, thus a backscattering involves a momentum transfer of $2\delta k_f$. The backscattering of the C fermion is described by

$$\mathcal{S} = \int d\tau dx \; uU(x) \left(C_L^\dagger C_R e^{2i\delta k_f x} + H.c. \right) \tag{3.15}$$

where $U(x)$ is the periodic potential along the wire due to the AA stacking islands. If the integral along the entire wire $\int dx U(x) e^{i2\delta k_f x}$ is nonzero, then this implies that

$2\delta k_f = \pm 2\pi/a$, where a is the lattice constant of the Moiré superlattice, or the distance between two AA stacking islands. This implies that there must be extra integer multiple of $\pm 2e$ charges between two AA islands on each wire (one C fermion carries charge $2e$). And if wires along two directions acquire $+2e$ between every two neighboring AA islands, and the wires along the third direction acquire $-2e$ between AA islands, the entire system becomes an insulator at half-filling away from charge neutrality with $+2e$ charge per unit cell on the superlattice. The insulator observed at the 1/4 filling should correspond to two particle backscattering, which is a much weaker effect. The backscattering will be more relevant with larger Luttinger parameter K.

We also notice that in experiment the resistivity at the same charge density can strongly depend on the displacement field [237]. This is a natural phenomenon in our formalism, because a stronger displacement field would lead to a larger gap in the quantum valley Hall insulator, and hence stronger localization of the electron wave function at the wires. Stronger localization of the domain wall states would lead to a stronger effective particle density-density interaction in the $(1+1)d$ CFT, and hence a larger Luttinger parameter K based on the standard bosonization formalism. A larger K would render the backscattering at the AA islands more relevant. This means that the Luttinger parameter K is tunable by the displacement field, and the field can potentially lead to a metal-insulator transition.

Summary: We study the correlated physics of the TBG based on a coupled wire framework. The low energy physics of the system is dominated by the conducting wires which are the domain walls between the AB/BA domains. These domains are enlarged due to lattice relaxation, and are driven into the quantum valley Hall insulators under a displacement field which can have multiple origins. The observed superconductivity and the correlated insulator of the system are interpreted as consequences of the Josephson tunneling and also backscattering at the AA stacking islands, which are the junctions

where the wires along three directions meet. One puzzle from the experiment is the weakness of the insulators at fractional fillings. In our description, the insulating behavior is due to the backscattering at the AA islands, which is still suppressed due to large momentum transfer (large momentum transfer orthogonal to the wire, which is still approximately defined due to the smoothness of the background potential), thus it will at most lead to a weak correlated insulator. In our formalism, a displacement field can tune the Luttinger parameter of the CFT, and hence affect the relevance of backscattering and also charge transport, as was observed experimentally.

3.2 Interaction-Driven Metal-Insulator Transition with Charge Fractionalization

3.2.1 Introduction

Many correlated phenomena have been observed in graphene-based moiré systems, such as high temperature superconductivity (compared with the bandwidth of the moiré bands), correlated insulators [2, 3, 129, 130, 131, 132, 133, 134, 135], and the strange metal phase [70, 136], etc. The most fundamental reason for the emergence of these correlated physics is that the slow modulating moiré potential leads to very narrow bandwidths [138, 139]. Great theoretical interests and efforts have been devoted to the graphene based moiré systems [290, 291, 248, 249, 292, 293, 294, 295, 254, 296, 297, 298, 299, 300, 301, 302, 303, 304]. But the theoretical description and understanding of the graphene based moiré systems may be complicated by the fact that in the noninteracting limit the moiré mini bands can have various types of either robust or fragile nontrivial topologies [305, 306, 307, 308, 309, 310, 311, 312, 313, 314], although the exact role of the band topology to the interacting physics at fractional filling is not entirely clear.

Hence similar narrow band systems with trivial band topology and unambiguous concise theoretical framework would be highly desirable. It was proposed that much of the correlated physics of the transition metal dichalcogenide (TMD) moiré heterostructure can be captured by an extended Hubbard model with an effective spin-1/2 electron on a triangular moiré lattice [146]

$$H = \sum_{\boldsymbol{r},\boldsymbol{r}',\alpha} -t_{\boldsymbol{r},\boldsymbol{r}'} c^{\dagger}_{\boldsymbol{r},\alpha} c_{\boldsymbol{r}',\alpha} + H.c. + \sum_{\boldsymbol{r}} U n_{\boldsymbol{r},\uparrow} n_{\boldsymbol{r},\downarrow} + \cdots \tag{3.16}$$

The electron operator $c_{\boldsymbol{r},\alpha}$ is constructed by states within a topologically trivial moiré mini band. Due to the strong spin-orbit coupling, the spin and valley degrees of freedom are locked with each other in the TMD moiré system. We will use $\alpha = \uparrow, \downarrow$ or $1, 2$ to denote two spin or equivalently two valley flavors. When a moiré band is partially filled, the correlated physics within the partially filled moiré mini bands may be well described by Eq. 3.16, which only contains half of the degrees of freedom of a mini band in a graphene based moiré system. The ellipsis in Eq. 3.16 can include further neighbor hopping, "spin-orbit" coupling terms allowed by symmetry [315], and further neighbor interaction. Note the "spin-orbit" coupling here refers to the hopping terms in Eq. 3.16 that depend on the spin index α and should not be confused with the bare spin-orbit coupling within the TMD system before the moiré superlattice is imposed. The TMD moiré systems are hence considered as a simulator for the extended Hubbard model on a triangular lattice [316].

Like the graphene-based moiré systems, the TMD moiré heterostructure is a platform for many correlated physics. This manuscript mainly concerns the metal-insulator transition (MIT) driven by interaction. The MIT of the Hubbard model on a triangular lattice has attracted much numerical efforts recently [317, 318]. The symmetry of the TMD moiré heterostructure is different from the simplest version of the Hubbard model,

hence even richer physics can happen in the system. Continuous MIT has been reported at half-filling of the moiré bands (electron filling $\nu = 1/2$, or one electron per moiré unit cell on average) in the TMD moiré system [4, 319]. The experimental tuning parameter of the MIT in the TMD heterostructure is the displacement field, i.e. an out-of-plane electric field, which tunes the width of the mini moiré bands, and hence the ratio between the kinetic and interaction energies in the effective Hubbard model. Correlated insulators have also been observed at various other fractional electron fillings, though the nature of the MITs at these fractional fillings have not been thoroughly inspected experimentally [320, 321, 322, 323]. In this manuscript we will mainly focus on $\nu = 1/2$, but other fractional fillings will also be briefly discussed.

The nature of an interaction driven MIT depends on the nature of the insulator phase near the MIT. The Hubbard model on the triangular lattice has one site per unit cell, which based on the generalized Lieb-Shultz-Matthis theorem [20, 22] demands that the insulator phase at half-filling should not be a trivial incompressible (gapped) state which preserves the translation symmetry. If the insulator phase has a semiclassical spin order that breaks the translation symmetry, the evolution between the metal and insulator could involve two transitions: at the first transition a semiclassical spin order develops, which reduces the Fermi surface to several Fermi pockets; and at the second transition the size of the Fermi pockets shrink to zero, and the system enters an insulator phase. A more interesting scenario of the MIT only involves one single transition [324, 86, 87], but then the insulator phase is not a semiclassical spin order, instead it is a spin liquid state with a spinon Fermi surface. An intuitive picture for this transition is that, at the MIT, the charge degrees of freedom are gapped, but the spins still behave as if there is a "ghost" Fermi surface. The spinon Fermi surface can lead to the Friedel oscillation just like the metal phase [325]. The structure of the Fermi surface does not change drastically across the transition.

In a purely two dimensional system, conductivity (or resistivity) is a dimensionless quantity, hence it can take universal value at the order of e^2/h (or h/e^2) in various scenarios. For example, the Hall conductivity of the quantum Hall state is precisely $\sigma_H = \nu e^2/h$; the conductivity (or resistivity) at a $(2+1)d$ quantum critical point also takes a universal value at the order of e^2/h (or h/e^2) [326]. One central prediction given by the theory above for interaction driven continuous MIT is that, there is a universal resistivity jump at the order of $\sim h/e^2$ at the MIT compared with the metal phase; and the critical resistivity at the MIT should also be close to the order of h/e^2 (we will review these predictions in the next section). In this manuscript we will argue that the current experimental observations suggest that the nature of the MIT in $MoTe_2/WSe_2$ moiré superlattice without twisting [4] is beyond the previous theory [324, 86, 87], and we propose an alternative candidate theory of MIT with further charge fractionalizations. We will discuss how the alternative theory can potentially address the experimental puzzles, and more predictions based on our theory will be made. Our assumption is that the MIT in this system is indeed driven by electron-electron interaction (as was suggested by Ref. 4); If the disorder plays the dominant role in this system, the MIT may be described by the picture discussed in Ref. 327.

The paper is organized as follows: In section 3.2.2 we introduce an alternative parton construction for systems described by the extended Hubbard model with a spin-orbit coupling, which naturally leads to charge fractionalization at the interaction-driven MIT even at half-filling; we also give an intuitive argument of physical effects caused by charge fractionalization at the MIT. In section 3.2.3, we will discuss the theory for MIT when the insulating phase spontaneously breaks the translation symmetry. Section 3.2.4 studies the theory of MIT when the insulating phase has different types of topological orders. In section 3.2.5 we discuss various experimental predictions based on our theory, for the MIT and also the phases nearby. We present the details of our theory in the appendix,

including the projective symmetry group, field theories, and calculation of DC resistivity, etc.

3.2.2 Two Parton Constructions

The previous theory for the interaction-driven continuous MIT for correlated electrons on frustrated lattices was based on a parton construction. The parton construction splits the quantum number of an electron into a bosonic parton which carries the electric charge, and a fermionic parton which carries the spin. In the current manuscript we compare two different parton constructions:

$$\mathrm{I} : c_{\boldsymbol{r},\alpha} = b_{\boldsymbol{r}} f_{\boldsymbol{r},\alpha}, \qquad \mathrm{II} : c_{\boldsymbol{r},\alpha} = b_{\boldsymbol{r},\alpha} f_{\boldsymbol{r},\alpha}. \tag{3.17}$$

In parton construction-I only one species of charged bosonic parton b is introduced for electrons with both spin/valley flavors; while in parton construction-II a separate charged bosonic parton b_α is introduced for each spin/valley flavor. As we will see later, the two different parton constructions will lead to very different observable effects. The construction-I is the standard starting point of the theory of MIT that was used in previous literature [324, 86, 87]; construction-II is usually unfavorable for systems with a full spin SU(2) invariance, because the parton construction itself breaks the spin rotation symmetry. But the construction-II is a legitimate parton construction for the system under study, whose band structure in general does not have full rotation symmetry between the two spin/valley flavors.

The time-reversal symmetry of the microscopic TMD system relates the two spin/valley flavors. But it is not enough to guarantee a full SU(2) rotation symmetry between the two flavors. In fact, since the two flavors can be tied to the two valleys of the TMD material, the trigonal warping of the TMD bands, which takes *opposite* signs for the

two different valleys, can lead to the breaking of such an SU(2) rotation symmetry. To estimate the trigonal warping effect in the Hubbard model, one can compare the k^2 term and the $k_x^3 - 2k_x k_y^2$ term in the electron dispersion of one of the two layers in the heterostructure expanded at one valley. Then the relative strength of the trigonal warping compared to the SU(2)-invariant hopping in Eq. 3.16 is given by the ratio between the lattice constant of the original TMD material and that of the morié superlattice. In addition, the natural microscopic origin of the interactions in the Hamiltonian Eq. 3.16 is the Coulomb interaction between the electrons. The Coulomb interaction when projected to the low-energy bands relevant to the moiré-scale physics is expected to contain SU(2)-breaking interaction terms. The momentum conservation only guarantees the valley U(1) symmetry. Assuming the unscreened Coulomb interaction between electrons before the projection to the low-energy bands, further neighbor interaction will appear in the extended Hubbard model. The relative strength of the SU(2)-breaking interaction terms obtained from the projection compared to the SU(2)-invariant interactions can again be estimated by the ratio between the lattice constant of the original TMD material and the moiré superlattice, as the Fourier transform of unscreened Coulomb interaction in $2d$ space is $V_q \sim 1/q$.

The most important difference between these two parton theories resides in the filling of the bosonic partons. Since each bosonic parton carries the same electric charge as an electron, the total number of bosonic partons should equal to the number of electrons. Hence at electron filling ν (meaning 2ν electrons per unit cell), the filling factor of boson b in construction-I is $\nu_b = 2\nu$, i.e. 2ν bosonic parton per unit cell; in construction-II the filling factor of boson b_α has filling factor $\nu_b^\alpha = \nu$ for each spin/valley flavor. Hence even with one electron per site (half-filing or $\nu = 1/2$ of the extended Hubbard model), the bosonic parton in construction-II is already at half filling for each spin/valley flavor. The half-filling will lead to nontrivial features inside the Mott insulator phase, as well

as at the MIT. Another more theoretical difference is that, in construction-I there is one dynamical emergent U(1) gauge field a_μ which couples to both b and f_α; while in construction-II there are two dynamical U(1) gauge fields $a_{\alpha,\mu}$, one for each spin/valley flavor.

In construction-I, the bosonic parton b is at integer filling, and the MIT is naturally interpreted as a superfluid to Mott insulator (SF-MI) transition of boson b. At the MIT, using the Ioffe-Larkin rule [328], the DC resistivity of system is $\rho = \rho_b + \rho_f$, where ρ_b and ρ_f are the resistivity contributed by the bosonic and fermionic partons respectively. ρ_f caused by disorder or interaction such as the Umklapp process is a smooth function of the tuning parameter, the drastic change of ρ across the MIT arises from ρ_b. In the metal phase, i.e. the "superfluid phase" of b, ρ_b is zero, and the total resistivity is just given by ρ_f. Also, in the superfluid phase of b, the U(1) gauge field a_μ that couples to both b and f_α is rendered massive due to the Higgs mechanism caused by the condensate of b. In the insulator phase, ρ_b and ρ are both infinity, and the system enters a spin liquid phase with a spinon Fermi surface of f_α that couples to the dynamical U(1) gauge field a_μ. The MIT which corresponds to the condensation of b belongs to the 3D XY universality class. The dynamical gauge field a_μ is argued to be irrelevant at the transition due to the overdamping of the gauge field that arises from the spinon Fermi surface [86, 87], and hence does not change the universality class of the SF-MI transition of b.

In parton construction-I, at the MIT the bosonic parton contribution to the resistivity ρ_b is given by $\rho_b = Rh/e^2$, where R is an order-1 universal constant. In the order of limit $T \to 0$ before $\omega \to 0$, R is associated to the 3D XY universality class [329], because the gauge field a_μ is irrelevant as mentioned above. This universal conductivity at the 3D XY transition has been studied through various analytical and numerical methods [326, 330, 331, 332, 333, 334, 335, 336, 337]. At finite T and zero frequency, the gauge field a_μ can potentially enhance the value R to $R' > R$, based on a large-$\mathbf{N}$

calculation in Ref. 111 ($\mathbf{N}$ is different from N in our work). The evaluation in Ref. 111 gave $R' \sim 7.92$, while we evaluate the same quantity to be $R' \sim 7.44$. Hence the prediction of the construction-I is that, the DC resistivity of the system right at the MIT has a universal jump compared with the resistivity at the metallic phase close to the MIT [86, 87], i.e. $\Delta\rho = \rho_b = R'h/e^2$. With moderate disorder, at the MIT ρ_b of the bosonic parton is supposed to dominate the resistivity ρ_f of the fermionic parton f_α, hence the total resistivity $\rho = \rho_b + \rho_f$ should be close to ρ_b.

In the experiment on the $MoTe_2/WSe_2$ moiré superlattice, it was reported that disorder in the system is playing a perturbative role, and the continuous MIT is mainly driven by the interaction [4]. However, the reported resistivity ρ increases rapidly with the tuning parameter (the displacement field) near the MIT. The bare value of ρ near and at the MIT is significantly greater than h/e^2 (and significantly larger than the computed value of $\rho_b \sim R'h/e^2$ mentioned above), and it is clearly beyond the Mott-Ioffe-Regel limit, i.e. the system near and at the MIT is a very "bad metal" [338, 339]. This suggests that the MIT is not a simple SF-MI transition of b, or in other words b should be "much less conductive" compared with what was predicted in construction-I considered in previous literature. We will demonstrate that construction-II can potentially address the large resistivity at the MIT. The most basic picture is that, since b_1 and b_2 are both at half-filling, the LSM theorem [20, 22] dictates that the Mott insulator phase of each flavor of boson cannot be a trivial insulator, namely the Mott insulator must either be a density wave that spontaneously breaks the translation symmetry, or have topological order. In either case, the MIT is not a simple 3D XY transition, and the most prominent feature of the transition is that, the bosonic parton number (or the electric charge) must further fractionalize.

The MIT with charge fractionalization will be discussed in detail in the next section using the dual vortex formalism, but the consequence of this charge fractionalization can

be understood from a rather intuitive picture. Suppose b fractionalizes into N parts at the MIT, meaning the charge carriers at the MIT have charge $e_* = e/N$, then each charge carrier will approximately contribute a resistivity at the order of $h/e_*^2 \sim N^2 h/e^2$ at the MIT; and if there are in total N_b species of the fractionalized charge carriers, at the MIT the bosonic parton will approximately contribute resistivity

$$\rho_b \sim \frac{N^2 h}{N_b e^2}. \tag{3.18}$$

There is a factor of N_b in the denominator because intuitively the total conductivity of b will be a sum of the conductivity of each species of fractionalized charge carriers, i.e. $\sigma_b = \sum_{j=1}^{N_b} \sigma_j$, in the unit of e^2/h (a more rigorous rule of combining transport from different partons will be discussed later). Hence when $N^2/N_b > 1$, the construction-II with inevitable charge fractionalization can serve as a natural explanation for the large ρ at the MIT, and it will also predict a large jump of resistivity $\Delta\rho$ at the MIT.

3.2.3 Mott Insulator with Translation Symmetry Breaking

General Formalism

In this section we will discuss the MIT following the parton construction-II discussed in the previous section. The MIT is still interpreted as the SF-MI transition of both spin/valley flavors of the bosonic parton b_α, although as we discussed previously the insulator cannot be a trivial incompressible state of b_α. In the superfluid phase of b_α, both U(1) gauge fields $a_{1,\mu}$ and $a_{2,\mu}$ that couple to the two flavors of partons are gapped out by the Higgs mechanism, and the system enters a metal phase of the electrons; b_1 and b_2 must undergo the SF-MI transition simultaneously, since the time-reversal or spatial reflection symmetries both interchange the two flavors of partons due to the spin-valley

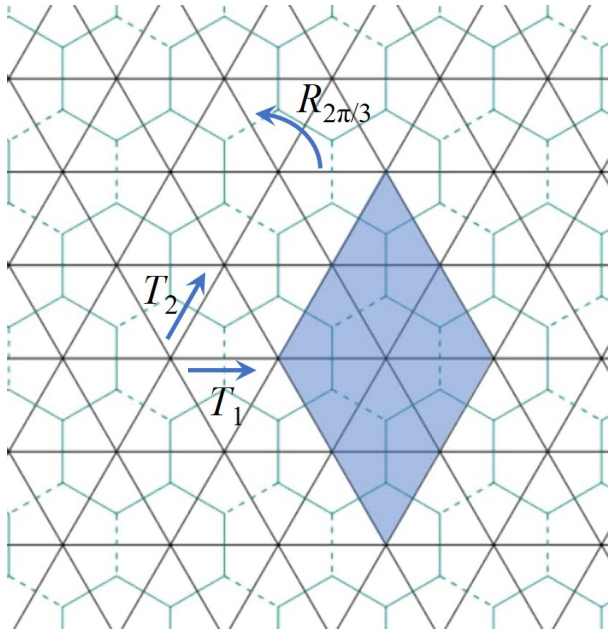

Figure 3.2: The triangular moiré lattice, and its dual honeycomb lattice. In the parton construction-II, the bosonic parton b_α is at half-filling for each spin/valley flavors, which becomes a $\pi-$flux of the dual gauge field A_μ through the hexagon of the dual honeycomb lattice. Hence the vortex ψ defined on the dual honeycomb lattice does not have a uniform hopping amplitude, the dashed links on the dual honeycomb lattice have negative hopping amplitudes. The symmetry of the lattice will be realized as a projective symmetry group. There are eight dual sites per unit cell (shaded area) in this gauge choice. At each spin/valley flavor, there are translation symmetries $T_{1,2}$, a rotation symmetry $R_{\frac{2\pi}{3}}$, and a product of reflection $P_x(x \to -x)$ and time-reversal $\mathcal{T}$. We also argue that P_y is a symmetry of the system as long as there is no valley mixing; and the six-fold rotation $R_{\pi/3}$ becomes a good approximate symmetry of the Hubbard model in the case of long moiré lattice constant.

locking.

The dual vortex theory [340, 18, 341] is the most convenient formalism that describes a transition between a superfluid and a nontrivial insulator of a boson at fractional filling. If we start with a boson b, after the boson-vortex duality, a vortex of the superfluid phase of b becomes a point particle that couples to a dynamical U(1) gauge field A_μ, which is the dual of the Goldstone mode of the superfluid (not to be confused with the U(1) gauge field a_μ mentioned before that couples to the bosonic parton b). In the dual picture, the superfluid phase of b (which corresponds to the metal phase of the electron) is the

insulator phase of the vortex field; while the Mott insulator phase of b corresponds to the condensate of the vortices, which "Higgses" the U(1) gauge field A_μ, and drives the boson b into a gapped insulator phase. If at low energy there is only one component of vortex field with gauge charge 1 under A_μ (which corresponds to integer filling of boson b), the insulator phase of b is a trivial insulator without any further symmetry breaking or topological order; if there are more than one component of the vortex fields at low energy, or if the vortex field carries multiple gauge charges of A_μ, the insulator must be of nontrivial nature.

For example, when b has a fractional filling $\nu_b = 1/q$ with integer q, Ref. 342, 105 studied the quantum phase transition between the bosonic SF and various MIs with commensurate density waves which spontaneously break the translation symmetry but have no topological order. The study is naturally generalized to filling factor $\nu_b = p/q$ with coprime integers (p, q). We can use this formalism in our system. Hereafter we focus on one spin/valley flavor α, and the index α will be hidden for conciseness. In this case the theory for the SF-MI transition at one spin/valley flavor is:

$$\mathcal{L}^{(1)} = \sum_{j=0}^{N-1} (|(\partial_\mu - \mathrm{i}A_\mu)\psi_j|^2 + r|\psi_j|^2) + u(\sum_{j=0}^{N-1} |\psi_j|^2)^2 + \frac{\mathrm{i}}{2\pi} A \wedge d(a + eA_{\mathrm{ext}}) + \cdots \tag{3.19}$$

Here ψ_j with $j \in \{0, \cdots N-1\}$ are N flavors of vortex fields of the boson b at low energy, and A_μ is the dual gauge field of boson b: $\frac{1}{2\pi} dA = J_b$, where J_b is the current of boson b. a_μ is the gauge field that couples to both b and f, and A_{ext} is the external electromagnetic field. The reason there are N flavors of the vortex field is that, the vortex which is defined on a dual honeycomb lattice will view the partially filled boson density as a fractional background flux of the dual gauge field A_μ through each hexagon, and the band structure of the vortex will have multiple minima in the momentum space. The degeneracy of the multiple minima is protected by the symmetry of the triangular

lattice. ψ_j transforms as a representation of the projective symmetry group (PSG) of the lattice. Notice that since Eq. 3.19 describes one of the two spin/valley flavors, the PSG that constrains Eq. 3.19 should include translation, and $2\pi/3$ rotation of the lattice ($R_{\frac{2\pi}{3}}$). There is another more subtle symmetry $P_x\mathcal{T}$ for each spin/valley flavor of the boson and vortex fields. P_x that takes $x \to -x$, and time-reversal $\mathcal{T}$ both exchange the two spin/valley indices, but their product will act on the same spin/valley species, and part of its role is to take momentum k_y to $-k_y$.

In the appendix we will argue that P_y which takes y to $-y$ within each valley is also a good symmetry of the system, as long as valley mixing is negligible. One consequence of the P_y symmetry is that the expectation value of gauge flux da can be set to zero for the theory Eq. 3.19, or equivalently the P_y symmetry ensures that the "chemical potential" term $\psi_j^*\partial_\tau\psi_j$ does not appear in Eq. 3.19, as P_y transforms a vortex to anti-vortex: $\psi_a \to U_{ab}\psi_b^*$. Also, with long moiré lattice constant, the trigonal warping $k_x^3 - 3k_xk_y^2$ in each valley of the original BZ of the system becomes less important compared with the leading order quadratic dispersion expanded at each valley, hence the six-fold rotation $R_{\pi/3}$ becomes a good approximate symmetry of the effective Hubbard model with long moiré lattice constant.

The theory in Eq. 3.19 also has an emergent particle-hole symmetry. The simplest choice of the particle-hole symmetry is $\psi_a \to U_{ab}\psi_b^*$, $A \to -A$, $a \to -a$ and $A_{\text{ext}} \to -A_{\text{ext}}$. Although we used the same transformation matrix U_{ab} as P_y, this emergent particle-hole symmetry is different from P_y as it does not involve any spatial transformations. Note that any (spatially uniform) P_y-symmetric terms involving only the "matter fields" ψ_j must also preserve this emergent particle-hole symmetry. Another potentially relevant particle-hole-symmetry-breaking perturbation that needs to be examined is given by the finite density of the fluxes dA. dA is tied to the physical U(1) charge density (compared to the charge density set by the fixed electron filling $\nu = 1/2$) and hence should have

a vanishing spatial average. At the SF-MI transition point, the translation symmetry of the theory Eq. 3.19 and the fact that dA has a vanishing spatial average guarantee that dA has a vanishing expectation value everywhere, which respects the particle-hole symmetry. Therefore, the particle-hole symmetry is a valid emergent symmetry at the SF-MI critical point described by Eq. 3.19. The same argument would also conclude the emergent particle-hole symmetry at the ordinary SF-MI transition in the Bose-Hubbard model.

For parton construction-II, when the electron has filling $\nu = 1/2$, both b_1 and b_2 are at filling $\nu_b^\alpha = 1/2$. For each flavor of b_α, the formalism in Ref. 105 would lead to a dual vortex theory with $N = 4$ components of vortex fields, i.e. there are four degenerate minima of the vortex band structure in the momentum space for each spin/valley index. This calculation is analogous to the frustrated Ising model on the honeycomb lattice [343, 344]. Using the gauge choice of Fig. 3.2, the four minima are located at the K and K' points of the reduced Brillouin zone (BZ), with two fold degeneracy at each point.

From $N = 4$ to "$N = \infty$"

Ref. 105 considered a specific band structure of the vortex, which only involved the nearest neighbor hopping of vortices on the dual honeycomb lattice. But there is no fundamental reason that further neighbor hopping of vortices should be excluded. Indeed, once we take into account of further neighbor hopping, the dual vortex theory has a much richer possibility. We have explored the phase diagram of the dual vortex theory up to seventh neighbor hopping, and we obtained the phase diagram in Fig. 3.3a. Further neighbor hopping of the vortex field can modify the band structure, and lead to $N = 6$ or $N = 12$ components of vortex fields by choosing different hopping amplitudes. The $N = 6$ minima are located at three inequivalent M points of the reduced BZ (Fig. 3.3), each M point again has two-fold degeneracy. The two-fold degeneracy at each M point

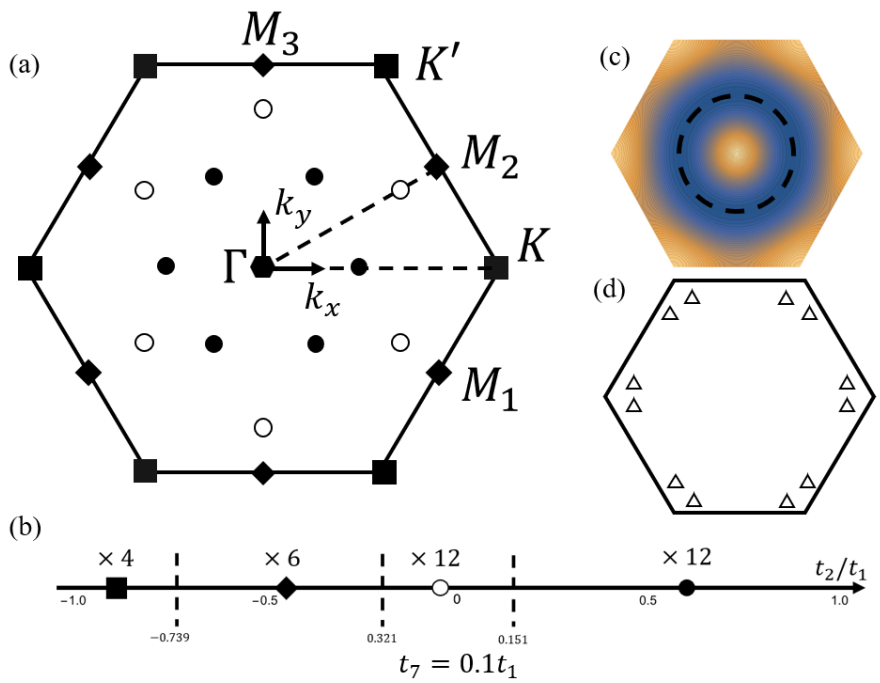

Figure 3.3: (a) The minima of the vortex band structure. With nearest neighbor vortex hopping on Fig. 3.2, the minima locate at the K and K' points of the Brillouin zone, each K point has two fold degeneracy; with further neighbor hoppings, the minima can shift to the three M points, still with two fold degeneracy at each M point. (b) The phase diagram of vortex modes with seventh neighbor hopping $t_7 = 0.1t_1$, and by tuning t_2 there are two regions in the phase diagram with $N = 12$ vortex modes at low energy. The 12 vortex modes are located either on the lines between Γ and K/K' or Γ and M. (c) With only t_1 and t_2, there is a large region of the phase diagram where there is a ring degeneracy of the vortex band structure. (d) All the symmetries (including approximate symmetries) of the system can protect up to 24 degenerate vortex modes, which locate at 12 incommensurate momenta in the BZ.

is protected by the translation symmetry of the triangular moiré lattice only, which is required by the LSM theorem. The shift of the vortex field minima from the K points to M points is similar to what was discussed in the context of frustrated quantum Ising models with further neighbor couplings [345, 346]. With symmetries $T_{1,2}$, $R_{\frac{2\pi}{3}}$ and $P_x\mathcal{T}$ at each spin/valley flavor, the degeneracy of the $N = 6$ minima at the M points are protected.

There are two regions in the phase diagram in Fig. 3.3b with $N = 12$ modes of vortex,

two at each momentum. The six incommensurate momenta at the minima of the vortex band structure can be located either on the lines between Γ and K/K' or Γ and M. With the $R_{\pi/3}$ symmetry that becomes a good approximate symmetry with long moiré lattice constant, the degeneracy of the $N = 12$ vortex modes is protected. In principle, all the symmetries together including $R_{\pi/3}$ can protect up to $N = 24$ degenerate minima, as shown in Fig. 3.3*d*.

For a theory with N components of vortex fields, the electric charge carried by the boson b will fractionalize. Under the boson-vortex duality $\frac{1}{2\pi}dA = J_b$, the boson number of b becomes the flux number of the dual gauge field A_μ. The gauge flux of A_μ is trapped at the vortex core of each field ψ_j (we denote the vortex of ψ_j as φ_j). With N components of the vortex fields, the vortex of each ψ_j field will carry $1/N$ flux quantum of the gauge field A_μ, hence the charge e_* of each fractionalized charge carrier should be e/N at the MIT. And there are in total $N_b = 2N$ species of the charge carriers (the factor of 2 comes from the two spin/valley flavors).

With just t_1 and t_2 (first and second neighbor vortex hopping), there is a large region of the parameter space where the minima of the vortex band structure form a ring. This one dimensional ring degeneracy is not protected by the symmetry of the system, but its effect may still be observable for a finite energy range. A ring degeneracy is analogous to $N = \infty$ in Eq. 3.19. Condensed matter systems with a ring degeneracy have attracted considerable interests [347, 348, 349, 350]. By integrating out the vortices with ring degeneracy, a "mass term" for the transverse component of A_μ is generated in the infrared limit [350] (in the limit of momentum goes to zero before frequency), meaning the fluctuation of A_μ is highly suppressed, which is consistent with the intuition of $N = \infty$.

The ellipsis in Eq. 3.19 includes other terms allowed by the PSG of the triangular lattice, but break the enlarged flavor symmetry of the CP^{N-1} model field theory. More

details about PSG, extra terms in the Lagrangian, coupling to fermionic parton f_α [351], and the possible valence bond solid orders with $N = 6$ will be discussed in appendix A and B. The exact fate of the critical theory in the infrared is complicated by these extra perturbations. It was shown previously that nonlocal interactions can drive a transition to a new fixed point [39, 352, 353], and here nonlocal interactions arise from coupling to the fermionic partons [351]. Hence the transition may eventually flow to a CFT different from the CP^{N-1} theory in Eq. 3.19, or be driven to a first order transition eventually. But as long as the first order nature is not strong, the charge fractionalization and large resistivity to be discussed in the next subsection is expected to hold at least for a considerable energy/temperature window.

So far we have not paid much attention to the dynamical gauge fields a_μ in parton construction-I or $a_{\alpha,\mu}$ in construction-II shared by the bosonic and fermionic partons, as the gauge coupling between b (b_α) and the gauge field is irrelevant at the MIT with a background spinon Fermi surface. Here we briefly discuss the fate of the spinon Fermi surface in the insulator phase. When the bosonic parton b is gapped, the theory of spinon Fermi surface coupled with the dynamical U(1) gauge field is a problem that has attracted a great deal of theoretical efforts [44, 45, 46, 48, 49, 50, 51]. These studies mostly rely on a "patch" theory approximation of the problem, which zooms in one or two patches of the Fermi surface. Then an interacting fixed point with a nonzero gauge coupling is found in the IR limit based on various analytical perturbative expansion methods.

Previous studies have also shown that the non-Fermi liquid obtained through coupling a Fermi surface to a dynamical bosonic field can be instable against BCS pairing of fermions [354, 355, 356, 357, 358, 359, 360]. If there is only one flavor of U(1) gauge field, the low energy interacting fixed point is expected to be robust against this pairing instability, because the U(1) gauge field leads to repulsive interaction between the spinons. However, when there are two flavors of U(1) gauge fields [360, 361], like the case in our

parton construction-II, the two U(1) gauge fields can lead to interflavor spinon pairing instability. This interflavor pairing can still happen at the MIT. But depending on the microscopic parameters this instability can happen at rather low energy scale.

Resistivity at the MIT

For low frequency and temperature, the resistivity of a system is usually written as $\rho(x)$ with $x = \omega/T$. The DC conductivity at zero temperature corresponds to $x = 0$, i.e. the limit $\omega \to 0$ before $T \to 0$. As we have mentioned, the interaction driven MIT has a jump of resistivity at the MIT compared with the metal phase near MIT, and this jump is given by the resistivity ρ_b of the bosonic parton b_α. For a bosonic system with an emergent particle-hole symmetry in the infrared, $\rho_b(x)$ with $x = 0$ or $x = \infty$ have attracted most studies. In general both $\rho_b(0)$ and $\rho_b(\infty)$ should be universal numbers at the order of $\sim h/e^2$. The reason $\rho_b(0)$ could be finite even without considering disorder and Umklapp process is that, with an emergent particle-hole symmetry in the infrared discussed in the previous subsection, there is zero overlap between the electric current and the conserved momentum density (extra subtleties about this from hydrodynamics will be discussed in section VI). The universal $\rho_b(0)$ was evaluated in Ref. 111 for the interaction-driven MIT without charge fractionalization. The calculation therein was based on Boltzmann equation in a theoretical large$-\mathbf{N}$ limit and eventually $\mathbf{N}$ was taken to 1 (we remind the readers that the $\mathbf{N}$ introduced in Ref. 111 was for technical reasons, it is not to be confused with N used in this work).

We have generalized the computation in Ref. 111 to our case with $N-$components of vortex fields and charge fractionalization. To proceed with the computation we need to turn on "easy plane" anisotropy to Eq. 3.19 and perform duality to the basis of fractional charge carriers φ_j (Eq. B.44). The φ_j will be coupled to multiple gauge fields which are the dual of the ψ_j fields. Eventually the total resistivity $\rho_b(0)$ is obtained through a

generalized Ioffe-Larkin rule, which combines the resistivity of each parton φ_j into ρ_b:

$$\rho_b = \frac{\hbar}{e^2}\left(\sum_{j=0}^{N-1}\rho_{b,j}\right). \tag{3.20}$$

$\rho_{b,j}$ is the resistivity of each charge carrier φ_j when its charge is taken to be 1. The detail of the computation is presented in the appendix, and we summarize the results here. For N flavors of vortices in Eq. 3.19, the resistivity $\rho_b(0)$ at the MIT roughly increases linearly with N, as was expected through the intuitive argument we gave before:

$$\rho_b(0) = \Delta\rho = \left(R^{(0)} + R^{(1)}(N-1)\right)\frac{h}{e^2}, \tag{3.21}$$

where $R^{(0)} \sim 3.62$, $R^{(1)} \sim 1.68$. We would like to compare our prediction with the previous theory of MIT without charge fractionalization. In the previous theory, the DC resistivity jump is evaluated to be $\Delta\rho \sim 7.92h/e^2$ [111] (we reproduced this calculation and our result at $N = N_b = 1$ is $7.44h/e^2$). Eq. 3.18 suggests that when $N \geq 4$, the resistivity jump in our case is indeed larger than that predicted by the previous theory of MIT.

We would also like to discuss the AC resistivity $\rho_b(\infty)$. One way to evaluate $\rho_b(\infty)$ is to again start with Eq. B.44, and follow the same strategy as the calculation of the DC resistivity. According to the generalized Ioffe-Larkin rule, the AC resistivity contributed by *each valley* is given by

$$\rho_b = N\frac{1}{\sigma_\varphi}\frac{\hbar}{e^2}, \qquad \sigma_\varphi = \lim_{\omega\to 0}\frac{1}{\mathrm{i}\omega}\langle J^\varphi_\omega J^\varphi_{-\omega}\rangle_{\vec{p}=0}, \tag{3.22}$$

where $J^\varphi = \mathrm{i}\varphi_j^*\nabla\varphi_j + h.c.$ is the current of the charge carrier φ_j. With the theoretical large-$\mathbf{N}$ limit mentioned above, the effects of all the dynamical gauge fields are sup-

pressed, and φ_j will contribute conductivity $\sigma_\varphi(\infty) = \frac{1}{16}$ (contrary to DC transport, $\sigma_\varphi(\infty)$ does not need collisions; the effects of dynamical gauge fields can be included through the $1/\mathbf{N}$ expansion). Eventually one would obtain resistivity from each valley

$$\rho_b = \frac{8N}{\pi}\frac{h}{e^2}, \tag{3.23}$$

the final resistivity of the system is half of Eq. 3.23 due to the two spin/valley flavors. With $N = 1$, the transition should belong to the ordinary 3D XY universality class, and the value given by Eq. 3.23 is not far from what was obtained through more sophisticated methods (see for instance Ref. 332, 331, 333, $\rho_b \sim 2.8h/e^2$). This should not be surprising as the 3D XY universality class can be obtained perturbatively from the free boson theory. In our current case with charge fractionalization, with $N \geq 4$, the total AC resistivity which is half of the value in Eq. 3.23 is larger than the universal resistivity at the 3D XY transition.

Another way to evaluate the resistivity of Eq. 3.19 is by integrating out ψ_j from Eq. 3.19, and an effective Lagrangian for A_μ is generated

$$\mathcal{L} \;=\; \sum_{p_\mu} \frac{Np}{16}\left(\delta_{\mu\nu} - \frac{p_\mu p_\nu}{p^2}\right) A_\mu(p) A_\nu(-p). \tag{3.24}$$

This effective action is supposed to be accurate in the limit of $N \to \infty$. The electric current carried by b is $J^b = \frac{e}{2\pi} dA$, hence the current-current correlation can be extracted from the photon Green's function based on the effective action Eq. 3.24:

$$\rho_{b,N\to\infty} = \frac{\pi N}{8}\frac{h}{e^2}. \tag{3.25}$$

Again the final resistivity of the system is half of Eq. 3.25 due to the two spin/valley flavors. The evaluation Eq. 3.25 is still proportional to N just like Eq. 3.23. These two

different evaluations discussed above give different values for $N = N_b = 1$, and compared with the known value of the universal resistivity at the 3D XY transition, the evaluation in Eq. 3.23 is much more favorable, though the evaluation Eq. 3.25 based on Eq. 3.24 is supposed to be accurate with large N.

When there is a ring of degeneracy in the vortex band structure, as we mentioned before the gauge field A_μ will acquire a "mass term" after integrating out ψ_j [350]. In this case the resistivity of the system at the MIT will be infinity, as the dynamics of A_μ is fully suppressed by the mass term in the infrared. One can also integrate out the action of A_μ with the mass term, and verify that the response theory of A_{ext} is no different from that of an insulator in the infrared limit. This is consistent with both Eq. 3.23,3.25 by naively taking N to infinity. In Ref. 350 when the boson field has a ring degeneracy, the phase is identified as a bose metal; this is because in Ref. 350 it is the boson with ring degeneracy that carries charges. But in Eq. 3.19 the electric charge is carried by the flux of A_μ.

3.2.4 Mott Insulator with Topological Order

As we explained in the previous subsection, due to the fractional filling of boson b_α, the vortex dynamics is frustrated by the background fractional flux through the hexagons. To drive the system into an insulator phase, the vortex can either condense at multiple minima in the BZ as was discussed in the previous section, or form a bound state that carries multiple gauge charge of A_μ and become "blind" to the background flux. In parton construction-II, with electron filling $\nu = 1/2$, each flavor of boson is at filling $\nu_b = 1/2$. The double-vortex, i.e. bound state of two vortices, or more generally the bound state of N vortices with even integer N, no longer see the background flux. Hence the N-vortex can condense at zero momentum, and its condensate will drive the system

into a Z_N topological order.

After the boson-vortex duality, the theory for the N-vortex condensation at one of the two spin/valley flavors is

$$\mathcal{L}^{(2)} = |(\partial_\mu - \mathrm{i}NA_\mu)\psi|^2 + r|\psi|^2 + g|\psi|^4 + \frac{\mathrm{i}}{2\pi}A \wedge d(a + eA_{\mathrm{ext}}) + \cdots \tag{3.26}$$

The condensate of ψ will break the U(1) gauge field to a Z_N gauge field, whose deconfined phase has a nontrivial Z_N topological order. In the Z_N topological order as well as at the MIT, the charge carrier is an anyon of the Z_N topological order, and it carries charge $e^* = e/N$. We still label the fractional charge carrier as φ. φ carries charge e/N, and is coupled to a Z_N gauge field originated from the Z_N topological order discussed in the previous paragraph.

In our case, in order to preserve the time-reversal symmetry, both spin/valley flavors should form a Z_N topological order simultaneously. Hence there is one species of φ_α field for each spin/valley flavor. The MIT can equally be described as the condensation of the φ_α field, and since the Z_N gauge field does not lead to singular correction in the infrared, the condensation of φ_α is a 3D XY* transition, and the transition for $N = 2$ was discussed in Ref. 197, 362, 22, 182, 183, 363. The b_α field is now a composite operator of φ_α. In the condensate of φ_α, the electron operator c_α is related to the fermionic parton operator f_α through $c_\alpha \sim \langle b_\alpha \rangle f_\alpha \sim \langle \varphi_\alpha^N \rangle f_\alpha$. The coupling between the two flavors of φ_α, i.e. the coupling $|\varphi_1|^2|\varphi_2|^2$ is irrelevant at the decoupled 3D XY* transition according to the known critical exponents of the 3D XY* transition. There are also couplings such as $|\varphi_\alpha|^2 f_\alpha^\dagger f_\alpha$ allowed by all the symmetries, but after formally integrating out the fermions, the generated couplings for φ_α is also irrelevant at the two decoupled 3D XY* universality class. The reason is that after formally integrating out the fermions, terms such as $\frac{|\omega|}{q}|\varphi_\alpha|^2_{\omega,\vec{q}}|\varphi_\beta|^2_{-\omega,-\vec{q}}$ can be generated, but this term is irrelevant knowing that the

standard critical exponent $\nu > 2/3$ for the 3D XY* transition.

Following the large$-\mathbf{N}$ calculation discussed before, the DC resistivity jump $\rho_b(0)$ would be $N^2/2$ times that of the previous theory [111], namely

$$\rho_b(0) \sim R^{(2)} N^2 \frac{h}{e^2}, \tag{3.27}$$

where $R^{(2)} = R'/2 \sim 3.7$ based on our evaluation. The AC resistivity jump at the MIT is enhanced by the same factor compared with the previous theory. We also note that the fractional universal conductivity at the transition between the superfluid and a Z_2 topological order was observed numerically in Ref. 363.

Another set of natural topological orders a boson at fractional filling can form are bosonic fractional quantum Hall (bFQH) states which are close analogues to the bosonic Laughlin's wave function. We would like to discuss this possibility as a general exploration, although this state breaks the P_y symmetry (but it still preserves the product $P_x\mathcal{T}$ symmetry). If we interpret the half-filled boson at each site as a quantum spin-1/2 system, this set of states are analogous to a chiral spin liquid [364, 365]. The Chern-Simons theory for this set of states at each valley reads

$$\mathcal{L}_{\text{cs}} = -\frac{\mathrm{i}k}{4\pi} A \wedge dA + \frac{\mathrm{i}}{2\pi} A \wedge d(a + A_{\text{ext}}), \tag{3.28}$$

with an even integer k and a dynamical Spin$_c$ U(1) gauge field A. The topological order characterized by this theory is the SU$(k)_1$ topological order. Here, the integer k needs to be even so that this theory is compatible with the LSM constraint imposed by the boson filling 1/2 on the lattice [366]. This is because the boson filling 1/2 requires the topological phase to contain an Abelian anyon that carries a fractional charge 1/2 (modulo integer). There should be one such anyon per unit cell to account for the boson filling 1/2 on the

lattice. The fact that such an anyon carries a fractional charge 1/2 implies that this anyon should generate under fusion an Abelian group $\mathbb{Z}_p$ with p an even number. Such a fusion rule is incompatible with any odd value of k. Therefore, k needs to be even in the theory given by Eq. 3.28. The time-reversal of the TMD moiré system demands that the bosonic parton b_α with opposite spin/valley index α forms a pair of time-reversal conjugate bFQH states. Or in other words if we take both spin/valley flavors together, this state is a fractional topological insulator, like the state discussed in Ref. 367.

The MIT is now a direct transition between the bFQH state and the superfluid of b_α. When the even integer k is $k = 2n^2$ with odd integer n, there is a natural theory for this direct continuous transition, and its simplest version with $n = 1$ was proposed in Ref. 368. The transition is a 3D QED with two flavors of Dirac fermions coupled to the dynamical U(1) Spin$_c$ gauge field A_μ (the dual of the Goldstone mode of the boson superfluid) with a Chern-Simons term at level-n^2, and the fermions have gauge charge-n:

$$\mathcal{L}^{(3)} = \sum_{j=1}^{2} \bar{\chi}_j \gamma \cdot (\partial - \mathrm{i}nA)\chi_j + M\bar{\chi}_j\chi_j - \frac{\mathrm{i}n^2}{4\pi} A \wedge dA + \frac{\mathrm{i}}{2\pi} A \wedge d(a + eA_{\mathrm{ext}}) + \cdots \tag{3.29}$$

In this theory, the fact that A is a Spin$_c$ U(1) gauge field and that n is odd guarantee that this theory describes the phases of a boson. A Spin$_c$ connection A_μ means a U(1) gauge field with a "charge-statistics relation": there is no fermionic object that is neutral under A_μ. When A_μ is a Spin$_c$ U(1) gauge field, and n is an odd integer in Eq. 3.29, Eq. 3.29 describes an interacting state of bosons that carries electric charge e. The charge$-e$ object of Eq. 3.29 that is also neutral under A_μ, is a composite of 2π flux of A_μ and n fermions χ. This composite is a boson as long as n being an odd integer, and this composite should be identified as b_α in Eq. 3.17. The ellipsis in this Lagrangian includes other terms such as the Maxwell term of the gauge field A_μ. Please note that this equation is for one of the two spin/valley flavors of the physical system. The mass

M of the Dirac fermions is the tuning parameter of the transition. With one sign of the mass term, after integrating out the Dirac fermions, the Spin_c U(1) gauge field A will acquire a Chern-Simons term at level $-2n^2$, which describes the $\text{SU}(k)_1$ topological order with $k = 2n^2$. With the opposite sign of M, there is no Chern-Simons term of the gauge field A after integrating out the Dirac fermions, and the Maxwell term of the gauge field A is the dual description of the superfluid phase. Hence by tuning M the system undergoes a transition between the $k = 2n^2$ bFQH state and the superfluid state of b (the metal phase of the original electron system).

The translation symmetry of the system actually guarantees that the two flavors of Dirac fermions are degenerate in Eq. 3.29. If these two Dirac fermions are not degenerate, an intermediate topological order is generated by changing the sign of the mass of one of the Dirac fermions in Eq. 3.29. Then after integrating out the fermions, the gauge field A acquires a total CS term with an odd level $-n^2$, which violates the LSM constraint imposed by the boson filling 1/2. Therefore, the masses of the two flavors of the Dirac fermions in Eq. 3.29 should be the same. In fact, for the simplest case with $n = 1$ ($k = 2$), an explicit parton construction of this transition can be given following the strategy in Ref. 368, and the two Dirac fermions in Eq. 3.29 are two Dirac cones of a $\pi-$flux state of χ on the triangular lattice. The degeneracy of these two Dirac fermions is protected by the translation symmetry of the triangular lattice. From the parton formalism one can also see that the boson b is constructed as a product of the two fermions χ_i.

At the transition $M = 0$, though it is difficult to compute the resistivity of Eq. 3.29 exactly, the resistivity $\rho(x)$ should scale as $1/k$ with large $k \sim n^2$, as after integrating out χ_j the entire effective action of A scales linearly as k. Then after integrating out A, the response theory to A_{ext} is proportional to $1/k$.

3.2.5 Summary of Predicted Physical Properties

So far we have discussed three different kinds of possible Mott insulators at half filling of the extended Hubbard model, based on the parton construction-II: (1) Mott insulators with translation symmetry breaking; (2) a Z_N topological order at each spin/valley flavor with even integer $N \geq 2$; and (3) a pair of conjugate bFQH states at two spin/valley flavors. For all scenarios, we have evaluated the bosonic parton contribution to the resistivity ρ_b at the MIT, which is also the universal jump of resistivity $\Delta\rho$. The predicted resistivity jump for the three scenarios are summarized in the table below.

Nature of Insulator	$\Delta\rho$, or ρ_b
(1) Density wave	$\rho_b(0) \sim (R^{(0)} + R^{(1)}(N-1))\frac{h}{e^2}$
(2) Z_N TO each flavor	$\rho_b(0) = R^{(2)}N^2\frac{h}{e^2}$
(3) Conjugate bFQH	$\rho_b(x) \sim \frac{1}{k}\frac{h}{e^2}$

Another observable effect predicted by the previous theory of interaction-driven MIT is the scaling of quasi-particle weight $\sqrt{Z}$ near the MIT [86, 87], where $\sqrt{Z} \sim r^{\beta_1} \sim |r|^{0.33}$. Our theory also gives a different prediction of the quasi-particle weight compared with the previous theory, and this is most conveniently evaluated for scenario (2). In the metal phase but close to the MIT, the quasi-particle weight scales as

$$\sqrt{Z} \sim \langle \varphi_\alpha^N \rangle \sim |r|^{\beta_N}, \tag{3.30}$$

where $\beta_N = \nu\Delta_N$. $\nu \sim 0.67$ is the standard correlation length exponent at the 3D XY* transition (it is the same as the 3D XY transition) and Δ_N is the scaling dimension of φ^N at the 3D XY transition. These exponents can be extracted from numerical simulation on the 3D XY and XY* transitions. For example, when $N = 2$, β_2 should be close to 0.8 [197, 362, 369], hence $\sqrt{Z} \sim |r|^{0.8}$. The scaling of quasi-particle weight can be checked in future experiments through the measurement of local density of states of electrons.

For scenario (1), i.e. where the insulator has translation symmetry breaking, the

scaling of quasiparticle weight can be estimated with large-N in Eq. 3.19. The boson creation operator $b^\dagger$ is a monopole operator of A_μ which creates a 2π gauge flux. With large-N in Eq. 3.19 the monopole operator has scaling dimension proportional to N [370, 371], hence the critical exponent β in the quasiparticle weight $\sqrt{Z} \sim |r|^\beta$ is expected to be proportional to N. The similar evaluation applies to Eq. 3.29, and the creation operator $b^\dagger$ has a scaling dimension proportional to k, which is also proportional to $\sqrt{Z}$.

As we explained, our theory provides a natural explanation of the anomalously large resistivity at the MIT. Another qualitative experimental feature reported in Ref. 4 is that, the resistivity drops rapidly as a function of temperature at the MIT where the charge gap vanishes. Our theory also provides a natural explanation for the temperature dependence of the critical resistivity. At zero temperature the bosonic chargeon parton b fractionalizes into multiple partons with smaller charges, and these partons will couple to extra gauge fields. These extra gauge fields will all confine at finite temperature. Hence at finite temperature, there is a crossover from transport with fractionalized charge to unfractionalized charge, which will cause a significant drop of resistivity with increasing temperature.

In the following paragraphs we discuss physics in phases near the MIT, based on our theory. These analysis can distinguish the three possible scenarios discussed to this point. Let us first discuss the insulator phase at fixed electron filling $\nu = 1/2$. The scenario (3) describes a topological order that is essentially a topological fractional quantum spin Hall insulator, hence this insulator phase, if does exists, must have nonchiral gapless modes localized at the boundary of the system. This nonchiral edge gapless modes should lead to similar experimental phenomena as the experiments on quantum spin Hall insulator [372]; but rather than edge conductance $2e^2/h$, the edge conductance of the fractional quantum spin Hall insulator should be $2e^2/(kh)$, which is twice of the edge conductance of the bFQH state with CS level-k. Also, the edge conductance should be

suppressed by external magnetic field, also analogous to what was observed in Ref. 372.

The insulating phase of scenario (1) and scenario (2) also lead to distinctive predictions. In scenario (1), the electric charges are only deconfined at the MIT, but still confined in the insulating phase, which has no topological order. Hence the charge deconfinement of scenario (1) is analogous to the original deconfined quantum critical point discussed in Ref. 182, 183. The confinement of fractional charges in scenario (1) happens even at zero temperature in the insulating phase. However, in scenario (2), the insulator phase has a Z_N topological order that supports deconfined fractional charge at zero temperature even in the insulator phase. While at finite temperature, the Z_N gauge field will lead to confinement of fractional charges with confinement length $\xi \sim \exp(c\Delta_m/T)$, where Δ_m is the gap of the fractionalized Z_N gauge fluxes, which is an anyon with nontrivial statistics with the fractional charges. If we look at the insulator phase close to the MIT, the gap of the fractional charge, i.e. the $e-$anyon of the Z_N topological order is suppsosed to be smaller than Δ_m, as the MIT corresponds to the condensation of the $e-$anyon, hence at very low temperature the thermally activated $e-$anyon has a much smaller distance l_e with each other compared with ξ. Then at low but finite temperature the transport is governed by charge carriers with gap Δ_e and charge $e_* = e/N$. The gap Δ_e can be extracted from fitting the low temperature transport data versus temperature. However, if one measures the tunnelling gap through tunnelling spectroscopy, since the external device can only inject a single electron which fractionalizes into multiple $e-$anyons, the tunneling gap should be approximately $N\Delta_e$. This contrast between tunneling gap and the thermally activated transport gap happens in scenario (2) but not scenario (1).

We also consider the metallic phase next to the insulator after charge doping, and we will see the scenario (2) also leads to very nontrivial predictions due to the deconfined nature of the Z_N topological order. In scenario (2), after some charge doping, we expect

a metallic state with charge fractionalization at low temperature. The bosonic charge carriers are coupled to the Z_N gauge field as well as the U(1) gauge field a_μ that are shared with the fermionic partons f_α. When the temperature is increased, the Z_N gauge field will confine, and due to the time-reversal symmetry, the confine-deconfine crossover should happen for both spin/valley flavors simultaneously. In the following, we shall only focus on one spin/valley. According to the Ioffe-Larkin composition rule, the total resistivity is composed of contributions from both bosonic and fermionic partons $\rho = \sigma^{-1} = \sigma_b^{-1} + \sigma_f^{-1}$. Let us assume the resistivity of both the bosonic and fermionic sectors are dominated by the scattering with the gauge field a_μ (this of course assumes that the momentum of the gauge field a_μ can relax through other mechanism such as disorder). This scattering mechanism was first evaluated in Ref. 373. The gauge-field propagator can be written as $D(\omega, \boldsymbol{q})^{-1} = i\gamma\omega/q + \chi_d q^2$, where the ω/q term is due to the Landau damping from the fermi-surface, and the "diamagnetic" χ_d is roughly a constant within the temperature window of interest. The scattering rate can then be estimated using the imaginary part of the boson/fermion self-energy:

$$\begin{aligned}\mathrm{Im}\Sigma_{b,f}(\omega, \boldsymbol{k}) = \int_0^\infty d\omega' \int \frac{d^2\boldsymbol{k}'}{(2\pi)^2}(1 + n_b(\omega'))(1 \pm n_{b,f}(\omega_{\boldsymbol{k}'})) \\ \frac{(k_\alpha + k'_\alpha)(k_\beta + k'_\beta)}{2m_{b,f}} \frac{\delta_{\alpha\beta} - q_\alpha q_\beta}{\boldsymbol{q}^2} \delta(\omega - \omega_{\boldsymbol{k}'} - \omega')\mathrm{Im}D(\omega', \boldsymbol{q}),\end{aligned} \tag{3.31}$$

where $\boldsymbol{q} = \boldsymbol{k}' - \boldsymbol{k}$, $n_{b,f}(\omega)$ denotes the Bose-Einstein (Fermi-Dirac) distribution function, and $m_{b,f}$ is the boson/fermion mass. We must stress that the expression of $\Sigma_{b,f}$ is valid for partons with gauge charge-1. When the Z_N gauge field is deconfined, each boson carries the gauge charge-$1/N$ of the gauge field a_μ, and therefore there is an additional factor $1/N^2$ in the self-energy. The integral was evaluated in Ref. 373, and the time-scale responsible for transport has an extra factor proportional to q^2 in the integral. After

taking these into account, we obtain the "transport" scattering rate for boson/fermion

$$\frac{1}{\tau_f} \sim T^{4/3}, \qquad \frac{1}{\tau_b} \approx \frac{k_B T}{m_b \chi_d}. \tag{3.32}$$

Comparing $1/\tau_b$ and $1/\tau_f$, we can see that the resistivity is dominated by the boson-gauge scattering at low temperature, and the bosonic partons are in a disordered phase rather than a quasi long range order at finite temperature due to their coupling to the dynamical gauge field a_μ. We take the Drude formula for the dilute Bose gas that we use to model the bosonic partons at finite temperature:

$$\rho \sim \frac{m_b}{n_* e_*^2} \frac{1}{\tau_b} \sim \frac{g_*^2}{n_* e_*^2} \frac{k_B T}{\chi_d}, \tag{3.33}$$

where $e_* = e/N$ and $g_* = 1/N$ denote the electric and gauge charges of bosons, and $n_* e_*$ is the doped physical electric charge density. Here, we have assumed that the resistivity ρ is dominated by the boson contribution because $(i.)$ the scattering rate of the boson is bigger compared to the fermions at low temperature as shown in Eq. 3.32, and $(ii.)$ the bosons have much lower density at low charge doping compared to the fermions which already has finite fermi surface at zero charge doping. In the following discussion, we will work under these assumptions at least up to the temperature scale T_c around which the Z_N gauge becomes fully confined.

The Z_N gauge field is fully confined when ξ is at the same order as the lattice constant; *i.e.* $T > T_c \sim \Delta_m$. Here we assume that the gauge field a_μ that is coupled to the fermionic parton is less prone to confinement due to its coupling to the large density of gapless fermoins. Above T_c, the charge carriers in the system carry charge-e. The equation above still hold with the substitutions $e_* \to e = Ne_*, g_* \to g = Ng_*, n_* \to n = n_*/N$. We expect there is a crossover from the deconfined value of resistivity $\rho(T \sim 0)$ to the

confined value $\rho(T \geq T_c)$:

$$\frac{(d\rho/dT)_{T\geq T_c}}{(d\rho/dT)_{T\sim 0}} \sim N, \tag{3.34}$$

This is an observable effect of scenario (2) that can be experimentally verified. Note that the crossover caused by confinement at the metallic phase is different from the critical point of the MIT; as transport at the critical point originates from rather different physics; for example both particles and holes will contribute to the charge transport at the critical point [374].

Contrary to the Ioffe-Larkin rule, the total thermal conductivity of the system is a sum of the contribution from the bosonic parton, fermionic parton, and also the gauge boson. With low charge doping away from $\nu = 1/2$, we expect the fermionic partons dominates the thermal transport according to Ref. 375: $\kappa_f \sim T^{1/3}$. As we discussed above, in scenario (2) the low-temperature charge transport is dominated by the boson contribution $\sigma_b \sim 1/T$, while the thermal transport is dominated by the fermion contribution $\kappa_f \sim T^{1/3}$. Due to the crossover of charge transport at finite temperature caused by the confinement of the Z_N gauge field in scenario (2), there is also an observable prediction one can make for the Lorentz number $L = \kappa/(T\sigma) \approx \kappa_f/(T\sigma_b)$:

$$\frac{(L/T^{1/3})_{T\geq T_c}}{(L/T^{1/3})_{T\sim 0}} \sim N. \tag{3.35}$$

3.2.6 Summary, Discussion, & Other Fractional Fillings

In this work we proposed a theory for a potentially continuous metal-insulator transition for the extended Hubbard model on the triangular lattice at half-filling (one electron per unit cell). The extended Hubbard model is simulated by the TMD moiré systems. We introduce a different parton construction from the previous literature, which leads

to a series of observable predictions. We demonstrated that our theory is more favorable given the current experiments on the heterobilayer TMD moiré systems. Although our theory was motivated by the recent experiments on $MoTe_2/WSe_2$ moiré superlattice [4], we envision our theory can have broad application given the recent rapid progresses in synthesizing pure two dimensional systems.

The moiré potential in the $MoTe_2/WSe_2$ moiré superlattice with no twisting is formed due to the mismatch of the lattice constants of the two layers. There is another experiment on MIT in twisted WSe_2 [319]. The situation in twisted WSe_2 seems rather different from $MoTe_2/WSe_2$ moiré superlattice. Inside the "insulator phase", the resistivity $\rho(T)$ at some displacement fields first increases with decreasing temperature, and eventually the plot seems to saturate at a finite value, which is much lower than the resistivity observed in the $MoTe_2/WSe_2$ moiré superlattice near the MIT. Hence the MIT of twisted WSe_2 could be of a different nature, between the metallic phase and the insulator phase, there could be an intermediate phase with an order at nonzero momentum and reduced size of electron Fermi pockets.

Correlated insulators at other fractional fillings $\nu = p/q$ have been reported in various TMD moiré systems [320, 321, 322, 323]. Although the nature of the MIT at these fillings has not been looked into carefully, here we briefly discuss the theory for the possible continuous MIT at general fractional filling $\nu = p/q$. As long as $q > 2$, even for parton construction-I, the bosonic parton b will have fractional filling, and hence the insulator phase of b cannot be a trivial incompressible state without translation symmetry breaking or topological order. Here we would like to acknowledge that charge fractionalization for interacting electron system at fractional electron number per unit cell was discussed in previous literature [376], using similar formalism as the parton construction-I. At electron filling $\nu = 1/q$, the boson filling $\nu_b = 2/q$; if we only consider nearest neighbor hopping of the vortex, the insulator has commensurate density wave that spontaneously breaks the

translation symmetry, and the MIT is described by Eq. 3.19 with $N = q$ for odd integer q; $N = q/2$ for $q = 4k + 2$; and $N = q$ for $q = 4k$. The electron charge will further fractionalize at the continuous MIT. In parton construction-I, there are in total N species of the charge carriers each carrying electric charge $e^* = e/N$. Hence the estimate of ρ_b is $\rho_b \sim Nh/e^2$.

For parton construction-II, with electron filling $\nu = 1/q$, the boson filling for each spin/valley flavor is $\nu_b = 1/q$. Again, if only nearest neighbor hopping of the vortices is considered, the MIT is described by Eq. 3.19 with $N = q$ for odd integer q; $N = 2q$ for even integer q. The field theory describing the MIT is two copies of Eq. 3.19: ψ_j, A_μ and a_μ should all carry a spin index α. There are in total $N_b = 2N$ species of the charge carriers each carrying electric charge $e^* = e/N$. Hence the estimate of ρ_b is $\rho_b \sim Nh/(2e^2)$. If we consider further neighbor hopping like section 3.2.3, the charge carriers may carry even smaller fractional charge, and hence larger ρ_b.

Here, we would like to discuss some subtlety regarding the conductivity σ_b of the bosonic parton. In a generic theory with momentum conservation, one expects a finite overlap between the electric current and the conversed momentum. Such a finite overlap would lead to a Drude peak in the (optical) conductivity (see Ref. 374 for a review) $\sigma(\omega) = \sigma_Q + \mathcal{D}\left(\frac{i}{\omega} + \delta(\omega)\right)$ where $\mathcal{D} > 0$ is the Drude weight and ω is the frequency. In a theory with an exact particle-hole symmetry, this overlap between the electric current and momentum is strictly zero and, consequently, the Drude weight $\mathcal{D}$ vanishes. In the MIT considered in this paper and previous literature such as Ref. 324, 86, 111, the theories that govern the bosonic partons all have an emergent particle-hole symmetry. This emergent particle-hole symmetry is expected to produce a Drude weight that vanishes at zero temperature, namely $\mathcal{D} \to 0$ as $T \to 0$. If there is a finite momentum relaxation time τ_p induced by for example disorder, the Drude peak should take the form $\frac{\mathcal{D}}{\tau_p^{-1} - i\omega}$ and should be viewed as an extra correction, when we take $\omega \to 0$, to the bosonic parton DC

conductivity σ_b calculated for the MIT. Since $\mathcal{D}$ vanishes as $T \to 0$ due to the emergent particle-hole symmetry, the DC limit, i.e. $\omega \to 0$, of the Drude peak becomes a small correction to the bosonic parton DC conductivity σ_b at low temperature.

There is another subtlety associated with the bosonic parton conductivity due to extra hydrodynamical corrections and the purely two dimensional nature of the system. It was known (see, for example, Ref. 377 for a review) that, when momentum is strictly conversed, even in the presence of particle-hole symmetry, hydrodynamical fluctuations lead to a logarithmic correction to the optical conductivity that scale as $\log(\tau_{\rm th}\omega)$. Here, $\tau_{\rm th}$ is the time scale of local thermalization [378] and can be estimated as $\sim T^{-1}$. This hydrodynamical correction to the conductivity diverges in the DC limit. This divergence is due to the long-lived hydrodynamical mode associated with the conserved momentum. As we mentioned before, in real systems disorder and Umklapp process always induce a finite momentum relaxation time τ_p. The diverging hydrodynamical correction is only valid when $\tau_p \gg \tau_{\rm th} \sim T^{-1}$, meaning momentum is strictly conserved over the thermalization time scale, where the hydrodynamical description becomes applicable. When the temperature T is low compared to τ_p^{-1}, hydrodynamical corrections are cut-off by τ_p^{-1} and are again expected to be small corrections to the bosonic parton conductivity calculated in the rest parts of this paper. In fact the divergent hydrodynamical correction may be already cut-off at a higher temperature scale that is favorable to us, as the crossover scale is suppressed by a large factor depending on the dimensionless entropy density of the system [378].

We would like to stress that the optical conductivity $\sigma(\infty)$ which is much easier to evaluate theoretically (see section.III for an example) is free of these subtleties, and we encourage future experiments to measure the optical conductivity at the MIT as well.

In recent years very impressive progresses have been made on numerically simulating interacting fermionic systems (for examples see Ref. 379, 380, 381, 382). It is conceivable

that an extended Hubbard model with spin-orbit coupling can be constructed on the triangular lattice, and by changing the parameter (for example the strength of the spin-orbit coupling), two types of interaction-driven MIT may be realized, one described by the original theory [324, 87], the other described by our current theory. Predictions made in these two theories, such as different universality classes and transport properties at the MIT, different scalings of quasiparticle weight, and the existence of the spinon Fermi surface in the insulator phase, can potentially be directly tested through various numerical methods on the extended Hubbard model. We will leave this to future exploration.

Chapter 4

Theoretical Constructions of Non-Fermi Liquids

In Sec. 1.3, we have seen examples of metallic states beyond Landau-Fermi liquid theory and the difficulties in their theoretical descriptions. This chapter collects some of our efforts in theoretically constructing metallic states with exotic properties, including quasiparticle breakdown, bad metal behavior, strange metal behavior, etc.

Non-fermi liquid and unconventional quantum critical points (QCP) with strong fractionalization are two exceptional phenomena beyond the classic condensed matter doctrines, both of which could occur in strongly interacting quantum many-body systems. Sec. 4.1 demonstrates that using a controlled method one can construct a non-fermi liquid within a considerable energy window based on the unique physics of unconventional QCPs. We will focus on the "nearly-marginal non-fermi liquid", defined as a state whose fermion self-energy scales as $\Sigma_f(\mathrm{i}\omega) \sim \mathrm{i}\mathrm{sgn}(\omega)|\omega|^\alpha$ with α close to 1 in a considerable energy window. The nearly-marginal non-fermi liquid is obtained by coupling an electron fermi surface to unconventional QCPs that are beyond the Landau paradigm. This mechanism relies on the observation that the anomalous dimension η of the order pa-

rameter of these unconventional QCPs can be close to 1, which is significantly larger than conventional Landau phase transitions, for example the Wilson-Fisher fixed points. The fact that $\eta \sim 1$ justifies a perturbative renormalization group calculation proposed earlier. Various candidate QCPs that meet this desired condition are proposed.

In Sec. 4.2, we discuss examples of two-dimensional metallic states with charge fractionalization, and we will demonstrate that the mechanism of charge fractionalization leads to exotic metallic behaviors at low and intermediate temperature. The simplest example of such a state is constructed by fermionic partons at finite density coupled to a Z_N gauge field, whose properties can be studied through rudimentary methods. This simple state has the following exotic features: *(1)* at low temperature this state is a "bad metal" whose resistivity can be much larger than the Mott-Ioffe-Regel limit; *(2)* while increasing temperature T the resistivity $\rho(T)$ is a nonmonotonic function, and it crosses over from a bad metal at low T to a good metal at relatively high T; *(3)* the optical conductivity $\sigma(\omega)$ has a small Drude weight at low T, and a larger Drude weight at intermediate T; *(4)* at low temperature the metallic state has a large Lorenz number, which strongly violates the Wiedemann-Franz law. A more complex example with fermionic partons at finite density coupled to a SU(N) gauge field will also be constructed.

In Sec. 4.3, we propose a lattice model for strongly interacting electrons with the potential to explain the main phenomenology of the strange metal phase in the cuprate high-temperature superconductors. Our model is motivated by the recently developed "tetrahedron" rank-3 tensor model that mimics much of the physics of the better-known Sachdev-Ye-Kitaev (SYK) model. Our electron model has the following advantageous properties: *(1)* it only needs one orbital per site on the square lattice; *(2)* it does not require any quenched random interaction; *(3)* it has local interactions and respects all the symmetries of the system; *(4)* the soluble limit of this model has a longitudinal DC resistivity that scales linearly with temperature within a finite temperature window; *(5)*

again the soluble limit of this model has a fermion pairing instability in the infrared, which can lead to either superconductivity or a "pseudogap" phase. The linear$-T$ longitudinal resistivity and the pairing instability originate from the generic scaling feature of the SYK model and the tetrahedron tensor model.

A variety of exotic non-fermi liquid (NFL) states have been observed in many condensed matter systems, with different scaling relations between transport coefficients and temperature. The "standard" approach to studying these NFLs is by coupling a fermi liquid to quantum critical fluctuations, which potentially can drive the system into a NFL. In Sec. 4.4, we seek for an alternative understanding of these various NFLs in a unified framework. We first construct two "elementary" *randomness-free* models with *four-fermion* interactions only, whose many properties can be analyzed exactly in a certain limit just like the Sachdev-Ye-Kitaev (SYK) model. The most important new feature of our models is that, the fermion scaling dimension in the conformal invariant solution in the infrared limit is tunable by charge density. Then based on these elementary models, we propose two versions of lattice models with four fermion interactions which give us non-fermi liquid behaviors with DC resistivity scaling $\varrho \sim T^{\alpha}$ in a finite temperature window, and $\alpha \in [1, 2)$ depends on the fermion density in the model, which is a rather universal feature observed in many experimental systems.

4.1 Fermi-Surface States Coupled to Non-Landau Critical Modes

4.1.1 Introduction

In the past few decades, a consensus has been gradually reached that quantum many-body physics with strong quantum entanglement can be much richer than classical physics

driven by thermal fluctuations [383, 384]. Classical phase transitions usually happen between a disordered phase with high symmetries, and an ordered phase which spontaneously breaks such symmetries. Typical classical phase transitions can be well described by the Landau's paradigm, but the Landau's paradigm may or may not apply to quantum phase transitions that happen at zero temperature. Generally speaking, the Landau's formalism can only describe the quantum phase transition between a direct-product quantum disordered state and a spontaneous symmetry breaking state; but it can no longer describe the quantum phase transition between two states when at least one of the states cannot be adiabatically connected to a direct product states, *i.e.* when this state is a topological order [221]; nor can the Landau's paradigm describe generic continuous quantum phase transitions between states with different spontaneous symmetry breakings [182, 183, 173].

Phenomenologically, in contrast with the ordinary Landau's transitions, non-Landau transitions often have a large anomalous dimension of order parameters, due to fractionalization or deconfinement of the order parameter [188, 189, 190, 191]. The ordinary Wilson-Fisher (WF) fixed point in $(2+1)d$ space-time (or three dimensional classical space) has very small anomalous dimensions [197], meaning that the Wilson-Fisher fixed point is not far from the mean field theory. In particular, in the large$-N$ limit, the anomalous dimension of the vector order parameter of the O(N) Wilson-Fisher fixed point is $\eta \sim 0$; while the CP^{N-1} model, the theory that describes a class of non-Landau quantum phase transition [182, 183], has $\eta \sim 1$ in the large-N limit [219]. Numerically it was also confirmed that the quantum phase transition between the Z_2 topological order and the superfluid phase has $\eta \sim 1.5$ [184, 185], as was predicted theoretically. The large anomalous dimension has been used as a strong signature when searching for unconventional QCPs numerically.

In this work we propose that the unique physics described above about the uncon-

ventional QCPs with strong fractionalization can be used to construct another broadly observed phenomenon beyond the classic Landau's theory: the non-Fermi liquid whose fermion self-energy scales $\Sigma_f(\mathrm{i}\omega) \sim \mathrm{i}\mathrm{sgn}(\omega)|\omega|^\alpha$ with $\alpha < 1$. When $\alpha = 1$, this non-fermi liquid is referred to as marginal fermi liquid [385]. Signature of marginal fermi liquid and nearly-marginal fermi liquid have been observed rather broadly in various materials [77, 386, 136]. In this work we will focus on the non-Fermi liquid that is "nearly-marginal", meaning α is close to 1.

We assume that there exists a field $\mathcal{O}(\boldsymbol{x}, \tau)$ in the unconventional QCP that carries zero momentum, and it couples to the fermi surface in the standard way: $\int d^2x d\tau\ g\psi^\dagger T\psi\mathcal{O}$, where T is a flavor matrix of the fermion. We assume that we first solve (or approximately solve) the bosonic part of the theory, *i.e.* the strongly interacting QCP without coupling to the fermi surface, and calculate the anomalous dimension η at the QCP:

$$\langle \mathcal{O}(\boldsymbol{q}, \omega)\mathcal{O}(-\boldsymbol{q}, -\omega)\rangle \sim \frac{1}{\Omega^{2-\eta}} \tag{4.1}$$

where $\Omega \sim \sqrt{v^2\boldsymbol{q}^2 + \omega^2}$. Then the fermion self-energy, the quantity of central interest to us, is computed perturbatively with the boson-fermion coupling g.

When the anomalous dimension η is close to 1, we can take $\eta = 1 - \epsilon$ with small ϵ. Ref. [387, 388, 389] developed a formalism for the boson-fermion coupled theory with an expansion of ϵ, though eventually one needs to extrapolate the calculation to $\epsilon = 1$ for the problems studied therein [387, 388, 389], and the convergence of the $\epsilon-$expansion at $\epsilon = 1$ is unknown, *i.e.* even if we start with a weak boson-fermion coupling, it would become nonperturbative under renormalization group (RG). But we will demonstrate in the next section that in the cases that we are interested in, ϵ is naturally small when η is close to 1, due to the fractionalized nature of many unconventional QCPs. To the leading nontrivial order, our problem can be naturally studied by the previously proposed

perturbative formalism with small ϵ.

Here we stress that our goal is to construct a scenario in which a non-Fermi liquid state within an energy window can be constructed using a controlled method. Recently many works have taken a similar spirit, and various non-Fermi liquid states especially a state that mimics the strange metal were constructed by deforming the soluble Sachdev-Ye-Kitaev (SYK) and related models [54, 55, 390, 391, 392]. Then within the energy window where the deformation remains perturbative, the system resembles the non-Fermi liquid [393, 394, 395, 396, 397, 398]. Our current work also starts with (approximately) soluble strongly interacting bosonic systems (in the sense that the gauge invariant order parameters in these systems are bosonic), and then we turn on perturbation, which in our case is the boson-fermion coupling. We will demonstrate that a non-Fermi liquid can be constructed based on the unique nature of the strongly interacting bosonic system.

4.1.2 ϵ-Expansion for Non-Fermi Liquids

A controlled reliable study of the non-Fermi liquid problem is generally considered as a very challenging problem, one example of the difficulties was discussed in Ref. [399]. Over the years various approximation methods were proposed. We begin by reviewing the $\epsilon-$expansion developed in Ref. [387, 388, 389], and demonstrate how perturbation of ϵ is naturally justified for some unconventional QCPs. It is often convenient to study interacting fermions with finite density by expanding at one patch of the Fermi surface. The low-energy theory of the fermions expanded at one patch of the fermi surface is

$$\mathcal{L}_f = \psi^\dagger(\xi\partial_\tau - \mathrm{i}v_F\partial_x - \kappa\partial_y^2)\psi, \tag{4.2}$$

where x is perpendicular to the fermion surface and y is the tangent direction. The initial value of ξ is $\xi_0 = 1$, and it will be renormalized by the fermion self-energy. Our

main goal is to evaluate the fermion self-energy to the leading nontrivial order of the boson-fermion coupling. We will show that this is equivalent to the leading nontrivial order of $\epsilon = 1 - \eta$. At this order of expansion of ϵ, for our purpose it is sufficient to consider a simple "effective action" of $\mathcal{O}(\boldsymbol{x}, \tau)$:

$$\mathcal{S}_{eff} \sim \int d^2x d\tau \ \mathcal{O}(\boldsymbol{x}, \tau)(-\partial_\tau^2 - v^2 \boldsymbol{\nabla}^2)^{1-\frac{\eta}{2}} \mathcal{O}(\boldsymbol{x}, \tau) \tag{4.3}$$

which will reproduce the correlation function of $\mathcal{O}(\boldsymbol{x}, \tau)$, assuming we have fully solved the interacting bosonic system first.

When the boson-fermion coupling is zero, i.e., $g = 0$, the system is at a Gaussian fixed point with the following scaling dimensions of spacetime coordinates and fields

$$[\tau] = -2, \qquad [x] = -2, \qquad [y] = -1, \tag{4.4}$$

$$[\psi(\boldsymbol{x}, \tau)] = \frac{3}{2}, \qquad [\mathcal{O}(\boldsymbol{x}, \tau)] = \frac{3}{2} + \frac{\eta}{2} = 2 - \frac{\epsilon}{2}. \tag{4.5}$$

We then turn on the boson-fermion interaction

$$\int d^2x d\tau \ g \psi^\dagger T \psi \mathcal{O} \tag{4.6}$$

and consider the perturbative RG at the Gaussian fixed point. We find that the scaling dimension of g is $[g] = \epsilon/2$, hence it is weakly relevant if ϵ is naturally small, and it may flow to a weakly coupled new fixed point in the infrared which facilitates perturbative calculations with expansion of ϵ. Indeed, the beta function of g^2 at the leading order of ϵ was derived in Ref. [387, 388, 389]:

$$\frac{dg^2}{d\log b} = \frac{\epsilon}{2} g^2 - \Upsilon g^4. \tag{4.7}$$

Thus there is a fixed point at weak coupling $g_*^2 = \epsilon/(2\Upsilon)$, where the parameter $\Upsilon \sim 1/(4\pi^2 v_F v)$.

Under the rescaling $x' = xb^{-1}$, namely after integrating out the short scale degrees of freedom, the fermion acquires a one-loop self-energy

$$\begin{aligned}\delta\Sigma_f\left(\mathrm{i}\omega, \boldsymbol{p}\right) &\sim g^2 \int d\nu d\boldsymbol{q} \langle \mathcal{O}^*_{\boldsymbol{q},\nu} \mathcal{O}_{\boldsymbol{q},\nu}\rangle G_f(\mathrm{i}\omega + \mathrm{i}\nu, \boldsymbol{q}+\boldsymbol{p}) \\ &\sim g^2 \int d\nu dq_x \int_{\frac{\Lambda}{\sqrt{b}}}^{\Lambda} dq_y \frac{1}{\left|v^2 q_x^2 + v^2 q_y^2 + \omega^2\right|^{\frac{1+\epsilon}{2}}} \frac{1}{\mathrm{i}\left(\omega+\nu\right) - v_F\left(p_x + q_x\right) - \kappa\left(p_y + q_y\right)^2}.\end{aligned} \tag{4.8}$$

In the boson correlation function, $v^2 q_x^2$ and ω^2 are irrelevant compared with $v^2 q_y^2$, hence we first integrate over q_x, and the fermion propagator contributes a factor $\mathrm{sgn}\left(\omega+\nu\right)\mathrm{i}/(2v_F)$. We then perform the ν integral and finally integrate q_y over the momentum shell $\Lambda b^{-1/2} < |q_y| < \Lambda$. The last integral is evaluated at $\epsilon = 0$, which is valid at the leading order perturbation of ϵ. This procedure leads to

$$\delta\Sigma_f\left(\mathrm{i}\omega, \boldsymbol{p}\right) = -\mathrm{i}\omega g^2 \Upsilon \log b + O\left(\epsilon^2\right). \tag{4.9}$$

Combining the calculations above, at the fixed point g_*^2, the renormalized $\mathrm{i}\xi(\omega)\omega$ in the Fermion Green's function reads

$$\mathrm{i}\xi(\omega)\omega \sim -\mathrm{i}\mathrm{sgn}\left(\omega\right)|\omega|^{1-\epsilon/2}. \tag{4.10}$$

The fermion self-energy, hence the decay rate of the fermion, scales in the same way as Eq. 4.10. The calculation above gives a nearly-marginal non-Fermi liquid behavior for small but finite ϵ. For small η such as the cases in the Wilson-Fisher fixed points, the calculation of the scaling of fermion self-energy is not reliable with the leading order expansion of ϵ described above.

Here we stress that, our main purpose is to compute $\mathrm{i}\xi(\omega)\omega$, or the fermion self-energy

to the leading order of boson-fermion coupling $g_*^2 \sim \epsilon$, assuming a weak initial coupling g. At higher order expansion of the boson-fermion coupling, corrections to the boson field self-energy (for example the standard RPA diagram) from the boson-fermion coupling needs to be considered. The RPA diagram is proportional to $\mathcal{L}_{\text{RPA}} \sim |\mathcal{O}_{\omega,\boldsymbol{q}}|^2 g^2 |\omega|/(v_F \kappa q)$. Several parameters can be tuned, including the weak coupling fixed point value of g_*^2, to make this term weak enough to allow an energy window where the calculations in this section apply. At the elementary level, we need the terms in Eq. 4.3 to dominate the RPA effect $|\mathcal{O}_{\omega,\boldsymbol{q}}|^2 g^2 |\omega|/(v_F \kappa q)$. A field $\mathcal{O}$ at momentum $\boldsymbol{q}$ should correspond to energy scale $\omega \sim vq$. For Eq. 4.3 at $\eta = 1$ to dominate the RPA effect, we need $q > g^2/(v_F \kappa)$, or $\omega > g^2 v/(v_F \kappa)$. If we start with a weak initial bare coupling constant g_0, and also $\epsilon \ll 1$ hence the fixed point value of g_* is also perturbative, there is a sufficiently large energy window for our result. Tuning the parameter v/v_F and κ can further expand the energy window. A full analysis of the term $\mathcal{L}_{\text{RPA}} \sim |\mathcal{O}_{\omega,\boldsymbol{q}}|^2 g^2 |\omega|/(v_F \kappa q)$ in the bosonic sector of the theory in the infrared limit requires more detailed analysis because $\mathcal{O}_{\omega,\boldsymbol{q}}$ is a composite operator in the field theories discussed in the next section.

4.1.3 Candidate Unconventional QCPs

Bosonic-QED-Chern-Simons Theory

In the following we will discuss candidate QCPs which suffice the desired condition $\eta \sim 1$, or $\epsilon \ll 1$. When we study the pure bosonic sector of the theory, we ignore the coupling to the fermions, assuming the boson-fermion coupling is weak, which is self-consistent with the conclusion in the previous review section that the boson-fermion interaction will flow to a weakly coupled fixed point $g_*^2 \sim \epsilon$. As we stated in the previous section, we will start with a weak boson-fermion coupling g, and eventually we only compute the fermion self-energy to the leading nontrivial order of the fixed point $g_*^2 \sim \epsilon$. In

the purely bosonic theory, the scaling of the space-time has the standard Lorentz invariance. To avoid confusion, we use "[ ]" to represent scaling dimensions under the scaling Eq. 4.5 of the one-patch theory in the previous section, and "{ }" represent the scaling dimension in the Lorentz invariant purely bosonic theory. At a QCP, multiple operators will become "critical", namely multiple operators can have power-law correlation. We will demand that the operator with the strongest correlation (smallest scaling dimension) satisfy the desired condition, since this is the operator that provides the strongest scattering with the electrons.

We consider $(2+1)d$ bosonic quantum electrodynamics (QED) with N flavors of bosons coupled to a noncompact U(1) gauge field with a Chern-Simons term:

$$\mathcal{L}_{\text{bQED}} = \sum_{\alpha=1}^{2}\sum_{a=1}^{N/2} |(\partial_\mu - \mathrm{i}b_\mu) z_{\alpha,a}|^2 + r(z^\dagger_{\alpha,a} z_{\alpha,a}) \tag{4.11}$$

$$+ u(\sum_{\alpha,a} |z_{\alpha,a}|^2)^2 + u' \sum_{\alpha=1}^{2}(\sum_{a=1}^{N/2} |z_{\alpha,a}|^2)^2 + \frac{\mathrm{i}kN}{4\pi} b \wedge db. \tag{4.12}$$

The following operators are gauge invariant composite fields, which we assume are all at zero momentum:

$$\mathcal{O}_0 = \sum_{\alpha=1}^{2}\sum_{a=1}^{N/2} z^\dagger_{\alpha,a} z_{\alpha,a}, \quad \mathcal{O}_{1,3} = \sum_{a=1}^{N/2} z^\dagger_a \sigma^{1,3} z_a. \tag{4.13}$$

Potential applications of this field theory to strongly correlated systems will be discussed later.

To compute their scaling dimensions, we introduce two Hubbard-Stratonovich(HS)

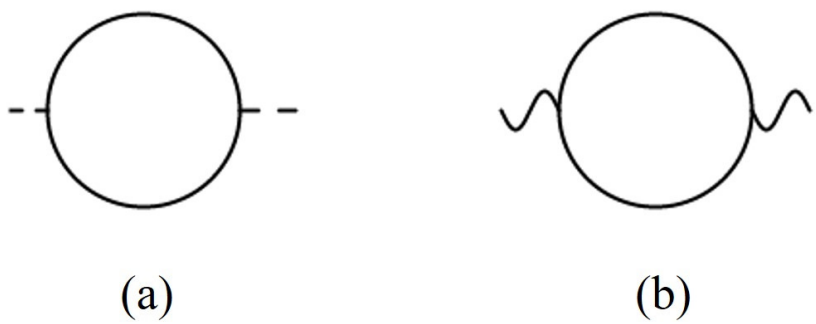

Figure 4.1: The self-energy of field σ_+ and gauge field b_μ in the large$-N$ limit.

fields to decouple the quartic potentials:

$$\mathcal{L}'_{\text{bQED}} = \sum_{\alpha=1}^{2}\sum_{a=1}^{N/2} |(\partial_\mu - \mathrm{i}b_\mu)z_{\alpha,a}|^2 + r(z^\dagger_{\alpha,a}z_{\alpha,a}) + \mathrm{i}\sigma_+\mathcal{O}_0 \tag{4.14}$$

$$+ \mathrm{i}\sigma_-\mathcal{O}_3 + \frac{1}{2u'+4u}\sigma_+^2 + \frac{1}{2u'}\sigma_-^2 + \frac{\mathrm{i}kN}{4\pi} b\wedge db. \tag{4.15}$$

We will consider the following two scenarios: (1) $u' \to 0, u > 0$, where σ_- is fully suppressed and the system has a full $\mathrm{SU}(N)\times\mathrm{U}(1)_T$ symmetry, where the $\mathrm{U}(1)_T$ is the "topological symmetry" that corresponds to the conservation of the gauge flux; and (2) $u, u' > 0$ when the $\mathrm{SU}(N)$ symmetry is broken down to $\mathrm{SU}(N/2)\times\mathrm{SU}(N/2)\times\mathrm{U}(1)\rtimes Z_2$, where the $\mathrm{U}(1)\rtimes Z_2$ is the symmetry within the Pauli matrix space in Eq. 4.13.

In scenario (1) with a full $\mathrm{SU}(N)$ symmetry, at the critical point $r = 0$, the field σ_+ acquires a self-energy in the large$-N$ limit

$$\Sigma_{\sigma_+}(p) = N\int \frac{d^3q}{(2\pi)^3}\frac{1}{q^2(q+p)^2} = \frac{N}{8p}. \tag{4.16}$$

Hence the propagator of field σ_+ in the large$-N$ limit reads

$$G_{\sigma_+}(p) = 1/\Sigma_{\sigma_+} = \frac{8p}{N}. \tag{4.17}$$

Similarly, for the gauge field, the self-energy in the large$-N$ limit is

$$\Sigma_{b,\mu\nu}(p) = -N \int \frac{d^3q}{(2\pi)^3} \frac{(2q+p)_\mu (2q+p)_\nu}{q^2(q+p)^2} = \frac{N}{16p}(p^2\delta_{\mu\nu} - p_\mu p_\nu). \tag{4.18}$$

When combined with the Chern-Simons term, in the Landau gauge, the gauge field has the following large$-N$ propagator [221]

$$G_{b,\mu\nu}(p) = \frac{1}{Np}\left(F\left(\delta_{\mu\nu} - \frac{p_\mu p_\nu}{p^2}\right) + H\frac{\epsilon_{\mu\nu\rho}p^\rho}{p}\right), \tag{4.19}$$

where

$$F = \frac{16\pi^2}{\pi^2 + 64k^2}, \qquad H = -\frac{128\pi k}{\pi^2 + 64k^2}. \tag{4.20}$$

After introducing the HS fields, the scaling dimension of the composite operator $\mathcal{O}_0$ of the original field theory Eq. 4.12 is "transferred" to the scaling dimension of the HS fields σ_+. To the order of $O(1/N)$, the Feynman diagrams in Fig. 4.2 contribute to the σ_+ self energy, which was computed in Ref. [221].

But it is evident that in the large$-N$ limit, the scaling dimension of σ_+ (and the scaling dimension of operator $\mathcal{O}_0$ of the original field theory Eq. 4.12) is $\lim_{N\to\infty}\{\mathcal{O}_0\} = 2$, hence it does not meet the desired condition. When $\mathcal{O}_0$ couples to the Fermi surface, the boson-fermion coupling will be irrelevant in the one patch theory discussed in the previous section according to the scaling of space-time Eq. 4.5.

The scaling dimension of $\sigma_{1,3}$ equal to each other with a full SU(N) symmetry, and unlike $\mathcal{O}_0$, they have scaling dimension 1 in the large$-N$ limit. The $1/N$ corrections to their anomalous dimensions come from diagram $(a)-(d)$ in Fig. 4.2, or equivalently

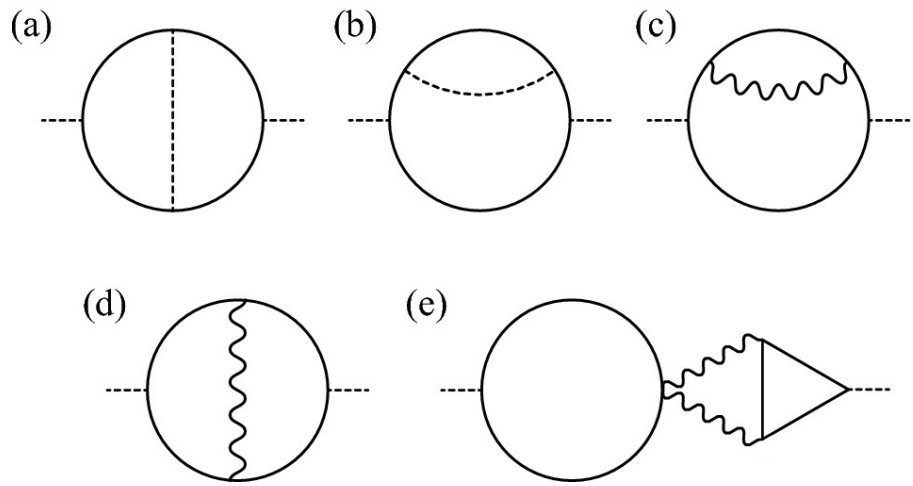

Figure 4.2: In scenario (1), diagrams $(a)-(e)$ contribute to the anomalous dimension of $\mathcal{O}_0$ in Eq. 4.12 or equivalently σ_+ in Eq. 4.15; while only diagrams $(a)-(d)$ contribute to the anomalous dimension of $\mathcal{O}_{1,3}$. The solid line represents the propagator of $z_{\alpha,a}$, the dashed and wavy lines represent the large$-N$ propagators of σ_+ and b_μ respectively.

through the standard momentum shell RG:

$$\{\mathcal{O}_{1,3}\} = 1 + \frac{16}{3\pi^2 N} - \frac{4}{3\pi^2 N} F. \tag{4.21}$$

Ref. [219] and references therein have computed scaling dimensions of gauge invariant operators for theories with matter fields coupled with a U(1) gauge field, without a Chern-Simons term. Our result is consistent with these previous references, since $\lim_{k\to 0}\{\mathcal{O}_{1,3}\} = 1 - 16/(\pi^2 N)$, which is the result of the CP^{N-1} model with a noncompact gauge field. Also, in the limit of $k \to +\infty$, our result is consistent with Ref. [219] when the fermion component is taken to be infinity, since both limits suppress the gauge field fluctuation completely. In general operators $\mathcal{O}_{1,3}$ have stronger correlations than $\mathcal{O}_0$, hence they will make stronger contributions to scattering when coupled with the fermi

surface. As an example, the anomalous dimension of $\mathcal{O}_{1,3}$ with $k = 1/2$ reads

$$\eta_{1,3} \sim 1 - \frac{0.57}{N}, \tag{4.22}$$

which is reasonably close to 1 even for the most physically relevant case with $N = 2$.

In scenario (2) we should keep both σ_+ and σ_- in the calculation, and both $\sigma_\pm$ (operator $\mathcal{O}_0$ and $\mathcal{O}_3$ in theory Eq. 4.12) have scaling dimension 2 in the large$-N$ limit [220]. Now $\mathcal{O}_1$ has the strongest correlation, and at the order of $O(1/N)$, its scaling dimension reads:

$$\{\mathcal{O}_1\} \;=\; 1 + \frac{8}{3\pi^2 N} - \frac{4}{3\pi^2 N} F. \tag{4.23}$$

When $k = 1$, its anomalous dimension reads

$$\eta_1 \sim 1 - \frac{0.037}{N}, \tag{4.24}$$

which is always very close to 1. Using the formalism reviewed in the previous section, by coupling to $\mathcal{O}_1$, the fermion self-energy would scale as $\Sigma_f\left(\mathrm{i}\omega, \boldsymbol{p}\right) \sim -\mathrm{i}\mathrm{sgn}\left(\omega\right)|\omega|^{0.99}$ for $N = 2$.

The field theory Eq. 4.12 describes a quantum phase transition from a topological order with Abelian anyons to an ordered phase that spontaneously breaks the global flavor symmetry. The flavor symmetry can be either a full $\mathrm{SU}(N)$ symmetry (scenario *1*) or $\mathrm{SU}(N/2) \times \mathrm{SU}(N/2) \times \mathrm{U}(1) \rtimes Z_2$ (scenario *2*). So far we have assumed that the gauge invariant $\mathcal{O}_{1,3}$ have zero momentum, hence they cannot be the ordinary antiferromagnetic Néel order parameter. They must be translational invariant order parameters with nontrivial representation under the internal symmetry group, for example they could be the quantum spin Hall order parameter for $N = 2$.

The topological order described by the Chern-Simons theory with $N = 2$, $k = 1$ is the most studied state in condensed matter theory. This topological order is the $\mathrm{U}(1)_2$ or equivalently the $\mathrm{SU}(2)_1$ topological order with semionic anyons. It is the most natural topological order that can be constructed from the slave particle formalism [106]. And recently it was conjectured that this topological order is also related to the parent state of the cuprates high temperature superconductor [400] motivated by the giant thermal Hall signal observed [401].

Another interesting scenario is when $N = 2$, $k = 0$ and $u > 0$. In this case Eq. 4.12 is the same field theory as the easy-plane deconfined QCP between the inplane antiferromagnetic Néel order and the valence bond solid state on the square lattice. Recent numerical studies have shown that this quantum phase transition may be continuous, and the scaling dimension of both $\mathcal{O}_0$ and $\mathcal{O}_3$ are fairly close to 1 based on numerical results [191, 402]. It has been proposed that this field theory is self-dual [218], and it is dual to the transition between the bosonic symmetry protected topological (SPT) phase and the trivial phase [98, 171], which is directly describe by a noncompact QED with $N = 2$ flavors of Dirac fermion matter fields [403, 404]. The tuning parameter for this topological transition is instead coupled to $\mathcal{O}_3$. Hence this SPT-trivial transition is also a candidate quantum phase transition which meets the desired criterion proposed in our paper that leads to a nearly-marginal fermi liquid. But in these cases there are other fields (for example the inplane Néel order parameter) with smaller scaling dimensions, and we need to assume that these operators carry finite lattice momentum hence couple to the Fermi surface differently.

Gross-Neveu-Yukawa QCP

Another candidate QCP that likely suffices the desired condition $\eta \sim 1$ is the Gross-Neveu-Yukawa QCP with $N-$flavors of Dirac fermion:

$$\mathcal{L}_{\text{GNY}} = \sum_{a=1}^{N} \bar{\chi}_a \gamma_\mu \partial_\mu \chi_a + g\phi\bar{\chi}_a\chi_a + (\partial\phi)^2 + r\phi^2 + u\phi^4. \tag{4.25}$$

At the critical point $r = 0$, both u and g flows to a fixed point. In our context, the QCP describes a bosonic or spin system, hence χ is viewed as a fermionic slave particle of spin, *i.e.* the spinon, and we assume that χ is coupled to a Z_2 gauge field, namely the system is a Z_2 spin liquid with fermionic spinons. But the dynamical Z_2 gauge field does not lead to extra singular corrections to low energy correlation functions of gauge invariant operators, hence the universality class of Eq. 4.25 is still identical to the Gross-Neveu-Yukawa (GNY) theory, as long as we only focus on gauge invariant operators.

The GNY QCP can still be solved in the large$-N$ limit, and the cases with finite N can approached through a $1/N$ expansion. At the GNY QCP coupled with a Z_2 gauge field, the gauge invariant operator with the lowest scaling dimension is ϕ, and its scaling dimension can be found in Ref. [405] and references therein:

$$\{\phi\} \sim 1 - \frac{16}{3\pi^2 N}. \tag{4.26}$$

Other gauge invariant operators such as $\bar{\chi}T\chi$ with a SU(N) matrix T have much larger scaling dimension at the GNY QCP, for example $\{\bar{\chi}T\chi\} = 2$ in the large$-N$ limit. If we replace the Z_2 gauge field by a U(1) gauge field, the U(1) gauge fluctuation will enhance the correlation of ϕ, hence increases $\epsilon = 1 - \eta$ compared with the situation with only a Z_2 gauge field. Hence a GNY QCP with a U(1) gauge field is less desirable according to our criterion.

The GNY QCP coupled with a Z_2 gauge field can be realized in various lattice model Hamiltonians for quantum antiferromagnet. For example, for SU(M) spin systems on the triangular lattice with a self-conjugate representation on each site, using the fermionic spinon formalism, when there is a $\pi-$flux through half of the triangles, there are $N = 2M$ components of Dirac fermions at low energy [406]. SU(M) quantum magnet may be realized in transition metal oxides with orbital degeneracies [407, 408, 409], and also cold atom systems with large hyperfine spins [410, 411, 412, 413]. Recently it was also proposed that an approximate SU(4) quantum antiferromagnet can be realized in some of the recently discovered Moiré systems [238, 414, 415], and a SU(4) quantum antiferromagnet on the triangular lattice may realize the Z_2-gauged GNY QCP with $N = 8$ (with lower spatial symmetry compared with SU(2) systems as was pointed out in Ref. [416]). On the other hand, a SU(M) spin systems on the honeycomb lattice can potentially realize the GNY QCP with $N = 2M$ (with zero flux through the hexagon) or $N = 4M$ (with $\pi-$flux through the hexagon).

The operator ϕ is odd under time-reversal and spatial reflection, hence physically ϕ corresponds to the spin chirality order. Hence the Z_2-gauged GNY QCP is a quantum phase transition between a massless spin liquid and a chiral spin liquid.

Non-Fermi liquid is often observed only at a finite temperature/energy window in experiments. At the infrared limit, the non-Fermi liquid is usually preempted by other instabilities, for example a dome of superconductor [417, 418, 419]. In Ref. [417] the instability of non-Fermi liquid towards the superconductor dome was systematically studied in the framework of the $\epsilon-$expansion. According to Ref. [417], when $\mathcal{O}$ is an order parameter at zero momentum, at $\epsilon = 0$ the superconductor instability will occur at an exponentially suppressed temperature/energy scale $\Delta_{\rm sc} \sim \Lambda_\omega \exp(-A/|g_0|)$, where g_0 is the bare boson-fermion coupling constant. In our case the estimate of the superconductor instability is complicated by the fact that $\mathcal{O}$ is a composite field, but the qualitative

exponentially-suppressed form of $\Delta_{\rm sc}$ is not expected to change because g is still at most a marginally relevant coupling. When $\epsilon = 0$, the imaginary part of the fermi self-energy (the inverse of quasi-particle life-time) scales linearly with ω. Because the bare electron dispersion has no imaginary part at all, the imaginary part of the self-energy should be much easier to observe compared with the real part, assuming other scattering mechanisms of the fermions are weak enough. The scaling behavior of the fermion self-energy is also observable numerically like Ref. 420. This linear scaling behavior of the imaginary part of self-energy is observable for fermionic excitations at energy scale $\omega > \Delta_{\rm sc}$, . Hence above the superconductor energy scale $\Delta_{\rm sc}$, the non-Fermi liquid behavior is observable. This result should still hold for small enough ϵ. [1]

4.1.4 Conclusion

In this work we proposed a mechanism based on which a nearly marginal non-fermi liquid can be constructed with a controlled method in an energy window. This mechanism demonstrates that two exceptional phenomena beyond the standard Landau's paradigm, *i.e.* the non-Landau quantum phase transitions and the non-fermi liquid may be connected: a non-Landau quantum phase transition can have a large anomalous dimension $\eta \sim 1$, which physically justifies and facilitates a perturbative calculation of the Boson-Fermion coupling fixed point. Several candidate QCPs that suffice this condition were proposed, including topological transitions from Abelian topological orders to an ordered phase, and a Gross-Neveu-Yukawa transition of Z_2 spin liquids.

We would like to compare our construction of non-fermi liquid states and the con-

[1] In Ref. [417], the non-Fermi liquid energy scale $E_{\rm nfl}$ is defined as the energy scale where the fermi velocity v_F is renormalized strongly from its bare value, hence $E_{\rm nfl}$ was defined based on the real part of the fermion self-energy. In other words the $E_{\rm nfl}$ was defined as the scale where the real part of self-energy dominates the bare energy in the Green's function. But since the bare dispersion of fermion is difficult to observe, and the bare fermion energy has no imaginary part at all, we prefer to use the imaginary part of fermion self-energy as a characteristic definition of non-Fermi liquid state.

structions based on the SYK related models. In the constructions based on SYK-like models, the existence of a strange-metal like phase was based on the fact that in the soluble limit, *i.e.* in the SYK model the scaling dimension of fermion is 1/4 (scaling with time only). But since the definition of the electric current operator in these constructions is proportional to the perturbation away from the SYK model, the current-current correlation function and the electrical conductivity is small in the energy window where the construction applies. Recently an improved construction was proposed which can produce the Planckian metal observed in cuprates materials [421]. In our construction, since the boson-fermion coupling will flow to a weakly coupled fixed point, the scattering rate of the fermion due to the boson-fermion coupling is expected to be low. We will further study if a Planckian metal like state can be constructed by developing our current approach. In this future exploration, a mechanism of momentum relaxation, for instance the disorder, or Umklapp process, needs to be introduced.

4.2 Transport in Metallic States with Charge Fractionalization

4.2.1 Introduction

Dimensionless quantities in nature can be universal, meaning they are insensitive to the microscopic details of the system. Dimensionless universal quantities can arise from two different mechanisms: either criticality, or topology. At a critical point (either classical or quantum critical point), the diverging correlation length renders most of the the microscopic details irrelevant to infrared physics, hence each universality class is characterized by a series of numbers referred to as critical exponents. Examples of these critical points include various two dimensional statistical mechanics models such as the

Ising model [422], the "Yang-Lee singularity" [423], and the Wilson-Fisher fixed points of three dimensional systems [424]. Topology can lead to universal quantities due to topological quantization. The simplest example of such is the magnetic flux quantization in Dirac monopole [425], and in superconductor [426, 427]. The Hall conductivity of quantum Hall systems (either integer or fractional) is a discrete universal number, it is related to the level of the Chern-Simons topological field theory [428, 429, 430, 431], which has to be quantized due to mathematical consistency.

Electrical resistivity/conductivity is a dimensionless quantity in two spatial dimensions, hence it can in principle take universal values that are independent of the microscopic details of the system. A universal resistivity can arise with various mechanisms. Besides the Hall resistivity of the quantum Hall states mentioned above, the resistivity of $(2+1)d$ quantum critical points with gapless charge degree of freedom [329, 326], the resistivity jump at $(2+1)d$ metal-insulator transition driven by interaction [86, 87, 111], and the criterion of the so-called "bad metal" in two dimensions [78, 79, 80] are all "universal". In all these examples, the resistivity (or the bound of resistivity) is always an order-unity dimensionless number times h/e^2.

This work concerns the metallic states with finite charge density and finite charge compressibility. The usual theory that describes the transport of a metal is the Boltzmann equation. The Boltzmann equation most conveniently applies when the concept of quasiparticles remains valid in the system [2], which usually requires that $l_{\mathrm{m}}k_F \gg 1$, where l_{m} is the mean free path, and k_F is the Fermi wave vector. When $l_{\mathrm{m}}k_F$ becomes order 1, the resistivity saturates the Mott-Ioffe-Regel (MIR) limit of a metal, and the system becomes a "bad metal" [78, 79, 80], where descriptions based on quasiparticles break down. For a purely two dimensional system, the condition of $l_{\mathrm{m}}k_F \sim l_{\mathrm{m}}n^{1/2} \sim 1$ implies

[2] A generalized quantum Boltzmann equation can be developed when well-defined quasiparticles are lost due to interaction with bosonic modes [432].

that the resistivity ρ should be at the order of h/e^2. When the measured resistivity ρ of a purely two dimensional metal is significantly larger than h/e^2, or in other words the estimated value of $l_{\mathrm{m}}k_F$ exceeds order unity for a $2d$ metal, one has to abandon the conventional description based on quasiparticles, and resort to other theoretical tools.

In real systems metallic states without quasiparticles usually arise from coupling electrons to bosonic gapless quantum critical modes. The theoretical formalism for these states usually start with a decoupled system with noninteracting electrons, and analyze how the fermion-boson coupling modifies the system [44, 45, 46, 48, 85, 50, 51]. Through various perturbative renormalization group methods, one can show that the coupling between the Fermi surface and the gapless bosonic modes is relevant, and potentially drive the system into a non-Fermi liquid fixed point without quasiparticles. In recent years, a new route of constructing non-Fermi liquid has been explored, which was based on models that are soluble in certain limit (such as the Sachdev-Ye-Kitaev model and other related models) [54, 55, 390, 391, 392]. These models have no notion of spatial dimensions, but solution of these models already have no quasiparticles. Lattice models built upon these soluble models quite naturally lead to non-Fermi liquids in various spatial dimensions [393, 433, 434, 394, 395, 396, 397, 435].

In this work we explore an alternative construction of exotic metallic states. The constructions used in this work are not based on soluble lattice models of interacting electrons, but there are sufficient theoretical arguments to show that these are indeed stable states. Though these examples are far from weakly interacting electrons with quasiparticles, the design of these states allows them to be studied through rudimentary theoretical tools.

4.2.2 Fractionalized Metal with Z_N Gauge Structure

The central idea of our construction is "charge fractionalization". Fractionalization of quantum numbers is most well-known and well established in particle physics [436], but it is also predicted and observed in condensed matter systems such as fractional quantum Hall states [437, 438, 439]. Quantum number fractionalization is also one of the signatory phenomena in quantum spin liquids [108, 440, 441, 442, 443]. Electric charge fractionalization was discussed in the context of Mott transition in systems with partially filled $3d$ pyrochlore lattice [376]. Recently, motivated by experiments on transition metal dichalcogenide (TMD) moiré heterostructures [4], effects of charge fractionalization at the metal-insulator transition in pure $2d$ systems have been discussed in Ref. 444, 351. In this work we will explore the consequences of charge fractionalization in a metallic state.

The first example we consider is a Z_N topological order enriched with a global U(1) symmetry, which corresponds to the ordinary electric charge conservation. The elementary anyon ψ_α of the Z_N topological order carries a Z_N gauge charge, and it is also a spin-1/2 fermion with fractional electric charge $e_* = e/N$. When N is an odd integer, the gauge invariant states of the system include fermions that carry odd integer electric charges and half-integer spins; as well as bosons with even integer charges and integer spins. This is the same Hilbert space as a many-body electron system.

It is known that the discrete gauge field at two spatial dimensions has a stable deconfined phase at zero temperature, in which the anyon ψ_α can be separated infinitely far from each other, hence the anyon ψ_α plays the role as the charge carriers in the system at least at zero temperature. Although we do not pursue an exactly soluble model based on electrons in this work, the state discussed here should be a stable state of electrons, given that a discrete gauge theory is free from confinement at zero temperature in $(2+1)d$.

At finite temperature the thermal equilibrium state of the system is in a confined phase, but at low temperature the observable physics should still crossover to the deconfined phase at zero temperature. In fact, the finite temperature confinement of the Z_N gauge field is caused by thermally activated population of gauge fluxes with nontrivial mutual statistics with ψ_α. The confinement length $\xi(T)$, i.e. the distance that a single ψ_α can be separated from the "crowd", takes the form of $\xi(T) \sim \exp(c\Delta/T)$, where Δ is the gap of Z_N gauge fluxes, and c is a constant. We argue that when $\xi(T)$ simultaneously satisfy two criteria, namely (*i.*) $\xi(T)$ is large compared with the distance between ψ_α anyons (assuming a sufficiently large charge density), and (*ii.*) $\xi(T)$ is large compared with the mean free path $l_{\rm m}$, the anyon ψ_α still plays the role of charge carrier in the nonequilibrium process of charge transport, as ψ_α does not travel long enough between two consecutive scatterings to "feel" the confinement.

Charge Transport

In the follows we will discuss various properties of the state described above. We first consider electrical resistivity at zero temperature. The key advantage of this construction is that, at zero temperature, the Z_N gauge field dynamics is gapped, and does not lead to any scattering to the gapless charged partons below the gap of the Z_N gauge fields. The main source of relaxation of electric current at zero temperature still comes from conventional mechanisms, such as impurities, which give the partons a mean free length $l_{\rm m}$. If we assume the electric charge density is en_e, in an ordinary system without fractionalization, the rudimentary semiclassical theory of transport breaks down when $l_{\rm m} n_e^{1/2} \sim 1$, i.e. $l_{\rm m} \sim 1/n_e^{1/2}$. Since the parton carries charge e/N, the density of the parton is $n_* = Nn_e$, hence the usual transport theory can be applicable for even smaller $l_{\rm m}$, i.e. $l_{\rm m} \sim 1/(n_*)^{1/2} \sim 1/(Nn_e)^{1/2}$. When $l_{\rm m}$ saturates this limit, the system should be

a "bad metal of partons", with an "upper bound" of resistivity

$$\rho_{max} \sim \frac{h}{e_*^2} \sim N^2 \frac{h}{e^2}. \tag{4.27}$$

When $l_{\rm m} \sim 1/(n_*)^{1/2} > 1$, rudimentary formalism of describing metallic states should still apply; the only difference is that now the charge carrier ψ_α carries charge $e_* = e/N$, and the density of ψ_α is higher than electric charge density.

At low temperature, a $2d$ Z_N gauge field will cause confinement in equilibrium. As we mentioned above, the confinement of a $2d$ Z_N gauge theory is caused by the thermally activated gauge fluxes, and the confinement length $\xi(T)$ is roughly the distance between two thermally activated gauge fluxes, hence $\xi(T) \sim \exp(c\Delta/T)$, where Δ is the energy gap for the Z_N gauge flux. We need to compare $\xi(T)$ with other length scales of the system: the distance between anyons ψ_α, which is given by $1/n_*^{1/2}$; the lattice constant a; and the mean free path $l_{\rm m}$. To ensure that the transport of the state can be studied with controlled methods, we assume that the mean free length $l_{\rm m}$ is at the order of, or larger than $N^{1/2}/n_e^{1/2}$; or equivalently $l_{\rm m} n_*^{1/2}$ is at the order of, or greater than N. In this limit, at least at low temperature, the following hierarchy of length scales holds: $\xi(T) > l_{\rm m} > 1/n_*^{1/2}$. In this limit the simple theory of metal, such as the Drude formula still applies. The conductivity at zero and low temperature would be

$$\sigma_0 = \frac{n_* e_*^2 l_{\rm m}}{m_* v_F^*} \sim \frac{e_*^2}{h}(l_{\rm m} n_*^{1/2}) \sim \frac{1}{N}\frac{e^2}{h}, \tag{4.28}$$

which can still be a bad metal, even with the choice of relatively long mean free length.

We assume that $l_{\rm m}$ mostly arises from scattering with impurities with a hard-sphere like potential, and hence is insensitive to temperature. With rising temperature, the resistivity first increases with conventional mechanism, such as scattering with phonon,

or interaction between the partons. These scattering are still suppressed due to the small electric charge carried by the partons. For example, the parton-phonon interaction is down by a factor of $1/N$ compared with the electron-phonon interaction, and the resistivity due to parton-phonon interaction is down by a factor of $1/N^2$. For short-range parton-parton interactions which presumably leads to Fermi liquid like scaling of resistivity (i.e. $\rho \sim \rho_0 + AT^2$), if the short-range interaction arises from screened Coulomb interaction, the interaction is suppressed by a factor of $1/N^2$ [3].

When temperature rises further, the confinement length $\xi(T)$ becomes shorter, and eventually at temperature scale T_1 where $\xi(T_1) \sim l_{\rm m}$, the semiclassical picture of ψ_α breaks down. At even higher temperature scale where the confinement length $\xi(T)$ is comparable with the lattice constant a, i.e. $T > T_2$ with $\xi(T_2) \sim a$, the partons are fully confined, and the charge carriers should still be viewed as electrons. The electron density is n_e, and since we assumed a hard-sphere like potential of the impurities, $l_{\rm m}$ from impurities remains approximately unchanged from before. The conductivity at temperature T_2 should be

$$\sigma(T_2) \sim \frac{n_e e^2 l_{\rm m}}{m v_F} \sim N^{1/2} \frac{e^2}{h}, \tag{4.29}$$

which can be a good metal. Hence with rising temperature, the resistivity evolves in a nonmonotonic way; it will crossover from a bad metal with $T < T_1$ to a good metal at $T \sim T_2$. The schematic behavior of $\rho(T)$ is sketched in Fig. 4.3.

We have chosen $l_{\rm m}$ so that the simple pictures of metal such as the Drude theory applies for both temperature ranges $T < T_1$ and $T > T_2$. In the low temperature range the semiclassical theory of metal with fractional charge carrier ψ_α becomes applicable; while with $T > T_2$ the system becomes a conventional metal with electrons. We lack the

[3] The screening of the Coulomb interaction is affected by the charge of the parton as well, which will complicate the estimate of the screened-short range interaction.

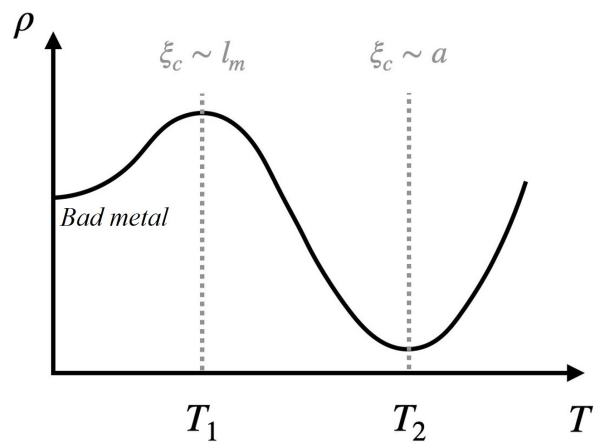

Figure 4.3: The schematic behavior of resistivity $\rho(T)$ constructed with fermionic partons carrying fractional charges coupled with a Z_N gauge field.

reliable theoretical tools to describe the intermediate temperature range $T_1 < T < T_2$, but sufficient argument can lead to the conclusion that the system crossover from a bad metal phase at low temperature range, to a good metal phase in the higher temperature range. Also, if the optical conductivity is measured, our construction implies that the Drude weight of the optical conductivity is small at $T < T_1$, but the Drude weight will crossover to a larger value proportional to $\sigma(T_2)$ at $T \sim T_2$.

Hall Effect

For both temperature ranges $T < T_1$ and $T > T_2$, the transport coefficients can be derived with the rudimentary semiclassical theory of metal. We take the semiclassical Boltzmann transport equation under the relaxation-time approximation

$$\frac{\partial g}{\partial t} + \dot{\boldsymbol{x}} \cdot \frac{\partial g}{\partial \boldsymbol{x}} + \dot{\boldsymbol{k}} \cdot \frac{\partial g}{\partial \boldsymbol{k}} = \left(\frac{\partial g}{\partial t}\right)_{\text{coll}} \approx -\frac{\delta g}{\tau}, \tag{4.30}$$

where $g(t, \boldsymbol{x}, \boldsymbol{k})$ denotes the non-equilibrium distribution function, and δg is its deviation from the equilibrium distribution $f(\epsilon)$. This Boltzman equation can be applied to the parton ψ_α at temperature $T < T_1$, and to electrons at temperature $T > T_2$.

At low temperature, according to the Ong's formula [445] based on the Jones-Zener solution to Eq. 4.30, the weak-field Hall conductivity in $2d$ metals has a geometric interpretation

$$\sigma_{xy} = \frac{e_*^2}{h} \frac{\mathcal{A}_l}{\pi (l_B^*)^2} \tag{4.31}$$

where $l_B^* = \sqrt{\hbar/(e_* B)}$ is the magnetic length for partons, and $\mathcal{A}_l$ is the area swept out by the vector $\boldsymbol{l}(\boldsymbol{k}) = \tau(\epsilon(\boldsymbol{k}))\boldsymbol{v}(\boldsymbol{k})$ when $\boldsymbol{k}$ moves around the FS, i.e.,

$$\mathcal{A}_l = \frac{\boldsymbol{B}}{B} \cdot \int_{\mathrm{FS}} d\boldsymbol{l}(\boldsymbol{k}) \times \boldsymbol{l}(\boldsymbol{k}) \sim l_{\mathrm{m}}^2. \tag{4.32}$$

If we assume electrons and partons share the same isotropic l_{m} and therefore the same area $\mathcal{A}_l$, there is a large ratio between σ_{xy} at low temperature and the second crossover temperature T_2:

$$\frac{\sigma_{xy}(T_2)}{\sigma_{xy}(T < T_1)} \sim N^3. \tag{4.33}$$

The situation is different in the strong field limit. In this limit the collision integral in Eq. 4.30 can be neglected. Taking the directions $\boldsymbol{B} = B\hat{z}$ and $\boldsymbol{E} = E\hat{y}$, one obtains the solution $\delta g = (\hbar k_x E/B)(\partial f/\partial \epsilon)$ which has no explicit dependence on N. In this case, the integral of $v_x(\boldsymbol{k})\delta g(\boldsymbol{k})$ over the Brillouin zone gives $n_* E/B$, which leads to the high-field Hall conductivity

$$\sigma_{xy} = \frac{n_* e_*}{B} = \frac{n_e e}{B}. \tag{4.34}$$

The answer only depends on the total charge density.

Thermoelectric Properties

In the presence of nonzero electric field $\boldsymbol{E}$ and temperature gradient $-\nabla T$, the linear response of electric current $\boldsymbol{J}^e$ and heat current $\boldsymbol{J}^h$ are usually organized in one equation

$$\begin{pmatrix} \boldsymbol{J}^e \\ \boldsymbol{J}^h \end{pmatrix} = \begin{pmatrix} \sigma & \alpha \\ T\alpha & \bar{\kappa} \end{pmatrix} \begin{pmatrix} \boldsymbol{E} \\ -\nabla T \end{pmatrix}. \tag{4.35}$$

The electrical conductivity σ and thermoelectric transport coefficients $\alpha, \bar{\kappa}$ are matrices of spatial coordinates. When $\boldsymbol{J}^e = 0$, the thermal conductivity is given by $\kappa = \bar{\kappa} - T\alpha\sigma^{-1}\alpha$. The semiclassical equation of motion of partons in electric and magnetic fields reads

$$\begin{aligned} \dot{\boldsymbol{x}} \equiv \boldsymbol{v}_n(\boldsymbol{k}) &= \frac{1}{\hbar}\frac{\partial \epsilon_n(\boldsymbol{k})}{\partial \boldsymbol{k}} - \dot{\boldsymbol{k}} \times \boldsymbol{\Omega}_n(\boldsymbol{k}), \\ \hbar\dot{\boldsymbol{k}} &= -e_*\boldsymbol{E}(\boldsymbol{x}) - e_*\dot{\boldsymbol{x}} \times \boldsymbol{B}(\boldsymbol{x}), \end{aligned} \tag{4.36}$$

where n is the band index, and $\boldsymbol{\Omega}_n(\boldsymbol{k})$ is the Berry curvature associated with each band.

We first evaluate the diagonal thermoelectric response by neglecting the magnetic field $\boldsymbol{B}$ and the Berry curvature $\boldsymbol{\Omega}_n$. With nonzero electric field and temperature gradient, the solution of the Boltzmann equation Eq. 4.30 for deconfined partons reads

$$\delta g = -\left(e_*\boldsymbol{E} + \frac{\epsilon(\boldsymbol{k}) - \mu}{T}\nabla T\right) \cdot \boldsymbol{v}(\boldsymbol{k})\tau(\epsilon(\boldsymbol{k}))\left(-\frac{\partial f}{\partial \epsilon}\right), \tag{4.37}$$

which leads to the diagonal transport coefficients

$$\begin{aligned} \sigma_{xx} &= e_*^2 \mathsf{s}_{xx}(\epsilon_F^*) \sim \frac{\mathsf{s}_{xx}(\epsilon_F^*)}{N^2}, \\ \alpha_{xx} &= -\frac{e_*}{T}\int d\epsilon \left(-\frac{\partial f}{\partial \epsilon}\right)(\epsilon - \mu)\mathsf{s}_{xx}(\epsilon) \sim \frac{T\mathsf{s}'_{xx}(\epsilon_F^*)}{N}, \\ \bar{\kappa}_{xx} &= \frac{1}{T}\int d\epsilon \left(-\frac{\partial f}{\partial \epsilon}\right)(\epsilon - \mu)^2 \mathsf{s}_{xx}(\epsilon) \sim T\mathsf{s}_{xx}(\epsilon_F^*), \end{aligned} \tag{4.38}$$

where we have used $(-\partial f/\partial\epsilon) \approx \delta(\epsilon - \epsilon_F^*)$ and $\mu \approx \epsilon_F^*$ at low temperature, and the function $\mathsf{s}_{ij}(\epsilon)$ is defined as

$$\mathsf{s}_{ij}(\epsilon) = \tau(\epsilon) \int \frac{d^2\boldsymbol{k}}{(2\pi)^2} \delta(\epsilon - \epsilon(\boldsymbol{k})) v_i(\boldsymbol{k}) v_j(\boldsymbol{k}). \tag{4.39}$$

Assuming the band mass is isotropic and $\boldsymbol{k}$-independent, one reproduces the Drude form for partons $\mathsf{s}_{ij} = \delta_{ij}\tau n_*/m_*$. The thermopower Q (i.e., Seebeck coefficient) of the charge fractionalized metal is given by:

$$Q(T < T_1) = \frac{\alpha_{xx}}{\sigma_{xx}} = -N\frac{\pi^2}{3}\frac{k_B^2 T}{e}\frac{\sigma'}{\sigma}. \tag{4.40}$$

Note that the mean free path l_{m} gets cancelled in the ratio.

Experimentally, one clear signature for a charge fractionalized metal is the strong violation of the Wiedemann-Franz law. The Lorentz number acquires a large factor due to charge fractionalization:

$$L(T < T_1) = \frac{\kappa_{xx}}{T\sigma_{xx}} = N^2\frac{\pi^2}{3}\frac{k_B^2}{e^2}. \tag{4.41}$$

This strong violation of the Wiedemann-Franz law can be naively understood by the fact that, though each fermionic parton carries a much smaller charge, it still carries the same entropy as an electron.

When the temperature reaches T_2 and the partons are fully confined, we expect these transport coefficients to decrease due to confinement

$$\frac{Q(T_2)}{Q(T < T_1)} \sim \frac{1}{N}, \qquad \frac{L(T_2)}{L(T < T_1)} \sim \frac{1}{N^2}. \tag{4.42}$$

For systems that break time-reversal symmetry such as a ferromagnetic metal, the

transport coefficients σ, α, κ could have nonzero off-diagonal terms even in the absence of $\boldsymbol{B}$. They receive intrinsic contributions from the Berry curvature in the band structure. Considering the nonzero Berry curvature $\boldsymbol{\Omega}(\boldsymbol{k})$ in Eq. 4.36, the parton wave packet acquires an anomalous velocity orthogonal to $\boldsymbol{E}$, which leads to the anomalous Hall conductivity

$$\sigma_{xy}(\epsilon) = \frac{e_*^2}{\hbar} \int \frac{d^2\boldsymbol{k}}{(2\pi)^2} \Theta(\epsilon - \epsilon(\boldsymbol{k}))\Omega^z(\boldsymbol{k}), \tag{4.43}$$

where $\Theta(\epsilon)$ is the Heaviside step function. Similar to their diagonal counterparts, the thermal Hall conductivity κ_{xy} is given by

$$\kappa_{xy}(\epsilon) = \frac{\pi^2}{3} \frac{k_B^2 T}{e_*^2} \sigma_{xy}(\epsilon). \tag{4.44}$$

At low temperature, the transverse Wiedemann-Franz law is still strongly violated due to charge fractionalization.

4.2.3 Fractionalized Metal with $\mathrm{SU}(N)$ Gauge Fields

In this section we consider a more complex example of metal with charge fractionalization. For simplicity we will consider spin polarized electrons, hence the electron operator no longer carries a spin index. The first step of our construction is a parton construction:

$$c_j \sim \sum_{\{\alpha_i\}} \epsilon_{\alpha_1,\alpha_2,\cdots\alpha_N} \psi_{j,\alpha_1} \psi_{j,\alpha_2} \cdots \psi_{j,\alpha_N}. \tag{4.45}$$

This parton construction introduces a $\mathrm{SU}(N)$ gauge degree of freedom with an odd integer N. The nonabelian gauge field was also first introduced for particle physics [446], but

later used broadly in the study of spin liquids (see for example Ref. 443), and other strongly correlated electron systems [447, 448]. The parton ψ_α with $\alpha = 1 \cdots N$ carries a fundamental representation of the SU(N) gauge group, and also physical electric charge $e_* = e/N$. The starting point of our analysis is the following Lagrangian:

$$\begin{aligned}
&\mathcal{L}_{\rm UV}[\psi^\dagger, \psi, a] = \mathcal{L}_{\rm UV}[\psi, a] + \mathcal{L}_{\rm UV}[a], \qquad \mathcal{L}_{\rm UV}[a] = -\frac{1}{4} F^I_{\mu\nu}(F^I)^{\mu\nu} \\
&\mathcal{L}_{\rm UV}[\psi, a] = \psi^\dagger(\mathrm{i}\partial_t + g a^I_0 \mathbf{t}^I + e_* A_0 + \mu)\psi - \frac{1}{2m}\psi^\dagger(-\mathrm{i}\nabla + g a^I_i \mathbf{t}^I + e_* A_i)^2 \psi
\end{aligned} \tag{4.46}$$

where $\psi = (\psi_1, \psi_2, ..., \psi_N)^\mathsf{T}$, $a^I_\mu = (a^I_0, \vec{a}^I)$ is the SU(N) gauge field with $\mu = 0, 1, 2$; $\mathbf{t}^I$ is the SU(N) Lie algebra in the fundamental representation, with $I = 1, 2, \ldots, N^2 - 1$. g is the strength of the gauge coupling, the non-Abelian gauge field stress tensor is $F^I_{\mu\nu} = \partial_\mu a^I_\nu - \partial_\nu a^I_\mu + g\epsilon^{IJK} a^J_\mu a^K_\nu$, and $A_\mu = (A_0, \vec{A})$ is the background U(1) electromagnetic field.

Just like all systems that involve nonabelian gauge fields, Eq. (4.46) needs gauge fixing. The systematic method of gauge fixing is through the Faddeev-Popov procedure [449], by introducing the ghost fields. Since our system does not have Lorentz invariance to begin with, we will consider the Coulomb gauge $\nabla \cdot \vec{a} = 0$. It was shown in Ref. 89 that the ghost fields are decoupled from the system in the infrared limit. Further more, the nondynamical component of the gauge field a_0 is suppressed by the Thomas-Fermi screening of the Fermi surface, hence will be dropped in the rest of the consideration.

Eq. 4.46 with a finite Fermi surface is a highly challenging theory to study. Starting with the Lagrangian Eq. 4.46, one standard approximate treatment is to construct the low energy effective theory assuming that the Fermi energy is the largest energy scale in the problem, and $T \ll E_F$. Below the cutoff Λ that satisfies $T \ll \Lambda \ll E_F$, the fermion operators can be expanded on two opposite patches of the Fermi surface. A patch model

can be constructed following the logic of Ref. 44, 45, 46, 48, 85, 50, 51, 354, 89. The patch lagrangian $\mathcal{L}_{\text{patch}}$ reads

$$\begin{aligned}\mathcal{L}_{\text{patch}}[\psi, a] &= \psi^\dagger \left[\mathrm{i}\eta\partial_t - \left(l v_F k_x + \frac{k_y^2}{2m} \right) \right] \psi - l g v_F \psi^\dagger a_x^I \mathbf{t}^I \psi, \\ \mathcal{L}_{\text{patch}}[a] &= \frac{1}{2} q_y^2 (a_x^I)^2. \end{aligned} \tag{4.47}$$

x and y are the local coordinates orthogonal and transverse to the patch Fermi surface of interest, $l = \pm 1$ labels the antipodal patches that can be connected by the transverse gauge fluctuations. The form of the patch Lagrangian implies the following scaling of space-time coordinates under coarse graining

$$\omega' = b^{z_\psi}\omega,\ k_x' = b k_x,\ k_y' = b^{1/2} k_y \tag{4.48}$$

with $z_\psi = 1$, and $b > 1$. Due to the different scaling dimensions of the x and y coordinate and the Coulomb gauge constraint, we find $\Delta_{a_y} = \Delta_{a_x} + 1/2$, where $\Delta_{\mathcal{O}}$ is the scaling dimension of a field or coupling $\mathcal{O}$, e.g. $a_y' = b^{\Delta_{a_y}} a_y$, $a_x' = b^{\Delta_{a_x}} a_x$. Due to the highly anisotropic scaling of space-time, the form of the Lagrangian of the patch theory Eq. 4.47 is very different from a standard Lorentz invariant theory.

Unlike the U(1) gauge theory, a non-Abelian gauge field has self-interactions. It can be argued within the framework of the patch theory [89] that the self-interaction between gauge bosons is irrelevant in the infrared, hence we can use Eq. 4.47 as the starting point of RG analysis. Note that the irrelevance of gauge field self-interactions is due to the highly anisotropic scaling of local coordinates x and y in Eq. 4.47. To get a controlled interacting RG fixed point, we need one more step of transformation of Eq. 4.47: we consider a small ϵ expansion by replacing q_y^2 with $q_y^{1+\epsilon}$, as was first introduced by Ref. 45, 46. At the leading order of ϵ, only the 1-loop diagrams contribute, which

leads to a weakly interacting RG fixed point [45, 46, 85]. The self-energy correction to the parton propagator $\mathrm{G} = -\mathrm{i}\langle T_t \psi \bar{\psi}\rangle$ obtained by integrating out modes from $q_y = \Lambda$ to $q_y = \Lambda/b^{1/2}$ reads

$$\delta\Sigma = -\mathrm{i}\omega \frac{g^2 v_F}{4\pi^2} \mathbb{c}_2 \mathbf{1} \ln b \tag{4.49}$$

where $\mathbb{c}_2\mathbf{1} = \sum_I \mathbf{t}^I \mathbf{t}^I = \frac{N^2-1}{2N}\mathbf{1}$, with $\mathbb{c}_2$ the quadratic Casimir operator for the fundamental representation of SU(N); and $\mathbf{1}$ is the identity matrix in the color space. The vertex correction vanishes at the leading order ϵ-expansion, as was argued in Ref. 85. Eventually the one-loop corrections lead to a new fixed point $g_*^2 = 2\pi^2\epsilon/(\mathbb{c}_2 v_F)$. The existence of this fixed point is physically due to the screening of the gauge coupling from matter fields with finite density of states.

Physical properties at this new fixed point can be self-consistently solved. To be general, we consider the gauge field kinetic energy as $k_y^2 \to |k_y|^{1+\epsilon}$, while ϵ is not necessarily small for the self-consistent calculation. Assuming that the parton self-energy does not depend on the momentum, which can be checked posteriori, the self-consistent equation reads

$$\begin{aligned}
&\Sigma_{\alpha\alpha'}(\mathrm{i}\omega, \boldsymbol{k}) = \sigma_\psi(\mathrm{i}\omega, \boldsymbol{k})\delta_{\alpha\alpha'}, \\
&\sigma_\psi(\mathrm{i}\omega, \boldsymbol{k}) = (-)g^2 v_F^2 \mathbb{c}_2 \int \frac{\mathrm{d}\nu \mathrm{d}q_x \mathrm{d}q_y}{(2\pi)^3} \frac{1}{\mathrm{i}(\omega+\nu) + \sigma_\psi(\omega+\nu) - \xi_{\boldsymbol{k}+\boldsymbol{q}}} \frac{1}{\mathrm{i}\nu + \pi_a(\mathrm{i}\nu, \boldsymbol{q}) + q_y^{1+\epsilon}}; \\
&\Pi_{IJ}(\mathrm{i}\nu, \boldsymbol{q}) = \pi(\mathrm{i}\nu, \boldsymbol{q})\delta_{IJ}, \\
&\pi(\mathrm{i}\nu, \boldsymbol{q}) = g^2 v_F^2 \mathbb{c} \int \frac{\mathrm{d}\boldsymbol{k}\mathrm{d}\omega}{(2\pi)^3} \frac{1}{\mathrm{i}\omega + \sigma_\psi(\omega) - \xi_{\boldsymbol{k}}} \frac{1}{\mathrm{i}(\omega+\nu) + \sigma_\psi(\omega+\nu) - \xi_{\boldsymbol{k}+\boldsymbol{q}}}.
\end{aligned} \tag{4.50}$$

The solution for the fermion and gauge boson self-energy is given by

$$\begin{aligned}\sigma_\psi(\omega) &= -\mathrm{i}\frac{\mathbb{C}_2\gamma^{-\epsilon/(2+\epsilon)}}{2(8\pi)^{\epsilon/(2+\epsilon)}}\csc\left(\frac{2\pi}{2+\epsilon}\right)\bar{g}^{\frac{2}{2+\epsilon}}E_f^{\frac{\epsilon}{2+\epsilon}}|\omega|^{\frac{2}{2+\epsilon}}\mathrm{sgn}(\omega),\\ \pi(\mathrm{i}\nu,\boldsymbol{q}) &= \frac{1}{v_F^{2+\epsilon}}\frac{\gamma}{8\pi}\bar{g}E_f^{1+\epsilon}\left|\frac{\nu}{\boldsymbol{q}}\right|.\end{aligned} \tag{4.51}$$

Here we have defined a dimensionless coupling constant $\bar{g} = \frac{g^2 v_F^{1-\epsilon}}{(2m)^\epsilon}$. One can see that the standard Landau damping term emerges in the self-consistent solution of the gauge boson self-energy. And the fermion self-energy takes the form of a non-Fermi liquid.

Confinement and Crossover at Finite Temperature

To evaluate transport properties at different temperature scales, like the Z_N gauge theory discussed earlier, we need to determine the two temperature scales T_1 and T_2 at which the confinement length satisfies $\xi_c(T_1) \sim l_\mathrm{m}$ and $\xi_c(T_2) \sim a$. When $\xi_c > l_\mathrm{m}$ the transport is governed by fractionalized charges. Like the case with the Z_N gauge field, here we need to evaluate the scaling of ξ_c with temperature at the fixed point discussed above, and in this section we are going to take $\epsilon = 1$. First of all, the gauge fields would become classical when $g_*^2\frac{|\nu_{n=1}|}{q} > q^2$, where ν_n is the n-th Matsubara frequency. This gives a quantum-classical crossover length $\xi_\mathrm{cl} \sim q_\mathrm{cl}^{-1} \sim (Tg_*^2)^{-\frac{1}{3}}$ above which the gauge field dynamics is classical. A classical gauge theory in $2d$ is described by the action

$$\mathcal{S}_\mathrm{classical} = \int \mathrm{d}\boldsymbol{x}\ \sum_I \frac{1}{Tg^2}(F_{\mu\nu}^I)^2 \tag{4.52}$$

The scaling dimension of Tg^2 now becomes $\Delta_{Tg^2} = 2$. At the confinement length ξ_c, Tg^2 renormalizes to $Tg^2 \sim 1$. We then find

$$\frac{Tg(\xi_c)^2}{Tg_*^2} \sim \frac{1}{Tg_*^2} \sim \left(\frac{\xi_c}{\xi_{\rm cl}}\right)^2 \quad \Longrightarrow \quad \xi_c(T) \sim (Tg_*^2)^{-5/6} \sim T^{-5/6}. \tag{4.53}$$

Hence at low temperature T, due to the Landau damping physics arising from the Fermi surface, when we observe the system with increasing length scale, physics of the gauge field will first crossover to classical at $\xi_{\rm cl} \sim (Tg_*^2)^{-1/3}$, then crossover to confinement at an even longer scale $\xi_c(T) \sim (Tg_*^2)^{-5/6}$. This analysis implies that the crossover temperature T_1 scales with the mean free path $T_1 \sim l_{\rm m}^{-6/5}$.

Transport Properties

At low temperature, we assume that the impurity still dominates the momentum relaxation. This assumption is valid at strictly zero temperature, and also valid at finite temperature with the artificial limit of small ϵ, since the fixed point gauge coupling $g_*^2 \sim \epsilon$, scattering with the gauge field is weak in this limit. The resistivity caused by gauge boson scattering can be computed following the procedure in Ref. 373. One key difference from the Z_N example we discussed before is that, there are N species of the fermionic partons now, each with the same density as the electron, and hence the same size of Fermi sea as the electron, *i.e.* $n_* = n_e$, and $k_F^* = k_F$. In this case, the conductivity of the fractionalized metal at zero temperature reads

$$\sigma(T=0) = N\left(\frac{n_* e_*^2 l_{\rm m}}{m_* v_F^*}\right) \sim \frac{1}{N}\frac{e^2}{h}(l_{\rm m} n_e^{1/2}), \tag{4.54}$$

which can still be a bad metal. Notice that in other parton constructions for example in Ref. 86, the total electrical conductivity is governed by the Ioeffe-Larkin rule [328]; while

in our case the conductivity should be a direct sum of conductivity of each parton. Once again, when the confinement length ξ_c becomes the order of lattice constant a (which occurs at temperature T_2 with $\xi_c(T_2) \sim a$), the partons are fully confined to electron, and the conductivity is given by the standard form $\sigma(T_2) = \frac{e^2}{h}(l_{\mathrm{m}} n_e^{1/2})$.

At low temperature, both the partons and the gauge bosons will contribute to the thermal transport. But it was shown that the gauge boson contribution is subdominant [450] compared with the fermionic partons, hence it will be ignored in the following discussion. At low temperature the thermal transport of the fermionic partons will also be mostly determined by their scattering with impurities:

$$\frac{\kappa}{T} = N\left(\frac{\pi^2}{3}\frac{k_B^2 n_* l_{\mathrm{m}}}{m_* v_F^*}\right) \sim N\frac{\pi^2}{3}\frac{k_B^2}{h}(l_{\mathrm{m}} n_e^{1/2}), \tag{4.55}$$

again we have taken into account of the fact that, there are N color species of the partons, and for each species $n_* = n_e$. There is still a strong violation of the Wiedmann Franz law same as the Z_N gauge field case Eq. (4.41) at zero temperature:

$$L(T=0) = \frac{\kappa_{xx}}{T\sigma_{xx}} = N^2\frac{\pi^2}{3}\frac{k_B^2}{e^2}. \tag{4.56}$$

4.2.4 Summary and Discussion

We proposed two constructions of exotic metallic phases based on the idea of charge fractionalization. It was proposed before that charge fractionalization may be playing an important role [444] in the metal-insulator transition (MIT) observed in transition metal dichalcogenide (TMD) moiré heterostructures [4], where an anomalously large resistivity was observed at low temperature near and at the MIT, followed by a rapid drop of resistivity at slightly higher temperature, analogous to the physics discussed between T_1 and T_2 in Fig. 4.3. Similar physics has also been observed in another TMD moiré

sample [451].

The two constructions discussed in this work are actually related to each other. The SU(N) gauge group always has a Z_N center, hence the SU(N) gauge field can be broken down to a Z_N gauge field by condensing Higgs fields [452, 453, 454] with the right representation. The condensed Higgs field is also expected to mix the different color species and lift the degeneracy of the fermionic parton Fermi surface. In fact, a spin liquid usually has a U(1) or even SU(2) gauge degrees of freedom in the UV, but the gauge group can be broken down to Z_2 through the Higgs mechanism, hence in the infrared the system becomes a Z_2 spin liquid [441, 442, 443].

4.3 Exactly Solvable Square-Lattice Models for Strange Metal

4.3.1 Introduction

Non-fermi liquid (NFL) state represents a family of exotic metallic states that do not have long-lived quasi-particles, and hence behave fundamentally differently from the standard Landau Fermi liquid theory [43, 44, 45, 46, 47, 48, 49, 50, 51, 52, 455]. The NFLs usually occur at certain quantum critical point in itinerant fermion systems, and the quantum critical fluctuations couple strongly with the fermions and hence "kill" the quasiparticles. But the most well-known (yet poorly understood) NFL, the "strange metal" phase at the optimal doping of the cuprate high temperature superconductors, seems more generic than the byproduct of a certain quantum critical point, because its anomalous temperature dependence of longitudinal DC resistivity ($\rho \sim T$) persists up to a rather high temperature in the phase diagram [63, 64, 65, 66, 67], which is presumably much higher than the ultraviolet cut-off of any possible quantum critical point in the

system. However, like many other NFLs [354, 355, 356, 357, 358, 359, 456], the strange metal phase is also preempted by a dome of "ordered phase" with pair condensate of fermions (high T_c superconductivity) at low temperature. Thus the strange metal phase is more fundamental than the superconductor phase itself: it is the "parent state" of the high T_c superconductor, just like the Fermi liquid is the parent state (or normal state) of conventional BCS superconductors. And we had better view this parent state as a generic non-Fermi liquid state, instead of a quantum critical behavior.

A series of toy models for NFL, despite their relatively unnatural forms, seem to capture the key universal features mentioned above. These models are the so-called Sachdev-Ye-Kitaev (SYK) model and its generalizations [54, 55, 457, 458, 390, 391, 392, 459]. *1.* the fermion Green's function in these models has a completely different scaling behavior from the noninteracting fermions in the infrared limit, thus it has no quasi-particle and by definition is a NFL. *2.* it was found that the SYK model has marginally relevant "pairing instability" just like the ordinary Fermi liquid state [460, 461], which is again consistent with one of the universal features of the NFLs observed experimentally. *3.* Recently measured charge density fluctuation of the strange metal [462] agrees with the unique scaling behavior of the SYK model [54]. *4.* Last but not least, recently a generalization based on the SYK model has shown linear-T resistivity for a large temperature window, and the scaling behavior of the SYK model is the key for the linear-T resistivity [393] (similar effect can be achieved in models with large$-N$ generalization of the electron-phonon coupling [433, 434, 463]). All these developments suggest that some version of the SYK model and its generalizations may indeed have to do with the strange metal phase.

More often than not, an exactly soluble model has to sacrifice reality to some extent by making some artificial assumptions. To ensure its solubility, the original SYK model has the following necessary ingredients that make it unlikely to be directly related to the

cuprates: *1.* It needs an all-to-all four-fermion interaction, while a natural Hamiltonian for a real condensed matter system usually has local interactions only; *2.* The four-fermion interaction is fully random with a Gaussian distribution, which is also far from the real system. *3.* So far the NFL models constructed based on generalizations of the SYK model all have a large number of fermion states on each unit-cell of the lattice with a fully random all-to-all intra unit-cell interaction [464, 465, 466, 467, 393, 394, 396], while the common wisdom is that the cuprate materials only have one active $d-$orbital on each copper site.

In this work we will construct two lattice models for strongly interacting electrons that are still motivated by the SYK physics, but are much closer to real systems. *1.* Our models only need one orbital per unit-cell on the square lattice; *2.* Our models have no quenched randomness; *3.* Our models still capture the most desired physics of the SYK model, such as the linear$-T$ scaling of the longitudinal DC resistivity, and pairing instability in the infrared. In the soluble limit, the solution of our model is identical to the SYK model, thus our analytical results largely rely on the known solution of the SYK model in for instance Ref. 457. But we will also check our analytical predictions based on the soluble limit by exact diagonalization of the minimal and most realistic version of our model away from the soluble limit, on a finite system. The phase diagram of our proposed model for the physics near the strange metal phase including the low energy phases induced by different perturbations considered in this paper are plotted in Fig. 4.4.

It was shown previously for the Sachdev-Ye model, that away from the exactly soluble large$-N$ limit [4], the SYK scaling still persists at finite energy scale (for example finite temperature), while instabilities due to $1/N$ corrections emerge at low energy which are suppressed (sub)exponentially with increasing$-N$ [468]. Although the exactly soluble

[4]Actually the original Sachdev-Ye model requires two parameters, N and M, be taken infinite. Here for simplicity we use large$-N$ to represent both limits.

version of our models still requires some large$-N$ limit, by evaluating the next order diagrams, we argue that for finite$-N$, the scaling behavior of the large$-N$ limit may still apply to an intermediate energy or temperature window, which is where the strange metal phase was observed in real systems.

4.3.2 The Hamiltonian

Let us first write down the most important term of the interacting electron Hamiltonian that we will study on the square lattice:

$$H = \sum_j H_j, \tag{4.57}$$
$$H_j = U\hat{n}_j^2 + \sum_{\hat{e}=\hat{x},\hat{y}} J\left(\vec{S}_j \cdot \vec{S}_{j+\hat{e}} - \frac{1}{4}\hat{n}_j\hat{n}_{j+\hat{e}}\right) - K\left(\epsilon_{\alpha\beta}\epsilon_{\gamma\sigma}c^\dagger_{j,\alpha}c^\dagger_{j+\hat{x}+\hat{y},\beta}c_{j+\hat{y},\gamma}c_{j+\hat{x},\sigma} + H.c.\right),$$

where $\epsilon_{\alpha\beta}$ is an 2×2 antisymmetric matrix in the spin space. Other terms, such as single particle hopping, will later be treated as perturbations. We will study this model with a fixed particle density both analytically and numerically. $\hat{n}_j = \hat{n}_{j,\uparrow} + \hat{n}_{j,\downarrow}$ is the total electron number on site j, $\vec{S}_j = \frac{1}{2}c_j^\dagger\vec{\sigma}c_j$ is the spin operator. Besides the standard charge density and spin interactions, we also turned on a "ring exchange" term with coefficient K, which takes a spin singlet pair of electrons on two diagonal sites of a plaquette to the two opposite diagonal sites of the same plaquette. This Hamiltonian preserves the square lattice symmetry (because this interaction only has parity-even and spin singlet pairing between fermions), and also spin SU(2) symmetry.

We will try to make connection between Eq. 4.57 and the SYK physics. As we explained previously, many necessary ingredients of the original SYK model are not very realistic. Instead of directly using the SYK model, our construction Eq. 4.57 is motivated by the randomness-free "tetrahedron" model (or the so-called rank-3 tensor

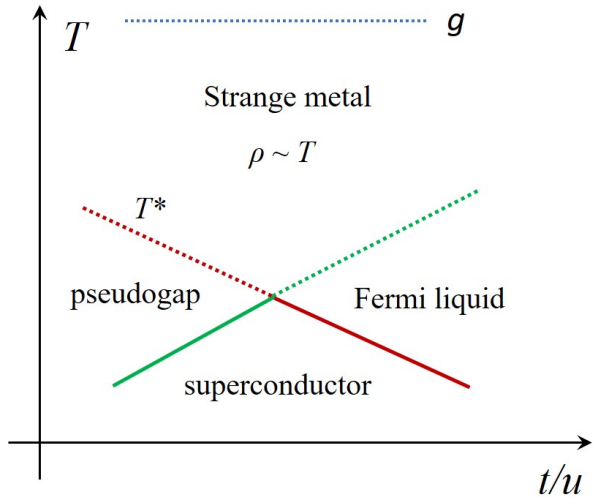

Figure 4.4: The schematic phase diagram of our Hamiltonian Eq. 4.57 or Eq. 4.80 plus single particle hopping parametrized by t and nearest neighbor perturbation H_u (Eq. 4.75) with coefficient u. The strange metal phase is dominated by Eq. 4.57 or Eq. 4.80 only, and is characterized by the non fermi liquid behavior and an anomalous linear$-T$ scaling of the DC resistivity. The pseudogap crossover temperature scale T^* is given by Eq. 4.77. The exact phase boundaries need further calculations.

model) [469, 391, 392]:

$$H_1^t = \frac{g}{(N_a N_b N_c)^{1/2}} c^\dagger_{a_1 b_1 c_1} c^\dagger_{a_2 b_2 c_1} c_{a_1 b_2 c_2} c_{a_2 b_1 c_2}. \tag{4.58}$$

$a_1, a_2 = 1 \cdots N_a$, $b_1, b_2 = 1 \cdots N_b$, and $c_1, c_2 = 1 \cdots N_c$. This model has a $\mathrm{U}(N_a) \times \mathrm{U}(N_b) \times \mathrm{O}(N_c)$ symmetry. It was shown in the literature that, in the large N_i limit, the dominant contribution to the Fermion Green's function comes from a series of "melon Feynman diagrams", which can be summed analytically by solving the Schwinger-Dyson equation.

To make connection to electron systems, the first step is to modify the tetrahedron

model as follows:

$$H_2^t = -\frac{g}{(N_a N_b N_c)^{1/2}} \mathcal{J}_{c_1,c_1'} \mathcal{J}_{c_2,c_2'} c^\dagger_{a_1 b_1 c_1} c^\dagger_{a_2 b_2 c_1'} c_{a_1 b_2 c_2} c_{a_2 b_1 c_2'}, \tag{4.59}$$

where $\mathcal{J}$ is the antisymmetric matrix associated with the $\mathrm{Sp}(N_c)$ group, and $\mathcal{J}_{ab} c_a c_b$ forms a $\mathrm{Sp}(N_c)$ singlet. The total symmetry of this model is now $\mathrm{U}(N_a) \times \mathrm{U}(N_b) \times \mathrm{Sp}(N_c)$. The solubility of this model is unchanged from Eq. 4.58 in the large$-N_i$ limit, and the single particle Green's function in this limit is identical to the disorder-averaged Green's function of the SYK model [457]:

$$G(\tau) = -\mathcal{B}(\theta)\, e^{-2\pi T \mathcal{E} \tau} \sqrt{\frac{\pi T}{2g \sin(\pi T \tau)}}, \tag{4.60}$$

$$G(i\omega)_{T=0} = \frac{\mathcal{B}(\theta)}{\sin\left(\frac{\pi}{4} + \theta\right)} \frac{e^{-i\mathrm{sgn}[\omega]\left(\frac{\pi}{2}+\theta\right)}}{|2g\omega|^{\frac{1}{2}}}, \tag{4.61}$$

where a real angle parameter $-\frac{\pi}{4} < \theta < \frac{\pi}{4}$ and the spectral asymmetry $\mathcal{E}$ have been introduced. Both parameters depend on the charge density, and they are related to each other by

$$e^{2\pi\mathcal{E}} = \frac{\sin\left(\frac{\pi}{4} + \theta\right)}{\sin\left(\frac{\pi}{4} - \theta\right)}. \tag{4.62}$$

The angle $\theta = 0$ corresponds to the case of half-filling. By solving consistent equations with the same method as Ref. 457, the coefficient $\mathcal{B}$ is found to be

$$\mathcal{B}(\theta) = \left(\frac{1}{\pi \cos(2\theta)}\right)^{\frac{1}{4}} \sin\left(\frac{\pi}{4} + \theta\right). \tag{4.63}$$

In Eq. 4.60, we have assumed $0 < \tau < \beta$ in the Green's function, and the Green's function with $-\beta < \tau < 0$ is determined by the standard relation $G(\tau + \beta) = -G(\tau)$.

Now we can draw connection between the modified tetrahedron model Eq. 4.59 and our original model Eq. 4.57. When $U = K = \eta J/2$ ($\eta = \pm 1$), the total Hamiltonian Eq. 4.57 is equivalent to the following model with $N = 3$ and $M = 2$:

$$H = \sum_{j} \sum_{r,r'=-(N-1)/2}^{(N-1)/2} \sum_{\alpha,\beta,\gamma,\sigma=1}^{M} -\frac{g\eta_{r,r'}}{N\sqrt{M}} \mathcal{J}_{\alpha\beta}\mathcal{J}_{\gamma\sigma} c^{\dagger}_{j_x,j_y,\alpha} c^{\dagger}_{j_x+r,j_y+r',\beta} c_{j_x,j_y+r',\gamma} c_{j_x+r,j_y,\sigma}. \quad (4.64)$$

Just like the tetrahedron model Eq. 4.59, every fermion still carries three indices: the $\mathrm{Sp}(M)$ spin, the $x-$coordinate, and $y-$coordinate. We will consider and numerically study two versions of the models with $\eta_{r,r'} = +1$ uniformly (when $N = 3$, $M = 2$ it corresponds to $U = K = -J/2$) and $\eta_{r,r'} = (-1)^{r+r'}$ (which corresponds to $U = K = +J/2$) respectively. Here we allow J to take both signs. Although an antiferromagnetic order is well-known in cuprates in the underdoped regime, ferromagnetism has also been discussed in the overdoped regime [470].

The minimal version of the model Eq. 4.64 with $N = 3$, $M = 2$, is identical to Eq. 4.57, which should be analogous to the case with $N_a = N_b = 3$ in Eq. 4.59. In analytical calculations, we always take the thermodynamics limit first (the sum of j is taken on a square lattice with infinite size). Then in the large$-N$ and large$-M$ limit, for both choices of $\eta_{r,r'}$, the fermion Green's function is still dominated by the "melon diagrams", and hence the Schwinger-Dyson equations, as well as their solutions, remain the same as models Eq. 4.58, and Eq. 4.59:

$$G_{j,j',\alpha,\beta}(\tau) = G(\tau)\,\delta_{j,j'}\delta_{\alpha,\beta}, \quad (4.65)$$

from which we can extract the fermion spectral function (local density of states)

$$\rho_f(\omega) = \sqrt{\frac{1}{gT}} \frac{\mathcal{B}(\theta)}{\sin\left(\frac{\pi}{4}+\theta\right)} \mathrm{Im}\left[\frac{ie^{-i\theta}}{2\pi} \frac{\Gamma\left(\frac{1}{4}+\frac{\beta(\omega-\omega_{\mathcal{S}})}{2\pi i}\right)}{\Gamma\left(\frac{3}{4}+\frac{\beta(\omega-\omega_{\mathcal{S}})}{2\pi i}\right)}\right]. \quad (4.66)$$

Here $\omega_{\mathcal{S}} = 2\pi\mathcal{E}T$. The Fermion Green's function has a form of local quantum criticality, and the scaling dimension of the fermion operator is $\Delta[c] = 1/4$.

We have introduced a fixed fermion density defined as

$$\mathcal{Q} = \frac{1}{M}\sum_{\alpha=1}^{M}\left\langle c_{j,\alpha}^{\dagger}c_{j,\alpha}\right\rangle. \tag{4.67}$$

The value of $\mathcal{Q}$ can be varied within the range $0 < \mathcal{Q} < 1$. Using the same method as Ref. 457, the relation between fermion density $\mathcal{Q}$ and the angle parameter θ in the Green's function is found to be

$$\mathcal{Q} = \frac{1}{2} - \frac{\theta}{\pi} - \frac{\sin(2\theta)}{4}, \qquad -\frac{\pi}{4} < \theta < \frac{\pi}{4}. \tag{4.68}$$

The fact that the Fermion Green's function Eq. 4.65 remains localized in space is due to the fact that the Hamiltonian Eq. 4.57 and Eq. 4.64 preserve the center-of-mass of the electrons on the square lattice. Any nonzero fermion correlation with a finite spatial separation would violate the center of mass conservation, thus the Fermion Green's function is fully localized in space. Single particle hopping will later be introduced as perturbation, which breaks center-of-mass conservation and leads to spatial correlation between fermions, and also charge transport.

For finite N and M, we need to estimate the corrections coming from the subdominant Feynman diagrams. For any diagram, if we evaluate it with the solution in the large$-N, M$ limit, it will roughly lead to a "marginal" correction, namely it will correct the large$-N, M$ solution with a logarithmic function of infrared cut-off, say the temperature. This is because in the large$-N, M$ soluble limit the coupling constant g becomes marginal, since the scaling dimension of the fermion operator is 1/4. Subdominant Feynman diagrams of SYK like models have been carefully calculated in Ref. 471, and the

result is consistent with our expectation. Thus we expect that any subdominant diagram will *at most* lead to corrections with the form $\sim 1/N^A 1/M^B (\log(\Lambda/T))^C$, where A, B and C are all positive numbers. This diagram will hence become significant only when

$$T \leq \Lambda \exp(-cN^{\frac{A}{C}} M^{\frac{B}{C}}), \tag{4.69}$$

where Λ is the ultraviolet cut-off of the system, which can be identified as g in our model. Thus we expect the correction to the NFL solution is suppressed rapidly with increasing N and M, hence it is possible that there is a finite energy window where the solution Eq. 4.65 applies. This is consistent with the expectation for the original Sachdev-Ye model away from the exactly soluble limit [468]. Away from the exactly soluble limit, the ground state has no finite entropy density.

4.3.3 Properties of the NFL

Longitudinal Conductivity

Assuming Eq. 4.65 applies to a finite energy window, we can use it to compute quantities at finite temperature within such energy window. Because Eq. 4.57 conserves the center of mass of the electrons, it is incapable of transporting electric charge. More formally, this interaction term does not couple to the zero momentum component of the external electromagnetic field, analogous to models studied previously with center of mass conservation [120, 472]. Thus the single particle hopping term is still responsible for charge transport. In cuprates both the nearest neighbor and second neighbor hoppings are important [473]. In the soluble large$-N, M$ limit, we formally generalize the electric

current density to the following form:

$$J_x = \frac{1}{\sqrt{NM}} \left(\sum_{\alpha} itc^{\dagger}_{j,\alpha} c_{j+\hat{x},\alpha} + \sqrt{\frac{N-1}{2}} itc^{\dagger}_{j,\alpha} c_{j+\hat{x}\pm\hat{y},\alpha} \right) + H.c. \tag{4.70}$$

This electric current density can be derived by designing a corresponding single electron hopping term in the large$-N, M$ limit (which involves both nearest and second neighbor hopping), and couple it to the external electromagnetic field.

Assuming the solution in the large$-N, M$ limit Eq. 4.65 applies to a finite energy window of the system, then according to the Kubo formula, the central task is to calculate the retarded current-current correlation function. The imaginary-time correlation function is defined as $C(J, J; \tau) = \langle \mathbb{T}_\tau J(\tau) J(0) \rangle$. We find $\langle J_x \; J_y \rangle$ correlation vanishes due to the symmetry of the model, and the leading order nonzero contribution to $\langle J_x \; J_x \rangle$ takes the form $C(J, J; \tau) = -2t^2 G(\tau) G(-\tau)$. Then we Fourier transform $C(J, J; \tau)$ to obtain the correlation function in the Matsubara frequency space:

$$C(J, J; i\omega_n) = 2t^2 \int_{\delta}^{\beta-\delta} d\tau e^{i\omega_n \tau} G(\tau) G(\beta - \tau), \tag{4.71}$$

where we have regulated the integral by introducing a small positive cut-off δ. After removing the divergent term $\log \delta$ (which does not contribute to the real part of the conductivity), we obtain the analytically continued correlation function

$$C(J, J; z) = -2\frac{t^2}{g} \mathcal{B}^2 e^{-2\pi\mathcal{E}} \psi\left(\frac{1}{2} + \frac{\beta z}{2\pi i}\right), \tag{4.72}$$

where $\psi(z) = \frac{d}{dz} \log \Gamma(z)$ is the polygamma function, and the complex frequency z satisfies $\mathrm{Im} z > 0$. The function $C(J, J; i\omega_n)$ can be obtained by setting $z \to i\omega_n$ on the above expression, and the retarded/advanced correlation function $C^{R/A}(J, J; \omega)$ is obtained by taking $z \to \omega \pm i0^+$. Finally, using the relation $\sigma(\omega) = \frac{1}{i\omega} C^R(J, J; \omega)$, we

find the real part of the optical conductivity

$$\mathrm{Re}\sigma\left(\omega\right)=\frac{\sqrt{\pi}t^{2}}{4gT}\Upsilon_{\sigma}\left(\mathcal{Q},\omega/T\right), \tag{4.73}$$

where

$$\Upsilon_{\sigma}\left(\mathcal{Q},\omega/T\right)=\sqrt{\cos\left(2\theta\left(\mathcal{Q}\right)\right)}\frac{\tanh\left(\omega/2T\right)}{\omega/2T} \tag{4.74}$$

is the scaling function of conductivity. From another perspective, Υ_σ can also be computed from the convolution of the scaling function of the fermion spectral function ρ_f in Eq. 4.66.

By our definition, Υ_σ depends on both the fermion density $\mathcal{Q}$ and the ratio ω/T. The $\mathcal{Q}$-dependence of the conductivity is contained in the coefficient $\sqrt{\cos\left(2\theta\right)}$ in the scaling function $\Upsilon_\sigma\left(\mathcal{Q},\omega/T\right)$, and the function $\theta\left(\mathcal{Q}\right)$ can be obtained by inverting Eq. 4.68. The half-filling $\theta=0$ gives the maximum conductivity, as one would naively expect. Once we fix the ratio ω/T (for example the DC limit with $\omega/T=0$), the longitudinal conductivity $\sigma(\omega,T)$ is proportional to $1/T$, which is the most important phenomenon of the strange metal phase.

In the calculation above we have assumed that the correlation function between current operators factorizes into a product of two Fermion Green's functions. This is true in the large$-N,M$ limit using the current operator Eq. 4.70, and the expression Eq. 4.73 is exact in this limit.

We also studied the minimal and most realistic version of our model, Eq. 4.57, with exact diagonalization on a small 3×4 lattice with periodic boundary condition, and a fixed particle number $N_p=4$. With our numerical method, it is most convenient to compare the quantity $F(\omega_c,T)=\int_0^\infty d\omega e^{-\omega/\omega_c}\omega\sigma(\omega,T)$ with the analytical result Eq. 4.73. We

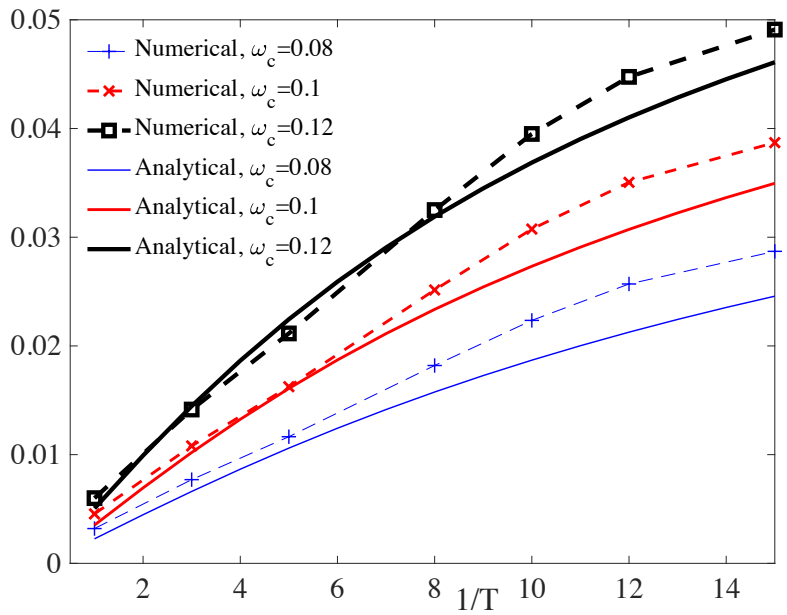

Figure 4.5: The quantity $F(\omega_c, T) = \int_0^\infty d\omega e^{-\omega/\omega_c}\omega\sigma(\omega, T)$ extracted from exact diagonalization of Eq. 4.64 on a 3×4 lattice, with $g = 1$, $M = 2$, $N = 3$, and a fixed particle number $N_p = 4$. The solid lines are the plot of the same quantity calculated based on the scaling function Eq. 4.73. In the definition of electric current we have also taken $N = 3$, $M = 2$, namely both the nearest neighbor and second neighbor hopping will contribute to conductivity. On this small system our data with a uniform $\eta_{r,r'} = +1$ compares better with the analytical solution in the large$-N, M$ limit.

found that the case with a uniform choice $\eta_{r,r'} = +1$ compares better with the solution in the large$-N, M$ limit. The general shape of the function $F(\omega_c, T)$ obtained numerically is similar to the analytical expression in the large$-N, M$ limit (Fig. 4.5), but further numerical evidences are demanded for larger system sizes, for both choices of $\eta_{r,r'}$.

The value of the DC conductivity is tunable by the parameter t in the definition of the electric current (which is determined by the size of the hopping term), and the overall energy scale g. Thus the resistivity in the minimal version of our model can easily exceed the Mott-Ioffe-Regel limit, *i.e.* it can naturally become the so-called "bad metal", which is another puzzling phenomenon observed in cuprate materials and has attracted a lot of attentions [78, 79, 80].

Pairing instability and "pseudogap"

Besides hopping, we can also turn on other perturbations on Eq. 4.57. For example, we can turn on the following perturbation on every link of the lattice:

$$H_u = \sum_{<i,j>} -\frac{u}{2M}\left(\Delta_{i,j}^\dagger \Delta_{i,j} + \Delta_{i,j}\Delta_{i,j}^\dagger\right). \tag{4.75}$$

Here $\Delta_{i,j} = \mathcal{J}_{\alpha\beta} c_{i,\alpha} c_{j,\beta}$ is a $\mathrm{Sp}(M)$ singlet pairing operator on a nearest neighbor link $< i, j >$. This term can be reorganized into a nearest neighbor density-density interaction and a Heisenberg interaction using the Fierz identity of the symplectic Lie algebra [474].

This interaction term is marginal at the large$-N, M$ limit by power-counting, again based on the fact that the fermion operator has scaling dimension 1/4, and in the large$-N, M$ limit all the renormalization from Eq. 4.64 to this term is contained in the renormalization of the fermion operator. In this limit, the RG equation of u can be computed through the standard loop diagram in the same way as Ref. 460, using the fermion Green's function in Eq. 4.61:

$$\frac{du}{d\ln l} = \frac{u^2}{\sqrt{g^2 \pi \cos(2\theta)}}. \tag{4.76}$$

Thus the u term is marginally relevant in this limit, and it will likely lead to the fermion pairing instability just like the BCS instability of the ordinary Fermi liquid.

H_u and single particle hopping will compete with each other under RG. H_u will become nonperturbative at scales T^*:

$$T^* \sim g \exp\left(-\sqrt{\pi \cos(2\theta)}\frac{g}{u}\right). \tag{4.77}$$

Assuming the single particle hopping becomes nonperturbative at scale E_0 (by naive

power-counting a single particle hopping is indeed relevant, and will become nonperturbative at scale $E_0 \sim t^2/g$), Then obviously there are two possible scenarios: If $E_0 > T^*$, the hopping term will dominate the low energy physics and generate a Fermi sea. And at low energy the RG flow of u will be controlled by the standard RG equation of interactions on the Fermi sea, and again u will be marginally relevant and lead to a pairing instability [42]. H_u and the band structure together will likely favor a $d-$wave superconductor [475, 476, 477] on the square lattice near half-filling.

The possibility of $T^* > E_0$, *i.e.* u becomes nonperturbative first under renomralization while lowering energy, is even more interesting. Without single electron hopping, based on the RG equation Eq. 4.76 alone, one cannot determine the pairing symmetry. In fact, in this case, while lowering temperature (energy scale), before forming a superconductor with global phase coherence, the system would favor to form Sp(M) spin singlet fermion pairings on as many nearest neighbor links as possible. At half-filling, a generalization of the Rokhsar's theorem [222] can be straightforwardly applied to our case, and the ground states of Eq. 4.75 in the large$-M$ limit are all the "dimerized" configurations with one quarter of the links occupied by $M/2$ pairs of fermions that each forms a Sp(M) singlet [5]. All these dimerized configurations are degenerate in the large$-M$ limit [222]. Weak disorder and $1/M$ correction could energetically select certain pattern of dimerization from the extensively degenerate configurations, as was observed experimentally [478]. This state has a single particle excitation gap which necessarily breaks a Sp(M) singlet on one of the links, but there is no global fermion-pair phase coherence. This case could be identified as the pseudogap phase in the cuprates phase diagram above the superconducting dome.

[5]Rokhsar's original theorem was proven for spin systems instead of fermion systems. But this theorem was formulated in the slave-fermion language, and the gauge constraint on the slave-fermions becomes less and less important with increasing N. In the large$-N$ limit, energetically the slave fermions become physical fermions, because the gauge field dynamics is completely suppressed in this limit.

The "pseudogap" crossover temperature T^* is given by Eq. 4.77, below which the system develops a nonzero expectation value of $\langle\Delta_{ij}\rangle = \Delta$ on a maximal possible number of links, based on our physical picture given above. With a nonzero Δ, for each pair of sites i and j coupled by the Sp(M) singlet pair, we consider the perturbation $\frac{u}{M}\Delta^*\left(\mathcal{J}_{\gamma\delta}c_{i,\gamma}c_{j,\delta}\right)+H.c.$ to the original model Eq. 4.59. Let us consider two sites ($j = 1, 2$) connected by a dimer. We introduce a $2M$-component fermion basis $\Psi = \left(c_{1,\alpha}\ ,\ c^\dagger_{2,\alpha}\right)^T$ and the $2M \times 2M$ Green's function matrix $\mathcal{G}(\tau) \equiv -\langle\mathbb{T}_\tau\Psi(\tau)\Psi(0)^\dagger\rangle$. To the first order of Δ, the Green's function in the imaginary-frequency domain is given by

$$\mathcal{G}^{-1}\left(i\omega_n\right) = \begin{bmatrix} G^{-1}\left(i\omega_n\right) & \frac{u}{M}\Delta\mathcal{J} \\ \frac{u}{M}\Delta^*\mathcal{J}^{\mathrm{T}} & -G^{-1}\left(-i\omega_n\right) \end{bmatrix}, \tag{4.78}$$

where $G\left(i\omega_n\right)$ is the original single fermion Green's function given by Eq. 4.61,Eq. 4.60. By inverting Eq. 4.78, we obtain the final Green's function $-\langle\mathbb{T}_\tau c_{1,\alpha}(\tau)c^\dagger_{1,\beta}(0)\rangle$:

$$\frac{\delta_{\alpha\beta}}{G^{-1}\left(i\omega_n\right) + \frac{u^2}{M^2}\left|\Delta\right|^2 G\left(-i\omega_n\right)}. \tag{4.79}$$

We can analytically continue this expression to real frequency to obtain the retarded Green's function on each site, whose imaginary part can be identified as the local density of states (see Fig. 4.6), where a "pseudogap" is manifest. In this calculation the Green's function only depends on the amplitude of $\langle\Delta_{ij}\rangle$, thus even if the phase angle of $\langle\Delta_{ij}\rangle$ is disordered the pseudogap in the local density of states is still expected to exist.

A schematic global phase diagram with the parent strange metal phase dominated by H_s, and the competition between perturbations H_u and single particle hopping parametrized by t is depicted in Fig. 4.4.

We must stress that all the analysis discussed in this section is based on the physics of the tetrahedron model in the soluble limit, which is identical to the disorder-averaged

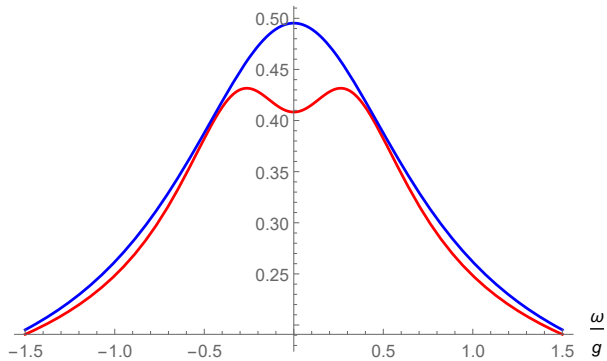

Figure 4.6: The local density of states at half filling ($\theta = 0$) with $T > T^*$ and $\langle \Delta_{ij} \rangle = 0$ (blue upper curve), and $T < T^*$ with nonzero $\langle \Delta_{ij} \rangle$ (red lower curve). In the former case we have chosen $g\beta = 2$; in the latter case we have chosen $g\beta = 4.5$ and $(u\Delta)/(gM) = 0.15$ for illustration.

physics of the SYK model. No matter how exactly the SYK physics is realized in the real system, these analysis always applies. Our Eq. 4.57 and Eq. 4.64 only give one possible realization of these physics. Very similar physics can be realized in another model discussed in the following section.

4.3.4 Another Possible Model

Another model which is slightly less natural but probably leads to very similar physics is also worth discussion. Again, the most important term (but not the only term) of the Hamiltonian reads

$$H = \sum_j H_j, \tag{4.80}$$

$$H_j = U\hat{n}_j^2 + \sum_{\hat{e}=\hat{e}_1,\hat{e}_2} J\left(\vec{S}_j \cdot \vec{S}_{j+\hat{e}} - \frac{1}{4}\hat{n}_j\hat{n}_{j+\hat{e}}\right) - K\left(\epsilon_{\alpha\beta}\epsilon_{\gamma\sigma}c^\dagger_{j,\alpha}c^\dagger_{j+\hat{e}_1+\hat{e}_2,\beta}c_{j+\hat{e}_2,\gamma}c_{j+\hat{e}_1,\sigma} + H.c.\right),$$

where $\hat{e}_1 = \hat{x} + \hat{y}$, and $\hat{e}_2 = \hat{x} - \hat{y}$. This term has no interaction between sublattice A and B yet, and like before we will consider the single particle hoppings and interactions that mix the two sublattices as perturbations.

The advantage of this model is that, we no longer needs a large$-N$ generalization of the hopping term. The ordinary nearest neighbor hopping bridges the two sublattices, *i.e.* it bridges two "SYK-clusters", similar to the previously studied coupled SYK cluster models [479, 480]. The nearest neighbor hopping with coefficient t is a relevant perturbation based on the scaling dimension of the fermion operator $\Delta[c_j] = 1/4$ in the soluble limit. The scaling dimension of t is $\Delta[t] = 1/2$. Thus with the perturbation of the nearest neighbor hopping, we expect the large$-N, M$ solution of the tetrahedron model to be applicable roughly to the energy window $(t^2/g,\ g)$, and within this window the longitudinal conductivity $\sigma(\omega, T)$ takes the same form as the previous case. Other analysis like the perturbation of H_u (Eq. 4.75) and pairing instability remains unchanged compared with the last model we considered.

4.3.5 Summary and Discussion

In this work we proposed two strongly interacting electron models on the square lattice, with one orbital per unit cell. And we demonstrated that in certain limit these models mimic the behavior of the "tetrahedron" tensor model, and hence can be solved. The physics in this limit is consistent with the main phenomenology of the strange metal non fermi liquid phase observed in the cuprates. We argue that away from this exactly soluble limit, there is still a finite energy window where the solution is applicable. We then checked our predictions numerically by exactly diagonalizing the minimal version of the proposed Hamiltonian (which is away from the soluble limit and hence takes a realistic form) on a small lattice. We also discussed effects of perturbations including the single particle hopping, and argued that depending on the competition between two perturbations, the system can develop either a $d-$wave superconductor, or a "pseudogap" phase at low temperature.

More numerical effort is demanded in the future to further analyze both our models Eq. 4.57, Eq. 4.80. Also, more predictions on thermodynamics and transport can be made below the crossover temperature T^* where the system enters the pseudogap phase driven by H_u. The exact phase boundaries in the phase diagram Fig. 4.4 also needs further detailed calculations. In this work we have treated single particle hopping as a perturbation on top of the SYK-like physics. A complete treatment of the interaction term Eq. 4.57, Eq. 4.80 together with a single particle hopping is demanded in the future in order to study the momentum space structure of our theory. We will leave these open questions to future studies.

4.4 Lattice Models for NFLs with Tunable Transport Scalings

4.4.1 Introduction

Non-fermi liquid (NFL) states represent a family of exotic metallic states that do not have long-lived quasi-particles, and hence behave fundamentally differently from the standard Landau Fermi liquid theory [81, 82, 43, 44, 45, 46, 47, 48, 49, 50, 51, 52, 455]. The most well-known NFL, the "strange metal" phase at the optimal doping of the cuprate high temperature superconductors, has a universal scaling of its DC resistivity $\varrho \sim T$ [63, 64, 65, 66, 67], while the standard Fermi liquid theory predicts $\varrho \sim T^2$. Recently the same strange metal behavior was observed in twisted bilayer graphene above the superconductor phase [70]. A consensus of the nature of the strange metal phase has not been reached yet, but a series of toy models, despite their relatively unnatural forms, seem to capture many of the key universal features of the strange metal phase. These models are the so-called Sachdev-Ye-Kitaev (SYK) model and its generalizations [54,

55, 457, 458, 390, 391, 392, 459]. For example, it was found that the SYK model has marginally relevant "pairing instability" just like the ordinary Fermi liquid state [460, 461], which is consistent with the fact that the non-Fermi liquid phase is often preempted by a dome of "ordered phase" with pair condensate of fermions (superconductivity) at low temperature [354, 355, 356, 357, 358, 359, 456]. Thus the "SYK phase" can be viewed as a candidate parent phase of superconductor. Also, the recently observed anomalous charge density fluctuation of the strange metal [462] suggests connection to the SYK model [54]. Last but not least, a series of generalizations based on the SYK model has shown linear-T resistivity for a large temperature window, and the scaling dimension of the fermion operators in the SYK model is the key for the linear-T scaling of the resistivity [393, 465, 394, 396]. But these models, in order to ensure solubility, require fully random four-fermion interactions with a Gaussian distribution and zero mean, which is unlikely to exist in real materials. More recently a model on the square lattice without random interaction was constructed [397], which in the soluble limit mimics the physics of the so called three-index tensor models [391, 392, 469], and gives us the same desirable physics such as linear$-T$ scaling of DC resistivity, and marginally relevant instability towards superconductor and other competing phases.

Most of the previously discussed generalizations of the SYK model aimed at constructing the strange metal phase with precisely linear$-T$ scaling of resistivity. But NFL can have much richer physics than the strange metal. In various systems with NFL behaviors, the DC resistivity can scale with temperature as $\varrho \sim T^{\alpha}$ with $1 \leq \alpha < 2$ [72, 73, 74, 75, 76, 77], and α is usually tunable by varying the charge density. As we mentioned in the previous paragraph, the linear$-T$ scaling of the DC resistivity is a direct consequence of the scaling dimension $\Delta_f = 1/4$ of the fermion operator in the SYK model after disorder average. To design a model with α between 1 and 2, we can in principle start with the SYK$_q$ model with $q > 4$. But these models require a $q-$body

interactions between the fermions, and hence are also not realistic for condensed matter systems. Thus to construct a relatively realistic NFL with $\varrho \sim T^{\alpha}$ and an arbitrary $\alpha \in [1, 2)$, we need to start with a model with *four-fermion interaction only* and *no randomness*, but with conformal solutions whose fermion scaling dimensions can be different from 1/4. And most ideally the fermion scaling dimension is tunable with charge density.

The standard approach of understanding these NFLs is by coupling the Fermi liquid state to a fluctuating bosonic quantum critical mode, and the relevant boson-fermion coupling can potentially drive the system into a NFL [81, 82, 43, 44, 45, 46, 47, 48, 49, 50, 51, 52, 455]. And the transport-temperature scaling would depend on the spatial dimensionality and also the momentum carried by the quantum critical mode. In this paper we take a different approach. We will first design two elementary models for interacting fermions that is free of randomness, whose solution in certain theoretical limit is a conformal field theory, and most importantly the fermion has a scaling dimension that depends on the charge density of the model. Then based on these elementary models we design two versions of lattice models which naturally give us $\varrho \sim T^{\alpha}$, and $\alpha \in [1, 2)$ is tunable by charge density. Our models provide an alternative approach of studying various experimentally observed NFLs in a unified framework.

4.4.2 Two Elementary Models

We first give a brief review of the "tetrahedron" three-index tensor model without any disorder, and in the large-N limit their solutions mimic the better-known SYK_4 model. As was discussed in Ref. 392, the original $\mathrm{U}(N_a) \times \mathrm{U}(N_b) \times \mathrm{O}(N_c)$ symmetric tetrahedron model can be written as

$$H = \frac{g}{\sqrt{N_a N_b N_c}} \psi^{\dagger}_{a_1 b_1 c_1} \psi^{\dagger}_{a_2 b_2 c_1} \psi_{a_1 b_2 c_2} \psi_{a_2 b_1 c_2}, \tag{4.81}$$

where $a = 1, \ldots, N_a$, $b = 1, \ldots, N_b$, $c = 1, \ldots, N_c$. One can prove that as long as

$$0 < \frac{N_a}{N_b}, \frac{N_b}{N_c}, \frac{N_c}{N_a} < \infty, \tag{4.82}$$

this tensor model is dominated by the melonic diagrams in the large-N_a, N_b, N_c limit (Fig. 4.7), and its solution is a conformal field theory fixed point in the infrared limit. At the conformal fixed point, the melonic diagrams can be summed by solving the Schwinger-Dyson equations which are identical to the original SYK_4 model for the complex fermions [54, 457, 55]:

$$G\left(i\omega_n\right) = \frac{1}{i\omega_n + \mu - \Sigma\left(i\omega_n\right)}, \tag{4.83}$$

$$\Sigma\left(\tau\right) = -4g^2 G\left(\tau\right)^2 G\left(-\tau\right), \tag{4.84}$$

where the two-point Green's function $G\left(\tau\right)$ is defined as

$$G\left(\tau\right)\delta_{aa'}\delta_{bb'}\delta_{cc'} = -\left\langle \mathbb{T}_\tau \psi_{abc}\left(\tau\right)\psi^\dagger_{a'b'c'}\left(0\right)\right\rangle \tag{4.85}$$

Σ is the self energy, ω_n is fermionic Matsubara frequency $\omega_n = \left(2n+1\right)\pi T, n \in \mathbb{Z}$, and τ is imaginary time. One key feature of this model is that in its conformal solution the fermions have the scaling dimension

$$\Delta_\psi = \frac{1}{4} \tag{4.86}$$

just like the SYK_4 model.

This model certainly has many variants with the same large-N solution. In Ref. 397 in order to make connection to the cuprates, we constructed a lattice model based on a

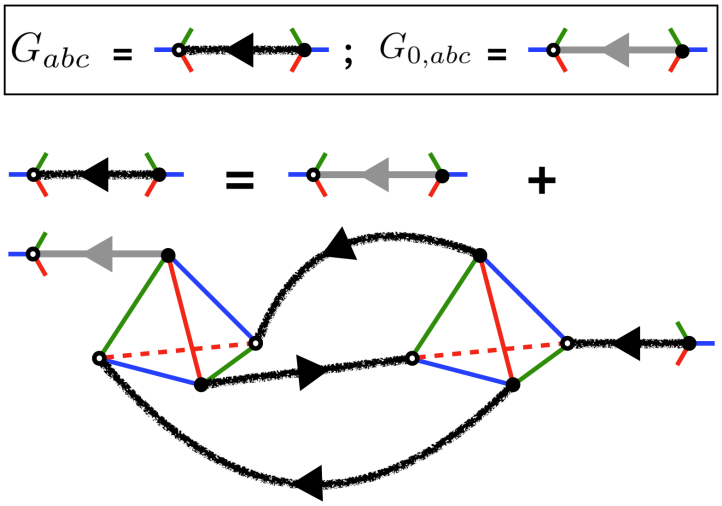

Figure 4.7: The large-N Schwinger-Dyson equation for various complex tetrahedron models.

modified tensor model with the form

$$H = \frac{g\mathcal{J}_{c_1c_1'}\mathcal{J}_{c_2c_2'}}{\sqrt{N_aN_bN_c}}\psi^\dagger_{a_1b_1c_1}\psi^\dagger_{a_2b_2c_1'}\psi_{a_1b_2c_2}\psi_{a_2b_1c_2'}, \tag{4.87}$$

where $\mathcal{J}$ is the antisymmetric matrix associated with the $\mathrm{Sp}\,(N_c)$ group and $\mathcal{J}_{cc'}\psi_c\psi_{c'}$ forms an $\mathrm{Sp}\,(N_c)$ singlet.

So far all the tetrahedron models are comprised of one-orbital of fermions with three indices and conformal dimension 1/4 in the soluble limit. In this paper, we consider generalizations to two versions of "elementary" models each with two orbitals (types) of fermions ψ and χ, and a mutual four-fermion interaction. The existence of multi-orbitals of fermions is analogous to the situation in many heavy fermion systems, where most of the NFLs were observed. This simple generalization leads to some important new features: the conformal dimensions Δ_χ and Δ_ψ can be tuned by changing the parameters, especially the particle density in the models. These elementary models enable us to build several lattice models for NFLs with different transport scalings with randomness-free four-fermion interactions.

Model A

The first "elementary model" we construct takes the following form:

$$H_0^A = \sum_{a_1,a_2,b_1,b_2=1}^{N} \sum_{c=1}^{M_1} \sum_{d=1}^{M_2} \frac{g}{N\sqrt{M}} \left(\psi^\dagger_{a_1,b_1,c} \psi_{a_2,b_2,c} \chi^\dagger_{a_1,b_2,d} \chi_{a_2,b_1,d} + h.c. \right), \tag{4.88}$$

where $M = \sqrt{M_1 M_2}$. ψ and χ are two orbitals (types) of fermions each carries three indices. The model above is the simplest model with the desired features. It has continuous symmetries just like the original tetrahedron model, but these symmetries are not essential to our results. There are also some discrete symmetries that are more important for the solution, which will be spelled out later.

In the large-N, M_1, M_2 limit, just like the three-index tensor models, only the "melonic diagrams" dominate. The sum of all the melonic diagrams must satisfy the coupled Schwinger-Dyson (S-D) equations:

$$G_\psi(i\omega_n) = \frac{1}{i\omega_n + \mu_\psi - \Sigma_\psi(i\omega)}, \tag{4.89}$$

$$G_\chi(i\omega_n) = \frac{1}{i\omega_n + \mu_\chi - \Sigma_\chi(i\omega)}, \tag{4.90}$$

and the self energies are

$$\Sigma^A_\psi(\tau) = -4g^2 \sqrt{\frac{M_2}{M_1}} G_\psi(\tau) G_\chi(\tau) G_\chi(-\tau), \tag{4.91}$$

$$\Sigma^A_\chi(\tau) = -4g^2 \sqrt{\frac{M_1}{M_2}} G_\chi(\tau) G_\psi(\tau) G_\psi(-\tau), \tag{4.92}$$

where we have introduced different chemical potentials μ_ψ, μ_χ for the two fermions to fix the particle densities.

Apparently, in this model the particle density of ψ and χ are separately conserved,

thus we can introduce filling factor $\mathcal{Q}_\psi, \mathcal{Q}_\chi \in (0,1)$ separately. $\mathcal{Q}_\psi$ is defined as

$$\mathcal{Q}_\psi = \frac{\sum_{a,b,c} \langle \psi^\dagger_{a,b,c} \psi_{a,b,c} \rangle}{N^2 M_1}, \tag{4.93}$$

and $\mathcal{Q}_\chi$ is defined accordingly. The role of the filling factors will be specified later and derived in detail in the supplementary material. With fixed filling factors $\mathcal{Q}_\psi$ and $\mathcal{Q}_\chi$, just like the original S-Y model Ref. 54, we should set $\Sigma\left(i\omega_n = 0\right) = \mu$. Thus, we can redefine the self energy as

$$\tilde{\Sigma}_{\psi/\chi}\left(i\omega_n\right) = \Sigma_{\psi/\chi}\left(i\omega_n\right) - \mu \tag{4.94}$$

Now in the infrared limit, assuming the self-energy always dominates the $i\omega_n$ term in the infrared, the S-D equations are simplified as

$$G_\psi\left(i\omega_n\right)\tilde{\Sigma}_\psi\left(i\omega_n\right) = G_\chi\left(i\omega_n\right)\tilde{\Sigma}_\chi\left(i\omega_n\right) = -1. \tag{4.95}$$

At general filling factors $\mathcal{Q}_\psi$ and $\mathcal{Q}_\chi$, and at zero temperature $T = 0$, we use the following power law ansatz at complex frequency z $\left(\mathrm{Im}\left(z\right) > 0, |z| \ll g\right)$ to solve the S-D equations

$$G_\psi\left(z\right) = C_\psi \frac{e^{-i\left(\pi\Delta_\psi + \theta_\psi\right)}}{z^{1-2\Delta_\psi}}, \tag{4.96}$$

$$G_\chi\left(z\right) = C_\chi \frac{e^{-i\left(\pi\Delta_\chi + \theta_\chi\right)}}{z^{1-2\Delta_\chi}}, \tag{4.97}$$

where the real parameters C, θ, Δ satisfy

$$C_\psi > 0, \qquad -\pi\Delta_\psi < \theta_\psi < \pi\Delta_\psi, \tag{4.98}$$

$$C_\chi > 0, \qquad -\pi\Delta_\chi < \theta_\chi < \pi\Delta_\chi. \tag{4.99}$$

There are in general six unknowns that we need to solve for: $C_{\psi/\chi}$, $\Delta_{\psi/\chi}$ and $\theta_{\psi/\chi}$. But through the S-D equations which are exact in the large-N, M_1, M_2 limit, we will be able to determine five of them: $C_\psi^2 C_\chi^2$, $\Delta_{\psi/\chi}$ and $\theta_{\psi/\chi}$. The scaling dimensions $\Delta_{\psi/\chi}$ are the most important quantities which will determine the scaling of the transport coefficients, as we will calculate explicitly later. In the large-N, M_1, M_2 limit, only the product $C_\psi^2 C_\chi^2$ is determined, while C_ψ and C_χ may be determined separately through subleading diagrams.

The S-D equation, or the melonic diagrams, demand that the self energies at complex frequency $z, \mathrm{Im}\,(z) > 0$ take the following form:

$$\tilde{\Sigma}_\psi^A(z) \propto C_\psi C_\chi^2 \sqrt{\frac{M_2}{M_1}} e^{i\left(\pi\Delta_\psi + \theta_\psi\right)} z^{1-2\Delta_\psi}, \tag{4.100}$$

$$\tilde{\Sigma}_\chi^A(z) \propto C_\chi C_\psi^2 \sqrt{\frac{M_1}{M_2}} e^{i\left(\pi\Delta_\chi + \theta_\chi\right)} z^{1-2\Delta_\chi}. \tag{4.101}$$

Eventually the coupled S-D equations Eq. 4.95 lead to the following self-consistent equations:

$$2g^2 C_\psi^2 C_\chi^2 \sqrt{\frac{M_2}{M_1}} \frac{\cos(2\pi\Delta_\psi) + \cos(2\theta_\chi)}{\pi(1-2\Delta_\psi)\sin(2\pi\Delta_\psi)} = 1, \tag{4.102}$$

$$2g^2 C_\chi^2 C_\psi^2 \sqrt{\frac{M_1}{M_2}} \frac{\cos(2\pi\Delta_\chi) + \cos(2\theta_\psi)}{\pi(1-2\Delta_\chi)\sin(2\pi\Delta_\chi)} = 1. \tag{4.103}$$

The conformal dimensions Δ_ψ and Δ_χ also must satisfy another relation, which physically

guarantee that the system is at a fixed point controlled by the four fermion interaction:

$$2\Delta_\psi + 2\Delta_\chi = 1. \tag{4.104}$$

Additionally, the filling factors $\mathcal{Q}_\psi$ and $\mathcal{Q}_\chi$ give further constraints on $\Delta_{\psi/\chi}$, and $\theta_{\psi/\chi}$ (please refer to the supplementary material):

$$\mathcal{Q}_\psi = \frac{1}{2} - \frac{\theta_\psi}{\pi} - \left(\frac{1}{2} - \Delta_\psi\right)\frac{\sin(2\theta_\psi)}{\sin(2\pi\Delta_\psi)}, \tag{4.105}$$

$$\mathcal{Q}_\chi = \frac{1}{2} - \frac{\theta_\chi}{\pi} - \left(\frac{1}{2} - \Delta_\chi\right)\frac{\sin(2\theta_\chi)}{\sin(2\pi\Delta_\chi)}. \tag{4.106}$$

The five equations above, *i.e.* Eq. 4.102 to Eq. 4.106 involve five unknown real numbers that we need to solve for: Δ_ψ, Δ_χ, θ_ψ, θ_χ, and $C_\psi^2 C_\chi^2$. These equations imply that the conformal dimension $\Delta_{\psi/\chi}$ can be tuned by the particle filling factors $\mathcal{Q}_\psi$ and $\mathcal{Q}_\chi$, as we will demonstrate explicitly later.

The imaginary time correlation function can be obtained by Fourier transforming Eq. 4.96 and Eq. 4.97:

$$G_{\psi/\chi}(\tau) = \frac{\mathcal{B}_{\psi/\chi}}{|\tau|^{2\Delta_{\psi/\chi}}} \qquad (\tau > 0), \tag{4.107}$$

$$G_{\psi/\chi}(\tau) = -\frac{\mathcal{B}'_{\psi/\chi}}{|\tau|^{2\Delta_{\psi/\chi}}} \qquad (\tau < 0). \tag{4.108}$$

Following the convention of the literatures on the complex SYK model (for example Ref. 457), we can introduce the spectral asymmetry $\mathcal{E}_{\psi/\chi}$

$$e^{2\pi\mathcal{E}_{\psi/\chi}} = \frac{\sin\left(\pi\Delta_{\psi/\chi} + \theta_{\psi/\chi}\right)}{\sin\left(\pi\Delta_{\psi/\chi} - \theta_{\psi/\chi}\right)}, \tag{4.109}$$

and the coefficient $\mathcal{B}_{\psi/\chi}$, $\mathcal{B}'_{\psi/\chi}$ is related to $C_{\psi/\chi}$ as

$$\mathcal{B}_{\psi/\chi} = -\frac{C_{\psi/\chi}\Gamma\left(2\Delta_{\psi/\chi}\right)\sin\left(\pi\Delta_{\psi/\chi}+\theta_{\psi/\chi}\right)}{\pi}, \tag{4.110}$$

$$\mathcal{B}'_{\psi/\chi} = -\frac{C_{\psi/\chi}\Gamma\left(2\Delta_{\psi/\chi}\right)\sin\left(\pi\Delta_{\psi/\chi}-\theta_{\psi/\chi}\right)}{\pi} = \mathcal{B}_{\psi/\chi}e^{-2\pi\mathcal{E}_{\psi/\chi}}. \tag{4.111}$$

Although we cannot determine C_ψ and C_χ separately from the S-D equations, dimensional analysis determines that $\mathcal{B}_{\psi/\chi} \sim C_{\psi/\chi} \sim g^{-2\Delta_{\psi/\chi}}$, thus $C_\psi^2 C_\chi^2 \sim 1/g^2$.

The finite temperature solution can be obtained by performing the conformal mapping $\tau \to \frac{1}{\pi T}\tan\left(\pi T\tau\right)$, where τ becomes a periodic imaginary time coordinate with periodicity $1/T$. Using the rules of reparametrization transformation, we obtain

$$G\left(\tau\right) = \begin{cases} \mathcal{B}e^{-2\pi\mathcal{E}T\tau}\left|\frac{\pi T}{\sin(\pi T\tau)}\right|^{2\Delta} & 0<\tau<\frac{1}{T} \\ -\mathcal{B}'e^{-2\pi\mathcal{E}T\tau}\left|\frac{\pi T}{\sin(\pi T\tau)}\right|^{2\Delta} & 0<-\tau<\frac{1}{T} \end{cases}, \tag{4.112}$$

Now we are ready to solve the equations from Eq. 4.102 to Eq. 4.106. In general an analytic solution would be very tedious. But for the simplified case where $M_1 = M_2$, there are only two parameters in this theory: $q_\psi = \mathcal{Q}_\psi - 1/2$ and $q_\chi = \mathcal{Q}_\chi - 1/2$, and all the relevant quantities can be expanded as a polynomial of q_ψ, q_χ. We also define $d = \Delta_\psi - 1/4 = 1/4 - \Delta_\chi$. Then Eq. 4.104 implies that $d_\psi = -d_\chi = d$. We will obtain analytic solutions for small q_ψ and q_χ.

In fact, in Eq. 4.106 and Eq. 4.105, we do not need to compute the exact prefactor before $\sin(2\theta_\psi)$ and $\sin(2\theta_\chi)$. Without loss of generality, we can assume the prefactor $f(\Delta,\theta)$ is a function of Δ and θ, and some general constraints of the its form would be sufficient for the lowest nontrivial order of solutions as a polynomial of $q_{\psi/\chi}$. For example, $f(\Delta,\theta)$ must be consistent with the results in Ref. 468. When $q_\psi = q_\chi$, there is a Z_2 symmetry that exchanges ψ and χ, hence in this case $\Delta_\psi = \Delta_\chi = 1/4$, or

$d = d_\psi = -d_\chi = 0$. And to be consistent with the result in Ref. 468, the $f(\Delta, \theta)$ function must satisfy

$$f(1/4, \theta) = 1/4, \tag{4.113}$$

and this statement is independent of θ. This is consistent with the result of Ref. 465 where it was found that $f(\Delta, \theta)$ does not depend on θ at all.

Under the particle-hole transformation, the Green's function $G(\tau)$ at filling factor q_ψ, q_χ will become $-G(-\tau)$ at filling factor $-q_\psi$, $-q_\chi$. This implies that d must be an even function of q_ψ and q_χ, while θ_ψ, θ_χ must be odd functions of q_ψ, q_χ. If we assume $q_\psi \sim q_\chi \sim q \ll 1$, to the lowest order expansion of q_ψ and q_χ, $d \sim (q_\psi^2 - q_\chi^2)$, which follows from the aforementioned fact that $d = 0$ when $q_\psi = q_\chi$. Thus to the lowest nontrivial order of expansion of q, we can just take $f(\Delta, \theta) = 1/4 + O(q_\psi^2 - q_\chi^2) + O(q^3)$.

All the five equations from Eq. 4.102 to Eq. 4.106 can be expanded as a polynomial of q_ψ and q_χ. And at the lowest nontrivial order, we obtain the following analytic solutions:

$$\theta_\psi = -\frac{2\pi q_\psi}{\pi + 2} + O(q^3), \tag{4.114}$$

$$\theta_\chi = -\frac{2\pi q_\chi}{\pi + 2} + O(q^3), \tag{4.115}$$

$$\Delta_\psi = \frac{1}{4} + d = \frac{1}{4} + \frac{2\pi^2(q_\psi^2 - q_\chi^2)}{(\pi + 2)^2(\pi - 2)} + O(q^4), \tag{4.116}$$

$$\Delta_\chi = \frac{1}{4} - d = \frac{1}{4} - \frac{2\pi^2(q_\psi^2 - q_\chi^2)}{(\pi + 2)^2(\pi - 2)} + O(q^4). \tag{4.117}$$

These solutions are consistent with all the previous observations, and also consistent with numerical solutions of the equations

Model B

Another elementary model that we will start with is also constructed with two orbitals of fermions, each with three indices. The Hamiltonian takes the following form:

$$H_0^B = \sum_{a_1,a_2,b_1,b_2=1}^{N} \sum_{c,c'=1}^{M_1} \sum_{d,d'=1}^{M_2} \frac{g}{N\sqrt{M}} \mathcal{J}^{\psi}_{c,c'} \mathcal{J}^{\chi}_{d,d'} \left(\psi^{\dagger}_{a_1,b_1,c} \psi^{\dagger}_{a_2,b_2,c'} \chi_{a_1,b_2,d} \chi_{a_2,b_1,d'} + h.c. \right), \quad (4.118)$$

Here ψ_c and χ_d form fundamental representation of $\mathrm{Sp}(M_1)$ and $\mathrm{Sp}(M_2)$ group. $\mathcal{J}^{\psi}_{c,c'}\psi_c\psi_{c'}$ and $\mathcal{J}^{\chi}_{d,d'}\chi_d\chi_{d'}$ form singlets under $\mathrm{Sp}(M_1)$ and $\mathrm{Sp}(M_2)$ respectively.

Although both model A and model B share a similar three-index structure, there are some fundamental differences between them. First of all, the particle density of ψ and χ are no longer separately conserved in model B. Only the total particle density is conserved. Thus, we should introduce

$$\mathcal{Q} = \frac{M_1 \mathcal{Q}_{\psi} + M_2 \mathcal{Q}_{\chi}}{M_1 + M_2} \in (0, 1) \quad (4.119)$$

as a "total" filling factor, Notice that Q_{ψ} and Q_{χ} are defined as the expectation values of ψ and χ fermion number operator (Eq. 4.93), while only $\mathcal{Q}$ is a conserved quantity in this case.

Secondly and very importantly, the self energies are different compared with those of model A, based on the melonic diagrams:

$$\Sigma^B_{\psi}(\tau) = -4g^2 \sqrt{\frac{M_2}{M_1}} G_{\chi}(\tau)^2 G_{\psi}(-\tau), \quad (4.120)$$

$$\Sigma^B_{\chi}(\tau) = -4g^2 \sqrt{\frac{M_1}{M_2}} G_{\psi}(\tau)^2 G_{\chi}(-\tau), \quad (4.121)$$

Again, we want to solve the coupled S-D equations Eq. 4.95 self-consistently in the conformal limit, and we still use the power law ansatz Eq. 4.96 and Eq. 4.97. We found

that the self energies $\tilde{\Sigma}^B_\psi, \tilde{\Sigma}^B_\chi$ can still be written as the form of Eq. 4.100, Eq. 4.101. But now the self-consistency of the S-D equation imposes another constraint on θ_ψ, θ_χ (for more details, please refer to Appendix. B.3.1):

$$\frac{\sin(\pi\Delta_\psi + \theta_\psi)}{\sin(\pi\Delta_\psi - \theta_\psi)} = \frac{\sin(\pi\Delta_\chi + \theta_\chi)}{\sin(\pi\Delta_\chi - \theta_\chi)}, \tag{4.122}$$

which implies that the two types of fermions have the same spectral asymmetry. Under this constraint, the S-D equation Eq. 4.95 leads to the same expressions as Eq. 4.102 and Eq. 4.103.

In addition, we have verified in the supplementary material that the expectation values of the particle numbers for ψ and χ fermions share the same expressions Eq. 4.105 and Eq. 4.106 as model A. The total filling factor $\mathcal{Q}$ imposes further constraints on $\Delta_{\psi/\chi}$, and $\theta_{\psi/\chi}$

$$\mathcal{Q} = \frac{1}{2} - \frac{M_1\theta_\psi + M_2\theta_\chi}{\pi(M_1+M_2)} - \frac{M_1\Delta_\chi \sin(2\theta_\psi) + M_2\Delta_\psi \sin(2\theta_\chi)}{\sin\left(2\pi\Delta_{\psi/\chi}\right)(M_1+M_2)}, \tag{4.123}$$

where $\Delta_{\psi/\chi}$ can be either Δ_ψ or Δ_χ due to Eq. 4.104.

Still, we have five equations that involve five unknown real quantities $\Delta_\psi, \Delta_\chi, \theta_\psi, \theta_\chi$, and $C^2_\psi C^2_\chi$. Compared to model A, the conditions that $\mathcal{Q}_\psi$ and $\mathcal{Q}_\chi$ are fixed separately is replaced by fixing $\mathcal{Q}$, together with the constraint Eq. 4.122. Now the conformal dimension $\Delta_{\psi/\chi}$ can be tuned by changing the total particle filling factor $\mathcal{Q}$.

4.4.3 Lattice Models for NFLs

Lattice model (1)

Based on the elementary models constructed in the previous section, we can construct lattice models with the desired resistivity scaling $\varrho \sim T^\alpha$ with $\alpha \in [1, 2)$. Our first lattice

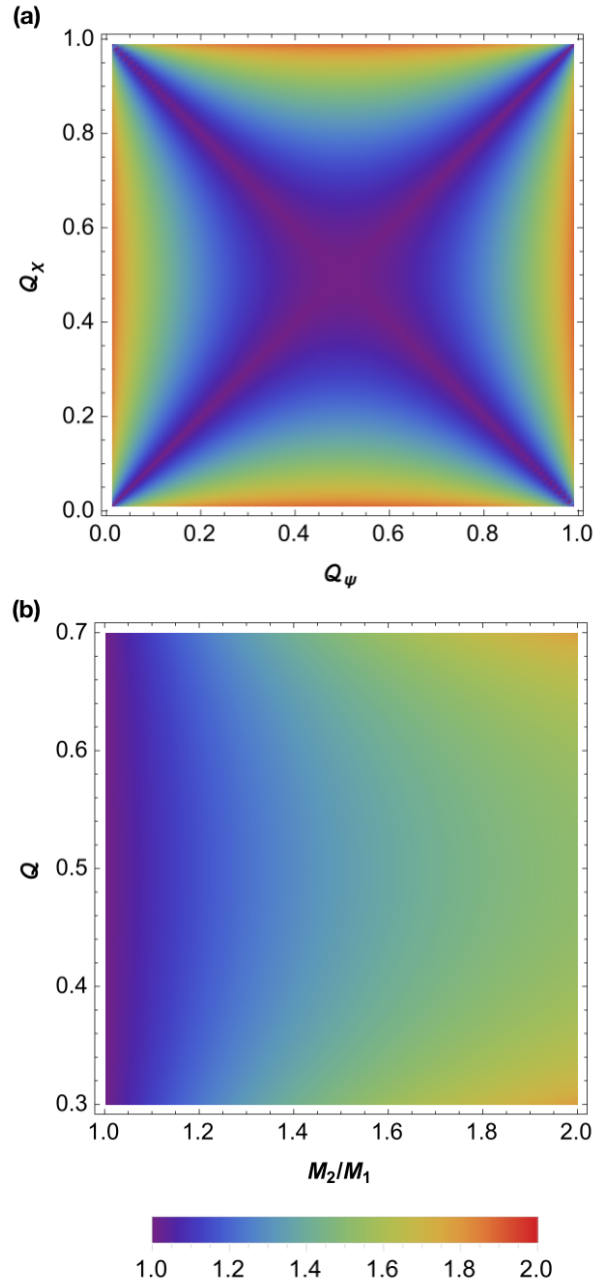

Figure 4.8: The relation between the transport scaling power α (defined as resistivity $\varrho \sim T^{\alpha}$) and parameters in the lattice models for NFLs. (a) α plotted against $\mathcal{Q}_\psi$ and $\mathcal{Q}_\chi$ with $M_2/M_1 = 1$ for the lattice model (1) with the on-cluster Hamiltonian $H_0^A(\boldsymbol{r})$; (b) α plotted against $\mathcal{Q}$ and M_2/M_1, for lattice model (1) with the on-cluster Hamiltonian $H_0^B(\boldsymbol{r})$; and also the lattice model (2) Eq. 4.134.

model is constructed with coupled clusters (following the previous efforts [393, 465, 394, 396] of constructing the strange metal phase with the SYK_4-like clusters), and the physics on each cluster $\boldsymbol{r}$ is described by Eq. 4.88 or Eq. 4.118, which is the leading energy scale of the system. Different clusters are coupled together through hoppings of both ψ and χ:

$$H = \sum_{\boldsymbol{r}} H_0^{A/B}(\boldsymbol{r}) - \sum_{\langle \boldsymbol{r}, \boldsymbol{r}' \rangle} \left(t_1 \psi_{\boldsymbol{r}}^\dagger \psi_{\boldsymbol{r}'} + t_2 \chi_{\boldsymbol{r}}^\dagger \chi_{\boldsymbol{r}'} \right) + \dots \tag{4.124}$$

The indices of ψ and χ are summed over in the equation above. Although the t-terms are expected to drive the system into a Fermi liquid state at low energy, our goal is to construct a NFL phase *at a finite energy/temperature window*, which is where most of the NFLs are observed experimentally. Thus let us focus on the finite energy window where $H_0^{A/B}$ is dominant, and the hopping term is perturbative.

The electric current operator of model Eq. 4.124 can be obtained by coupling the model to the external electromagnetic field, and perform functional derivative of the external field:

$$J_{\boldsymbol{\delta}} = \sum_{\boldsymbol{r}} i t_1 \psi_{\boldsymbol{r}}^\dagger \psi_{\boldsymbol{r}+\boldsymbol{\delta}} + i t_2 \chi_{\boldsymbol{r}}^\dagger \chi_{\boldsymbol{r}+\boldsymbol{\delta}} + \mathrm{H.c.} \tag{4.125}$$

In order to compute the electric conductivity, we define the imaginary-time current-current correlation function as $C(J, J; \tau) = \langle \mathbb{T}_\tau J(\tau) J(0) \rangle$. The leading order nonzero contribution takes the form

$$\frac{C(J, J; \tau)}{\mathcal{N}} = -2t_1^2 G_\psi(\tau) G_\psi(-\tau) - 2t_2^2 G_\chi(\tau) G_\chi(-\tau), \tag{4.126}$$

where $\mathcal{N}$ is $\mathcal{N} = N^2 M V$ with V being the size of the lattice.

Then we perform Fourier transformation of $C(J, J; \tau)$ to obtain correlation function

in the Matsubara frequency space:

$$\frac{C\left(J,J;i\omega_n\right)}{\mathcal{N}}=\frac{C_\psi\left(J,J;i\omega_n\right)}{\mathcal{N}}+\frac{C_\chi\left(J,J;i\omega_n\right)}{\mathcal{N}}, \tag{4.127}$$

where C_ψ is calculated as

$$\frac{C_\psi\left(J,J;i\omega_n\right)}{\mathcal{N}}=2t_1^2\int_0^{\frac{1}{T}}d\tau e^{i\omega_n\tau}G_\psi\left(\tau\right)G_\psi\left(\frac{1}{T}-\tau\right), \tag{4.128}$$

which is exact in the large$-N, M_1, M_2$ limit, and C_χ has a similar expression.

When $0<\Delta_\psi<1/4$, the integral Eq. 4.128 has a finite expression, but it diverges when $1/4\leq\Delta_\psi<1/2$. For $1/4\leq\Delta_\psi<1/2$, we regulate the integral by introducing a small positive cutoff $\delta>0$:

$$\int_0^{\frac{1}{T}}\rightarrow\int_\delta^{\frac{1}{T}-\delta}. \tag{4.129}$$

There is a $\mathcal{O}\left(\log\delta\right)$ divergence when $\Delta_\psi=1/4$, and a $\mathcal{O}\left(1/\delta^{4\Delta-1}\right)$ divergence when $1/4<\Delta_\psi<1/2$. The divergence is in the real part but not the imaginary part of the correlation function, hence does not contribute to the conductivity, thus the divergence can be removed in order to calculate the conductivity. The retarded/advanced correlation function $C^{R/A}\left(J,J;\omega\right)$ can then be derived by taking $z\rightarrow\omega\pm i0^+$. And eventually using the relation $\sigma\left(\omega\right)=\frac{1}{i\omega}C^R\left(J,J;\omega\right)$, we find the real part of the optical conductivity

$$\mathrm{Re}[\sigma\left(\omega\right)]\sim\frac{t_1^2\mathcal{B}_\psi^2e^{-2\pi\mathcal{E}_\psi}}{T^{2-4\Delta_\psi}}\Upsilon\left(\Delta_\psi,\frac{\omega}{T}\right)+\frac{t_2^2\mathcal{B}_\chi^2e^{-2\pi\mathcal{E}_\chi}}{T^{2-4\Delta_\chi}}\Upsilon\left(\Delta_\chi,\frac{\omega}{T}\right), \tag{4.130}$$

where we have introduced the scaling function

$$\Upsilon\left(\Delta,\frac{\omega}{T}\right)=\frac{\left(2\pi\right)^{4\Delta-1}}{\Gamma\left(4\Delta\right)\cos\left(2\pi\Delta\right)}\frac{2\pi T}{\omega}\mathrm{Im}\left[\frac{\Gamma\left(2\Delta+\frac{\omega}{i2\pi T}\right)}{\Gamma\left(1-2\Delta+\frac{\omega}{i2\pi T}\right)}\right]\quad\left(0<\Delta<1/2\right). \tag{4.131}$$

One can check that when $\Delta = 1/4$, the scaling function above reproduces the scaling function for SYK_4-like models [397]

$$\Upsilon\left(\Delta = 1/4, \omega/T\right) = \frac{\pi \tanh\left(\omega/2T\right)}{\omega/2T}. \tag{4.132}$$

The DC limit $\omega \to 0$ of the scaling function $\Upsilon\left(\Delta, 0\right)$ is a function of Δ which takes finite positive values for $\Delta \in (0, 1/2)$. Since $2\Delta_\psi + 2\Delta_\chi = 1$, the final result of the DC conductivity takes the following form

$$\mathrm{Re}[\sigma] \sim \frac{A}{T^{2-4\Delta}} + \frac{B}{T^{4\Delta}}, \tag{4.133}$$

where Δ takes values in $0 < \Delta < 1/2$. The constants $A \sim t_1^2 \mathcal{B}_\psi^2 \sim t_1^2/g^{4\Delta}$, and $B \sim t_2^2 \mathcal{B}_\chi^2 \sim t_2^2/g^{2-4\Delta}$. Hence when $T < g$, the $A/T^{2-4\Delta}$ part of the DC conductivity will dominate for $0 < \Delta < 1/4$, and $B/T^{4\Delta}$ dominates for $1/4 < \Delta < 1/2$. Thus, in a finite temperature window for T lower than the dominant energy scale g, and higher than the infrared scale below which the hopping terms become nonperturbative, we are able to realize non-fermi liquid behaviors with resistivity $\varrho \sim T^\alpha$, and $\alpha \in [1, 2)$ depends on parameters in the theory, especially the filling factors in the model.

The relation between α and the filling factors is plotted in Fig. 4.8. If we start with model A on every cluster, α will depend on both Q_χ and Q_ψ even when $M_1 = M_2$; if we start with model B, then α depends on the total filling factor Q when $M_1 \neq M_2$.

Lattice model (2)

In this section we we propose another different construction of lattice model for NFL, by relating two of the three tensor indices to the lattice site coordinates of a two dimensional square lattice.

The dominant interaction in this model is

$$H = \sum_j \sum_{r,r'=-(N-1)/2}^{(N-1)/2} \sum_{c,c'=1}^{M_1} \sum_{d,d'=1}^{M_2} \frac{g\mathcal{J}^{\psi}_{c,c'}\mathcal{J}^{\chi}_{d,d'}}{N\sqrt{M}} \left(\psi^{\dagger}_{j_x,j_y,c}\psi^{\dagger}_{j_x+r,j_y+r',c'}\chi_{j_x,j_y+r',d}\chi_{j_x+r,j_y,d'} + h.c.\right). \quad (4.134)$$

This Hamiltonian is motivated by and resembles H_0^B. (j_x, j_y) represents the x and y coordinates of the lattice site j. Physically ψ_c and χ_d can be thought of as two types of fermions with $M_1 = 2J_1 + 1$ and $M_2 = 2J_2 + 1$ total angular momentum components, and the Hamiltonian represents the process of tunnelling between the pair singlets of χ and ψ. The cluster model in the previous section is insensitive to the spatial dimensions, while the construction of Eq. 4.134 most naturally applies to a two dimensional system.

In Eq. 4.134, we always take the thermodynamics limit first (the sum of j is taken on a square lattice with infinite size). Then in the large-N (in this model larger$-N$ means longer range interaction) and large-M_1, M_2 limit, the fermion Green's function is still dominated by the "melonic diagrams" and hence the Schwinger-Dyson equations, and their solutions, remain the same as model H_0^B. Notice that the single fermion Green's function is completely local in space, which is guaranteed by the fact that the Eq. 4.134 conserves the center of mass.

In addition to the dominant interaction, we will also turn on a single-particle hopping term as perturbations. Because Eq. 4.134 conserves the center of mass of the electrons, the interaction Eq. 4.134 alone cannot transport electric charge. Thus the electric current operator only comes from the electron hopping terms. In the soluble large-(N, M_1, M_2) limit, we formally generalize the electric current operator to the following form

$$\begin{aligned} J_x = &\frac{it_1}{\sqrt{NM_1}}\left(\sum_c \psi^{\dagger}_{j,c}\psi_{j+\hat{x},c} + \sqrt{\frac{N-1}{2}}\psi^{\dagger}_{j,c}\psi_{j+\hat{x}\pm\hat{y},c}\right) \\ &+ \frac{it_2}{\sqrt{NM_2}}\left(\sum_d \chi^{\dagger}_{j,d}\chi_{j+\hat{x},d} + \sqrt{\frac{N-1}{2}}\chi^{\dagger}_{j,d}\chi_{j+\hat{x}\pm\hat{y},d}\right) + H.c. \end{aligned} \quad (4.135)$$

This electric current density can be derived by designing a corresponding single-electron hopping term in the large-(N, M_1, M_2) limit (which involves both nearest- and second-neighbor hopping) and coupling it to the external electromagnetic field.

Using the large-(N, M_1, M_2) solution of Eq. 4.134, we can repeat all the calculations for conductivity as we did for the previous model (1), and we arrive at the same expression of conductivity Eq. 4.130. Thus, we again have tunability of transport scalings within this construction. The exponent α of $\varrho \sim T^\alpha$ is plotted against the filling factor Q and M_2/M_1 in Fig. 4.8*b*.

4.4.4 Summary and Discussion

We constructed two examples of lattice models for non-fermi liquid states whose DC resistivity scalings are tunable by adjusting the charge density, which is a phenomenon observed in many physical systems. Our lattice models are based on two versions of "elementary" models with *randomness free four fermion interactions*, which are soluble in certain theoretical limit just like the SYK model and the fermion tensor models. But unlike the previous models, our elementary models have tunable fermion scaling dimensions in their conformal solutions.

In this work we assumed that both orbitals (types) of the fermions in the model carry electric charges. But at least for model A, where the number of each type of fermions is conserved separately, we can also assume that one of the two types of fermions are charge neutral slave particles, which comes from "fractionalizing" the localized spins. This perspective is similar to the the case in the original Sachdev-Ye model [54], and also similar to a series of recent studies [465, 394, 396]. In this case, the slave fermions will be coupled to a U(1) gauge field, whose effect in the large$-N$ limit is expected to be suppressed, and the solution of our model in the large$-N$ limit remains unchanged. In

this case the electric transport only comes from one of the two orbitals of the fermions, and it is still tunable by changing the charge density of the system.

In Ref. 460, 397, it was shown that the SYK-type of models are instable against extra marginally relevant four-fermion interactions, and these perturbations can lead to instability at low energy/temperature. In experiment, many of the observed NFLs are preempted by ordered phases (for example superconductivity) at low temperature. Also, it was shown in Ref. 468 that the $1/N$ effect of the original Sachdev-Ye model plays a role only at an exponentially suppressed energy scale, and at finite temperature there is a wide window where the conformal solution of the Sachdev-Ye model applies. Similar effects were shown for the SYK model and also the three-index tensor models by studying the subleading order of the Feynmann diagrams [471]. All these analysis can be performed for our models as well, which we will defer to future study.

Chapter 5

Characterizations of Symmetries and Anomalies

In Sec. 1.5, we have seen the important role of generalized symmetries and anomalies in the modern understanding of quantum phases and phase transitions. This chapter presents our understanding of how to unambiguously characterize generalized symmetries at quantum phase transitions, and some applications of generalized anomalies in condensed matter systems.

In Sec. 5.1, we study the concept of "categorical symmetry" introduced recently, which in the most basic sense refers to a pair of dual symmetries, such as the Ising symmetries of the $1d$ quantum Ising model and its self-dual counterpart. In this manuscript, we study discrete categorical symmetry at higher dimensional critical points and gapless phases. At these selected gapless states of matter, we can evaluate the behavior of categorical symmetries analytically. We analyze the categorical symmetry in the following examples of criticality: (*i.*) $(2+1)d$ Lifshit critical point of a quantum Ising system; (*ii.*) $(3+1)d$ photon phase as an intermediate gapless phase between the topological order and the confined phase of $3d$ Z_2 quantum gauge theory; (*iii.*) $2d$ and $3d$ examples of systems

with both categorical symmetries (either 0-form or 1-form categorical symmetries) and subsystem symmetries. We demonstrate that at some of these gapless states of matter the categorical symmetries have very different behavior from the nearby gapped phases.

In Sec. 5.2, we investigate the behavior of higher-form symmetries at various quantum phase transitions. We consider discrete 1-form symmetries, which can be either part of the generalized concept "categorical symmetry" (labeled as $\tilde{Z}_N^{(1)}$) introduced recently, or an explicit $Z_N^{(1)}$ 1-form symmetry. We demonstrate that for many quantum phase transitions involving a $Z_N^{(1)}$ or $\tilde{Z}_N^{(1)}$ symmetry, the following expectation value $\langle(\log O_{\mathcal{C}})^2\rangle$ takes the form $\langle(\log O_{\mathcal{C}})^2\rangle \sim -\frac{A}{\epsilon}P + b\log P$, where $O_{\mathcal{C}}$ is an operator defined associated with loop $\mathcal{C}$ (or its interior $\mathcal{A}$), which reduces to the Wilson loop operator for cases with an explicit $Z_N^{(1)}$ 1-form symmetry. P is the perimeter of $\mathcal{C}$, and the $b\log P$ term arises from the sharp corners of the loop $\mathcal{C}$, which is consistent with recent numerics on a particular example. b is a universal microscopic-independent number, which in $(2+1)d$ is related to the universal conductivity at the quantum phase transition. b can be computed exactly for certain transitions using the dualities between $(2+1)d$ conformal field theories developed in recent years. We also compute the "strange correlator" of $O_{\mathcal{C}}$: $S_{\mathcal{C}} = \langle 0|O_{\mathcal{C}}|1\rangle/\langle 0|1\rangle$ where $|0\rangle, |1\rangle$ are many-body states with different topological nature.

In Sec. 5.3, we discuss physical constructions and boundary properties of various symmetry-protected topological phases that involve 1-form symmetries, from one spatial dimension ($1d$) to four spatial dimensions ($4d$). For example, the prototype $3d$ boundary state of $4d$ SPT states involving 1-form symmetries can be either a gapless photon phase (quantum electrodynamics) or gapped topological order enriched by 1-form symmetries, namely the loop excitations of these topological orders carry nontrivial 1-form symmetry charges. This study also serves the purpose of diagnosing anomalies of $3d$ states of matter. The connection between SPT states with 1-form symmetries and condensed matter systems such as quantum dimer models at one lower dimension will also be discussed.

Whether a quantum dimer model can have a trivial gapped phase or not depends on the nature of its corresponding bulk state in one higher dimension.

5.1 Order Diagnosis Operators and Categorical Symmetries at Criticality

5.1.1 Basics of Categorical Symmetry

Categorical symmetry is a new concept introduced in Ref. 481, which expanded the conventional notion of symmetries in physics, and how one should think about them. The basic examples of categorical symmetry correspond to a pair of dual symmetries, whose local symmetry charges in general do not commute with each other. The simplest example of such, are the Z_2 and $\tilde{Z}_2$ dual symmetry of the $1d$ quantum Ising model:

$$H = \sum_j -K\sigma_j^3\sigma_{j+1}^3 - h\sigma_j^1 \quad \leftrightarrow \quad H_d = \sum_{\tilde{j}} -K\tau_{\tilde{j}}^1 - h\tau_{\tilde{j}}^3\tau_{\tilde{j}+1}^3. \tag{5.1}$$

This model has a well-known self-duality point $K = h$; σ_j^3 and $\tau_{\tilde{j}}^3$ are order parameters of the original Z_2 and the dual $\tilde{Z}_2$ symmetry. Let us label the entire categorical symmetries of the $1d$ quantum Ising model as $Z_2 \star \tilde{Z}_2$.

For the convenience of generalizing to higher dimensional systems with higher form symmetries and more exotic subsystem symmetries that we will discuss in this manuscript, we will introduce the concept "Order Diagnosis Operator" (ODO) for each symmetry. The expectation value of the ODO diagnoses the behavior of its corresponding symmetry. An ODO should commute with all the *conserved global* symmetry charges (which implies that the expectation value of the ODO is in general nonzero [1]), but creates *local* charges

[1]The expectation value of ODOs should not be viewed as an analogue of order parameter, they

of the corresponding symmetry. For the Z_2 and $\tilde{Z}_2$ symmetries of the $1d$ quantum Ising model, the ODOs are respectively

$$O_{i,j} = \sigma_i^3 \sigma_j^3, \qquad \tilde{O}_{\tilde{i},\tilde{j}} = \tau_{\tilde{i}}^3 \tau_{\tilde{j}}^3 = \prod_{i<k<j} \sigma_k^1. \tag{5.2}$$

$O_{i,j}$ creates a pair of Z_2 charges at sites i and j (but it preserves/commutes with the global Z_2 charge $\prod_j \sigma_j^1$), while $\tilde{O}_{\tilde{i},\tilde{j}}$ creates a pair of domain walls of σ^3 at $\tilde{i}$ and $\tilde{j}$, which are local charges of the $\tilde{Z}_2$ symmetry.

When $K > h$, there is a long range correlation of σ^3, short range correlation of τ^3 (long range expectation value of ODO $O_{i,j}$, and short range expectation value of $\tilde{O}_{\tilde{i},\tilde{j}}$); hence this is a phase that spontaneously breaks Z_2, but preserves $\tilde{Z}_2$. When $K < h$, there is a long range correlation of τ^3, but short range correlation of σ^3 (long range expectation value of $\tilde{O}_{\tilde{i},\tilde{j}}$, short range expectation value of $O_{i,j}$); hence this is a phase that spontaneously breaks $\tilde{Z}_2$, but preserves Z_2. Whether a symmetry is preserved or spontaneously broken, can be defined by the behavior of its ODO. When $K = h$, both order parameters have power-law correlation, hence this is a criticality which preserves both symmetries.

In what sense is $\tilde{Z}_2$ a symmetry, and in what sense is there a spontaneous symmetry breaking (SSB) of $\tilde{Z}_2$? In the $1d$ quantum Ising model, without changing the physical Ising Hilbert space, the SSB phase of the $\tilde{Z}_2$ symmetry does not lead to ground state degeneracy (GSD), after all it is just a quantum disordered phase of the Ising model. However, with some global constraint on the physical Hilbert space, or when we view the $1d$ system as the boundary of a $2d$ topological order [481], neither phase ($K > h$ or $K < h$) has GSD. *Hence we no longer view GSD as a criterion for SSB. The SSB should*

should be viewed as analogue of correlation of order parameters. The ODOs were studied as the "patch symmetry operators" of the categorical symmetry in Ref. 481.

be defined solely by the behavior of $\langle O\rangle$ *and* $\langle\tilde{O}\rangle$.

In higher dimensions, the possible categorical symmetries are much richer. In the $2d$ quantum Ising model, there is a $Z_2 \star \tilde{Z}_2^{(1)}$ symmetry. Here $\tilde{Z}_2^{(1)}$ is a 1-form symmetry as a generalization of ordinary symmetries introduced in recent years (see for instance Ref. 482, 483, 484, 485, 486, 117, 487, 488, 489):

$$\begin{aligned} H &= \sum_{\langle \mathbf{x},\mathbf{x}'\rangle} -K\sigma^3_{\mathbf{x}}\sigma^3_{\mathbf{x}'} - \sum_{\mathbf{x}} h\sigma^1_{\mathbf{x}} \qquad \leftrightarrow \\ H_d &= \sum_{\tilde{\mathbf{x}},\hat{\mu}} -K\tau^1_{\tilde{\mathbf{x}},\hat{\mu}} - \sum_{\tilde{\mathbf{x}}} h\tau^3_{\tilde{\mathbf{x}},\hat{x}}\tau^3_{\tilde{\mathbf{x}},\hat{y}}\tau^3_{\tilde{\mathbf{x}}+\hat{x},\hat{y}}\tau^3_{\tilde{\mathbf{x}}+\hat{y},\hat{x}}. \end{aligned} \tag{5.3}$$

The lattice site $\mathbf{x}$ and dual lattice site $\tilde{\mathbf{x}}$ are illustrated in Fig. 5.1. The subscripts $(\tilde{\mathbf{x}},\hat{x})$ and $(\tilde{\mathbf{x}},\hat{y})$ label the links of the dual lattice. The ODO of the Z_2 symmetry is still $O_{\mathbf{x},\mathbf{x}'} = \sigma^3_{\mathbf{x}}\sigma^3_{\mathbf{x}'}$; while the ODO of $\tilde{Z}_2^{(1)}$ symmetry is

$$\tilde{O}^{(1)}_{\mathcal{C}} = \prod_{\tilde{l}\in\mathcal{C}} \tau^3_{\tilde{l}} = \prod_{\mathbf{x}\in\mathcal{A},\ \partial\mathcal{A}=\mathcal{C}} \sigma^1_{\mathbf{x}}. \tag{5.4}$$

Here $\tilde{l}$ also labels a link in the dual lattice, which belongs to the contractible loop $\mathcal{C}$. $\tilde{O}^{(1)}_{\mathcal{C}}$ creates an Ising domain wall of σ^3, the one dimensional domain wall carries the dual $\tilde{Z}_2^{(1)}$ 1-form symmetry charge. Here $\mathcal{A}$ is a finite $2d$ patch on the dual lattice, $\mathcal{C}$ is the boundary of $\mathcal{A}$, which is a contractible loop. Again, the ODO $\tilde{O}^{(1)}_{\mathcal{C}}$ commutes with all the conserved 1-form symmetry charges, which is defined as a product of τ^1 along any closed $1d$ loop $\mathcal{C}'$. Notice that $\mathcal{C}'$ always intersects with the contractible $\mathcal{C}$ for even times, hence the ODO $\tilde{O}^{(1)}_{\mathcal{C}}$ commutes with the conserved 1-form symmetry charges $\prod_{\tilde{l}\in\mathcal{C}'} \tau^1_{\tilde{l}}$.

There are again two phases with K/h greater or smaller than a critical value. These two phases have the following known behaviors of the ODOs [490], which can be computed

through a reliable perturbation theory due to the gap in the spectrum of both phases

$$\begin{aligned} K/h \gg 1: &\qquad \langle O_{\mathbf{x},\mathbf{x}'}\rangle \sim \text{Const}, \qquad \langle \tilde{O}^{(1)}_{\mathcal{C}}\rangle \sim e^{-\alpha_1 \log(K/h)\mathcal{A}}; \\ K/h \ll 1: &\qquad \langle O_{\mathbf{x},\mathbf{x}'}\rangle \sim e^{-|\mathbf{x}-\mathbf{x}'|/\xi}, \qquad \langle \tilde{O}^{(1)}_{\mathcal{C}}\rangle \sim e^{-\alpha_2 (K/h)^2 \mathcal{C}}. \end{aligned} \tag{5.5}$$

α_i are order 1 numbers. Hence in the phase $K \gg h$, the $\tilde{Z}_2^{(1)}$ symmetry $\tilde{O}^{(1)}_{\mathcal{C}}$ decays with an area law; while in the phase $K \ll h$, the domain walls proliferate/condense, and $\tilde{O}^{(1)}_{\mathcal{C}}$ has a perimeter law. Again, in the phase $h \gg K$, even though the domain walls proliferate/condense, there is no GSD. This is in stark contrast with ordinary 1-form symmetry SSB state, which would lead to topological degeneracy. Hence here we should view the behavior of $\langle \tilde{O}^{(1)}_{\mathcal{C}}\rangle$ as a criterion of SSB of $\tilde{Z}_2^{(1)}$, rather than the GSD.

At the $(2+1)d$ Ising critical point, the Z_2 order parameter has a power-law correlation (the expectation value of $O_{\mathbf{x},\mathbf{x}'}$ falls off as a power-law), hence the Z_2 symmetry is not broken. Intuitively, since $O_{\mathbf{x},\mathbf{x}'}$ has a power-law correlation, the expectation value of the dual ODO $\tilde{O}^{(1)}_{\mathcal{C}}$ should be stronger than the area law deep in the $K \gg h$ phase, but weaker than the perimeter law deep in the $K \ll h$ phase. But the exact behavior of $\tilde{O}^{(1)}_{\mathcal{C}}$ is difficult to compute analytically at the $3D$ Ising critical point, and in other lattice models that will be discussed in the following sections. The main goal of this manuscript is to find critical points (or fine-tuned critical points) where the ODOs of the categorical symmetries can be evaluated analytically. The strategy we will generally take is that, we embed the target lattice model into a larger "parent" system where the ODOs of the original system have a clear representation. Then we tune the parent system to a multi-critical point, or even a gapless phase, where we can use tools in the continuum limit to compute ODOs defined in both sides of the duality. Since many of the states we discuss in this manuscript do not have Lorentz invariance, we will focus on expectation value of time-independent operators at static states.

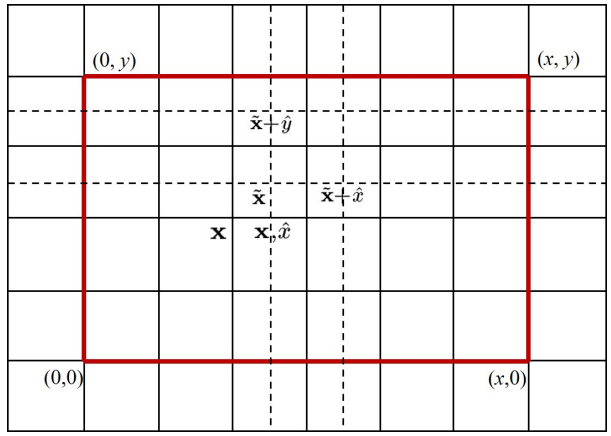

Figure 5.1: The $2d$ square lattice, and its dual lattice. The lattice site is labelled as $\mathbf{x}$, and the dual lattice site (the plaquette of the original lattice) is labelled as $\tilde{\mathbf{x}}$. The links of the lattice are labelled as $(\mathbf{x}, \hat{\mu})$, while the links of the dual lattice are labelled as $(\tilde{\mathbf{x}}, \hat{\mu})$.

5.1.2 Ising Categorical Symmetries at Criticality

$2d$ Lifshitz Point

We can embed the target $2d$ quantum Ising model into a parent system described by a U(1) quantum "rotor":

$$H = \sum_{\mathbf{x},\mu} -t \cos\left(\nabla_\mu \hat{\theta}(\mathbf{x})\right) + \sum_{\mathbf{x}} \frac{U}{2} \hat{n}(\mathbf{x})^2 - g \cos\left(2\hat{\theta}(\mathbf{x})\right). \tag{5.6}$$

$\hat{\theta}(\mathbf{x})$ and $\hat{n}(\mathbf{x})$ are a pair of conjugate variables, i.e. $[\hat{n}(\mathbf{x}), \hat{\theta}(\mathbf{x}')] = \mathrm{i}\delta_{\mathbf{x},\mathbf{x}'}$. $\hat{n}(\mathbf{x})$ takes discrete integer eigenvalues, while $\hat{\theta}(\mathbf{x})$ is periodically defined: $\hat{\theta}(\mathbf{x}) = \hat{\theta}(\mathbf{x}) + 2\pi$. The last g term in Eq. 5.6 breaks the U(1) symmetry down to Z_2. The operators $\sigma^3_{\mathbf{x}}$ and $\sigma^1_{\mathbf{x}}$ of the Ising model correspond to the operators in the parent U(1) theory:

$$\sigma^3_{\mathbf{x}} = e^{\mathrm{i}\hat{\theta}(\mathbf{x})}, \qquad \sigma^1_{\mathbf{x}} = e^{\mathrm{i}\pi\hat{n}(\mathbf{x})}. \tag{5.7}$$

If the g term is ignored, the U(1) model is dual to a lattice QED:

$$H_d = \sum_{\tilde{\mathbf{x}}} -t\cos\left(\hat{\vec{e}}(\tilde{\mathbf{x}})\right) + \sum_{\tilde{\mathbf{x}}} \frac{U}{2}\left(\vec{\nabla}\times\hat{\vec{a}}(\tilde{\mathbf{x}})\right)^2,$$
$$\hat{\vec{e}}(\tilde{\mathbf{x}}) = \hat{z}\times\vec{\nabla}\hat{\theta}(\mathbf{x}), \qquad \vec{\nabla}\times\hat{\vec{a}}(\tilde{\mathbf{x}}) = \hat{n}(\mathbf{x}). \tag{5.8}$$

The electric field $\hat{\vec{e}}_\mu$ and gauge vector potential $\hat{\vec{a}}_\mu$ were defined on the links $(\tilde{\mathbf{x}},\hat{x})$, $(\tilde{\mathbf{x}},\hat{y})$ of the dual lattice, but we can also equivalently define $\hat{\vec{e}}(\tilde{\mathbf{x}}) = (\hat{\vec{e}}_x(\tilde{\mathbf{x}}),\hat{\vec{e}}_y(\tilde{\mathbf{x}})) = (\hat{\vec{e}}_{\tilde{\mathbf{x}},\hat{x}},\hat{\vec{e}}_{\tilde{\mathbf{x}},\hat{y}})$, $\hat{\vec{a}}(\tilde{\mathbf{x}}) = (\hat{\vec{a}}_x(\tilde{\mathbf{x}}),\hat{\vec{a}}_y(\tilde{\mathbf{x}})) = (\hat{\vec{a}}_{\tilde{\mathbf{x}},\hat{x}},\hat{\vec{a}}_{\tilde{\mathbf{x}},\hat{y}})$. In the parent U(1) system, the Z_2 and $\tilde{Z}_2^{(1)}$ ODO are

$$O_{\mathbf{x},\mathbf{x}'} = e^{\mathrm{i}\hat{\theta}(\mathbf{x})}e^{-\mathrm{i}\hat{\theta}(\mathbf{x}')},$$
$$\tilde{O}_{\mathcal{C}}^{(1)} = \prod_{\mathcal{A},\ \partial\mathcal{A}=\mathcal{C}} \sigma^1_{\mathbf{x}} = \exp\left(i\pi\sum_{\mathbf{x}\in\mathcal{A}}\hat{n}(\mathbf{x})\right) = \exp\left(i\pi\oint_{\mathcal{C}}\hat{\vec{a}}\cdot d\vec{l}\right). \tag{5.9}$$

In model Eq. 5.6, there is a critical point at critical value $(U/t)_c$. Without the g term, the transition in Eq. 5.6 is a $3D$ XY transition between the superfluid phase with small U/t and a boson Mott insulator phase at large U/t. While with the g term, it is expected that the $3D$ XY critical point will flow to the $3D$ Ising fixed point, because g is obviously relevant at the $3D$ XY fixed point. However, one can fine-tune the critical point to reach a Lifshitz point described by the following field theory Hamiltonian and action in the continuum limit

$$H = \int d^2x\frac{U}{2}\hat{n}(\mathbf{x})^2 + \frac{\rho}{2}\left(\nabla^2\hat{\theta}(\mathbf{x})\right)^2,$$
$$\mathcal{S} = \int d^2x d\tau\frac{1}{2U}(\partial_\tau\theta)^2 + \frac{\rho}{2}(\nabla^2\theta)^2. \tag{5.10}$$

It is known that the g operator can be irrelevant at the $(2+1)d$ Lifshitz Gaussian fixed point for certain range of U and ρ, more precisely for large enough U/ρ [491, 492]. The

irrelevance of g guarantees that the continuum limit field theory description in terms of θ is applicable at this Lifshitz fixed point. One can also compute the expectation value of O, which is the equal-time correlation function between σ^3:

$$\langle O_{0,\mathbf{x}}\rangle = \langle e^{\mathrm{i}\hat{\theta}(0)} e^{-\mathrm{i}\hat{\theta}(\mathbf{x})}\rangle \sim \frac{1}{|\mathbf{x}|^{2\Delta_\theta}}, \qquad \Delta_\theta \sim \sqrt{\frac{U}{\rho}}. \tag{5.11}$$

Hence at the Lifshitz point, the Z_2 symmetry is preserved.

The situation is rather different for the $Z_2^{(1)}$ ODO $\tilde{O}_{\mathcal{C}}$. The dual Hamiltonian and action of the Lifshitz theory Eq. 5.10 is

$$\begin{aligned} H_d &= \int d^2\tilde{x} \frac{U}{2}\left(\vec{\nabla}\times\hat{\vec{a}}\right)^2 + \frac{\rho}{2}\left((\nabla_x \hat{\vec{e}}_y)^2 + (\nabla_y \hat{\vec{e}}_x)^2\right), \\ \mathcal{S}_d &= \int d^2\tilde{x} d\tau \frac{1}{2\rho}\left(\hat{\vec{a}}_x \frac{\partial_\tau^2}{\partial_y^2}\hat{\vec{a}}_x + \hat{\vec{a}}_y \frac{\partial_\tau^2}{\partial_x^2}\hat{\vec{a}}_y\right) + \frac{U}{2}(\vec{\nabla}\times\hat{\vec{a}})^2. \end{aligned} \tag{5.12}$$

This is the same Hamiltonian and action describing the $2d$ quantum dimer model at the Rohksar-Kivelson point [493, 494]. The correlation function of $\vec{a}_{\vec{q},\omega}$ is

$$\langle \hat{\vec{a}}_\mu(-\omega,-\vec{q})\hat{\vec{a}}_\nu(\omega,\vec{q})\rangle \sim \frac{\rho(q^2\delta_{\mu\nu} - q_\mu q_\nu)}{\omega^2 + \rho U q^4}, \qquad \langle \hat{\vec{a}}_\mu(0,0)\hat{\vec{a}}_\nu(0,\mathbf{x})\rangle \sim \sqrt{\frac{\rho}{U}}\frac{1}{|\mathbf{x}|^2}. \tag{5.13}$$

The expectation of $\tilde{O}_{\mathcal{C}}^{(1)}$ can be evaluated using the Gaussian theory of the gauge field:

$$\langle \exp(\mathrm{i}\pi \oint_{\mathcal{C}} \hat{\vec{a}}\cdot d\vec{l})\rangle \sim \exp\left(-\frac{\pi^2}{2}\oint_{\mathcal{C}}\oint_{\mathcal{C}} \langle \hat{\vec{a}}_\mu(\mathbf{x})\hat{\vec{a}}_\nu(\mathbf{x}')\rangle dx^\mu dx'^\nu\right). \tag{5.14}$$

Power-counting suggests that this is still a perimeter law: the $1/|\mathbf{x}|^2$ decay of the correlation function of the gauge fields do not lead to extra divergence with large loop size, the expectation value of $\tilde{O}_{\mathcal{C}}^{(1)}$ is dominated by small distance correlation of the gauge field. Since in the gapped phase $h \gg K$ (Eq. 5.3) where the domain walls clearly proliferates, $\tilde{O}_{\mathcal{C}}^{(1)}$ follows a perimeter law, we will use the perimeter law of $\tilde{O}_{\mathcal{C}}^{(1)}$ as a criterion of SSB

of $\tilde{Z}_2^{(1)}$. Then this Lifshitz point still spontaneously breaks the $\tilde{Z}_2^{(1)}$ symmetry, while preserving the Z_2 symmetry. One can also see that when the expectation value of $O_{\mathbf{x},\mathbf{x}'}$ is stronger (smaller Δ_θ at smaller U/ρ), the expectation value of $\tilde{O}_{\mathcal{C}}^{(1)}$ becomes weaker (larger ρ/U). The results of this section are summarized in the table below.

$2d$ Quantum Ising theory	$K \gg h$ in Eq. 5.3	$K \ll h$ in Eq. 5.3	Fine-tuned Lifshitz Point
$O_{\mathbf{x},\mathbf{x}'}$	Long range	Short Range	Power law
$\tilde{O}_{\mathcal{C}}^{(1)}$	Area law	Perimeter law	Perimeter law

$3d$ Z_2 Quantum Gauge Theory

It was well-known that the $3d$ lattice Z_2 gauge theory has a self-dual structure [490, 495, 496]:

$$\begin{aligned} H &= \sum_{\mathbf{x},\hat{\mu},\hat{\nu}} -K\sigma^3_{\mathbf{x},\hat{\mu}}\sigma^3_{\mathbf{x},\hat{\nu}}\sigma^3_{\mathbf{x}+\hat{\mu},\hat{\nu}}\sigma^3_{\mathbf{x}+\hat{\nu},\hat{\mu}} - h\sigma^1_{\mathbf{x},\hat{\mu}} \\ \leftrightarrow \quad H_d &= \sum_{\tilde{\mathbf{x}},\hat{\mu},\hat{\nu}} -K\tau^1_{\tilde{\mathbf{x}},\hat{\mu}} - h\tau^3_{\tilde{\mathbf{x}},\hat{\mu}}\tau^3_{\tilde{\mathbf{x}},\hat{\nu}}\tau^3_{\tilde{\mathbf{x}}+\hat{\mu},\hat{\nu}}\tau^3_{\tilde{\mathbf{x}}+\hat{\nu},\hat{\mu}}. \end{aligned} \tag{5.15}$$

This system has a $Z_2^{(1)} \star \tilde{Z}_2^{(1)}$ categorical symmetry. The ODOs for $Z_2^{(1)}$ and $\tilde{Z}_2^{(1)}$ are

$$O_{\mathcal{C}}^{(1)} = \prod_{l\in\mathcal{C}} \sigma^3_l, \qquad \tilde{O}_{\mathcal{C}}^{(1)} = \prod_{\tilde{l}\in\mathcal{C}} \tau^3_{\tilde{l}}. \tag{5.16}$$

The $O_{\mathcal{C}}^{(1)}$ and $\tilde{O}_{\mathcal{C}}^{(1)}$ are products of the K and h terms of Eq. 5.15 within $2d$ patch $\mathcal{A}$ with $\partial\mathcal{A} = \mathcal{C}$.

There are two phases of this model: for $K \gg h$, $\langle O_{\mathcal{C}}^{(1)}\rangle$ decays with a perimeter law, while $\langle \tilde{O}_{\mathcal{C}}^{(1)}\rangle$ decays with an area law; this is a phase with SSB of $Z_2^{(1)}$ but preserves $\tilde{Z}_2^{(1)}$.

In the opposite limit $h \gg K$, $\langle O_{\mathcal{C}}^{(1)}\rangle$ decays with an area law, while $\langle \tilde{O}_{\mathcal{C}}^{(1)}\rangle$ decays with an perimeter law; this is the phase with SSB of $\tilde{Z}_2^{(1)}$ but preserves $Z_2^{(1)}$.

Unfortunately, model Eq. 5.15 does not have a second order transition between the two phases, hence there is no critical point in model Eq. 5.15 where $Z_2^{(1)}$ and $\tilde{Z}_2^{(1)}$ are

on equal footing. But we can embed the Z_2 gauge theory Eq. 5.15 into a QED model with $U(1)^{(1)} \star \tilde{U}(1)^{(1)}$ symmetries, and this QED model has a gapless photon phase. In this gapless photon phase, both $O_{\mathcal{C}}^{(1)}$ and $O_{\mathcal{C}'}^{(1)}$ in Eq. 5.16 can be computed using the Gaussian fixed point theory of the $U(1)$ gauge field, and its self-dual $\tilde{U}(1)$ gauge field. The Gaussian theory of the $U(1)$ and $\tilde{U}(1)$ gauge bosons indicates that both $O_{\mathcal{C}}$ and $\tilde{O}_{\mathcal{C}}$ follow a perimeter law. Since in the gapped phases of Eq. 5.15 $O_{\mathcal{C}}$ and $\tilde{O}_{\mathcal{C}}$ at most have a perimeter law, we view the gapless photon phase of the $U(1)$ gauge field as a phase which spontaneously breaks both $Z_2^{(1)}$ and $\tilde{Z}_2^{(1)}$ symmetries. This gapless QED would still have $Z_2^{(1)} \star \tilde{Z}_2^{(1)}$ as the UV symmetry, while the $U(1)^{(1)} \star \tilde{U}(1)^{(1)}$ symmetry are IR emergent symmetries. The IR emergent symmetries are spontaneously broken, which still leads to gapless photons as their Goldstone modes [2].

One can also fine-tune the QED to a Lifshitz point with non-Lorentz invariant dispersions of the $U(1)$ gauge bosons. However, we have checked and verified that, at various Lifshitz points (meaning fine-tuned states with different non-Lorentz invariant dispersion), at least one of the $Z_2^{(1)}$ and $\tilde{Z}_2^{(1)}$ symmetries is spontaneously broken, i.e. one of $O_{\mathcal{C}}$ and $\tilde{O}_{\mathcal{C}}$ must have a perimeter law.

5.1.3 Examples of Subsystem Categorical Symmetries

$2d$ Example

Let us consider a special $2d$ lattice Z_2 quantum gauge theory, which can be constructed in Josephson arrays of superconductor and ferromagnet deposited on top of a quantum

[2] Spontaneous breaking of emergent higher form symmetries in the infrared would still lead to gapless Goldstone modes, this is very different from the scenario of ordinary 0-form symmetries.

spin Hall insulator [497]:

$$H = \sum_{\mathbf{x}} -K\sigma^3_{\mathbf{x},\hat{x}}\sigma^3_{\mathbf{x},\hat{y}}\sigma^3_{\mathbf{x}+\hat{x},\hat{y}}\sigma^3_{\mathbf{x}+\hat{y},\hat{x}} - J\sigma^1_{\mathbf{x},\hat{x}}\sigma^1_{\mathbf{x}+\hat{x},\hat{x}} - J\sigma^1_{\mathbf{x},\hat{y}}\sigma^1_{\mathbf{x}+\hat{y},\hat{y}}. \tag{5.17}$$

The last two terms of this model are actually identical, due to the Z_2 Gauss law gauge constraint $\sigma^1_{\mathbf{x}-\hat{x},\hat{x}}\sigma^1_{\mathbf{x},\hat{x}}\sigma^1_{\mathbf{x}-\hat{y},\hat{y}}\sigma^1_{\mathbf{x},\hat{y}} = 1$, which we will impose strictly on the Hilbert space of the system.

This model has an ordinary $Z_2^{(1)}$ 1-form symmetry, and extra $Z_2^{(\text{sub})}$ subsystem symmetries. The subsystem symmetry grants the system a series of conserved quantities:

$$\Sigma_{\hat{x},y} = \prod_{y=\text{Const}} \sigma^3_{\mathbf{x},\hat{x}}, \qquad \Sigma_{\hat{y},x} = \prod_{x=\text{Const}} \sigma^3_{\mathbf{x},\hat{y}}. \tag{5.18}$$

x and y are the two coordinates of $\mathbf{x}$. The subsystem symmetries of Eq. 5.17 guarantee that $\Sigma_{\hat{x},y}$ and $\Sigma_{\hat{y},x}$ are conserved for arbitrary x and y. The ODO for $Z_2^{(1)}$, and its expectation value in the topological ordered phase $K \gg J$ is

$$O^{(1)}_{\mathcal{C}} = \prod_{l\in\mathcal{C}} \sigma^3_l, \qquad \langle O^{(1)}_{\mathcal{C}}\rangle \sim e^{-\alpha_3 (J/K)^2 N_{\mathcal{C}}}. \tag{5.19}$$

The $O^{(1)}_{\mathcal{C}}$ commutes with conserved quantities $\Sigma_{\hat{x},y}$ and $\Sigma_{\hat{y},x}$, hence it meets the criterion of ODO we introduced in the first section. Due to the conservation of the extra quantities $\Sigma_{\hat{x},y}$ and $\Sigma_{\hat{y},x}$, the ODO has a generic "corner law" instead of perimeter law, where $N_{\mathcal{C}}$ is the number of corners of loop $\mathcal{C}$. For example, in Fig. 5.1, the rectangular loop $\mathcal{C}$ has four corners, And $O^{(1)}_{\mathcal{C}}$ is a product of finite segments of $\Sigma_{\hat{x},y}$ and $\Sigma_{\hat{y},x}$. The expectation value of the rectangular $O^{(1)}_{\mathcal{C}}$ does not decay with the length of $\mathcal{C}$. Because $\Sigma_{\hat{x},y}$ and $\Sigma_{\hat{y},x}$ are conserved when the product is along an infinitely straight line, then for a generic $\mathcal{C}$, if we compute the expectation value of $O^{(1)}_{\mathcal{C}}$ through a perturbation of J/K like Ref. 490,

the value can only decay when $\mathcal{C}$ "takes a turn".

In the other limit of the model, $K \ll J$, the ODO $O_{\mathcal{C}}^{(1)}$ decays as an area law like the ordinary confined phase of a Z_2 lattice gauge theory, and there is a SSB of the subsystem symmetries $Z_2^{(\text{sub})}$. The most convenient way to study this limit, is to take the dual Hamiltonian of Eq. 5.17, which still has subsystem $\tilde{Z}_2^{(\text{sub})}$ symmetries:

$$H_d = \sum_{\tilde{\mathbf{x}}} -K\tau^1_{\tilde{\mathbf{x}}} - 2J\tau^3_{\tilde{\mathbf{x}}}\tau^3_{\tilde{\mathbf{x}}+\hat{x}}\tau^3_{\tilde{\mathbf{x}}+\hat{y}}\tau^3_{\tilde{\mathbf{x}}+\hat{x}+\hat{y}}. \tag{5.20}$$

The duality mapping between σ^i and τ^i is the same as the standard $2d$ Ising-Gauge duality discussed in the previous section. $\tilde{Z}_2^{(\text{sub})}$ inherits and contains $Z_2^{(\text{sub})}$, but is slightly larger: $\tilde{Z}_2^{(\text{sub})}$ includes another $\tilde{Z}_2$ element which changes the sign of all $\tau^3_{\tilde{\mathbf{x}}}$. This extra $\tilde{Z}_2$ element is the dual of $Z_2^{(1)}$, and it does not change σ^1_l in Eq. 5.17.

The ODO of $\tilde{Z}_2^{(\text{sub})}$ is a product of τ^3 on four corners of a rectangle:

$$\tilde{O}^{(\text{sub})}_{x,y} = \tau^3_{0,0}\tau^3_{x,0}\tau^3_{0,y}\tau^3_{x,y}. \tag{5.21}$$

The ODO defined above is also a product of the J term in Eq. 5.17 within the rectangle. In the original topological order $K \gg J$, $\tilde{O}^{(\text{sub})}_{x,y}$ can be computed through a perturbation of J/K, and it decays as an exponential of the area of the rectangle; while at the SSB phase of $\tilde{Z}_2^{(\text{sub})}$ ($K \ll J$), $\tilde{O}^{(\text{sub})}_{x,y}$ has long range expectation value [498].

Like the previous section, we can embed the dual model Eq. 5.20 into a model with $\tilde{U}(1)^{(\text{sub})}$ symmetry:

$$H_d = \int d^2\tilde{x}\ \frac{U}{2}\hat{n}(\tilde{\mathbf{x}})^2 - t\cos\left(\nabla_x\nabla_y\hat{\theta}(\tilde{\mathbf{x}})\right) - g\cos\left(2\hat{\theta}(\tilde{\mathbf{x}})\right). \tag{5.22}$$

The relation between the operators of the $\tilde{Z}_2^{(\text{sub})}$ theory Eq. 5.20 and the $\tilde{U}(1)^{(\text{sub})}$ theory

Eq. 5.22 is

$$\tau^x_{\tilde{\mathbf{x}}} = \exp\left(\mathrm{i}\pi\hat{n}(\tilde{\mathbf{x}})\right), \qquad \tau^z_{\tilde{\mathbf{x}}} = \exp\left(\mathrm{i}\hat{\theta}(\tilde{\mathbf{x}})\right) \tag{5.23}$$

When g is relevant, it will break the $\tilde{U}(1)^{(\mathrm{sub})}$ down to $\tilde{Z}_2^{(\mathrm{sub})}$.

However, as was studied before [499], the g term can only flow strong and become non-perturbative under renormalization group through "assistance" from some other terms such as $\gamma(2\nabla_\mu\theta)$. If we tune γ to zero, then there exists a stable gapless phase of the model Eq. 5.22 with a larger $\tilde{U}(1)^{(\mathrm{sub})}$ symmetry, and the g term is irrelevant. And in this gapless phase the system is described by the following action:

$$\mathcal{S}_d = \int d\tau d^2\tilde{x}\ \frac{1}{2U}(\partial_\tau\theta)^2 + \frac{t}{2}(\nabla_x\nabla_y\theta)^2, \tag{5.24}$$

where θ can be viewed as a free boson instead of a compact boson. The $\tilde{U}(1)^{(\mathrm{sub})}$ reads

$$\theta(\tilde{\mathbf{x}}) \to \theta(\tilde{\mathbf{x}}) + f(\tilde{x}) + g(\tilde{y}). \tag{5.25}$$

This gapless phase can also be described by a $U(1)$ gauge theory, which can be viewed as the parent theory where the original Z_2 lattice gauge theory Eq. 5.17 is embedded to:

$$H = \int d^2x\ \frac{U}{2}(\vec{\nabla}\times\hat{\vec{a}})^2 + \frac{t}{4}\left((\nabla_x\hat{\vec{e}}_x)^2 + (\nabla_y\hat{\vec{e}}_y)^2\right). \tag{5.26}$$

In this gapless phase, the expectation value of the ODO of the original Z_2 gauge theory $O^{(1)}_{\mathcal{C}}$ will depend on the shape of $\mathcal{C}$, but it no longer follows the "corner law" Eq. 5.19 of the gapped topological ordered phase $K \gg J$ in Eq. 5.17. In the gapless

phase, the ODO $O_{\mathcal{C}}^{(1)}$ can be written as

$$\langle O_{\mathcal{C}}^{(1)} \rangle = \langle \prod_{\tilde{\mathbf{x}} \in \mathcal{A}, \partial \mathcal{A} = \mathcal{C}} \tau_{\tilde{\mathbf{x}}}^{1} \rangle \sim \langle e^{\sum_{\tilde{\mathbf{x}} \in \mathcal{A}} \mathrm{i}\pi \hat{n}(\tilde{\mathbf{x}})} \rangle. \tag{5.27}$$

In order to evaluate $\langle O_{\mathcal{C}}^{(1)} \rangle$ we will make use of another duality of Eq. 5.22 and Eq. 5.24:

$$H_{d2} = \int d^2x \, \frac{U}{2} (\nabla_x \nabla_y \hat{\phi}(\mathbf{x}))^2 - t \cos\left(\hat{N}(\mathbf{x})\right). \tag{5.28}$$

Now $\hat{\phi}(\mathbf{x})$ and $\hat{N}(\mathbf{x})$ are still defined on the sites of the original lattice $\mathbf{x}$ (Fig. 5.1):

$$\nabla_x \nabla_y \hat{\theta}(\tilde{\mathbf{x}}) = -\hat{N}(\mathbf{x}), \qquad \nabla_x \nabla_y \hat{\phi}(\mathbf{x}) = \hat{n}(\tilde{\mathbf{x}}). \tag{5.29}$$

The gapless phase has a new dual description in terms of the continuum limit model of $\hat{\phi}(\mathbf{x})$:

$$\mathcal{S}_{2d} = \int d^2x d\tau \, \frac{1}{2t} (\partial_\tau \phi)^2 + \frac{U}{2} (\nabla_x \nabla_y \phi)^2. \tag{5.30}$$

In this gapless phase, if we consider a loop $\mathcal{C}$ which is a rectangle with four corners at $(0,0)$, $(x,0)$, $(0,y)$, (x,y) (Fig. 5.1), the expectation value $O_{\mathcal{C}}^{(1)}$ is

$$\begin{aligned}
&\langle O_{\mathcal{C}}^{(1)} \rangle = \langle \prod_{\tilde{\mathbf{x}} \in \mathcal{A}, \partial \mathcal{A} = \mathcal{C}} \tau_{\tilde{\mathbf{x}}}^{1} \rangle \sim \langle \exp\left(\sum_{\tilde{\mathbf{x}} \in \mathcal{A}} \mathrm{i}\pi \hat{n}(\tilde{\mathbf{x}}) \right) \rangle \\
&= \langle \exp\left(\mathrm{i}\pi (\hat{\phi}_{0,0} - \hat{\phi}_{x,0} - \hat{\phi}_{0,y} + \hat{\phi}_{x,y}) \right) \rangle \\
&\sim \exp\left(\pi^2 (\langle \hat{\phi}_{0,0} \hat{\phi}_{x,0} \rangle + \langle \hat{\phi}_{0,0} \hat{\phi}_{0,y} \rangle + \langle \hat{\phi}_{x,y} \hat{\phi}_{x,0} \rangle + \langle \hat{\phi}_{x,y} \hat{\phi}_{0,y} \rangle - \langle \hat{\phi}_{0,0} \hat{\phi}_{x,y} \rangle - \langle \hat{\phi}_{0,y} \hat{\phi}_{x,0} \rangle) \right) \\
&\sim \exp\left(-c\pi^2 \sqrt{\frac{t}{U}} \log|x| \log|y| \right).
\end{aligned} \tag{5.31}$$

This is a faster decay compared with the corner law in the gapped topologically ordered phase $K \gg J$ in Eq. 5.17. In the same gapless phase, the expectation value of $\tilde{O}_{x,y}^{\mathrm{sub}}$ defined

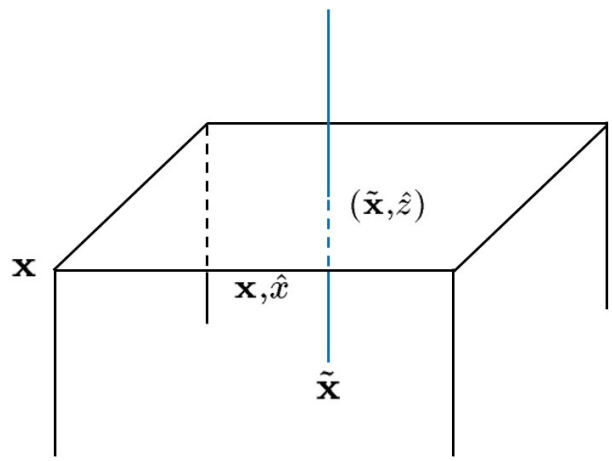

Figure 5.2: The cubic lattice and the dual lattice for models considered in section 5.1.3.

in Eq. 5.21 decays in a similar way as Eq. 5.31, rather than a long range expectation value as the phase $K \ll J$. Hence this gapless phase described by Eq. 5.24, Eq. 5.26, Eq. 5.30 can be viewed as a symmetric phase for both $Z_2^{(1)}$ and $\tilde{Z}_2^{\text{sub}}$ symmetries.

The special double logarithmic scaling in Eq. 5.31 arises from the subsystem symmetries Eq. 5.25 of the parent $U(1)$ theory. More technically, in order to evaluate $O_{\mathcal{C}}^{(1)}$, we need to compute the equal-time correlation function $\langle \hat{\phi}_{0,0}\hat{\phi}_{x,y}\rangle$, which in the momentum space is [499] $G_{k_x,k_y} \sim \int d\omega\ \omega t/(\omega^2 + tUk_x^2k_y^2) \sim 1/|k_xk_y|$. The double linear divergence at $k_x \to 0$ and $k_y \to 0$ leads to the special double logarithmic scaling in real space. The results of this subsection is summarized in the table below.

Special $2d$ Z_2 Gauge theory Eq. 5.17	$K \gg J$	$K \ll J$	Gapless Phase
$O_{\mathcal{C}}^{(1)}$	Corner law	Area law	$\exp\left(-c\pi^2\sqrt{t/U}\ \log\lvert x\rvert\log\lvert y\rvert\right)$ for rect. $\mathcal{C}$
$\tilde{O}_{x,y}^{\text{sub}}$	Area law	Long range	$\exp\left(-\tilde{c}\pi^2\sqrt{U/t}\ \log\lvert x\rvert\log\lvert y\rvert\right)$

$3d$ Example

We now consider a $3d$ Z_2 lattice gauge theory defined on the cubic lattice, which has both the 1-form symmetry, and subsystem symmetries:

$$\begin{aligned} H &= \sum_{\mathbf{x},\hat{\mu},\hat{\nu}} -K\sigma^3_{\mathbf{x},\hat{\mu}}\sigma^3_{\mathbf{x},\hat{\nu}}\sigma^3_{\mathbf{x}+\hat{\mu},\hat{\nu}}\sigma^3_{\mathbf{x}+\hat{\nu},\hat{\mu}} - J\sigma^1_{\mathbf{x},\hat{\mu}}\sigma^1_{\mathbf{x}+\hat{\mu},\hat{\mu}} \\ \leftrightarrow \quad H_d &= \sum_{\tilde{\mathbf{x}},\hat{\mu},\hat{\nu}} -K\tau^1_{\tilde{\mathbf{x}},\hat{\mu}} - \sum_{\hat{\rho}\perp\hat{\mu},\hat{\nu}} J\hat{\mathcal{B}}_{\tilde{\mathbf{x}},\hat{\mu}\hat{\nu}}\hat{\mathcal{B}}_{\tilde{\mathbf{x}}+\hat{\rho},\hat{\mu}\hat{\nu}}. \end{aligned} \tag{5.32}$$

where $\hat{\mathcal{B}}_{\tilde{\mathbf{x}},\hat{\mu}\hat{\nu}} = \tau^3_{\tilde{\mathbf{x}},\hat{\mu}}\tau^3_{\tilde{\mathbf{x}},\hat{\nu}}\tau^3_{\tilde{\mathbf{x}}+\hat{\mu},\hat{\nu}}\tau^3_{\tilde{\mathbf{x}}+\hat{\nu},\hat{\mu}}$. The theory H has an ordinary $Z_2^{(1)}$ symmetry like Eq. 5.15, plus subsystem symmetries with conserved quantities:

$$\Sigma_{\hat{x};(y,z)} = \prod_{y,z=\text{Const}} \sigma^3_{\mathbf{x},\hat{x}}, \quad \Sigma_{\hat{y};(x,z)} = \prod_{x,z=\text{Const}} \sigma^3_{\mathbf{x},\hat{y}}, \quad \Sigma_{\hat{z};(x,y)} = \prod_{x,y=\text{Const}} \sigma^3_{\mathbf{x},\hat{z}}. \tag{5.33}$$

x, y, z are the three coordinates of $\mathbf{x}$. The ODO of the $Z_2^{(1)}$ 1-form symmetry is the same as Eq. 5.15: $O^{(1)}_{\mathcal{C}} = \prod_{l\in\mathcal{C}} \sigma^3_l$. Due to the extra subsystem conserved quantities in Eq. 5.33, and since $O^{(1)}_{\mathcal{C}}$ is a product of segments of these extra conserved quantities, the expectation value of $O^{(1)}_{\mathcal{C}}$ in the phase $K \gg J$ also decays with a corner law, i.e. the expectation value of $O^{(1)}_{\mathcal{C}}$ decays only when $\mathcal{C}$ takes a turn; in the phase $K \ll J$, there is a SSB of the subsystem symmetry, and the expectation value of $O^{(1)}_{\mathcal{C}}$ decays with an area law.

The dual Hamiltonian H_d has the same $\tilde{Z}_2^{(1)}$ symmetry as the dual of the ordinary Z_2 quantum lattice gauge theory, with extra subsystem symmetries as well. The ODO we will consider for H_d is

$$\tilde{O}^{(1)}_{\mathcal{C},\mathcal{C}'} = \prod_{\tilde{l}\in\mathcal{C}} \tau^3_{\tilde{l}} \prod_{\tilde{l}\in\mathcal{C}'} \tau^3_{\tilde{l}}. \tag{5.34}$$

There are still subsystem symmetries in H_d of Eq. 5.32, with conserved subsystem symmetry charges such as

$$\tilde{\Sigma}_{\hat{z};(\tilde{y},\tilde{z})} = \prod_{\tilde{y},\tilde{z}=\text{Const}} \tau^1_{\tilde{\mathbf{x}},\hat{z}}, \qquad \tilde{\Sigma}_{\hat{z};(\tilde{x},\tilde{z})} = \prod_{\tilde{x},\tilde{z}=\text{Const}} \tau^1_{\tilde{\mathbf{x}},\hat{z}}, \qquad \cdots \tag{5.35}$$

These conserved subsystem charges are not entirely independent from each other due to the Gauss-law gauge constraint imposed on τ^1. Due to these subsystem symmetries in the dual model, we restrict our discussions to the cases when $\mathcal{C}$ and $\mathcal{C}'$ in $\tilde{O}^{(1)}_{\mathcal{C},\mathcal{C}'}$ are completely parallel with each other, and separated along the direction orthogonal to both loops, (for example, $\mathcal{C}$ and $\mathcal{C}'$ can be identical squares in two XY planes, but separated along the $\hat{z}$ direction), because only then would the ODO commute with all the conserved 1-form charges of the dual model Eq. 5.15, and also commute with the subsystem conserved charges $\tilde{\Sigma}$. When $\mathcal{C}$ and $\mathcal{C}'$ are identical loops in XY planes separated along the $\hat{z}$ direction, $\tilde{O}^{(1)}_{\mathcal{C},\mathcal{C}'}$ is also a product of $J\sigma^1_{\mathbf{x},\hat{z}}\sigma^1_{\mathbf{x}+\hat{z},\hat{z}}$ in H of Eq. 5.32 within the $3d$ region sandwiched between $\mathcal{C}$ and $\mathcal{C}'$; while $O^{(1)}_{\mathcal{C}}$ is still a product of the K term enclosed by $\mathcal{C}$.

In the phase $K \ll J$, the expectation value of $\tilde{O}^{(1)}_{\mathcal{C},\mathcal{C}'}$ can again be computed through a perturbation of K/J: it decays as a perimeter law of $\mathcal{C}$ (or equivalently $\mathcal{C}'$), but it does not decay with the distance between $\mathcal{C}$ and $\mathcal{C}'$. In the phase $K \gg J$, the expectation value of $\tilde{O}^{(1)}_{\mathcal{C},\mathcal{C}'}$ would decay exponentially with the distance between $\mathcal{C}$ and $\mathcal{C}'$, and also exponentially with the area of $\mathcal{C}$ (or $\mathcal{C}'$).

It is unknown whether model Eq. 5.32 has a second order transition between the two phases mentioned above or not. But again we can embed the models into a parent model with $U(1)^{(1)}$ and $\tilde{U}(1)^{(1)}$ symmetries. For instance, the H_d in Eq. 5.32 can be embedded into

$$H_d = \int d^3\tilde{x} \sum_{\mu} \frac{U}{2} \hat{e}^2_{\tilde{\mathbf{x}},\hat{\mu}} - t\cos(\nabla_z(\nabla_x \hat{\tilde{a}}_y - \nabla_y \hat{\tilde{a}}_x)) + (\text{permute } x,y,z) - g\cos(2\hat{\tilde{a}}_\mu). \tag{5.36}$$

$\hat{\vec{e}}$ and $\hat{\vec{a}}$ are defined on the dual lattice links $(\tilde{\mathbf{x}}, \hat{\mu})$, which are also the plaquettes of the original cubic lattice (Fig. 5.2). This model admits a gapless phase described by the following action:

$$\mathcal{S}_d = \int d^3\tilde{x} d\tau \ \frac{1}{2U}(\partial_\tau \vec{a})^2 + \frac{t}{2}\left(\nabla_z(\nabla_x a_y - \nabla_y a_x)\right)^2 + (\text{permute } x, y, z). \tag{5.37}$$

In this gapless phase, the ODO Eq. 5.34 becomes

$$\tilde{O}^{(1)}_{\mathcal{C},\mathcal{C}'} = \prod_{\tilde{l}\in\mathcal{C}} \tau^3_{\tilde{l}} \prod_{\tilde{l}\in\mathcal{C}'} \tau^3_{\tilde{l}} \sim \exp\left(\mathrm{i} \oint_{\mathcal{C}} \hat{\vec{a}}_\mu dx^\mu\right) \exp\left(-\mathrm{i} \oint_{\mathcal{C}'} \hat{\vec{a}}_\nu dx^\nu\right). \tag{5.38}$$

The expectation value of $\tilde{O}^{(1)}_{\mathcal{C},\mathcal{C}'}$ can be evaluated with the continuum limit action Eq. 5.37.

Our goal is to show that, the behavior of $\tilde{O}^{(1)}_{\mathcal{C},\mathcal{C}'}$ is different from the gapped phases. This effect can be readily shown by considering the simple case when both $\mathcal{C}$ and $\mathcal{C}'$ are unit plaquettes in the XY planes, separated in the z direction by distance Z. Then

$$\begin{aligned}\tilde{O}^{(1)}_{\mathcal{C},\mathcal{C}'}(Z) &\sim \exp\left(\langle(\nabla_x \hat{\vec{a}}_y - \nabla_y \hat{\vec{a}}_x)_{z=0}(\nabla_x \hat{\vec{a}}_y - \nabla_y \hat{\vec{a}}_x)_{z=Z}\rangle\right) \\ &\sim \exp\left(-c_1\sqrt{\frac{U}{t}}\log Z\right) \sim \frac{1}{|Z|^{2\Delta_{\mathcal{C},\mathcal{C}'}}}, \qquad \Delta_{\mathcal{C},\mathcal{C}'} \sim \sqrt{\frac{U}{t}}.\end{aligned} \tag{5.39}$$

This power-law decay along the z direction originates from the fact that the correlation function $\langle(\nabla_x \hat{\vec{a}}_y - \nabla_y \hat{\vec{a}}_x)_{z=0}(\nabla_x \hat{\vec{a}}_y - \nabla_y \hat{\vec{a}}_x)_{z=Z}\rangle$ has a singularity $1/k_z$ in the momentum space near $k_z = 0$. This power-law scaling along z is already very different from the expectation value of $\tilde{O}^{(1)}_{\mathcal{C},\mathcal{C}'}(Z)$ in the gapped phases of the models in Eq. 5.32. We also made efforts to compute $\tilde{O}^{(1)}_{\mathcal{C},\mathcal{C}'}$ for $\mathcal{C}$, $\mathcal{C}'$ with more general shapes, this calculation is presented in Appendix. B.4.1.

To evaluate $O^{(1)}_{\mathcal{C}}$, again it is more convenient to use a third dual description of the

theory:

$$H_{d2} = \int d^3x \, \frac{U}{2} \left(\nabla_x \nabla_y (\hat{\phi}_x(\mathbf{x}) - \hat{\phi}_y(\mathbf{x})) \right)^2 - t \cos\left(\hat{N}_z(\mathbf{x}) \right) + (\text{permute } x, y, z) \quad (5.40)$$

The operators in Eq. 5.40 are related to the operators in Eq. 5.36 through the mapping (the duality between H_d and H_{d2} was first discussed in Ref. 500)

$$\begin{aligned} &\hat{\vec{e}}_{\tilde{\mathbf{x}},\hat{z}} = \nabla_x \nabla_y (\hat{\phi}_x(\mathbf{x}) - \hat{\phi}_y(\mathbf{x})), \quad \text{and permutation of } x, y, z; \\ &\nabla_z (\nabla_x \hat{\vec{a}}_{\tilde{\mathbf{x}},\hat{y}} - \nabla_y \hat{\vec{a}}_{\tilde{\mathbf{x}},\hat{x}}) = -\hat{N}_z(\mathbf{x}), \quad \text{and permutation of } x, y, z. \end{aligned} \quad (5.41)$$

The gapless phase is described by the following action:

$$\mathcal{S}_{d2} = \int d^3x d\tau \, \frac{U}{2} (\nabla_x \nabla_y (\phi_x - \phi_y))^2 + \frac{1}{2t} (\partial_\tau \phi_z)^2 + (\text{permute } x, y, z) \quad (5.42)$$

$\hat{\phi}_i(\mathbf{x})$ and $\hat{N}_i(\mathbf{x})$ are three pairs of conjugate variables defined on the sites of the original cubic lattice $\mathbf{x}$. Let us assume that the loop $\mathcal{C}$ in $O_{\mathcal{C}}^{(1)}$ is a rectangle in the XY plane, then

$$\begin{aligned} O_{\mathcal{C}}^{(1)} &= \prod_{l \in \mathcal{C}} \sigma_l^3 = \prod_{(\tilde{\mathbf{x}},\hat{z}) \in \mathcal{A}} \tau^1_{\tilde{\mathbf{x}},\hat{z}} = \prod_{(\tilde{\mathbf{x}},\hat{z}) \in \mathcal{A}} \exp(\mathrm{i}\pi \hat{\vec{e}}_{\tilde{\mathbf{x}},\hat{z}}) \\ &= \prod_{\mathbf{x} \in \mathcal{A}} \exp\left(\mathrm{i}\pi \nabla_x \nabla_y (\hat{\phi}_x(\mathbf{x}) - \hat{\phi}_y(\mathbf{x})) \right) = \exp\left(\mathrm{i}\pi \sum_{\mathbf{x} \in \mathcal{A}} \nabla_x \nabla_y (\hat{\phi}_x(\mathbf{x}) - \hat{\phi}_y(\mathbf{x})) \right) \\ &= \exp\left(\begin{array}{c} \mathrm{i}\pi(\hat{\phi}_x(0,0) - \hat{\phi}_x(x,0) - \hat{\phi}_x(0,y) + \hat{\phi}_x(x,y)) \\ -\mathrm{i}\pi(\hat{\phi}_y(0,0) - \hat{\phi}_y(x,0) - \hat{\phi}_y(0,y) + \hat{\phi}_y(x,y)) \end{array} \right). \end{aligned} \quad (5.43)$$

Again since our goal is to show that $O_{\mathcal{C}}^{(1)}$ has different behavior from the two gapped phases $K \gg J$ and $K \ll J$, it is sufficient to consider a special "narrow rectangular" shape of $\mathcal{C}$, i.e. $y = 1$, but $x \gg 1$. $\langle O_{\mathcal{C}}^{(1)} \rangle$ in this case is evaluated as $\exp(\pi^2 \langle \nabla_y (\phi_x -$

$\phi_y)_{0,0}\nabla_y(\phi_x-\phi_y)_{x,0}\rangle)$. The key correlation function $\langle\nabla_y(\phi_x-\phi_y)_{0,0}\nabla_y(\phi_x-\phi_y)_{x,0}\rangle$ has an infrared singularity as $1/|k_x|$ near $k_x=0$. $O^{(1)}_{\mathcal{C}}$ with a narrow rectangular $\mathcal{C}$ scales as

$$\langle O^{(1)}_{\mathcal{C}}\rangle \sim \frac{1}{|x|^{\Delta_{\mathcal{C}}}}, \qquad \Delta_{\mathcal{C}} \sim \sqrt{\frac{t}{U}}. \tag{5.44}$$

The power law decay of $O^{(1)}_{\mathcal{C}}$ is very different from the two gapped phases of Eq. 5.32. The results of this subsection are summarized in the table below.

Special $3d$ Z_2 Gauge theory Eq. 5.32	$K \gg J$	$K \ll J$	Gapless Phase
$O^{(1)}_{\mathcal{C}}$ with rect. $\mathcal{C}$ in XY	Corner law	Area law	$\frac{1}{\lvert x\rvert^{\Delta_{\mathcal{C}}}}$, with $y=1$ and $x\gg 1$.
$\tilde{O}^{(1)}_{\mathcal{C},\mathcal{C}'}$ parallel $\mathcal{C}$, $\mathcal{C}'$ in XY; separated along $\hat{z}$	Area law of $\mathcal{C}$, $\mathcal{C}'$; exponential decay with Z	Perimeter law of $\mathcal{C}$; long range with Z	$\frac{1}{\lvert Z\rvert^{2\Delta_{\mathcal{C},\mathcal{C}'}}}$, for unit square $\mathcal{C},\mathcal{C}'$ separated along z

5.1.4 Summary

In this manuscript we analyzed the behavior of order diagnosis operators (ODO), at fine-tuned critical points or gapless phases of lattice systems with microscopic discrete categorical symmetries. The symmetries on both sides of the duality of the lattice models are constituents of the entire categorical symmetry of the system. We demonstrate that at these selected criticalities, the behavior of ODOs of categorical symmetries can be evaluated analytically, and they could have rather different scalings from the gapped phases of these models, where the ODO can be computed using the perturbation theory. The existence of subsystem symmetries of some of the systems intrinsically modify the behavior of ODOs at both the gapped phases, and the criticalities. And in examples with subsystem symmetries, we found that at these criticalities the scaling of ODOs defined on

both sides of the duality of the lattice models is substantially different from the gapped phases.

While preparing for our manuscript, we became aware of a work that numerically computed the behavior of ODO of $\tilde{Z}_2^{(1)}$ at the $3D$ Ising critical point, combined with theoretical comparison with free field theories [501]. The conclusion in this work is that, the $\tilde{Z}_2^{(1)}$ symmetry is still spontaneously broken at the $3D$ Ising critical point. The conclusion is similar to ours at the fine-tuned Lifshitz criticality of $2d$ lattice quantum Ising systems.

5.2 Universal Features of Higher-Form Symmetries at Phase Transitions

5.2.1 Introduction

The concept of symmetry is the most fundamental concept in physics, and has profound implications and constraints on physical phenomena. In recent years various generalizations of the concept of symmetry have been explored. For example, ordinary symmetries in a $d-$dimensional system are associated with the global conservation of the symmetry charges, and the symmetry charges localized within a $d-$dimensional subsystem of the space can only change through the Noether current flowing across the surface of the subsystem. In recent years the concept of 1-form symmetry (more generally higher form symmetry) was proposed (see for example Ref. 502, 482, 483, 484, 485, 486, 117, 487, 488, 489), and the concept of 1-form symmetry is associated with conserved "flux" through a $(d-1)-$dimensional subsystem; and the flux can only change through the flowing of a 2-form symmetry current across the edge of the $(d-1)-$dimensional subsystem. The concept of 1-form symmetry was proven highly useful when analyzing gauge fields. Using

this new concept of symmetry and its 't Hooft anomaly, it was proven that gauge fields with certain topological term cannot be trivially gapped [503], which is an analogue of the Lieb-Shultz-Mattis theorem in condensed matter systems [20, 22].

Lagrangians are often used to describe a physical system, and the form of the Lagrangian depends on one's choice of "local degrees of freedom" of the system, and other degrees of freedom may become nonlocal topological defects in the Lagrangian. When we select another set of local degrees of freedom of the same system to construct the Lagrangian, it will take a new form, and the new form of Lagrangian is related to the original Lagrangian through a "duality transformation". It was realized in recent years that, in some examples, duality transformation of the Lagrangian, along with the explicit symmetry of the Lagrangian, could be embedded into a larger symmetry group [504, 505], which may only emerge in the infrared limit, and is not explicit unless one takes into account of all the dual forms of the Lagrangian.

Most recently a new generalization of symmetry was developed which also involves the dual description of a system. It is well-known that certain models of theoretical physics have a dual description, and the dual model has symmetries that are inexplicit in the original model. A concept called "categorical symmetry" was developed which unifies the explicit symmetry of a system and the inexplicit symmetry of its dual model, and treat them on an equal footing [118]. To diagnose the behavior of the categorical symmetries, and most importantly to diagnose the explicit symmetry and the inexplicit dual symmetry on an equal footing, a concept of "order diagnosis operator" (ODO) was introduced, whose expectation value reduces to the correlation function between order parameters for an explicit 0-form symmetry, and reduces to a Wilson loop for an explicit 1-form symmetry [506]. The ODO was also referred to as the patch operator in Ref. 118. For example, the ODO for the Z_2 symmetry of the $2d$ quantum Ising model is $O_{ij} = \sigma_i^z \sigma_j^z$, while the ODO for the dual $\tilde{Z}_2^{(1)}$ 1-form symmetry is $\tilde{O}_{\mathcal{C}} = \prod_{j \in \mathcal{A}, \partial \mathcal{A} = \mathcal{C}} \sigma_j^x$,

where σ^z transforms under the explicit Z_2 symmetry. $\tilde{O}_{\mathcal{C}}$ creates a domain wall of σ^z along a closed loop $\mathcal{C}$ by flipping the sign of σ^z on a patch $\mathcal{A}$, which is the interior of $\mathcal{C}$. ODOs for systems with special symmetries such as subsystem symmetries may have special forms and behaviors, and examples with these special symmetries were discussed in Ref. 506.

The expectation value of O_{ij} and $\tilde{O}_{\mathcal{C}}$ in the $2d$ quantum Ising system characterizes different phases of the system. In the two gapped phases, i.e. the ordered and disordered phase of σ^z, the behavior of $\langle O_{ij}\rangle$ and $\langle \tilde{O}_{\mathcal{C}}\rangle$ are relatively easy to evaluate, since they can be computed through perturbation [490], which is protected by the gap of the phases. In the ordered phase of σ^z, $\langle O_{ij}\rangle$ saturates to a constant when $|i-j| \to \infty$, and $\langle \tilde{O}_{\mathcal{C}}\rangle$ decays with an area law; in the disordered phase of σ^z, $\langle O_{ij}\rangle$ decays exponentially with $|i-j|$, while $\langle \tilde{O}_{\mathcal{C}}\rangle$ decays with a perimeter law. But at the critical point of the system, i.e. the $(2+1)d$ quantum Ising phase transition, the behavior of the ODO $\tilde{O}_{\mathcal{C}}$ is more difficult to evaluate. Ref. 501 evaluated $\langle \tilde{O}_{\mathcal{C}}\rangle$ numerically, and the result indicates that in addition to a leading term linear with the perimeter of $\mathcal{C}$, a subleading term which is logarithmic of the perimeter arises for a *rectangular* shaped loop $\mathcal{C}$. The logarithmic subleading contribution may be a universal feature of ODO at a critical point, and the Z_2 ODO can be mapped to the 2nd Renyi entanglement entropy of a *free* boson/fermion system [501]. Tt is known that there is a corner induced logarithmic contribution for the Renyi entropy in a general conformal field theory [507, 508, 509, 510]. However, for *interacting* systems the exact relation between entanglement entropy and ODO is not clear yet.

In this work we demonstrate that, for a $2d$ quantum system with either an explicit 1-form symmetry $Z_N^{(1)}$, or an inexplicit symmetry $\tilde{Z}_N^{(1)}$ (which is dual to a 0-form ordinary Z_N symmetry), the following quantity $\langle(\log O_{\mathcal{C}})^2\rangle$ or $\langle(\log \tilde{O}_{\mathcal{C}})^2\rangle$ take a universal form $-\frac{A}{\epsilon}P + b\log P$ at many quantum critical points. Here P is the perimeter of the loop $\mathcal{C}$. b

is a universal number which arises from a sharp angle of the loop $\mathcal{C}$; b is proportional to the universal conductivity of the $2d$ quantum critical point, and it is a universal function of the angle θ. We demonstrate this result for various examples of quantum critical points. We also comment on the connection between ODO and entanglement entropy in the end of the manuscript.

We also compute a quantity called the "strange correlator" of the 1-form ODO $O_{\mathcal{C}}$. The strange correlator was introduced as a tool to diagnose the symmetry protected topological (SPT) states based on the bulk wave function instead of the edge states [511], and it was shown to be effective in many examples [512, 513, 514, 515, 516, 517, 518, 519, 520]. In the current work we study the strange correlator for one example of 1-form SPT state, but we expect similar studies are worth pursuing for more general cases.

5.2.2 Systems with Dual $\tilde{Z}_N^{(1)}$ Symmetry

Example 1: Z_N order-disorder transition

We first consider cases when the system has an explicit Z_N (0-form) symmetry, and it has an inexplicit dual $\tilde{Z}_N^{(1)}$ 1-form symmetry. The simplest example of quantum phase transition, is the order-disorder transition of the Z_N symmetry. The lattice model with Z_N symmetry, can be embedded into an ordinary U(1) rotor model:

$$H = \sum_{\langle i,j \rangle} -t\cos(\hat{\theta}_i - \hat{\theta}_j) + V(\hat{n}_i) - 2u\cos(N\hat{\theta}_i), \tag{5.45}$$

where $[\hat{n}_i,\ \hat{\theta}_j] = \mathrm{i}\delta_{ij}$, and $\hat{\theta}_j$ prefers to take values $\hat{\theta}_j = 2\pi k/N$ with $k = 0, \cdots N-1$ due to the u-term. The potential $V(\hat{n})$ has a minimum at $\hat{n} = 0$. The order-disorder

transition of the Z_N symmetry is described by the Landau-Ginzburg action

$$\begin{aligned}\mathcal{S} &= \int d^2x d\tau \ |\partial\Phi|^2 + r|\Phi|^2 + g|\Phi|^4 + u(\Phi^N + h.c.) \quad \leftrightarrow \\ \mathcal{S}_d &= \int d^2x d\tau \ |(\partial - \mathrm{i}a)\phi|^2 + \tilde{r}|\phi|^2 + \tilde{g}|\phi|^4 + u(\mathrm{M}^N + h.c.). \end{aligned} \tag{5.46}$$

Φ is the complex order parameter. The second line of the equation is the well-known boson-vortex dual description of the phase transition [340, 18, 341], and $r \sim -\tilde{r}$ is the tuning parameter of the transition: $r > 0$ ($r < 0$) corresponds to the gapped (condensed) phase of Φ and condensed (gapped) phase of ϕ. The Φ^N term is the Z_N anisotropy on Φ which breaks the U(1) symmetry of Φ to Z_N. The Φ^N is dual to the $N-$fold monopole operator (M^N) in the dual theory. It is known that when $N \geq 4$, the u term (Z_N anisotropy) is an irrelevant perturbation at the $(2+1)d$ XY transition, and there will be an emergent U(1) symmetry at the quantum phase transition.

As was discussed before, a system with Z_N symmetry has an inexplicit dual $\tilde{Z}_N$ 1-form symmetry, the Z_N and $\tilde{Z}_N^{(1)}$ symmetry together constitute the "categorical symmetry" of the system [118]. In order to describe the behavior of the $\tilde{Z}_N^{(1)}$ symmetry, Ref. 506 introduced the "order diagnosis operator" $\tilde{O}_{\mathcal{C}}$. Represented in terms of lattice operators, the ODO for the dual $Z_N^{(1)}$ symmetry reads

$$\tilde{O}_{\mathcal{C}} = \exp\left(\mathrm{i}\frac{2\pi}{N}\sum_{j\in\mathcal{A}}\hat{n}_j\right), \tag{5.47}$$

where $\partial\mathcal{A} = \mathcal{C}$ is a patch of the $2d$ lattice enclosed by contractible loop $\mathcal{C}$, and the ODO was also called patch operator in Ref. 118. $\tilde{O}_{\mathcal{C}}$ creates a Z_N domain wall. In the ordered and disordered phase of the Z_N symmetry, the expectation value of $\tilde{O}_{\mathcal{C}}$ decays with an area law and perimeter law respectively.

At the order-disorder phase transition, to extract the universal feature of the ODO

$\tilde{O}_{\mathcal{C}}$, we evaluate $\langle(\log \tilde{O}_{\mathcal{C}})^2\rangle$ [3], which in the dual theory reduces to

$$\langle(\log \tilde{O}_{\mathcal{C}})^2\rangle = -\frac{1}{N^2}\int_{\mathcal{C}} dl^{\mu}\int_{\mathcal{C}'} dl'^{\nu}\langle a_{\mu}(\mathbf{x})a_{\nu}(\mathbf{x}')\rangle. \tag{5.48}$$

The relation between a_μ and the original Landau-Ginzburg theory is $J = \frac{\mathrm{i}}{2\pi} * da$, where J is the current of the emergent U(1) symmetry at the Z_N order-disorder transition. The correlation of a_μ is dictated by the correlation of J whose scaling dimension *does not* renormalize at a general conformal field theory. The correlation between currents J is proportional to the universal conductivity at a $(2+1)d$ conformal field theory:

$$\langle J_{\mu}(0)J_{\nu}(\mathbf{x})\rangle = \sigma\frac{I_{\mu\nu}(\mathbf{x})}{|\mathbf{x}|^4}, \tag{5.49}$$

where the matrix $I_{\mu\nu}(\mathbf{x})$ is given by $I_{\mu\nu}(\mathbf{x}) = \delta_{\mu\nu} - 2x_\mu x_\nu/|\mathbf{x}|^2$, and σ is C_J in (for example) Ref. 521. The universal conductivity at a $(2+1)d$ XY transition was predicted in Ref. 329, and it can be computed using various theoretical and numerical methods, and also measured experimentally (see for example Ref 326, 330, 331, 333, 335, 336, 337, the universal conductivity in some of the references was computed/measured with strong disorder).

It is straightforward to verify that the gauge field propagator can be written as

$$\langle a_{\mu}(0)a_{\nu}(\mathbf{x})\rangle = \sigma\pi^2\frac{\delta_{\mu\nu} - \zeta I_{\mu\nu}(\mathbf{x})}{|\mathbf{x}|^2}, \tag{5.50}$$

[3] log is a multivalued function. Since $\tilde{O}_{\mathcal{C}} = \prod_j \tilde{O}_{j\in\mathcal{A},\partial\mathcal{A}=\mathcal{C}}$, where $\tilde{O}_j = e^{\mathrm{i}2\pi\hat{n}_j/N}$, we define $\log\tilde{O}_{\mathcal{C}} = \sum_{j\in\mathcal{A}}\log\tilde{O}_j$, and demand $\mathrm{Arg}[\tilde{O}_j] = \log\tilde{O}_j \in (-\pi,\pi] \sim 2\pi\hat{n}_j/N$, the $V(\hat{n}_i)$ term in the Hamiltonian Eq. 5.45 restricts $\hat{n}_j$ to largely fluctuate around its minimum $\hat{n}_j \sim 0$.

The parameter ζ is introduced by a nonlocal gauge fixing term

$$\frac{1}{8\pi^6\sigma}\frac{1}{1-\zeta}\int d^3\mathbf{x}d^3\mathbf{y}\frac{\partial_\mu a^\mu(\mathbf{x})\partial_\nu a^\nu(\mathbf{y})}{|\mathbf{x}-\mathbf{y}|^2}, \tag{5.51}$$

which contributes to a total derivative $I_{\mu\nu}(\mathbf{x})/|\mathbf{x}|^2 = \frac{1}{2}\partial_\mu\partial_\nu \log|\mathbf{x}|^2$ in the gauge field propagator.

In the explicit calculation of Eq. 5.48, one should be very careful about how to set the UV cut-off. A hard cut-off on the integration interval $|\mathbf{x}-\mathbf{x}'|$ along $\mathcal{C}$ will spoil the gauge invariance. To guarantee that $\mathcal{C}$ and $\mathcal{C}'$ are both complete loops in the integral (hence gauge invariance is preserved), a good method is to set a small distance between $\mathcal{C}$ and $\mathcal{C}'$ along the temporal direction by distance $\tau = \epsilon > 0$, and this small splitting serves as a small real-space UV cut-off. The integral is then performed along the closed loop $\mathcal{C}$ (and its duplicate $\mathcal{C}'$) in the x-y plane. For a smooth loop $\mathcal{C}$ with perimeter P, the evaluation of $\langle(\log O_{\mathcal{C}})^2\rangle$ simply yields a perimeter law, *i.e.* proportional to P with a UV-dependent coefficient. For example, when $\mathcal{C}$ is a circle with radius R, the integral in Eq. 5.48 gives

$$-\langle(\log \tilde{O}_{\mathcal{C}})^2\rangle = \frac{\sigma\pi^2}{N^2}\left(\frac{2\pi^2 R}{\epsilon} - 2\pi^2 + \frac{3\pi^2\epsilon}{4R}\right) + \mathcal{O}(\epsilon^2). \tag{5.52}$$

There are two observations. First, the final result is independent of the gauge choice ζ. Second, the large-R scaling is only given by a linear term which depends on the UV cut-off.

However, if the loop $\mathcal{C}$ has sharp corners, the situation is very different, and some universal feature that does not depend on the UV cut-off emerges. Let us first consider $\mathcal{C}$ being a spatial square with four corners $(0,0), (L,0), (L,L), (0,L)$. There are three types of integrals that are involved. The linear contribution is from the correlation along

the same edge of $\mathcal{C}$

$$\int_0^L dx \int_0^L dx' \frac{(1+\zeta)(x-x')^2 + (1-\zeta)\epsilon^2}{((x-x')^2+\epsilon^2)^2} = \frac{\pi L}{\epsilon} - 2(1+\zeta)\log(L/\epsilon) + \mathcal{O}(1). \tag{5.53}$$

It is important to notice that there is a $\log(L/\epsilon)$ term, which also shows up in the integral for two neighboring edges that are perpendicular to each other

$$\int_0^L dx \int_0^L dy' \frac{2\zeta x y'}{(x^2+y'^2+\epsilon^2)^2} = \zeta \log(L/\epsilon). \tag{5.54}$$

The integral from two parallel edges is a finite number which does not grow with L

$$\int_0^L dx \int_0^L dx' \frac{(\zeta+1)(x-x')^2 + (1-\zeta)(L^2+\epsilon^2)}{-(L^2+(x-x')^2+\epsilon^2)^2} = \mathcal{O}(1) \tag{5.55}$$

Combining all contributions together, we find the gauge invariant result

$$-\langle(\log \tilde{O}_{\mathcal{C}})^2\rangle = \frac{\sigma\pi^2}{N^2}\left(\frac{\pi 4L}{\epsilon} - 8\log(L/\epsilon)\right) + \mathcal{O}(1). \tag{5.56}$$

The ζ-independence of the $\mathcal{O}(1)$ term has also been verified. This result is similar to the evaluation of a square Wilson loop for free QED in $(3+1)$ dimensions. In both the two cases above, we find that the linear term in $-\langle(\log \tilde{O}_{\mathcal{C}})^2\rangle$ is $\frac{\sigma\pi^2}{N^2}\frac{\pi P}{\epsilon}$ where $P = 2\pi R$ for the circle and $P = 4L$ for the square.

Let us now generalize Eq. 5.54 to the case of two straight lines with an arbitrary angle θ with $0 < \theta < \pi$. For convenience, we choose the gauge $\zeta = 0$ in the following calculations. We could parametrize the two straight lines by $t(\cos(\theta/2), -\sin(\theta/2))$ and $s(\cos(\theta/2), \sin(\theta/2))$ where $0 < s, t < L$. To extract the angle-dependence of the

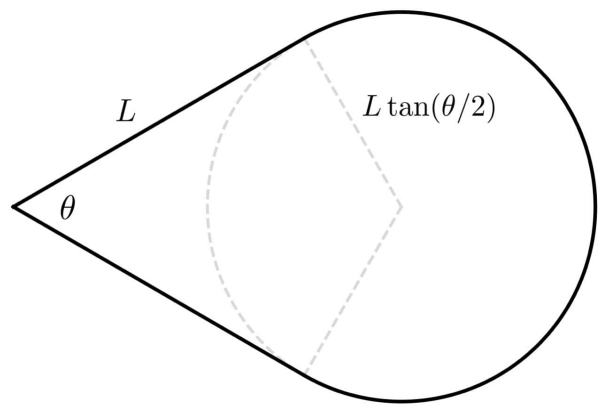

Figure 5.3: The shape of $\mathcal{C}$ with only one angle $0 < \theta < \pi$. As a concrete example, we consider a circle with two tangent lines that intersect at a point. Each tangent line has the length L, the radius of the circle is therefore $L\tan(\theta/2)$ and the perimeter of $\mathcal{C}$ is given by $P = (2 + (\pi + \theta)\tan(\theta/2))L$.

logarithmic divergence, we use the trick in Ref. 522, 523

$$\int_0^L ds \int_0^L dt \frac{-\cos\theta}{s^2 + t^2 - 2st\cos\theta + \epsilon^2} = \int_0^L d\ell \int_0^1 d\lambda \left[\frac{\ell}{\ell^2 + \epsilon^2} \frac{-\cos\theta}{\lambda^2 + (1-\lambda)^2 - 2\lambda(1-\lambda)\cos\theta} + \mathcal{O}(\epsilon^2/\ell^3)\right], \tag{5.57}$$

where we have changed the integration variables to $s = \ell\lambda, t = \ell(1-\lambda)$, and the $\mathcal{O}(\epsilon^2/\ell^3)$ part does not contribute to any logarithmic divergence. The λ-integral can be evaluated exactly, which gives $-(\pi - \theta)\cot\theta$. The $\log(L/\epsilon)$ divergence then arises from the ℓ-integral. There is another logarithmic contribution from correlation within the same line. Combining all the contributions together, eventually we obtain

$$-\langle(\log\tilde{O}_{\mathcal{C}})^2\rangle = \frac{\sigma\pi^2}{N^2}\left(\frac{\pi P}{\epsilon} - f(\theta)\log P\right) + \mathcal{O}(1) \tag{5.58}$$

$$f(\theta) = 2(1 + (\pi - \theta)\cot(\theta)) \tag{5.59}$$

for any shape of $\mathcal{C}$ with a single corner, where P is the perimeter of $\mathcal{C}$. We observe that the universal logarithmic term vanishes when $\theta = \pi$, and only the linear term remains,

as expected. To double check the analytical expression Eq. 5.58, we consider the shape of $\mathcal{C}$ as shown in FIG. 5.3, and the numerical evaluation for $-\langle(\log \tilde{O}_{\mathcal{C}})^2\rangle$ for different angles are shown in FIG. 5.4. For fixed values of L, ϵ, the angle dependence for both the linear and the logarithmic terms agree with Eq. 5.58 and Eq. 5.59.

We computed $-\langle(\log \tilde{O}_{\mathcal{C}})^2\rangle$, which is the second order expansion of $2\langle\tilde{O}_{\mathcal{C}}\rangle$. We have not proven whether higher order expansion in $\langle\tilde{O}_{\mathcal{C}}\rangle$ leads to different corner contribution from $\langle(\log \tilde{O}_{\mathcal{C}})^2\rangle$ or not. We would also like to mention that the entanglement entropy of a patch $\mathcal{A}$ with corners in a $(2+1)d$ CFT is related to another universal quantity C_T from the correlation of the stress-energy tensor $T_{\mu\nu}$. As discussed in Ref. 507, 508, 509, 510, the entanglement entropy takes the form $S = \frac{B}{\epsilon}P - a(\theta)\log P + \mathcal{O}(1)$, where B/ϵ depends on the UV details, and the universal coefficient $a(\theta)$ is proportional to C_T. The function $a(\theta)$ proposed for entanglement entropy [507, 508] is also proportional to $f(\theta)$ in our result.

Example 2: Z_N SPT-trivial transition

Now let us still assume the system has a Z_N symmetry, but the system undergoes a transition between a $2d$ Z_N symmetry protected topological (SPT) state and a trivial state. Both states are disordered states of the Z_N symmetry, hence in both states the ODO $\tilde{O}_{\mathcal{C}}$ should obey a perimeter law. Our main interest focuses on the trivial-SPT phase transition, especially the universal features of $\tilde{O}_{\mathcal{C}}$ at this transition. This example, and the next few examples will be described by a class of similar theories:

$$\mathcal{S} = \int d^2x d\tau \sum_{\alpha=1}^{N_f} \bar{\psi}_\alpha \gamma \cdot (\partial - iNa)\psi_\alpha + m\bar{\psi}\psi + \frac{\mathrm{i}k}{4\pi} a da + \cdots \tag{5.60}$$

with integer N_f and N, and in general these theories will be labelled as $\mathrm{QED}_{(N_f,N,k)}$. The trivial-SPT transition corresponds to $\mathrm{QED}_{(2,1,0)}$, i.e. $N_f = 2$, $N = 1$ and $k = 0$ [404, 403],

θ	L	$\log L$	$1/L$	const.
$\pi/20$	7.10018	-40.0651	14.6678	38.1625
$\pi/10$	8.00282	-19.4447	21.0523	-1.35483
$3\pi/20$	9.00801	-12.474	17.0716	-10.7626
$\pi/5$	10.1315	-8.93462	12.4601	-14.3023
$\pi/4$	11.3933	-6.70427	11.2763	-16.2376

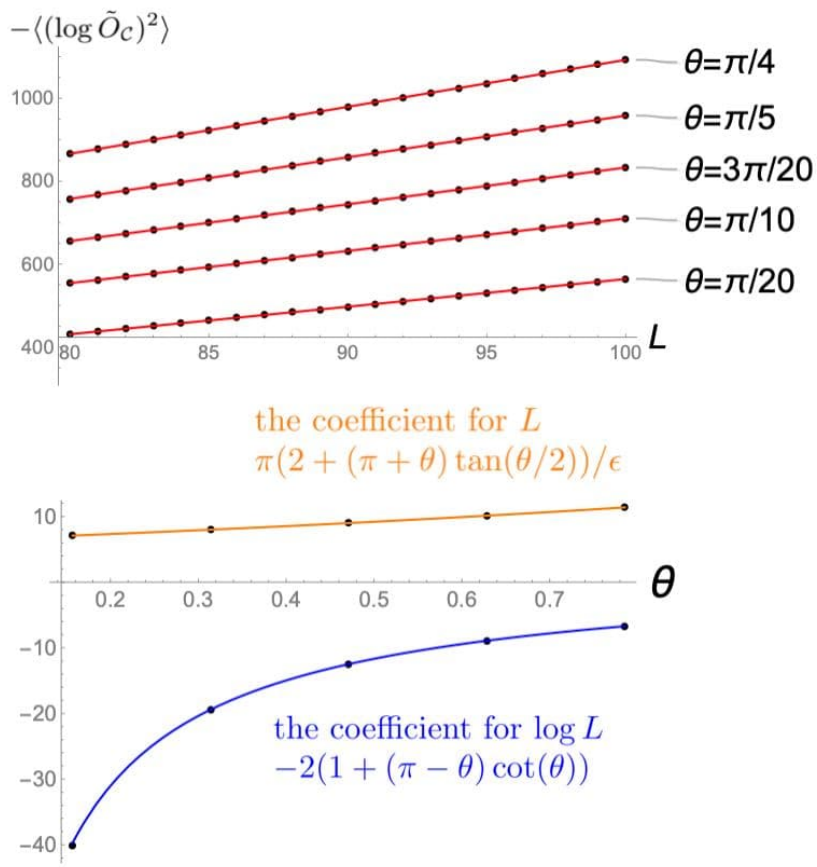

Figure 5.4: The numerical results of $-\langle(\log \tilde{O}_{\mathcal{C}})^2\rangle$ (in the unit of $\sigma\pi^2/N^2$) for the shape in FIG. 5.3 with different angles. The UV cut-off is set to be $\epsilon = 1$. The large-L scaling is fitted by the function $-\langle(\log \tilde{O}_{\mathcal{C}})^2\rangle = aL/\epsilon + b\log L + c/L + d$, and the fitting parameters a, b agree with the analytical expressions Eq. 5.58 and Eq. 5.59.

plus Chern-Simons terms of background gauge fields which are not written explicitly in Eq. 5.60. The trivial-SPT transition needs certain fine-tuning to reach the critical point described by this field theory, hence this field theory is a multi-critical point between the two states. This multi-critical point is self-dual [168, 524, 169] and also dual to the easy-plane deconfined quantum critical point [171, 504, 525, 505]. The Dirac fermion mass term m in Eq. 5.60 is the tuning parameter between the trivial and SPT phases.

In the theory $\text{QED}_{(2,1,0)}$, the current of the U(1) symmetry in which the microscopic Z_N symmetry is embedded, is $J = \frac{\mathrm{i}}{2\pi} * da$, and the ODO of the system is given by Eq. 5.47. The angle dependence of the ODO is still give by Eq. 5.59, with σ replaced by the counterpart at the trivial-SPT (multi-)critical point $\text{QED}_{(2,1,0)}$. The universal conductivity can be computed using various methods such as $1/N_f$ expansion.

5.2.3 Systems with Explicit $Z_N^{(1)}$ Symmetry

Topological transition at the boundary of a $3d$ SPT with $Z_N^{(1)} \times \text{U}(1)^{(0)}$ symmetry

Here we consider an example with an explicit $Z_N^{(1)}$ 1-form symmetry. The infrared of this example is described by $\text{QED}_{(1,2N,0)}$ of Eq. 5.60, i.e. it is a single massless Dirac fermion ψ with charge$-2N$ coupled with a U(1) gauge field. In our construction of theory $\text{QED}_{(1,2N,0)}$ we also need a charge$-N$ fermion ψ' in the background, hence the system only has a $Z_N^{(1)}$ 1-form symmetry, i.e. the electric flux of the gauge field through any closed surface is conserved mod Z_N. We also demand that the magnetic flux of the $\text{QED}_{(1,2N,0)}$ is conserved, which corresponds to another $\text{U}(1)^{(0)}$ symmetry. There is a mixed anomaly between the $Z_N^{(1)}$ and $\text{U}(1)^{(0)}$ symmetries. Hence the field theory $\text{QED}_{(1,2N,0)}$ can be realized at the boundary of a $3d$ SPT state with $Z_N^{(1)}$ and $\text{U}(1)^{(0)}$ symmetry [526]. In the following paragraphs we spell out this construction of the $3d$ bulk SPT state. [4]

[4] This is one possible construction of the $3d$ bulk, the field theory $\text{QED}_{(1,2N,0)}$ maybe realized as the boundary theory of other $3d$ 1-form SPT states too.

To construct the boundary theory $\mathrm{QED}_{(1,2N,0)}$, we first consider a $3d$ bulk with an ordinary photon phase of gauge field a_μ, and only charge$-N$ and charge$-2N$ fermionic matter field is dynamical, although all the integer-charge Wilson loops are allowed in the theory. Hence the system has a $Z_N^{(1)}$ 1-form symmetry. All the fermionic matters are in a topologically trivial band structure in $3d$. Then we bind the Dirac monopole of $\vec{a}$ with another gauge neutral boson with global $\mathrm{U}(1)^{(0)}$ conservation, and condense the bound state. The $3d$ bulk is a SPT state with $Z_N^{(1)} \times \mathrm{U}(1)^{(0)}$ symmetry [526]. The natural $2d$ boundary of the system is a $(2+1)d$ photon phase. To create a gauge flux at the $2d$ boundary, one needs to move a Dirac monopole from outside of the system, into the $3d$ bulk; since in the $3d$ bulk the bound state between the Dirac monopole and the $\mathrm{U}(1)^{(0)}$ boson is condensed, the 2π magnetic flux at the boundary must also carry the $\mathrm{U}(1)^{(0)}$ boson. Hence the photons at the $2d$ boundary is the dual of the Goldstone modes of the $\mathrm{U}(1)^{(0)}$ symmetry. Notice that the bulk is fully gapped and has no spontaneous breaking of the $\mathrm{U}(1)^{(0)}$ symmetry, because the condensed bound state in the bulk is coupled to the dual gauge field while carrying the $\mathrm{U}(1)^{(0)}$ charge. The condensate is still gapped due to the Higgs mechanism.

At the $2d$ boundary, the charge$-2N$ fermion ψ is tuned close to the transition between a trivial insulator and a Chern insulator with Chern number $+1$. Due to the fermi-doubling in $2d$, there must be another massive Dirac cone of ψ in the band structure that affects the dynamics of a_μ. Hence we need to design a background band structure of the charge$-N$ fermion ψ' with Chern number -2. The Chern-Simons term of a_μ generated from ψ' will cancel the Chern-Simons term generated by the band structure of fermion ψ.

Now we have arrived at the theory $\mathrm{QED}_{(1,2N,0)}$. The $\mathrm{QED}_{(1,2N,0)}$ is a transition between two different topological states tuned by the mass of the Dirac fermion ψ, these two topological orders are described by the CS term for a_μ with level $k = \pm 2N^2$, which is

free of $Z_N^{(1)}$ 1-form symmetry anomaly. The ODO for the $Z_N^{(1)}$ symmetry is the charge-1 Wilson loop $O_{\mathcal{C}} = \exp(\mathrm{i}\int d\vec{l}\cdot\vec{a})$. In this case the quantity $\langle(\log O_{\mathcal{C}})^2\rangle$ at the critical point $m = 0$ can be evaluated exactly, based on the fermion-vortex duality developed recently [527, 528, 529, 216, 530]:

$$\mathrm{QED}_{(1,2N,0)} \quad \leftrightarrow \quad \bar{\chi}\gamma\cdot\partial\chi \text{ coupled to } Z_N \text{ gauge theory} + \cdots \tag{5.61}$$

The detailed and exact form of the duality can be found in Ref. 530. The right hand side of the duality is a Dirac fermion coupled with a Z_N gauge field. The duality relation we will exploit is

$$J_\chi = \mathrm{i}\frac{2N}{4\pi} * da, \tag{5.62}$$

where J_χ is the current carried by χ. Although χ is coupled with a Z_N gauge field, since the Z_N gauge field is gapped, in the infrared the correlation of J_χ is identical to that of the free Dirac fermion, and can be computed exactly:

$$\langle J_{\chi,\mu}(0)J_{\chi,\nu}(\mathbf{x})\rangle = \frac{1}{8\pi^2}\frac{I_{\mu\nu}(\mathbf{x})}{|\mathbf{x}|^4}. \tag{5.63}$$

One can determine the propagator of the dual gauge field accordingly. Considering again the $\mathcal{C}$ in FIG. 5.3, we find

$$-\langle(\log O_{\mathcal{C}})^2\rangle = \frac{1}{8N^2}\left(\frac{\pi P}{\epsilon} - f(\theta)\log P\right) + \mathcal{O}(1), \tag{5.64}$$

where $f(\theta)$ is given in Eq. 5.59.

$\mathbf{QED}_{(N_f,N,k)}$ with explicit $Z_N^{(1)}$ symmetry and Chern-Simons term

We consider the theory $\mathrm{QED}_{N_f,N,k}$ with large$-N_f$ and level $k = qN^2$, where q is an integer at the order of N_f. $\mathrm{QED}_{(N_f,N,k)}$ with even integer N_f, and a CS term with level k being integer multiple of N^2 can be constructed in $2d$ with $Z_N^{(1)}$ 1-form symmetry [5]. At low energy, the dynamics of gauge field is significantly modified by the one-loop polarization diagram of fermion ψ. In the momentum space, the loop diagram integral gives

$$|a_\mu(\vec{p})|^2 \frac{N_f N^2}{16} \frac{|p|^2 \delta_{\mu\nu} - p_\mu p_\nu}{|p|} \tag{5.65}$$

which gives an order N_f contribution to the gauge field self-energy. To the leading order in $1/N_f$, the gauge field propagator in the momentum space is given by

$$\frac{16}{N_f N^2} \frac{1}{|p|} \left(\frac{\cos \hat{\boldsymbol{K}}}{|\boldsymbol{K}|} \left(\delta_{\mu\nu} - \zeta \frac{p_\mu p_\nu}{|p|^2} \right) + \frac{\sin \hat{\boldsymbol{K}}}{|\boldsymbol{K}|} \frac{\varepsilon_{\mu\nu\sigma} p_\sigma}{|p|} \right), \tag{5.66}$$

where $|\boldsymbol{K}|, \hat{\boldsymbol{K}}$ denote the magnitude and the angle of the two-dimensional vector $\boldsymbol{K} = (1, \frac{-16k}{2\pi N_f N^2})$. The Fourier transformation to real space gives

$$\langle a_\mu(0) a_\nu(\mathbf{x}) \rangle = \frac{8}{N_f N^2} \frac{1}{\pi^2 |\mathbf{x}|^2} \times \left(\frac{\cos \hat{\boldsymbol{K}}}{|\boldsymbol{K}|} \frac{\delta_{\mu\nu} - \zeta I_{\mu\nu}(\mathbf{x})}{|\mathbf{x}|^2} + \frac{\sin \hat{\boldsymbol{K}}}{|\boldsymbol{K}|} \frac{\mathrm{i}\pi}{2} \frac{\varepsilon_{\mu\nu\sigma} x_\sigma}{|\mathbf{x}|} \right), \tag{5.67}$$

[5] We can verify that the absence of the anomaly associated to the Z_N 1-form symmetry in this QED theory by considering the its massive phases. For example, when a positive mass of the Dirac fermion is turned on, one obtains a U(1) CS theory of level $(q + N_f/2)N^2$. In this massive phase, the Z_N 1-form symmetry is generated by the anyon line operator carrying U(1) charge $(q + Nf/2)N$. When N is odd, we should in fact view the U(1) gauge field a as a spin$_c$ gauge field. Consequently, this charge-$(q+N_f/2)N$ anyon always has bosonic self-statistics, which indicates the absence of anomaly associated with the Z_N 1-form symmetry. When N is even, the QED (and its massive phases) intrinsically resides in a fermionic Hilbert space. The gauge field a is now a regular U(1) gauge field. In this case, the charge-$(q + N_f/2)N$ anyon can have either bosonic or fermionic self-statistics depending on the value of $(q + N_f/2)N$. However, neither case leads to any anomaly associated to the Z_N 1-form symmetry because the self-statistics of the charge-$(q + N_f/2)N$ anyon can be made bosonic by attaching extra neutral fermions in the Hilbert space.

which has an imaginary part due to the Chern-Simons term. The parameter ζ is introduced by gauge fixing.

The ODO for the $Z_N^{(1)}$ symmetry is still the charge-1 Wilson loop $O_{\mathcal{C}} = \exp(\mathrm{i}\int d\vec{l}\cdot\vec{a})$. As for the shape of $\mathcal{C}$ with a sharp corner in FIG. 5.3, our calculation leads to the gauge invariant result

$$-\langle(\log O_{\mathcal{C}})^2\rangle = \frac{8N^2N_f}{64k^2+\pi^2N^4N_f^2}\left(\frac{\pi P}{\epsilon} - f(\theta)\log P\right) + \mathcal{O}(1), \tag{5.68}$$

where $f(\theta)$ is given in Eq. 5.59. The imaginary antisymmetric part of $\langle a_\mu a_\nu\rangle$ does not contribute, and the final result has the similar form as before. In the large$-N_f$ limit the universal conductivity of the current $J = \frac{1}{2\pi} * da$ can be computed exactly.

5.2.4 The "Strange Correlator" of ODO

Following the argument from Ref. 531, if a state $|\Omega\rangle$ is the ground state described by a Lagrangian $\mathcal{L}(\Phi(\mathbf{x}))$, the matrix elements between $|\Omega\rangle$ and two different field configurations $|\Phi(\mathbf{x})\rangle$ and $|\Phi'(\mathbf{x})\rangle$ is given by the path integral:

$$\langle\Phi(\mathbf{x})|\Omega\rangle\langle\Omega|\Phi'(\mathbf{x})\rangle \sim \int_{\Phi(\mathbf{x},\tau=-\infty)=\Phi'(\mathbf{x})}^{\Phi(\mathbf{x},\tau=+\infty)=\Phi(\mathbf{x})} D\Phi(\mathbf{x},\tau)\exp\left(-\int_{-\infty}^{+\infty} d\tau d^dx\ \mathcal{L}(\Phi(\mathbf{x},\tau))\right), \tag{5.69}$$

knowing the matrix element, Ref. 531 was able to derive the ground state wave function based on the Lagrangian description of various SPT states.

Based on the information of the ground state wave function of SPT state derived from its Lagrangian, the quantity "strange correlator" was introduced and designed to diagnose a SPT state based on its bulk wave function [511]. Let us assume that $|0\rangle$ and $|1\rangle$ are the trivial state and SPT state defined within the same bosonic Hilbert space in a two dimensional real space, and both systems have the same symmetry. The

strange correlator is the quantity $S(\mathbf{x}, \mathbf{x}') = \langle 0|\Phi(\mathbf{x})\Phi(\mathbf{x}')|1\rangle/\langle 0|1\rangle$, where $\Phi(\mathbf{x})$ is the order parameter of the symmetry that defines the systems.

For a class of Langrangians $\mathcal{L}$, using the derived wave functions for both the SPT state $|1\rangle$ and trivial state $|0\rangle$, one would see that the strange correlator $S(\mathbf{x}, \mathbf{x}')$ cannot have a trivial short range correlation at least for $d = 2$. Another picture to see this is that, if the Lagrangian $\mathcal{L}$ has an emergent Lorentz invariant description, after the space-time rotation, the strange correlator which was purely defined in space, becomes a space-time correlation function at the one dimensional spatial interface between $|0\rangle$ and $|1\rangle$. This picture is similar to the construction of fractional quantum Hall wave function using conformal blocks [532]. Because the spatial interface between $|0\rangle$ and $|1\rangle$ cannot be trivially gapped, the strange correlator $S(\mathbf{x}, \mathbf{x}')$ must be either long ranged, or have a power-law. Hence the strange correlator can be viewed as a tool to diagnose a SPT state based on its bulk wave function, and it has been shown to be effective for many examples [512, 513, 514, 515, 516, 517, 518, 519, 520].

ODO is the generalization of correlation functions of 0-form symmetries. Here we generalize the strange correlator to the ODO of 1-form symmetry i.e. we evaluate the following quantity

$$S(\mathcal{C}) = \langle 0|O_{\mathcal{C}}|1\rangle/\langle 0|1\rangle, \tag{5.70}$$

where $|0\rangle$ and $|1\rangle$ are trivial state and SPT state with 1-form symmetry respectively. SPT states protected by 1-form symmetries have attracted great interests in the last few years [368, 117, 533, 534, 489, 535, 536, 537, 538, 539, 540, 541, 526], we expect this general question of evaluating strange correlator of ODO to be a new direction that is worth a deep exploration. In the current work we consider a typical $3d$ SPT state protected by the $Z_N^{(1)}$ 1-form symmetry as an example. This SPT state can be described

by the following Lagrangian [542]

$$\mathcal{L} = \frac{1}{2g}\mathrm{tr}[F \wedge *F] + \frac{\mathrm{i}\Theta}{8\pi^2}\mathrm{tr}[F \wedge F]. \tag{5.71}$$

F is the curvature tensor of the SU(N) gauge field. To guarantee there is a $Z_N^{(1)}$ 1-form symmetry, we only allow dynamical (but massive) matter fields of the SU(N) gauge field which carries an adjoint representation of the gauge field, while closed Wilson loops with other representations of the gauge field are still allowed. The SPT state corresponds to $\Theta = 2\pi$, while the trivial state corresponds to $\Theta = 0$ in the Lagrangian. The interface between $\Theta = 0$ and $\Theta = 2\pi$ is a $2d$ topological order described by SU$(N)_1$ Chern-Simons theory with topological degeneracy. For both $\Theta = 0$ or 2π, the coupling constant g in the Lagrangian is expected to flow to infinity under renormalization group, hence the $\Theta-$term is what remains in the infrared limit. The $\Theta-$term is a total derivative, hence

$$\begin{aligned}\langle A(\mathbf{x})|1\rangle\langle 1|A'(\mathbf{x})\rangle &\sim \int_{A(\mathbf{x},\tau=-\infty)=A'(\mathbf{x})}^{A(\mathbf{x},\tau=+\infty)=A(\mathbf{x})} DA(\mathbf{x},\tau)\exp\left(-\int_{-\infty}^{+\infty} d\tau d^3x\mathcal{L}(A)_{g\to+\infty}\right)\\ &\sim \exp\left(\int d^3x\frac{\mathrm{i}}{4\pi}\mathrm{CS}[A] - \frac{\mathrm{i}}{4\pi}\mathrm{CS}[A']\right),\end{aligned} \tag{5.72}$$

Hence the wave function of the SPT state $|1\rangle$, and the trivial state $|0\rangle$ (corresponds to $\Theta = 0$) in the limit $g \to +\infty$ are schematically

$$|0\rangle \sim \int DA|A\rangle, \tag{5.73}$$

$$|1\rangle \sim \int DA\exp\left(\int d^3x\frac{\mathrm{i}}{4\pi}\mathrm{CS}[A]\right)|A\rangle. \tag{5.74}$$

Now the evaluation of the strange correlator of ODO, which is a purely $3d$ spatial quantity, is mathematically equivalent to evaluating world lines of anyons in $(2+1)d$ SU$(N)_1$ CS

field theory:

$$S(\mathcal{C}) \sim \int DA \ \mathrm{tr}[e^{\mathrm{i}\int_{\mathcal{C}} d\vec{l}\cdot\vec{A}}] \exp\left(\int d^3x \frac{\mathrm{i}}{4\pi}\mathrm{CS}[A]\right). \tag{5.75}$$

Then if the ODO is a Wilson loop with the fundamental representation of the gauge group, and $\mathcal{C}$ contains two loops with a link, then this evaluation is identical to the braiding process of two anyons of the $\mathrm{SU}(N)_1$ topological order, and it yields phase $\exp(\mathrm{i}2\pi/N^2)$ for $S(\mathcal{C})$.

5.2.5 Discussion

In this work we studied the behavior of the "order diagnosis operator" of 1-form symmetries (for either explicit 1-form symmetry, or inexplicit 1-form symmetry as a dual of a 0-form symmetry) at various $(2+1)d$ quantum phase transitions. We demonstrate that for a class of transitions there is a universal logarithmic contribution to the ODO arising from the corners of the loop upon which the ODO is defined. For this class of transitions, the universal logarithmic contribution is related to the universal conductivity at the critical points, and in some cases can be computed exactly using the duality between conformal field theories.

This logarithmic contribution is similar to the corner contribution to the entanglement entropy, in fact this relation can be made exact for free boson/fermion systems [501]. For general systems, the ODO associated with certain 1-form symmetry and the entanglement entropy can be studied in a unified framework. To study the Renyi entropy, one needs to use the replica trick, and duplicate $n-$copies of the system. Then the system is granted an extra "swapping symmetry" between replica indices. The Renyi entropy reduces to evaluating the ODO of the 1-form dual of the swapping symmetry [543, 544]. Hence we can start with the duplicated system, and just study the ODO of all the

symmetries of the duplicated system, to extract the information of both the intrinsic symmetries, and the entanglement entropy simultaneously. One remark worth making is that, when computing Renyi entropy for ordinary systems with a Hamiltonian and translation invariance, there is no interaction between different duplicated systems, hence each duplicated copy has its own conservation laws.

In this work we also computed the strange correlator of the 1-form ODO for a particular example. SPT states protected by 1-form symmetries have attracted great efforts and interests in the last few years, and we believe the strange correlator of the 1-form ODO can be applied to many related systems. We will leave the more general discussion of this topic to future studies.

5.3 SPT Phases Involving Higher-Form Symmetries and LSM Theorems

5.3.1 Introduction

The symmetry protected topological (SPT) phases [157, 158] have greatly enriched our understanding of quantum states of matter. With certain symmetries, the boundary of these SPT states cannot be trivially gapped without degeneracy. Especially, many exotic states of matter can be realized at the $2d$ boundary of $3d$ bosonic SPT states. For example, exotic quantum critical points (QCP) in $2d$ with spatial symmetries (both on the square or triangular lattice) can be realized at the boundary of certain $3d$ SPT states [161, 173], and the conjectured emergent symmetry of the deconfined QCP matches well with the bulk symmetry of the SPT state, sometimes these emergent symmetries are only revealed through certain dualities [504, 505] between $(2+1)d$ quantum field theories. The analysis of the SPT state in the $(d+1)$-dimensional bulk can also be

used as a diagnose of the "Lieb-Schultz-Mattis theorem" in d-dimensional systems with spatial symmetries, i.e. whether or not the d-dimensional system can be gapped without degeneracy [91, 92, 93, 95, 90, 94] is related to the nature of the corresponding bulk state in one higher dimension.

In recent years it was realized that the very concept of symmetry can be generalized to higher dimensional objects rather than just point like operators [482, 483, 484, 485, 486, 117, 487, 488, 489]. Examples of SPT states that involve these generalized symmetries were discussed in previous literatures [368, 117, 533, 534, 489, 535, 536, 537, 538, 539, 540]. For example a classification of SPT states based on generalized cobordism theory was given in Ref. 537, 538, exactly soluble lattice models for a class of SPT states were constructed in Ref. 539, 540. In the current manuscript we focus on physical construction and boundary properties of a series of SPT states with generalized concepts of symmetries, from $(1+1)$-dimension to $(4+1)$-dimension. We do not seek for exactly soluble models, instead we will focus on general physical pictures of these states. For example, the prototype $4d$ (or $(4+1)d$) SPT state we will discuss can be constructed by "decorated Dirac monopole loop" picture, which is analogous to the flux attachment construction in $2d$ SPT state. And the prototype $3d$ boundary state of the $4d$ SPT state is a photon phase with various constraints of dynamics, quantum numbers, and statistics on the electric and magnetic charges. We assume that the gauge invariant objects/excitations, i.e. objects that do not couple to *dynamical* gauge field, are always bosonic. These include point particles and higher dimensional excitations such as loops.

The 1-form symmetry transformation acts on loop-like operators such as the Wilson loop or 't Hooft loop of a dynamical gauge field. The existence of an electric 1-form symmetry demands that the electric charge of the gauge field is infinitely heavy. In condensed matter systems the quantum dimer model [493] naturally fits this criterion. It is well-known that the quantum dimer model can be mapped to a lattice gauge field [545].

In a quantum dimer model, every site of the lattice is connected to a fixed number of dimers, which implies that there is a background electric charge distribution, but no dynamical charge in the system. Hence the quantum dimer model naturally has a 1-form symmetry. The quantum dimer model on certain d-dimensional lattice may be mapped to the boundary of a $(d+1)$-dimensional SPT state with 1-form symmetry in certain limit, and the spatial symmetries of the quantum dimer model is mapped to the onsite symmetry of the bulk SPT state. The analysis of the SPT state in the bulk has strong indications on the allowed phenomena of the quantum dimer model at d-dimension.

Due to the inevitable complexity of notations used in this manuscript, we will keep a self-consistent conventions of notations (*1-6*): (*1*) The $N-$form symmetry G will be labelled as $G^{(N)}$, such as $\mathrm{U}(1)^{(1)}$, $Z_n^{(1)}$, etc. Ordinary 0-form symmetry will be labelled without superscript. (*2*) Gauge symmetries associated with *dynamical* gauge field will be labelled as $u(1)^{(1)}$, $z_n^{(2)}$, etc. depending on the nature of the gauge fields. A topological order which corresponds to a dynamical discrete gauge field will also be labelled as, for example, a z_n topological order. (*3*) Gauge symmetries associated with *background* gauge fields will be labelled as $\mathcal{U}(1)^{(1)}$, $\mathcal{Z}_n^{(2)}$, etc. (*4*) Classifications of SPT states will be labelled as $\mathbb{Z}$, $\mathbb{Z}_n$, etc. (*5*) For space and space-time dimensions, for example, $3d$ space refers to three spatial dimensions; $(3+1)d$ refers to the space-time dimension, which is the same as $4D$ Euclidean space-time. Also, QED_4 refers to quantum electrodynamics in $(3+1)d$ or $4D$ space-time dimension. (*6*) For a QED_4, there are point like particles such as electric charge, and Dirac monopole. We label bosonic (fermionic) electric charges as e_b (e_f), and bosonic (fermionic) Dirac monopoles as m_b (m_f). Some of these point excitations have no dynamics (infinitely heavy) due to the 1-form symmetries, we will label these immobile point particles as e_{0b}, e_{0f}, etc. A QED_4 with bosonic electric charge and fermionic Dirac monopole is labelled as "$\mathrm{QED}_4\{e_b, m_f\}$".

5.3.2 Building Bricks–$1d$ SPT State with 1-Form Symmetries

The simplest SPT state that involves a 1-form symmetry exists in $1d$ space or $(1+1)d$ space-time. $1d$ SPT state with a 1-form symmetry is analogous to an ordinary SPT state in $0d$ space. For a $\mathrm{U}(1)^{(1)}$ 1-form symmetry, a SPT state in $1d$ simply corresponds to a state with integer electric flux through the system. Let us take a $1d$ chain with electric field operators defined on the links. Due to the Gauss law constraint, $\nabla_x \hat{e}(x) = 0$, the electric field $\hat{e}(x)$ takes a uniform integer eigenvalue on the entire chain (in a compact $u(1)$ lattice gauge theory, the electric field operator $\hat{e}(x)$ takes discrete integer value, while its conjugate operator $\hat{a}(x)$ is periodically defined), hence for a $\mathrm{U}(1)^{(1)}$ 1-form symmetry, the classification of $1d$ SPT states is $\mathbb{Z}$, which corresponds to different integer eigenvalues of $\hat{e}(x)$. It is analogous to the $\mathbb{Z}$ classification of a zero dimensional ordinary SPT state with U(1) symmetry [157, 158].

The Hamiltonian of a $1d$ lattice U(1) gauge field is also very simple, for example:

$$H = \sum_x g\left(\hat{e}(x) - k\right)^2 . \tag{5.76}$$

Due to the Gauss law constraint, a Hamiltonian must be invariant under gauge transformation $\hat{a} \to \hat{a} + \nabla_x f(x)$, where $\hat{a}$ is the conjugate operator of $\hat{e}$. A local $1d$ Hamiltonian that involves $\hat{a}$ cannot be gauge invariant, hence a local gauge invariant Hamiltonian is only a function of $\hat{e}$. In Eq. 5.76 k can take continuous values. When k is half integer, the system is at the transition between two SPT states, and the ground state of the Hamiltonian is two-fold degenerate with $\hat{e}(x) = k \pm 1/2$, namely the transition is a level crossing between two eigenvalues of $\hat{e}(x)$. This transition should be viewed as a first order transition.

One can also couple the electric field to a background 2-form $\mathcal{U}(1)^{(2)}$ gauge field:

$$S = \int d\tau dx \ \mathrm{i} f_{\mu\nu} B_{\mu\nu} \tag{5.77}$$

In $(1+1)d$ the stress tensor of the $u(1)$ gauge field is just the electric field: $f_{10} - f_{01} = e(x)$, and $B_{01} = -B_{10}$ is a Lagrange multiplier. Hence the $(1+1)d$ topological response theory for the SPT state is

$$S_{\mathrm{1d-topo}} = \int_{(1+1)d} \mathrm{i} k B, \tag{5.78}$$

which is a $(1+1)d$ Chern-Simons action of the 2-form gauge field B, and its level k takes only integer values. For each integer level$-k$, the electric field (the 1-form symmetry charge)

$$e(x) = \frac{\delta S_{\mathrm{1d-topo}}}{\mathrm{i}\delta B(x)} = k. \tag{5.79}$$

The $1d$ SPT state with 1-form symmetries will be the building bricks for SPT states in higher dimensions. Suppose we break the $\mathrm{U}(1)^{(1)}$ down to $Z_n^{(1)}$ symmetry, the topological response theory Eq. 5.78 still applies, but B is now a 2-form $\mathcal{Z}_n^{(2)}$ background gauge field. The classification of the SPT state will reduce to $\mathbb{Z}_n$, which means that in Eq. 5.78 the integer $k + n = k$.

5.3.3 $4d$ SPT States with $G_1^{(1)} \times G_2^{(1)}$ Symmetry

Parent $4d$ SPT state with $\mathrm{U}(1)^{(1)} \times \mathrm{U}(1)^{(1)}$ symmetry

We now discuss SPT states in $4d$ space that involves 1-form symmetries. This discussion is useful for diagnosing anomalies of $3d$ states of matter, namely some $3d$ states

of matter can only be realized at the boundary of a $4d$ SPT state. The parent SPT state that we will start with is the $(4+1)d$ state with the $\mathrm{U}(1)^{(1)} \times \mathrm{U}(1)^{(1)}$ 1-form symmetry. With two $\mathrm{U}(1)^{(1)}$ 1-form symmetries, the system can couple to two background $\mathcal{U}(1)^{(2)}$ 2-form gauge fields B^1 and B^2, and the response theory in $(4+1)d$ reads

$$S_{\mathrm{4d-topo}} = \int_{(4+1)d} \frac{\mathrm{i}k}{4\pi} \epsilon_{IJ} B^I \wedge dB^J, \tag{5.80}$$

where $\epsilon_{IJ} = \mathrm{i}\sigma^y$. For each integer k, Eq. 5.80 is a different Chern-Simons theory, and the system should correspond to a different SPT state, hence these SPT states described by Eq. 5.80 have a $\mathbb{Z}$ classification. The $(3+1)d$ boundary of this state is a QED_4 without dynamical electric or magnetic charge (Dirac monopole). This QED_4 has a $\mathrm{U}(1)^{(1)} \times \mathrm{U}(1)^{(1)}$ mixed 't Hooft anomaly as was derived in previous literatures [368, 117, 489].

To construct this $4d$ SPT state, we can start with two $(4+1)d$ $u(1)$ gauge fields $\vec{a}^1$ and $\vec{a}^2$. These two gauge fields both have *electric* 1-form $\mathrm{U}(1)^{(1)}$ symmetry, namely both gauge fields have no dynamical electric charges, i.e. the Gauss law constraint on the electric field is strictly enforced. This is equivalent to tuning the electric charges in the $4d$ bulk to be infinitely heavy. Both $u(1)$ gauge fields allow dynamical Dirac monopole loop/line defects in the $4d$ space. We will first discuss the cases where the charges of $\vec{a}^1$ and $\vec{a}^2$ are both bosons, otherwise $\vec{a}^1$ and $\vec{a}^2$ would be Spin^C connections. Situations with fermionic gauge charges of $\vec{a}^1$ and $\vec{a}^2$ will be discussed later.

We use the analogue of the "flux attachment" (or "decorated defect") construction of the SPT state which was used to construct $2d$ bosonic SPT state [546]. In $2d$ space, a $\mathrm{U}(1) \times \mathrm{U}(1)$ SPT state (the parent state of many $2d$ SPT states) can be constructed by binding the vortex defect of one $\mathrm{U}(1)$ symmetry with the charge of the other $\mathrm{U}(1)$ symmetry, and condense the bound state, which drives the system into a gapped SPT phase. In $4d$ space, the analogue of the vortex defect of an ordinary $\mathrm{U}(1)$ 0-form symmetry, is

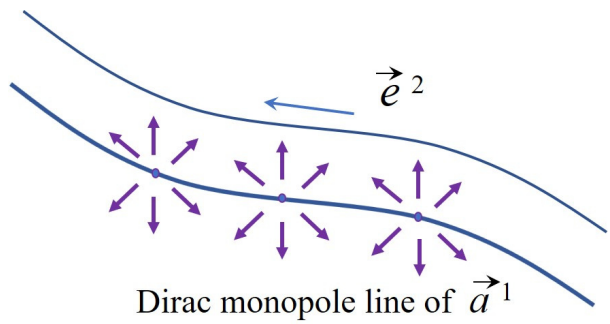

Figure 5.5: The decorated Dirac monopole loop construction of the parent SPT state in $4d$ space. The Dirac monopole loop of gauge field $\vec{a}^1$ is decorated with the $1d$ SPT state of the $\mathrm{U}(1)^{(1)}$ 1-form symmetry associated with gauge field $\vec{a}^2$. After the condensation of the decorated Dirac monopole loops, the $4d$ system is driven into a SPT state described by response theory Eq. 5.80.

the Dirac monopole loop/line of a $u(1)$ gauge field. We decorate the Dirac monopole loop of $\vec{a}^1$ with the $1d$ SPT state defined with the 1-form symmetry associated with $\vec{a}^2$ with level $(+k)$ in Eq. 5.78, and condense/proliferate the decorated loops (Fig. 5.5). Once the bound state between the monopole loop of $\vec{a}^1$ and the $(+k)$ unit of electric flux of $\vec{a}^2$ is condensed, the monopole loop of $\vec{a}^2$ will be automatically bound with $(-k)$ unit of electric flux of $\vec{a}^1$.

Condensation of Dirac monopole loops would normally drive a $(4{+}1)d$ $u(1)$ gauge field to the gapped confined phase (the loop excitation is coupled to a dual dynamical 2-form gauge field, and the condensate is gapped due to the Higgs mechanism). But because the Dirac monopole loop is decorated with another SPT state with $1-$form symmetry in our case, after the condensation of the decorated monopole loops, the phase in the $4d$ bulk is not an ordinary confined phase, it is actually a SPT phase described by Eq. 5.80. In fact, Eq. 5.80 directly implies that the 1-form symmetry charge (electric field) $\vec{e}^2(x)$, which is the variation $\delta S_{4\mathrm{d-topo}}/(\mathrm{i}\delta B^2_{01})$, equals to the flux of B^1, which is attached to the monopole of $\vec{a}^1$.

The $3d$ boundary of the $4d$ SPT state is most naturally a $(3+1)d$ QED_4 with both

magnetic and electric 1-form symmetries. The electric 1-form symmetry of the boundary QED_4 is inherited from the 1-form symmetry of $\vec{a}^1$ in the bulk, while the magnetic 1-form symmetry of the QED_4 corresponds to the electric 1-form symmetry of $\vec{a}^2$ in the bulk, because the Dirac monopole line of $\vec{a}^1$ in the $4d$ bulk is bound/decorated with the electric 1-form symmetry charge of $\vec{a}^2$. As we mentioned previously, we will first discuss the situation with bosonic point particles, hence in this QED_4 the infinitely heavy electric charge and Dirac monopoles are both bosons. We label this QED_4 as $\mathrm{QED}_4\{e_{0b}, m_{0b}\}$. Even though these point particles have infinite mass, their statistics still matter, because their Wilson loops (or 't Hooft loops) still exist. If these point particles are fermions, the Wilson loop will need a framing structure, and the Wilson loop or 't Hooft loop with a twist will acquire a minus sign.

Descendant $4d$ SPT state with $\mathrm{U}(1)^{(1)} \times Z_n^{(1)}$ symmetry

Now we break one of the $\mathrm{U}(1)^{(1)}$ 1-form symmetry down to the $Z_n^{(1)}$ symmetry. The topological response theory remains unchanged from Eq. 5.80, although one of the background 2-form gauge fields will become a $\mathcal{Z}_n^{(2)}$ background 2-form gauge field. The decorated monopole line construction discussed in the previous section still applies here. One key difference is that, because the $1d$ SPT phase with $Z_n^{(1)}$ 1-form symmetry has a $\mathbb{Z}_n$ classification itself, the flux attachment or decorated defect construction mentioned in the previous subsection will naturally lead to a $\mathbb{Z}_n$ classification of the $4d$ SPT state also. Namely, when $k = n$ in Eq. 5.80, this bulk SPT state will be trivialized, because the $1d$ SPT state decorated on the Dirac monopole line is trivial.

We can always start with the QED_4 as a candidate boundary state. Now since the magnetic 1-form symmetry is only $Z_n^{(1)}$, it means that there are dynamical Dirac monopoles with $n-$magnetic charges (Dirac monopole with $2\pi n$ flux quantum). As we mentioned before we first focus on the cases where the point excitations are bosons,

then we can condense the $n-$magnetic charge at the $3d$ boundary without breaking any symmetry. The condensate of the $2\pi n$ Dirac monopole will drive the boundary into a $3d$ z_n topological order.

An ordinary $3d$ z_n topological order is the deconfined phase of a dynamical $z_n^{(1)}$ gauge field. In an ordinary $3d$ z_n topological order, normally there are two types of excitations: a point particle which is the remnant of the 2π Dirac monopole; and also another line/loop excitation which is coupled to a $z_n^{(2)}$ 2-form gauge field. If the loop excitation is condensed (proliferated in $4D$ Euclidean space), the z_n topological order is trivialized, and the system becomes gapped and nondegenerate.

The dynamics of the loop excitation can be schematically described by the following Hamiltonian

$$H_{\text{loop}} = \sum_{\mathcal{C}} -t_{\mathcal{C}} \cos\left(\sum_{\vec{l}\in\mathcal{C}} \hat{c}_{\vec{l}} - \sum_{\vec{p}\in\mathcal{A}_{\mathcal{C}}} \hat{b}_{\vec{p}}\right) + \cdots \tag{5.81}$$

In this equation, $\mathcal{C}$ represents certain loop configuration; $\vec{l}$ is a link which is part of this loop, and $\mathcal{A}_{\mathcal{C}}$ is a membrane whose boundary is the loop $\mathcal{C}$ ($\partial\mathcal{A}_{\mathcal{C}} = \mathcal{C}$); $\vec{p}$ is a plaquette that belongs to $\mathcal{A}_{\mathcal{C}}$. $\Psi_{\vec{l}}^{\dagger} \sim \exp(\mathrm{i}\hat{c}_{\vec{l}})$ is the creation operator of the loop segment on link $\vec{l}$, and $\hat{b}_{\vec{p}}$ is a 2-form gauge field defined on plaquette $\vec{p}$. The direction of the link and the unit plaquette can be absorbed into the definition of $\hat{c}$ and $\hat{b}$ and render them a 1-form and 2-form fields.

For an ordinary z_n topological order, both $\hat{c}_{\vec{l}}$ and $\hat{b}_{\vec{p}}$ take eigenvalues $2\pi N/n$ with integer N. Hence the "condensation" of the loop excitation will not lead to degeneracy because of the existence of the $z_n^{(2)}$ 2-form gauge field $\hat{b}$. Or in other words, the condensation of the loop excitation will be fully "Higgsed" due to the coupling to the $z_n^{(2)}$ dynamical gauge field $\hat{b}$, and this Higgs phase is the confined phase of the $z_n^{(1)}$ gauge theory.

However, if the loop excitation carries a $\mathrm{U}(1)^{(1)}$ 1-form charge, the situation would be very different. Now $\hat{c}_{\bar{l}}$ can take continuous values between 0 and 2π. Condensing the loop would just drive the system back into a gapless photon phase. Physically because the loop excitation carries a $\mathrm{U}(1)^{(1)}$ 1-form charge, condensing the loop excitations would lead to spontaneous $\mathrm{U}(1)^{(1)}$ 1-form symmetry breaking, whose "Goldstone mode" is precisely the photon.

With the bulk response action Eq. 5.80, the loop excitation of $3d$ boundary carries charge quantum k/n of the $\mathrm{U}(1)^{(1)}$ 1-form symmetry. However, when $k = n$, the quantum number of the loop excitation can be screened by binding with unfractionalized integer 1-form symmetry charge, hence the loop excitations become completely neutralized. Then when $k = n$ the neutralized loop excitation can proliferate and drive the boundary to a fully gapped and nondegenerate state, just like the case of an ordinary $z_n^{(1)}$ gauge theory. This argument again leads to a $\mathbb{Z}_n$ classification.

Descendant $4d$ SPT state with $Z_q^{(1)} \times Z_n^{(1)}$ symmetry

We can further break the left $\mathrm{U}(1)^{(1)}$ 1-form symmetry down to $Z_q^{(1)}$ from the previous example. Now in the condensate of the $2\pi n$ Dirac monopole, the loop excitation will carry k/n unit of the $Z_q^{(1)}$ 1-form symmetry charge, and the loop excitation is coupled to a dual $z_n^{(2)}$ gauge field. Our interest is to ask when this $3d$ boundary can be fully gapped without degeneracy.

Let us start with the simple example with $k = 1$, $q = 3$, and $n = 2$. Following the discussion in the previous subsection, we consider the z_2 topological order after condensing the 4π Dirac monopole at the boundary QED_4 (The $2\pi n$ monopole has dynamics and can condense). There is a loop excitation of this z_2 topological order, which couples to a dual $z_2^{(2)}$ gauge field, and carries half charge of the $Z_3^{(1)}$ 1-form symmetry. Now consider

a loop excitation whose creation operator is $P_{\mathcal{C}}^{\dagger}$:

$$P_{\mathcal{C}}^{\dagger} \sim \prod_{\vec{l}\in\mathcal{C}} \Psi_{\vec{l}}^{\dagger} \sim \exp(\mathrm{i}\sum_{\vec{l}\in\mathcal{C}} \hat{c}_{\vec{l}}). \tag{5.82}$$

$P_{\mathcal{C}}^{\dagger}$ carries half charge under $Z_3^{(1)}$, and it also couples to a dual $z_2^{(2)}$ gauge field. Under both the $Z_3^{(1)}$ symmetry and the $z_2^{(2)}$ gauge symmetry, $\mathcal{C}$ transforms as

$$Z_3^{(1)} : P_{\mathcal{C}}^{\dagger} \to e^{\mathrm{i}\frac{1}{2}\frac{2\pi N}{3}} P_{\mathcal{C}}^{\dagger}, \qquad z_2^{(2)}\text{-gauge} : P_{\mathcal{C}}^{\dagger} \to -P_{\mathcal{C}}^{\dagger}, \tag{5.83}$$

with integer N. One can check that by combining the loop operator $P_{\mathcal{C}}$ with unfractionalized integer 1-form charges, the $Z_3^{(1)}$ transformation can be completely cancelled by a $z_2^{(2)}$ gauge transformation. In other words the fractional $Z_3^{(1)}$ charge carried by the $P_{\mathcal{C}}^{\dagger}$ can be "neutralized" by binding a gauge invariant $Z_3^{(1)}$ charge, and the $3d$ boundary system can be driven into a trivial gapped phase by condensing this $Z_3^{(1)}$ neutral loop excitation.

The discussions above can be generalized to other q and n. With $k = 1$ in Eq. 5.80, after condensing the $2\pi n$ monopole, the $3d$ boundary system is driven into a z_n topological order whose loop excitation carries $1/n$ fractional $Z_q^{(1)}$ 1-form symmetry charge. Our interest is to check, when this fractional 1-form symmetry charge can be "neutralized" by integer 1-form symmetry charge, namely by binding integer 1-form symmetry charge the $Z_q^{(1)}$ transformation can be completely absorbed/cancelled by the dual $z_n^{(2)}$ gauge transformation.

Under a $Z_q^{(1)}$ transformation, the loop creation operator $P_{\mathcal{C}}$ acquires phase angle $2\pi/(nq)$; after binding with Q units of integer $Z_q^{(1)}$ charge, the loop would acquire phase angle $2\pi/(nq) + 2\pi Q/q$. Now we seek for a pair of integer (Q, N) which suffices the

following equation:

$$\frac{1}{nq} + \frac{Q}{q} = \frac{N}{n}. \tag{5.84}$$

This would mean that the $Z_q^{(1)}$ transformation can be totally absorbed/cancelled by a gauge transformation. For $(q, n) = (3, 2)$ one can choose $(Q, N) = (1, 1)$. In general the question is equivalent to finding a pair of integers (Q, N) that satisfies $Nq - Qn = 1$, which is only possible when q and n are coprime. When q and n are not coprime, the loop quantum number can be fully neutralized when $k = \gcd(q, n)$. This implies a $\mathbb{Z}_{\gcd(q,n)}$ classification.

— *More States*

All the SPT states discussed so far have bosonic electric charge and Dirac monopoles at its boundary QED_4, namely the boundary of all the SPT states are $\mathrm{QED}_4\{e_{0b}, m_{0b}\}$ states. Let us revisit the starting point of our bulk construction of Eq. 5.80. The two $u(1)$ gauge fields $\vec{a}^1$ and $\vec{a}^2$ can have either bosonic or fermionic electric charges with infinite mass in the bulk, which become the static electric charges and Dirac monopoles of the boundary QED_4. Hence logically there will also be $\mathrm{QED}_4\{e_{0b}, m_{0f}\}$, $\mathrm{QED}_4\{e_{0f}, m_{0b}\}$, $\mathrm{QED}_4\{e_{0f}, m_{0f}\}$ states that we need to discuss. As we pointed out before, the statistics of static particles still affect the Wilson/'t Hooft loops. We defer discussions of these states to section 5.3.5.

5.3.4 $4d$ SPT State with $\mathrm{U}(1)^{(1)} \times G$ Symmetry

Here we consider $4d$ SPT states with both a $\mathrm{U}(1)^{(1)}$ symmetry and an ordinary 0-form symmetry G. The decorated defect construction in the previous section can be generalized here: we start with one $(4+1)d$ $u(1)$ gauge field $\vec{a}$ with a 1-form electric symmetry, and decorate its Dirac monopole line with the $1d$ SPT state with symmetry

G, then condense the monopole line in the bulk. A prototype $4d$ SPT state with such construction was discussed previously, whose G symmetry is SO(3), and its topological response theory is [547]

$$\mathcal{S}_{\text{4d}-\text{topo}} = \mathrm{i}\pi \int_{(4+1)d} w_2[A^{\text{SO}(3)}] \cup \frac{dB}{2\pi}, \tag{5.85}$$

where $A^{\text{SO}(3)}$ is the external 1-form SO(3) gauge field.

Generally speaking the discussion of $4d$ SPT state with 1-form symmetry has implications on properties of $3d$ systems with loop-like excitations. If in certain limit a $3d$ system with spatial symmetries can be mapped to the boundary of a $4d$ state with onsite symmetries, then whether or not the $4d$ bulk is a nontrivial SPT state has strong implication on whether the $3d$ system can be trivially gapped or not, i.e. the nature of the $4d$ bulk helps us prove a Lieb-Schultz-Mattis (LSM) theorem [20, 22] of the $3d$ system. In recent years much progress has been made in understanding the LSM theorems for quantum spin systems using the anomaly analysis of its corresponding higher dimensional bulk states [548, 91, 92, 93, 95, 90, 94]. In condensed matter theories the quantum dimer model is an example of systems with loop like excitations. Dimers are defined on the links of the lattice, and each site of the lattice is connected to a fixed number of dimers. Previous literature has shown that, the $3d$ quantum dimer model can be mapped to a QED_4 without dynamical electric charge [549], but its monopole can carry nontrivial quantum number under spatial group due to the Berry phase, and in particular, for the quantum dimer model on the cubic lattice, the monopole of the QED_4 carries a "spin-1/2" representation (projective representation) of an emergent SO(3) symmetry [550, 551]. Hence this quantum dimer model is analogous to the boundary of a $4d$ SPT state with symmetry $\text{U}(1)^{(1)} \times \text{SO}(3)$, and there should be a LSM theorem for this quantum dimer model.

This LSM theorem for the quantum dimer model is consistent with the LSM theorem for spin-1/2 systems on the cubic lattice. In Ref. 91, various quantum spin systems on the cubic lattice were considered. For example, a SU(N) spin system on the cubic lattice with fundamental and antifundamental representations on the two sublattices of the cubic lattice has a LSM theorem for even integer N, but there is no LSM theorem for odd integer N, i.e. the quantum spin system described above with odd integer N can have a featureless gapped ground state on the cubic lattice. However, a quantum dimer model on the cubic lattice could be the low energy effective description of all these systems, since two nearest neighbor AB sites can always form a dimer (spin singlet), regardless of even or odd integer N.

One simple extension of Eq. 5.85 is that, when we break SO(3) down to its subgroup $\mathrm{U}(1) \rtimes Z_2$, Eq. 5.85 reduces to

$$S_{\mathrm{4d-topo}} = \mathrm{i}\frac{\Theta}{(2\pi)^2}\int_{(4+1)d} dB \wedge dA, \tag{5.86}$$

where A is the background U(1) gauge field. The integral in Eq. 5.86 is quantized, hence Θ is periodically defined: $\Theta = \Theta + 2\pi$. Under the Z_2 subgroup of SO(3), A changes sign, hence a symmetric response theory demands $\Theta = k\pi$ with integer k. Eq. 5.86 with $k = 1$ corresponds to the nontrivial $4d$ SPT phase.

Eq. 5.86 also describes the corresponding $4d$ bulk state if instead we consider a quantum dimer model defined on a $3d$ tetragonal lattice, here the U(1) symmetry is further reduced to a Z_4 symmetry, and the Z_4 corresponds to the rotation of the square lattice in each layer. In this case in the topological response theory Eq. 5.86, A is a background Z_4 gauge field. Eq. 5.86 still describes a nontrivial $4d$ SPT state with 1-form symmetry.

The situation will be very different if we consider a quantum dimer model on a $3d$ bipartite lattice with an effective $Z_3 \rtimes Z_2 = S^3$ symmetry. The Z_3 should correspond to

a three fold rotation C_3 in the XY plane, and Z_2 is a π-rotation about the x-axis. Such quantum dimer models can potentially be mapped to the boundary of a $4d$ system with $\mathrm{U}(1)^{(1)} \times S^3$ symmetry. But there is no $1d$ SPT state with the S^3 symmetry, hence the $4d$ bulk with the $\mathrm{U}(1)^{(1)} \times S^3$ symmetry is also trivial as a descendant state of the SPT state described by Eq. 5.86. Hence there should be no LSM theorem for these quantum dimer models, i.e. these quantum dimer models can in general have a gapped ground state without degeneracy, unless this model has higher symmetries than the lattice itself.

5.3.5 Other $4d$ SPT States

With just a $\mathrm{U}(1)^{(1)}$ symmetry, there is already a nontrivial $4d$ SPT phase, whose boundary is a QED_4 with a 1-form electric symmetry, and the Dirac monopole is a fermion (labelled as m_f). The unit electric charge (labelled as e_{0b}) is infinitely heavy at the boundary QED_4 due to the $\mathrm{U}(1)^{(1)}$ symmetry. We label this boundary QED_4 as state $\mathrm{QED}_4\{e_{0b}, m_f\}$. The bulk is a nontrivial SPT state, namely its boundary QED_4 cannot be trivially gapped. One can condense a Cooper pair of the fermionic Dirac monopole m_f, and drive the QED_4 to a "monopole superconductor", which is also a z_2 topological order. The loop excitation of the z_2 topological order will carry a fractional half charge of the $\mathrm{U}(1)^{(1)}$ 1-form symmetry, and hence cannot lead to a fully gapped and nondegenerate state after condensation for the reasons explained previously in this manuscript. Although the electric charges are infinitely heavy due to the 1-form symmetry, its statistics still matters to physical observables such as the Wilson loops of the QED_4. And in this QED_4 the infinitely heavy electric charge is a boson.

This state remains a nontrivial SPT after breaking the $\mathrm{U}(1)^{(1)}$ down to $Z_n^{(1)}$ with even integer n, the cases with $n = 2, 4$ were discussed in Ref. 537, 538. But this state will be trivialized if n is an odd integer. For odd integer n, in the monopole superconductor

constructed above, the loop excitation carries half charge of the $Z_n^{(1)}$ 1-form symmetry, and it can be "neutralized" by binding unfractionalized 1-form symmetry charge, i.e. the $Z_n^{(1)}$ transformation on the loop excitation can be completely cancelled by the $z_2^{(2)}$ gauge transformation on the loop excitation, then the condensation of the neutralized loop can lead to a trivially gapped phase.

There is even a nontrivial bosonic SPT state in $4d$ space without any symmetry; its boundary is a QED_4 whose both electric charge and Dirac monopole (including their bound state dyon) are fermions [552, 553]. We label this QED as $\text{QED}_4\{e'_f, m'_f\}$ state. We view the $\text{QED}_4\{e_{0b}, m_f\}$ and $\text{QED}_4\{e'_f, m'_f\}$ as two root states, and by "gluing" these two QED_4 states together, another new state can be constructed. One can condense the bound state of the Dirac monopoles (labelled as (m_f, m'_f)) of both QED_4 systems, then the gauge fields from both QED_4 will be identified due to the Higgs mechanism, and e_{0b} and e_f are both confined since they both have nontrivial statistics with the condensed bound state of monopoles. Although e_{0b} is infinitely heavy, its confinement can still be defined by the behavior of Wilson loop of its gauge field. In the condensed phase of bound state (m_f, m'_f), the Wilson loop of each individual gauge field obeys the area law. But the bound state $(e_{0b}, -e'_f)$, which has trivial mutual statistics with (m_f, m'_f), remains deconfined, though it is still infinitely heavy. This new QED state has infinitely heavy fermionic electric charge, and dynamical fermionic Dirac monopole. This new state is labelled as $\text{QED}_4\{e_{0f}, m_f\}$. One can also exchange e and m, and label the state as $\text{QED}_4\{e_f, m_{0f}\}$, i.e. a state with dynamical fermionic gauge charge, but infinitely heavy fermionic Dirac monopole.

Summary of 4d SPT states with 1-form symmetries:

Let us reinvestigate the states discussed in the end of section 5.3.3. As we briefly discussed there, besides the states $\text{QED}_4\{e_{0b}, m_{0b}\}$, logically there should also be $\text{QED}_4\{e_{0b}, m_{0f}\}$,

$\mathrm{QED}_4\{e_{0f}, m_{0b}\}$, $\mathrm{QED}_4\{e_{0f}, m_{0f}\}$, which can all be boundary states of $(4+1)d$ SPT bulk. It turns out that these states can be constructed by gluing states in section 5.3.3 and 5.3.5. For example, starting with the state $\mathrm{QED}_4\{e_{0b}, m_{0b}\}$ discussed in section 5.3.3 (we label its gauge field as $\vec{a}$), one can combine it with the state $\mathrm{QED}_4\{e'_{0b}, m'_f\}$ (with gauge field $\vec{a}'$) discussed in section 5.3.5, and consider the charge bound state $(e_{0b}, -e'_{0b})$. This bound state carries zero total gauge charge of $\vec{a}$ and $\vec{a}'$. We assume that there is only one $\mathrm{U}(1)^{(1)}$ 1-form symmetry, hence the charge bound state $(e_{0b}, -e'_{0b})$, which carries zero total gauge charge, is no longer necessarily infinitely heavy and can acquire dynamics and condense. Its condensate would render $\vec{a} = \vec{a}'$ through the Higgs mechanism, and in the condensate the monopole bound state (m_{0b}, m'_f) remains deconfined, as it has trivial mutual statistics with $(e_{0b}, -e'_{0b})$. The final state is identical to state $\mathrm{QED}_4\{e_{0b}, m_{0f}\}$ discussed in section 5.3.3. Following the same argument, through gluing $\mathrm{QED}_4\{e_{0b}, m_{0f}\}$ and state $\mathrm{QED}_4\{e'_f, m'_{0f}\}$ discussed in section 5.3.5 (by condensing the bound state $(m_{0f}, -m'_{0f})$), one can obtain another state $\mathrm{QED}_4\{e_{0f}, m_{0f}\}$ discussed in section 5.3.3.

The construction of all these states discussed so far can be summarized mathematically in a single unified topological response theory in the $(4+1)d$ bulk:

$$S_{\mathrm{4d-topo}} = \int_{(4+1)d} \frac{\mathrm{i}k_0}{2\pi} B^1 \wedge dB^2 + \frac{\mathrm{i}k_1}{2} dB^1 \cup w_2 + \frac{\mathrm{i}k_2}{2} dB^2 \cup w_2 + \mathrm{i}\pi k_3 w_2 \cup w_3. \quad (5.87)$$

w_2 and w_3 are the second and third Stiefel-Whitney class of the space-time manifold. k_0 takes arbitrary integer values, while k_1, k_2 and k_3 only take value 0 and 1, since the Stiefel-Whitney class is defined mod 2. This topological response theory is equivalent to the discussion based on the cobordism theory in Ref. 537, 538.

The classification of $4d$ SPT states discussed so far is summarized as follows:

$$\begin{aligned}
\mathrm{U}(1)^{(1)}: &\quad \mathbb{Z}_2 \otimes \mathbb{Z}_2; \\
Z_n^{(1)}: &\quad \mathbb{Z}_2 \otimes \mathbb{Z}_{\gcd(2,n)}; \\
\mathrm{U}(1)^{(1)} \times \mathrm{U}(1)^{(1)}: &\quad \mathbb{Z} \otimes \mathbb{Z}_2^3; \\
\mathrm{U}(1)^{(1)} \times Z_n^{(1)}: &\quad \mathbb{Z}_n \otimes \mathbb{Z}_2^2 \otimes \mathbb{Z}_{\gcd(2,n)}; \\
Z_q^{(1)} \times Z_n^{(1)}: &\quad \mathbb{Z}_{\gcd(q,n)} \otimes \mathbb{Z}_{\gcd(2,q)} \otimes \mathbb{Z}_{\gcd(2,n)} \otimes \mathbb{Z}_2.
\end{aligned} \tag{5.88}$$

5.3.6 $3d$ SPT State with $G_1^{(1)} \times G_2$ Symmetry

Parent $3d$ SPT state with $\mathrm{U}(1)^{(1)} \times \mathrm{U}(1)$ symmetry

The parent $3d$ SPT state we will consider, is a state with $\mathrm{U}(1)^{(1)} \times \mathrm{U}(1)$ symmetry. We can couple its symmetry currents to a background 2-form gauge field B, and a 1-form gauge field A. The response theory for this SPT state is

$$S_{\mathrm{3d-topo}} = \int \frac{\mathrm{i}k}{2\pi} B \wedge dA = \int \frac{\mathrm{i}k}{2\pi} A \wedge dB. \tag{5.89}$$

To construct such state, again one can rely on the decorated defect picture. We can start with a photon phase with an electric $\mathrm{U}(1)^{(1)}$ 1-form symmetry, namely there is no dynamical electric charge, or equivalently the electric charge is infinitely heavy, but there are dynamical Dirac monopoles. Then we decorate the Dirac monopole with a zero dimensional bosonic SPT state with U(1) symmetry, which is a bosonic charge with U(1) symmetry. This zero dimensional bosonic SPT state has $\mathbb{Z}$ classification, which correspond to states with integer charges of a boson with U(1) symmetry. These states can also be equivalently constructed by decorating the vortex line of the U(1) order parameter with a $1d$ SPT state with $\mathrm{U}(1)^{(1)}$ 1-form symmetry, i.e. the building bricks

discussed in section 5.3.2.

After condensing the decorated Dirac monopole, the $3d$ bulk of the system is driven into a fully gapped state without degeneracy. The $2d$ boundary of the system would most naturally be a QED_3 whose dynamical $u(1)$ gauge field $\vec{a}$ has no dynamical gauge charge, but its magnetic flux carries conserved U(1) quantum number that couples to A. The QED_3 is a dual of the superfluid phase with spontaneous breaking of the U(1) symmetry. And the assumption that there is no dynamical electric charge of gauge field $\vec{a}$ is equivalent to the statement that there is no dynamical vortex of the dual superfluid, hence the superfluid cannot be disordered by condensing the vortices.

Descendant $3d$ SPT state with $\text{U}(1)^{(1)} \times Z_n$ symmetry

We can break the U(1) 0-form symmetry coupled to A in Eq. 5.89 down to a Z_n symmetry, now the entire symmetry becomes $\text{U}(1)^{(1)} \times Z_n$. The topological response theory Eq. 5.89 still applies, but now A becomes a $\mathcal{Z}_n^{(1)}$ background gauge field. The decorated defect construction in the previous case would lead to a $\mathbb{Z}_n$ classification, because the zero dimensional SPT state with Z_n symmetry decorated at the Dirac monopole has a $\mathbb{Z}_n$ classification.

This classification can be understood at the boundary as well. The $(2+1)d$ boundary is a QED_3 whose flux carries k units of the Z_n quantum number, where k is given in Eq. 5.89. With $k = n$, the flux of the QED_3 basically carries trivial quantum number, and the QED_3 can be driven into a trivial confined phase. This boundary state is similar to the quantum dimer model on a $2d$ bipartite lattice, such as the square lattice. The quantum dimer model can be mapped to a compact QED_3 with no electric charge (the quantum dimer constraint, i.e. every site is connected to precisely one dimer, is strictly enforced), but the flux of the compact QED_3 carries nontrivial lattice quantum number. The description of the quantum dimer model in terms of QED_3 is analogous to the

boundary of the $3d$ SPT state with $\mathrm{U}(1)^{(1)} \times Z_4$ symmetry at $k = 1$. It is well-known that the confined phase of the quantum dimer model on the square lattice cannot be a trivial gapped phase, instead it must have ground degeneracy due to spontaneous breaking of lattice symmetry. But in the quantum dimer model because the Z_4 symmetry is a non-onsite lattice symmetry, the quantum dimer model exists as a well defined system in $2d$.

This effect is inherited from the LSM theorem for spin-1/2 systems on the square lattice. There is no LSM theorem for a spin-2 system on the square lattice, and a spin-2 system can be viewed as four copies of spin-1/2 systems glued together, or a system with four spin-1/2s in each unit cell. All these observations are consistent with the $\mathbb{Z}_4$ classification of the $3d$ SPT state with $\mathrm{U}(1)^{(1)} \times Z_4$ symmetry discussed in this section.

Descendant $3d$ SPT state with $Z_q^{(1)} \times \mathrm{U}(1)$ symmetry

Next we consider the $3d$ SPT states as descendant states of Eq. 5.89 with $Z_q^{(1)} \times \mathrm{U}(1)$ symmetry. Again we will first consider the cases where all the point particles in the bulk are bosons. When we break the $\mathrm{U}(1)^{(1)}$ symmetry down to $Z_q^{(1)}$, the $2d$ boundary is a QED_3 whose flux carries U(1) quantum number, and there are dynamical $q-$fold electric charges. The boundary can only be driven to a z_q topological order by condensing the $q-$fold electric charge. One of the point like anyons of this topological order is the remnant of the $2\pi/q$ flux of the QED_3, which carries k/q charges of the U(1) symmetry quantum number. When $k = q$ this anyon carries unfractionalized quantum number, hence can be neutralized by binding with gauge invariant integer charge of the U(1) symmetry. This neutralized anyon is a self-boson, and after condensation it drives the boundary into a trivial gapped state. Hence this $3d$ SPT state should have a $\mathbb{Z}_q$ classification.

To facilitate further discussions let us also consider a different $3d$ bulk state with

U(1) global symmetry only. This is a QED_4 whose electric charge is fermion, and Dirac monopole is a boson (using the notations introduced before, this bulk state is $\mathrm{QED}_4\{e_f, m_b\}$). Again one can bind the Dirac monopole with another boson that carries U(1) quantum number, and condense the bound state in the $3d$ bulk. Then the bulk is gapped and nondegenerate, while the $2d$ boundary is a QED_3 whose electric charge is a fermion, while the gauge flux carries U(1) quantum number. However, this $3d$ bulk is not a SPT state, since one can put the electric charge at the boundary in a $2d$ Chern insulator with Hall conductivity 1, then the $2d$ boundary is gapped without breaking any symmetry. This is consistent with the classification of ordinary SPT states without higher form symmetries. With only U(1) symmetry, there is no nontrivial SPT state in $3d$. One needs another time-reversal symmetry to construct a $3d$ bosonic SPT state, since the boundary Chern insulator of the fermionic gauge charge as we constructed above necessarily breaks the time-reversal.

One can again glue the $2d$ boundary states in the previous two paragraphs together. Let us recall that the boundary of a nontrivial $3d$ SPT state with $Z_q^{(1)} \times \mathrm{U}(1)$ symmetry is a QED_3 whose flux carries U(1) quantum number, and its bosonic electric charges are infinitely heavy; the boundary of the trivial state discussed in the last paragraph is a QED_3 whose flux also carries U(1) quantum number, and its electric charge is a fermion with nonzero dynamics. Once we couple the two $2d$ systems together, the tunnelling between the gauge fluxes between the two QED_3 will be turned on, which identifies the two gauge fields. Now the $2d$ boundary state is a QED_3 whose gauge flux still carries U(1) quantum number, but its static electric charge is a fermion. This state is not a new SPT state since it can be constructed by gluing the $2d$ boundaries of the two systems discussed above.

Descendant $3d$ SPT state with $Z_q^{(1)} \times Z_n$ symmetry

Finally we can break the $\mathrm{U}(1)^{(1)}$ 1-form symmetry in Eq. 5.89 to $Z_q^{(1)}$. Again we can start with the QED_3 state at the $(2+1)d$ boundary. In this case there are dynamical q-fold electric charge of the $u(1)$ gauge field, and the magnetic flux of the $u(1)$ gauge field still carries Z_n quantum number. One can condense the charge$-q$ bound state, and drive the $2d$ boundary into a $2d$ z_q topological order. In an ordinary $2d$ z_q topological order, there are two sets of anyons. The e anyon is a remnant of the unit charge excitation of the QED_3 before the condensation of the q-fold electric charge, and the m anyon is a $2\pi/q$ flux quantum of the $u(1)$ gauge flux. Both e and m anyons are self-bosons, but have a mutual $2\pi/q$ statistical angle. In our current case, due to the $Z_q^{(1)}$ 1-form symmetry, the e anyons are not dynamical, and a m anyon carries a fractional quantum number $1/q$ of the Z_n symmetry (assuming $k = 1$ in Eq. 5.89). Both e and m anyons are coupled to z_q gauge fields. Following the arguments in section 5.3.3, we can demonstrate that when q and n are coprime, the fractional quantum number of the m anyon can always be "neutralized" by binding with integer charges of the Z_n symmetry, in the sense that the Z_n transformation on the decorated m anyon can always be cancelled by a z_q gauge transformation. When q and n are not coprime, the quantum number of the m anyon can be neutralized when $k = \gcd(q, n)$. The neutralized m anyon can condense and drive the $2d$ boundary to a trivial gapped state without degeneracy. Hence as a descendant state of Eq. 5.89, the classification of the $3d$ SPT state with $Z_q^{(1)} \times Z_n$ symmetry is $\mathbb{Z}_{\gcd(q,n)}$.

Summary of 3d SPT states with 1-form symmetries:

Here we summarize the classification of $3d$ SPT states that are descendants of Eq. 5.89. If there are special SPT states that cannot be described by Eq. 5.89, such as some of the

states discussed in Ref. 539, 540, they are not included in this list.

$$\begin{aligned} \mathrm{U}(1)^{(1)} \times \mathrm{U}(1): &\quad \mathbb{Z}; \\ Z_q^{(1)} \times \mathrm{U}(1): &\quad \mathbb{Z}_q; \\ \mathrm{U}(1)^{(1)} \times Z_n: &\quad \mathbb{Z}_n; \\ Z_q^{(1)} \times Z_n: &\quad \mathbb{Z}_{\gcd(q,n)}. \end{aligned} \tag{5.90}$$

5.3.7 $2d$ SPT State with $G_1^{(1)} \times Z_2^T$ Symmetry

Several different $(2+1)d$ SPT states that involve 1-form symmetries can be described by the following topological response term:

$$S_{\mathrm{2d-topo}} = \int_{(2+1)d} \frac{\mathrm{i}\Theta}{2\pi} dB \tag{5.91}$$

In principle Θ can take arbitrary value, because dB is gauge invariant. But some extra symmetry can pin Θ to a specific value, like the Θ term of the ordinary topological insulator [554] and bosonic SPT state [161].

As an example of such states, we assume that the 2-form background gauge field B is unchanged under time-reversal transformation, this means that the 1-form symmetry charge will change sign under time-reversal. This implies that the total symmetry of the system is a direct product between the 1-form symmetry and time-reversal. Θ is clearly defined periodically, namely $\Theta + 2\pi = \Theta$, hence the time-reversal invariant states correspond to $\Theta = \pi k$ with arbitrary integer k.

For even integer k, the $(2+1)d$ topological response theory Eq. 5.91 reduces to a boundary topological term that is identical to the topological response theory with $1d$

SPT state with a 1-form symmetry (section 5.3.2). This means that, for even integer k, the boundary corresponds to a well-defined $1d$ state, hence an even integer k would correspond to a trivial state in $(2+1)d$. On the other hand, for odd integer k, the boundary is a "half" $1d$ SPT state with 1-form symmetry $G^{(1)}$. Then the $(2+1)d$ bulk could be a SPT state.

As we mentioned before, due to the strict constraint $\nabla_x \hat{e}(x) = 0$ for 1-form charge in one dimension, a $1d$ system with 1-form symmetry is analogous to a $0d$ system with ordinary 0-form symmetry. Then whether there is a $(2+1)d$ SPT state with $G^{(1)} \times Z_2^T$ symmetry can also be determined by the existence of projective representation of $G \times Z_2^T$. And there is a 2-dimensional projective representation of $\mathrm{U}(1) \times Z_2^T$, but not for $\mathrm{U}(1) \rtimes Z_2^T$. Indeed, if the symmetry of the system is $G^{(1)} \rtimes Z_2^T$, namely B is odd under time-reversal, the Θ coefficient is unchanged under time-reversal, hence time-reversal will not pin Θ to any specific value.

To summarize our result in two spatial dimensions, there is a nontrivial $2d$ SPT state with $\mathrm{U}(1)^{(1)} \times Z_2^T$ symmetry, and this state remains nontrivial when $\mathrm{U}(1)^{(1)}$ is broken down to $Z_q^{(1)}$ with even integer q.

The decorated defect construction also applies in this scenario, which is analogous to what was discussed in Ref. 555 for ordinary SPT states. We can construct the SPT state with $k = 1$ in Eq. 5.91, by first creating a domain wall of time-reversal symmetry, then embed each domain wall with a $1d$ SPT state described by Eq. 5.78, and finally proliferate the domain walls. Besides construction from $1d$ SPT state, we can also obtain this $2d$ SPT state by reduction from higher dimensions. For example, starting with the $3d$ SPT state with $\mathrm{U}(1)^{(1)} \times \mathrm{U}(1)$ symmetry described by the response theory Eq. 5.89, one can compactify one of the three spatial dimensions (the $3d$ space R^3 becomes $\mathrm{R}^2 \otimes S^1$), and insert a $\pi-$flux of the 1-form gauge field A through S^1. Then the response theory Eq. 5.89 reduces to Eq. 5.91 with $k = 1$. This is the same procedure of dimensional

reduction introduced in Ref. 554.

5.3.8 Discussion

In this work we discussed the classification, construction, and boundary properties of SPT states involving higher symmetries, from one to four spatial dimensions. Our discussion is mostly based on physical arguments. As an application of our discussion, we make connection between the SPT states with 1-form symmetry to quantum dimer model at one lower dimension. Quantum dimer model with spatial symmetries can be mapped to the boundary of a bulk state with onsite symmetries. Some of the universal features of the quantum dimer model is dictated by the nature of the corresponding bulk state.

In this work we only discussed quantum dimer models on bipartite lattices, which can be mapped to a QED with $\mathrm{U}(1)^{(1)}$ 1-form symmetry. It is well known that some other dimer models can be naturally mapped to a z_2 gauge field, such as quantum dimer model on the triangular lattice [556]. Then these models would be examples of systems with $Z_2^{(1)}$ 1-form symmetry, and they can also be potentially mapped to the boundary of one higher dimensions. Insights for these systems gained from higher dimensions will be studied in later works.

Chapter 6

Summary and Discussion

The main body of this dissertation presents our series of works on quantum matter beyond the two cornerstones [1]. There are diverse research projects, including understanding experimentally motivated questions, constructing exotic quantum matter, and exploring novel theoretical concepts. Finally, I would like to finish this dissertation by commenting on related topics that may deserve better understanding in future studies. Below is just an incomplete list that I personally found interesting.

In Sec. 2.3, we have found novel 2+1D fixed points involving non-local interactions. The non-locality associated with boundaries and defects is due to the coupling to a gapless bulk in 3+1D. Similar nonlocal terms could arise from the coupling between bosonic order parameters and fermi-surface hot spots in 2+1D systems. It opens the possibilities of constructing exotic quantum phase transitions in metals.

In all the examples we have considered in Chap. 2, the critical bulk only involves bosonic degrees of freedom. So far, we do not have a good understanding of boundary theories of fermi-surface states. For example, it would be nice to work out the boundary theory of the Halperin-Lee-Read theory [88] for the half-filled Landau level. It should

[1] Landau's Fermi liquid theory and symmetry-breaking theory of conventional phase transitions

lead to experimentally relevant predictions.

The analysis of emergent symmetries and anomalies could shed new light on old problems. For example, the Luttinger theorem has recently been rationalized in Ref. [58] using the 't Hooft anomaly of an emergent loop-group symmetry. (The emergent symmetry can be intuitively understood as the charge conservation associated with each patch of the fermi surface.) Since controlled calculations are hard to achieve in strongly correlated metals, it would be nice to have more theoretical constraints on their kinematic properties from emergent symmetries and anomalies.

The non-linear bosonization of fermi liquids has been recently developed in Ref. [59], which states that the emergent anomaly in Ref. [58] is from the linear approximation of a non-linearly realized symmetry preserved under fermi-surface evolution. It would be interesting to see whether this new formulation can help develop a controlled framework for non-fermi liquids under certain assumptions.

In Sec. 5.1, we have seen the ODOs for subsystem symmetries can have exotic scaling behaviors (involving logarithmic factor) other than perimeter law and power law. A similar feature shows up in fermi-surface states, where the ODO (which is related to the bipartite charge fluctuations in literature) scales as $L\log(L)$ with the linear system size L in 2+1D. Both fermi-surface states and states with subsystem symmetries have a large number of conserved quantities, and they both involve UV-IR mixing in certain scenarios. It is tantalizing to explore a deep relationship between the two.

As for material realizations of exotic quantum phases, experimentalists are actively building "quantum LEGO" using Moiré heterostructures, and highly entangled synthetic matter using Rydberg atoms. There will be a lot more systems to study for theorists.

I would like to continue these lines of research in the future.

Appendix A

Appendix to Chapter 1 (Introduction)

A.1 Conformal Perturbation Theory

Conformal perturbation theory is a standard method in the literature. This section serves as a short introduction.

A.1.1 Conformal Fixed Points

Let's briefly summarize some properties of a conformal RG fixed point. Due to emergent scale invariance, the two-point correlation function of any physical observable $\mathcal{O}(x)$ should obey the power law

$$\langle \mathcal{O}(x)\mathcal{O}(y)\rangle = \frac{\text{const.}}{|x-y|^{2\Delta_{\mathcal{O}}}}, \tag{A.1}$$

where $\Delta_{\mathcal{O}}$ is the scaling dimension of $\mathcal{O}$. In this section, all the correlation functions should be understood as time-ordered [1].

The scale invariance at a RG fixed point is often enlarged to conformal invariance (see e.g. [100]), and quasi-primary fields $\mathcal{O}(x)$ transform irreducibly as

$$\mathcal{O}_j(x) \to \left|\det\frac{\partial x'}{\partial x}\right|^{\Delta_j/D} \mathcal{O}_j(x'), \tag{A.2}$$

where $D = d + 1$ is the total spacetime dimensions. The conformal symmetry further restricts the form of two-point functions

$$\langle \mathcal{O}_1(x_1)\mathcal{O}_2(x_2)\rangle = \begin{cases} \frac{C_{12}}{|x_1-x_2|^{\Delta_1+\Delta_2}} & \Delta_1 = \Delta_2 \\ 0 & \Delta_1 \neq \Delta_2 \end{cases}, \tag{A.3}$$

where the coefficient C_{12} can be set to 1 by redefining the operators $\mathcal{O}$'s. It resembles an orthogonal relation for quasi-primary fields with different scaling dimensions. The three-point functions are restricted to be

$$\langle \mathcal{O}_1(x_1)\mathcal{O}_2(x_2)\mathcal{O}_3(x_3)\rangle = \frac{C_{123}}{|x_{12}|^{\Delta_{12}}\,|x_{23}|^{\Delta_{23}}\,|x_{31}|^{\Delta_{31}}}, \tag{A.4}$$

where $x_{ij} = x_i - x_j$ and $\Delta_{ij} = \Delta_i + \Delta_j - \Delta_k$ with $i, j, k = 1, 2, 3$. The coefficient C_{123} is a universal number that characterizes the fixed point.

Operator product expansion (OPE) is a statement about the product of two nearby local operators $\mathcal{O}_i, \mathcal{O}_j$ is equivalent to a suitable linear combination of the operators $\{\mathcal{O}_k\}$

$$\lim_{x_i\to x_j} \mathcal{O}_i(x_i)\mathcal{O}_j(x_j) = \lim_{x_i\to x_j} \sum_k \frac{\widetilde{C}_{ijk}}{|x_i - x_j|^{\Delta_i+\Delta_j-\Delta_k}} \mathcal{O}_k\left(x_k\right), \tag{A.5}$$

[1] In CFT, the "time" is defined with respect to certain spacetime foliation.

where $x_k = \lambda x_i + (1-\lambda)\, x_j$ with $0 \leq \lambda \leq 1$ can be any point between x_i and x_j. Any OPE equation $\texttt{left} = \texttt{right}$ should be understood as the equivalence of operators inside correlation functions $\langle \texttt{left}\,(\ldots)\rangle = \langle \texttt{right}\,(\ldots)\rangle$, where $\ldots$ can be any other operators that are far away from x_i and x_j. This is basically saying that they produce the same UV singularity under $x_i \to x_j$, and hence the OPE method is useful in extracting logarithmic UV-divergence in practical RG calculations.

One can show that the OPE coefficients $\widetilde{C}_{ijk}$ are the same as the coefficients C_{ijk} of the three-point functions. Let's consider $\langle \mathcal{O}_i(x_i)\mathcal{O}_j(x_j)\mathcal{O}_l(x_l)\rangle$ and use the OPE of $\mathcal{O}_i\mathcal{O}_j$

$$\begin{aligned}
&\lim_{x_i\to x_j} \langle \mathcal{O}_i(x_i)\mathcal{O}_j(x_j)\mathcal{O}_l(x_l)\rangle = \lim_{x_i\to x_j} \sum_k \frac{\widetilde{C}_{ijk}}{|x-y|^{\Delta_i+\Delta_j-\Delta_k}} \langle \mathcal{O}_k(x_k)\mathcal{O}_l(x_l)\rangle \\
&= \lim_{x_i\to x_j} \frac{\widetilde{C}_{ijl}}{|x_{ij}|^{\Delta_i+\Delta_j-\Delta_l}} \frac{1}{|x_{kl}|^{2\Delta_l}} = \lim_{x_i\to x_j} \frac{\widetilde{C}_{ijl}}{|x_{ij}|^{\Delta_i+\Delta_j-\Delta_l}} \frac{1}{|x_{il}|^{\Delta_l+\Delta_i-\Delta_j}} \frac{1}{|x_{jl}|^{\Delta_l+\Delta_j-\Delta_i}},
\end{aligned} \tag{A.6}$$

where the convention $C_{kl} = \delta_{kl}$ is assumed, and we have used $x_{kl} = x_{il} = x_{jl}$ under the limit $x_i \to x_j$. It is clear that we can identify $\widetilde{C}_{ijk} = C_{ijk}$ for normalized operators with $C_{ij} = \delta_{ij}$. Formally, we can regard an OPE as a fusion algebra of operators approaching each other, which has the conventional notation

$$[\mathcal{O}_i] \times [\mathcal{O}_j] = \sum_k C_{ijk}\, [\mathcal{O}_k]\,. \tag{A.7}$$

A.1.2 Real-Space RG & OPEs

The OPE provides a natural way to calculate RG flow at any given conformal fixed point [30]. Let $\mathcal{S}_{\text{CFT}}$ be a fixed-point action in D Euclidean dimensions. We turn on a set of general perturbations parametrized by a complete set of quasi-primary fields $\{\mathcal{O}_j\}$

$$\mathcal{S} = \mathcal{S}_{\text{CFT}} + \delta\mathcal{S} = \mathcal{S}_{\text{CFT}} + \int \mathrm{d}^D x \sum_j u_j a^{\Delta_j - D} \mathcal{O}_j(x), \tag{A.8}$$

where $\{u_j\}$ is the set of dimensionless coupling constants, $a = 1/\Lambda$ is the UV regulator in real space (i.e., Λ is the UV cut-off in momentum space), and Δ_j denotes the scaling dimension of each field $\mathcal{O}_j$. The partition function can be formally evaluated as

$$\mathcal{Z} = \mathrm{Tr} e^{-\mathcal{S}_{\mathrm{CFT}} - \delta\mathcal{S}} = \mathcal{Z}_{\mathrm{CFT}} \left\langle e^{-\delta\mathcal{S}} \right\rangle, \tag{A.9}$$

where $\mathcal{Z}_{\mathrm{CFT}} = \mathrm{Tr} e^{-\mathcal{S}_{\mathrm{CFT}}}$ is the CFT partition function, and $\langle \ldots \rangle = \mathcal{Z}_{\mathrm{CFT}}^{-1} \mathrm{Tr}(e^{-\mathcal{S}_{\mathrm{CFT}}}(\ldots))$ denotes the expectation value of $(\ldots)$ evaluated at the fixed point. We could perform a Taylor expansion of the partition function

$$\begin{aligned}
\frac{\mathcal{Z}}{\mathcal{Z}_{\mathrm{CFT}}} &= \left\langle e^{-\delta\mathcal{S}} \right\rangle = \sum_{n=0}^{\infty} \frac{(-1)^n}{n!} \left\langle (\delta\mathcal{S})^n \right\rangle \\
&= 1 + \sum_{n=1}^{\infty} \frac{(-1)^n}{n!} \sum_{j_1,\ldots,j_n} \left(\prod_{r=1}^{n} \int \frac{\mathrm{d}^D x_{j_r}}{a^{D-\Delta_{j_r}}} u_{j_r} \right) \left\langle \mathcal{O}_{j_1}(x_{j_1}) \ldots \mathcal{O}_{j_n}(x_{j_n}) \right\rangle \\
&= 1 - \sum_j \int \frac{\mathrm{d}^D x}{a^{D-\Delta_j}} u_j \left\langle \mathcal{O}_j(x) \right\rangle + \frac{1}{2!} \sum_{i,j} \int \frac{\mathrm{d}^D x_i \mathrm{d}^D x_j}{a^{2D-\Delta_i-\Delta_j}} u_i u_j \left\langle \mathcal{O}_i(x_i) \mathcal{O}_j(x_j) \right\rangle \\
&\quad - \frac{1}{3!} \sum_{i,j,k} \int \frac{\mathrm{d}^D x_i \mathrm{d}^D x_j \mathrm{d}^D x_k}{a^{3D-\Delta_i-\Delta_j-\Delta_k}} u_i u_j u_k \left\langle \mathcal{O}_i(x_i) \mathcal{O}_j(x_j) \mathcal{O}_k(x_k) \right\rangle + O(u^4).
\end{aligned} \tag{A.10}$$

In all the integrals, we should assume $\Delta x = |x_i - x_j| > a$ for any pair of coordinates, which is equivalent to imposing a momentum cut-off $\Lambda = 1/a$. We implement the real-space RG transformations by rescaling the real-space cut-off $a \to a e^{\delta\ell}$ where $\delta\ell \ll 1$. The original integral can be split as

$$\int_{a<\Delta x} = \int_{a e^{\delta\ell} < \Delta x} + \int_{a < \Delta x < a e^{\delta\ell}}, \tag{A.11}$$

In the first term, the leading-order RG flow of u_j from pure rescaling can be obtained via

$$\begin{aligned} & u_j a^{\Delta_j - D} \text{ invariant: } a^{\Delta_j - D} \to a^{\Delta_j - D} e^{\delta\ell(\Delta_j - D)} \\ \Longrightarrow \quad & u_j \to u_j e^{-\delta\ell(\Delta_j - D)} = u_j - u_j(\Delta_j - D)\delta\ell. \end{aligned} \tag{A.12}$$

In addition, the integral over the thin shell $a < \Delta x < ae^{\delta\ell}$ may also contribute. In this case, any two points are fairly close to each other, and hence OPEs can be applied.

Two-point RG The first order term is going to be generated by two-point OPEs

$$\begin{aligned} & \frac{1}{2!}\sum_{i,j}\int_{\text{shell}} \frac{\mathrm{d}^D x_i \mathrm{d}^D x_j}{a^{2D-\Delta_i-\Delta_j}} u_i u_j \left\langle \mathcal{O}_i(x_i)\mathcal{O}_j(x_j)\right\rangle \\ = & \frac{1}{2!}\sum_{i,j}\int_{\text{shell}} \frac{\mathrm{d}^D x_i \mathrm{d}^D x_j}{a^{2D-\Delta_i-\Delta_j}} u_i u_j \sum_k \frac{C_{ijk}}{a^{\Delta_i+\Delta_j-\Delta_k}} \left\langle \mathcal{O}_k(x_i)\right\rangle \\ = & \frac{1}{2!}\sum_{i,j,k} C_{ijk} u_i u_j S_{D-1}\delta\ell \int \frac{\mathrm{d}^D x}{a^{D-\Delta_k}} \left\langle \mathcal{O}_k(x)\right\rangle, \end{aligned} \tag{A.13}$$

where the surface area $S_{D-1} = 2\pi^{D/2}/\Gamma(D/2)$ of $(D-1)$-sphere is introduced. Consequently, we have the beta function of u_j to order $O(u^2)$

$$\begin{aligned} & \frac{\mathrm{d}u_j}{\mathrm{d}\ell} = (D-\Delta_j)u_j - \frac{S_{D-1}}{2}\sum_{i,k} C_{ikj} u_i u_k + O(u^3) \\ \xlongequal[\text{rescale } u]{\frac{S_{D-1}}{2}u\to u} & \frac{\mathrm{d}u_j}{\mathrm{d}\ell} = (D-\Delta_j)u_j - \sum_{i,k} C_{ikj} u_i u_k + O(u^3). \end{aligned} \tag{A.14}$$

Notice that $C_{ikj} = C_{kij}$ and the contributions where $i \neq k$ are counted twice in the summation. The perturbative RG flow is determined by the universal data of CFT (including scaling dimensions and OPE coefficients). For Landau-Ginzburg-Wilson-Fisher (LGWF) theory, the " two-point RG" identifies the "one-loop RG" in standard terminology, since the OPE $[\phi^4]\times[\phi^4] \sim [\phi^4] + \ldots$ only involves one-loop Feynman diagram. Although some

two-point OPEs may involve higher loop diagrams, the final result is only valid to the first order $O(\epsilon)$ in ϵ-expansion.

New fixed point The relevant perturbations may drive the system flow to a new fixed point $\{u_j^*\}$ that satisfies $\mathrm{d}u_j/\mathrm{d}\ell = 0$ for all operators $\mathcal{O}_j$. At the new fixed point, the scaling dimension Δ_j^* of $\mathcal{O}_j$ can be obtained via

$$\begin{cases} (u_j^* + \delta u_j)\mathcal{O}_j e^{\delta\ell(\Delta_j^* - D)} = u_j^* \mathcal{O}_j \\ \delta u_j = \mathrm{d}u_j/\mathrm{d}\ell|_{u=u^*}\, \delta\ell \end{cases} \Longrightarrow$$

$$\Delta_j^* = D - \frac{1}{u_j}\frac{\mathrm{d}u_j}{\mathrm{d}\ell}\bigg|_{u=u^*} = \Delta_j + \sum_{i,k} C_{ikj}\frac{u_i^* u_k^*}{u_j^*} + O(u^2). \tag{A.15}$$

A.1.3 Wilson-Fisher Fixed Points

In this section, we use conformal perturbation theory to reproduce some standard results that can be found in textbooks (also see [30]).

Ising model Let's apply the conformal perturbation theory to the LGWF theory. We first analyze the simplest case, the Ising model

$$\mathcal{S} = \int d^D x \frac{1}{2}\left(\partial\phi\right)^2 + a^{-1-D/2} h\phi + a^{-2} r\phi^2 + a^{D-4} u\phi^4 + \ldots, \tag{A.16}$$

where the bare scaling dimension of the free field is $\Delta_\phi = D/2 - 1$. The composite operator $\Phi_n =: \phi^n :$ with the scaling dimension $\Delta_n = n\Delta_\phi$ satisfies

$$\langle \Phi_n(x)\Phi_n(y)\rangle = \langle : \phi^n(x) :: \phi^n(y) : \rangle = \frac{\text{const.}}{|x-y|^{2n\Delta_\phi}}, \tag{A.17}$$

which can be easily understood through the Wick contractions of n pairs of ϕ fields. Furthermore, the expression of Φ_n can be obtained directly from the Wick theorem

$$\begin{aligned}
\Phi_1 &=: \phi := \phi - \langle\phi\rangle = \phi, \\
\Phi_2 &=: \phi^2 := \phi^2 - \langle\phi^2\rangle, \\
\Phi_4 &=: \phi^4 := \phi^4 - 6\langle\phi^2\rangle\phi^2.
\end{aligned} \tag{A.18}$$

Their OPEs can be obtained by counting the symmetry factors of Feynman diagrams

$$\begin{aligned}
&[\Phi_1]\times[\Phi_1] = [1] + [\Phi_2]\,, \quad [\Phi_1]\times[\Phi_2] = 2\,[\Phi_1] + [\Phi_3]\,, \\
&[\Phi_2]\times[\Phi_2] = 2\,[1] + 4\,[\Phi_2] + [\Phi_4]\,, \quad [\Phi_2]\times[\Phi_4] = 12\,[\Phi_2] + 8\,[\Phi_4]\,, \\
&[\Phi_4]\times[\Phi_4] = 24\,[1] + 96\,[\Phi_2] + 72\,[\Phi_4]\,, \quad [\Phi_1]\times[\Phi_4] = 4\,[\Phi_3]\,,
\end{aligned} \tag{A.19}$$

where we only keep the UV-divergent terms with potentially relevant operators. Using Eq. A.14, we could write down the one-loop beta functions of h, r, u directly

$$\begin{aligned}
\frac{dh}{dl} &= (D/2+1)h - 4hr + \dots \\
\frac{dr}{dl} &= 2r - h^2 - 4r^2 - 24ru - 96u^2 + \dots \\
\frac{du}{dl} &= (4-D)u - r^2 - 16ru - 72u^2 + \dots
\end{aligned} \tag{A.20}$$

To leading order in $\epsilon = 4 - D$, the Wilson-Fisher fixed point is found to be $h^* = 0, r^* = 0, u^* = \epsilon/72$. We can see the scaling dimension of r is $2 - 24u^* = 2 - \epsilon/3$, which implies $\Delta[\Phi_2] = 2 + \epsilon/3$ at the WF fixed point.

O(N) model Let us generalize the discussions to O(N) model with N-component real vector $\boldsymbol{\phi}$. We can focus on Φ_2 and Φ_4 which have the expressions

$$\Phi_2 =: \boldsymbol{\phi}^2 := \boldsymbol{\phi}^2 - N\langle\phi^2\rangle, \quad \Phi_4 =: (\boldsymbol{\phi}^2)^2 := (\boldsymbol{\phi}^2)^2 - 2(N+2)\langle\phi^2\rangle\boldsymbol{\phi}^2, \tag{A.21}$$

where $\boldsymbol{\phi}^2 = \sum_{a=1}^{N}\phi_a^2$. Their OPEs are evaluated as

$$\begin{aligned}
&[\Phi_2]\times[\Phi_2] = 2\,[1] + 4\,[\Phi_2] + [\Phi_4]\,, \quad [\Phi_2]\times[\Phi_4] = 4(N+2)\,[\Phi_2] + 8\,[\Phi_4]\,,\\
&[\Phi_4]\times[\Phi_4] = 8(N^2+2)\,[1] + 32(N+2)\,[\Phi_2] + 8(N+8)\,[\Phi_4]\,,
\end{aligned} \tag{A.22}$$

where we still only keep the UV-divergent terms with potentially relevant operators. Using Eq. A.14, we can directly write down the RG flow of O(N) model

$$\begin{aligned}
\frac{dr}{dl} &= 2r - 4r^2 - 8(N+2)ru - 32(N+2)u^2 + \dots\\
\frac{du}{dl} &= (4-D)u - r^2 - 16ru - 8(N+8)u^2 + \dots
\end{aligned} \tag{A.23}$$

To leading order in $\epsilon = 4 - D$, the WF fixed point is at $r^* = O(\epsilon^2), u^* = \frac{\epsilon}{8(N+8)} + O(\epsilon^2)$. The scaling dimension of r is now $2 - 8(N+2)u^* = 2 - \frac{N+2}{N+8}\epsilon$, and accordingly the scaling dimension of Φ_2 is $\Delta[\Phi_2] = 2 + \frac{N+2}{N+8}\epsilon$.

U(N) model For the U(N) model with N-component complex vectors $\boldsymbol{\phi}^\dagger$ and $\boldsymbol{\phi}$, we are interested in the operators

$$\begin{aligned}
&\Phi_2 =: \boldsymbol{\phi}^\dagger\boldsymbol{\phi} := \boldsymbol{\phi}^\dagger\boldsymbol{\phi} - N\langle\phi^\dagger\phi\rangle, \quad \Psi_2 =: \boldsymbol{\phi}^2 := \boldsymbol{\phi}^2,\\
&\Phi_4 =: (\boldsymbol{\phi}^\dagger\boldsymbol{\phi})^2 := (\boldsymbol{\phi}^\dagger\boldsymbol{\phi})^2 - 2(N+1)\langle\phi^2\rangle\boldsymbol{\phi}^\dagger\boldsymbol{\phi},
\end{aligned} \tag{A.24}$$

where $\boldsymbol{\phi}^\dagger\boldsymbol{\phi} = \sum_{a=1}^N \phi_a^\dagger\phi_a$ and $\boldsymbol{\phi}^2 = \sum_{a=1}^N \phi_a^2$. In addition to the charge operator Φ_2, we also turned on paring operator Ψ_2. They satisfy the following OPEs

$$
\begin{aligned}
&[\Phi_2]\times[\Phi_2] = [1] + 2\,[\Phi_2] + [\Phi_4]\,, \quad [\Phi_2]\times[\Phi_4] = 2(N+1)\,[\Phi_2] + 4\,[\Phi_4]\,,\\
&[\Phi_4]\times[\Phi_4] = 2(N^2+1)\,[1] + 8(N+1)\,[\Phi_2] + 4(N+4)\,[\Phi_4]\,,\\
&[\Psi_2]\times[\Phi_4] = 2\,[\Psi_2] + \dots
\end{aligned}
\tag{A.25}
$$

Let us still assume the coupling constants of Φ_2, Φ_4 are r, u, and introduce the coupling w for Ψ_2. Based on Eq. A.14, their beta functions are obtained as

$$
\begin{aligned}
\frac{dr}{dl} &= 2r - 2r^2 - 4(N+1)ru - 8(N+1)u^2 + \dots\\
\frac{du}{dl} &= (4-D)u - r^2 - 8ru - 4(N+4)u^2 + \dots\\
\frac{dw}{dl} &= 2w - 4uw + \dots
\end{aligned}
\tag{A.26}
$$

To leading order in $\epsilon = 4 - D$, the U(N) WF fixed point is located at $r^* = O(\epsilon^2), u^* = \frac{\epsilon}{4(N+4)} + O(\epsilon^2)$ and $w^* = O(\epsilon^2)$. Using Eq. A.15, we have the scaling dimensions of the charge operator Φ_2 and the pairing operator Ψ_2

$$
\begin{aligned}
\Delta[\Phi_2] &= (D-2) + 4(N+1)u^* = (2-\epsilon) + \frac{N+1}{N+4}\epsilon,\\
\Delta[\Psi_2] &= (D-2) + 4u^* = (2-\epsilon) + \frac{\epsilon}{N+4}.
\end{aligned}
\tag{A.27}
$$

The result about Φ_2 here is indeed consistent with the analog in O($2N$) model.

A.1.4 Bulk-Boundary OPEs

For a critical system with boundaries, Eq. A.14 can not be applied directly, since two-point functions are no longer as simple as Eq. A.1. But we still can define the OPE

for any two operators close to each other

$$\lim_{x_i \to x_j} \mathcal{O}_i(x_i)\mathcal{O}_j(x_j) = \lim_{x_i \to x_j} \sum_k \mathscr{C}_{ijk}(x_i; x_j)\mathcal{O}_k(x_k), \tag{A.28}$$

where $x_k = \lambda x_i + (1-\lambda)\, x_j$ with $0 \leq \lambda \leq 1$ is any point between x_i and x_j, and $\mathcal{O}_j$ can be boundary operators or bulk operators. The OPE coefficient $\mathscr{C}_{ijk}$ may depend on the details of the boundary (analyzed by the method of images for certain cases). But the Taylor expansion Eq. A.10 is always valid. Thus we could obtain one-loop RG flow (through the same logic as in Eq. A.13) by considering how the first-order term is generated by the second order term via OPEs between all operators (including bulk-bulk and bulk-boundary OPEs). In the calculations below, we consider a $D = d+1$ dimensional system parametrized by the coordinate $x = (\mathtt{x}, y)$ where $\mathtt{x} \in \mathbb{R}^d, y > 0$.

The bulk OPEs often reduce back to the standard form, i.e.,

$$\mathscr{C}_{ijk}(x_i, x_j) = C_{ijk} / \left|x_i - x_j\right|^{\Delta_i + \Delta_j - \Delta_k} \tag{A.29}$$

and Eq. A.13 can be directly applied. But the bulk-boundary OPEs need to be calculated case by case, i.e.,

$$\begin{aligned} &\frac{1}{2!}\sum_{i,j}\int_{\text{half-shell}} \frac{\mathrm{d}^d\mathtt{x}_i \mathrm{d}y \mathrm{d}^d\mathtt{x}_j}{a^{2d+1-\Delta_i-\Delta_j}} u_i u_j \left\langle \mathcal{O}_i(\mathtt{x}_i, y)\mathcal{O}_j(\mathtt{x}_j, 0)\right\rangle \\ =&\frac{1}{2!}\sum_{i,j}\int_{\text{half-shell}} \frac{\mathrm{d}^d\mathtt{x}_i \mathrm{d}y \mathrm{d}^d\mathtt{x}_j}{a^{2d+1-\Delta_i-\Delta_j}} u_i u_j \sum_k \mathscr{C}_{ijk}(\mathtt{x}_i, y; \mathtt{x}_j, 0) \left\langle \mathcal{O}_k(\mathtt{x}_j, 0)\right\rangle \end{aligned} \tag{A.30}$$

where $\int \mathrm{d}^d\mathtt{x}_i \mathrm{d}y \mathcal{O}_i(\mathtt{x}_i, y)$ is a bulk operator, $\int \mathrm{d}^d\mathtt{x}_i \mathrm{d}y \mathcal{O}_j(\mathtt{x}_j, 0)$ is boundary operator, and the integral is over the real-space half-shell $a < ((\mathtt{x}_i - \mathtt{x}_j)^2 + y^2)^{1/2} < ae^{\delta\ell}, y > 0$ near the boundary. We proceed with the integral of $\mathscr{C}_{ijk}(\mathtt{x}_i, y; \mathtt{x}_j, 0)$ over $\mathtt{x}_i$ and y. The result should be a constant independent of $\mathtt{x}_j$, owing to the translational invariance

along $\mathtt{x}$-directions. In addition, the result should be proportional to $a^{d+1-\Delta_i-\Delta_j+\Delta_k}\delta\ell$ by dimensional analysis. Thus, we could introduce a dimensionless number Υ_{ijk} (determined by bulk-boundary correlation functions) such that

$$\int_{\text{shell}} \mathrm{d}^d\mathtt{x}_i \mathrm{d}y \mathscr{C}_{ijk}(\mathtt{x}_i, y; \mathtt{x}_j, 0) = C_{ijk}\Upsilon_{ijk}S_d a^{d+1-\Delta_i-\Delta_j+\Delta_k}\delta\ell, \tag{A.31}$$

where C_{ijk} is the standard OPE coefficient (determined by Wick contractions), and $S_d = 2\pi^{\frac{d+1}{2}}/\Gamma(\frac{d+1}{2})$ is the surface area of d-sphere. Schematically, we can write down how the boundary operators are generated under RG

$$\begin{aligned} &\frac{1}{2!}\sum_{i,j}\int_{\text{shell}} \frac{\mathrm{d}^d\mathtt{x}_i dy \mathrm{d}^d\mathtt{x}_j}{a^{2d+1-\Delta_i-\Delta_j}} u_i u_j \left\langle \mathcal{O}_i(\mathtt{x}_i, y)\mathcal{O}_j(\mathtt{x}_j, 0)\right\rangle \\ &= \frac{S_d}{2}\sum_{i,j,k}\Upsilon_{ijk}C_{ijk}u_i u_j \delta\ell \int \frac{\mathrm{d}^d\mathtt{x}}{a^{d-\Delta_k}} \left\langle \mathcal{O}_k(\mathtt{x}, 0)\right\rangle . \end{aligned} \tag{A.32}$$

If we define $\Upsilon_{ijk} = 1$ for all bulk OPEs, then the one-loop beta functions of all coupling constants (for both bulk and boundary operators) can be written compactly as

$$\frac{\mathrm{d}u_j}{\mathrm{d}\ell} = (D - \Delta_j)\, u_j - \sum_{i,k}\Upsilon_{ikj}C_{ikj}u_i u_k + O(u^3), \tag{A.33}$$

where we have rescaled the coupling constant $uS_d/2 \to u$ as in Eq. A.14. Notice that $C_{ikj} = C_{kij}$ and the contributions where $i \neq k$ are counted twice in the summation.

A.2 Ricci Flow & RG of NLSM

This appendix introduces some well-known standard results relevant to Sec. 1.1. In two dimensions, a generic bosonic non-linear sigma model (NLSM) reads

$$\mathcal{S}[\varphi] = \frac{1}{2}\int g_{ab}(\varphi)\mathrm{d}\varphi^a \wedge \star\mathrm{d}\varphi^b + h_{ab}(\varphi)\mathrm{d}\varphi^a \wedge \mathrm{d}\varphi^b, \tag{A.34}$$

where where $\varphi^a \in \mathbb{R}$ and $g_{ab} \in \mathbb{R}$ are the coordinate and the metric on the target manifold, and $h_{ab} = -h_{ba}$ gives Wess-Zumino-Witten (WZW) term. The RG of NLSM+WZW actually has a very elegant geometric interpretation. The RG flow corresponds to the Ricci flow [557, 558] in the target manifold which has torsion induced by WZW term [559] (also see Ref. [560] and references therein).

Riemann geometry The Christoffel symbol is obtained from g_{ab} via ($\partial_a = \frac{\partial}{\partial\varphi^a}$)

$$\Gamma^a_{\ bc} = \frac{1}{2}g^{ae}\left(-\partial_e g_{bc} + \partial_c g_{be} + \partial_b g_{ce}\right). \tag{A.35}$$

It gives the Riemann curvature without torsion

$$R^a_{\ b} = \mathrm{d}\Gamma^a_{\ b} + \Gamma^a_{\ c} \wedge \Gamma^c_{\ b} \quad \Longleftrightarrow \quad R^a_{\ bcd} = \partial_c\Gamma^a_{\ db} - \partial_d\Gamma^a_{\ cb} + \Gamma^a_{\ ce}\Gamma^e_{\ db} - \Gamma^a_{\ de}\Gamma^e_{\ cb}, \tag{A.36}$$

where $\Gamma^a_{\ b} = \Gamma^a_{\ cb}dx^c$ is the connection and $R^a_{\ b} = \frac{1}{2}R^a_{\ bcd}\mathrm{d}x^c \wedge \mathrm{d}x^d$ is the Riemann curvature. In addition, the WZW form $h = \frac{1}{2}h_{ab}\mathrm{d}\varphi^a \wedge \mathrm{d}\varphi^b$ gives us a contorsion K_{abc}

$$K = \mathrm{d}h \quad \Longleftrightarrow \quad K_{abc} = \frac{1}{2}(\partial_a h_{bc} + \partial_b h_{ca} + \partial_c h_{ab}). \tag{A.37}$$

Now, we can define the generalized affine connection with torsion

$$\hat{\Gamma}^a{}_{bc} = \Gamma^a{}_{bc} + K^a{}_{bc}. \tag{A.38}$$

The generalized Riemann curvature with torsion $\hat{R}^a{}_b = \frac{1}{2}\hat{R}^a{}_{bcd}\mathrm{d}x^c \wedge \mathrm{d}x^d$ can be still calculated from its standard relation to the connection $\hat{\Gamma}^a{}_b = \hat{\Gamma}^a{}_{cb}\mathrm{d}x^c$:

$$\hat{R}^a{}_b = \mathrm{d}\hat{\Gamma}^a{}_b + \hat{\Gamma}^a{}_c \wedge \hat{\Gamma}^c{}_b \quad \Longleftrightarrow \quad \hat{R}^a{}_{bcd} = \partial_c\hat{\Gamma}^a{}_{db} - \partial_d\hat{\Gamma}^a{}_{cb} + \hat{\Gamma}^a{}_{ce}\hat{\Gamma}^e{}_{db} - \hat{\Gamma}^a{}_{de}\hat{\Gamma}^e{}_{cb}. \tag{A.39}$$

The Ricci tensor is defined as the contraction of Riemann curvature, and the Ricci scalar is its full contraction, i.e.,

$$\mathcal{R}_{ab} = \hat{R}^c{}_{acb}, \qquad \mathcal{R} = g^{ab}\mathcal{R}_{ab}. \tag{A.40}$$

RG of NLSM + WZW The one-loop bata functions for g_{ab} and h_{ab} are

$$\frac{\mathrm{d}g_{ab}}{\mathrm{d}\ell} = -\frac{1}{2\pi}\mathcal{R}_{(ab)} + \ldots, \qquad \frac{\mathrm{d}h_{ab}}{\mathrm{d}\ell} = -\frac{1}{2\pi}\mathcal{R}_{[ab]} + \ldots, \tag{A.41}$$

where $\mathcal{R}_{(ab)} = \frac{1}{2}(\mathcal{R}_{ab} + \mathcal{R}_{ba})$ and $\mathcal{R}_{[ab]} = \frac{1}{2}(\mathcal{R}_{ab} - \mathcal{R}_{ba})$. The proof of Ricci flow using covariant background field method, as well as higher-loop results can be found in Ref. [560]. In addition to the geometric interpretation of RG flow, the fixed points are shown to correspond to the metrics satisfying generalized Einstein equation [557, 558]. Here is remark about the Einstein manifold. This is when the Ricci tensor is proportional to the metric $\mathcal{R}_{ab} \propto g_{ab}$. In this case, the RG flow of coupling constant is easy to read from the Ricci flow. There are many manifolds are within this category, like anti-de Sitter space, de Sitter space, complex projective space, etc.

RG of O(N) NLSM Using the powerful method of Ricci flow, we can in principle calculate the RG flow of any NLSM with constrain $\sum_{i=1}^{N}(n^i)^2 = 1$. (Namely, one could consider O(N) NLSM with anisotropies. One example with applications to twisted bilayer graphene Moiré superlattice has been considered in Ref. [561].) To use the machinery, we need to first get rid of the constrain by introducing constraint-free variables φ (Goldstone modes), then consider the NLSM of φ, and get the beta function from Ricci flow. In $D = 2 + \epsilon$ expansion, the flow of the target-space metric reads

$$\mathcal{S}[\mathbf{n}] = \frac{1}{2}\int \mathrm{d}^{2+\epsilon}x\rho_{ij}\partial_\mu n^i\partial_\mu n^j = \mathcal{S}[\varphi] = \frac{1}{2}\int \mathrm{d}^{2+\epsilon}x g_{ab}(\varphi)\partial_\mu\varphi^a\partial_\mu\varphi^b,$$
$$\frac{\mathrm{d}g_{ab}}{\mathrm{d}\ell} = \epsilon g_{ab} - \frac{1}{2\pi}\mathcal{R}_{ab} + \dots. \tag{A.42}$$

Without the WZW term, the manifold is torsion free, and the Ricci tensor $\mathcal{R}_{ab} = \mathcal{R}_{(ab)}$ is symmetric. There are many non-linear transformations to reparametrize the theory. For example, one can introduce the coordinates

$$n^1 = \varphi^1, \qquad \dots\dots \qquad n^{N-1} = \varphi^{N-1}, \qquad n^N = \sqrt{1 - \sum_{a=1}^{N-1}(\varphi^a)^2}. \tag{A.43}$$

For the standard symmetric O(N) NLSM with $\rho_{ij} = \rho\delta_{ij}$, things are much easier. We obtain the metric on target manifold $g_{ab} = \rho\hat{g}_{ab}$ (and $g^{ab} = \hat{g}^{ab}/\rho$) where

$$\hat{g}_{ab} = \delta_{ab} + \frac{\varphi^a\varphi^b}{1 - |\varphi|^2}, \qquad \hat{g}^{ab} = \delta^{ab} - \varphi^a\varphi^b, \qquad \det\hat{g}_{ab} = \frac{1}{1 - |\varphi|^2}, \tag{A.44}$$

which leads to the affine connection $\Gamma^a_{bc} = \varphi^a\hat{g}_{bc}$, and the Riemann curvature $R_{abcd} = \hat{g}_{ac}\hat{g}_{bd} - \hat{g}_{ad}\hat{g}_{bc}$, as well as the Ricci curvature $\mathcal{R}_{ab} = (\dim[\varphi] - 1)\hat{g}_{ab} = (N-2)\hat{g}_{ab}$. We find the Ricci flow method indeed reproduces the standard results for O(N) NLSM (see

Polyakov [562], or Fradkin [13] or Kardar [563])

$$\begin{aligned}
&\frac{\mathrm{d}(\rho\hat{g}_{ab})}{\mathrm{d}\ell} = \epsilon(\rho\hat{g}_{ab}) - \frac{(N-2)\hat{g}_{ab}}{2\pi} \qquad \Longrightarrow \\
&\frac{\mathrm{d}\rho}{\mathrm{d}\ell} = \epsilon\rho - \frac{N-2}{2\pi} \quad \Longleftrightarrow \quad \frac{\mathrm{d}\rho^{-1}}{\mathrm{d}\ell} = -\epsilon\rho^{-1} + \frac{N-2}{2\pi}\rho^{-2}.
\end{aligned} \tag{A.45}$$

For $N > 2$ and $D > 2$ (such that $\epsilon > 0$), there is a new fixed point at

$$\rho_*^{-1} = \frac{2\pi\epsilon}{N-2}. \tag{A.46}$$

For $N > 2$ in two dimensions (such that $\epsilon = 0$), ρ^{-1} has a positive beta function and will flow strong. The $\rho^{-1} \to +\infty$ phase is the disordered phase. Therefore we find there is no spontaneous O(N) symmetry breaking (with $N > 2$) in two dimensions. For O(2) = U(1), the one-loop beta function is zero, but one could realize the Kosterlitz-Thouless transition, which is beyond the conventional symmetry-breaking paradigm.

A.3 Non-Fermi Liquids in QCD$_3$

In this appendix, we discuss the non-fermi liquid (NFL) fixed-point (or fixed-hyperplane in general) for the fermi-surface (FS) state in non-abelian gauge theory. It serves as a generalization of the NFL fixed point introduced in Sec. 1.3.2 and used in Sec. 4.1. A shorter version of the discussion (in slightly different notations) can be found in Sec. 4.2.

A.3.1 Single-Patch Theory

The expansion of the fermion energy dispersion $\epsilon_{\boldsymbol{k}+\boldsymbol{k}_F} \approx v_F k_\perp + \kappa \boldsymbol{k}_\parallel^2$ at the fermi wave vector $\boldsymbol{k}_F \in \mathrm{FS}$ leads to the low-energy theory on each patch

$$\mathcal{S}_F = \int \mathrm{d}\tau \mathrm{d}x_\perp \mathrm{d}^{d-1}\boldsymbol{x}_\parallel \sum_{I=1}^{N_f} \psi_I^\dagger (\eta \partial_\tau - \mathtt{i} v_F \nabla_\perp - \kappa \boldsymbol{\nabla}_\parallel^2)\psi_I, \tag{A.47}$$

where $x_\perp$ denotes the normal direction of the FS and $\boldsymbol{x}_\parallel$ is a $(d-1)$-dimensional vector in the tangent space of the FS manifold. To be general, we have introduced a fermion flavor number N_f, which may come from certain global symmetry of the system (e.g., $\mathrm{SU}(N_f)$ global symmetry). We have also introduced a temporal coefficient η for generic scenarios. For FLs we simply set $\eta = 1$, and we will allow η to renormalize for NFLs. At the free-fermion UV fixed point, we have anisotropic scalings of spacetime coordinates

$$\tau' = \tau e^{-\ell}, \qquad x'_\perp = x_\perp e^{-\ell}, \qquad \boldsymbol{x}'_\parallel = \boldsymbol{x}_\parallel e^{-\ell/2}, \tag{A.48}$$

and accordingly the fermion operator has the scaling dimension

$$\psi'(\tau', x'_\perp, \boldsymbol{x}'_\parallel) = e^{\ell(d+1)/4}\psi(\tau, x_\perp, \boldsymbol{x}_\parallel) \quad \Longrightarrow \quad \Delta[\psi] = \frac{d+1}{4}. \tag{A.49}$$

Then we couple the FS state to a non-abelian gauge theory with a gauge group G

$$\begin{aligned}\mathcal{S}[\psi^\dagger, \psi, a, \lambda, c^\dagger, c] = &\int \mathrm{d}\tau \mathrm{d}x_\perp \mathrm{d}^{d-1}\boldsymbol{x}_\parallel \sum_{I=1}^{N_f} \psi_I^\dagger (\eta \mathrm{D}_\tau - \mathtt{i} v_F \mathrm{D}_\perp - \kappa \mathrm{D}_\parallel^2)\psi_I \\ &+ \frac{1}{\mathbb{x}}\mathrm{Tr}\int \frac{N_f}{2g^2} f \wedge \star f + \mathtt{i}\mathtt{k}\mathrm{CS}[a] + \frac{\zeta}{2}\lambda \wedge \star\lambda + \nabla\lambda \wedge \star a + \nabla c^\dagger \wedge \star \mathrm{D}c,\end{aligned} \tag{A.50}$$

where we have included a Chern-Simons term at level-k when $d = 2$

$$\mathrm{CS}[a] = \frac{1}{4\pi}\mathrm{Tr}(a \wedge \mathrm{d}a - a \wedge a \wedge a). \tag{A.51}$$

Given a set of group generators $\{\mathbf{t}_\mathsf{a}\}$ under certain representation, the 1-form gauge field connection is defined by $a = a_\mu \mathrm{d}x^\mu = a^\mathsf{a}_\mu \mathbf{t}_\mathsf{a} \mathrm{d}x^\mu$, the 2-form curvature is then $f = \mathrm{d}a - \mathtt{i}a \wedge a$, and the gauge covariant derivative reads $\mathrm{D} = \mathrm{d} - \mathtt{i}a$. The bosonic auxiliary fields $\lambda = \lambda^\mathsf{a}\mathbf{t}_\mathsf{a}$ are introduced to implement the gauge fixing (e.g., the Coulomb gauge $\nabla \cdot \boldsymbol{a} = 0$), and the Faddeev-Popov determinant is taken care of by the fermionic ghost fields $c = c^\mathsf{a}\mathbf{t}_\mathsf{a}$. As for the gauge group generators $\{\mathbf{t}_\mathsf{a}\}$, we denote the Lie algebra and the normalization convention by

$$[\mathbf{t}_\mathsf{a}, \mathbf{t}_\mathsf{b}] = \mathtt{i}\mathbb{f}^\mathsf{c}_\mathsf{ab}\mathbf{t}_c, \qquad \mathrm{Tr}(\mathbf{t}_\mathsf{a}\mathbf{t}_\mathsf{b}) = \mathbb{x}\delta_\mathsf{ab}, \qquad \mathsf{a}, \mathsf{b} = 1, 2, \ldots, \mathrm{dim}G, \tag{A.52}$$

where $\mathbb{f}^\mathsf{c}_\mathsf{ab}$ is the the structure constant, and $\mathbb{x}$ is the Dynkin index of the representation (e.g., one often choose $\mathbb{x} = 1/2$ for the fundamental representation of $\mathrm{SU}(N)$). We assume each fermion flavor $I = 1, \ldots, N_f$ carries a representation of the gauge group G. For convenience, we have rescaled the gauge coupling constant $g^2 \to g^2/N_f$. There are many terms in Eq. A.52 that are actually irrelevant in the patch theory. We present some diagrammatic calculations and scaling analyses in general dimensions here, and we will focus on $2 + 1$ dimensions eventually.

Boson self-energy and Landau damping of chromo-magnetic field Considering the Yukawa-type coupling $v_F\psi^\dagger a_\perp \psi$, we have the one-loop boson self-energy $\Sigma_\perp$

$\Sigma_\perp^{\mathsf{ab}}(\mathtt{i}\omega, \boldsymbol{p}) =$ 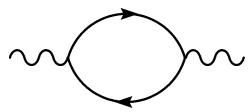 $= v_F^2 \int \frac{\mathrm{d}\nu \mathrm{d}^d \boldsymbol{k}}{(2\pi)^{d+1}} \mathrm{Tr}[G_{\psi,0}(\mathtt{i}\nu, \boldsymbol{k})\mathbf{t}_{\mathsf{a}} G_{\psi,0}(\mathtt{i}\nu + \mathtt{i}\omega, \boldsymbol{k}+\boldsymbol{p})\mathbf{t}_{\mathsf{b}}]$

$$
\begin{aligned}
&= N_f v_F^2 \mathrm{Tr}(\mathbf{t}_{\mathsf{a}}\mathbf{t}_{\mathsf{b}}) \int \frac{\mathrm{d}\nu \mathrm{d}k_\perp \mathrm{d}^{d-1}\boldsymbol{k}_\parallel}{(2\pi)^{d+1}} \frac{1}{\mathtt{i}\eta\nu - v_F k_\perp - \kappa \boldsymbol{k}_\parallel^2} \frac{1}{\mathtt{i}\eta(\nu+\omega) - v_F(k_\perp + p_\perp) - \kappa(\boldsymbol{k}_\parallel + \boldsymbol{p}_\parallel)^2} \\
&= N_f \delta_{\mathsf{ab}} \mathbb{x} v_F^2 \int \frac{\mathrm{d}\nu \mathrm{d}^{d-1}\boldsymbol{k}_\parallel}{(2\pi)^d} \frac{\mathtt{i}(\mathrm{sgn}(\omega+\nu) - \mathrm{sgn}(\nu))}{2v_F(\mathtt{i}\eta\omega - v_F p_\perp - \kappa \boldsymbol{p}_\parallel^2 - 2\kappa \boldsymbol{p}_\parallel \cdot \boldsymbol{k}_\parallel)} \\
&= N_f \delta_{\mathsf{ab}} \mathbb{x} \frac{|\omega| v_F}{2\pi} \int \frac{\mathrm{d}^{d-1}\boldsymbol{k}_\parallel}{(2\pi)^{d-1}} \frac{\mathtt{i}}{\mathtt{i}\eta\omega - v_F p_\perp - \kappa \boldsymbol{p}_\parallel^2 - 2\kappa \boldsymbol{p}_\parallel \cdot \boldsymbol{k}_\parallel} \\
&= N_f \delta_{\mathsf{ab}} \mathbb{x} \frac{|\omega|}{|\boldsymbol{p}_\parallel|} \frac{v_F}{8\pi\kappa} \int \frac{\mathrm{d}^{d-2}\boldsymbol{k}_\parallel}{(2\pi)^{d-2}} = N_f \delta_{\mathsf{ab}} \mathbb{x} \frac{|\omega|}{|\boldsymbol{p}_\parallel|} \frac{v_F}{8\pi\kappa} \frac{S_{d-3}}{(2\pi)^{d-2}} \Lambda^{d-2},
\end{aligned}
\tag{A.53}
$$

where $S_d = 2\pi^{\frac{d+1}{2}}/\Gamma(\frac{d+1}{2})$ is the spherical surface area. When $d = 2$, the one-loop integral is universal and independent of the UV cut off Λ. An important lesson from the above calculation is that the low-energy fermion modes only couple strongly to the boson modes $a_\perp$ with momenta $\boldsymbol{p}_\parallel$ tangent to the fermi surface. Another feature worth our attention is that the one-loop $\Sigma_\perp$ does not depend on the temporal coefficient η.

Debye screening of chromo-electric field Due to the finite density of fermions ψ, the temporal gauge fields a_τ^{a} are screened and therefore gapped. Consequently, the Chern-Simons term is irrelevant under RG, which is similar to the situation in the Halperin-Lee-Read story [88] for the half-filled Landau level problem.

Scaling analysis in patch theory Including the Landau damping term, the action of the transverse gauge boson $a_\perp$ can be written as

$$
\mathcal{S}_\perp = \frac{N_f}{2g^2} \int \frac{\mathrm{d}\omega \mathrm{d}p_\perp \mathrm{d}^{d-1}\boldsymbol{p}_\parallel}{(2\pi)^{d+1}} \left(\gamma \frac{|\omega|}{|\boldsymbol{p}_\parallel|} + |\boldsymbol{p}_\parallel|^{z_\perp - 1} + \dots \right) |a_\perp(\omega, \boldsymbol{p})|^2 + \dots \tag{A.54}
$$

where $z_\perp = 3$ is the dynamic critical exponent of $a_\perp$, and the coefficient $\gamma \sim g^2\Lambda^{d-2}v_F/\kappa$ has been introduced. We did not write down $p_\perp$-dependence, since $p_\perp$ is not as relevant as $\boldsymbol{p}_\parallel$. By power counting, we find the UV scaling dimensions

$$\Delta[a_\perp/g] = 1 + \frac{d - z_\perp}{4}, \qquad \Delta[\boldsymbol{a}_\parallel/g] = \frac{3}{2} + \frac{d - z_\perp}{4}, \qquad \Delta[c] = \frac{d+1}{4}, \tag{A.55}$$

where the scaling dimension of $\boldsymbol{a}_\parallel$ is fixed by the Coulomb gauge $\nabla_\perp a_\perp + \nabla_\parallel \cdot \boldsymbol{a}_\parallel = 0$, and $\Delta[c]$ is determined by the most relevant kinetic term $c^\dagger \nabla_\parallel^2 c$ of ghost fields. Considering the Yukawa-type boson-fermion interaction $\psi^\dagger a_\perp \psi = g\psi^\dagger(a_\perp/g)\psi$, we obtain the bare scaling dimension of the coupling g

$$\Delta[g] = 1 + 1 + \frac{d-1}{2} - 2\Delta[\psi] - \Delta[a_\perp/g] = \frac{z_\perp - d}{4} = \frac{\epsilon}{4}, \tag{A.56}$$

which is weakly relevant when $\epsilon = z_\perp - d > 0$ is small, and a perturbative RG calculation looks desirable. (In $d = 2$, $\epsilon = 1$ is not really a small number, and we may lose the analytical control.) We can easily check the scaling dimensions of gluon self-interactions and gluon-ghost interactions, e.g.,

$$\Delta[\nabla_\parallel a_\perp a_\perp a_\parallel/g^2] = 4 + \frac{\epsilon}{2}, \quad \Delta[a_\perp a_\parallel a_\perp a_\parallel/g^2] = 5 + \frac{\epsilon}{2}, \quad \Delta[c^\dagger \nabla \cdot \boldsymbol{a} c] = \frac{d+5}{2}. \tag{A.57}$$

All of them are larger than $\Delta[\mathrm{d}\tau \mathrm{d}x_\perp \mathrm{d}^{d-1}\boldsymbol{x}_\parallel] = (d+3)/2$ when $d \leq 5$, and therefore are irrelevant. In addition, one can check that the fermion-gluon interactions other than $\psi^\dagger a_\perp \psi$ are all irrelevant, e.g.,

$$\begin{aligned} &\Delta[\psi^\dagger \nabla \cdot \boldsymbol{a}\psi] = \Delta[\psi^\dagger a_\perp a_\perp \psi] = \frac{d+5}{2}, \\ &\Delta[\psi^\dagger a_\parallel \psi] = \frac{d+4}{2}, \quad \Delta[\psi^\dagger a_\parallel a_\parallel \psi] = \frac{d+7}{2}. \end{aligned} \tag{A.58}$$

Thus, we can safely ignore all of them in the perturbative RG calculation, and the total action is significantly simplified in $d = 2$

$$\begin{aligned}\mathcal{S}[\psi^\dagger, \psi, a_\perp] = &\int \mathrm{d}\tau \mathrm{d}x_\perp \mathrm{d}^{d-1}\boldsymbol{x}_\parallel \sum_{I=1}^{N_f} \psi_I^\dagger \left(\eta\partial_\tau - \mathtt{i}v_F\nabla_\perp - \kappa\boldsymbol{\nabla}_\parallel^2 + v_F \sum_{\mathsf{a}=1}^{\dim G} a_\perp^{\mathsf{a}} \mathbf{t}_{\mathsf{a}} \right) \psi_I \\ &+ \frac{N_f}{2g^2} \int \frac{\mathrm{d}\omega \mathrm{d}p_\perp \mathrm{d}^{d-1}\boldsymbol{p}_\parallel}{(2\pi)^{d+1}} \left(\gamma \frac{|\omega|}{|\boldsymbol{p}_\parallel|} + |\boldsymbol{p}_\parallel|^{z_\perp - 1} \right) \sum_{\mathsf{a}=1}^{\dim G} |a_\perp^{\mathsf{a}}(\omega, \boldsymbol{p})|^2 , \end{aligned} \tag{A.59}$$

where only Landau-damped transverse modes of chromo-magnetic field remain in the low-energy theory. The non-abelian gauge structure is effectively quasi-abelianized.

Fermion self-energy and logarithmic UV-divergence Before going to the ϵ-expansion in $2+1$ dimensions, let's evaluate the one-loop fermion self-energy with a generic value of $z_\perp$ in $d+1$ dimensions and see how the logarithmic UV-divergence shows up

$\Sigma_\psi(\mathtt{i}\omega, \boldsymbol{p}) =$ 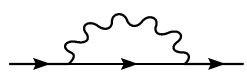

$$\begin{aligned} &= -\mathbf{t}_{\mathsf{a}}\mathbf{t}_{\mathsf{a}} v_F^2 \int \frac{\mathrm{d}\nu \mathrm{d}q_\perp \mathrm{d}^{d-1}\boldsymbol{q}_\parallel}{(2\pi)^{d+1}} \frac{g^2/N_f}{\gamma|\nu|/|\boldsymbol{q}_\parallel| + |\boldsymbol{q}_\parallel|^{z_\perp - 1}} \frac{1}{\mathtt{i}\eta(\omega+\nu) - v_F(p_\perp + q_\perp) - \kappa(\boldsymbol{p}_\parallel - \boldsymbol{q}_\parallel)^2} \\ &= \mathbf{t}_{\mathsf{a}}\mathbf{t}_{\mathsf{a}} v_F^2 \frac{g^2}{N_f} \frac{1}{\mathtt{i}2v_F} \int \frac{\mathrm{d}\nu \mathrm{d}^{d-1}\boldsymbol{q}_\parallel}{(2\pi)^d} \frac{\mathrm{sgn}(\omega+\nu)}{\gamma|\nu|/|\boldsymbol{q}_\parallel| + |\boldsymbol{q}_\parallel|^{z_\perp - 1}} \\ &= \mathbf{t}_{\mathsf{a}}\mathbf{t}_{\mathsf{a}} v_F^2 \frac{g^2}{N_f} \frac{\mathrm{sgn}(\omega)}{\mathtt{i}2\pi v_F \gamma} \int \frac{\mathrm{d}^{d-1}\boldsymbol{q}_\parallel}{(2\pi)^{d-1}} |\boldsymbol{q}_\parallel| \log(1 + \gamma|\omega|/|\boldsymbol{q}_\parallel|^{z_\perp}) \\ &= \mathbb{c}_2 \mathbf{1} \frac{S_{d-2}}{(2\pi)^{d-1}} \frac{g^2}{N_f} \frac{v_F \mathrm{sgn}(\omega)}{\mathtt{i}2\pi\gamma} \int_0^{+\infty} \mathrm{d}q q^{d-1} \log(1 + \gamma|\omega|/q^{z_\perp}) \\ &\overset{d<z_\perp}{\Longrightarrow} \mathbb{c}_2 \mathbf{1} \frac{S_{d-2}}{(2\pi)^{d-1}} \frac{g^2}{N_f} \frac{-\mathtt{i}v_F \mathrm{sgn}(\omega)\, |\omega|^{d/z_\perp}}{2\gamma^{1-d/z_\perp} d \sin(\pi d/z_\perp)} \end{aligned} \tag{A.60}$$

where the quadratic Casimir operator $\mathbf{t}_{\mathsf{a}}\mathbf{t}_{\mathsf{a}}$ is proportional to the group identity $\mathbf{1}$ with the coefficient $\mathbb{c}_2$ (e.g., $\mathbb{c}_2 = \frac{N^2-1}{2N}$ for the fundamental representation of $\mathrm{SU}(N)$). Therefore, the fermion self-energy Σ_ψ is diagonal in both color space and flavor space. Notice that the denominator vanishes $\sin(\pi d/z_\perp) \to 0$ under the limit $z_\perp \to d$, and the result becomes divergent. If we define an expansion parameter $\epsilon > 0$ by $z_\perp = d + \epsilon$, the leading order

result of fermion self-energy can be written as

$$\Sigma_\psi(\mathtt{i}\omega, \boldsymbol{p}) = -\mathtt{i}\frac{1}{N_f}\frac{g^2}{\epsilon}\frac{v_F}{\gamma^{\epsilon/d}}\frac{S_{d-2}\mathbb{C}_2\mathbf{1}}{(2\pi)^d}\mathrm{sgn}(\omega)|\omega|^{1-\epsilon/d}. \tag{A.61}$$

For a finite N_f and a small but finite ϵ, g is weakly relevant and we expect the system will flow to a perturbative NFL fixed point. The perturbation in terms of g^2 is justified by $g^2 \sim \epsilon N_f$ being small. Another observation is that the ϵ^{-1}-divergence in dimensional regularization corresponds to the logarithmic UV-divergence, which means the dynamical exponent of fermions will be renormalized and receive an ϵ-order correction. Everything seems self-consistent so far, and we are ready to consider the perturbative RG treatment.

A.3.2 Perturbative NFLs

In this section, we will closely follow Ref. [85, 354]

Wilson RG approach The single-patch theory is highly anisotropic in space, and we introduce two momentum cut-offs for the width $\Lambda_\parallel$ and the thickness $\Lambda_\perp$ respectively, such that

$$\Lambda_\parallel \ll k_F \qquad \text{and} \qquad \Lambda_\perp \sim \Lambda_\parallel^2/k_F \ll \Lambda_\parallel \ll k_F. \tag{A.62}$$

In the Wilson RG approach, we should integrate out the bosonic modes within $\Lambda_\parallel e^{-\ell/2} < |\boldsymbol{q}_\parallel| < \Lambda_\parallel$ and the fermionic modes within $\Lambda_\perp e^{-\ell} < |q_\perp| < \Lambda_\perp$, followed by the rescaling $q_\perp \to q_\perp e^\ell$ and $\boldsymbol{q}_\parallel \to \boldsymbol{q}_\parallel e^{\ell/2}$. Notice that integrating out fermionic modes on the FS is illegal, and the meaning of $\Lambda_\parallel \to \Lambda_\parallel b^{-1/2}$ for the fermion part is only a repartition of the FS into smaller patches. (In this section, we ignore the pairing instability of fermions, and we only need to worry about integrating out bosonic modes.) We also want to

mention there are at least two conventions for the RG procedure: (1) one can fix v_F and let η flow as in Ref. [85]; (2) one can also fix $\eta = 1$ and let v_F flow as in Ref. [354]. They are physically equivalent in renormalizing the fermion dynamical exponent. But the final effective Lagrangians may look different, i.e., $\mathcal{L} \sim \mathtt{i}\mathrm{sgn}(\omega)|\omega|^{1/z_\psi} - p_\perp$ and $\mathcal{L} \sim \mathtt{i}\omega - \mathrm{sgn}(p_\perp)|p_\perp|^{z_\psi}$. In this note, we choose the first RG convention.

Emergent rotational symmetry One can show the non-renormalization of the FS curvature κ (or more precisely κ/v_F, if one allows v_F to flow in another RG convention). Let's consider two base points $\boldsymbol{k}_F, \boldsymbol{k}'_F \in \mathrm{FS}$ for the same patch theory, where $|\boldsymbol{k}_F - \boldsymbol{k}'_F| < \Lambda_\parallel$. The physical momentum $\boldsymbol{K}$ of fermions has two different expansions

$$\boldsymbol{K} = \boldsymbol{k}_F + \boldsymbol{p}\,(= \boldsymbol{k}_F + p_\perp \hat{\boldsymbol{v}}_F + \boldsymbol{p}_\parallel) = \boldsymbol{k}'_F + \boldsymbol{p}'\,(= \boldsymbol{k}'_F + p'_\perp \hat{\boldsymbol{v}}'_F + \boldsymbol{p}'_\parallel). \tag{A.63}$$

Within the same patch, we can take the approximations $k_F \approx k'_F (v_F \approx v'_F)$ and $\kappa \approx \kappa'$. Then the two coordinates $(p'_\perp, \boldsymbol{p}'_\parallel)$ and $(p_\perp, \boldsymbol{p}_\parallel)$ are related by a shift of $\delta\boldsymbol{k}_F = \boldsymbol{k}'_F - \boldsymbol{k}_F$, followed by a rotation by the angle between $\hat{\boldsymbol{k}}'_F$ and $\hat{\boldsymbol{k}}_F$ (i.e., the angle between $\hat{\boldsymbol{v}}'_F$ and $\hat{\boldsymbol{v}}_F$). To leading order in $\delta\boldsymbol{k}_F$, one has

$$p'_\perp = p_\perp - \delta k_\perp + \frac{2\kappa}{v_F}\delta\boldsymbol{k}_\parallel \cdot (\boldsymbol{p}_\parallel - \delta\boldsymbol{k}_\parallel), \qquad \boldsymbol{p}'_\parallel = \boldsymbol{p}_\parallel - \delta\boldsymbol{k}_\parallel, \tag{A.64}$$

where the coordinate $(\delta k_\perp, \delta\boldsymbol{k}_\parallel)$ of $\delta\boldsymbol{k}_F$ is defined with respect to the coordinate system at $\boldsymbol{k}_F$ (i.e., $\delta\boldsymbol{k}_F = \hat{\boldsymbol{v}}_F\delta k_\perp + \delta\boldsymbol{k}_\parallel$). Since $\boldsymbol{k}'_F$ is on the FS, one must have $v_F(\delta k_\perp) + \kappa(\delta\boldsymbol{k}_\parallel)^2 = 0$. Then one can directly verify the invariant $v_F(p'_\perp) + \kappa(\boldsymbol{p}'_\parallel)^2 = v_F(p_\perp) + \kappa(\boldsymbol{p}_\parallel)^2$. We expect physical quantities are independent of which base point we choose on the FS. It leads to the noncompact rotational symmetry introduced by Ref. [50]

$$\psi(x_\perp, \boldsymbol{x}_\parallel) \to e^{-\mathtt{i}(\kappa/v_F)(2\boldsymbol{\theta}\cdot\boldsymbol{x}_\parallel + \boldsymbol{\theta}^2 x_\perp)}\psi(x_\perp, \boldsymbol{x}_\parallel + \boldsymbol{\theta}), \tag{A.65}$$

where $\boldsymbol{\theta} \in \mathbb{R}^{d-1}$ has the same scaling dimension as $\boldsymbol{p}_{\parallel}$. If one believe the rotational symmetry is preserved under RG, then the FS curvature κ/v_F can not be renormalized.

Wave-function renormalization In $d = 2$, the one-loop fermion self-energy is

$$\Sigma_\psi(\mathtt{i}\omega, \boldsymbol{p}) =$$

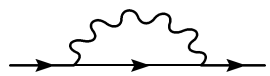

$$\begin{aligned} &= \mathbb{c}_2 \frac{\Omega_{d-2}}{(2\pi)^{d-1}} \frac{g^2}{N_f} \frac{v_F \mathrm{sgn}(\omega)}{\mathtt{i}2\pi\gamma} \int_{\Lambda_\parallel e^{-\ell/2}}^{\Lambda_\parallel} \mathrm{d}q q^{d-1} \log(1 + \gamma|\omega|/q^{d+\epsilon}) \\ &= -\mathtt{i}\omega \frac{g^2}{N_f} \frac{v_F \mathbb{c}_2}{4\pi^2} \ell + \Lambda_\parallel\text{-dependent terms} + \mathcal{O}(\epsilon^2), \end{aligned} \tag{A.66}$$

where $\mathbb{c}_2$ denotes the quadratic Casimir in the gauge theory. We have only kept the leading order terms in small-ϵ expansion, and we checked that $\Lambda_\parallel$-dependent terms vanish under the limit $\Lambda_\parallel \to +\infty$. Notice that the result of Σ_ψ is consistent with Eq. A.61 under the limit $d \to 2, \epsilon \to 0^+$, where $1/\epsilon$ in the dimensional regularization scheme corresponds to $\ell/2$ in the momentum cut-off scheme. To significantly simplify the notation in the scaling analysis, we introduce a constant Υ by

$$\Sigma_\psi(\mathtt{i}\omega, \boldsymbol{p}) = -\mathtt{i}\omega g^2 \Upsilon \ell + \ldots, \qquad \text{where} \qquad \Upsilon = \frac{v_F \mathbb{c}_2}{4\pi^2 N_f}. \tag{A.67}$$

Vertex correction In addition, one can show the vertex correction vanishes [85]

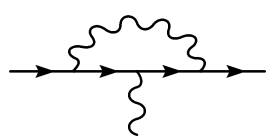

$$= 0. \tag{A.68}$$

RG flow of gauge coupling Due to the logarithmically divergent fermion self-energy, the ω-dependence in the fermion propagator changes to $\omega' = \omega b^{1+g^2\Upsilon}$. In other word, the

spacetime scalings are modified as

$$\tau' = \tau b^{-z_\psi} = \tau b^{-(1+g^2\Upsilon)}, \qquad x'_\perp = x_\perp b^{-1}, \qquad \boldsymbol{x}'_\parallel = \boldsymbol{x}_\parallel b^{-1/2}, \tag{A.69}$$

where $z_\psi = 1+g^2\Upsilon$ is the fermion dynamical exponent. At the potential new fixed point, we have the scaling dimensions of fermions and bosons in $d = 2$

$$\begin{aligned} \Delta[\psi] &= \frac{d-1+2z_\psi}{4} = \frac{d+1+2g^2\Upsilon}{4}, \\ \Delta[a_\perp/g] &= \frac{d+2+2z_\psi - z_\perp}{4} = \frac{d+4+2g^2\Upsilon - z_\perp}{4}. \end{aligned} \tag{A.70}$$

To be consistent with the gauge covariant derivative reads $D_\perp = \partial_\perp - \mathtt{i}a_\perp$, the scaling dimension $\Delta[a_\perp] = \Delta[x_\perp] = 1$ is fixed. The scaling dimension of g is therefore $\Delta[g] = (z_\perp - d - 2g^2\Upsilon)/4 = (\epsilon - 2g^2\Upsilon)/4$, which gives the beta function of g^2

$$\frac{\mathrm{d}g^2}{\mathrm{d}\ell} = \frac{\epsilon}{2}g^2 - \Upsilon g^4 = \frac{\epsilon}{2}g^2 - \frac{v_F\mathbb{C}_2}{4\pi^2 N_f}g^4. \tag{A.71}$$

Thus, we indeed self-consistently find a new fixed point at weak coupling

$$g_*^2 = \frac{\epsilon}{2\Upsilon} = \frac{2\pi^2 N_f \epsilon}{v_F\mathbb{C}_2}. \tag{A.72}$$

NFL fixed-point propagators Notice that η also need to rescale under RG, which gives $\frac{\mathrm{d}\eta}{\mathrm{d}\ell} = \eta g^2\Upsilon$. Combining the two beta functions, we have $\frac{\mathrm{d}(\eta g^2)}{\mathrm{d}\ell} = \frac{\epsilon}{2}\eta g^2$. Thus we arrive at a simple rescaling relation $\eta(\ell)g^2(\ell) = \eta(0)g^2(0)e^{\ell\epsilon/2}$, that can be used to find the fixed point value of η, where $g^2(0)$ and $\eta(0)$ are bare values in the UV. As in Ref.

[85], if we set $e^\ell \sim \Lambda^2/\omega$ for the perturbative fixed point, we ought to have the IR value

$$\begin{aligned} \eta_* &= \frac{g^2(0)}{g_*^2}\frac{\Lambda^\epsilon}{|\omega|^{\epsilon/2}} = \frac{2\Upsilon g^2(0)}{\epsilon}|\omega|^{-\epsilon/2} \\ \Longrightarrow \quad -\mathtt{i}\eta_*\omega &= -\mathtt{i}\frac{1}{N_f}\frac{g^2(0)}{\epsilon}\frac{v_F\mathbb{C}_2}{2\pi^2}\mathrm{sgn}(\omega)|\omega|^{1-\epsilon/2}, \end{aligned} \tag{A.73}$$

where the factor $\Lambda^\epsilon = 1 + \epsilon\log\Lambda + \ldots$ is only kept to leading order. We can see $-\mathtt{i}\eta_*\omega$ indeed reproduces the result of fermion self-energy Eq. A.61 under $d \to 2$ and $\gamma^{\epsilon/d} \to 1$ (to leading order). Replacing the bare coupling constant $g^2(0)$ by the fixed-point value g_*^2, we have the boson and fermion propagators at the NFL fixed point

$$\begin{aligned} G_\perp(\mathtt{i}\omega, \boldsymbol{p}) &= \frac{g_*^2}{N_f}\frac{1}{\gamma_*|\omega|/|p_\parallel| + |p_\parallel|^{1+\epsilon}}, \\ G_\psi(\mathtt{i}\omega, \boldsymbol{p}) &= \frac{1}{\mathtt{i}\mathrm{sgn}(\omega)|\omega|^{1-\epsilon/2} - v_F p_\perp - \kappa p_\parallel^2}, \end{aligned} \tag{A.74}$$

where $g_*^2 \sim N_f\epsilon/v_F$ and $\gamma_* \sim g_*^2 v_F/\kappa \sim N_f\epsilon/\kappa$.

Remark on spacetime scaling Let us summarize some technical details. The fermion dynamical exponent is renormalized by logarithmic UV-divergence, while the boson dynamical exponent is not renormalized (which is common for nonlocal/singular propagators). The spacetime scaling in the patch theory is determined by the fermion part.

Generalization to multiple gauge coupling constants So far, the calculation applies to the $G = \mathrm{SU}(N)$ gauge group. The generalization for other gauge groups should be straightforward. Namely, one could consider $G = \mathrm{SU}(N)\times\mathrm{SU}(M)$ or $G = \mathrm{U}(N)$ which has a U(1) part and a SU(N) part. In general, we assume the total gauge group is

$$G = \bigotimes_A G_A \tag{A.75}$$

and the coupling constant for G_A-gauge field is g_A. Each gauge field has a contribution in the wave-function renormalization of the fermion dynamical exponent z_ψ. In total, we have

$$z_\psi = 1 + \sum_A \Bigg[\quad \Bigg]_A = 1 + \sum_A g_A^2 \Upsilon^A, \quad \Upsilon^A = \frac{v_F \mathbb{c}_2(G_A)}{4\pi^2 N_f}, \tag{A.76}$$

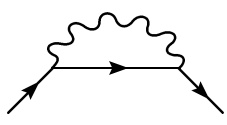

where $\mathbb{c}_2(G_A)$ denotes the quadratic Casimir in the representation of G_A. Suppose all the gauge fields share the same dynamical exponent $z_\perp$, then they also have the same scaling dimension at the potential new fixed point

$$\Delta[g_A] = \frac{(z_\perp - d) - 2(z_\psi - 1)}{4} = \frac{\epsilon - 2\sum_B \Upsilon^B g_B^2}{4}, \tag{A.77}$$

which leads to the coupled RG flow of all gauge coupling constants g_A^2

$$\frac{dg_A^2}{d\log b} = \frac{\epsilon}{2} g_A^2 - \sum_B \Upsilon^B g_B^2 g_A^2. \tag{A.78}$$

We self-consistently find a nontrivial IR fixed-hyperplane at weak coupling

$$\sum_A \Upsilon^A g_A^2 = \sum_A \frac{v_F \mathbb{c}_2(G_A)}{4\pi^2 N_f} g_A^2 = \frac{\epsilon}{2}. \tag{A.79}$$

The ratio between any two gauge couplings g_A and g_B is RG invariant, which is simply due to $\Delta[g_A] = \Delta[g_B]$. The particular examples of $G = \mathrm{U}(1) \times \mathrm{U}(1)$ and $G = \mathrm{U}(2)$ have been discussed in Ref. [89].

A.4 Explicit and Inexplicit Symmetries

The purpose of this appendix [2] is to clarify the rudimentary concepts used in this dissertation. The standard definition of a global symmetry of a quantum system is associated with a global conserved quantity $\hat{G}$ that commutes with the entire Hamiltonian of the system. Normally when we say a system has a global symmetry, it implies the following two qualities of the system:

(1) the dynamics allowed by the symmetry, for example the evolution generated by the Hamiltonian of the system does not change the quantum number of quantity $\hat{G}$;

(2) states with different quantum numbers of $\hat{G}$ are all present in the Hilbert space.

To exemplify these two qualities, let us still start with the basic example of transverse-field Ising chain: $H = \sum_j -K\sigma_j^z\sigma_{j+1}^z - h\sigma_j^x$. Here the conserved quantity of the $\mathbb{Z}_2$ Ising spin symmetry is $\hat{G} = \prod_j \sigma_j^x$, and any physical process allowed by the symmetry does not change the quantum number of $\hat{G}$ (only processes that flip even number of spins σ_j^x are allowed); but states with $\hat{G} = \pm 1$ all exist in the Hilbert space. Hence both qualities *(1)* and *(2)* mentioned above are perfectly satisfied by the $\mathbb{Z}_2$ spin symmetry.

It is often stated that the transverse-field Ising chain is "self-dual" under the Kramers-Wannier duality, namely if we introduce dual operators $\tau_{\tilde{j}}^{z,x}$ as $\sigma_j^z\sigma_{j+1}^z = \tau_{\tilde{j}}^x$, $\sigma_j^x = \tau_{\tilde{j}-1}^z\tau_{\tilde{j}}^z$, the Hamiltonian of the dual model formally takes the form $H = \sum_{\tilde{j}} -K\tau_{\tilde{j}}^x - h\tau_{\tilde{j}}^z\tau_{\tilde{j}+1}^z$. Physically τ^x is the kink of the original operator σ^z. There appears to be another dual $\tilde{\mathbb{Z}}_2$ symmetry, whose conserved quantity $\tilde{\hat{G}}$ is formally $\prod_{\tilde{j}} \tau_{\tilde{j}}^x$. However, if we take a periodic boundary condition of the original quantum Ising model, $\tilde{\hat{G}}$ is a trivial quantity in the original Ising spin Hilbert space, because $\tilde{\hat{G}}$ always equals to $+1$, or in other words within the original Ising spin Hilbert space, only states with even number of kinks are allowed. Hence although the "$\tilde{\mathbb{Z}}_2$ symmetry" satisfies quality *(1)* above, it does NOT meet *(2)*.

[2] The appendix has previously published (on 18 August 2021) in SciPost Phys. 11, 033 (2021).

The dual "$\tilde{\mathbb{Z}}_2$ symmetry", though does not meet quality *(2)*, still leads to nontrivial conservation law of kinks of σ^z: the kink number is unchanged under any physical process for the Ising model with periodic boundary condition. As was pointed out by previous references such as Ref. 118, both the $\mathbb{Z}_2$ and $\tilde{\mathbb{Z}}_2$ can be made real symmetries (meaning they both satisfy qualities *(1)* and *(2)*) if we embed the $1d$ quantum Ising model as the boundary of a $2d$ toric code model (of course, there were other previously known ways such as introducing different boundary conditions to interpret the $\tilde{\mathbb{Z}}_2$ symmetry, but introducing the bulk as Ref. 118 has the most natural generalizations to higher dimensions and higher form dimensions). The Ising spin excitation corresponds to the e anyon of the toric code, and the kink corresponds to the m anyon. The two sets of conservation laws (quality *(1)*) of the Ising spins and kinks arise from the fusion rules of the anyons: $e \times e = 1$, $m \times m = 1$; now both the $\mathbb{Z}_2$ and $\tilde{\mathbb{Z}}_2$ symmetries also satisfy quality *(2)*: both the Ising spin number and the kink number can be either even or odd at the $1d$ boundary, because one can create a pair of e (or m) anyons, and move only one anyon of the pair to the $1d$ boundary.

Since the original quantum Ising model has conservation laws for dynamics of both the Ising spins and the kinks, in our main text we call the original $\mathbb{Z}_2$ spin symmetry of the quantum Ising model as an explicit symmetry (meaning quality *(1)* and *(2)* are both satisfied), while the $\tilde{\mathbb{Z}}_2$ symmetry is called an "inexplicit symmetry", as only quality *(1)* is satisfied. As we mentioned in the last paragraph, both $\mathbb{Z}_2$ and $\tilde{\mathbb{Z}}_2$ symmetries can be made explicit by embedding the system to the boundary of a $2d$ toric code model.

These definitions and notions can be generalized to higher dimensions with higher form discrete symmetries. As a practice let us also consider the $2d$ quantum $\mathbb{Z}_2$ gauge theory, which is often stated to be dual to a $2d$ quantum Ising model, though these two models have different symmetries. To clarify what this duality means exactly, we consider the standard Hamiltonian for the $2d$ quantum $\mathbb{Z}_2$ gauge theory on a $2d$ torus:

$H = \sum_{\square} -K \prod_{\langle ij\rangle \in \square} \sigma^z_{ij} - \sum_{\langle ij\rangle} h\sigma^x_{ij}$, where $\langle ij\rangle$ is a link of a square lattice; $\sigma^{z,x}_{ij}$ is a qubit defined on the link. $\prod_{\langle ij\rangle \in \square} \sigma^z_{ij}$ is a product of σ^z_{ij} on the four links around each square plaquette. The Hilbert space of the quantum $\mathbb{Z}_2$ gauge theory is subject to a local constraint $\prod_{\langle ij\rangle \in v} \sigma^x_{ij} = +1$, where $\langle ij\rangle \in v$ represent four links around a vertex/site of the square lattice. This model has a $\mathbb{Z}_2^{(1)}$ 1-form symmetry, which corresponds to the $\mathbb{Z}_2$ conservation of $\mathbb{Z}_2$ electric field penetrating any contractible loop $\mathcal{C}$: $\hat{G}_{\mathcal{C}} = \prod_{\langle ij\rangle \perp \mathcal{C}} \sigma^x_{ij}$ ($\langle ij\rangle \perp \mathcal{C}$ corresponds to all the links on loop $\mathcal{C}$ and orthogonal to $\mathcal{C}$ locally). But if the system is a torus, then $\hat{G}_{\mathcal{C}}$ for a noncontractible loop $\mathcal{C}$ can take values ± 1, which can be interpreted as either the topological sector, or the ground state degeneracy of spontaneous breaking of the $\mathbb{Z}_2^{(1)}$ 1-form symmetry. Hence the $\mathbb{Z}_2^{(1)}$ 1-form symmetry is an explicit symmetry that satisfies both *(1)* and *(2)* mentioned previously.

The dual $2d$ quantum Ising model can be formally derived by introducing the dual operators on the dual lattice sites $\bar{i}$ and $\bar{j}$, which are located on the center of the plaquette squares of the original square lattice: $\tau^x_{\bar{i}} = \prod_{\langle ij\rangle \text{around } \bar{i}} \sigma^z_{ij}$, $\tau^z_{\bar{i}}\tau^z_{\bar{j}} = \sigma^x_{ij}$ for $\langle \bar{i}\bar{j}\rangle \perp \langle ij\rangle$. The dual Hamiltonian reads $H = \sum_{\bar{i}} -K\tau^x_{\bar{i}} - \sum_{\langle \bar{i}\bar{j}\rangle} h\tau^z_{\bar{i}}\tau^z_{\bar{j}}$. However, the conserved quantity of the dual Ising model $\tilde{\hat{G}} = \prod_{\bar{i}} \tau^x_{\bar{i}}$ is always $+1$ in the original Hilbert space of the $\mathbb{Z}_2$ gauge theory, although a physical process can only create even number of $\tau^x_{\bar{i}}$ (which corresponds to the m anyon of the original quantum $\mathbb{Z}_2$ gauge theory) hence there is a $\mathbb{Z}_2$ conservation of τ^x. Therefore the dual Ising model has a $\tilde{\mathbb{Z}}_2$ symmetry that satisfies quality *(1)* but not *(2)*, hence according to our convention it is an inexplicit symmetry.

Let us also discuss the converse example, and start with a real $2d$ quantum Ising spin model on a square lattice: $H = \sum_{\langle i,j\rangle} -K\sigma^z_i\sigma^z_j - \sum_j h\sigma^x_j$, which is formally dual to a $2d$ quantum $\mathbb{Z}_2$ gauge theory, with the electric field defined on the dual link $\langle \bar{i}\bar{j}\rangle \perp \langle ij\rangle$ as $\tau^x_{\bar{i}\bar{j}} = \sigma^z_i\sigma^z_j$. The $2d$ quantum Ising model also has two sets of conservation laws: the conservation of the original Ising spin, and the conservation law of the Ising domain walls. The latter corresponds to a $\tilde{\mathbb{Z}}_2^{(1)}$ 1-form "inexplicit symmetry": there is a conservation

law of the dynamics of Ising domain wall, namely the Ising domain walls always penetrate any closed contractible loop even times (quality *(1)*); but within the Ising spin Hilbert space the product of $\tau^x_{\bar{ij}} = \sigma^z_i \sigma^z_j$ with $\langle ij \rangle \perp \langle \bar{i}\bar{j} \rangle$ is always $+1$ along a noncontractible cycle $\mathcal{C}$ orthogonal to the dual lattice link $\langle \bar{i}\bar{j} \rangle$. But for a real $2d$ $\mathbb{Z}_2$ gauge theory, as we discussed above, the corresponding product of electric field can take value ± 1, which can be either interpreted as different topological sectors, or as ground state degeneracy caused by spontaneous breaking of the $\mathbb{Z}_2^{(1)}$ 1-form symmetry. Hence in the Ising spin Hilbert space, only the $\mathbb{Z}_2$ symmetry satisfies qualities *(1)* and *(2)* together, while $\tilde{\mathbb{Z}}_2^{(1)}$ satisfies *(1)* only. But both $\mathbb{Z}_2$ and $\tilde{\mathbb{Z}}_2^{(1)}$ can be made explicit symmetries, i.e. they can satisfy both *(1)* and *(2)* when the quantum Ising model is embedded as the boundary of a $3d$ topological order.

The quantity order diagnosis operator (ODO) was introduced in Ref. 121 to characterize the behavior of the explicit and inexplicit symmetries, especially the notion of spontaneous symmetry breaking of both the explicit and the inexplicit symmetries defined above. The ODO reduces to previously introduced concepts in specific cases. For example, for the Ising models, the ODO of the dual inexplicit symmetry is the disorder operator discussed in Ref. 564. But the phrase "disorder operator" implies that when it condenses, the original symmetry would be restored or the system should enter a disordered phase of the original symmetry. This is indeed true for the Ising spin models. But in some cases that involve higher form symmetries both the symmetry and the dual symmetry can be spontaneously broken simultaneously, namely both the explicit symmetry and its dual inexplicit symmetry can enter the ordered phase simultaneously under proper generalizations. For example, a $3d$ system with $\mathbb{Z}_2^{(1)}$ 1-form symmetry can enter a gapless photon phase where the Wilson loop and the corresponding "disorder operator" of the $\mathbb{Z}_2^{(1)}$ 1-form symmetry both have perimeter laws, which is the criterion of spontaneous symmetry breaking of 1-form symmetries. Hence we feel a generalized

notion is necessary. In fact, a notion of "patch operator" was introduced in Ref. 118 as a generalization of the the disorder operator to higher form symmetries. The notion of order diagnosis operator used in this manuscript also reduces to the "patch operator" in Ref. 118 for systems without subsystem symmetries. But for systems with a more exotic subsystem symmetries [121] the proper form of the ODO is not always defined on a simple patch of the lattice.

Appendix B

Appendix to Chapter 3,4,5 (Main Text)

B.1 Appendix to Sec. 3.1

B.1.1 Exchange Energy of Two-Particle Wave Functions

Let us evaluate the exchange energy of two-particle wave functions in more detail in this appendix. The wave function $\Psi_A(\mathbf{x}_1, \mathbf{x}_2)$ considered in the main tex has the interaction energy

$$E_{int} \sim \int d\mathbf{x}_1 d\mathbf{x}_2 \Psi_A^*(\mathbf{x}_1, \mathbf{x}_2) V_{\mathbf{x}_1,\mathbf{x}_2} \Psi_A(\mathbf{x}_1, \mathbf{x}_2) = E_0 + E_{ex}, \tag{B.1}$$

where $V_{\mathbf{x}_1,\mathbf{x}_2}$ is the (screened) Coulomb interaction. Both integrals $\int d\mathbf{x}_1$, $\int d\mathbf{x}_2$ are performed in the $2d$ space.

$$E_0 = \int d\mathbf{x}_1 d\mathbf{x}_2 |\varphi_{L,1}(\mathbf{x}_1)|^2 |\varphi_{R,2}(\mathbf{x}_2)|^2 V_{\mathbf{x}_1,\mathbf{x}_2} + \cdots \tag{B.2}$$

E_{ex} is the exchange energy, and it involves six integrals

$$
\begin{aligned}
I_{ex,1} &\sim -\int d\mathbf{x}_1 d\mathbf{x}_2 \varphi^*_{L,1}(\mathbf{x}_1)\varphi_{L,2}(\mathbf{x}_1)V_{\mathbf{x}_1,\mathbf{x}_2}\varphi^*_{R,2}(\mathbf{x}_2)\varphi_{R,1}(\mathbf{x}_2) + c.c, \\
I_{ex,2} &\sim +\int d\mathbf{x}_1 d\mathbf{x}_2 \varphi^*_{L,1}(\mathbf{x}_1)\varphi_{R,1}(\mathbf{x}_1)V_{\mathbf{x}_1,\mathbf{x}_2}\varphi^*_{R,2}(\mathbf{x}_2)\varphi_{L,2}(\mathbf{x}_2) + c.c, \\
I_{ex,3} &\sim -\int d\mathbf{x}_1 d\mathbf{x}_2 \varphi^*_{L,1}(\mathbf{x}_1)\varphi_{R,2}(\mathbf{x}_1)V_{\mathbf{x}_1,\mathbf{x}_2}\varphi^*_{R,2}(\mathbf{x}_2)\varphi_{L,1}(\mathbf{x}_2) + c.c, \\
I_{ex,4} &\sim -\int d\mathbf{x}_1 d\mathbf{x}_2 \varphi^*_{L,2}(\mathbf{x}_1)\varphi_{R,1}(\mathbf{x}_1)V_{\mathbf{x}_1,\mathbf{x}_2}\varphi^*_{R,1}(\mathbf{x}_2)\varphi_{L,2}(\mathbf{x}_2) + c.c, \\
I_{ex,5} &\sim +\int d\mathbf{x}_1 d\mathbf{x}_2 \varphi^*_{L,2}(\mathbf{x}_1)\varphi_{R,2}(\mathbf{x}_1)V_{\mathbf{x}_1,\mathbf{x}_2}\varphi^*_{R,1}(\mathbf{x}_2)\varphi_{L,1}(\mathbf{x}_2) + c.c, \\
I_{ex,6} &\sim -\int d\mathbf{x}_1 d\mathbf{x}_2 \varphi^*_{R,1}(\mathbf{x}_1)\varphi_{R,2}(\mathbf{x}_1)V_{\mathbf{x}_1,\mathbf{x}_2}\varphi^*_{L,2}(\mathbf{x}_2)\varphi_{L,1}(\mathbf{x}_2 + c.c, \\
E_{ex} &= \sum_{i=1}^{6} I_{ex,i}.
\end{aligned}
\tag{B.3}
$$

The single-particle wave functions are roughly (for example) $\varphi_{L,1}(\mathbf{x}) \sim \exp(iK_1 x)F_{L,1}(y)$, etc. where $F_{L,1}(y)$ is an envelop function of the coordinate y orthogonal to the wire, and localized at the wire. $F_{L,1}(y)$ should carry an approximately conserved large momentum, which inherits from the crystal momentum of one of the two valleys, assuming the domain wall is smooth enough compared with the lattice scale. In all these exchange energy integrals, $I_{ex,2-5}$ are expected to be considerably smaller than $I_{ex,1}$ and $I_{ex,6}$, because they involve large momentum transfer, *i.e.* integrals like $\int d\mathbf{x}_1 \varphi^*_{L,1}(\mathbf{x}_1)\varphi_{R,1}(\mathbf{x}_1)$, These integrals are highly suppressed because $\varphi_{L,1}(\mathbf{x}_1)$ and $\varphi_{R,1}(\mathbf{x}_1)$ come from two valleys in the original honeycomb lattice, the two valleys have very large momentum difference.

$I_{ex,1} + I_{ex,6}$ is the main exchange energy gained by Ψ_A, both integrals do not involve large momentum transfer, and they both conserve the total momentum along the wire (time-reversal symmetry guarantees that $K_1 = -K_2'$, $K_2 = -K_1'$), assuming we focus on a single wire without junction. With the Coulomb interaction, or the standard form of screened Coulomb interaction, $I_{ex,1} + I_{ex,6}$ is negative. The exchange energy of Ψ_B is very

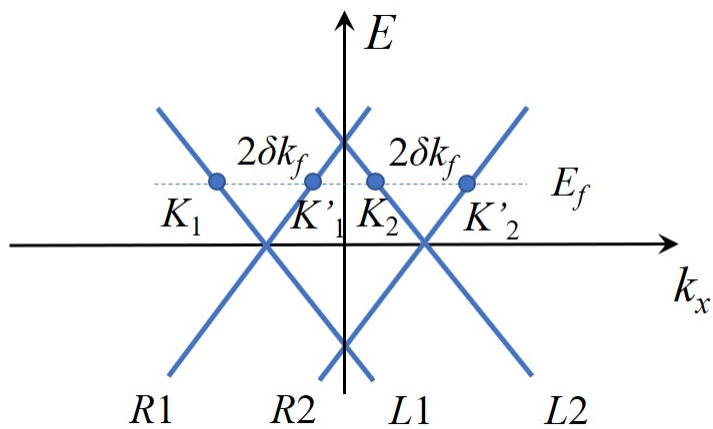

Figure B.1: Schematic dispersion of the $1d$ domain wall states after doping. K_1 and K_2 come from the same valley $\mathbf{Q}$ in the $2d$ Brillouin zone. Time-reversal symmetry guarantees that $K_1 = -K_2'$, $K_2 = -K_1'$.

similar, and both wave functions are "channel" singlet states.

One can also run the same test on other two-particle wave functions which are symmetric in the channel space, such as

$$\begin{aligned}
\Psi_C(\mathbf{x}_1,\mathbf{x}_2) &\sim \varphi_{L,1}(\mathbf{x}_1)\varphi_{R,2}(\mathbf{x}_2) + \varphi_{L,2}(\mathbf{x}_1)\varphi_{R,1}(\mathbf{x}_2) - \varphi_{R,1}(\mathbf{x}_1)\varphi_{L,2}(\mathbf{x}_2) - \varphi_{R,2}(\mathbf{x}_1)\varphi_{L,1}(\mathbf{x}_2),\\
\Psi_D(\mathbf{x}_1,\mathbf{x}_2) &\sim \varphi_{L,1}(\mathbf{x}_1)\varphi_{R,1}(\mathbf{x}_2) - \varphi_{L,2}(\mathbf{x}_1)\varphi_{R,2}(\mathbf{x}_2) + \varphi_{R,1}(\mathbf{x}_1)\varphi_{L,1}(\mathbf{x}_2) - \varphi_{R,2}(\mathbf{x}_1)\varphi_{L,2}(\mathbf{x}_2),\\
&\ldots\ldots
\end{aligned} \tag{B.4}$$

None of these wave functions gain as much exchange energy compared with Ψ_A and Ψ_B, because their exchange energy integrals either involve large momentum transfer, or violate total momentum conservation along the wire. For example, for $\Psi_D(\mathbf{x}_1,\mathbf{x}_2)$, its exchange energy contains terms like

$$-\int d\mathbf{x}_1 d\mathbf{x}_2 \varphi^*_{L,1}(\mathbf{x}_1)\varphi_{L,2}(\mathbf{x}_1) V_{\mathbf{x}_1,\mathbf{x}_2} \varphi^*_{R,1}(\mathbf{x}_2)\varphi_{R,2}(\mathbf{x}_2), \tag{B.5}$$

this integral represents the physical process of moving two particles at momenta K_2 and

K_2' to momenta K_1 and K_1' (Fig. B.1), which is suppressed because in general it violates total momentum conservation along the wire. This total momentum conservation can be viewed as a $U(1)$ symmetry in the channel space, *i.e.* $N_{L,1} + N_{R,1} - N_{L,2} - N_{R,2}$ must be a conserved quantity, where (for example) $N_{L,1}$ is the number of left moving particles at channel 1.

B.1.2 Fermion Bilinears as CFT Fields

In the main text, we obtain the CFT field expressions of the fermion mass operator Eq. 5 using the non-Abelian bosonization of $U(4)_1$ and the decomposition $U(4)_1 \sim U(1)_4 \otimes SU(2)_2^s \otimes SU(2)_2^c$. For the Cooper pair operator Eq. 6, we first define a new basis of fermions such that the Cooper pair operator acts as a fermion mass operator in the new basis. Then, we conduct a similar non-Abelian bosonization and the decomposition of $U(4)_1$ to obtain its CFT field expression. In this section, we study a different method to obtain the CFT field expressions of the fermion mass operator and the Cooper pair operator while treating them in equal footing.

We first rewrite the left/right-moving complex fermions $\psi_{L,c,\alpha}$, $\psi^\dagger_{L,c,\alpha}$, $\psi_{R,c,\alpha}$, and $\psi^\dagger_{R,c,\alpha}$ in a Majorana fermion basis $\chi_{L/R}$ where each of χ_L and χ_R is an 8-component Majorana spinor. The Majorana fermion basis is chosen such that the generators of the symmetries $U(1)^e$, $SU(2)^s$ and $SU(2)^c$ are given by

$$\begin{aligned} U(1)^e &: \sigma^{y00}, \\ SU(2)^s &: \sigma^{0xy},\ \sigma^{0zy},\ \sigma^{0y0}, \\ SU(2)^c &: \sigma^{0yx},\ \sigma^{0yz},\ \sigma^{00y}, \end{aligned} \tag{B.6}$$

where $\sigma^{x,y,z}$ are the Pauli matrices and σ^0 is the 2×2 identity matrix. Here, we've adopted

the notation $\sigma^{abc\cdots} \equiv \sigma^a \otimes \sigma^b \otimes \sigma^c \otimes \ldots$. The left and right-moving Majorana fermions can be described by the $O(8)_1$ CFT. More precisely, we can bosonize these Majorana femions and describe them using a non-linear sigma model with the group $O(8)$ and with a Wess-Zumino-Witten term at level 1. Following the non-Abelian bosonization procedure given by Ref. 565, we can identify the fermion bilinears $\chi_L \chi_R^T$ with the field $h \in O(8)$ of the non-linear sigma model. The fermion mass operator in Eq. 5 and the Cooper pair operator Eq. 6 are included in $\chi_L \chi_R^T$ and hence can be expressed in terms of $h \in O(8)$ when bosonized. In the following, we will study the specific form of field $h \in O(8)$ which represents the fermion mass and the Cooper pair operators.

First of all, both of the fermion mass and the Cooper pair operators are $SU(2)^c$ singlets. Hence, we focus only on the field $h \in O(8)$ such that h commutes with the $SU(2)^c$ generators given in Eq. B.6. The field h that satisfy this condition takes the general form

$$h = W(\tilde{h} \otimes \sigma^0)W^\dagger \tag{B.7}$$

where $W = \frac{1}{\sqrt{2}}(1 + i\sigma^{0yy})$ and $\tilde{h}$ is a 4×4 matrix. Since $h \in O(8)$, h has to be a real matrix, which implies

$$\sigma^{0y}\tilde{h}\sigma^{0y} = \tilde{h}^*. \tag{B.8}$$

This condition implies that $\tilde{h}$ decompose into a linear superposition of the following basis

matrices with real coefficients:

$$\begin{aligned}
&\sigma^{00},\ i\sigma^{0x},\ i\sigma^{0y},\ i\sigma^{0z}\\
&i\sigma^{y0},\ \sigma^{yx},\ \sigma^{yy},\ \sigma^{yz}\\
&\sigma^{x0},\ i\sigma^{xx},\ i\sigma^{xy},\ i\sigma^{xz}\\
&\sigma^{z0},\ i\sigma^{zx},\ i\sigma^{zy},\ i\sigma^{zz}.
\end{aligned} \tag{B.9}$$

Both the fermion mass and the Cooper pair operators transform non-trivially under the left and right $U(1)^e$ and $SU(2)^s$ actions. For the field h, the left and right $U(1)^e$ and $SU(2)^s$ actions are given by the left and right multiplication of $U(1)^e$ and $SU(2)^s$ matrices generated the generators given in Eq. B.6. Hence, we should organize the basis of $\tilde{h}$ such that h transforms properly under the left and right $U(1)^e$ and $SU(2)^s$ actions:

$$\tilde{h} = \alpha(\cos\phi + i\sin\phi\sigma^y)\otimes g + \beta(\cos\theta\sigma^x + \sin\theta\sigma^z)\otimes g', \tag{B.10}$$

where α, β are real number, ϕ and θ are two angular variables, and $g, g' \in SU(2)$ are 2×2 $SU(2)$ matrices. Note that $\tilde{h}$ contains two terms. Their transformations under the left and right $U(1)^e$ symmetries allow us to identify them as the fermion mass operator and the Cooper pair operators respectively. The angular variables ϕ and θ are then naturally identify with the ϕ and θ fields of the $U(1)^e_4$ CFT fields discussed in the main text. Finally, we need to consider the constrain of $h^T h = 1$ on $\tilde{h}$:

$$\alpha^2 + \beta^2 = 1, \qquad gg' = g'g. \tag{B.11}$$

To treat the fermion mass operator and the Cooper pair operator in equal footing, we should choose $\alpha = \beta = \frac{1}{\sqrt{2}}$. The second equation is naturally satisfy by setting $g = g' \in$

$SU(2)$. Now, we can conclude that the most generic form of $\tilde{h}$ that captures the fermion mass operators and Cooper pair operators in equal footing is given by

$$\tilde{h} = \frac{1}{\sqrt{2}}(\cos\phi + i\sin\phi\sigma^y) \otimes g + \frac{1}{\sqrt{2}}(\cos\theta\sigma^x + \sin\theta\sigma^z) \otimes g. \tag{B.12}$$

Using this form of $\tilde{h}$, we can obtain the expression of h. We can furthermore transform the basis from $\chi_{L/R}$ back to the complex fermions $\psi_{L,c,\alpha}$, $\psi^\dagger_{L,c,\alpha}$, $\psi_{R,c,\alpha}$. After the basis transformation, we see that the two terms in h (that comes from the two terms in $\tilde{h}$) agree respectively with the CFT field expressions of the fermion mass operator Eq. 5 and of the Cooper pair operator Eq. 6 in the main text.

B.2 Appendix to Sec. 3.2

B.2.1 Field Theories for $N = 6$ and $N = 12$ of Scenario (1)

In the next section we will derive the projective symmetry group transformation for the low energy vortex modes of scenario (1). For $N = 6$, with symmetries $R_{2\pi/3}$, translation, $P_x\mathcal{T}$, and P_y, the PSG-invariant interactions between the vortex fields ψ_a beyond Eq. 3.19 take the following form:

$$\begin{aligned}
\mathcal{L}^{(1)\prime}[\psi_a] &= u_1 \sum_{a=0}^{2}(|\psi_{2a}|^2 + |\psi_{2a+1}|^2)^2 + u_2 \left(\sum_{a=0}^{5}|\psi_a|^2\right)^2 \\
&+ v_1 \left(\sum_{a=0}^{5}\psi_a^2\right)\left(\sum_{a=0}^{5}(\psi_a^*)^2\right) + v_2 \sum_{a=0}^{2}(\psi_{2a}^2 + \psi_{2a+1}^2)((\psi_{2a}^*)^2 + (\psi_{2a+1}^*)^2) \\
&+ w_1 \sum_{a=0}^{2}(|\psi_{2a}|^2 - |\psi_{2a+1}|^2)(\psi_{2a+2}\psi_{2a+3}^* + \psi_{2a+2}^*\psi_{2a+3}) \\
&+ w_2 \left(\sum_{a=0}^{2}(\psi_{2a}^2 - \psi_{2a+1}^2)\psi_{2a+2}^*\psi_{2a+3}^* + c.c.\right) + \dots
\end{aligned} \tag{B.13}$$

Here the dots stand for terms higher than the quartic order. The parameters $\{u_1, u_2, v_1, v_2, w_1, w_2\}$ in (B.13) are all real, and the index a for ψ_a is regarded as cyclic modulo 6.

In addition to the quartic terms, the gauge invariant density wave order parameter can couple to the Fermi surface of the fermionic partons, and quartic terms of ψ_a with singularity in the frequency space can be generated as was pointed out by Ref. 351, such as $|\omega||S_{\omega,q}|^2$, where $S_{\omega,q}$ is a bilinear of ψ_a. This coupling only arises for scenario (1). For scenario (2) discussed in the main text, the 3D XY* fixed point should be stable against symmetry allowed perturbations; the field theory Eq. 3.29 is also stable against coupling to the fermionic parton Fermi surface.

Although we do not aim to give a full discussion of the fate of the infrared limit of scenario (1), in the current work we establish the formalism for this problem that one can use in the future. As we explained in the previous paragraph, after integrating out the fermion that is connected by the finite momentum of the density wave order parameter, a term is generated $\sim |\omega||S_{\omega,q}|^2$, where $S = \psi^\dagger T \psi$ and T is an $N \times N$ matrix. One can introduce a new field Φ through the Hubbard-Stratonovich transformation, and ψ_a will interact with the Φ field [566]. We start with the first line of Eq. B.13. The field theory Eq. 3.19 with u_1 and u_2 in Eq. B.13 can be reformulated by introducing multiple Lagrange multipliers λ_i:

$$\mathcal{L}^{(1)} = \sum_{a=0}^{N-1} |(\partial - \mathrm{i}A)\psi_a|^2 + \mathrm{i}\sum_{i=1}^{N_1} \lambda_i \left(\sum_{\tau=1}^{N_2} |\psi_{\tau,i}|^2 \right) + \mathrm{i}\Phi\psi^\dagger T\psi; \tag{B.14}$$

$$\langle \lambda_i(\vec{q})\lambda_{i'}(-\vec{q})\rangle = \frac{8}{N_2}|q|\delta_{i,i'}, \tag{B.15}$$

$$\langle A_\mu(\vec{q})A_\nu(-\vec{q})\rangle = \frac{16}{N}\left(\frac{\delta_{\mu\nu} - q_\mu q_\nu/q^2}{|q|}\right), \tag{B.16}$$

$$\langle \Phi(\vec{q})\Phi(-\vec{q})\rangle = g|\omega|. \tag{B.17}$$

Here $N = N_1 N_2$, and for the real system with $N = 6$, $N_1 = 3$ and $N_2 = 2$. Introducing

λ_i for each index i physically means that we are investigating the theory near the point with a SU(N_2) symmetry for each index i, rather than the original CP^{N-1} theory with a large SU(N) flavor symmetry. This is analogous to the "easy-plane bosonic QED$_3$" considered in Ref. 567. The actions of λ_i and the transverse component of gauge field A are generated by integrating out the fields ψ_a. One possible way to proceed with the calculation is that, we can fix N_1, and take $1/N_2$ as a small parameter. When g is the same order of $1/N_2$, the interaction between ψ_a and the Φ field will lead to the contribution comparable with that arising from coupling to λ_i and A. The calculation would be analogous to the one formulated in Ref. 353, where the nonlocal interaction on top of a bosonic QED flows to a new fixed point. One can evaluate the scaling behaviors (such as relevance/irrelevance in the IR) of the v and w terms in the second and third lines in Eq. B.17 at this new fixed point. By exploring the parameter space of g, $1/N_2$, and different choice of matrix T, it is possible to identify a finite region where Eq. B.17 corresponds to a stable fixed point where the v and w terms in Eq. B.13 are irrelevant.

The same strategy can be applied to the situation with $N = 12$. With long moiré lattice constants, the 6-fold rotation $R_{\pi/3}$ also becomes a good approximate symmetry. Together with $R_{\pi/3}$, the quartic terms in the field theory for $N = 12$ (please refer to the phase diagram in Fig. 3.3) are:

$$\begin{aligned}
\mathcal{L}^{(1)\prime}[\psi_{\sigma,\tau,i}] &= u_1 \sum_{\sigma,i} \left(\sum_{\tau} |\psi_{\sigma,\tau,i}|^2 \right)^2 + u_2 \left(\sum_{\sigma\tau i} |\psi_{\sigma\tau i}|^2 \right)^2 \\
&+ v_1 \sum_{\sigma, i\neq i'} \left(\sum_{\tau} |\psi_{\sigma,\tau,i}|^2 \right) \left(\sum_{\tau'} |\psi_{\sigma,\tau',i'}|^2 \right) + v_2 \sum_{i} \left(\sum_{\tau} |\psi_{+,\tau,i}|^2 \right) \left(\sum_{\tau'} |\psi_{-,\tau',i}|^2 \right) \\
&+ w_1 \left| \sum_{i,\tau} \psi_{+,\tau,i} \psi_{-,\tau,i} \right|^2 + \mathrm{i} w_2 \left(\sum_{i,\tau,\tau'} \psi^*_{+,\tau,i+1} \psi^*_{-,\tau,i+1} \psi_{+,\tau',i} \psi_{-,\tau',i} - h.c. \right)
\end{aligned} \tag{B.18}$$

Here the 12 modes are labelled by $\psi_{\sigma,\tau,i}$ in which $\tau = \pm$ labels two degenerate modes at the same momentum, $\sigma = \pm$ labels two sets of momenta that are each connected by

$R_{2\pi/3}$, and $i = 0, 1, 2 \mod 3$ labels these three momenta within each set.

We can again start with the first line of Eq. B.18, and introduce Lagrange multiplier $\lambda_{\sigma,i}$ which couples to the ψ_a fields as $\sum_{\tau=1}^{N_2} \lambda_{\sigma,i}|\psi_{\sigma,\tau,i}|^2$. Notice that we have generalized τ to $1 \cdots N_2$. Then the Hubbard-Stratonovich transformation can introduce new fields that couple to ψ_a to account for the singular terms generated through interacting with the Fermi surface. A combined perturbation theory of $1/N_2$ and g can again determine the relevance/irrelevance of the second and third lines of Eq. B.18. In particular, the two terms in the second line of Eq. B.18 are indeed irrelevant with large-N_2, as the scaling dimension of $\sum_\tau |\psi_{\sigma,\tau,i}|^2$ is 2 with large-N_2.

B.2.2 The PSG Transformation for $N = 6$ in Scenario (1)

Under the boson-vortex duality, the dual vortex theory on the hexagonal lattice takes the form

$$H = \sum_{\langle ij \rangle} -t_{ij}\phi_i^*\phi_j + H'_\phi + V_\phi + \ldots, \quad t_{ij} = te^{-\mathrm{i}A_{ij}} \tag{B.19}$$

Here H'_ϕ describes hopping terms between further neighbors. The potential V_ϕ includes a quadratic term $\sum_i r|\phi_i|^2$ which tunes through the phase transition.

When t_{ij} is nonzero only for nearest neighbor links on the dual honeycomb lattice, and it takes positive sign on the solid links and negative sign on the dashed links in Fig. 3.2 due to the π flux of A_μ through each hexagon, there are four minima of the vortex band structure in the Brillouin zone (Fig. 3.3). We label the four minimum modes from 0 to 3, each have momentum (k_x, k_y)

$$\mathbf{Q}_{0,1} = \mathbf{K} = \left(\frac{2\pi}{3\sqrt{3}}, 0\right), \quad \mathbf{Q}_{2,3} = \mathbf{K}' = \left(\frac{\pi}{3\sqrt{3}}, \frac{\pi}{3}\right). \tag{B.20}$$

With further neighbor vortex hopping (please refer to the phase diagram in Fig. 3.3),

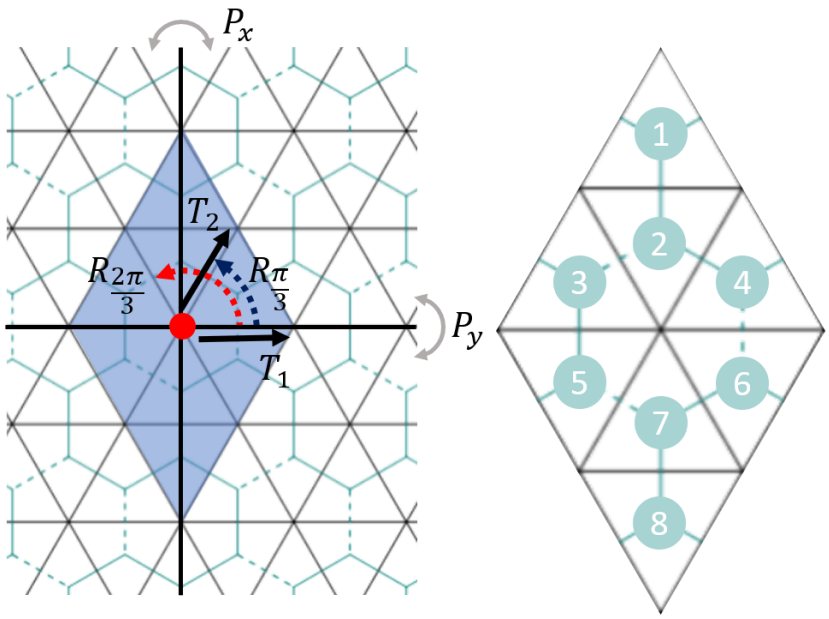

Figure B.2: Crystal symmetry of the triangular lattice, the nearest neighbor hopping amplitudes of the vortices, and the unit cell after taking into account of the sign of t_{ij}.

the minima of the vortex band structure can shift to the M points, similar to Ref. 345. When the degenerate minima are shifted to the M points (Fig. 3.3), the six corresponding momenta are

$$\mathbf{Q}_{0,1} = \left(\frac{\pi}{2\sqrt{3}}, -\frac{\pi}{6}\right), \ \mathbf{Q}_{2,3} = \left(\frac{\pi}{2\sqrt{3}}, \frac{\pi}{6}\right), \ \mathbf{Q}_{4,5} = \left(0, \frac{\pi}{3}\right). \tag{B.21}$$

Similar to the four minima case, the vortex field can be expanded using these six modes as

$$\phi_{n,\mathbf{r}} \sim \sum_{a=0}^{5} \psi_a v_{a,n} e^{\mathrm{i}\mathbf{Q}_a \cdot \mathbf{r}}. \tag{B.22}$$

The coefficients $v_{a,n}$ are solved from the band structure.

The symmetries of the theory for one single valley must include translation T_1, T_2, three-fold rotation $R_{2\pi/3}$, $P_x\mathcal{T}$. These transformations do not mix the two valleys. In the following we derive the PSG matrices of these symmetries. We first need the form of

the transformations when acting on the 8 sites in each unit cell:

$$T_{1,2}(\phi_{n,\mathbf{k}}) = \sum_m (t_{1,2})_{nm}\phi_{m,\mathbf{k}}, \tag{B.23}$$

$$t_1 = \begin{pmatrix} 0 & 0 & 0 & 0 & 0 & 0 & 1 & 0 \\ 0 & 0 & 0 & 0 & 0 & 0 & 0 & 1 \\ 0 & 0 & 0 & -1 & 0 & 0 & 0 & 0 \\ 0 & 0 & 1 & 0 & 0 & 0 & 0 & 0 \\ 0 & 0 & 0 & 0 & 0 & 1 & 0 & 0 \\ 0 & 0 & 0 & 0 & -1 & 0 & 0 & 0 \\ -1 & 0 & 0 & 0 & 0 & 0 & 0 & 0 \\ 0 & -1 & 0 & 0 & 0 & 0 & 0 & 0 \end{pmatrix}, \quad t_2 = \begin{pmatrix} 0 & 0 & 1 & 0 & 0 & 0 & 0 & 0 \\ 0 & 0 & 0 & 0 & 1 & 0 & 0 & 0 \\ -1 & 0 & 0 & 0 & 0 & 0 & 0 & 0 \\ 0 & 0 & 0 & 0 & 0 & 0 & -1 & 0 \\ 0 & -1 & 0 & 0 & 0 & 0 & 0 & 0 \\ 0 & 0 & 0 & 0 & 0 & 0 & 0 & 1 \\ 0 & 0 & 0 & 1 & 0 & 0 & 0 & 0 \\ 0 & 0 & 0 & 0 & 0 & -1 & 0 & 0 \end{pmatrix} \tag{B.24}$$

and

$$R_{2\pi/3}(\phi_{n,\mathbf{k}}) = (r_{\pi/3})_{nm}\phi_{m,R_{2\pi/3}\mathbf{k}}, \quad r_{2\pi/3} = \begin{pmatrix} 1 & 0 & 0 & 0 & 0 & 0 & 0 & 0 \\ 0 & 0 & 0 & 0 & 1 & 0 & 0 & 0 \\ 0 & 0 & 0 & 0 & 0 & 0 & 1 & 0 \\ 0 & 0 & 1 & 0 & 0 & 0 & 0 & 0 \\ 0 & 0 & 0 & 0 & 0 & 1 & 0 & 0 \\ 0 & 1 & 0 & 0 & 0 & 0 & 0 & 0 \\ 0 & 0 & 0 & 1 & 0 & 0 & 0 & 0 \\ 0 & 0 & 0 & 0 & 0 & 0 & 0 & 1 \end{pmatrix}, \tag{B.25}$$

$$P_x\mathcal{T}(\phi_{n,\mathbf{k}}) = (p_x t)_{nm}\phi_{m,-P_x\mathbf{k}}, \quad (p_x t)_{ab} = \begin{pmatrix} 1 & 0 & 0 & 0 & 0 & 0 & 0 & 0 \\ 0 & 1 & 0 & 0 & 0 & 0 & 0 & 0 \\ 0 & 0 & 0 & -1 & 0 & 0 & 0 & 0 \\ 0 & 0 & -1 & 0 & 0 & 0 & 0 & 0 \\ 0 & 0 & 0 & 0 & 0 & 1 & 0 & 0 \\ 0 & 0 & 0 & 0 & 1 & 0 & 0 & 0 \\ 0 & 0 & 0 & 0 & 0 & 0 & -1 & 0 \\ 0 & 0 & 0 & 0 & 0 & 0 & 0 & -1 \end{pmatrix}. \tag{B.26}$$

Besides these symmetries, here we argue that, if the system does have an effective Hubbard model description with two local Wannier orbitals per unit cell (one for each valley), P_y is also a good symmetry of the Hubbard model, as long as the valley mixing is negligible, which is a justified assumption with long wavelength moiré potential

modulation. Let us first assume there is no valley mixing, then for each valley the band structure of the moiré mini band is described by a tight binding model with one orbital per site on the moiré triangular lattice. The hopping amplitude $t(\theta)$ along angle θ must satisfy the following relations based on the explicit $P_x\mathcal{T}$ and translation symmetry:

$$t(\theta) = t^*(\pi - \theta), \quad t^*(\theta) = t(\pi + \theta), \tag{B.27}$$

we can easily show that $t(\theta) = t(-\theta)$, namely the system should have a P_y symmetry.

However, when there is valley mixing, t becomes a 2×2 matrix with off-diagonal terms that mix two valleys. A 2×2 hopping matrix t should satisfy four symmetries, P_x, $\mathcal{T}$, translation, and $R_{2\pi/3}$ rotation. A natural choice of P_x and $\mathcal{T}$ on t is

$$P_x : t(\theta) \to \sigma^x t(\pi - \theta)\sigma^x; \quad \mathcal{T} : t(\theta) \to (\mathrm{i}\sigma^y)t^*(-\mathrm{i}\sigma^y); \tag{B.28}$$

and the translation symmetry plus hermicity demands $t^\dagger(\theta) = t(\pi + \theta)$. P_y does not change the valley indices; if P_y takes $t(\theta)$ to $t(-\theta)$, there exists a valley mixing term $t(\theta) \sim \mathrm{i}\sigma^x \sin(3\theta)$ that preserves all the symmetries mentioned above, but breaks P_y; while if P_y takes $t(\theta)$ to $\sigma^z t(-\theta)\sigma^z$ this term becomes $t(\theta) \sim \mathrm{i}\sigma^y \cos(3\theta)$.

P_y acts on the ϕ bosons as

$$P_y(\phi_{n,\mathbf{k}}) = (p_y)_{nm}\phi^*_{m,-P_y\mathbf{k}}, \qquad (p_y)_{ab} = \begin{pmatrix} 0 & 0 & 0 & 0 & 0 & 0 & 0 & 1 \\ 0 & 0 & 0 & 0 & 0 & 0 & 1 & 0 \\ 0 & 0 & 0 & 0 & 1 & 0 & 0 & 0 \\ 0 & 0 & 0 & 0 & 0 & 1 & 0 & 0 \\ 0 & 0 & 1 & 0 & 0 & 0 & 0 & 0 \\ 0 & 0 & 0 & 1 & 0 & 0 & 0 & 0 \\ 0 & 1 & 0 & 0 & 0 & 0 & 0 & 0 \\ 1 & 0 & 0 & 0 & 0 & 0 & 0 & 0 \end{pmatrix}. \tag{B.29}$$

Furthermore, in the case with long moiré lattice constant, we additionally have the

six-fold rotation $R_{\pi/3}$

$$R_{\pi/3}(\phi_{n,\mathbf{k}}) = (r_{\pi/3})_{nm}\phi_{m,R_{\pi/3}\mathbf{k}}, \qquad (r_{\pi/3})_{ab} = \begin{pmatrix} 0 & 0 & 0 & 0 & 0 & 0 & 0 & -1 \\ 0 & 0 & -1 & 0 & 0 & 0 & 0 & 0 \\ 0 & 0 & 0 & 0 & 1 & 0 & 0 & 0 \\ 0 & 1 & 0 & 0 & 0 & 0 & 0 & 0 \\ 0 & 0 & 0 & 0 & 0 & 0 & -1 & 0 \\ 0 & 0 & 0 & -1 & 0 & 0 & 0 & 0 \\ 0 & 0 & 0 & 0 & 0 & 1 & 0 & 0 \\ 1 & 0 & 0 & 0 & 0 & 0 & 0 & 0 \end{pmatrix}. \tag{B.30}$$

In the position space, the transformation rules can be summarized as

$$G(\phi_{n,\mathbf{r}}) = \sum_{m=1}^{8} g_{n,m}\phi_{m,\mathbf{r}'_m} \tag{B.31}$$

in which $\mathbf{r}'_m$ is the center of the unit cell of field ϕ_m which is obtained by certain site in the original unit cell (centered at $\mathbf{r}$) after transformation under symmetry operation G. For example, under T_1, $\mathbf{r}'_7 = \mathbf{r}'_8 = \mathbf{r} + 2\mathbf{a}_2$, because sites 1 and 2 at unit cell $\mathbf{r}$ are transformed into sites 7 and 8 in the nearby enlarged unit cell which is centered at $\mathbf{r}+2\mathbf{a}_2$. In general, we can write the transformation as $\mathbf{r}'_m = G\mathbf{r} + \vec{\Delta}_{G,m}$, in which $\vec{\Delta}_{G,m}$ is a constant that does not depend on $\mathbf{r}$, and $G\mathbf{r}$ is the coordinate of the center of the unit cell after spacial symmetry G.

Now we plug in the low energy expansions of $\phi_{n_\mathbf{k}}$ around the minima into the equation, which yields

$$\sum_{a=0}^{N-1} G(\psi_a)v_{a,n}e^{\mathbf{i}\mathbf{Q}_a\cdot\mathbf{r}} = \sum_{a=0}^{N-1}\sum_{m=1}^{8} \psi_a g_{nm} v_{m,a} e^{\mathbf{i}\mathbf{Q}_a\cdot\mathbf{r}'_m}. \tag{B.32}$$

The relation can be viewed as a vector identity with n being the vector index on both sides. Because all the vectors $v_{a,n}(a = 0, \ldots, N-1)$ are orthogonal to each other, we can

multiply the conjugated vector $v^*_{b,n}$ on both sides and sum over n:

$$G(\psi_b)e^{\mathrm{i}\mathbf{Q}_b\cdot\mathbf{r}} = \sum_{a=0}^{N-1}\sum_{m,n=1}^{8} \psi_a v^*_{b,n} g_{n,m} v_{a,m} e^{\mathrm{i}\mathbf{Q}_a\cdot\mathbf{r}'_m}. \tag{B.33}$$

For this equation to hold for all $\mathbf{r}$, the RHS needs to have the same momentum. This requires $\mathbf{Q}_b = G^{-1}\mathbf{Q}_a$, which can only be satisfied by two possible choices of a (recall that in the convention of eight-site unit cell, each momentum $\mathbf{Q}_a$ always has two fold degeneracy for all N), denoted by a_1 and a_2. Thus we eventually have

$$G(\psi_b) = \sum_{m,n=1}^{8} v^\dagger_{b,n} g_{nm} v_{a_1,m} e^{\mathrm{i}\mathbf{Q}_{a_1}\cdot\vec{\Delta}_{G,m}} \times \psi_{a_1} + \sum_{m,n=1}^{8} v^\dagger_{b,n} g_{nm} v_{a_2,m} e^{\mathrm{i}\mathbf{Q}_{a_2}\cdot\vec{\Delta}_{G,m}} \times \psi_{a_2} \tag{B.34}$$

The final results can be organized into $N \times N$ matrices. For $N = 6$, the transformations read

$$T_{1,2}(\psi_a) = (\mathfrak{t}_{1,2})_{ab}\psi_b, \quad (\mathfrak{t}_1)_{ab} = \begin{pmatrix} -1 & 0 & 0 & 0 & 0 & 0 \\ 0 & 1 & 0 & 0 & 0 & 0 \\ 0 & 0 & 0 & 1 & 0 & 0 \\ 0 & 0 & 1 & 0 & 0 & 0 \\ 0 & 0 & 0 & 0 & 0 & 1 \\ 0 & 0 & 0 & 0 & -1 & 0 \end{pmatrix}, \quad (\mathfrak{t}_2)_{ab} = \begin{pmatrix} 0 & 1 & 0 & 0 & 0 & 0 \\ -1 & 0 & 0 & 0 & 0 & 0 \\ 0 & 0 & 1 & 0 & 0 & 0 \\ 0 & 0 & 0 & -1 & 0 & 0 \\ 0 & 0 & 0 & 0 & 0 & -1 \\ 0 & 0 & 0 & 0 & -1 & 0 \end{pmatrix}, \tag{B.35}$$

$$R_{2\pi/3}(\psi_a) = (\mathfrak{R}_{2\pi/3})_{ab}\psi_b, \qquad P_x\mathcal{T}(\psi_a) = (\mathfrak{P}_x\mathfrak{T})_{ab}\psi_b, \tag{B.36}$$

$$(\mathfrak{R}_{2\pi/3})_{ab} = \begin{pmatrix} 0 & 0 & 0 & 0 & 1 & 0 \\ 0 & 0 & 0 & 0 & 0 & 1 \\ -1 & 0 & 0 & 0 & 0 & 0 \\ 0 & -1 & 0 & 0 & 0 & 0 \\ 0 & 0 & 1 & 0 & 0 & 0 \\ 0 & 0 & 0 & 1 & 0 & 0 \end{pmatrix}, \qquad (\mathfrak{P}_x\mathfrak{T})_{ab} = \frac{1}{\sqrt{2}}\begin{pmatrix} 0 & 0 & 1 & -1 & 0 & 0 \\ 0 & 0 & -1 & -1 & 0 & 0 \\ 1 & -1 & 0 & 0 & 0 & 0 \\ -1 & -1 & 0 & 0 & 0 & 0 \\ 0 & 0 & 0 & 0 & 1 & -1 \\ 0 & 0 & 0 & 0 & -1 & -1 \end{pmatrix}. \tag{B.37}$$

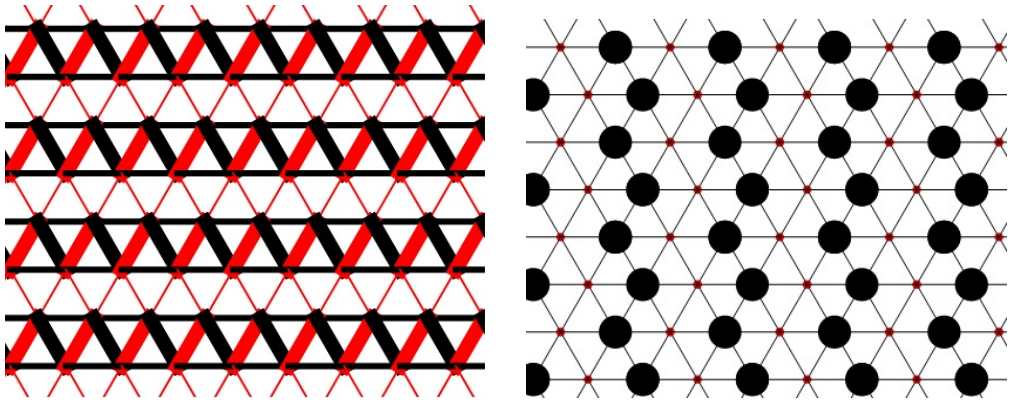

Figure B.3: Some possible density wave patterns of the original boson that correspond to different condensate of ψ_a with $a = 0, \cdots 5$. The left and right patterns correspond to $\vec{\Psi} \sim (1, 0, 0, 0, 0, 0)$ and $\vec{\Psi} \sim (0, 1/\sqrt{2}, 1/2, -1/2, 0, 0)$ respectively.

and

$$P_y(\psi_a) = (\mathfrak{P}_y)_{ab}\psi_b^*, \qquad R_{\pi/3}(\psi_a) = (\mathfrak{R}_{\pi/3})_{ab}\psi_b, \tag{B.38}$$

$$(\mathfrak{P}_y)_{ab} = \frac{1}{\sqrt{2}}\begin{pmatrix} 0 & 0 & 1 & 1 & 0 & 0 \\ 0 & 0 & 1 & -1 & 0 & 0 \\ 1 & 1 & 0 & 0 & 0 & 0 \\ 1 & -1 & 0 & 0 & 0 & 0 \\ 0 & 0 & 0 & 0 & 1 & 1 \\ 0 & 0 & 0 & 0 & 1 & -1 \end{pmatrix}, \qquad (\mathfrak{R}_{\pi/3})_{ab} = \begin{pmatrix} 0 & 0 & 0 & -1 & 0 & 0 \\ 0 & 0 & 1 & 0 & 0 & 0 \\ 0 & 0 & 0 & 0 & 0 & 1 \\ 0 & 0 & 0 & 0 & -1 & 0 \\ 0 & 1 & 0 & 0 & 0 & 0 \\ -1 & 0 & 0 & 0 & 0 & 0 \end{pmatrix}. \tag{B.39}$$

Deep inside the vortex condensate phase with $r \ll 0$ in equation Eq. 3.19, the vector $\vec{\Psi} = (\psi_0, \psi_1, \psi_2, \psi_3, \psi_4, \psi_5)$ can have different condensates depending on the parameters in Eq. B.13. Without loss of generality we set $\sum_{a=0}^{5} |\psi_a|^2 = 1$. The two figures in Eq. B.3 illustrate the density waves of the bosonic parton centered at the bonds and the sites on the moiré triangular lattice that correspond to two different possible condensates of $\vec{\Psi}$. The density on the bond l is inferred from $t_{ij}\langle\phi_i^*\phi_j\rangle$, with ij being the link on the dual honeycomb lattice that is dual to l, and t_{ij} takes the sign according to the gauge convention of Fig. 3.2. The operator $t_{ij}\langle\phi_i^*\phi_j\rangle$ is the energy density in terms of vortex fields, and the modulation of this operator should correspond to the valence bond solid of the original bosonic parton. We also consider an operator centered on site p of the original

lattice (plaquette of the dual lattice): $\sum_{\langle ij\rangle\in p} t_{ij}\langle\phi_i^*\phi_j\rangle$, with the summation over the links that surround the plaquette p on the dual honeycomb lattice, whose center hosts the site p of the original moiré triangular lattice. In both cases, $\langle\phi_i^*\phi_j\rangle$ is evaluated using Eq. B.22 and the value of $\vec{\Psi}$ which minimizes the quartic energy. The left pattern in Eq. B.3 is a rather common valence bond solid configuration for either spin-1/2 system or hard core boson on the triangular lattice. If one started with the construction-I of the parton construction, the discussion in this section corresponds to the original electron system with an average 1/2 electron per unit cell (the filling considered in Ref. 321); while for construction-II, the discussion here applies to one electron per unit cell, and the analysis in this section corresponds to one of the two spin/valley flavors of the system.

B.2.3 Dual of the Vortex Theory

Here we derive the Lagrangian written in terms of the fractionally charged bosonic partons for scenario (1). We start with Eq. 3.19 in our paper:

$$\mathcal{L}^{(1)} = \sum_{j=0}^{N-1} |(\partial_\mu - \mathrm{i}A_\mu)\psi_j|^2 + r|\psi_j|^2 + \frac{\mathrm{i}}{2\pi} A\wedge d(a+eA_{\mathrm{ext}}) + \cdots \tag{B.40}$$

To facilitate the calculation of the DC resistivity which will be discussed in the next subsection, we need to "dual back" to the charge-carriers, which requires deforming Eq. B.40 with an easy-plane anisotropy $\sum_j |\psi_j|^4$. The bosonic fractional charge carriers φ_j are the vortices of the vortex fields ψ_j. We first take the standard duality for ψ_j, and Eq. B.40 becomes:

$$\mathcal{L}^{(1)} = \sum_{j=0}^{N-1} |(\partial - \mathrm{i}\tilde{A}_j)\varphi_j|^2 + \tilde{r}|\varphi_j|^2 + \frac{\mathrm{i}}{2\pi}\tilde{A}_j\wedge dA + \frac{\mathrm{i}}{2\pi} A\wedge d(a+eA_{\mathrm{ext}}) + \cdots \tag{B.41}$$

The basic duality relation is that the current of ψ_j, *i.e.* $J_{\psi_j} \sim d\tilde{A}_j$. Now integrating out A would lead to the following constraint for the rest of the gauge fields:

$$\sum_j \tilde{A}_j - a - eA_{\text{ext}} = 0. \tag{B.42}$$

From this constraint we can take $\tilde{A}_j$ as

$$\tilde{A}_j = \tilde{a}_j + \frac{1}{N}a + \frac{e}{N}A_{\text{ext}}, \quad \sum_j \tilde{a}_j = 0. \tag{B.43}$$

Hence the dual of the dual theory becomes

$$\mathcal{L}^{(1)} = \sum_{j=0}^{N-1} |(\partial - \mathrm{i}\tilde{a}_j - \mathrm{i}\frac{1}{N}a - \mathrm{i}\frac{e}{N}A_{\text{ext}})\varphi_j|^2 + \tilde{r}|\varphi_j|^2 + \cdots . \tag{B.44}$$

The gauge fields $\tilde{a}_j$ are still subject to the constraint $\sum_j \tilde{a}_j = 0$. φ_j carries e/N charge of external EM gauge field; it also carries charge $1/N$ of gauge field a which is shared with the fermionic parton f_α.

For scenario (2) the theory in terms of fractional parton φ is much simpler: there is only one flavor of φ for each valley, and there is no extra continuous gauge fields $\tilde{a}$ besides gauge field a: Following the calculation in Ref. 111, one can generalize this one flavor of φ in each valley to an $\mathbf{N}$ component of bosons:

$$\mathcal{L}^{(2)} = \sum_{l=1}^{\mathbf{N}} |(\partial - \mathrm{i}\frac{1}{N}a - \mathrm{i}\frac{e}{N}A_{\text{ext}})\varphi^l|^2 + \mathrm{i}\lambda|\varphi^l|^2 + \cdots \tag{B.45}$$

and the bosons will scatter with both gauge field a and field λ which is introduced as a Lagrange multiplier. The fact that φ^l carries charge $1/N$ of gauge field a does not change the scattering rate through the large-$\mathbf{N}$ calculation, as the gauge charge cancels out in the calculation of scattering rate through the large-$\mathbf{N}$ approach. Compared with

scenario (2), in scenario (1) the parton φ_j is also coupled to extra gauge fields $\tilde{a}_j$, which will lead to extra scattering to the charge carriers.

When computing the resistivity, especially the DC resistivity of scenario (1), we also rely on a large$-\mathbf{N}$ generalization, namely we need to introduce an extra $l = 1 \cdots \mathbf{N}$ index for each component of fractional charge field: φ_j^l.

B.2.4 DC Resistivity Jump in Scenario (1)

In this section we present a detailed computation of the DC resistivity jump in the scenario (1) of MIT, i.e. the scenario when the insulator has a density wave. We start with Eq. B.44. The resistivity jump at the MIT is given by the universal resistivity of the bosonic sector of the system ρ_b at the MIT. First of all, one can prove a generalized Ioffe-Larkin rule, which combines the resistivity of each parton φ_j into ρ_b:

$$\rho_b = \frac{\hbar}{e^2}\left(\sum_{j=0}^{N-1} \rho_{b,j}\right), \tag{B.46}$$

where $\rho_{b,j}$ is the resistivity of each parton φ_j, when the charge of φ_j is taken to be 1. This generalized Ioffe-Larkin rule can be proven by formally integrating out φ_j, gauge fields $\tilde{a}_j$ and a from Eq. B.44, and eventually arriving at a response function of A_{ext}. At each level of the path integral, we keep a quadratic form of the action, i.e. the random phase approximation. This Ioffe-Larkin rule is independent of the assignment of electric charges on each parton.

To compute ρ_b, we formulate the quantum Boltzmann equation (QBE) for the φ_j fields of a given valley. The computation follows that for ρ_b at the MIT without charge fractionalization [111], where the gauge field dynamics needs to be modified due to the charge fractionalization, which we explain in detail below for comparison. Note that ρ_b can be finite without momentum relaxation due to the emergent particle-hole symmetry.

Furthermore, the two-in two-out scatterings among the φ_j fields are enough to relax the current and generate finite DC resistivity. For simplicity, we consider the scattering between the φ_j and emergent gauge fields in Eq. (B.44), where the gauge fields are in thermal equilibrium and their dynamics is acquired due to the coupling with the matter fields φ_j and f. Here, we argue that treating the gauge fields as in thermal equilibrium is a legitimate approximation. First, the gauge field a couples to the spinon field f, which is sensitive to impurities and relaxes momentum fast. Second, diagrammatically, the two-in two-out scatterings between the φ_j fields that give finite DC resistivity can be captured by the φ_j scattering with the emergent gauge fields.

To simplify the computation of the gauge field dynamics, it is convenient to express Eq. B.44 in terms of the gauge field $\tilde{A}_j$ (Eq. B.42), together with the effective action for the spinon field, the dual theory reads

$$\begin{aligned}\mathcal{L}^{(1)} &= \sum_{j=0}^{N-1} |(\partial - \mathrm{i}\tilde{A}_j)\varphi_j|^2 + \tilde{r}|\varphi_j|^2 \\ &+ \bar{f}\left(\partial_\tau - \mu - \mathrm{i}\sum_{j=0}^{N-1}\tilde{A}_{j,0} + \mathrm{i}eA_{\mathrm{ext},0} + \frac{1}{2m}(\nabla - \mathrm{i}\sum_{j=0}^{N-1}\tilde{\mathbf{A}}_j + \mathrm{i}e\mathbf{A}_{\mathrm{ext}})^2\right) f + \cdots . \end{aligned} \tag{B.47}$$

Integrating out φ_j and f fields, the gauge field propagators read

$$D_{ij}^{(\tilde{A})} = -\mathrm{i}\langle \mathrm{T}_t \tilde{A}_i \tilde{A}_j\rangle = \begin{cases} \frac{\Pi_b^J + (N-1)\Pi_f^J}{(\Pi_b^J)^2 + N\Pi_b^J\Pi_f^J} & \text{if } i = j \\ \frac{-\Pi_f^J}{(\Pi_b^J)^2 + N\Pi_b^J\Pi_f} & \text{if } i \neq j \end{cases}, \tag{B.48}$$

where Π_b^J, Π_f^J is the current-current correlation function for φ_j and f fields, respectively.

For a controlled systematic calculation of transport, we introduce a large number of (complex) rotor and spinon flavors $\mathbf{N}$ with the constraint $\sum_{l=1}^{\mathbf{N}} |\varphi_j^l|^2 = 1$ for all $j = 0, 1, ..., N-1$, and only the $l = 1$ component couples to A_{ext}. The $\mathbf{N} = 1$ limit will be

taken at the end. The effective action for the extended model becomes

$$\mathcal{L} = \sum_{j=0}^{N-1}\left(\sum_{l=1}^{\mathbf{N}}|(\partial - \mathrm{i}\tilde{A}_j)\varphi_j^l|^2 + \mathrm{i}\lambda_j(\sum_{l=1}^{\mathbf{N}}|\varphi_j^l|^2 - 1) + \frac{1}{2g^2}(\epsilon_{\mu\nu\lambda}\partial_\nu\tilde{A}_{j,\lambda})^2\right) \tag{B.49}$$
$$+\sum_{l=1}^{\mathbf{N}}\bar{f}_l\left(\partial_\tau - \mu - \mathrm{i}\sum_{j=0}^{N-1}\tilde{A}_{j,0} + \mathrm{i}eA_{\mathrm{ext},0}\delta_{l,1} + \frac{1}{2m}(\nabla - \mathrm{i}\sum_{j=0}^{N-1}\tilde{\mathbf{A}}_j + \mathrm{i}e\mathbf{A}_{\mathrm{ext}}\delta_{l,1})^2\right)f_l + \cdots .$$

Using the Fourier expansion for the electrically charged rotor $\varphi_j^{l=1}$ in terms of the holons (+) and doublons (-),

$$\varphi_j^{l=1} = \int_{\mathbf{k}}\alpha_{+,j}(t,\mathbf{k})e^{\mathrm{i}\mathbf{k}\cdot\mathbf{x}} + \alpha_{-,j}(t,\mathbf{k})e^{-\mathrm{i}\mathbf{k}\cdot\mathbf{x}}, \tag{B.50}$$

the conductivity $\sigma_{b,j} = \rho_{b,j}^{-1}$ can be obtained as

$$\sigma_{b,j} = \langle J_{x,j}\rangle/E_x, \quad \langle J_{x,j}\rangle = \int_{\mathbf{k}}\sum_{s=\pm}s\frac{\mathbf{k}}{\epsilon_{\mathbf{k}}}f_{s,j}(t,\mathbf{k}), \tag{B.51}$$

where we define the distribution for holon ($s = +$) and doublon ($s = -$) as $f_{s,j} = \langle\alpha_{s,j}^\dagger(t,\mathbf{k})\alpha_{s,j}(t,\mathbf{k})\rangle$, and they satisfy the QBE as

$$(\partial_t + s\mathbf{E}\cdot\partial_{\mathbf{k}})f_{s,j}(t,\mathbf{k}) = \frac{1}{2\mathbf{N}}(I_{\lambda_j}[f_{\pm,j}] + I_{\tilde{A}_j}[f_{\pm,j}]). \tag{B.52}$$

Note that the gauge choice in Eq. B.47 ensures that $f_{s,j}$ are decoupled and equal for different j within the approximation that $\tilde{A}_j$ is in thermal equilibrium, so the subindex j will be dropped unless there is ambiguity. The RHS of Eq. B.52 reads

$$\mathrm{RHS} = \frac{1}{2\mathbf{N}}\int_0^\infty\frac{\mathrm{d}\Omega}{\pi}\int\frac{\mathrm{d}^2\mathbf{q}}{(2\pi)^2}\{\tau_\lambda\,\mathrm{Im}\,D^{(\lambda)}(\Omega,\mathbf{q}) + \tau_{\tilde{A}}\,\mathrm{Im}\,D_{ii}^{(\tilde{A})}(\Omega,\mathbf{q})\} \tag{B.53}$$
$$\times\{\frac{2\pi\delta(\epsilon_{\mathbf{k}} - \epsilon_{\mathbf{k}+\mathbf{q}} + \Omega)}{4\epsilon_{\mathbf{k}}\epsilon_{\mathbf{k}+\mathbf{q}}}[f_s(t,\mathbf{k})(1 + f_s(t,\mathbf{k}+\mathbf{q}))n_{\mathbf{q}}(\Omega) - (1 + f_s(t,\mathbf{k}))f_s(t,\mathbf{k}+\mathbf{q})(1 + n_{\mathbf{q}}(\Omega))]$$
$$+\frac{2\pi\delta(\epsilon_{\mathbf{k}} - \epsilon_{\mathbf{k}+\mathbf{q}} - \Omega)}{4\epsilon_{\mathbf{k}}\epsilon_{\mathbf{k}+\mathbf{q}}}[f_s(t,\mathbf{k})(1 + f_s(t,\mathbf{k}+\mathbf{q}))(1 + n_{\mathbf{q}}(\Omega)) - (1 + f_s(t,\mathbf{k}))f_s(t,\mathbf{k}+\mathbf{q})n_{\mathbf{q}}(\Omega)]$$
$$+\frac{2\pi\delta(-\epsilon_{\mathbf{k}} - \epsilon_{\mathbf{k}+\mathbf{q}} + \Omega)}{4\epsilon_{\mathbf{k}}\epsilon_{\mathbf{k}+\mathbf{q}}}[f_s(t,\mathbf{k})f_s(t,\mathbf{k}+\mathbf{q})(1 + n_{\mathbf{q}}(\Omega)) - (1 + f_s(t,\mathbf{k}))(1 + f_s(t,\mathbf{k}+\mathbf{q}))n_{\mathbf{q}}(\Omega)]\},$$

where $\tau_\lambda = -1$ and $\tau_{\tilde{A}} = (2\mathbf{k} \times \hat{\mathbf{q}})^2$ come from the bare vertex functions.

N	1	2	3	4	5	6	...	∞
$\sigma_{b,j}(e^2/\hbar)$	0.021	0.029	0.034	0.036	0.038	0.039		0.047
$\rho_b(h/e^2)$	3.72	5.41	7.09	8.76	10.44	12.11		$(3.62 + 1.68(N-1))$

Table B.1: Rotor conductivity ($\sigma_{b,j}$) and resistivity jump ρ_b at the MIT with fractionally charged bosonic parton $e_* = e/N$.

$\mathrm{Im}\, D^{(\lambda)}, \mathrm{Im}\, D^{(\tilde{A})}$ physically denote the density of states of the emergent fields that scatter with φ, which are broad in the $(\Omega, \mathbf{q})$ space due to the couplings with the φ fields. Below, we ignore the bare dynamics. $D^{(\lambda),(\tilde{A})}$ in the large-$\mathbf{N}$ limit reads

$$\begin{aligned} D^{(\lambda)}(\Omega, \mathbf{q}) &= \frac{1}{\Pi_b}, \\ D^{(\tilde{A})}_{ii}(\Omega, \mathbf{q}) &= \frac{\Pi_b^J + (N-1)\Pi_f^J}{(\Pi_b^J)^2 + N\Pi_b^J\Pi_f^J} = \frac{N-1}{N}\frac{1}{\Pi_b^J} + \frac{1}{N}\frac{1}{\Pi_b^J + N\Pi_f^J}, \end{aligned} \tag{B.54}$$

where $D^{(\tilde{A})}_{ii}$ reduces to the MIT without charge fractionalization as discussed in Ref. 111 when $N = 1$. For $N > 1$, as only the linear combination of $\tilde{A}_j$, i.e. $\sum_{j=0}^{N-1} \tilde{A}_j$ couples to the spinon field f and is Landau damped, there is a factor $\frac{1}{N}$ for the Landau damped component of the gauge field propagator $D^{(\tilde{A})}_{ii}$, which may also be understood as the a component of gauge field in Eq. (B.44). The rest part is not Landau damped, and is determined solely by Π_b^J. Note that as $\mathrm{Im}\,\Pi_f^J \gg \mathrm{Im}\,\Pi_b^J$ in the limit $\mu \gg T$, the Landau damped component can be approximated as $\frac{1}{N}\frac{1}{\Pi_b^J + N\Pi_f^J} \approx \frac{1}{N}\frac{1}{\Pi_b^J(\Omega=0,\mathbf{q}) + N\Pi_f^J(\Omega,\mathbf{q})}$, and be treated in the same way as Ref. 111 for the gauge field a. On the other hand, the first term in $D^{(\tilde{A})}_{ii}$ should be determined for generic $\Omega, \mathbf{q}$. Using the standard expression for

polarizations Π,

$$\begin{aligned}
\Pi_b(\Omega,\mathbf{q}) &= \frac{T}{2}\sum_m \int_{\mathbf{k}} \tau_\lambda \frac{1}{(\nu_m+\Omega_n)^2+\epsilon^2_{\mathbf{k}+\mathbf{q}}}\frac{1}{\nu_m^2+\epsilon^2_{\mathbf{k}}}|_{\mathrm{i}\Omega_n\to\Omega+\mathrm{i}\delta} \\
\Pi_b^J(\Omega,\mathbf{q}) &= \frac{T}{2}\sum_m \int_{\mathbf{k}} \tau_{\tilde{A}} \frac{1}{(\nu_m+\Omega_n)^2+\epsilon^2_{\mathbf{k}+\mathbf{q}}}\frac{1}{\nu_m^2+\epsilon^2_{\mathbf{k}}}|_{\mathrm{i}\Omega_n\to\Omega+\mathrm{i}\delta} \\
\Pi_f^J(\Omega,\mathbf{q}) &= -\frac{T}{2}\sum_m \int_{\mathbf{k}} \frac{(2\mathbf{k}\times\hat{\mathbf{q}})^2}{(2m)^2}\frac{1}{\mathrm{i}(\omega_m+\Omega_n)-\xi_{\mathbf{k}+\mathbf{q}}}\frac{1}{\mathrm{i}\omega_m-\xi_{\mathbf{k}}}|_{\mathrm{i}\Omega_n\to\Omega+\mathrm{i}\delta},
\end{aligned} \tag{B.55}$$

Eq. (B.52) can be solved self-consistently. In Tab. B.1, we show $\sigma_{b,j}$ and the final resistivity $\rho_b = (N\sigma_{b,j}^{-1})/2$ at different N, again the factor of 1/2 arises from the two spin/valley flavors. ρ_b increases roughly linearly with N, and the fit of the data points at different N gives

$$\rho_b = \left(R^{(0)} + R^{(1)}(N-1)\right)\frac{h}{e^2} = (3.62 + 1.68(N-1))\frac{h}{e^2}. \tag{B.56}$$

B.3 Appendix to Sec. 4.4

B.3.1 More Details about Self Energies

Model A Using the S-D equations, the fermion self-energies $\Sigma^A_{\psi/\chi}$ in imaginary time reads

$$\begin{aligned}
\tilde{\Sigma}^A_\psi(\tau) &= -2g^2 C_\psi C_\chi^2 \sqrt{\frac{M_2}{M_1}}\frac{(\cos(2\pi\Delta_\psi)+\cos(2\theta_\chi))\,\Gamma(1-2\Delta_\psi)\sin(\pi\Delta_\psi+\mathrm{sgn}(\tau)\,\theta_\psi)}{\pi^2\sin(2\pi\Delta_\psi)}\frac{\mathrm{sgn}(\tau)}{|\tau|^{2-2\Delta_\psi}}, \\
\tilde{\Sigma}^A_\chi(\tau) &= -2g^2 C_\chi C_\psi^2 \sqrt{\frac{M_1}{M_2}}\frac{(\cos(2\pi\Delta_\chi)+\cos(2\theta_\psi))\,\Gamma(1-2\Delta_\chi)\sin(\pi\Delta_\chi+\mathrm{sgn}(\tau)\,\theta_\chi)}{\pi^2\sin(2\pi\Delta_\chi)}\frac{\mathrm{sgn}(\tau)}{|\tau|^{2-2\Delta_\chi}}.
\end{aligned} \tag{B.57}$$

After Fourier transformation, the self-energy at complex frequency $z, \mathrm{Im}\,(z) > 0$ reads

$$\tilde{\Sigma}^A_\psi(z) = -2g^2 C_\psi C_\chi^2 \sqrt{\frac{M_2}{M_1}} \frac{\cos(2\pi\Delta_\psi) + \cos(2\theta_\chi)}{\pi(1-2\Delta_\psi)\sin(2\pi\Delta_\psi)} e^{i\left(\pi\Delta_\psi+\theta_\psi\right)} z^{1-2\Delta_\psi},$$
$$\tilde{\Sigma}^A_\chi(z) = -2g^2 C_\chi C_\psi^2 \sqrt{\frac{M_1}{M_2}} \frac{\cos(2\pi\Delta_\chi) + \cos(2\theta_\psi)}{\pi(1-2\Delta_\chi)\sin(2\pi\Delta_\chi)} e^{i(\pi\Delta_\chi+\theta_\chi)} z^{1-2\Delta_\chi}. \tag{B.58}$$

We can see that the self-energy for model A automatically takes the form $\Sigma^A(z) \propto e^{i(\pi\Delta+\theta)} z^{1-2\Delta}$ with a real factor.

Model B We then consider model B. Using the S-D equations, the self-energies $\Sigma^B_{\psi/\chi}$ in imaginary time are

$$\tilde{\Sigma}^B_\psi(\tau) = -4g^2 C_\psi C_\chi^2 \sqrt{\frac{M_2}{M_1}} \frac{\cos^2(\pi\Delta_\psi - \mathrm{sgn}(\tau)\theta_\chi)\sin(\pi\Delta_\psi - \mathrm{sgn}(\tau)\theta_\psi)\Gamma(1-2\Delta_\psi)}{\pi^2\sin(2\pi\Delta_\psi)} \frac{\mathrm{sgn}(\tau)}{|\tau|^{2-2\Delta_\psi}},$$
$$\tilde{\Sigma}^B_\chi(\tau) = -4g^2 C_\chi C_\psi^2 \sqrt{\frac{M_1}{M_2}} \frac{\cos^2(\pi\Delta_\chi - \mathrm{sgn}(\tau)\theta_\psi)\sin(\pi\Delta_\chi - \mathrm{sgn}(\tau)\theta_\chi)\Gamma(1-2\Delta_\chi)}{\pi^2\sin(2\pi\Delta_\chi)} \frac{\mathrm{sgn}(\tau)}{|\tau|^{2-2\Delta_\chi}}. \tag{B.59}$$

Again, after Fourier transformation, the self-energy with imaginary frequency reads:

$$\tilde{\Sigma}^B_\psi(z) = -g^2 C_\psi C_\chi^2 \sqrt{\frac{M_2}{M_1}} \frac{e^{-i2\left(\pi\Delta_\psi+\theta_\chi+\theta_\psi\right)}\left(\left(-1+e^{4i\theta_\chi}\right)e^{2i\left(\pi\Delta_\psi+\theta_\psi\right)} + 2e^{2i\left(\pi\Delta_\psi+\theta_\chi\right)} + e^{4i\pi\Delta_\psi}+1\right)}{\pi(1-2\Delta_\psi)\sin(2\pi\Delta_\psi)} e^{i\left(\pi\Delta_\psi+\theta_\psi\right)} z^{1-2\Delta_\psi},$$
$$\tilde{\Sigma}^B_\chi(z) = -g^2 C_\chi C_\psi^2 \sqrt{\frac{M_1}{M_2}} \frac{e^{-i2\left(\pi\Delta_\chi+\theta_\chi+\theta_\psi\right)}\left(\left(-1+e^{4i\theta_\psi}\right)e^{2i\left(\pi\Delta_\chi+\theta_\chi\right)} + 2e^{2i\left(\pi\Delta_\chi+\theta_\psi\right)} + e^{4i\pi\Delta_\chi}+1\right)}{\pi(1-2\Delta_\chi)\sin(2\pi\Delta_\chi)} e^{i\left(\pi\Delta_\chi+\theta_\chi\right)} z^{1-2\Delta_\chi}. \tag{B.60}$$

The self-consistency of the S-D equation demands the self-energy take the form $\Sigma^B(z) = -C^{-1}e^{i(\pi\Delta+\theta)}z^{1-2\Delta}$ with a real pre-factor C. Demanding the imaginary part of C vanish leads to

$$\cos(\theta_\chi+\theta_\psi)\left(\sin^2(\pi\Delta_\psi)\sin(\theta_\chi)\cos(\theta_\psi) - \cos^2(\pi\Delta_\psi)\cos(\theta_\chi)\sin(\theta_\psi)\right) = 0, \tag{B.61}$$
$$\cos(\theta_\chi+\theta_\psi)\left(\sin^2(\pi\Delta_\chi)\sin(\theta_\psi)\cos(\theta_\chi) - \cos^2(\pi\Delta_\chi)\cos(\theta_\psi)\sin(\theta_\chi)\right) = 0. \tag{B.62}$$

These equations can be simplified as

$$\frac{\tan\left(\theta_\psi\right)}{\tan\left(\pi\Delta_\psi\right)} = \frac{\tan\left(\theta_\chi\right)}{\tan\left(\pi\Delta_\chi\right)}, \tag{B.63}$$

where we have used $\Delta_\psi + \Delta_\chi = 1/2$ to simplify the equations. In fact, we can rewrite Eq. B.63 as

$$\frac{\sin\left(\pi\Delta_\psi + \theta_\psi\right)}{\sin\left(\pi\Delta_\psi - \theta_\psi\right)} = \frac{\sin\left(\pi\Delta_\chi + \theta_\chi\right)}{\sin\left(\pi\Delta_\chi - \theta_\chi\right)}, \tag{B.64}$$

which implies that the two types of fermions have the same spectral asymmetry.

The S-D equation also requires

$$C_\psi^{-2} C_\chi^{-2} = 2g^2 \sqrt{\frac{M_2}{M_1}} \frac{\cos\left(2\pi\Delta_\psi\right)\cos\left(2\left(\theta_\chi + \theta_\psi\right)\right) + \cos\left(2\theta_\psi\right)}{\pi\left(1 - 2\Delta_\psi\right)\sin\left(2\pi\Delta_\psi\right)}, \tag{B.65}$$

$$C_\chi^{-2} C_\psi^{-2} = 2g^2 \sqrt{\frac{M_1}{M_2}} \frac{\cos\left(2\pi\Delta_\chi\right)\cos\left(2\left(\theta_\chi + \theta_\psi\right)\right) + \cos\left(2\theta_\chi\right)}{\pi\left(1 - 2\Delta_\chi\right)\sin\left(2\pi\Delta_\chi\right)}. \tag{B.66}$$

Imposing the constraints Eq. 4.122 or Eq. B.64, we recover exactly the same self-consistent equations Eq. 4.102 and Eq. 4.103 as the model A.

B.3.2 Luttinger-Ward Calculation

Let us generalize the discussion by Georges-Parcollet-Sachdev [468] to our model, and the goal is to establish the relation between the filling factors (particle density) $\mathcal{Q}_\psi, \mathcal{Q}_\chi$ of model A, and $\mathcal{Q}$ of model B to the most relevant quantities such as $\Delta_{\psi/\chi}$ and $\theta_{\psi/\chi}$.

In the real-time formalism, at zero temperature, the filling factor can be evaluated by computing the following integral [468]

$$i\mathbb{P}\int_{-\infty}^{+\infty} \frac{d\omega}{2\pi} e^{i\omega 0^+} \left(\partial_\omega \log G\left(\omega\right) - G\left(\omega\right)\partial_\omega \tilde{\Sigma}\left(\omega\right)\right), \tag{B.67}$$

where $G\left(\omega\right) = G^R\left(\omega\right)\Theta\left(\omega\right) + G^A\left(\omega\right)\Theta\left(-\omega\right)$ is the time-ordered Green function with

$\Theta(\omega)$ being the Heaviside step function, and $G^{R/A}(\omega) = G(\omega \pm i0^+)$ is the real-time retarded/advanced Green's function obtained by replacing $i\omega_n$ by $\omega \pm i0^+$ in the imaginary-time Green's function. We use $\mathbb{P}$ to denote the the principal value of the integral $\mathbb{P}\int_{-\infty}^{+\infty} = \int_{-\infty}^{-\delta} + \int_{+\delta}^{+\infty}$ with a small positive cut off $\delta > 0$ [468].

Through the same line of arguments in Appendix A of Ref. 468 (also see Appendix D of Ref. 465), the filling factors for both fermions ψ and χ are

$$\mathcal{Q}_\psi = \frac{1}{2} - \frac{\theta_\psi}{\pi} - i\mathbb{P}\int_{-\infty}^{+\infty} \frac{d\omega}{2\pi} e^{i\omega 0^+} G_\psi(\omega)\, \partial_\omega \tilde{\Sigma}_\psi(\omega)\,, \tag{B.68}$$

$$\mathcal{Q}_\chi = \frac{1}{2} - \frac{\theta_\chi}{\pi} - i\mathbb{P}\int_{-\infty}^{+\infty} \frac{d\omega}{2\pi} e^{i\omega 0^+} G_\chi(\omega)\, \partial_\omega \tilde{\Sigma}_\chi(\omega)\,. \tag{B.69}$$

We are going to calculate the integral

$$\mathcal{I}_{\psi/\chi}^{A/B} = i\mathbb{P}\int_{-\infty}^{+\infty} \frac{d\omega}{2\pi} e^{i\omega 0^+} G_{\psi/\chi}(\omega)\, \partial_\omega \tilde{\Sigma}_{\psi/\chi}^{A/B}(\omega) \tag{B.70}$$

for two fermions ψ, χ in both model A and model B. To do so, we will use the properties of the spectral functions

$$\mathscr{A}_\psi(\omega) = \frac{C_\psi}{\pi}\frac{S_{\psi,\pm}}{|\omega|^{1-2\Delta_\psi}}, \quad \mathscr{A}_\chi(\omega) = \frac{C_\chi}{\pi}\frac{S_{\chi,\pm}}{|\omega|^{1-2\Delta_\chi}}, \tag{B.71}$$

where the notation $S_\pm$ stands for $S_\pm = \sin(\pi\Delta \pm \theta)$, and $\pm$ depends on the sign of ω. Our convention here is

$$\mathscr{A}(\omega) = \mp\frac{1}{\pi}\mathrm{Im}G^{R/A}(\omega)\,, \qquad G(z) = \int_{-\infty}^{+\infty} d\omega \frac{\mathscr{A}(\omega)}{z-\omega}. \tag{B.72}$$

Model A Using the melonic S-D equation, we obtain the Fourier transformation of $\tilde{\Sigma}_{\psi}^{A}(\tau)$

$$\begin{aligned}\tilde{\Sigma}_{\psi}^{A}(\omega) &= -4g^2\sqrt{\frac{M_2}{M_1}}\int_{-\infty}^{+\infty}\frac{d\nu_1}{2\pi}\frac{d\nu_2}{2\pi}\frac{d\nu_3}{2\pi}G_{\psi}(\nu_1)G_{\chi}(\nu_2)G_{\chi}(\nu_3)2\pi\delta(\nu_1+\nu_2-\nu_3-\omega)\\ &= -4g^2\sqrt{\frac{M_2}{M_1}}\int_{\{\omega_1^+,\omega_2^+,\omega_3^-\}\cup\{\omega_1^-,\omega_2^-,\omega_3^+\}}d\omega_1 d\omega_2 d\omega_3\frac{\mathscr{A}_{\psi}(\omega_1)\mathscr{A}_{\chi}(\omega_2)\mathscr{A}_{\chi}(\omega_3)}{\omega_1+\omega_2-\omega-\omega_3+i0^+\mathrm{sgn}(\omega_3)},\end{aligned} \tag{B.73}$$

where the notation $\{\omega_1^+,\omega_2^+,\omega_3^-\}$ means the integration domain $\{\omega_1>0,\omega_2>0,\omega_3<0\}$. Accordingly, the integral Eq. B.70 for ψ reads

$$\begin{aligned}\mathcal{I}_{\psi}^{A} &= i\mathbb{P}\int_{-\infty}^{+\infty}\frac{d\omega d\omega_0}{2\pi}\frac{\mathscr{A}_{\psi}(\omega_0)e^{i\omega 0^+}}{\omega-\omega_0+i0^+\mathrm{sgn}(\omega_0)}\partial_{\omega}\tilde{\Sigma}_{\psi}^{A}(\omega)\\ &= \frac{4g^2}{2\pi i}\sqrt{\frac{M_2}{M_1}}\int_{\Gamma}d\omega_0 d\omega_1 d\omega_2 d\omega_3\mathscr{A}_{\psi}(\omega_0)\mathscr{A}_{\psi}(\omega_1)\mathscr{A}_{\chi}(\omega_2)\mathscr{A}_{\chi}(\omega_3)\Phi_{\delta}\left(\omega_1+\omega_2-\omega_3-i0^+\mathrm{sgn}\omega_1,\omega_0-i0^+\mathrm{sgn}\omega_0\right).\end{aligned} \tag{B.74}$$

The integration domain of $\mathcal{I}_{\psi}^{A}$ is $\Gamma=\Gamma_1\cup\Gamma_2\cup\Gamma_3\cup\Gamma_4$ where

$$\begin{aligned}\Gamma_1 &= \{\omega_0^+,\omega_1^+,\omega_2^+,\omega_3^-\}, \qquad \Gamma_2 = \{\omega_0^-,\omega_1^+,\omega_2^+,\omega_3^-\},\\ \Gamma_3 &= \{\omega_0^+,\omega_1^-,\omega_2^-,\omega_3^+\}, \qquad \Gamma_4 = \{\omega_0^-,\omega_1^-,\omega_2^-,\omega_3^+\}.\end{aligned} \tag{B.75}$$

We have also used the function

$$\Phi_{\delta}(a+i\epsilon_a,b+i\epsilon_b) = \mathbb{P}\int_{-\infty}^{+\infty}dz\frac{e^{i\omega 0^+}}{(z-a-i\epsilon_a)^2(z-b-i\epsilon_b)} \tag{B.76}$$

where $a,b\in\mathbb{R}$ and $\epsilon_a,\epsilon_b\to 0$. The expression of Φ_{δ} is explicitly calculated as Eq. A8 in Ref. 468. In the following, we will only use its property $\Phi_{\delta}(-a-i\epsilon_a,-b-i\epsilon_b)=$

$-\Phi_\delta\left(a+i\epsilon_a, b+i\epsilon_b\right)$. By changing of variables, we could write the integral as

$$\mathcal{I}_\psi^A = \frac{4g^2}{2\pi i}\sqrt{\frac{M_2}{M_1}}\int_{x_i>0}\prod_{i=0}^{3}dx_i \left(\begin{array}{c} \left(\begin{array}{c}\mathscr{A}_\psi\left(x_1\right)\mathscr{A}_\chi\left(x_2\right)\mathscr{A}_\chi\left(-x_3\right)\mathscr{A}_\psi\left(-x_0\right)\\ -\mathscr{A}_\psi\left(-x_1\right)\mathscr{A}_\chi\left(-x_2\right)\mathscr{A}_\chi\left(x_3\right)\mathscr{A}_\psi\left(x_0\right)\end{array}\right)\\ \times\Phi_\delta\left(x_1+x_2+x_3-i\epsilon_1, -x_0+i\epsilon_0\right)+\\ \left(\begin{array}{c}\mathscr{A}_\psi\left(x_1\right)\mathscr{A}_\chi\left(x_2\right)\mathscr{A}_\chi\left(-x_3\right)\mathscr{A}_\psi\left(x_0\right)\\ -\mathscr{A}_\psi\left(-x_1\right)\mathscr{A}_\chi\left(-x_2\right)\mathscr{A}_\chi\left(x_3\right)\mathscr{A}_\psi\left(-x_0\right)\end{array}\right)\\ \times\Phi_\delta\left(x_1+x_2+x_3-i\epsilon_1, x_0-i\epsilon_0\right)\end{array}\right). \tag{B.77}$$

Using the expressions Eq. B.71, we have

$$\begin{aligned}&\mathscr{A}_\psi\left(x_1\right)\mathscr{A}_\chi\left(x_2\right)\mathscr{A}_\chi\left(-x_3\right)\mathscr{A}_\psi\left(-x_0\right)-\mathscr{A}_\psi\left(-x_1\right)\mathscr{A}_\chi\left(-x_2\right)\mathscr{A}_\chi\left(x_3\right)\mathscr{A}_\psi\left(x_0\right)\\ =&\frac{C_\psi^2C_\chi^2}{\pi^4}\frac{S_{\psi,+}S_{\chi,+}S_{\chi,-}S_{\psi,-}-S_{\psi,-}S_{\chi,-}S_{\chi,+}S_{\psi,+}}{\left|x_0\right|^{1-2\Delta_\psi}\left|x_1\right|^{1-2\Delta_\psi}\left|x_2\right|^{1-2\Delta_\chi}\left|x_3\right|^{1-2\Delta_\chi}}=0.\end{aligned} \tag{B.78}$$

Thus, the first term vanishes, and we only need to calculate the second term

$$\mathcal{I}_\psi^A = \frac{4g^2}{2\pi i}\sqrt{\frac{M_2}{M_1}}\frac{C_\psi^2C_\chi^2}{\pi^4}\int_{u_i>0}\prod_{i=0}^{3}du_i\frac{S_{\psi,+}^2S_{\chi,+}S_{\chi,-}-S_{\psi,-}^2S_{\chi,-}S_{\chi,+}}{\left|u_0u_1\right|^{1-2\Delta_\psi}\left|u_2u_3\right|^{1-2\Delta_\chi}}\Phi_{\delta=1}\left(u_1+u_2+u_3-i\epsilon_1, u_0-i\epsilon_0\right), \tag{B.79}$$

where we have introduced new variables $x_i = u_i\delta$ to take the limit $\delta\to 0^+$.

Before calculating the integral, we want to show $\mathcal{I}_\psi^A$ does not depend on M_1, M_2. On one hand, the straightforward calculation gives

$$S_{\psi,+}^2S_{\chi,+}S_{\chi,-}-S_{\psi,-}^2S_{\chi,-}S_{\chi,+}=\frac{1}{2}\sin\left(2\pi\Delta_\psi\right)\sin\left(2\theta_\psi\right)\left(\cos\left(2\theta_\chi\right)-\cos\left(2\pi\Delta_\chi\right)\right). \tag{B.80}$$

On the other hand, we read from the S-D equation

$$C_\psi^2C_\chi^2=\frac{1}{2g^2}\sqrt{\frac{M_1}{M_2}}\frac{\pi\left(1-2\Delta_\psi\right)\sin\left(2\pi\Delta_\psi\right)}{\cos\left(2\pi\Delta_\psi\right)+\cos\left(2\theta_\chi\right)}. \tag{B.81}$$

They together give us

$$\mathcal{I}_{\psi}^{A}=\frac{1}{i\pi^{4}}F^{A}\left(\Delta_{\psi}\right)\left(\frac{1}{2}-\Delta_{\psi}\right)\sin^{2}\left(2\pi\Delta_{\psi}\right)\sin\left(2\theta_{\psi}\right), \tag{B.82}$$

where

$$F^{A}\left(\Delta_{\psi}\right)=\int_{u_{i}>0}\prod_{i=0}^{3}du_{i}\frac{\Phi_{\delta=1}\left(u_{1}+u_{2}+u_{3}-i\epsilon_{1},u_{0}-i\epsilon_{0}\right)}{\left|u_{0}u_{1}\right|^{1-2\Delta_{\psi}}\left|u_{2}u_{3}\right|^{2\Delta_{\psi}}}. \tag{B.83}$$

Then we define $x=u_{0},y=u_{1}+u_{2}+u_{3}$, and integrate over u_{2},u_{3}. The result is

$$F\left(\Delta_{\psi}\right)=\frac{\pi}{\left(1-2\Delta_{\psi}\right)\sin\left(2\pi\Delta_{\psi}\right)}\int_{0}^{\infty}dxdy\left(\frac{y}{x}\right)^{1-2\Delta_{\psi}}\Phi_{\delta=1}\left(y-i\epsilon_{1},x-i\epsilon_{0}\right). \tag{B.84}$$

We proceed to calculate the integral in the following way

$$\begin{aligned}&\int_{0}^{\infty}dxdy\left(\frac{y}{x}\right)^{1-2\Delta_{\psi}}\Phi_{\delta=1}\left(y-i\epsilon_{1},x-i\epsilon_{0}\right)\\&=\int_{0}^{\infty}dxdy\left(\frac{y}{x}\right)^{1-2\Delta_{\psi}}\mathbb{P}_{\delta=1}\int_{-\infty}^{+\infty}dz\frac{e^{i\omega0^{+}}}{\left(z-y+i\epsilon_{1}\right)^{2}\left(z-x+i\epsilon_{0}\right)}\\&=\pi^{2}\frac{\left(1-2\Delta_{\psi}\right)}{\sin^{2}\left(2\pi\Delta_{\psi}\right)}\mathbb{P}_{\delta=1}\int_{-\infty}^{+\infty}dz\frac{e^{iz0^{+}}}{z}=i\pi^{3}\frac{\left(1-2\Delta_{\psi}\right)}{\sin^{2}\left(2\pi\Delta_{\psi}\right)}.\end{aligned} \tag{B.85}$$

Thus, we have

$$F\left(\Delta_{\psi}\right)=\frac{i\pi^{4}}{\sin^{3}\left(2\pi\Delta_{\psi}\right)}\quad\Longrightarrow\quad\mathcal{I}_{\psi}=\left(\frac{1}{2}-\Delta_{\psi}\right)\frac{\sin\left(2\theta_{\psi}\right)}{\sin\left(2\pi\Delta_{\psi}\right)}. \tag{B.86}$$

In conclusion, we arrive at the result Eq. 4.105, which is consistent with the expression $\mathcal{Q}\left(\theta,\Delta\right)$ in Ref 465 for the complex SYK_{q} model with the conformal dimension $\Delta=1/q$.

Through similar calculations based on

$$\mathcal{I}_{\chi}^{A}=\frac{4g^{2}}{2\pi i}\sqrt{\frac{M_{1}}{M_{2}}}\frac{C_{\psi}^{2}C_{\chi}^{2}}{\pi^{4}}\int_{u_{i}>0}\prod_{i=0}^{3}du_{i}\frac{S_{\chi,+}^{2}S_{\psi,+}S_{\psi,-}-S_{\chi,-}^{2}S_{\psi,-}S_{\psi,+}}{\left|u_{0}u_{1}\right|^{1-2\Delta_{\psi}}\left|u_{2}u_{3}\right|^{1-2\Delta_{\chi}}}\Phi_{\delta=1}\left(u_{1}+u_{2}+u_{3}-i\epsilon_{1},u_{0}-i\epsilon_{0}\right), \tag{B.87}$$

we obtain the identical expression Eq. 4.106 for χ fermion. In model A, θ_ψ, θ_χ are two independent variables, and U (1) charges for ψ, χ are conserved separately.

Model B The expression of $\tilde{\Sigma}^B$ is a bit different from $\tilde{\Sigma}^A$

$$\begin{aligned}\tilde{\Sigma}^B_\psi(\omega) =& -4g^2\sqrt{\frac{M_2}{M_1}}\int_{-\infty}^{+\infty}\frac{d\nu_1}{2\pi}\frac{d\nu_2}{2\pi}\frac{d\nu_3}{2\pi}G_\chi(\nu_1)G_\chi(\nu_2)G_\psi(\nu_3)2\pi\delta(\nu_1+\nu_2-\nu_3-\omega)\\ =& -4g^2\sqrt{\frac{M_2}{M_1}}\int_{\{\omega_1^+,\omega_2^+,\omega_3^-\}\cup\{\omega_1^-,\omega_2^-,\omega_3^+\}}d\omega_1 d\omega_2 d\omega_3\frac{\mathscr{A}_\chi(\omega_1)\mathscr{A}_\chi(\omega_2)\mathscr{A}_\psi(\omega_3)}{\omega_1+\omega_2-\omega-\omega_3+i0^+\mathrm{sgn}(\omega_3)}.\end{aligned} \tag{B.88}$$

Now the integral Eq. B.70 for ψ reads

$$\mathcal{I}^B_\psi = \frac{4g^2}{2\pi i}\sqrt{\frac{M_2}{M_1}}\int_\Gamma d\omega_0 d\omega_1 d\omega_2 d\omega_3 \mathscr{A}_\psi(\omega_0)\mathscr{A}_\chi(\omega_1)\mathscr{A}_\chi(\omega_2)\mathscr{A}_\psi(\omega_3)\Phi_\delta\left(\omega_1+\omega_2-\omega_3-i0^+\mathrm{sgn}\omega_1, \omega_0-i0^+\mathrm{sgn}\omega_0\right) \tag{B.89}$$

with the same integration domain as $\mathcal{I}^A_\psi$. By changing of variables, we could write the integral as

$$\mathcal{I}^B_\psi = \frac{4g^2}{2\pi i}\sqrt{\frac{M_2}{M_1}}\int_{x_i>0}\prod_{i=0}^{3}dx_i\left(\begin{array}{c}\left(\begin{array}{c}\mathscr{A}_\chi(x_1)\mathscr{A}_\chi(x_2)\mathscr{A}_\psi(-x_3)\mathscr{A}_\psi(-x_0)\\ -\mathscr{A}_\chi(-x_1)\mathscr{A}_\chi(-x_2)\mathscr{A}_\psi(x_3)\mathscr{A}_\psi(x_0)\end{array}\right)\\ \times\Phi_\delta(x_1+x_2+x_3-i\epsilon_1, -x_0+i\epsilon_0)+\\ \left(\begin{array}{c}\mathscr{A}_\chi(x_1)\mathscr{A}_\chi(x_2)\mathscr{A}_\psi(-x_3)\mathscr{A}_\psi(x_0)\\ -\mathscr{A}_\chi(-x_1)\mathscr{A}_\chi(-x_2)\mathscr{A}_\psi(x_3)\mathscr{A}_\psi(-x_0)\end{array}\right)\\ \times\Phi_\delta(x_1+x_2+x_3-i\epsilon_1, x_0-i\epsilon_0)\end{array}\right). \tag{B.90}$$

Using the expressions Eq. B.71, we have

$$\begin{aligned}&\mathscr{A}_\chi(x_1)\mathscr{A}_\chi(x_2)\mathscr{A}_\psi(-x_3)\mathscr{A}_\psi(-x_0)-\mathscr{A}_\chi(-x_1)\mathscr{A}_\chi(-x_2)\mathscr{A}_\psi(x_3)\mathscr{A}_\psi(x_0)\\ =&\frac{C_\psi^2C_\chi^2}{\pi^4}\frac{S_{\chi,+}S_{\chi,+}S_{\psi,-}S_{\psi,-}-S_{\chi,-}S_{\chi,-}S_{\psi,+}S_{\psi,+}}{|x_0|^{1-2\Delta_\psi}|x_1|^{1-2\Delta_\chi}|x_2|^{1-2\Delta_\chi}|x_3|^{1-2\Delta_\psi}},\end{aligned} \tag{B.91}$$

which seems nonzero at first glance. But it indeed vanishes due to the constraint Eq. 4.122, and we only need to calculate the second term

$$\mathcal{I}_{\psi}^{B}=\frac{4g^{2}}{2\pi i}\sqrt{\frac{M_{2}}{M_{1}}}\frac{C_{\psi}^{2}C_{\chi}^{2}}{\pi^{4}}\int_{u_{i}>0}\prod_{i=0}^{3}du_{i}\frac{S_{\chi,+}^{2}S_{\psi,-}S_{\psi,+}-S_{\chi,-}^{2}S_{\psi,+}S_{\psi,-}}{\left|u_{0}u_{3}\right|^{1-2\Delta_{\psi}}\left|u_{1}u_{2}\right|^{1-2\Delta_{\chi}}}\Phi_{\delta=1}\left(u_{1}+u_{2}+u_{3}-i\epsilon_{1},u_{0}-i\epsilon_{0}\right), \tag{B.92}$$

where we have again used new variables $x_i = u_i\delta$. We proceed to analyze the coefficient. The straightforward calculation gives

$$S_{\chi,+}^{2}S_{\psi,+}S_{\psi,-}-S_{\chi,-}^{2}S_{\psi,-}S_{\psi,+}=\frac{1}{2}\sin\left(2\pi\Delta_{\chi}\right)\sin\left(2\theta_{\chi}\right)\left(\cos\left(2\theta_{\psi}\right)-\cos\left(2\pi\Delta_{\psi}\right)\right). \tag{B.93}$$

By using the expression Eq. B.81 of $C_{\psi}^{2}C_{\chi}^{2}$ and the constraint Eq. 4.122, we are able to obtain a similar form comparing to Eq. B.82

$$\mathcal{I}_{\psi}^{B}=\frac{1}{i\pi^{4}}F^{B}\left(\Delta_{\psi}\right)\left(\frac{1}{2}-\Delta_{\psi}\right)\sin^{2}\left(2\pi\Delta_{\psi}\right)\sin\left(2\theta_{\psi}\right), \tag{B.94}$$

where

$$F^{B}\left(\Delta_{\psi}\right)=\int_{u_{i}>0}\prod_{i=0}^{3}du_{i}\frac{\Phi_{\delta=1}\left(u_{1}+u_{2}+u_{3}-i\epsilon_{1},u_{0}-i\epsilon_{0}\right)}{\left|u_{0}u_{3}\right|^{1-2\Delta_{\psi}}\left|u_{1}u_{2}\right|^{2\Delta_{\psi}}}. \tag{B.95}$$

The definition of $F^{B}\left(\Delta\right)$ here differs from $F^{A}\left(\Delta\right)$ by exchanging $u_1 \leftrightarrow u_3$. Notice that $\epsilon_1 = -\epsilon_3$ which makes the definition looks nonequivalent. However, after defining $x = u_0, y = u_1+u_2+u_3$, and integrating over u_2, u_3, we still have the expression Eq. B.84. Thus, we have exactly the same result Eq. 4.105 for $\langle\mathcal{Q}_{\psi}^{B}\rangle$.

Through similar calculations for χ fermion

$$\mathcal{I}_{\chi}^{B}=\frac{4g^{2}}{2\pi i}\sqrt{\frac{M_{1}}{M_{2}}}\frac{C_{\psi}^{2}C_{\chi}^{2}}{\pi^{4}}\int_{u_{i}>0}\prod_{i=0}^{3}du_{i}\frac{S_{\psi,+}^{2}S_{\chi,-}S_{\chi,+}-S_{\psi,-}^{2}S_{\chi,+}S_{\chi,-}}{\left|u_{0}u_{3}\right|^{1-2\Delta_{\psi}}\left|u_{1}u_{2}\right|^{1-2\Delta_{\chi}}}\Phi_{\delta=1}\left(u_{1}+u_{2}+u_{3}-i\epsilon_{1},u_{0}-i\epsilon_{0}\right), \tag{B.96}$$

we again obtain exactly the same expression Eq. 4.106 for $\mathcal{Q}_{\chi}^{B}$. Despite the similarity in expressions, only the total $\mathrm{U}\left(1\right)$ charge filling factor Eq. 4.119 is a conserved quantity in

model B.

B.4 Appendix to Sec. 5.1

B.4.1 More Calculations for $\tilde{O}^{(1)}_{\mathcal{C},\mathcal{C}'}$

Let's first analyze the expectation value of $\tilde{O}^{(1)}_{\mathcal{C},\mathcal{C}'}$ defined in Eq. 5.34, which can be calculated using the continuous gauge theory Eq. 5.37 via

$$\langle \widetilde{O}^{(1)}_{\mathcal{C},\mathcal{C}'} \rangle \sim \exp\left[\left(\oint_{\mathcal{C}} \oint_{\mathcal{C}'} - \frac{1}{2} \oint_{\mathcal{C}} \oint_{\mathcal{C}} - \frac{1}{2} \oint_{\mathcal{C}'} \oint_{\mathcal{C}'} \right) \langle a_\mu(\mathbf{x}) a_\nu(\mathbf{x}') \rangle \, dx^\mu dx'^\nu \right]. \tag{B.97}$$

With a Faddeev-Popov type gauge fixing ζ term, the gauge field propagator $D_{\mu\nu}(\omega, \mathbf{k})$ is given by

$$D^{-1}_{\mu\nu}(\omega, \mathbf{k}) = \begin{pmatrix} \omega^2/U + 2tk_y^2 k_z^2 & -tk_x k_y k_z^2 & -tk_x k_z k_y^2 \\ -tk_x k_y k_z^2 & \omega^2/U + 2tk_z^2 k_x^2 & -tk_y k_z k_x^2 \\ -tk_x k_z k_y^2 & -tk_y k_z k_x^2 & \omega^2/U + 2tk_x^2 k_y^2 \end{pmatrix} - \zeta^{-1} k_\mu k_\nu. \tag{B.98}$$

Our gauge choice is $\zeta \to 0$. Since we are interested in the expectation value of ODO of a static state, we will use the equal time Green's function. Directly using the full form of $D_{\mu\nu}$ would be tedious, but we observe that D_{xx} has linear singularity at $k_y \to 0$, and $k_z \to 0$, which will dominate IR behavior of the Green's function. We can extract the most singular part of the Green's function, then D_{xx} at $\tau = 0$ reads

$$D_{xx}(\tau = 0, \mathbf{k}) = \int \frac{d\omega}{2\pi} D_{xx}(\omega, \mathbf{k}) = \sqrt{\frac{U}{t}} \frac{1}{\sqrt{6}} \left(\frac{k_y^2}{\left(k_x^2 + k_y^2\right)^{3/2}} \frac{1}{|k_z|} + \frac{k_z^2}{\left(k_x^2 + k_z^2\right)^{3/2}} \frac{1}{|k_y|} \right) + \cdots \tag{B.99}$$

This approximate form of Green's function captures the singularity at $k_y \to 0$ and $k_z \to 0$ separately. There is an extra singularity when multiple momenta approach zero simultaneously. But since this extra singularity occurs at a much smaller measure of the

momentum space compared with the singularities captured by Eq. B.99, we take the approximate form of Green's function Eq. B.99. Further analysis may be demanded to address all singularities in the Green's function.

Similarly, we approximate the off-diagonal term D_{xy} around its singularity $k_z = 0$

$$D_{xy}(\tau = 0, \mathbf{k}) = \sqrt{\frac{U}{t}} \frac{-k_x k_y}{\sqrt{6}\left(k_x^2 + k_y^2\right)^{3/2}} \frac{1}{|k_z|} + \cdots . \tag{B.100}$$

Other components of $D_{\mu\nu}$ can be obtained by the permutations of k_x, k_y, k_z. The real-space expression of the Green's function is then obtained through Fourier transformation:

$$D_{\mu\nu}(\tau = 0, \mathbf{x}) = \sqrt{\frac{U}{t}} \frac{-1}{2\sqrt{6}\pi^2} \begin{pmatrix} \frac{x^2 \log|z\delta|}{(x^2+y^2)^{3/2}} + \frac{x^2 \log|y\delta|}{(x^2+z^2)^{3/2}} & \frac{xy \log|z\delta|}{(x^2+y^2)^{3/2}} & \frac{xz \log|y\delta|}{(x^2+z^2)^{3/2}} \\ \frac{xy \log|z\delta|}{(x^2+y^2)^{3/2}} & \frac{y^2 \log|x\delta|}{(y^2+z^2)^{3/2}} + \frac{y^2 \log|z\delta|}{(y^2+x^2)^{3/2}} & \frac{yz \log|x\delta|}{(y^2+z^2)^{3/2}} \\ \frac{xz \log|y\delta|}{(x^2+z^2)^{3/2}} & \frac{yz \log|x\delta|}{(y^2+z^2)^{3/2}} & \frac{z^2 \log|y\delta|}{(z^2+x^2)^{3/2}} + \frac{z^2 \log|x\delta|}{(z^2+y^2)^{3/2}} \end{pmatrix}, \tag{B.101}$$

where $\delta > 0$ is a small IR cut-off, which is needed in the Fourier transformation of $1/|k|$. This is the effective real-space Green function that can be used to calculate the scaling behaviors of $\langle \tilde{O}^{(1)}_{\mathcal{C},\mathcal{C}'} \rangle$.

Let's consider two identical squares $\mathcal{C}, \mathcal{C}'$ that are completely parallel to each other. We assume $\mathcal{C}$ has four corners $(0,0,0), (L,0,0), (L,L,0), (0,L,0)$, and $\mathcal{C}'$ has four corners $(0,0,Z), (L,0,Z), (L,L,Z), (0,L,Z)$. Based on the real-space Green function Eq. B.101, an integral over $\mathcal{C}, \mathcal{C}'$ leads to

$$-\log\langle \tilde{O}^{(1)}_{\mathcal{C},\mathcal{C}'} \rangle = \sqrt{\frac{U}{t}} \frac{4L}{\sqrt{6}\pi^2} \begin{pmatrix} \left(2(\sqrt{L^2+Z^2} - Z)/L + \log(\sqrt{L^2+Z^2} - L)\right) \log(L/\epsilon) + \log L \left(\log L - 3\log\epsilon\right) \\ -\log(LZ) + \left(\sqrt{2} - \sinh^{-1}(1)\right) \log(Z/\epsilon) + 2\log\epsilon(\log\epsilon + 1) \end{pmatrix}. \tag{B.102}$$

where $\epsilon > 0$ is a small UV cut-off. It is important to notice that, although the real space Green's function has a dependence on the IR cut-off δ, the final result of $\tilde{O}^{(1)}_{\mathcal{C},\mathcal{C}'}$ is free from any IR-divergence. We are most interested in the behaviors of $\langle \tilde{O}^{(1)}_{\mathcal{C},\mathcal{C}'} \rangle$ under

the large-L and large-Z limits:

$$\langle \tilde{O}^{(1)}_{\mathcal{C},\mathcal{C}'} \rangle \sim \begin{cases} e^{-\sqrt{\frac{U}{t}}\frac{4}{\sqrt{6}\pi^2}L\left(\log(L/\epsilon)+\sqrt{2}-1-\sinh^{-1}(1)\right)\log Z} = e^{-c_1\sqrt{\frac{U}{t}}\log Z} & L<+\infty, Z\to+\infty \\ e^{-\sqrt{\frac{U}{t}}\frac{4}{\sqrt{6}\pi^2}(2\log(Z/\epsilon)+1-\log 2)L\log L} = e^{-c_2\sqrt{\frac{U}{t}}L\log L} & Z<+\infty, L\to+\infty \end{cases}, \quad \text{(B.103)}$$

where c_1 and c_2 are two numerical coefficients which depend on the UV cut-off ϵ.

Bibliography

[1] S Kasahara, T Shibauchi, K Hashimoto, K Ikada, S Tonegawa, R Okazaki, H Shishido, H Ikeda, H Takeya, K Hirata, et al. Evolution from non-fermi-to fermi-liquid transport via isovalent doping in $BaFe_2(As_{1-x}P_x)_2$ superconductors. *Physical Review B*, 81(18):184519, 2010.

[2] Yuan Cao, Valla Fatemi, Ahmet Demir, Shiang Fang, Spencer L. Tomarken, Jason Y. Luo, Javier D. Sanchez-Yamagishi, Kenji Watanabe, Takashi Taniguchi, Efthimios Kaxiras, and et al. Correlated insulator behaviour at half-filling in magic-angle graphene superlattices. *Nature*, 556(7699):80–84, Mar 2018.

[3] Yuan Cao, Valla Fatemi, Shiang Fang, Kenji Watanabe, Takashi Taniguchi, Efthimios Kaxiras, and Pablo Jarillo-Herrero. Unconventional superconductivity in magic-angle graphene superlattices. *Nature*, 556(7699):43–50, Mar 2018.

[4] Tingxin Li, Shengwei Jiang, Lizhong Li, Yang Zhang, Kaifei Kang, Jiacheng Zhu, Kenji Watanabe, Takashi Taniguchi, Debanjan Chowdhury, Liang Fu, and et al. Continuous Mott transition in semiconductor moiré superlattices. *Nature*, 597(7876):350–354, Sep 2021.

[5] Fernando Gargiulo and Oleg V Yazyev. Structural and electronic transformation in low-angle twisted bilayer graphene. *2D Materials*, 5(1):015019, 2018.

[6] Jonathan S. Alden, Adam W. Tsen, Pinshane Y. Huang, Robert Hovden, Lola Brown, Jiwoong Park, David A. Muller, and Paul L. McEuen. Strain solitons and topological defects in bilayer graphene. *Proceedings of the National Academy of Sciences*, 110(28):11256–11260, 2013.

[7] S. S. Sunku, G. X. Ni, B. Y. Jiang, H. Yoo, A. Sternbach, A. S. McLeod, T. Stauber, L. Xiong, T. Taniguchi, K. Watanabe, P. Kim, M. M. Fogler, and D. N. Basov. Photonic crystals for nano-light in moiré graphene superlattices. *to appear on Science*, 362(6419):1153–1156, 2018.

[8] LD Landau. On the theory of the fermi liquid. *Sov. Phys. JETP*, 8(1):70, 1959.

[9] Lev Davidovich Landau. On the theory of phase transitions. i. *Zh. Eksp. Teor. Fiz.*, 11:19, 1937.

[10] Sidney Coleman, Julius Wess, and Bruno Zumino. Structure of phenomenological lagrangians. i. *Physical Review*, 177(5):2239, 1969.

[11] Curtis G Callan Jr, Sidney Coleman, Julius Wess, and Bruno Zumino. Structure of phenomenological lagrangians. ii. *Physical Review*, 177(5):2247, 1969.

[12] Subir Sachdev. *Quantum Phase Transitions*. Cambridge University Press, 2 edition, 2011.

[13] Eduardo Fradkin. *Field Theories of Condensed Matter Physics*. Cambridge University Press, 2 edition, 2013.

[14] Chong Wang, Adam Nahum, Max A Metlitski, Cenke Xu, and T Senthil. Deconfined quantum critical points: symmetries and dualities. *Physical Review X*, 7(3):031051, 2017.

[15] Hendrik A Kramers and Gregory H Wannier. Statistics of the two-dimensional ferromagnet. part i. *Physical Review*, 60(3):252, 1941.

[16] Wenjie Ji and Xiao-Gang Wen. Categorical symmetry and noninvertible anomaly in symmetry-breaking and topological phase transitions. *Physical Review Research*, 2(3):033417, 2020.

[17] Michael E Peskin. Mandelstam-'t hooft duality in abelian lattice models. *Annals of Physics*, 113(1):122–152, 1978.

[18] C. Dasgupta and B. I. Halperin. Phase transition in a lattice model of superconductivity. *Physical Review Letters*, 47:1556, Nov 1981.

[19] MB Halpern. Field-strength and dual variable formulations of gauge theory. *Physical Review D*, 19(2):517, 1979.

[20] E. H. Lieb, T. D. Schultz, and D. C. Mattis. Two soluble models of an antiferromagnetic chain. *Ann. Phys.*, 16(3):407, 1961.

[21] Masaki Oshikawa. Commensurability, excitation gap, and topology in quantum many-particle systems on a periodic lattice. *Physical Review Letters*, 84:1535–1538, Feb 2000.

[22] M. B. Hastings. Lieb-Schultz-Mattis in higher dimensions. *Physical Review B*, 69(10):104431, Mar 2004.

[23] F Duncan M Haldane. O(3) nonlinear σ model and the topological distinction between integer-and half-integer-spin antiferromagnets in two dimensions. *Physical Review Letters*, 61(8):1029, 1988.

[24] N Read and Subir Sachdev. Valence-bond and spin-peierls ground states of low-dimensional quantum antiferromagnets. *Physical Review Letters*, 62(14):1694, 1989.

[25] N Read and Subir Sachdev. Spin-peierls, valence-bond solid, and néel ground states of low-dimensional quantum antiferromagnets. *Physical Review B*, 42(7):4568, 1990.

[26] Nathan Seiberg, T Senthil, Chong Wang, and Edward Witten. A duality web in $2+1$ dimensions and condensed matter physics. *Annals of Physics*, 374:395–433, 2016.

[27] T Senthil, Dam Thanh Son, Chong Wang, and Cenke Xu. Duality between $(2+1)d$ quantum critical points. *Physics Reports*, 827:1–48, 2019.

[28] Lorenzo Di Pietro, Davide Gaiotto, Edoardo Lauria, and Jingxiang Wu. 3d abelian gauge theories at the boundary. *Journal of High Energy Physics*, 2019(5):1–60, 2019.

[29] Tudor Dimofte, Davide Gaiotto, and Sergei Gukov. Gauge theories labelled by three-manifolds. *Communications in Mathematical Physics*, 325(2):367–419, 2014.

[30] John Cardy. *Scaling and Renormalization in Statistical Physics*. Cambridge Lecture Notes in Physics. Cambridge University Press, 1996.

[31] Hans Werner Diehl. *Field-theoretic Approach to Critical Behaviour at Surfaces*. in Phase Transitions and Critical Phenomena, edited by C. Domb and J. L. Lebowitz. Academic Press, 1986.

[32] Hans Werner Diehl. The theory of boundary critical phenomena. *International Journal of Modern Physics B*, 11(30):3503–3523, 1997.

[33] Thomas Scaffidi, Daniel E. Parker, and Romain Vasseur. Gapless symmetry-protected topological order. *Phys. Rev. X*, 7:041048, Nov 2017.

[34] Ruben Verresen, Nick G. Jones, and Frank Pollmann. Topology and edge modes in quantum critical chains. *Physical Review Letters*, 120:057001, Jan 2018.

[35] Ruben Verresen, Ryan Thorngren, Nick G Jones, and Frank Pollmann. Gapless topological phases and symmetry-enriched quantum criticality. *Physical Review X*, 11(4):041059, 2021.

[36] Guo-Yi Zhu, Tao Xiang, and Guang-Ming Zhang. Unconventional surface critical behavior induced by a quantum phase transition from the two-dimensional Affleck-Kennedy-Lieb-Tasaki phase to a Néel-ordered phase. *arXiv:1806.07535*, 118:087201, Feb 2018.

[37] Lukas Weber, Francesco Parisen Toldin, and Stefan Wessel. Nonordinary edge criticality of two-dimensional quantum critical magnets. *Physical Review B*, 98:140403, Oct 2018.

[38] Lukas Weber and Stefan Wessel. Nonordinary criticality at the edges of planar spin-1 Heisenberg antiferromagnets. *Physical Review B*, 100:054437, Aug 2019.

[39] Tarun Grover and Ashvin Vishwanath. Quantum criticality in topological insulators and superconductors: Emergence of strongly coupled majoranas and supersymmetry. *arXiv e-prints*, page arXiv:1206.1332, June 2012.

[40] Ruben Verresen. Topology and edge states survive quantum criticality between topological insulators. *arXiv preprint arXiv:2003.05453*, 2020.

[41] Max Metlitski. Boundary criticality of the O(N) model in $d = 3$ critically revisited. *SciPost Physics*, 12(4):131, 2022.

[42] R. Shankar. Renormalization-group approach to interacting fermions. *Rev. Mod. Phys.*, 66:129–192, Jan 1994.

[43] Hilbert v. Löhneysen, Achim Rosch, Matthias Vojta, and Peter Wölfle. Fermi-liquid instabilities at magnetic quantum phase transitions. *Rev. Mod. Phys.*, 79:1015–1075, Aug 2007.

[44] Joseph Polchinski. Low-energy dynamics of the spinon-gauge system. *Nuclear Physics B*, 422(3):617–633, 1994.

[45] Chetan Nayak and Frank Wilczek. Non-fermi liquid fixed point in $2 + 1$ dimensions. *Nuclear Physics B*, 417(3):359–373, 1994.

[46] Chetan Nayak and Frank Wilczek. Renormalization group approach to low temperature properties of a non-fermi liquid metal. *Nuclear Physics B*, 430(3):534–562, 1994.

[47] Vadim Oganesyan, Steven A. Kivelson, and Eduardo Fradkin. Quantum theory of a nematic fermi fluid. *Physical Review B*, 64:195109, Oct 2001.

[48] Sung-Sik Lee. Low-energy effective theory of fermi surface coupled with U(1) gauge field in $2 + 1$ dimensions. *Physical Review B*, 80:165102, Oct 2009.

[49] David F. Mross, John McGreevy, Hong Liu, and T. Senthil. Controlled expansion for certain non-fermi-liquid metals. *Physical Review B*, 82:045121, Jul 2010.

[50] Max A. Metlitski and Subir Sachdev. Quantum phase transitions of metals in two spatial dimensions. i. ising-nematic order. *Physical Review B*, 82:075127, Aug 2010.

[51] Max A. Metlitski and Subir Sachdev. Quantum phase transitions of metals in two spatial dimensions. ii. spin density wave order. *Physical Review B*, 82:075128, Aug 2010.

[52] Andres Schlief, Peter Lunts, and Sung-Sik Lee. Exact critical exponents for the antiferromagnetic quantum critical metal in two dimensions. *Phys. Rev. X*, 7:021010, Apr 2017.

[53] Sung-Sik Lee. Recent developments in non-fermi liquid theory. *Annual Review of Condensed Matter Physics*, 9:227–244, 2018.

[54] S. Sachdev and J. Ye. Gapless spin-fluid ground state in a random quantum Heisenberg magnet. *Physical Review Letters*, 70:3339–3342, May 1993.

[55] A. Kitaev. A simple model of quantum holography. `http://online.kitp.ucsb.edu/online/entangled15/kitaev/`,`http://online.kitp.ucsb.edu/online/entangled15/kitaev2/`., 2015. Talks at KITP, April 7, 2015 and May 27, 2015.

[56] Debanjan Chowdhury, Antoine Georges, Olivier Parcollet, and Subir Sachdev. Sachdev-Ye-Kitaev models and beyond: A window into non-Fermi liquids. *arXiv preprint arXiv:2109.05037*, 2021.

[57] Xiao-Gang Wen. Low-energy effective field theories of fermion liquids and the mixed $\mathrm{U}(1) \times \mathbb{R}^d$ anomaly. *Physical Review B*, 103(16):165126, 2021.

[58] Dominic V Else, Ryan Thorngren, and T Senthil. Non-fermi liquids as ersatz fermi liquids: general constraints on compressible metals. *Physical Review X*, 11(2):021005, 2021.

[59] Luca V Delacretaz, Yi-Hsien Du, Umang Mehta, and Dam Thanh Son. Nonlinear bosonization of fermi surfaces: The method of coadjoint orbits. *arXiv preprint arXiv:2203.05004*, 2022.

[60] Andrea Damascelli, Zahid Hussain, and Zhi-Xun Shen. Angle-resolved photoemission studies of the cuprate superconductors. *Reviews of modern physics*, 75(2):473, 2003.

[61] S-C Wang, H-B Yang, AKP Sekharan, Hong Ding, Jan R Engelbrecht, Xi Dai, Ziqiang Wang, A Kaminski, Tonica Valla, T Kidd, et al. Quasiparticle line shape of Sr_2RuO_4 and its relation to anisotropic transport. *Physical Review Letters*, 92(13):137002, 2004.

[62] T Valla, AV Fedorov, PD Johnson, BO Wells, SL Hulbert, Qiang Li, GD Gu, and N Koshizuka. Evidence for quantum critical behavior in the optimally doped cuprate $Bi_2Sr_2CaCu_2O_{8+\delta}$. *Science*, 285(5436):2110–2113, 1999.

[63] M. Gurvitch and A. T. Fiory. Resistivity of $La_{1.825}Sr_{0.175}CuO_4$ and $YBa_2Cu_3O_7$ to 1100 k: Absence of saturation and its implications. *Physical Review Letters*, 59:1337–1340, Sep 1987.

[64] S. W. Tozer, A. W. Kleinsasser, T. Penney, D. Kaiser, and F. Holtzberg. Measurement of anisotropic resistivity and Hall constant for single-crystal $YBa_2Cu_3O_{7-x}$. *Physical Review Letters*, 59:1768–1771, Oct 1987.

[65] S. Martin, A. T. Fiory, R. M. Fleming, L. F. Schneemeyer, and J. V. Waszczak. Temperature dependence of the resistivity tensor in superconducting $Bi_2Sr_{2.2}Ca_{0.8}Cu_2O_8$ crystals. *Physical Review Letters*, 60:2194–2197, May 1988.

[66] S. Martin, A. T. Fiory, R. M. Fleming, L. F. Schneemeyer, and J. V. Waszczak. Normal-state transport properties of $Bi_{2+x}Sr_{2-y}CuO_{6+\delta}$ crystals. *Physical Review B*, 41:846–849, Jan 1990.

[67] C. M. Varma, P. B. Littlewood, S. Schmitt-Rink, E. Abrahams, and A. E. Ruckenstein. Phenomenology of the normal state of cu-o high-temperature superconductors. *Physical Review Letters*, 63:1996–1999, Oct 1989.

[68] Chandra M Varma. Colloquium: Linear in temperature resistivity and associated mysteries including high temperature superconductivity. *Reviews of Modern Physics*, 92(3):031001, 2020.

[69] GR Stewart. Addendum: Non-fermi-liquid behavior in d-and f-electron metals. *Reviews of Modern Physics*, 78(3):743, 2006.

[70] Yuan Cao, Debanjan Chowdhury, Daniel Rodan-Legrain, Oriol Rubies-Bigorda, Kenji Watanabe, Takashi Taniguchi, T Senthil, and Pablo Jarillo-Herrero. Strange metal in magic-angle graphene with near planckian dissipation. *Physical Review Letters*, 124(7):076801, Feb 2020.

[71] Alexandre Jaoui, Ipsita Das, Giorgio Di Battista, Jaime Díez-Mérida, Xiaobo Lu, Kenji Watanabe, Takashi Taniguchi, Hiroaki Ishizuka, Leonid Levitov, and Dmitri K Efetov. Quantum critical behaviour in magic-angle twisted bilayer graphene. *Nature Physics*, pages 1–6, 2022.

[72] ND Mathur, FM Grosche, SR Julian, IR Walker, DM Freye, RKW Haselwimmer, and GG Lonzarich. Magnetically mediated superconductivity in heavy fermion compounds. *Nature*, 394(6688):39–43, 1998.

[73] H. Q. Yuan, F. M. Grosche, M. Deppe, G. Sparn, C. Geibel, and F. Steglich. Non-fermi liquid states in the pressurized $CeCu_2(Si_{1-x}Ge_x)_2$ system: Two critical points. *Physical Review Letters*, 96:047008, Feb 2006.

[74] N. Tsujii, H. Kitazawa, T. Aoyagi, T. Kimura, and G. Kido. Non-fermi liquid behavior in $YbCu_2Si_2$. *Journal of Magnetism and Magnetic Materials*, 310(2, Part 1):349–351, 2007. Proceedings of the 17th International Conference on Magnetism.

[75] H.Q. Yuan and F. Steglich. Unconventional superconductivity and quantum criticality in pressurized $CeCu_2(Si_{1-x}Ge_x)_2$. *Physica C: Superconductivity and its Applications*, 460-462:141–144, 2007. Proceedings of the 8th International Conference on Materials and Mechanisms of Superconductivity and High Temperature Superconductors.

[76] O. Stockert and F. Steglich. Unconventional quantum criticality in heavy-fermion compounds. *Annual Review of Condensed Matter Physics*, 2(1):79–99, 2011.

[77] Hilbert v. Löhneysen, Achim Rosch, Matthias Vojta, and Peter Wölfle. Fermi-liquid instabilities at magnetic quantum phase transitions. *Rev. Mod. Phys.*, 79:1015–1075, Aug 2007.

[78] N. E. Hussey, K. Takenaka, and H. Takagi. Universality of the Mott-Ioffe-Regel limit in metals. *Philosophical Magazine*, 84(27):2847–2864, 2004.

[79] H. Takagi, B. Batlogg, H. L. Kao, J. Kwo, R. J. Cava, J. J. Krajewski, and W. F. Peck. Systematic evolution of temperature-dependent resistivity in $La_{2-x}Sr_xCuO_4$. *Physical Review Letters*, 69:2975–2978, Nov 1992.

[80] V. J. Emery and S. A. Kivelson. Superconductivity in bad metals. *Physical Review Letters*, 74:3253–3256, Apr 1995.

[81] John A. Hertz. Quantum critical phenomena. *Physical Review B*, 14:1165–1184, Aug 1976.

[82] A. J. Millis. Effect of a nonzero temperature on quantum critical points in itinerant fermion systems. *Physical Review B*, 48:7183–7196, Sep 1993.

[83] Ar Abanov and Andrey V Chubukov. Spin-fermion model near the quantum critical point: one-loop renormalization group results. *Physical Review Letters*, 84(24):5608, 2000.

[84] Ar Abanov and Andrey Chubukov. Anomalous scaling at the quantum critical point in itinerant antiferromagnets. *Physical Review Letters*, 93(25):255702, 2004.

[85] David F. Mross, John McGreevy, Hong Liu, and T. Senthil. Controlled expansion for certain non-fermi-liquid metals. *Physical Review B*, 82:045121, Jul 2010.

[86] T. Senthil. Critical fermi surfaces and non-fermi liquid metals. *Physical Review B*, 78:035103, Jul 2008.

[87] T. Senthil. Theory of a continuous Mott transition in two dimensions. *Physical Review B*, 78:045109, Jul 2008.

[88] Bertrand I Halperin, Patrick A Lee, and Nicholas Read. Theory of the half-filled Landau level. *Physical Review B*, 47(12):7312, 1993.

[89] Liujun Zou and Debanjan Chowdhury. Deconfined metallic quantum criticality: A U(2) gauge-theoretic approach. *Physical Review Research*, 2:023344, Jun 2020.

[90] Yuan Yao, Chang-Tse Hsieh, and Masaki Oshikawa. Anomaly matching and symmetry-protected critical phases in SU(N) spin systems in $1+1$ dimensions. *Physical Review Letters*, 123(18):180201, 2019.

[91] Chao-Ming Jian, Zhen Bi, and Cenke Xu. Lieb-Schultz-Mattis theorem and its generalizations from the perspective of the symmetry-protected topological phase. *Physical Review B*, 97(5):054412, Feb 2018.

[92] Gil Young Cho, Chang-Tse Hsieh, and Shinsei Ryu. Anomaly manifestation of Lieb-Schultz-Mattis theorem and topological phases. *Physical Review B*, 96(19):195105, 2017.

[93] Max A. Metlitski and Ryan Thorngren. Intrinsic and emergent anomalies at deconfined critical points. *Physical Review B*, 98(8):085140, Aug 2018.

[94] Dominic V Else and Ryan Thorngren. Topological theory of Lieb-Schultz-Mattis theorems in quantum spin systems. *Physical Review B*, 101(22):224437, 2020.

[95] Meng Cheng. Fermionic Lieb-Schultz-Mattis theorems and weak symmetry-protected phases. *arXiv:1804.10122*, 99(7):075143, February 2018.

[96] Michael Levin and Todadri Senthil. Deconfined quantum criticality and néel order via dimer disorder. *Physical Review B*, 70(22):220403, 2004.

[97] Adam Nahum, P Serna, JT Chalker, M Ortuño, and AM Somoza. Emergent so (5) symmetry at the néel to valence-bond-solid transition. *Physical Review Letters*, 115(26):267203, 2015.

[98] Chong Wang, Adam Nahum, Max A Metlitski, Cenke Xu, and T Senthil. Deconfined quantum critical points: symmetries and dualities. *Physical Review X*, 7(3):031051, 2017.

[99] T Senthil and Matthew PA Fisher. Competing orders, nonlinear sigma models, and topological terms in quantum magnets. *Physical Review B*, 74(6):064405, 2006.

[100] David Poland, Slava Rychkov, and Alessandro Vichi. The conformal bootstrap: Theory, numerical techniques, and applications. *Reviews of Modern Physics*, 91(1):015002, 2019.

[101] Po-Shen Hsin and Nathan Seiberg. Level/rank duality and Chern-Simons-matter theories. *Journal of High Energy Physics*, 2016(9):1–30, 2016.

[102] Francesco Benini, Po-Shen Hsin, and Nathan Seiberg. Comments on global symmetries, anomalies, and duality in $(2+1)d$. *Journal of High Energy Physics*, 2017(4):1–39, 2017.

[103] Matthew PA Fisher, Peter B Weichman, Geoffrey Grinstein, and Daniel S Fisher. Boson localization and the superfluid-insulator transition. *Physical Review B*, 40(1):546, 1989.

[104] Leon Balents, Lorenz Bartosch, Anton Burkov, Subir Sachdev, and Krishnendu Sengupta. Putting competing orders in their place near the mott transition. *Physical Review B*, 71(14):144508, 2005.

[105] A. A. Burkov and Leon Balents. Superfluid-insulator transitions on the triangular lattice. *Physical Review B*, 72:134502, Oct 2005.

[106] Xiao-Gang Wen. Quantum orders and symmetric spin liquids. *Physical Review B*, 65:165113, Apr 2002.

[107] JC Slater. Magnetic effects and the Hartree-Fock equation. *Physical Review*, 82(4):538, 1951.

[108] P. Anderson. Resonating valence bonds: A new kind of insulator? *Phys. Rev.*, 109(2):1492, 1958.

[109] Nevill F Mott. Metal-insulator transition. *Reviews of Modern Physics*, 40(4):677, 1968.

[110] Tetsuya Furukawa, Kazuhiko Kobashi, Yosuke Kurosaki, Kazuya Miyagawa, and Kazushi Kanoda. Quasi-continuous transition from a fermi liquid to a spin liquid in κ-$(ET)_2Cu_2(CN)_3$. *Nature communications*, 9(1):1–7, 2018.

[111] William Witczak-Krempa, Pouyan Ghaemi, T. Senthil, and Yong Baek Kim. Universal transport near a quantum critical Mott transition in two dimensions. *Physical Review B*, 86:245102, Dec 2012.

[112] Y Shimizu, K Miyagawa, K Kanoda, M Maesato, and G Saito. Spin liquid state in an organic mott insulator with a triangular lattice. *Physical Review Letters*, 91(10):107001, 2003.

[113] Minoru Yamashita, Norihito Nakata, Yoshinori Senshu, Masaki Nagata, Hiroshi M Yamamoto, Reizo Kato, Takasada Shibauchi, and Yuji Matsuda. Highly mobile gapless excitations in a two-dimensional candidate quantum spin liquid. *Science*, 328(5983):1246–1248, 2010.

[114] Björn Miksch, Andrej Pustogow, Mojtaba Javaheri Rahim, Andrey A Bardin, Kazushi Kanoda, John A Schlueter, Ralph Hübner, Marc Scheffler, and Martin Dressel. Gapped magnetic ground state in quantum spin liquid candidate κ-(BEDT-TTF)$_2$Cu$_2$(CN)$_3$. *Science*, 372(6539):276–279, 2021.

[115] John McGreevy. Generalized symmetries in condensed matter. *arXiv preprint arXiv:2204.03045*, 2022.

[116] Clay Cordova, Thomas T Dumitrescu, Kenneth Intriligator, and Shu-Heng Shao. Snowmass white paper: Generalized symmetries in quantum field theory and beyond. *arXiv preprint arXiv:2205.09545*, 2022.

[117] Davide Gaiotto, Anton Kapustin, Nathan Seiberg, and Brian Willett. Generalized global symmetries. *Journal of High Energy Physics*, 2015(2), Feb 2015.

[118] Wenjie Ji and Xiao-Gang Wen. Categorical symmetry and noninvertible anomaly in symmetry-breaking and topological phase transitions. *Physical Review Research*, 2(3):033417, 2020.

[119] Chi-Ming Chang, Ying-Hsuan Lin, Shu-Heng Shao, Yifan Wang, and Xi Yin. Topological defect lines and renormalization group flows in two dimensions. *Journal of High Energy Physics*, 2019(1):1–85, 2019.

[120] Arun Paramekanti, Leon Balents, and Matthew P. A. Fisher. Ring exchange, the exciton Bose liquid, and bosonization in two dimensions. *Physical Review B*, 66:054526, Aug 2002.

[121] Xiao-Chuan Wu, Wenjie Ji, and Cenke Xu. Categorical symmetries at criticality. *Journal of Statistical Mechanics: Theory and Experiment*, 2021(7):073101, 2021.

[122] Xiao-Chuan Wu, Chao-Ming Jian, and Cenke Xu. Universal features of higher-form symmetries at phase transitions. *SciPost Phys.*, 11:33, 2021.

[123] F. D. M. Haldane. Stability of chiral luttinger liquids and abelian quantum hall states. *Physical Review Letters*, 74:2090–2093, Mar 1995.

[124] Michael Levin. Protected edge modes without symmetry. *Phys. Rev. X*, 3:021009, May 2013.

[125] Maissam Barkeshli, Chao-Ming Jian, and Xiao-Liang Qi. Theory of defects in abelian topological states. *Physical Review B*, 88(23):235103, 2013.

[126] T. Senthil. Symmetry-protected topological phases of quantum matter. *Annual Review of Condensed Matter Physics*, 6(1):299–324, 2015.

[127] KS Novoselov, o A Mishchenko, o A Carvalho, and AH Castro Neto. 2d materials and van der waals heterostructures. *Science*, 353(6298):aac9439, 2016.

[128] Andre K Geim and Irina V Grigorieva. Van der waals heterostructures. *Nature*, 499(7459):419–425, 2013.

[129] Zhong Wang, Xiao-Liang Qi, and Shou-Cheng Zhang. Evidence of a gate-tunable Mott insulator in a trilayer graphene moiré superlattice. *Physical Review Letters*, 105(3):256803, Jan 2010.

[130] Matthew Yankowitz, Shaowen Chen, Hryhoriy Polshyn, Yuxuan Zhang, K. Watanabe, T. Taniguchi, David Graf, Andrea F. Young, and Cory R. Dean. Tuning superconductivity in twisted bilayer graphene. *Science*, 363(6431):1059–1064, Jan 2019.

[131] Yu Saito, Jingyuan Ge, Kenji Watanabe, Takashi Taniguchi, and Andrea F. Young. Independent superconductors and correlated insulators in twisted bilayer graphene. *Nature Physics*, 16(9):926–930, Jun 2020.

[132] Xiaobo Lu, Petr Stepanov, Wei Yang, Ming Xie, Mohammed Ali Aamir, Ipsita Das, Carles Urgell, Kenji Watanabe, Takashi Taniguchi, Guangyu Zhang, Adrian Bachtold, Allan H. MacDonald, and Dmitri K. Efetov. Untying the insulating and superconducting orders in magic-angle graphene. *arXiv:1903.06513*, 583(7816):375–378, Jul 2019.

[133] Zhong Wang, Xiao-Liang Qi, and Shou-Cheng Zhang. Signatures of tunable superconductivity in a trilayer graphene moiré superlattice. *Physical Review B*, 85(7768):165126, Jul 2012.

[134] Xiaomeng Liu, Zeyu Hao, Eslam Khalaf, Jong Yeon Lee, Yuval Ronen, Hyobin Yoo, Danial Haei Najafabadi, Kenji Watanabe, Takashi Taniguchi, Ashvin Vishwanath, and et al. Tunable spin-polarized correlated states in twisted double bilayer graphene. *Nature*, 583(7815):221–225, Jul 2020.

[135] Yuan Cao, Daniel Rodan-Legrain, Oriol Rubies-Bigorda, Jeong Min Park, Kenji Watanabe, Takashi Taniguchi, and Pablo Jarillo-Herrero. Tunable correlated states and spin-polarized phases in twisted bilayer-bilayer graphene. *Nature*, 583(7815):215–220, May 2020.

[136] H. Polshyn, M. Yankowitz, S. Chen, Y. Zhang, K. Watanabe, T. Taniguchi, C. R. Dean, and A. F. Young. Large linear-in-temperature resistivity in twisted bilayer graphene. *arXiv:1902.00763*, 15(10):1011–1016, Aug 2019.

[137] Dante M Kennes, Martin Claassen, Lede Xian, Antoine Georges, Andrew J Millis, James Hone, Cory R Dean, DN Basov, Abhay N Pasupathy, and Angel Rubio. Moiré heterostructures as a condensed-matter quantum simulator. *Nature Physics*, 17(2):155–163, 2021.

[138] Rafi Bistritzer and Allan H. MacDonald. Moiré bands in twisted double-layer graphene. *Proceedings of the National Academy of Sciences*, 108(30):12233–12237, 2011.

[139] J. M. B. Lopes dos Santos, N. M. R. Peres, and A. H. Castro Neto. Continuum model of the twisted graphene bilayer. *Physical Review B*, 86:155449, Oct 2012.

[140] Liujun Zou, Hoi Chun Po, Ashvin Vishwanath, and T. Senthil. Band structure of twisted bilayer graphene: Emergent symmetries, commensurate approximants, and wannier obstructions. *Physical Review B*, 98:085435, Aug 2018.

[141] Hoi Chun Po, Liujun Zou, T Senthil, and Ashvin Vishwanath. Faithful tight-binding models and fragile topology of magic-angle bilayer graphene. *Physical Review B*, 99(19):195455, 2019.

[142] Patrick J Ledwith, Eslam Khalaf, and Ashvin Vishwanath. Strong coupling theory of magic-angle graphene: A pedagogical introduction. *Annals of Physics*, 435:168646, 2021.

[143] JT Chalker and PD Coddington. Percolation, quantum tunnelling and the integer Hall effect. *Journal of Physics C: Solid State Physics*, 21(14):2665, 1988.

[144] C.-M. Ho and J. T. Chalker. Models for the integer quantum Hall effect: The network model, the Dirac equation, and a tight-binding Hamiltonian. *Physical Review B*, 54:8708–8713, Sep 1996.

[145] Dmitry K. Efimkin and Allan H. MacDonald. Helical network model for twisted bilayer graphene. *Physical Review B*, 98:035404, Jul 2018.

[146] Fengcheng Wu, Timothy Lovorn, Emanuel Tutuc, and A. H. MacDonald. Hubbard model physics in transition metal dichalcogenide moiré bands. *Physical Review Letters*, 121:026402, Jul 2018.

[147] Dragana Popović, AB Fowler, and S Washburn. Metal-insulator transition in two dimensions: Effects of disorder and magnetic field. *Physical Review Letters*, 79(8):1543, 1997.

[148] Hans Bethe. Zur theorie der metalle. *Zeitschrift für Physik*, 71(3):205–226, 1931.

[149] A.A. Belavin, A.M. Polyakov, and A.B. Zamolodchikov. Infinite conformal symmetry in two-dimensional quantum field theory. *Nuclear Physics B*, 241(2):333–380, 1984.

[150] Xiao-Gang Wen. Choreographed entanglement dances: Topological states of quantum matter. *Science*, 363(6429):1641–1648, 2019.

[151] Long Zhang and Fa Wang. Unconventional surface critical behavior induced by a quantum phase transition from the two-dimensional Affleck-Kennedy-Lieb-Tasaki phase to a Néel-ordered phase. *Physical Review Letters*, 118:087201, Feb 2017.

[152] Chengxiang Ding, Long Zhang, and Wenan Guo. Engineering surface critical behavior of (2+1)-dimensional O(3) quantum critical points. *Physical Review Letters*, 120:235701, Jun 2018.

[153] Anders W. Sandvik. Ground states of a frustrated quantum spin chain with long-range interactions. *Physical Review Letters*, 104:137204, Mar 2010.

[154] Sibin Yang, Dao-Xin Yao, and Anders W. Sandvik. Deconfined quantum criticality in spin-1/2 chains with long-range interactions. *arXiv e-prints*, page arXiv:2001.02821, January 2020.

[155] Ian Affleck, Tom Kennedy, Elliott H. Lieb, and Hal Tasaki. Rigorous results on valence-bond ground states in antiferromagnets. *Physical Review Letters*, 59:799–802, Aug 1987.

[156] Oleg A. Starykh and Leon Balents. Dimerized phase and transitions in a spatially anisotropic square lattice antiferromagnet. *Physical Review Letters*, 93:127202, Sep 2004.

[157] Xie Chen, Zheng-Cheng Gu, Zheng-Xin Liu, and Xiao-Gang Wen. Symmetry protected topological orders and the group cohomology of their symmetry group. *Physical Review B*, 87(15):155114, 2013.

[158] Xie Chen, Zheng-Cheng Gu, Zheng-Xin Liu, and Xiao-Gang Wen. Symmetry-protected topological orders in interacting bosonic systems. *Science*, 338(6114):1604–1606, 2012.

[159] Zheng-Xin Liu and Xiao-Gang Wen. Symmetry-protected quantum spin Hall phases in two dimensions. *Physical Review Letters*, 110(6):067205, 2013.

[160] Yichen Xu, Xiao-Chuan Wu, Chao-Ming Jian, and Cenke Xu. Topological Edge and Interface states at Bulk disorder-to-order Quantum Critical Points. *arXiv e-prints*, page arXiv:2002.10479, February 2020.

[161] Ashvin Vishwanath and T Senthil. Physics of three-dimensional bosonic topological insulators: Surface-deconfined criticality and quantized magnetoelectric effect. *Physical Review X*, 3(1):011016, 2013.

[162] Cenke Xu. Three-dimensional symmetry-protected topological phase close to antiferromagnetic Néel order. *Physical Review B*, 87(14):144421, 2013.

[163] John Cardy. *Scaling and Renormalization in Statistical Physics*. Cambridge Lecture Notes in Physics, 1996.

[164] S. Dietrich and H. W. Diehl. The effects of surfaces on dynamic critical behavior. *Zeitschrift für Physik B Condensed Matter*, 51(4):343–354, Dec 1983.

[165] H. W. Diehl and S. Dietrich. Field-theoretical approach to static critical phenomena in semi-infinite systems. *Zeitschrift für Physik B Condensed Matter*, 42(1):65–86, Mar 1981.

[166] J Reeve and A J Guttmann. Renormalisation group calculations of the critical exponents of the n-vector model with a free surface. *Journal of Physics A: Mathematical and General*, 14(12):3357–3366, dec 1981.

[167] H. W. Diehl. The theory of boundary critical phenomena. *International Journal of Modern Physics B*, 11(30):3503–3523, 1997.

[168] Cenke Xu and Yi-Zhuang You. Self-dual quantum electrodynamics as boundary state of the three-dimensional bosonic topological insulator. *Physical Review B*, 92:220416, Dec 2015.

[169] Po-Shen Hsin and Nathan Seiberg. Level/rank duality and Chern-Simons-matter theories. *Journal of High Energy Physics*, 2016(9):1–30, 2016.

[170] David F. Mross, Jason Alicea, and Olexei I. Motrunich. Explicit derivation of duality between a free dirac cone and quantum electrodynamics in $(2+1)$ dimensions. *Physical Review Letters*, 117:016802, Jun 2016.

[171] Andrew C. Potter, Chong Wang, Max A. Metlitski, and Ashvin Vishwanath. Realizing topological surface states in a lower-dimensional flat band. *Physical Review B*, 96(23):235114, Dec 2017.

[172] T Senthil, Dam Thanh Son, Chong Wang, and Cenke Xu. Duality between $(2+1)d$ quantum critical points. *Physics Reports*, 827:1–48, 2019.

[173] Chao-Ming Jian, Alex Thomson, Alex Rasmussen, Zhen Bi, and Cenke Xu. Deconfined quantum critical point on the triangular lattice. *Physical Review B*, 97(19):195115, May 2018.

[174] Nicolas Laflorencie, Ian Affleck, and Mona Berciu. Critical phenomena and quantum phase transition in long range Heisenberg antiferromagnetic chains. *Journal of Statistical Mechanics: Theory and Experiment*, 2005(12):P12001, 2005.

[175] Michael Hermele, T Senthil, and Matthew PA Fisher. Algebraic spin liquid as the mother of many competing orders. *Physical Review B*, 72(10):104404, 2005.

[176] Sung-Sik Lee. Emergence of supersymmetry at a critical point of a lattice model. *Physical Review B*, 76:075103, Aug 2007.

[177] Alexei M. Tsvelik Alexander O. Gogolin, Alexander A. Nersesyan. *Bosonization and Strongly Correlated Systems*. Cambridge University Press, 2004.

[178] Anders W. Sandvik, Leon Balents, and David K. Campbell. Ground state phases of the half-filled one-dimensional extended Hubbard model. *Physical Review Letters*, 92:236401, Jun 2004.

[179] Brenden Roberts, Shenghan Jiang, and Olexei I. Motrunich. Deconfined quantum critical point in one dimension. *Physical Review B*, 99:165143, Apr 2019.

[180] Shenghan Jiang and Olexei Motrunich. Ising ferromagnet to valence bond solid transition in a one-dimensional spin chain: Analogies to deconfined quantum critical points. *Physical Review B*, 99:075103, Feb 2019.

[181] XIAO-GANG WEN. Theory of the edge states in fractional quantum Hall effects. *International Journal of Modern Physics B*, 06(10):1711–1762, 1992.

[182] T. Senthil, Ashvin Vishwanath, Leon Balents, Subir Sachdev, and M. P. A. Fisher. Deconfined quantum critical points. *Science*, 303(5663):1490, 2004.

[183] T. Senthil, Leon Balents, Subir Sachdev, Ashvin Vishwanath, and Matthew P. A. Fisher. Quantum criticality beyond the Landau-Ginzburg-Wilson paradigm. *Physical Review B*, 70(14):144407, Oct 2004.

[184] Sergei V Isakov, Matthew B Hastings, and Roger G Melko. Topological entanglement entropy of a Bose-Hubbard spin liquid. *Nature Physics*, 7(10):772–775, 2011.

[185] Sergei V Isakov, Roger G Melko, and Matthew B Hastings. Universal signatures of fractionalized quantum critical points. *Science*, 335(6065):193–195, 2012.

[186] Andrey V. Chubukov, Subir Sachdev, and T. Senthil. Quantum phase transitions in frustrated quantum antiferromagnets. *Nuclear Physics B*, 426(3):601–643, 1994.

[187] CENKE XU. Unconventional quantum critical points. *International Journal of Modern Physics B*, 26(18):1230007, 2012.

[188] Anders W. Sandvik. Evidence for deconfined quantum criticality in a two-dimensional Heisenberg model with four-spin interactions. *Physical Review Letters*, 98:227202, Jun 2007.

[189] Hui Shao, Wenan Guo, and Anders W. Sandvik. Quantum criticality with two length scales. *Science*, 352(6282):213–216, 2016.

[190] Roger G. Melko and Ribhu K. Kaul. Scaling in the fan of an unconventional quantum critical point. *Physical Review Letters*, 100:017203, Jan 2008.

[191] Yan Qi Qin, Yuan-Yao He, Yi-Zhuang You, Zhong-Yi Lu, Arnab Sen, Anders W. Sandvik, Cenke Xu, and Zi Yang Meng. Duality between the deconfined quantum-critical point and the bosonic topological transition. *Phys. Rev. X*, 7:031052, Sep 2017.

[192] John L. Cardy and Eliezer Rabinovici. Scaling and renormalization in statistical physics. *Nucl. Phys. B*, 205:1, 1982.

[193] John L. Cardy. Conformal invariance and surface critical behavior. *Nuclear Physics B*, 240(4):514–532, 1984.

[194] N. Read and Subir Sachdev. large-N expansion for frustrated quantum antiferromagnets. *Physical Review Letters*, 66:1773–1776, Apr 1991.

[195] Subir Sachdev and N. Read. Large-N expansion for frustrated and doped quantum antiferromagnets. *International Journal of Modern Physics B*, 05(01n02):219–249, 1991.

[196] Congjun Wu, Jiang-ping Hu, and Shou-cheng Zhang. Exact SO(5) symmetry in the spin-3/2 fermionic system. *Physical Review Letters*, 91:186402, Oct 2003.

[197] Pasquale Calabrese, Andrea Pelissetto, and Ettore Vicari. The critical behavior of magnetic systems described by Landau-Ginzburg-Wilson field theories. *arXiv:cond-mat/0306273*, 2003.

[198] Eduardo Fradkin and Leonard Susskind. Order and disorder in gauge systems and magnets. *Physical Review D*, 17:2637–2658, May 1978.

[199] T. Senthil. Theory of a continuous Mott transition in two dimensions. *Physical Review B*, 78:045109, Jul 2008.

[200] Long Zhang and Fa Wang. Unconventional surface critical behavior induced by a quantum phase transition from the two-dimensional Affleck-Kennedy-Lieb-Tasaki phase to a Néel-ordered phase. *Physical Review Letters*, 118:087201, Feb 2017.

[201] Thomas Scaffidi, Daniel E. Parker, and Romain Vasseur. Gapless symmetry-protected topological order. *Phys. Rev. X*, 7:041048, Nov 2017.

[202] C. L. Kane and E. J. Mele. Quantum Spin Hall Effect in Graphene. *Physical Review Letter*, 95:226801, 2005.

[203] C. L. Kane and E. J. Mele. Z_2 Topological Order and the Quantum Spin Hall Effect. *Physical Review Letter*, 95:146802, 2005.

[204] Liang Fu, Charles L Kane, and Eugene J Mele. Topological insulators in three dimensions. *Physical Review Letters*, 98(10):106803, 2007.

[205] J. E. Moore and L. Balents. Topological invariants of time-reversal-invariant band structures. *Physical Review B*, 75:121306(R), 2007.

[206] Andreas P Schnyder, Shinsei Ryu, Akira Furusaki, and Andreas WW Ludwig. Classification of topological insulators and superconductors. In *AIP Conference Proceedings*, volume 1134, pages 10–21. American Institute of Physics, 2009.

[207] Shinsei Ryu, Andreas P Schnyder, Akira Furusaki, and Andreas WW Ludwig. Topological insulators and superconductors: tenfold way and dimensional hierarchy. *New Journal of Physics*, 12(6):065010, 2010.

[208] Alexei Kitaev. Periodic table for topological insulators and superconductors. In *AIP conference proceedings*, volume 1134, pages 22–30. American Institute of Physics, 2009.

[209] Lukasz Fidkowski, Xie Chen, and Ashvin Vishwanath. Non-abelian topological order on the surface of a $3d$ topological superconductor from an exactly solved model. *Physical Review X*, 3(4):041016, 2013.

[210] Xie Chen, Lukasz Fidkowski, and Ashvin Vishwanath. Symmetry enforced non-abelian topological order at the surface of a topological insulator. *Physical Review B*, 89(16):165132, 2014.

[211] Parsa Bonderson, Chetan Nayak, and Xiao-Liang Qi. A time-reversal invariant topological phase at the surface of a 3d topological insulator. *Journal of Statistical Mechanics: Theory and Experiment*, 2013(09):P09016, 2013.

[212] Chong Wang, Andrew C Potter, and T Senthil. Gapped symmetry preserving surface state for the electron topological insulator. *Physical Review B*, 88(11):115137, 2013.

[213] Max A Metlitski, CL Kane, and Matthew PA Fisher. Symmetry-respecting topologically ordered surface phase of three-dimensional electron topological insulators. *Physical Review B*, 92(12):125111, 2015.

[214] Chong Wang and T Senthil. Boson topological insulators: A window into highly entangled quantum phases. *Physical Review B*, 87(23):235122, 2013.

[215] Meng Cheng, Michael Zaletel, Maissam Barkeshli, Ashvin Vishwanath, and Parsa Bonderson. Translational symmetry and microscopic constraints on symmetry-enriched topological phases: A view from the surface. *Physical Review X*, 6(4):041068, 2016.

[216] Nathan Seiberg, T. Senthil, Chong Wang, and Edward Witten. A duality web in $2+1$ dimensions and condensed matter physics. *Annals of Physics*, 374:395–433, Nov 2016.

[217] Zhen Bi, Alex Rasmussen, and Cenke Xu. Classification and description of bosonic symmetry protected topological phases with semiclassical nonlinear sigma models. *Physical Review B*, 91:134404, Apr 2015.

[218] Olexei I Motrunich and Ashvin Vishwanath. Emergent photons and transitions in the O(3) sigma model with hedgehog suppression. *Physical Review B*, 70(7):075104, 2004.

[219] Ribhu K. Kaul and Subir Sachdev. Quantum criticality of U(1) gauge theories with fermionic and bosonic matter in two spatial dimensions. *Physical Review B*, 77:155105, Apr 2008.

[220] Sergio Benvenuti and Hrachya Khachatryan. Easy-plane qed3's in the large nf limit. *Journal of High Energy Physics*, 2019(5):214, May 2019.

[221] Xiao-Gang Wen and Yong-Shi Wu. Transitions between the quantum Hall states and insulators induced by periodic potentials. *Physical Review Letters*, 70:1501–1504, Mar 1993.

[222] Daniel S. Rokhsar. Quadratic quantum antiferromagnets in the fermionic large-N limit. *Physical Review B*, 42:2526–2531, Aug 1990.

[223] N. Read and Subir Sachdev. Some features of the phase diagram of the square lattice SU(N) antiferromagnet. *Nuclear Physics B*, 316(3):609–640, 1989.

[224] Ian Affleck and J. Brad Marston. large-N limit of the Heisenberg-Hubbard model: Implications for high-T_c superconductors. *Physical Review B*, 37:3774–3777, Mar 1988.

[225] Walter Rantner and Xiao-Gang Wen. Electron spectral function and algebraic spin liquid for the normal state of underdoped high T_c superconductors. *Physical Review Letters*, 86:3871–3874, Apr 2001.

[226] Cenke Xu and Subir Sachdev. Square-lattice algebraic spin liquid with SO(5) symmetry. *Physical Review Letters*, 100:137201, Apr 2008.

[227] H. Nonne, M. Moliner, S. Capponi, P. Lecheminant, and K. Totsuka. Symmetry-protected topological phases of alkaline-earth cold fermionic atoms in one dimension. *EPL (Europhysics Letters)*, 102(3):37008, 2013.

[228] V. Bois, S. Capponi, P. Lecheminant, M. Moliner, and K. Totsuka. Phase diagrams of one-dimensional half-filled two-orbital SU(N) cold fermion systems. *Physical Review B*, 91:075121, Feb 2015.

[229] S. Capponi, P. Lecheminant, and K. Totsuka. Phases of one-dimensional SU(N) cold atomic fermi gases from molecular luttinger liquids to topological phases. *Annals of Physics*, 367:50–95, 2016.

[230] Kasper Duivenvoorden and Thomas Quella. Topological phases of spin chains. *Physical Review B*, 87:125145, Mar 2013.

[231] Ying Ran, Yi Zhang, and Ashvin Vishwanath. One-dimensional topologically protected modes in topological insulators with lattice dislocations. *Nature Physics*, 5:298, 2009.

[232] Jeffrey C. Y. Teo and C. L. Kane. Topological defects and gapless modes in insulators and superconductors. *Physical Review B*, 82:115120, Sep 2010.

[233] Wladimir A. Benalcazar, B. Andrei Bernevig, and Taylor L. Hughes. Quantized electric multipole insulators. *Science*, 357(6346):61–66, 2017.

[234] Guorui Chen, Lili Jiang, Shuang Wu, Bosai Lyu, Hongyuan Li, Bheema Lingam Chittari, Kenji Watanabe, Takashi Taniguchi, Zhiwen Shi, Jeil Jung, et al. Evidence of gate-tunable Mott insulator in rrilayer graphene-boron nitride Moiré superlattice. *arXiv preprint arXiv:1803.01985*, 2018.

[235] Yuan Cao, Valla Fatemi, Ahmet Demir, Shiang Fang, Spencer L Tomarken, Jason Y Luo, Javier D Sanchez-Yamagishi, Kenji Watanabe, Takashi Taniguchi, Efthimios Kaxiras, et al. Correlated insulator behaviour at half-filling in magic-angle graphene superlattices. *Nature*, 556(7699):80–84, 2018.

[236] Yuan Cao, Valla Fatemi, Shiang Fang, Kenji Watanabe, Takashi Taniguchi, Efthimios Kaxiras, and Pablo Jarillo-Herrero. Unconventional superconductivity in magic-angle graphene superlattices. *Nature*, 556(7699):43–50, 2018.

[237] Matthew Yankowitz, Shaowen Chen, Hryhoriy Polshyn, Yuxuan Zhang, K. Watanabe, T. Taniguchi, David Graf, Andrea F. Young, and Cory R. Dean. Tuning superconductivity in twisted bilayer graphene. *Science*, 363(6431):1059–1064, 2019.

[238] Cenke Xu and Leon Balents. Topological superconductivity in twisted multilayer graphene. *Physical Review Letters*, 121(8):087001, 2018.

[239] Hoi Chun Po, Liujun Zou, Ashvin Vishwanath, and T. Senthil. Origin of Mott insulating behavior and superconductivity in twisted bilayer graphene. *Phys. Rev. X*, 8:031089, Sep 2018.

[240] Maissam Barkeshli, Hong Yao, and Steven A. Kivelson. Phases of a phenomenological model of twisted bilayer graphene. *Physical Review B*, 87:140402(R), Aug 2013.

[241] Noah F. Q. Yuan and Liang Fu. Model for the metal-insulator transition in graphene superlattices and beyond. *Physical Review B*, 98:045103, Jul 2018.

[242] Jian Kang and Oskar Vafek. Symmetry, maximally localized wannier states, and a low-energy model for twisted bilayer graphene narrow bands. *Phys. Rev. X*, 8:031088, Sep 2018.

[243] Bikash Padhi, Chandan Setty, and Philip W. Phillips. Doped twisted bilayer graphene near magic angles: proximity to Wigner crystallization, not Mott insulation. *Nano Letters*, 18(10):6175–6180, 2018. PMID: 30185049.

[244] Bikash Padhi and Philip Phillips. Pressure-induced metal-insulator transition in twisted bilayer graphene. *arXiv:1810.00884*, 99:205141, May 2018.

[245] Ganapathy Baskaran. Theory of emergent josephson lattice in neutral twisted bilayer graphene (moiré is different). *arXiv preprint arXiv:1804.00627*, 2018.

[246] Cheng-Cheng Liu, Li-Da Zhang, Wei-Qiang Chen, and Fan Yang. Chiral spin density wave and $d+id$ superconductivity in the magic-angle-twisted bilayer graphene. *Physical Review Letters*, 121:217001, Nov 2018.

[247] Louk Rademaker and Paula Mellado. Charge-transfer insulation in twisted bilayer graphene. *Physical Review B*, 98:235158, Dec 2018.

[248] Hiroki Isobe, Noah F. Q. Yuan, and Liang Fu. Unconventional superconductivity and density waves in twisted bilayer graphene. *Phys. Rev. X*, 8:041041, Dec 2018.

[249] Mikito Koshino, Noah F. Q. Yuan, Takashi Koretsune, Masayuki Ochi, Kazuhiko Kuroki, and Liang Fu. Maximally localized Wannier orbitals and the extended Hubbard model for twisted bilayer graphene. *Phys. Rev. X*, 8:031087, Sep 2018.

[250] Yi-Zhuang You and Ashvin Vishwanath. Superconductivity from valley fluctuations and approximate SO(4) symmetry in a weak coupling theory of twisted bilayer graphene. *npj Quantum Materials*, 4(1):1–12, 2019.

[251] Fengcheng Wu, A. H. MacDonald, and Ivar Martin. Theory of phonon-mediated superconductivity in twisted bilayer graphene. *Physical Review Letters*, 121:257001, Dec 2018.

[252] Biao Lian, Zhijun Wang, and B. Andrei Bernevig. Twisted bilayer graphene: A phonon-driven superconductor. *Physical Review Letters*, 122:257002, Jun 2019.

[253] Huaiming Guo, Xingchuan Zhu, Shiping Feng, and Richard T. Scalettar. Pairing symmetry of interacting fermions on a twisted bilayer graphene superlattice. *Physical Review B*, 97:235453, Jun 2018.

[254] Ya-Hui Zhang and T. Senthil. Band structure of twisted bilayer graphene: Emergent symmetries, commensurate approximants, and wannier obstructions. *arXiv:1809.05110*, 98:085435, Aug 2018.

[255] Q. K. Tang, L. Yang, D. Wang, F. C. Zhang, and Q. H. Wang. Spin-triplet f-wave pairing in twisted bilayer graphene near $\frac{1}{4}$-filling. *arXiv:1809.06772*, 99:094521, Mar 2018.

[256] Alex Thomson, Shubhayu Chatterjee, Subir Sachdev, and Mathias S. Scheurer. Triangular antiferromagnetism on the honeycomb lattice of twisted bilayer graphene. *Physical Review B*, 98:075109, Aug 2018.

[257] Kasra Hejazi, Chunxiao Liu, Hassan Shapourian, Xiao Chen, and Leon Balents. Multiple topological transitions in twisted bilayer graphene near the first magic angle. *Physical Review B*, 99:035111, Jan 2019.

[258] Jianpeng Liu, Junwei Liu, and Xi Dai. Pseudo Landau level representation of twisted bilayer graphene: Band topology and implications on the correlated insulating phase. *arXiv:1810.03103*, 99:155415, Apr 2018.

[259] Rafi Bistritzer and Allan H. MacDonald. Moiré bands in twisted double-layer graphene. *Proceedings of the National Academy of Sciences*, 108(30):12233–12237, 2011.

[260] E. Suárez Morell, J. D. Correa, P. Vargas, M. Pacheco, and Z. Barticevic. Flat bands in slightly twisted bilayer graphene: Tight-binding calculations. *Physical Review B*, 82:121407, Sep 2010.

[261] Shiang Fang and Efthimios Kaxiras. Electronic structure theory of weakly interacting bilayers. *Physical Review B*, 93:235153, Jun 2016.

[262] G. Trambly de Laissardière, D. Mayou, and L. Magaud. Numerical studies of confined states in rotated bilayers of graphene. *Physical Review B*, 86:125413, Sep 2012.

[263] Philip Kim. Ferromagnetic superconductivity in twisted double bilayer graphene. `http://online.kitp.ucsb.edu/online/bands_m19/kim/`, 2019. Talks at KITP, Jan 15, 2019.

[264] Guorui Chen, Aaron L Sharpe, Patrick Gallagher, Ilan T Rosen, Eli J Fox, Lili Jiang, Bosai Lyu, Hongyuan Li, Kenji Watanabe, Takashi Taniguchi, et al. Signatures of tunable superconductivity in a trilayer graphene moiré superlattice. *Nature*, 572(7768):215–219, 2019.

[265] Ya-Hui Zhang, Dan Mao, Yuan Cao, Pablo Jarillo-Herrero, and T. Senthil. Nearly flat chern bands in moiré superlattices. *Physical Review B*, 99:075127, Feb 2019.

[266] Ya-Hui Zhang and T. Senthil. Bridging Hubbard model physics and quantum Hall physics in trilayer graphene/$h-$BN moiré superlattice. *arXiv:1809.05110*, 99:205150, May 2018.

[267] Bheema Lingam Chittari, Guorui Chen, Yuanbo Zhang, Feng Wang, and Jeil Jung. Gate-tunable topological flat bands in trilayer graphene boron-nitride moiré superlattices. *Physical Review Letters*, 122:016401, Jan 2019.

[268] Hoi Chun Po, Liujun Zou, T Senthil, and Ashvin Vishwanath. Faithful tight-binding models and fragile topology of magic-angle bilayer graphene. *Physical Review B*, 99(19):195455, 2019.

[269] Fan Zhang, Allan H. MacDonald, and Eugene J. Mele. Valley chern numbers and boundary modes in gapped bilayer graphene. *Proceedings of the National Academy of Sciences*, 110(26):10546–10551, 2013.

[270] Ivar Martin, Ya. M. Blanter, and A. F. Morpurgo. Topological confinement in bilayer graphene. *Physical Review Letters*, 100:036804, Jan 2008.

[271] Zhenhua Qiao, Jeil Jung, Qian Niu, and Allan H. MacDonald. Electronic highways in bilayer graphene. *Nano Letters*, 11(8):3453–3459, 2011. PMID: 21766817.

[272] Abolhassan Vaezi, Yufeng Liang, Darryl H. Ngai, Li Yang, and Eun-Ah Kim. Topological edge states at a tilt boundary in gated multilayer graphene. *Phys. Rev. X*, 3:021018, Jun 2013.

[273] Bor-Yuan Jiang, Guang-Xin Ni, Zachariah Addison, Jing K. Shi, Xiaomeng Liu, Shu Yang Frank Zhao, Philip Kim, Eugene J. Mele, Dimitri N. Basov, and Michael M. Fogler. Plasmon reflections by topological electronic boundaries in bilayer graphene. *Nano Letters*, 17(11):7080–7085, 2017. PMID: 28967761.

[274] Long-Jing Yin, Hua Jiang, Jia-Bin Qiao, and Lin He. Direct imaging of topological edge states at a bilayer graphene domain wall. *Nature Communications*, 7(11760):11760, 2016.

[275] Long Ju, Zhiwen Shi, Nityan Nair, Yinchuan Lv, Chenhao Jin, Jairo Velasco, Claudia Ojeda-Aristizabal, Hans A Bechtel, Michael C Martin, Alex Zettl, et al. Topological valley transport at bilayer graphene domain walls. *Nature*, 520(7549):650–655, 2015.

[276] E. C. Marino, Leandro O. Nascimento, Van Sérgio Alves, and C. Morais Smith. Interaction induced quantum valley Hall effect in graphene. *Phys. Rev. X*, 5:011040, Mar 2015.

[277] Hongki Min, Giovanni Borghi, Marco Polini, and A. H. MacDonald. Pseudospin magnetism in graphene. *Physical Review B*, 77:041407, Jan 2008.

[278] Rahul Nandkishore and Leonid Levitov. Quantum anomalous Hall state in bilayer graphene. *Physical Review B*, 82:115124, Sep 2010.

[279] Rahul Nandkishore and Leonid Levitov. Spontaneously ordered states in bilayer graphene. *Physica Scripta*, 2012(T146):014011, 2012.

[280] Mikito Koshino, Kyoka Sugisawa, and Edward McCann. Interaction-induced insulating states in multilayer graphenes. *Physical Review B*, 95:235311, Jun 2017.

[281] Kai Sun, Hong Yao, Eduardo Fradkin, and Steven A. Kivelson. Topological insulators and nematic phases from spontaneous symmetry breaking in 2d fermi systems with a quadratic band crossing. *Physical Review Letters*, 103:046811, Jul 2009.

[282] Pablo San-Jose and Elsa Prada. Helical networks in twisted bilayer graphene under interlayer bias. *Physical Review B*, 88:121408, Sep 2013.

[283] Peter Rickhaus, John Wallbank, Sergey Slizovskiy, Riccardo Pisoni, Hiske Overweg, Yongjin Lee, Marius Eich, Ming-Hao Liu, Kenji Watanabe, Takashi Taniguchi, Thomas Ihn, and Klaus Ensslin. Transport through a network of topological channels in twisted bilayer graphene. *Nano Letters*, 18(11):6725–6730, 2018. PMID: 30336041.

[284] Ian Affleck and F. D. M. Haldane. Critical theory of quantum spin chains. *Physical Review B*, 36:5291–5300, Oct 1987.

[285] Ian Affleck. On the realization of chiral symmetry in $1 + 1$ dimensions. *Nuclear Physics B*, 265(3):448–468, 1986.

[286] Ian Affleck. Exact critical exponents for quantum spin chains, non-linear σ-models at $\theta = \pi$ and the quantum hall effect. *Nuclear Physics B*, 265(3):409–447, 1986.

[287] Tin-Lun Ho. Spinor Bose condensates in optical traps. *Physical Review Letters*, 81:742–745, Jul 1998.

[288] Tetsuo Ohmi and Kazushige Machida. Bose-Einstein condensation with internal degrees of freedom in alkali atom gases. *Journal of the Physical Society of Japan*, 67(6):1822–1825, 1998.

[289] Subroto Mukerjee, Cenke Xu, and J. E. Moore. Topological defects and the superfluid transition of the $s = 1$ spinor condensate in two dimensions. *Physical Review Letters*, 97:120406, Sep 2006.

[290] Cenke Xu and Leon Balents. Topological superconductivity in twisted multilayer graphene. *Physical Review Letters*, 121(8):087001, 2018.

[291] Noah F. Q. Yuan and Liang Fu. Model for the metal-insulator transition in graphene superlattices and beyond. *Physical Review B*, 98:045103, Jul 2018.

[292] Alex Thomson, Shubhayu Chatterjee, Subir Sachdev, and Mathias S. Scheurer. Triangular antiferromagnetism on the honeycomb lattice of twisted bilayer graphene. *Physical Review B*, 98:075109, Aug 2018.

[293] J. F. Dodaro, S. A. Kivelson, Y. Schattner, X. Q. Sun, and C. Wang. Phases of a phenomenological model of twisted bilayer graphene. *Physical Review B*, 98:075154, Aug 2018.

[294] Hoi Chun Po, Liujun Zou, Ashvin Vishwanath, and T. Senthil. Origin of Mott insulating behavior and superconductivity in twisted bilayer graphene. *Phys. Rev. X*, 8:031089, Sep 2018.

[295] Jian Kang and Oskar Vafek. Symmetry, maximally localized wannier states, and a low-energy model for twisted bilayer graphene narrow bands. *Phys. Rev. X*, 8:031088, Sep 2018.

[296] Yi-Zhuang You and Ashvin Vishwanath. Superconductivity from valley fluctuations and approximate SO(4) symmetry in a weak coupling theory of twisted bilayer graphene. *npj Quantum Materials*, 4(1), apr 2019.

[297] Nick Bultinck, Shubhayu Chatterjee, and Michael P. Zaletel. Ground state and hidden symmetry of magic-angle graphene at even integer filling. *arXiv:1901.08110*, 10:031034, Aug 2019.

[298] Nick Bultinck, Shubhayu Chatterjee, and Michael P. Zaletel. Mechanism for anomalous hall ferromagnetism in twisted bilayer graphene. *Physical Review Letters*, 124:166601, Apr 2020.

[299] Fengcheng Wu and Sankar Das Sarma. Theory of phonon-mediated superconductivity in twisted bilayer graphene. *arXiv:1906.07302*, 121:257001, Dec 2019.

[300] Biao Lian, Zhijun Wang, and B. Andrei Bernevig. Twisted bilayer graphene: A phonon-driven superconductor. *Physical Review Letters*, 122:257002, Jun 2019.

[301] Jong Yeon Lee, Eslam Khalaf, Shang Liu, Xiaomeng Liu, Zeyu Hao, Philip Kim, and Ashvin Vishwanath. Theory of correlated insulating behaviour and spin-triplet superconductivity in twisted double bilayer graphene. *Nature Communications*, 10(1):5333, Nov 2019.

[302] Eslam Khalaf, Shubhayu Chatterjee, Nick Bultinck, Michael P. Zaletel, and Ashvin Vishwanath. Charged skyrmions and topological origin of superconductivity in magic-angle graphene. *Science Advances*, 7(19):eabf5299, May 2021.

[303] Yichen Xu, Xiao-Chuan Wu, Chao-Ming Jian, and Cenke Xu. Orbital order and possible non-fermi liquid in moiré systems. *Physical Review B*, 101:205426, May 2020.

[304] Rafael M. Fernandes and Jörn W. F. Venderbos. Nematicity with a twist: Rotational symmetry breaking in a moiré superlattice. *Science Advances*, 6(32):eaba8834, Aug 2020.

[305] Bheema Lingam Chittari, Guorui Chen, Yuanbo Zhang, Feng Wang, and Jeil Jung. Gate-tunable topological flat bands in trilayer graphene boron-nitride moiré superlattices. *Physical Review Letters*, 122:016401, Jan 2019.

[306] M. Serlin, C. L. Tschirhart, H. Polshyn, Y. Zhang, J. Zhu, K. Watanabe, T. Taniguchi, L. Balents, and A. F. Young. Intrinsic quantized anomalous Hall effect in a moiré heterostructure. *Science*, 367(6480):900–903, Dec 2019.

[307] Ya-Hui Zhang, Dan Mao, Yuan Cao, Pablo Jarillo-Herrero, and T. Senthil. Nearly flat chern bands in moiré superlattices. *Physical Review B*, 99:075127, Feb 2019.

[308] Guorui Chen, Aaron L. Sharpe, Eli J. Fox, Ya-Hui Zhang, Shaoxin Wang, Lili Jiang, Bosai Lyu, Hongyuan Li, Kenji Watanabe, Takashi Taniguchi, and et al. Tunable correlated chern insulator and ferromagnetism in a moiré superlattice. *Nature*, 579(7797):56–61, Mar 2020.

[309] Cécile Repellin and T Senthil. Chern bands of twisted bilayer graphene: Fractional chern insulators and spin phase transition. *Physical Review Research*, 2(2):023238, 2020.

[310] Petr Stepanov, Ming Xie, Takashi Taniguchi, Kenji Watanabe, Xiaobo Lu, Allan H. MacDonald, B. Andrei Bernevig, and Dmitri K. Efetov. Competing zero-field chern insulators in superconducting twisted bilayer graphene. *Physical Review Letters*, 127:197701, Nov 2021.

[311] Shaowen Chen, Minhao He, Ya-Hui Zhang, Valerie Hsieh, Zaiyao Fei, K. Watanabe, T. Taniguchi, David H. Cobden, Xiaodong Xu, Cory R. Dean, and et al. Electrically tunable correlated and topological states in twisted monolayer-bilayer graphene. *Nature Physics*, 17(3):374–380, Oct 2020.

[312] Andrew T Pierce, Yonglong Xie, Jeong Min Park, Eslam Khalaf, Seung Hwan Lee, Yuan Cao, Daniel E Parker, Patrick R Forrester, Shaowen Chen, Kenji Watanabe, et al. Unconventional sequence of correlated chern insulators in magic-angle twisted bilayer graphene. *Nature Physics*, 17(11):1210–1215, 2021.

[313] Xiao-Chuan Wu, Yichen Xu, Chao-Ming Jian, and Cenke Xu. Interacting valley chern insulator and its topological imprint on moiré superconductors. *Physical Review B*, 100:155138, Oct 2019.

[314] Xiao-Chuan Wu, Yichen Xu, Chao-Ming Jian, and Cenke Xu. Interacting valley chern insulator and its topological imprint on moiré superconductors. *Physical Review B*, 100:155138, Oct 2019.

[315] Haining Pan, Fengcheng Wu, and Sankar Das Sarma. Band topology, Hubbard model, Heisenberg model, and Dzyaloshinskii-Moriya interaction in twisted bilayer wse_2. *Physical Review Research*, 2:033087, Jul 2020.

[316] Yanhao Tang, Lizhong Li, Tingxin Li, Yang Xu, Song Liu, Katayun Barmak, Kenji Watanabe, Takashi Taniguchi, Allan H MacDonald, Jie Shan, et al. WSe_2/WS_2 moiré superlattices: a new Hubbard model simulator. *arXiv preprint arXiv:1910.08673*, 2019.

[317] Aaron Szasz, Johannes Motruk, Michael P. Zaletel, and Joel E. Moore. Chiral spin liquid phase of the triangular lattice Hubbard model: A density matrix renormalization group study. *Phys. Rev. X*, 10:021042, May 2020.

[318] Aaron Szasz and Johannes Motruk. Phase diagram of the anisotropic triangular lattice Hubbard model. *Physical Review B*, 103:235132, Jun 2021.

[319] Augusto Ghiotto, En-Min Shih, Giancarlo S. S. G. Pereira, Daniel A. Rhodes, Bumho Kim, Jiawei Zang, Andrew J. Millis, Kenji Watanabe, Takashi Taniguchi, James C. Hone, and et al. Quantum criticality in twisted transition metal dichalcogenides. *Nature*, 597(7876):345–349, Sep 2021.

[320] Emma C. Regan, Danqing Wang, Chenhao Jin, M. Iqbal Bakti Utama, Beini Gao, Xin Wei, Sihan Zhao, Wenyu Zhao, Zuocheng Zhang, Kentaro Yumigeta, and et al. Mott and generalized Wigner crystal states in WSe_2/WS_2 moiré superlattices. *Nature*, 579(7799):359–363, Mar 2020.

[321] Chenhao Jin, Zui Tao, Tingxin Li, Yang Xu, Yanhao Tang, Jiacheng Zhu, Song Liu, Kenji Watanabe, Takashi Taniguchi, James C. Hone, and et al. Stripe phases in WSe_2/WS_2 moiré superlattices. *Nature Materials*, 20(7):940–944, Mar 2021.

[322] Yang Xu, Song Liu, Daniel A. Rhodes, Kenji Watanabe, Takashi Taniguchi, James Hone, Veit Elser, Kin Fai Mak, and Jie Shan. Correlated insulating states at fractional fillings of moiré superlattices. *Nature*, 587(7833):214–218, Nov 2020.

[323] Xiong Huang, Tianmeng Wang, Shengnan Miao, Chong Wang, Zhipeng Li, Zhen Lian, Takashi Taniguchi, Kenji Watanabe, Satoshi Okamoto, Di Xiao, and et al. Correlated insulating states at fractional fillings of the WS_2/WSe_2 moiré lattice. *Nature Physics*, 17(6):715–719, Feb 2021.

[324] Sung-Sik Lee and Patrick A. Lee. U(1) gauge theory of the Hubbard model: Spin liquid states and possible application to $\kappa - \mathrm{BEDTTTF_2Cu_2CN_3}$. *Physical Review Letters*, 95:036403, Jul 2005.

[325] David F. Mross and T. Senthil. Charge Friedel oscillations in a Mott insulator. *Physical Review B*, 84:041102, Jul 2011.

[326] Min-Chul Cha, Matthew P. A. Fisher, S. M. Girvin, Mats Wallin, and A. Peter Young. Universal conductivity of two-dimensional films at the superconductor-insulator transition. *Physical Review B*, 44:6883–6902, Oct 1991.

[327] B. Spivak, S. V. Kravchenko, S. A. Kivelson, and X. P. A. Gao. Colloquium: Transport in strongly correlated two dimensional electron fluids. *Reviews of Modern Physics*, 82(2):1743–1766, May 2010.

[328] L. B. Ioffe and A. I. Larkin. Gapless fermions and gauge fields in dielectrics. *Physical Review B*, 39:8988–8999, May 1989.

[329] Matthew P. A. Fisher, G. Grinstein, and S. M. Girvin. Presence of quantum diffusion in two dimensions: Universal resistance at the superconductor-insulator transition. *Physical Review Letters*, 64:587–590, Jan 1990.

[330] Rosario Fazio and Dario Zappalà. ϵ expansion of the conductivity at the superconductor-Mott-insulator transition. *Physical Review B*, 53:R8883–R8886, Apr 1996.

[331] Jurij Šmakov and Erik Sørensen. Universal scaling of the conductivity at the superfluid-insulator phase transition. *Physical Review Letters*, 95:180603, Oct 2005.

[332] William Witczak-Krempa, Erik S. Sorensen, and Subir Sachdev. The dynamics of quantum criticality revealed by quantum monte carlo and holography. *Nature Physics*, 10(5):361, Mar 2014.

[333] Kun Chen, Longxiang Liu, Youjin Deng, Lode Pollet, and Nikolay Prokof'ev. Universal conductivity in a two-dimensional superfluid-to-insulator quantum critical system. *Physical Review Letters*, 112:030402, Jan 2014.

[334] Shai M. Chester, Walter Landry, Junyu Liu, David Poland, David Simmons-Duffin, Ning Su, and Alessandro Vichi. Carving out ope space and precise O(2) model critical exponents. *Journal of High Energy Physics*, 2020(6):142, Jun 2020.

[335] D. B. Haviland, Y. Liu, and A. M. Goldman. Onset of superconductivity in the two-dimensional limit. *Physical Review Letters*, 62:2180–2183, May 1989.

[336] Y. Liu, K. A. McGreer, B. Nease, D. B. Haviland, G. Martinez, J. W. Halley, and A. M. Goldman. Scaling of the insulator-to-superconductor transition in ultrathin amorphous bi films. *Physical Review Letters*, 67:2068–2071, Oct 1991.

[337] S. J. Lee and J. B. Ketterson. Critical sheet resistance for the suppression of superconductivity in thin mo-c films. *Physical Review Letters*, 64:3078–3081, Jun 1990.

[338] V. J. Emery and S. A. Kivelson. Superconductivity in bad metals. *Physical Review Letters*, 74:3253–3256, Apr 1995.

[339] N. E. Hussey, K. Takenaka, and H. Takagi. Universality of the Mott-Ioffe-Regel limit in metals. *Philosophical Magazine*, 84(27):2847–2864, 2004.

[340] Michael E Peskin. Mandelstam-'t hooft duality in abelian lattice models. *Annals of Physics*, 113(1):122–152, 1978.

[341] Matthew P. A. Fisher and D. H. Lee. Correspondence between two-dimensional bosons and a bulk superconductor in a magnetic field. *Physical Review B*, 39:2758, Feb 1989.

[342] Leon Balents, Lorenz Bartosch, Anton Burkov, Subir Sachdev, and Krishnendu Sengupta. Competing orders and non-Landau-Ginzburg-Wilson criticality in (Bose) Mott transitions. *Progress of Theoretical Physics Supplement*, 160:314–336, 2005.

[343] R. Moessner and S. L. Sondhi. Ising models of quantum frustration. *Physical Review B*, 63:224401, May 2001.

[344] Cenke Xu and Subir Sachdev. Global phase diagrams of frustrated quantum antiferromagnets in two dimensions: Doubled Chern-Simons theory. *Physical Review B*, 79:064405, Feb 2009.

[345] Kevin Slagle and Cenke Xu. Quantum phase transition between the Z_2 spin liquid and valence bond crystals on a triangular lattice. *Physical Review B*, 89:104418, Mar 2014.

[346] Cenke Xu and Leon Balents. Quantum phase transitions around the staggered valence-bond solid. *Physical Review B*, 84:014402, Jul 2011.

[347] Cong-Jun Wu, Ian Mondragon-Shem, and Xiang-Fa Zhou. Unconventional Bose-Einstein condensations from spin-orbit coupling. *Chinese Physics Letters*, 28(9):097102, sep 2011.

[348] Chunji Wang, Chao Gao, Chao-Ming Jian, and Hui Zhai. Spin-orbit coupled spinor Bose-Einstein condensates. *Physical Review Letters*, 105:160403, Oct 2010.

[349] Xiao-Tian Zhang and Gang Chen. Infinity scatter infinity: Infinite critical boson non-Fermi liquid. *arXiv e-prints*, page arXiv:2102.09272, February 2021.

[350] Ethan Lake, T. Senthil, and Ashvin Vishwanath. Bose-Luttinger liquids. *Physical Review B*, 104:014517, Jul 2021.

[351] Seth Musser, T Senthil, and Debanjan Chowdhury. Theory of a continuous Mott transition in two dimensions. *arXiv preprint arXiv:2111.09894*, 2021.

[352] Yichen Xu, Xiao-Chuan Wu, Chao-Ming Jian, and Cenke Xu. Topological edge and interface states at bulk disorder-to-order quantum critical points. *Physical Review B*, 101:184419, May 2020.

[353] Chao-Ming Jian, Yichen Xu, Xiao-Chuan Wu, and Cenke Xu. Continuous Néel-VBS Quantum Phase Transition in Non-Local one-dimensional systems with SO(3) Symmetry. *SciPost Phys.*, 10:33, 2021.

[354] Max A. Metlitski, David F. Mross, Subir Sachdev, and T. Senthil. Cooper pairing in non-fermi liquids. *Physical Review B*, 91:115111, Mar 2015.

[355] Yuxuan Wang and Andrey V. Chubukov. Enhancement of superconductivity at the onset of charge-density-wave order in a metal. *Physical Review B*, 92:125108, Sep 2015.

[356] Ipsita Mandal. Superconducting instability in non-fermi liquids. *Physical Review B*, 94:115138, Sep 2016.

[357] S. Lederer, Y. Schattner, E. Berg, and S. A. Kivelson. Enhancement of superconductivity near a nematic quantum critical point. *Physical Review Letters*, 114:097001, Mar 2015.

[358] Yuxuan Wang, Artem Abanov, Boris L. Altshuler, Emil A. Yuzbashyan, and Andrey V. Chubukov. Superconductivity near a quantum-critical point: The special role of the first matsubara frequency. *Physical Review Letters*, 117:157001, Oct 2016.

[359] Samuel Lederer, Yoni Schattner, Erez Berg, and Steven A. Kivelson. Superconductivity and non-fermi liquid behavior near a nematic quantum critical point. *Proceedings of the National Academy of Sciences*, 114(19):4905–4910, 2017.

[360] Liujun Zou and Debanjan Chowdhury. Deconfined metallic quantum criticality: A U(2) gauge-theoretic approach. *Physical Review Research*, 2(2):023344, Jun 2020.

[361] Ipsita Mandal. Critical fermi surfaces in generic dimensions arising from transverse gauge field interactions. *Physical Review Research*, 2:043277, Nov 2020.

[362] Sergei V. Isakov, Arun Paramekanti, and Yong Baek Kim. Exotic phase diagram of a cluster charging model of bosons on the kagome lattice. *Physical Review B*, 76:224431, Dec 2007.

[363] Yan-Cheng Wang, Meng Cheng, William Witczak-Krempa, and Zi Yang Meng. Fractionalized conductivity and emergent self-duality near topological phase transitions. *Nature Communications*, 12(1), Sep 2021.

[364] V. Kalmeyer and R. B. Laughlin. Equivalence of the resonating-valence-bond and fractional quantum Hall states. *Physical Review Letters*, 59:2095–2098, Nov 1987.

[365] Vadim Kalmeyer and R. B. Laughlin. Theory of the spin liquid state of the Heisenberg antiferromagnet. *Physical Review B*, 39:11879–11899, Jun 1989.

[366] Meng Cheng, Michael Zaletel, Maissam Barkeshli, Ashvin Vishwanath, and Parsa Bonderson. Translational symmetry and microscopic constraints on symmetry-enriched topological phases: A view from the surface. *Physical Review X*, 6(4):041068, 2016.

[367] Michael Levin and Ady Stern. Fractional topological insulators. *Physical Review Letters*, 103:196803, Nov 2009.

[368] Maissam Barkeshli and John McGreevy. Continuous transition between fractional quantum Hall and superfluid states. *Physical Review B*, 89(16):235116, Jun 2014.

[369] S. V. Isakov, R. G. Melko, and M. B. Hastings. Universal signatures of fractionalized quantum critical points. *Science*, 335(6065):193–195, Jan 2012.

[370] Silviu S. Pufu and Subir Sachdev. Monopoles in $2+1$-dimensional conformal field theories with global U(1) symmetry. *Journal of High Energy Physics*, 2013(9):127, Sep 2013.

[371] Ethan Dyer, Márk Mezei, Silviu S. Pufu, and Subir Sachdev. Scaling dimensions of monopole operators in the $\mathbb{CP}^{N_b-1}$ theory in $2+1$ dimensions. *Journal of High Energy Physics*, 2015(6):37, June 2015.

[372] Markus König, Steffen Wiedmann, Christoph Brüne, Andreas Roth, Hartmut Buhmann, Laurens W. Molenkamp, Xiao-Liang Qi, and Shou-Cheng Zhang. Quantum spin Hall insulator state in HgTe quantum wells. *Science*, 318(5851):766–770, Nov 2007.

[373] Patrick A. Lee and Naoto Nagaosa. Gauge theory of the normal state of high-t_c superconductors. *Physical Review B*, 46:5621–5639, Sep 1992.

[374] Sean A. Hartnoll, Andrew Lucas, and Subir Sachdev. *Holographic Quantum Matter*. The MIT Press, 2018.

[375] Cody P. Nave and Patrick A. Lee. Transport properties of a spinon fermi surface coupled to a U(1) gauge field. *Physical Review B*, 76:235124, Dec 2007.

[376] Gang Chen, Hae-Young Kee, and Yong Baek Kim. Fractionalized charge excitations in a spin liquid on partially filled pyrochlore lattices. *Physical Review Letters*, 113:197202, Nov 2014.

[377] Pavel Kovtun. Lectures on hydrodynamic fluctuations in relativistic theories. *Journal of Physics A Mathematical General*, 45(47):473001, November 2012.

[378] Luca V. Delacretaz. Heavy operators and hydrodynamic tails. *SciPost Phys.*, 9:34, 2020.

[379] Yoni Schattner, Samuel Lederer, Steven A. Kivelson, and Erez Berg. Ising nematic quantum critical point in a metal: A monte carlo study. *Phys. Rev. X*, 6:031028, Aug 2016.

[380] Xiao Yan Xu, Kai Sun, Yoni Schattner, Erez Berg, and Zi Yang Meng. Non-fermi liquid at $(2+1)d$ ferromagnetic quantum critical point. *Phys. Rev. X*, 7:031058, Sep 2017.

[381] Hong-Chen Jiang and Thomas P. Devereaux. Superconductivity in the doped Hubbard model and its interplay with next-nearest hopping t'. *Science*, 365(6460):1424–1428, sep 2019.

[382] Aaron Szasz, Johannes Motruk, Michael P. Zaletel, and Joel E. Moore. Chiral spin liquid phase of the triangular lattice Hubbard model: A density matrix renormalization group study. *Phys. Rev. X*, 10:021042, May 2020.

[383] X. G. WEN. Topological orders in rigid states. *International Journal of Modern Physics B*, 04(02):239–271, 1990.

[384] Xiao-Gang Wen. Choreographed entanglement dances: Topological states of quantum matter. *Science*, 363(6429), 2019.

[385] C. M. Varma, P. B. Littlewood, S. Schmitt-Rink, E. Abrahams, and A. E. Ruckenstein. Phenomenology of the normal state of cu-o high-temperature superconductors. *Physical Review Letters*, 63:1996–1999, Oct 1989.

[386] Yuan Cao, Debanjan Chowdhury, Daniel Rodan-Legrain, Oriol Rubies-Bigordï¿œ, Kenji Watanabe, Takashi Taniguchi, T. Senthil, and Pablo Jarillo-Herrero. Strange metal in magic-angle graphene with near planckian dissipation. *arXiv:1901.03710*, 124:076801, Feb 2019.

[387] Chetan Nayak and Frank Wilczek. Non-fermi liquid fixed point in $2+1$ dimensions. *Nuclear Physics B*, 417(3):359–373, 1994.

[388] Chetan Nayak and Frank Wilczek. Renormalization group approach to low temperature properties of a non-fermi liquid metal. *Nuclear Physics B*, 430(3):534–562, 1994.

[389] David F. Mross, John McGreevy, Hong Liu, and T. Senthil. Controlled expansion for certain non-fermi-liquid metals. *Physical Review B*, 82:045121, Jul 2010.

[390] J. Maldacena and D. Stanford. Remarks on the Sachdev-Ye-Kitaev model. *Physical Review D*, 94(10):106002, November 2016.

[391] Edward Witten. An syk-like model without disorder. *Journal of Physics A: Mathematical and Theoretical*, 52(47):474002, October 2019.

[392] Igor R. Klebanov and Grigory Tarnopolsky. Uncolored random tensors, melon diagrams, and the Sachdev-Ye-Kitaev models. *Physical Review D*, 95:046004, Feb 2017.

[393] Xue-Yang Song, Chao-Ming Jian, and Leon Balents. Strongly correlated metal built from Sachdev-Ye-Kitaev models. *Physical Review Letters*, 119:216601, Nov 2017.

[394] Aavishkar A. Patel, John McGreevy, Daniel P. Arovas, and Subir Sachdev. Magnetotransport in a model of a disordered strange metal. *Phys. Rev. X*, 8:021049, May 2018.

[395] Aavishkar A. Patel and Subir Sachdev. Critical strange metal from fluctuating gauge fields in a solvable random model. *Physical Review B*, 98:125134, Sep 2018.

[396] Debanjan Chowdhury, Yochai Werman, Erez Berg, and T. Senthil. Translationally invariant non-fermi-liquid metals with critical fermi surfaces: Solvable models. *Phys. Rev. X*, 8:031024, Jul 2018.

[397] Xiaochuan Wu, Xiao Chen, Chao-Ming Jian, Yi-Zhuang You, and Cenke Xu. Candidate theory for the strange metal phase at a finite-energy window. *Physical Review B*, 98:165117, Oct 2018.

[398] Xiao-Chuan Wu, Chao-Ming Jian, and Cenke Xu. Lattice models for non-fermi liquids with tunable transport scalings. *Physical Review B*, 100:075101, Aug 2019.

[399] Sung-Sik Lee. Low-energy effective theory of fermi surface coupled with U(1) gauge field in $2+1$ dimensions. *Physical Review B*, 80:165102, Oct 2009.

[400] Rhine Samajdar, Mathias S Scheurer, Shubhayu Chatterjee, Haoyu Guo, Cenke Xu, and Subir Sachdev. Enhanced thermal Hall effect in the square-lattice Néel state. *Nature Physics*, 15(12):1290–1294, 2019.

[401] Gaël Grissonnanche, Anaëlle Legros, Sven Badoux, Etienne Lefrançois, Victor Zatko, Maude Lizaire, Francis Laliberté, Adrien Gourgout, J-S Zhou, Sunseng Pyon, et al. Giant thermal Hall conductivity in the pseudogap phase of cuprate superconductors. *Nature*, 571(7765):376–380, 2019.

[402] Nikhil Karthik and Rajamani Narayanan. Scale invariance of parity-invariant three-dimensional QED. *Physical Review D*, 94:065026, Sep 2016.

[403] Tarun Grover and Ashvin Vishwanath. Quantum phase transition between integer quantum Hall states of bosons. *Physical Review B*, 87:045129, Jan 2013.

[404] Yuan-Ming Lu and Dung-Hai Lee. Quantum phase transitions between bosonic symmetry-protected topological phases in two dimensions: Emergent QED_3 and anyon superfluid. *Physical Review B*, 89(19):195143, May 2014.

[405] Rufus Boyack, Ahmed Rayyan, and Joseph Maciejko. Deconfined criticality in the QED_3 Gross-Neveu-Yukawa model: The $1/N$ expansion revisited. *Physical Review B*, 99:195135, May 2019.

[406] Yuan-Ming Lu. Symmetric Z_2 spin liquids and their neighboring phases on triangular lattice. *Physical Review B*, 93:165113, Apr 2016.

[407] Swapan K. Pati, Rajiv R. P. Singh, and Daniel I. Khomskii. Alternating spin and orbital dimerization and spin-gap formation in coupled spin-orbital systems. *Physical Review Letters*, 81:5406–5409, Dec 1998.

[408] Y. Q. Li, Michael Ma, D. N. Shi, and F. C. Zhang. SU(4) theory for spin systems with orbital degeneracy. *Physical Review Letters*, 81:3527–3530, Oct 1998.

[409] Y. Tokura and N. Nagaosa. Orbital physics in transition-metal oxides. *Science*, 288(5465):462–468, 2000.

[410] Congjun Wu, Jiang-ping Hu, and Shou-cheng Zhang. Exact SO(5) symmetry in the spin-3/2 fermionic system. *Physical Review Letters*, 91:186402, Oct 2003.

[411] Congjun Wu. Competing orders in one-dimensional spin-3/2 fermionic systems. *Physical Review Letters*, 95:266404, Dec 2005.

[412] CONGJUN WU. Hidden symmetry and quantum phases in spin-3/2 cold atomic systems. *Modern Physics Letters B*, 20(27):1707–1738, 2006.

[413] Alexey Vyacheslavovich Gorshkov, M Hermele, V Gurarie, C Xu, Paul S Julienne, J Ye, Peter Zoller, Eugene Demler, Mikhail D Lukin, and AM Rey. Two-orbital SU(N) magnetism with ultracold alkaline-earth atoms. *Nature physics*, 6(4):289–295, 2010.

[414] Xiao-Chuan Wu, Anna Keselman, Chao-Ming Jian, Kelly Ann Pawlak, and Cenke Xu. Ferromagnetism and spin-valley liquid states in moiré correlated insulators. *Physical Review B*, 100(2):024421, 2019.

[415] Constantin Schrade and Liang Fu. Spin-valley density wave in moiré materials. *Physical Review B*, 100(3):035413, 2019.

[416] Ya-Hui Zhang, Dan Mao, and T Senthil. Twisted bilayer graphene aligned with hexagonal boron nitride: anomalous Hall effect and a lattice model. *Physical Review Research*, 1(3):033126, 2019.

[417] Max A. Metlitski, David F. Mross, Subir Sachdev, and T. Senthil. Cooper pairing in non-fermi liquids. *Physical Review B*, 91:115111, Mar 2015.

[418] S. Lederer, Y. Schattner, E. Berg, and S. A. Kivelson. Enhancement of superconductivity near a nematic quantum critical point. *Physical Review Letters*, 114:097001, Mar 2015.

[419] Jérôme Rech, Catherine Pépin, and Andrey V. Chubukov. Quantum critical behavior in itinerant electron systems: Eliashberg theory and instability of a ferromagnetic quantum critical point. *Physical Review B*, 74:195126, Nov 2006.

[420] Xiao Yan Xu, Avraham Klein, Kai Sun, Andrey V. Chubukov, and Zi Yang Meng. Extracting non-Fermi liquid fermionic self-energy at $T = 0$ from quantum Monte Carlo data. *arXiv e-prints*, page arXiv:2003.11573, March 2020.

[421] Aavishkar A. Patel and Subir Sachdev. Theory of a planckian metal. *Physical Review Letters*, 123:066601, Aug 2019.

[422] C. N. Yang. The spontaneous magnetization of a two-dimensional ising model. *Phys. Rev.*, 85:808–816, Mar 1952.

[423] T. D. Lee and C. N. Yang. Statistical theory of equations of state and phase transitions. ii. lattice gas and ising model. *Phys. Rev.*, 87:410–419, Aug 1952.

[424] Kenneth G. Wilson and Michael E. Fisher. Critical exponents in 3.99 dimensions. *Physical Review Letters*, 28:240–243, Jan 1972.

[425] Paul Adrien Maurice Dirac. Quantised singularities in the electromagnetic field,. *Proceedings of the Royal Society of London. Series A, Containing Papers of a Mathematical and Physical Character*, 133(821):60–72, 1931.

[426] Bascom S. Deaver and William M. Fairbank. Experimental evidence for quantized flux in superconducting cylinders. *Physical Review Letters*, 7:43–46, Jul 1961.

[427] Bascom S. Deaver and William M. Fairbank. Experimental evidence for quantized flux in superconducting cylinders. *Physical Review Letters*, 7:43–46, Jul 1961.

[428] S. C. Zhang, T. H. Hansson, and S. Kivelson. Effective-field-theory model for the fractional quantum Hall effect. *Physical Review Letters*, 62:82–85, Jan 1989.

[429] X. G. Wen and Q. Niu. Ground-state degeneracy of the fractional quantum Hall states in the presence of a random potential and on high-genus Riemann surfaces. *Physical Review B*, 41:9377–9396, May 1990.

[430] SHOU CHENG ZHANG. The Chern–Simons–Landau–Ginzburg theory of the fractional quantum Hall effect. *International Journal of Modern Physics B*, 06(01):25–58, 1992.

[431] X. G. WEN. Topological orders in rigid states. *International Journal of Modern Physics B*, 04(02):239–271, 1990.

[432] Yong Baek Kim, Patrick A. Lee, and Xiao-Gang Wen. Quantum Boltzmann equation of composite fermions interacting with a gauge field. *Physical Review B*, 52:17275–17292, Dec 1995.

[433] Yochai Werman, Steven A. Kivelson, and Erez Berg. Non-quasiparticle transport and resistivity saturation: a view from the large-N limit. *npj Quantum Materials*, 2(1), Feb 2017.

[434] Yochai Werman and Erez Berg. Mott-Ioffe-Regel limit and resistivity crossover in a tractable electron-phonon model. *Physical Review B*, 93:075109, Feb 2016.

[435] Xiao-Chuan Wu, Chao-Ming Jian, and Cenke Xu. Lattice models for non-fermi liquids with tunable transport scalings. *Physical Review B*, 100:075101, Aug 2019.

[436] M. Gell-Mann. A schematic model of baryons and mesons. *Physics Letters*, 8(3):214–215, 1964.

[437] R. B. Laughlin. Anomalous quantum Hall effect: an incompressible quantum fluid with fractionally charged excitations. *Physical Review Letters*, 50:1395–1398, May 1983.

[438] R. de Picciotto, M. Reznikov, M. Heiblum, V. Umansky, G. Bunin, and D. Mahalu. Direct observation of a fractional charge. *Nature*, 389:162–164, 1997.

[439] L. Saminadayar, D. C. Glattli, Y. Jin, and B. Etienne. Observation of the $e/3$ fractionally Charged Laughlin quasiparticle. *Physical Review Letters*, 79:2526–2529, Sep 1997.

[440] V. Kalmeyer and R. B. Laughlin. Equivalence of the resonating-valence-bond and fractional quantum Hall states. *Physical Review Letters*, 59:2095–2098, Nov 1987.

[441] X. G. Wen, Frank Wilczek, and A. Zee. Chiral spin states and superconductivity. *Physical Review B*, 39:11413–11423, Jun 1989.

[442] N. Read and Subir Sachdev. large-N expansion for frustrated quantum antiferromagnets. *Physical Review Letters*, 66:1773–1776, Apr 1991.

[443] Xiao-Gang Wen. Quantum orders and symmetric spin liquids. *Physical Review B*, 65:165113, Apr 2002.

[444] Yichen Xu, Zhu-Xi Luo, Chao-Ming Jian, and Cenke Xu. Metal-insulator transition with charge fractionalization. *arXiv preprint arXiv:2106.14910*, 2021.

[445] N. P. Ong. Geometric interpretation of the weak-field Hall conductivity in two-dimensional metals with arbitrary Fermi surface. *Physical Review B*, 43:193–201, Jan 1991.

[446] C. N. Yang and R. L. Mills. Conservation of isotopic spin and isotopic gauge invariance. *Phys. Rev.*, 96:191–195, Oct 1954.

[447] Ribhu K. Kaul, Yong Baek Kim, Subir Sachdev, and T. Senthil. Algebraic charge liquids. *Nature Physics*, 4(1):28–31, dec 2007.

[448] Cenke Xu and Subir Sachdev. Majorana liquids: The complete fractionalization of the electron. *Physical Review Letters*, 105:057201, Jul 2010.

[449] L.D. Faddeev and V.N. Popov. Feynman diagrams for the Yang-Mills field. *Physics Letters B*, 25(1):29–30, 1967.

[450] Cody P. Nave and Patrick A. Lee. Transport properties of a spinon fermi surface coupled to a U(1) gauge field. *Physical Review B*, 76:235124, Dec 2007.

[451] Mingjie Zhang, Xuan Zhao, Kenji Watanabe, Takashi Taniguchi, Zheng Zhu, Fengcheng Wu, Yongqing Li, and Yang Xu. Pomeranchuk effect and tunable quantum phase transitions in 3l-mote2/wse2, 2022.

[452] Peter W. Higgs. Broken symmetries and the masses of gauge bosons. *Physical Review Letters*, 13:508–509, Oct 1964.

[453] F. Englert and R. Brout. Broken symmetry and the mass of gauge vector mesons. *Physical Review Letters*, 13:321–323, Aug 1964.

[454] G. S. Guralnik, C. R. Hagen, and T. W. B. Kibble. Global conservation laws and massless particles. *Physical Review Letters*, 13:585–587, Nov 1964.

[455] Yoni Schattner, Samuel Lederer, Steven A. Kivelson, and Erez Berg. Ising nematic quantum critical point in a metal: A monte carlo study. *Phys. Rev. X*, 6:031028, Aug 2016.

[456] Eduardo Fradkin, Steven A. Kivelson, and John M. Tranquada. Colloquium. *Rev. Mod. Phys.*, 87:457–482, May 2015.

[457] S. Sachdev. Bekenstein-Hawking entropy and strange metals. *Physical Review X*, 5(4):041025, October 2015.

[458] Joseph Polchinski and Vladimir Rosenhaus. The spectrum in the Sachdev-Ye-Kitaev model. *Journal of High Energy Physics*, 2016(4):1–25, 2016.

[459] David J Gross and Vladimir Rosenhaus. A generalization of sachdev-ye-kitaev. *Journal of High Energy Physics*, 2017(2):1–38, 2017.

[460] Zhen Bi, Chao-Ming Jian, Yi-Zhuang You, Kelly Ann Pawlak, and Cenke Xu. Instability of the non-Fermi-liquid state of the Sachdev-Ye-Kitaev model. *Physical Review B*, 95(20):205105, 2017.

[461] Zhihuang Luo, Yi-Zhuang You, Jun Li, Chao-Ming Jian, Dawei Lu, Cenke Xu, Bei Zeng, and Raymond Laflamme. Quantum simulation of the non-fermi-liquid state of Sachdev-Ye-Kitaev model. *npj Quantum Information*, 5(1):1–6, 2019.

[462] M. Mitrano, A. A. Husain, S. Vig, A. Kogar, M. S. Rak, S. I. Rubeck, J. Schmalian, B. Uchoa, J. Schneeloch, R. Zhong, G. D. Gu, and P. Abbamonte. Anomalous density fluctuations in a strange metal. *Proceedings of the National Academy of Sciences*, 115(21):5392–5396, 2018.

[463] Yochai Werman, Steven A. Kivelson, and Erez Berg. Quantum chaos in an electron-phonon bad metal. *arXiv:1705.07895*, 2017.

[464] Yingfei Gu, Xiao-Liang Qi, and Douglas Stanford. Local criticality, diffusion and chaos in generalized Sachdev-Ye-Kitaev models. *Journal of High Energy Physics*, 2017(5):125, May 2017.

[465] Richard A. Davison, Wenbo Fu, Antoine Georges, Yingfei Gu, Kristan Jensen, and Subir Sachdev. Thermoelectric transport in disordered metals without quasiparticles: The Sachdev-Ye-Kitaev models and holography. *Physical Review B*, 95:155131, Apr 2017.

[466] Shao-Kai Jian and Hong Yao. Solvable Sachdev-Ye-Kitaev models in higher dimensions: from diffusion to many-body localization. *Physical Review Letters*, 119:206602, Nov 2017.

[467] Chao-Ming Jian, Zhen Bi, and Cenke Xu. Model for continuous thermal metal to insulator transition. *Physical Review B*, 96:115122, Sep 2017.

[468] A. Georges, O. Parcollet, and S. Sachdev. Quantum fluctuations of a nearly critical Heisenberg spin glass. *Physical Review B*, 63:134406, Mar 2001.

[469] Razvan Gurau. Colored group field theory. *Communications in mathematical physics*, 304(1):69–93, 2011.

[470] Angela Kopp, Amit Ghosal, and Sudip Chakravarty. Competing ferromagnetism in high-temperature copper oxide superconductors. *Proceedings of the National Academy of Sciences*, 104(15):6123–6127, 2007.

[471] Stéphane Dartois, Harold Erbin, and Swapnamay Mondal. Conformality of $1/N$ corrections in Sachdev-Ye-Kitaev-like models. *Physical Review D*, 100(12), Dec 2019.

[472] Leon Balents and Arun Paramekanti. Xy ring-exchange model on the triangular lattice. *Physical Review B*, 67(13):134427, 2003.

[473] R. S. Markiewicz, S. Sahrakorpi, M. Lindroos, Hsin Lin, and A. Bansil. One-band tight-binding model parametrization of the high-T_c cuprates including the effect of k_z dispersion. *Physical Review B*, 72:054519, Aug 2005.

[474] Subir Sachdev and N. Read. Large-N expansion for frustrated and doped quantum antiferromagnets. *International Journal of Modern Physics B*, 05(01n02):219–249, 1991.

[475] Gabriel Kotliar and Jialin Liu. Superexchange mechanism and d-wave superconductivity. *Physical Review B*, 38:5142–5145, Sep 1988.

[476] DJ Scalapino, E Loh Jr, and JE Hirsch. D-wave pairing near a spin-density-wave instability. *Physical Review B*, 34(11):8190, 1986.

[477] F C Zhang, C Gros, T M Rice, and H Shiba. A renormalised hamiltonian approach to a resonant valence bond wavefunction. *Superconductor Science and Technology*, 1(1):36, 1988.

[478] Y. Kohsaka, C. Taylor, K. Fujita, A. Schmidt, C. Lupien, T. Hanaguri, M. Azuma, M. Takano, H. Eisaki, H. Takagi, S. Uchida, and J. C. Davis. An intrinsic bond-centered electronic glass with unidirectional domains in underdoped cuprates. *Science*, 315(5817):1380–1385, 2007.

[479] Sumilan Banerjee and Ehud Altman. Solvable model for a dynamical quantum phase transition from fast to slow scrambling. *Physical Review B*, 95:134302, Apr 2017.

[480] Xin Chen, Ruihua Fan, Yiming Chen, Hui Zhai, and Pengfei Zhang. Competition between chaotic and nonchaotic phases in a quadratically coupled Sachdev-Ye-Kitaev model. *Physical Review Letters*, 119:207603, Nov 2017.

[481] Wenjie Ji and Xiao-Gang Wen. Categorical symmetry and noninvertible anomaly in symmetry-breaking and topological phase transitions. *Physical Review Research*, 2(3):033417, 2020.

[482] Ofer Aharony, Nathan Seiberg, and Yuji Tachikawa. Reading between the lines of four-dimensional gauge theories. *Journal of High Energy Physics*, 2013(8), Aug 2013.

[483] Sergei Gukov and Anton Kapustin. Topological quantum field theory, nonlocal operators, and gapped phases of gauge theories. *arXiv preprint arXiv:1307.4793*, 2013.

[484] Anton Kapustin and Ryan Thorngren. Topological field theory on a lattice, discrete theta-angles and confinement. *Advances in Theoretical and Mathematical Physics*, 18(5):1233–1247, 2014.

[485] Anton Kapustin and Ryan Thorngren. Higher symmetry and gapped phases of gauge theories. In *Algebra, geometry, and physics in the 21st century*, pages 177–202. Springer, 2017.

[486] Anton Kapustin and Nathan Seiberg. Coupling a QFT to a TQFT and duality. *Journal of High Energy Physics*, 2014(4), Apr 2014.

[487] Po-Shen Hsin, Ho Tat Lam, and Nathan Seiberg. Comments on one-form global symmetries and their gauging in $3d$ and $4d$. *SciPost Physics*, 6(3), Mar 2019.

[488] Nathan Seiberg. Field theories with a vector global symmetry. *SciPost Physics*, 8(4), Apr 2020.

[489] Clay Córdova, Thomas T. Dumitrescu, and Kenneth Intriligator. Exploring 2-group global symmetries. *Journal of High Energy Physics*, 2019(2):184, February 2019.

[490] Leonard Susskind. Order and disorder in gauge systems and magnets. *arXiv:1412.8483*, 17:2637–2658, May 2014.

[491] C L Henley. From classical to quantum dynamics at rokhsar-kivelson points. *Journal of Physics: Condensed Matter*, 16(11):S891CS898, Mar 2004.

[492] Eduardo Fradkin, David A. Huse, R. Moessner, V. Oganesyan, and S. L. Sondhi. Bipartite rokhsar-kivelson points and cantor deconfinement. *Physical Review B*, 69(22), Jun 2004.

[493] Daniel S. Rokhsar and Steven A. Kivelson. Superconductivity and the quantum hard-core dimer gas. *Physical Review Letters*, 61:2376–2379, Nov 1988.

[494] Eduardo Fradkin and STEVEN Kivelson. Short range resonating valence bond theories and superconductivity. *Modern Physics Letters B*, 04(03):225–232, 1990.

[495] John B. Kogut. An introduction to lattice gauge theory and spin systems. *Rev. Mod. Phys.*, 51:659–713, Oct 1979.

[496] Robert Savit. Duality in field theory and statistical systems. *Rev. Mod. Phys.*, 52:453–487, Apr 1980.

[497] Cenke Xu and Liang Fu. Fractionalization in Josephson junction arrays hinged by quantum spin Hall edges. *Physical Review B*, 81:134435, Apr 2010.

[498] Cenke Xu and Joel E Moore. Strong-weak coupling self-duality in the two-dimensional quantum phase transition of $p + ip$ superconducting arrays. *Physical Review Letters*, 93(4):047003, 2004.

[499] Arun Paramekanti, Leon Balents, and Matthew P. A. Fisher. Ring exchange, the exciton Bose liquid, and bosonization in two dimensions. *Physical Review B*, 66(5), Aug 2002.

[500] Cenke Xu and Matthew PA Fisher. Bond algebraic liquid phase in strongly correlated multiflavor cold atom systems. *Physical Review B*, 75(10):104428, 2007.

[501] Jiarui Zhao, Zheng Yan, Meng Cheng, and Zi Yang Meng. Higher-form symmetry breaking at ising transitions. *Physical Review Research*, 3(3):033024, 2021.

[502] Zohar Nussinov and Gerardo Ortiz. A symmetry principle for topological quantum order. *Annals of Physics*, 324(5):977–1057, May 2009.

[503] Davide Gaiotto, Anton Kapustin, Zohar Komargodski, and Nathan Seiberg. Theta, time reversal and temperature. *Journal of High Energy Physics*, 2017(5), May 2017.

[504] Chong Wang, Adam Nahum, Max A Metlitski, Cenke Xu, and T Senthil. Deconfined quantum critical points: symmetries and dualities. *Physical Review X*, 7(3):031051, 2017.

[505] T Senthil, Dam Thanh Son, Chong Wang, and Cenke Xu. Duality between $(2+1)d$ quantum critical points. *Physics Reports*, 827:1–48, 2019.

[506] Xiao-Chuan Wu, Wenjie Ji, and Cenke Xu. Categorical symmetries at criticality. *Journal of Statistical Mechanics: Theory and Experiment*, 2021(7):073101, 2021.

[507] H Casini and M Huerta. Remarks on the entanglement entropy for disconnected regions. *Journal of High Energy Physics*, 2009(03):048–048, mar 2009.

[508] Brian Swingle. Mutual information and the structure of entanglement in quantum field theory. *arXiv preprint arXiv:1010.4038*, 2010.

[509] Pablo Bueno, Robert C Myers, and William Witczak-Krempa. Universality of corner entanglement in conformal field theories. *Physical Review Letters*, 115(2):021602, 2015.

[510] Thomas Faulkner, Robert G. Leigh, and Onkar Parrikar. Shape dependence of entanglement entropy in conformal field theories. *Journal of High Energy Physics*, 2016(4):88, April 2016.

[511] Yi-Zhuang You, Zhen Bi, Alex Rasmussen, Kevin Slagle, and Cenke Xu. Wave function and strange correlator of short-range entangled states. *Physical Review Letters*, 112:247202, Jun 2014.

[512] Keola Wierschem and Pinaki Sengupta. Quenching the haldane gap in spin-1 Heisenberg antiferromagnets. *Physical Review Letters*, 112:247203, Jun 2014.

[513] Keola Wierschem and Pinaki Sengupta. Strange correlations in spin-1 Heisenberg antiferromagnets. *Physical Review B*, 90:115157, Sep 2014.

[514] Keola Wierschem and Pinaki Sengupta. Characterizing the haldane phase in quasi-one-dimensional spin-1 Heisenberg antiferromagnets. *Modern Physics Letters B*, 28(32):1430017, 2014.

[515] Zohar Ringel and Steven H. Simon. Hidden order and flux attachment in symmetry-protected topological phases: A Laughlin-like approach. *Physical Review B*, 91:195117, May 2015.

[516] Zohar Ringel. Using weak measurements to extract the Z_2 index of a topological insulator. *Physical Review B*, 91:241109, Jun 2015.

[517] Thomas Scaffidi and Zohar Ringel. Wave functions of symmetry-protected topological phases from conformal field theories. *Physical Review B*, 93:115105, Mar 2016.

[518] Han-Qing Wu, Yuan-Yao He, Yi-Zhuang You, Cenke Xu, Zi Yang Meng, and Zhong-Yi Lu. Quantum monte carlo study of strange correlator in interacting topological insulators. *Physical Review B*, 92(16), Oct 2015.

[519] K. Wierschem and K. S. D. Beach. Detection of symmetry-protected topological order in AKLT states by exact evaluation of the strange correlator. *Physical Review B*, 93:245141, Jun 2016.

[520] Ari M. Turner, Yi Zhang, and Ashvin Vishwanath. Mapping topological to conformal field theories through strange correlators. *Physical Review B*, 82:241102R, Oct 2010.

[521] Simone Giombi, Grigory Tarnopolsky, and Igor R. Klebanov. On C_J and C_T in conformal QED. *Journal of High Energy Physics*, 2016(8), Aug 2016.

[522] G.P. Korchemsky and A.V. Radyushkin. Renormalization of the wilson loops beyond the leading order. *Nuclear Physics B*, 283:342–364, 1987.

[523] Richard A. Brandt, Filippo Neri, and Masa-aki Sato. Renormalization of loop functions for all loops. *Physical Review D*, 24:879–902, Aug 1981.

[524] David F Mross, Jason Alicea, and Olexei I Motrunich. Explicit derivation of duality between a free dirac cone and quantum electrodynamics in $2+1$ dimensions. *Physical Review Letters*, 117(1):016802, 2016.

[525] Yan Qi Qin, Yuan-Yao He, Yi-Zhuang You, Zhong-Yi Lu, Arnab Sen, Anders W. Sandvik, Cenke Xu, and Zi Yang Meng. Duality between the deconfined quantum-critical point and the bosonic topological transition. *Physical Review X*, 7(3), Sep 2017.

[526] Chao-Ming Jian, Xiao-Chuan Wu, Yichen Xu, and Cenke Xu. Physics of symmetry protected topological phases involving higher symmetries and its applications. *Physical Review B*, 103(6):064426, 2021.

[527] Dam Thanh Son. Is the composite fermion a Dirac particle? *Physical Review X*, 5(3):031027, 2015.

[528] Max A Metlitski and Ashvin Vishwanath. Particle-vortex duality of two-dimensional dirac fermion from electric-magnetic duality of three-dimensional topological insulators. *Physical Review B*, 93(24):245151, 2016.

[529] Chong Wang and T Senthil. Dual dirac liquid on the surface of the electron topological insulator. *Physical Review X*, 5(4):041031, 2015.

[530] Clay Cordova, Po-Shen Hsin, and Nathan Seiberg. Time-reversal symmetry, anomalies, and dualities in $(2+1)d$. *SciPost Phys.*, 5:6, 2018.

[531] Cenke Xu and T. Senthil. Wave functions of bosonic symmetry protected topological phases. *Physical Review B*, 87(17):174412, May 2013.

[532] N. Read and G. Moore. Fractional Quantum Hall Effect and Nonabelian Statistics. *Prog. Theor. Phys. Supplement*, 107:157–166, 01 1992.

[533] Ryan Thorngren and Curt von Keyserlingk. Higher SPT's and a generalization of anomaly in-flow. *arXiv preprint arXiv:1511.02929*, 2015.

[534] Chenchang Zhu, Tian Lan, and Xiao-Gang Wen. Topological nonlinear σ-model, higher gauge theory, and a systematic construction of $(3+1)d$ topological orders for boson systems. *Physical Review B*, 100:045105, Jul 2019.

[535] Cenke Xu and Yi-Zhuang You. Bosonic short-range entangled states beyond group cohomology classification. *Physical Review B*, 91(5), Feb 2015.

[536] Peng Ye and Zheng-Cheng Gu. Vortex-line condensation in three dimensions: a physical mechanism for bosonic topological insulators. *Physical Review X*, 5(2):021029, 2015.

[537] Zheyan Wan and Juven Wang. Higher anomalies, higher symmetries, and cobordisms i: classification of higher-symmetry-protected topological states and their boundary fermionic/bosonic anomalies via a generalized cobordism theory. *Annals of Mathematical Sciences and Applications*, 4(2):107–311, 2019.

[538] Zheyan Wan, Juven Wang, and Yunqin Zheng. Higher anomalies, higher symmetries, and cobordisms ii: Lorentz symmetry extension and enriched bosonic/fermionic quantum gauge theory. *arXiv preprint arXiv:1912.13504*, 2019.

[539] Xiao-Gang Wen. Emergent anomalous higher symmetries from topological order and from dynamical electromagnetic field in condensed matter systems. *Physical Review B*, 99:205139, May 2019.

[540] Lokman Tsui and Xiao-Gang Wen. Lattice models that realize $\mathbb{Z}_n$-1 symmetry-protected topological states for even n. *Physical Review B*, 101:035101, Jan 2020.

[541] Chao-Ming Jian and Cenke Xu. Note on generalized symmetries, gapless excitations, generalized symmetry protected topological states, and anomaly. *Journal of Statistical Mechanics: Theory and Experiment*, 2021(3):033102, 2021.

[542] Po-Shen Hsin, Ho Tat Lam, and Nathan Seiberg. Comments on one-form global symmetries and their gauging in $3d$ and $4d$. *SciPost Physics*, 6(3), Mar 2019.

[543] H Casini, C D Fosco, and M Huerta. Entanglement and alpha entropies for a massive dirac field in two dimensions. *Journal of Statistical Mechanics: Theory and Experiment*, 2005(07):P07007, Jul 2005.

[544] H Casini and M Huerta. Entanglement entropy in free quantum field theory. *Journal of Physics A: Mathematical and Theoretical*, 42(50):504007, Dec 2009.

[545] EDUARDO FRADKIN and STEVEN KIVELSON. Short range resonating valence bond theories and superconductivity. *Modern Physics Letters B*, 04(03):225–232, 1990.

[546] Michael Levin and T. Senthil. Deconfined quantum criticality and Néel order via dimer disorder. *Physical Review B*, 70:220403, Dec 2004.

[547] Chao-Ming Jian and Cenke Xu. Note on generalized symmetries, gapless excitations, generalized symmetry protected topological states, and anomaly. *Journal of Statistical Mechanics: Theory and Experiment*, 2021(3):033102, 2021.

[548] Meng Cheng, Michael Zaletel, Maissam Barkeshli, Ashvin Vishwanath, and Parsa Bonderson. Translational symmetry and microscopic constraints on symmetry-enriched topological phases: A view from the surface. *Physical Review X*, 6(4):041068, 2016.

[549] R. Moessner and S. L. Sondhi. Three-dimensional resonating-valence-bond liquids and their excitations. *Physical Review B*, 68:184512, Nov 2003.

[550] OI Motrunich and T Senthil. Origin of artificial electrodynamics in three-dimensional bosonic models. *Physical Review B*, 71(12):125102, 2005.

[551] Gang Chen, Jan Gukelberger, Simon Trebst, Fabien Alet, and Leon Balents. Coulomb gas transitions in three-dimensional classical dimer models. *Physical Review B*, 80(4):045112, 2009.

[552] Chong Wang, Andrew C Potter, and T Senthil. Classification of interacting electronic topological insulators in three dimensions. *Science*, 343(6171):629–631, 2014.

[553] Shauna Kravec, John McGreevy, and Brian Swingle. All-fermion electrodynamics and fermion number anomaly inflow. *Physical Review D*, 92(8):085024, 2015.

[554] Xiao-Liang Qi, Taylor L Hughes, and Shou-Cheng Zhang. Topological field theory of time-reversal invariant insulators. *Physical Review B*, 78(19):195424, 2008.

[555] Xie Chen, Yuan-Ming Lu, and Ashvin Vishwanath. Symmetry-protected topological phases from decorated domain walls. *Nature communications*, 5(1):1–11, 2014.

[556] R. Moessner and S. L. Sondhi. Resonating valence bond phase in the triangular lattice quantum dimer model. *Physical Review Letters*, 86:1881–1884, Feb 2001.

[557] Daniel Friedan. Nonlinear models in $2 + \epsilon$ dimensions. *Physical Review Letters*, 45(13):1057, 1980.

[558] Daniel Harry Friedan. Nonlinear models in $2 + \epsilon$ dimensions. *Annals of physics*, 163(2):318–419, 1985.

[559] Thomas L Curtright and Cosmas K Zachos. Geometry, topology, and supersymmetry in nonlinear models. *Physical Review Letters*, 53(19):1799, 1984.

[560] Sergei V Ketov. *Quantum non-linear sigma-models: from quantum field theory to supersymmetry, conformal field theory, black holes and strings*. Springer Science & Business Media, 2000.

[561] Xiao-Chuan Wu, Kelly Ann Pawlak, Chao-Ming Jian, and Cenke Xu. Emergent superconductivity in the weak mott insulator phase of bilayer graphene moiré superlattice. *arXiv preprint arXiv:1805.06906*, 2018.

[562] Aleksandr Michajlovič Polyakov. *Gauge fields and strings*. Taylor & Francis, 1987.

[563] Mehran Kardar. *Statistical Physics of Fields*. Cambridge University Press, 2007.

[564] Leo P. Kadanoff and Horacio Ceva. Determination of an operator algebra for the two-dimensional ising model. *Physical Review B*, 3:3918–3939, Jun 1971.

[565] Edward Witten. Nonabelian bosonization in two dimensions. *Comm. Math. Phys.*, 92(4):455–472, 1984.

[566] Ribhu K. Kaul and Subir Sachdev. Quantum criticality of U(1) gauge theories with fermionic and bosonic matter in two spatial dimensions. *Physical Review B*, 77:155105, Apr 2008.

[567] Sergio Benvenuti and Hrachya Khachatryan. Easy-plane QED_3 in the large N_f limit. *Journal of High Energy Physics*, 2019(5):1–43, 2019.